UNIVERSITÉ AIX-MARSEILLE

Centre de Recherche et d'Enseignement de Géosciences de l'Environnement

CARACTÉRISATION DE LA DÉFORMATION TECTONIQUE RÉCENTE DU SYSTÈME DE FAILLES DE BELLEDONNE ET DE L'AVANT-PAYS ALPIN (VALLÉE DU RHÔNE) : APPORTS D'UNE APPROCHE PLURIDISCIPLINAIRE

THESE

Pour obtenir le grade de

DOCTEUR DE L'UNIVERSITÉ AIX-MARSEILLE

Discipline : Géosciences de l'environnement

Présentée et soutenue publiquement par

Jérémy BILLANT

Le 10 mars 2016

JURY

M. LARROQUE Christophe	Maître de conférence, Université de Reims	Rapporteur
M. SCHWARTZ Stéphane	Maître de conférence, Université de Grenoble	Rapporteur
M. BOLLINGER Laurent	Ingénieur-chercheur, CEA	Examinateur
M. CAMELBEECK Thierry	Professeur invité, Université Libre de Bruxelles	Examinateur
M. RITZ Jean-François	Directeur de Recherche, CNRS	Examinateur
M. SUE Christian	Professeur, Université de Franche-Comté	Examinateur
M. MANCHUEL Kevin	Ingénieur-chercheur, EDF-DIN-CEIDRE TEGG/SGG	Invité
M. BELLIER Olivier	Professeur, Université Aix-Marseille	Directeur de thèse
M. HIPPOLYTE Jean-Claude	Chargé de Recherche, CNRS	Directeur de thèse

Résumé

Le but de cette étude est de caractériser, grâce une approche multi-disciplinaire (rendue nécessaire du fait des faibles taux de déformation et des forts taux d'érosion de la zone d'étude) les déformations tectoniques récentes (Plio-Quaternaire) associées au système de failles de Belledonne. Ce système de failles est localisé dans les Alpes occidentales et s'étend sur environ 150 km. Il est composé de plusieurs décrochements qui sont du NE au SW :

- la faille dextre de l'Arcalod orientée NE-SW dans le massif des Bauges,
- la faille bordière de Belledonne, dextre et orientée NE-SW, en bordure SE de la vallée du Grésivaudan,
- la faille sénestre antithétique du Brion orientée NW-SE en terminaison SW de la faille bordière de Belledonne,
- la faille dextre du Jasneuf orientée NE-SW dans le massif du Vercors.

La détermination des états de contraintes tardi-Cénozoique montre que le champ de contrainte actuel, responsable entre autre de la cinématique en décrochement le long du sytème de faille de Belledonne, date de la fin du Pliocène supérieur/Pléistocène et a succéder au champ de contrainte causé par la collision alpine.

Des marqueurs morphologiques décalés mais ambigües et d'âge incertain (probablement anté-Rissiens) ont été trouvés le long des failles de l'Arcalod et du Brion empéchant une détermination précise des vitesses de glissement. La trace de la faille bordière de Belledonne n'a pu être déterminé, suggérant que la déformation en surface associée à cette dernière soit accomodée dans une large bande de cisaillement.

La faille du Jasneuf décale des morphologies d'âges supposés messiniens et anté-Rissiens. La vitesse de cette faille intégrée depuis le messinien serait de 0,13±0,03 mm/an. En prenant en compte que cette faille semble limitée à la couverture et en excluant qu'une partie de la déformation soit accomodée asismiquement, elle pourrait générer des séismes de magnitude 5,7 avec un temps de retour ~500 ans.

L'accomodation de la déformation actuelle dans l'avant-pays a été étudié dans la vallée de Toulaud (SW de Valence) où une faille tardi-hercynienne recoupe le canyon messinien du Rhône. Les premiers résultats indiquent que la faille décale verticalement le canyon, attestant d'une tectonique Plio-Quaternaire le long de cet accident.

TABLE DES MATIÈRES

I - INTRODUCTION

Même si à l'échelle mondiale, le SE de la France est caractérisé par un aléa sismique modéré, il n'en demeure pas moins, à l'échelle nationale, l'une des régions les plus concernées par le risque sismique. Comme en témoigne son histoire, sa sismicité historique est une des plus importantes du territoire métropolitain, avec depuis le XVème siècle plusieurs séismes d'intensité égale ou supérieure à VIII, impliquant l'existence de failles actives ayant un potentiel sismogénique élevé (magnitudes potentielles de 6,0). La densité de population y est localement très importante (métropoles de Grenoble, Montpelliers, Nîmes, Nice et Marseille). Si l'intensité des séismes historiques est relativement élevée dans le SE de la France (intensité maximale entre VI à IX à périodicité séculaire), ce domaine ne subit qu'une faible activité microsismique, hormis le domaine alpin sensu stricto.

L'origine et les caractéristiques de cette sismicité et la prise en compte de ce risque sont, mal connues : Pourquoi et comment des séismes d'intensités importantes se produisent-ils dans cette zone alors que la déformation aux limites est très faible ? Comment appréhender le risque sismique dans des régions à aléa modéré ? Les études engagées ces dernières années ont contribué à répondre à certaines de ces questions, par une meilleure compréhension du comportement sismogénique des failles, notamment en Provence. Le plus souvent les résultats les plus probants ont été obtenus par l'utilisation de démarches consistant à croiser les approches géologiques et géophysiques (Chardon et al., 2005; Cushing et al., 2008; Larroque et al., 2011; Schlupp et al., 2001). Toutefois, il nous reste des efforts à faire en ce qui concerne d'autres régions françaises.

Cette étude se focalise sur un système de failles que nous appellerons système de Belledonne, qui constitue un alignement d'accidents orientés NE-SW qui comprend, entre autre, la faille bordière de Belledonne soulignée par un essaim de microsismicité bordant la vallée de l'Isère entre les cluses de Grenoble et de Chambéry (Fig. I.1, Thouvenot et al., 2003). Aucune étude géologique ou morphotectonique n'a permis, à ce jour, de mettre en évidence cette faille en surface. Cette faille pourrait appartenir aux systèmes d'accidents de socle d'orientation NE-SW, d'âge Varisque (hérité de la phase tardi-hercynienne), qui affectent le sud-est de la France et dont l'histoire géologique et structurale est longue et complexe (e.g., failles de Nîme, de la Moyenne Durance, etc.). Sa proximité de grandes agglomérations peri-Alpines en fait un objet d'étude privilégié pour l'évaluation de l'aléa sismique en France. Alors que des séismes de la période instrumentale sont connus avec des magnitudes relativement faibles (3.5, Laffrey, 1999 ; 4.9, Monteynard, 1963) la longueur de ce linéament suggère qu'il pourrait produire des événements de magnitude 6 (Thouvenot et al., 2003). En outre cet accident se situe en bordure de la vallée de

l'Isère, dont le remplissage de plus de 500 m de sédiments récents pourrait être un facteur aggravant en terme de risque en cas de séisme (effet de site, liquéfaction...).

I.1 - Présentation de la zone d'étude

I.1.1 - Principaux traits structuraux et morphologique

Dans la partie alpine, l'aire d'étude se situe à la limite de deux domaines : les massifs cristallins externes et les massifs subalpins correspondant respectivement au socle anté-triassique et sa couverture sédimentaire mésozoïque (Fig. I.1). Du nord au sud, les massifs cristallins sont les massifs des Aiguilles Rouges, du Mont Blanc, de Belledonne et du Pelvoux. Les massifs subalpins sont les massifs des Bornes, des Aravis, des Bauges, de la Chartreuse, du Vercors, du Diois et des Baronnies. Les massifs des Bauges et de la Chartreuse sont aujourd'hui séparés du massif de Belledonne par la vallée du Grésivaudan où s'écoule l'Isère.

Les failles principales de cette zone sont orientées NE-SW et recoupent les massifs cristallins externes (par exemple, la faille du Synclinal Médian). Ces failles sont héritées de la collision Varisque durant laquelle elles étaient de grands décrochements dextres recoupant l'ensemble de la croûte comme l'atteste l'injection de magma provenant du manteau lithosphérique dans certaines d'entre elles (Guillot and Ménot, 2009). Ces zones de faiblesse crustale ont pu être réactivées durant les phases tectoniques suivantes, notamment en tant que failles normales durant l'extension téthysienne (Guillot and Ménot, 1999; Lemoine et al., 1981) et en tant que failles décrochantes dextres ou failles inverses durant la collision alpine (Debelmas and Kerckhove, 1980; Lemoine et al., 1981).

Du Trias supérieur (Barféty and Gidon, 1990) au Dogger, l'extension téthysienne a permis la création d'hémi-graben le long de failles normales crustales à regard SE (Barféty et al., 1979; Lemoine et al., 1986, 1981). De l'Oligocène au Miocène supérieur (Beck et al., 1998; Bellahsen et al., 2014; Dumont et al., 2008), la collision alpine a affecté les domaines alpins les plus externes (massifs cristallins et subalpins). La compression engendrée a conduit dans les massifs cristallins externes à la verticalisation des failles normales téthysiennes (Gidon, 2001; Lemoine et al., 1981). Elle a également permis le chevauchement vers le nord-ouest et à la surrection des massifs cristallins externes (Fig.I.2 Bellahsen et al., 2014).

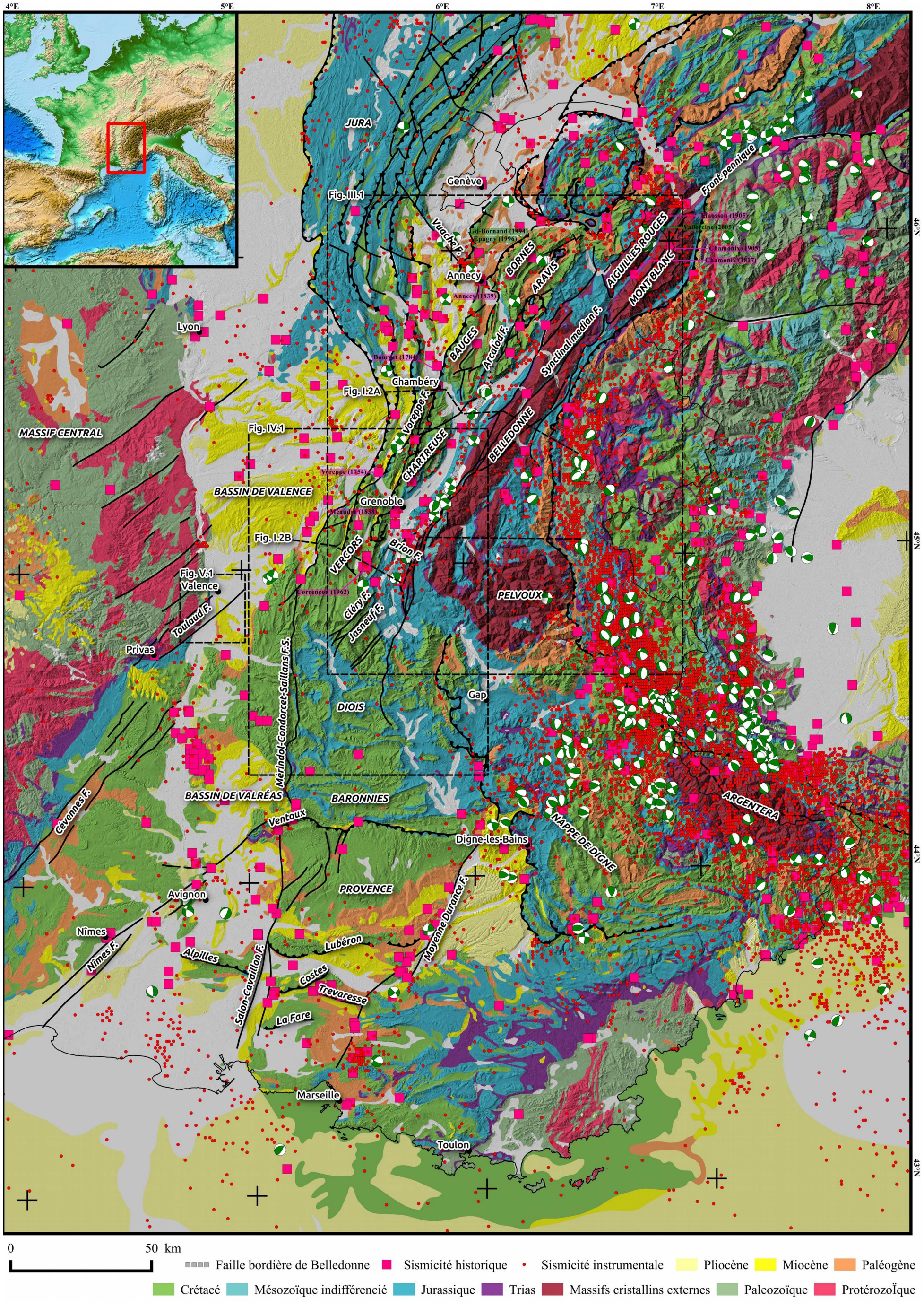

Figure I.1: Carte géologique simplifiée et de la sismicité. Mécanismes au foyer dessinés avec le module complémentaire qBeachball pour QGIS (en développement).

Dans les massifs subalpins, la collision a engendré la formation de plis et chevauchements orienté N-S à N20° (Chiron and Kerrien, 1980; Debelmas et al., 1979), les chevauchements s'enracinant dans les unités liassiques ou triassiques à la base de la pile sédimentaire (Fig. I.2, Arpin, 1988; Deville and Chauvière, 2000; Philippe et al., 1998). Ces plis et chevauchements sont recoupés par des failles dextres orientées NE-SW (Gidon, 1999, 1996, 1990, 1981; Kerckhove and Antoine, 1964). La dominance des décrochements dextres par rapport à ceux sénestres semble indiquer qu'il ne s'agit pas simplement de failles de transfert mais que ces dernières ont permis l'accommodation du cisaillement dextre de l'ensemble des massifs subalpin (Gidon, 1990) du fait de la rotation de la plaque apulienne (Collombet, 2001; Gidon, 1974). La limite occidentale des massifs du Vercors, du Diois et des Baronnies correspond au système de failles N-S de Mérindol-Condorcet-Saillans, limité à la couverture (Rangin et al., 2011a), long de ~80 km et s'étendant jusqu'au chaînon Ventoux-Lure au sud.

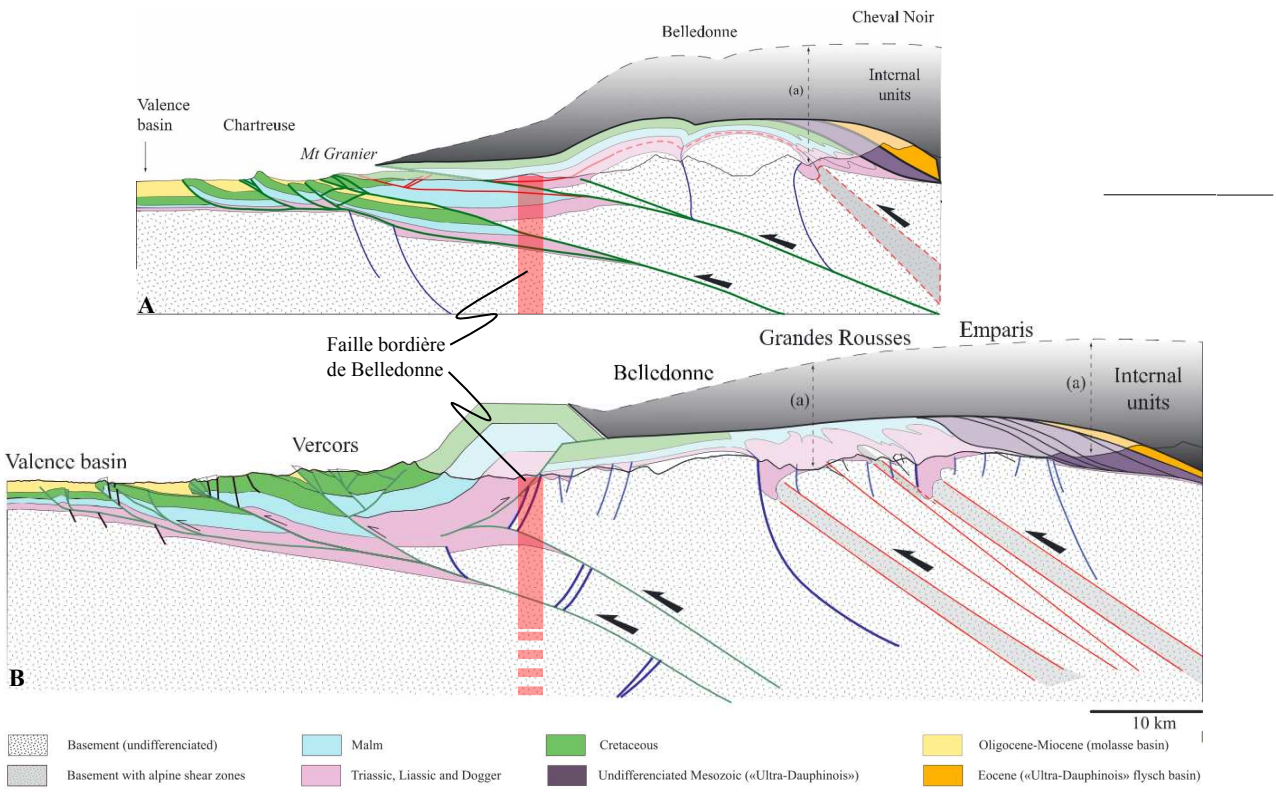

Figure I.2: Coupes géologiques équilibrées au travers du massif de Belledonne et A) du massif de la Chartreuse (Deville and Chauvière (2000) équilibrée par Bellahsen et al. (2014)) et B) du Vercors (Bellahsen et al., 2012). Location en figure I.1.

L'avant pays (bassin de Valence et de Valréas) est principalement constitué des dépôts de molasses miocènes marines et continentales recouvertes localement de dépôts continentaux plio-quaternaires (Chiron and Kerrien, 1980; Rouire et al., 1980). À l'ouest de la vallée du Rhône se trouve le Massif Central découpé par des décrochements NE-SW tardi-hercyniens (Arthaud and Matte, 1975). Parmi ces failles se trouve la faille des Cévennes. Longue de ~155 km, elle sépare le Massif Central du bassin du sud-est. Elle a été réactivée en tant que faille normale durant l'extension mésozoïque et en décrochement sénestre durant la collision pyrénéenne (Arthaud and Laurent, 1995). Elle a été inversée à nouveau en faille normale durant l'extension oligocène (Sanchis and Séranne, 2000).

I.1.2 - Déformation actuelle des Alpes de l'Ouest

I.1.2.1 - Sismicité de la zone d'étude

I.1.2.1.1 - Sismicité historique

La sismicité historique est diffuse, la plupart des événements ont une intensité (MSK) inférieure à V (base de donnée SISFRANCE) et ne peuvent être associés de manière certaine à la réactivation d'une faille en particulier. Quelques séismes notables présentent une intensité élevée, par exemple (localisation en fig. I.1) :

- les séismes du Lac du Bourget (15/10/1784, I = 6,5), de Voreppe (12/01/1754, I = 6,5) et celui de Méaudre (22/05/1838, I = 6,5) proches du front chevauchant des massifs subalpins.

- le séisme d'Annecy (11/08/1839, I = 7), ressenti à plus de 30 km et probablement causé par la faille du Vuache (Baize et al., 2011).

- les deux séismes de Chamonix (11/03/1817, I = 7 et 13/08/1905, I = 7) et le séisme d'Émosson (29/04/1905) localisés dans les massifs cristallins externes des Aiguilles Rouges et du Mont Blanc.

Un des événements les plus récents et des plus notables est le séisme de Corrençon-en-Vercors (25/04/1962, I = 7,5). Il fut ressenti à plus de 140 km et causa de graves dommages à la ville éponyme (Fig. I.3).

Figure I.3: Dégâts causés par le séisme de Corrençon-en-Vercors (25/04/1962, I = 7,5) : tombes ouvertes, murs craquelés et maisons effondrées. La pendule, tombée en panne lors du séisme, indique l'heure de ce dernier. Sources : http://fresques.ina.fr/rhone-alpes/fiche-media/Rhonal00357/un-tremblement-de-terre-a-correncon-en-vercors.html et http://www.ledauphine.com/isere-sud/2009/10/12/seisme-1962-correncon

I.1.2.1.2 - Sismicité instrumentale

La sismicité instrumentale (catalogue Si-HEX, Cara et al. (2015)) souligne deux arcs de sismicité séparés par les massifs cristallins externes déjà identifiés par Thouvenot (1996). Le premier arc sismique est limité à l'ouest par le front pennique. Dans ce domaine, les séismes ont principalement des magnitudes inférieures à 4 et leurs hypocentres sont principalement dans les dix premiers kilomètres de la croûte. Les mécanismes au foyer dont les axes T sont perpendiculaires à la chaîne indiquent des cinématiques en faille normale (Fig. I.1, Delacou et al., 2004; Eva and Solarino, 1998; Sue et al., 1999; Thouvenot, 1996)).

Le deuxième arc de sismicité est délimité, à l'ouest, par le front des massifs subalpins et à l'est, par les massifs cristallins externes. La sismicité y est plus diffuse (Fig. I.1). Les séismes se produisent aussi principalement dans les dix premiers kilomètres de la croûte et ont des magnitudes inférieures à 4. Les mécanismes au foyer dans ce domaine indiquent des cinématiques de failles en décrochement et en compression et présentent pour leur part des axes P perpendiculaires à la chaîne (Fig. I.1, Delacou et al., 2004; Kastrup et al., 2004; Maurer et al., 1997; Sue et al., 1999).

La faille bordière de Belledonne (localisation en figure I.1) compte parmi les quelques failles actives reconnues sur le territoire de France métropolitaine. Elle a été identifiée et caractérisée « sismologiquement » (microsismicité et mécanismes focaux) par Thouvenot et al. (2003). Elle correspond à un alignement d'environ 150 épicentres de séismes de magnitude 0 à 3,5, d'orientation NE-SW (environ N30°E), qui s'étend sur près de 50 km de La Mure (près de Grenoble) à Montmélian (près de Chambéry).

L'alignement des épicentres des séismes, de direction N30°E, confirme l'orientation NE-SW de la faille. Les foyers (hypocentres), localisés autour de 0 à 16 km de profondeur (seulement deux séismes présentent des profondeurs de 20 et 22 km), suggèrent qu'il pourrait s'agir d'une faille de socle (Fig. I.2), alors que les mécanismes au foyer calculés (Fig. I.1) sont caractérisés par des axes P orientés ENE-WSW et indiquent un mouvement de faille à composante décrochante dextre.

I.1.2.2 - Déformation mesurée par géodésie

À l'échelle des Alpes, les mesures de déplacement par GPS n'indique aucune convergence entre les plaques européenne et apulienne (Nocquet, 2012). En revanche, ces mêmes mesures indiquent que la plaque apulienne subit une rotation anti-horaire, de 0,3°/Ma à 0,5°/Ma autour d'un pôle de rotation situé dans la plaine du Pô (Calais et al., 2002; Caporali and Martin, 2000; D'Agostino et al., 2008). Cette rotation, dans un modèle de plaque rigide, impliquerait une limite en

décrochement dextre dans les Alpes occidentales accommodant environ 1 mm/an de mouvement relatif (Nocquet and Calais, 2004).

Les premières mesures de taux de déformation locaux dans les Alpes ont pu être effectuées par comparaison des différentes triangulations effectuées en France ou par comparaison de triangulations et de mesures effectués par GPS. Il a ainsi été déterminé que le Jura se déplaçait de 4 à 5 mm/an vers l'ouest par rapport à son front (Jouanne et al., 1994), des taux de raccourcissement E-W de 5 ± 2,5 $mm.an^{-1}$ (pour une cellule de 20*20 km) dans la région grenobloise (Martinod et al., 2001) et des taux E-W d'extension atteignant jusqu'à 4 $mm.an^{-1}$ (pour ~10 km) dans le Briançonnais (Sue et al., 2000). Les mesures effectuées par GPS par la suite, notamment grâce aux stations permanentes, ont permis de déterminer que des axes de déformations cohérents avec les études préliminaires, mais que les vitesses proposées étaient surestimées d'un facteur 4 à 10 (Calais et al., 2002; Nocquet, 2002; Walpersdorf et al., 2015, 2006). Les taux de déformation dans les Alpes occidentales sont donc de l'ordre de 0,1 à 1 mm/an (pour ~10 km).

I.2 - Objectifs et méthodologie de l'étude

Les Alpes occidentales, sont donc soumises à des déformations crustales modérées. Elles ont été et sont encore, soumises à une érosion importante. Cela rend l'étude de la déformation actuelle difficile par des méthodes classiquement utilisées en domaine de déformation plus rapide. En effet, les catalogues de sismicité ne renseigne pas sur le cycle sismique complet (temps de récurrence des forts séismes inconnu mais long) et les indices de déformations récentes sont souvent ambigües ; citons par exemple les failles normales actives des Grands Moulins (Baize et al., 2002; Bordet, 1970) réinterprétées comme des sackungs (Hippolyte et al., 2006b), la morphologie du balcon de Belledonne comme résultant de failles normales actives (Darmendrail et al., 1994) réinterprétée comme résultant de l'érosion glaciaire (Billant et al., 2015) ou encore le bassin de Séchilienne interprété comme un bassin en pull-appart entre deux failles actives sénestres (Pothérat et Effendiantz, 2009) réinterprété comme résultant uniquement de processus érosifs (Le Roux et al., 2010).

En France, des travaux récents ont permis de valider la démarche pluri-disciplinaire, consistant notamment à croiser les approches géologiques, géomorphologiques, géochronologiques et géophysiques (par exemple, Baize et al., 2011; Cushing et al., 2008; Larroque et al., 2011). Il faut donc favoriser et améliorer les approches pluri-disciplinaires dans les zones actives complexes à faible taux de déformation et aléa modéré, mais à risque potentiellement élevé. L'objectif de ce

travail est de caractériser la géométrie, la cinématique et le potentiel sismogénique du faisceau d'accidents de Belledonne et son interaction avec l'avant-pays alpin et les failles cévenols. Les structures tectoniques observées en surface dans le quart sud-est de la France résultent d'une histoire tectonique complexe (tectoniques superposées d'âge « téthysien », « pyrénéen », oligocène et « alpin »), marquée par l'héritage structural d'une histoire géologique depuis 250 Ma et qui a interféré au Cénozoïque avec des périodes de morphogénèses contrastées caractérisées par des phases alternées d'aplanissement, de remblaiement et de dissection. Les structures qui en résultent sont partiellement réactivées actuellement. Pour ces raisons, et parce que les traces de déformation récente en surface sont généralement de faible amplitude, il est nécessaire de mettre en place une approche pluri-échelle (dans le temps et l'espace) et donc multi-disciplinaire afin de mettre en évidence et de quantifier les processus géologiques, en surface et à l'échelle de la croûte, qui contrôlent l'architecture actuelle du substratum géologique et des failles actives. Cette approche pluri-échelle a également pour objectif de caractériser les processus qui contrôlent la morphogenèse tout en identifiant les processus de dégradation des indices morphologiques. Des actions de recherche dans les domaines suivants ont donc été développées :

- Tectonique et analyse structurale : analyse tectonique, géologie structurale, cartographie des accidents (à partir de documents planaires : cartes géologiques et topographiques, photo aériennes), de MNT et de données de terrains.

- Cinématique de failles et état de contrainte : mesure de fracturation et des vecteurs glissement sur les plans de faille récent en vue de déterminer l'état de contrainte récent responsable des déformations fini-tertiaires et quaternaires. Les états de contrainte ainsi déterminés peuvent être comparés à ceux définis par l'inversion de mécanismes au foyer.

- Géomorphologie qualitative et quantitative : analyse de photographies aériennes, acquisition et analyse de MNT, étude des marqueurs de déformation dans les terrains récents et d'anomalie de drainage.

- Géologie du quaternaire et géomorphologie plio-quaternaire (étude des terrasses alluviales, dépôts glaciaires). Une attention particulière sera portée à l'interaction entre les failles potentiellement actives et les marqueurs de la crise messinienne. L'activité récente des failles peut en effet être caractérisée par l'étude des canyons messiniens du Rhône et de ces affluents dont les marqueurs morphologiques et sédimentaires permettent la mise en évidence de déformations récentes (Clauzon et al., 2011; Molliex, 2009; Schlupp et al., 2001).

Les résultats de ce travail sont présentés sous la forme d'une série d'articles publiés, soumis ou en préparation formant les quatre chapitres de cette thèse :

- Le premier chapitre présente les cinématiques de faille et états de contraintes méso-cénozoïque du quart sud-est de la France. Les données sont issues d'une synthèse bibliographique complétée de travaux de terrain. Ce chapitre permettra également de présenter l'histoire géodynamique de la région.

- Le deuxième chapitre est consacré à l'analyse morphostructurale effectuée, du nord-est au sud-ouest, le long de la faille d'Arcalod, de la faille bordière de Belledonne et de sa faille antithétique, la faille du Brion.

- Le troisième chapitre présente les résultats de l'analyse morphostructurale effectuée sur la faille du Jasneuf située dans le prolongement sud-ouest de la faille bordière de Belledonne. Des points méthodologiques portant sur la mesure de décalage morphologique sont présentés.

- Enfin, dans le quatrième chapitre sont exposés les résultats préliminaires portant sur la faille de socle de Toulaud, située dans le Massif Central (à l'ouest de Valence), dont je tente de déterminer l'activité post-messinienne grâce à l'analyse de la morphologie de surface et de subsurface (canyon messinien du Rhône).

II - MESO-CENOZOIC STRESS STATE VARIATIONS IN THE WESTERN ALPS, FRANCE.

Un des premiers objectifs de cette étude pluridisciplinaire est de contraindre la cinématique actuelle du système de failles de Belledonne et de l'avant pays alpin, l'état de contrainte responsable des déformations et de remettre l'ensemble dans un contexte régional. Du fait des faibles taux de déformation, les déformations récentes sont souvent mal exprimées. La bonne caractérisation des régimes de déformation tardi-cénozoiques à actuels nécessite donc de bien connaître régionalement les contextes tectoniques du passé.

Dans cette optique et après avoir constaté qu'il n'existait pas de base de donnée des études de cinématique de faille et état de contrainte, nous avons effectué une synthèse des données de microtectonique des travaux précédents sur le quart sud-est de la France qui regroupe pour l'instant ~1700 tenseurs de contraintes. Cette base de données n'est pour l'instant pas exhaustive mais nous espérons pouvoir l'étendre dans le futur au reste de la France et à ses orogènes.

Cette base de donnée a été complétée par nos travaux le long du système de failles de Belledonne ainsi qu'en bordure Ouest des massifs du Vercors (avant-pays, Vallée du Rhône), du Diois et des Baronnies (dont une partie a été acquise durant les stages de Sébastien Baixas et d'Alexandra Heape, étudiants en deuxième année de master).

Les états de contrainte déduits de l'inversion des mécanismes au foyer ont également été pris en compte et comparés aux états de contrainte récents à actuels déduits des mesures de stries pour vérifier leur cohérence.

L'ensemble de ces données est présenté ci-après, sous forme d'un article en préparation. Il nous permettra également de présenter l'histoire géodynamique de notre zone d'étude depuis le début du secondaire.

II.1 - Introduction

In order to better understand the context of active tectonics and fault kinematics of the Belledonne fault system and Western Alps, we need to know the stress state variations in space and time at a regional scale. In this purpose, we made a bibliographic review of the existing stress state extending laterally from the eastern border of the Central massif to the western Inner Alps and longitudinally from the southern Jura to the Mediterranean coast. This review was completed by field surveys, mainly around the Mérindol-Condorcet-Saillans (MCS) fault system bordering to the West the Vercors, Diois and Baronnies massifs in order to better constrain the relationship between active tectonics of Alpine and Pyreneo-Provençal realms and to complete the lack of knowledge about the modern stress state in this area.

After the presentation of the method and the key sites of our field survey allowing the determination of stress states ages and/or chronologies, we discuss the stress states in the geodynamical frame.

II.2 - Stress state determination

After the formulation of the Wallace (1951) and Bott (1959) assumptions, it appears to tectonicians that fault striations could be used to determine the strain and/or stress state responsible of the deformation (e.g. Angelier, 1975; Arthaud, 1969; Carey and Brunier, 1974; Ritz and Taboada, 1993). This method was then extended to the determination of the stress state from focal mechanisms (Carey-Gailhardis and Mercier, 1987; Gephart and Forsyth, 1984). Since, this method has been used successfully to determine past and present stress state (e.g., Bellier and Zoback, 1995; Bergerat, 1981; Hippolyte et al., 2012a; Homberg et al., 2002; Mercier et al., 1991). Assuming that the shear stress applied on a fault plane has the same direction than the slip on this fault, most of the stress inversion methods compute a best fitting reduced stress tensor for a fault population. This computation is generally based on minimizing the angle between the measured striae and the computed slip vector resulting from the application on each fault plane of the computed stress tensor. Such an analysis therefore implies that striae and their kinematics must be constrained for a fault population corresponding to a single stress state.

II.2.1 - Stress determination method from fault kinematics analysis

II.2.1.1 - Data collection and inversion method

The first step is to collect fault slip data during field surveys. Fault slip data are defined by the strike and dip of the fault plane and by the trend and plunge of the striae measured on faults of any scale. Sense of slip is determined using sense criterion e.g., ploughing of striating elements (Fig. II.1), crystalline steps, Riedel fractures or tensile fractures (Petit, 1987; Petit et al., 1983).

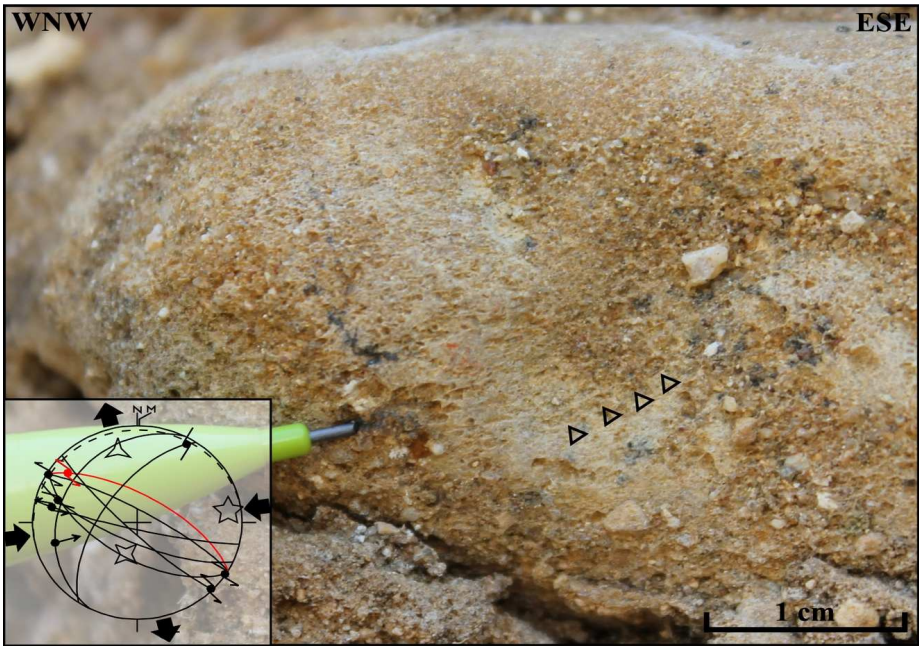

Figure II.1: Calcareous pebble striated by quartzitic sand in the upper Pliocene conglomerates at the BOZONS measurements site. Penetration of the sand indicates a left-lateral kinematics along the near vertical face of the pebble. Triangles underline one of the striae. Schmidt's diagrams with computed stress tensors of the BOZONS site: solid lines for fault planes (in red for the one of the photography), dashed lines for bedding planes. σ1, σ2, and σ3 as five branches, four branches and three branches stars respectively.

Fault slip data are then reported in a database. If several deformation stages are revealed on a site during field survey by incompatibles fault slips, each stage is separated in different subsets mainly based on field observations (see II.2.1.2). Here, a plot in a Schmidt's diagram can help to separate faults from different deformation stages in different subsets. We then performed stress inversion using the INVD method proposed by Angelier (1990) which gives reliable results in most

cases (Hippolyte et al., 2012b). The results of the stress inversion include the orientation (azimuth and plunge) of the three principal stress axes σ_1, σ_2 and σ_3 (maximum, intermediate and minimum compressional stress axes) of a stress tensor, and the stress ellipsoid shape ratio (R or $\varphi=(\sigma_2-\sigma_3)/(\sigma_1-\sigma_3)$). The α and RUP misfit parameters are also provided for each stria. α is the angle in the fault plane between the computed and the measured stria (range between 0 and 180°) and RUP is the magnitude of the difference between the unit vector along the computed shear stress and a scalar product of a unit slip vector along the stria (range between 0% and 200%). According to Angelier (1990), striations with α and RUP respectively of ≤22.5° and ≤50% are in good agreement with the modeled stress tensor whereas values of ≥45° and ≥75% must be rejected. Intermediate values must be considerated carrefully but can be good in the case of large fault slip dispersion. Analysis of this misfit parameters yields to exclude striae that do not correspond to the determined stress state but can also allow the separation between two fault subsets according to their dispersion. Finally, if necessary, faults and stress solution are back-tilted according to the structure of the site (in many cases, it consits to tilt the data of a value equal to the dip but in an opposite direction).

II.2.1.2 - Age and relative chronology of the stress states

For fault striations, it is usually difficult to constrain the absolute age of fault slips more precisely than younger than the age of the rocks affected by the faults.

It is possible that at one measurement site, different stress states affected the rocks. In this case, aim is to determine the chronology between the different stress states by using cross-cutting relationship between markers of the different stages, e.g. crystalline step growing from the flank of a corrugation (Fig. II.2) or one fault offsetting another fault. Even if it is rather rare to observe clear chronologies between two different faulting events, the chronologies observed at one site can be extrapolated at other sites (several close stress state over an area are supposed to have the same age and to be regionally significant).

At a measurement site, strata dip is also measured and we can estimate if the formation of a stria occurred before, during or after the tilting (Hippolyte et al., 2012b). If the relative or absolute age of the folding is known, it can allow the determination of the age of faulting and the associated stress state. Field observations are then compared with the result of the stress inversion. Stress axes are supposed to follow Andersonian orientation (i.e., two principal stress directions included in the plane defined by the earth surface). After the inversion, we can see if the stress axes are in such orientations. If not, and if two axes are included in or closed to the plane defined by the strata dip, it could imply that the stress state was prior to the tilting of the strata (e.g. normal faulting of the

SAILLANS2 site, fig. II.2). Stress state can also be registered during the tilting of the strata. In such a case, only one stress axis might be included in or closed to the great circle of the bedding plane. In the case of chronologies inferred from strata tilting, we look carefully to the geological structure in which we made measurements in order to determine for example, if the site is located at a fold termination or within a fault zone.

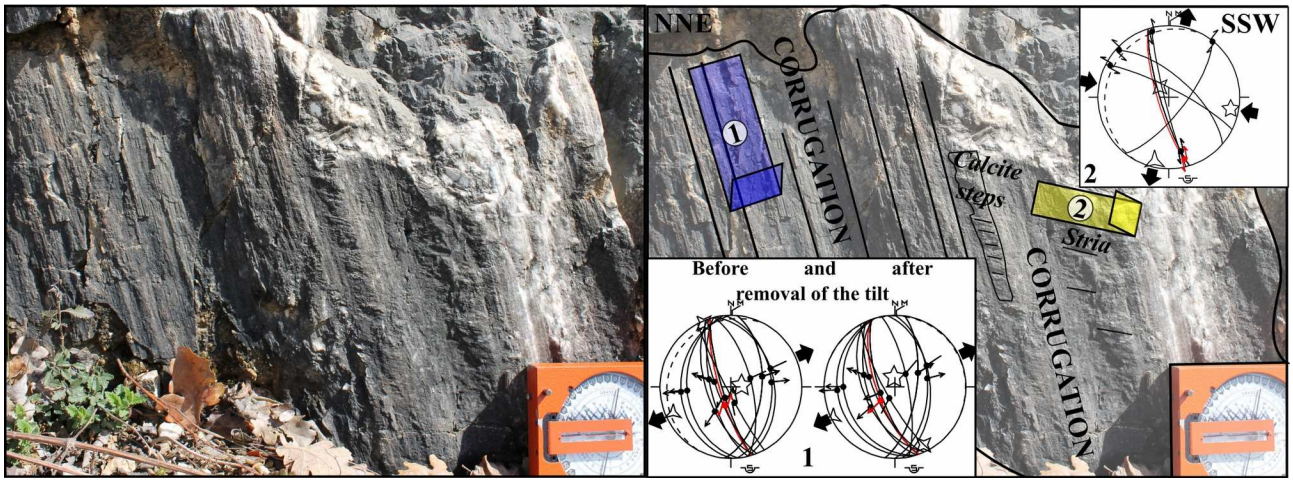

Figure II.2: Example of chronological indication between two fault slips at the SAILLANS2 measurement site (Tithonian limestone). Fault corrugations indicate normal faulting. A second left lateral strike-slip has generated calcite steps growing from one side of the corrugation and has striated the other side. Schmidt's diagrams with computed stress tensors for both fault kinematics. Same legend as fig. II.1.

II.2.2 - Stress determination method from focal mechanisms analysis

In this case, the problem is to determine which of the two nodal planes was the fault plane or the auxiliary plane (Carey-Gailhardis and Mercier, 1987; Gephart and Forsyth, 1984). For this, a first stress state is determined from the whole focal plane dataset using the Right Dihedron method which do not need a choice between the two nodal planes but which do not use the slip vectors (Angelier and Mechler, 1977). In most case, for a given stress tensor, the shear stress do not correspond to the slip along both focal planes. It allows the separation of the focal planes considering that for each focal mechanisms, the focal plane displaying the lowest misfit parameters is the fault plane. Finally, a last stress inversion is performed using only the fault planes. In this work, we used the method proposed by Delvaux and Sperner (2003). A first stress tensor is determined using the Right Dihedron method. Then for each focal mechanism, a counting deviation is computed. It corresponds to the ratio of the counting net of a focal mechanism with the average counting net. Focal mechanisms displaying abnormal counting deviations, i.e. higher than the mean

counting deviation +2σ, are rejected of the dataset. This method allows the identification of the focal mechanisms that are mostly incompatible with the dataset. Then, the same method as described above is applied to determine the stress state. The previously rejected focal mechanisms are finally test with the determined stress state and included in the inversion if one of their focal plane is in agreement with the computed solution according with the chosen misfit parameters.

II.3 - Stress state database

In order to well constrain the past stress fields and compare our results with the surrounding area, we built a database (Annexe 1) from the previous works including ~1700 stress tensors (Baroux, 2000; Bergerat, 1985, 1981; Billant et al., 2015, submit (Chapter IV), in prep. (Chapter V); Casagrande Fioretti, 1985; Champagnac et al., 2004; Combes, 1984; Fournier et al., 2008; Grosjean et al., 2004; Hippolyte et al., 2012a, 2006b; Homberg et al., 2013, 1999; Larroque et al., 2011; Le Roux et al., 2010; Philippe, 1995; Rebaï, 1988; Ritz, 1991; Sue and Tricart, 2003) but also ~100 deformation axes (François, 1981). Each measurement includes the more information provided by authors. Most includes the tectonic regime, the trend and plunge of the stress axes, the R ratio, the quality parameters of the inversion and the deformation stage proposed by the authors. When available, the age, kind and dip of the rock at the measurement site were added as well as the relative chronology of the stress state compare to strata tiliting and the pre-tilt inversion of the stress tensor.

II.4 - Field survey and observations

To complete the previous works, we performed field survey mainly around the Mérindol-Condorcet-Saillans fault zone. More than 1400 slickenslides and dip were measured at 70 different sites. It allows the definition of 97 stress tensors (Tab. II.1,Fig. II.3) including 15 compressional, 5 transpressional, 72 strike-slip, 1 transtensional and 3 tensional stress regimes.

Site	Lat.	Long.	Lithology	Age	Dip direction	Dip	Faulting/ tilt timing	Tectonic regime	σ_1 trend	σ_1 plunge	σ_2 trend	σ_2 plunge	σ_3 trend	σ_3 plunge	R	N	ANGLE	RUP
Jurassic Extension																		
SAILLANS2	5.2024	44.7168	Limestone	Tithonian	297	12	Before	T	174	-79	154	10	64	-4	0.368	15	11	33
Cretaceous Extension																		
BENIV	5.191	44.2933	Limestone	Up. Kimmeridgian-Tithonian	172	58	?	T	65	-73	137	5	45	16	0.319	10	9	30
Eocene Compression																		
BOUVIERE1	5.239	44.5078	Marly limestone	Barremian	173	46	Before	SS	17	-11	62	75	109	-11	0.729	9	9	32
BOUVIERE2	5.2271	44.5127	Marly limestone	Barremian-Bedoulian	251	65	Before	C	139	-10	47	-10	93	76	0.621	5	15	37
CHIFFE	4.8945	44.664	Marly limestone	Barremian-Bedoulian	152	10	After	SS	140	-5	59	62	48	-27	0.167	11	17	42
CROSAIG	4.45	44.3707	Limestone	Bedoulian	158	22	After	C	162	-16	70	-6	141	73	0.767	11	9	24
CROSAIG	4.45	44.3707	Limestone	Bedoulian	158	22	After	SS	148	-3	158	87	57	1	0.748	7	12	30
CURNIER	5.2227	44.3901	Marl and limestone	Berriasian	177	28	?	SS	21	15	101	-35	131	52	0.144	12	9	35
ESTABLET	5.4318	44.5159	Marl and limestone	Hauterivian-Low. Barremian	140	6	After	SS	138	-23	90	58	39	-21	0.271	6	11	43
FELINES3	5.0388	44.5823	Marl and limestone	Barremian	214	19	Before	SS	150	-4	59	-22	70	68	0.091	9	11	36
GLEYZOLLE	5.2912	44.6376	Limestone	Tithonian	236	38	?	SS	24	-3	74	85	114	-4	0.884	14	13	31
GUIERS	5.8125	45.4243	Limestone	Up. Barremian	88	31	Before	C	144	-14	35	-53	64	34	0.139	23	10	33
JONCHER1	5.4081	44.5684	Limestone	Tithonian	145	18	?	SS	14	-12	30	78	105	-3	0.574	18	7	21
MONTJOUX	5.09	44.501	Limestone	Turonian	227	32	Before	SS	160	-4	32	-82	70	5	0.218	5	5	21
RECH	5.1879	44.6748	Wackstone	Tithonian	229	16	Before	SS	166	10	14	79	77	-5	0.376	9	7	22
SAVASSE	4.7593	44.6161	Marly limestone	Barremian-Bedoulian	334	19	After	SS	18	-5	124	-73	106	16	0.615	4	6	37
TON2	5.1825	44.5786	Limestone	Barremian-Bedoulian	252	22	?	TP	19	3	106	-42	113	48	0.169	13	9	44
VROM2	5.0776	44.2382	Limestone	Neocomian	245	21	Before	SS	166	-12	169	78	76	1	0.608	4	3	37
Oligocene Extension																		
BATAILLE	5.249	44.901	Limestone	Albian	142	10	?	TT	58	52	26	-34	126	-16	0.567	8	10	32
CROSAIG	4.45	44.3707	Limestone	Bedoulian	158	22	After	T	155	71	67	-1	157	-19	0.301	5	9	28
Aquitanian Compression																		
AUTICHAM	4.9649	44.6813	Limestone	Oligocene	0	6	?	SS	15	0	111	-87	105	3	0.693	10	10	34
FELINES2	5.0403	44.5822	Marl and limestone	Barremian	175	6	After	SS	22	-10	5	79	112	3	0.732	10	10	30
PEROUSES	4.9802	44.6783	Limestone	Oligocene	289	18	Before	SS	38	1	116	-84	128	6	0.407	9	2	16
TON3	5.1859	44.5796	Limestone	Barremian	95	20	Before	SS	49	-4	157	-78	138	11	0.056	4	6	24

Site	Lat.	Long.	Lithology	Age	Dip direction	Dip	Faulting/ tilt timing	Tectonic regime	σ_1 trend	σ_1 plunge	σ_2 trend	σ_2 plunge	σ_3 trend	σ_3 plunge	R	N	ANGLE	RUP
Mio-Pliocene Compression																		
30PAS1	5.21	44.4443	Calcarenite	Turonian-Low. Coniacian	120	34	?	SS	91	23	101	-67	3	-3	0.256	13	12	32
30PAS2	5.212	44.4538	Calcarenite	Turonian-Low. Coniacian	~183	20	Before	SS	87	10	17	-63	172	-25	0.525	9	8	22
30PAS3	5.2132	44.4664	Limestone	Turonian	90	10	After	SS	91	-6	97	84	1	1	0.582	12	10	25
ARNAYON1	5.354	44.4736	Mudstone	Up. Tithonian-Berriasian	249	52	Before	TP	65	8	151	-25	171	64	0.162	9	15	43
ARNAYON2	5.3564	44.4689	Mudstone	Up. Tithonian-Berriasian	234	43	After	TP	81	26	17	-42	149	-37	0.098	4	11	45
BEDIOIS	5.268	44.6692	Limestone	Low. Valaginian	225	22	Before	SS	88	-22	122	64	3	13	0.743	7	7	24
BELLGARD	5.4185	44.5425	Marly limestone	Up. Tithonian-Berriasian	243	50	After	SS	73	-16	119	68	168	15	0.2	17	15	35
BEZAUDUN1	5.1716	44.6007	Limestone	Barremian	198	26	Before	SS	74	-16	122	66	169	-17	0.477	12	7	29
BEZAUDUN2	5.1697	44.5968	Limestone	Barremian-Bedoulian	221	19	Before	SS	94	3	149	-86	4	-4	0.297	10	6	20
BOUVIERE1	5.239	44.5078	Marly limestone	Barremian	173	46	Before	SS	109	-6	147	82	19	5	0.415	4	7	33
BOUVIERE2	5.2271	44.5127	Marly limestone	Barremian-Bedoulian	251	65	During	SS	87	24	53	-62	171	-14	0.332	7	10	40
CHAV1	5.2144	44.7443	Marly limestone	Low. Valaginian			?	TP	81	7	177	40	162	-49	0.712	7	9	39
CHAV2	5.2119	44.7427	Marly limestone	Low. Valaginian	238	60	After	TP	73	-23	149	29	15	52	0.36	10	7	31
CHAV2	5.2119	44.7427	Marly limestone	Low. Valaginian	238	60	After	SS	69	-18	127	59	167	-25	0.303	7	8	32
CHAV4	5.2229	44.7507	Limestone	Berriasian	358	26	Before	SS	83	-21	62	68	170	7	0.166	12	12	31
CHAV5	5.2209	44.7676	Marl and limestone	Up. Hauterivian	104	63	Before	SS	100	-21	69	65	5	-11	0.211	17	14	36
CRESTET	5.0837	44.2136	Calcarenite	Burdigalian	245	33	Before	SS	103	-10	178	57	20	31	0.222	24	8	26
CRUPIES1	5.1771	44.5516	Marly limestone	Barremian	146	35	After	SS	80	3	3	-76	169	-14	0.548	40	13	38
CRUPIES2	5.1878	44.5453	Marly limestone	Hauterivian	135	18	Before	SS	73	-1	141	88	163	-1	0.265	18	6	26
CURNIER	5.2227	44.3901	Marl and limestone	Berriasian	177	28	?	SS	99	6	25	-68	6	21	0.622	8	13	26
FELINES4	5.0374	44.5822	Marl and limestone	Barremian	208	29	Before	SS	67	1	154	-76	157	14	0.096	5	5	23
FOURNET	6.0572	45.5791	Limestone	Urgonian	90	39	After	SS	129	-23	50	25	1	-55	0.087	4	0	46
GLEYZOLLE	5.2912	44.6376	Limestone	Tithonian	236	38	?	SS	108	-9	63	78	16	-9	0.126	37	10	36
GUIERS	5.8125	45.4243	Limestone	Up. Barremian	88	31	After	SS	84	-13	174	-2	92	77	0.294	6	6	16
ISSARTEL	4.9336	44.693	Conglomerates	Stampian	340	12	Before	SS	127	11	62	-65	32	22	0.054	26	10	27
JONCHER1	5.4081	44.5684	Limestone	Tithonian	145	18	?	SS	81	-12	42	75	169	9	0.373	43	12	31
JONCHER2	5.4075	44.5705	Limestone	Tithonian	129	32	?	SS	88	6	164	-67	1	-22	0.515	10	8	21
MOIR	5.2001	44.671	Marly limestone	Kimmeridgian-Berriasian	134	60	After	SS	96	-31	61	54	176	17	0.401	9	14	39
MOLLANS	5.195	44.2392	Calcarenite	Burdigalian	138	31	Before	SS	17	-7	80	76	109	-12	0.18	34	9	24

Site	Lat.	Long.	Lithology	Age	Dip direction	Dip	Faulting/ tilt timing	Tectonic regime	σ_1 trend	σ_1 plunge	σ_2 trend	σ_2 plunge	σ_3 trend	σ_3 plunge	R	N	ANGLE	RUP
Mio-Pliocene Compression (continuation)																		
NYONS1	5.1416	44.3576	Sandstone	Burdigalian	283	24	Before	C	97	7	8	-10	155	-78	0.548	25	9	22
NYONS2	5.1229	44.3469	Conglomerates	Mid.-Up. Helvetian	271	39	Before	C	110	3	20	-12	7	77	0.351	29	9	26
NYONS2	5.1229	44.3469	Conglomerates	Mid.-Up. Helvetian	271	39	During	C	98	10	6	11	48	-75	0.5	9	9	20
NYONS2	5.1229	44.3469	Conglomerates	Mid.-Up. Helvetian	271	39	After	C	97	14	7	0	96	-76	0.519	11	6	17
NYONS3	5.1439	44.3606	Calcarenite	Burdigalian	271	66	Before	C	108	7	19	-8	160	-79	0.448	12	3	18
PENAS	5.1315	44.3193	Calcarenite	Burdigalian	212	77	After	C	78	-20	167	4	67	70	0.073	27	14	38
PEROUSES	4.9802	44.6783	Limestone	Oligocene	289	18	After	SS	119	-2	39	83	19	-6	0.42	8	8	28
PRAFEUX	6.2818	45.7462	Limestone	Up. Aptian-Albian	75	55	During	SS	104	21	86	-68	11	6	0.256	4	8	41
PROPIAC	5.1938	44.2729	Limestone	Up. Oxfordian-Low. Kimmeridgian	171	41	Before	SS	75	-12	133	67	169	-19	0.61	10	8	36
RECH	5.1879	44.6748	Wackstone	Tithonian	229	16	Before	SS	68	14	88	-75	159	5	0.913	26	6	21
RICOU	5.1405	44.3212	Marl and limestone	Barremian-Bedoulian	223	35	Before	SS	103	5	104	-85	13	0	0.446	7	5	19
RIMON	5.3154	44.665	Marly limestone	Kimmeridgian	225	13	After	SS	85	-3	47	86	174	2	0.43	13	6	21
ROCMAUR	4.7133	44.5959	Conglomerates	Oligocene	343	18	After	SS	105	3	61	-86	15	3	0.267	19	7	19
SAILLANS	5.2138	44.6914	Limestone	Kimmeridgian	283	53	After	C	79	-6	169	7	31	81	0.566	12	7	16
SAILLANS2	5.2024	44.7168	Limestone	Tithonian	297	12	After	SS	96	17	119	-73	7	-3	0.614	9	11	38
SAVEL	5.3009	44.6524	Marly limestone	Kimmeridgian	205	33	After	SS	80	-18	62	71	168	5	0.33	13	6	20
STGCOMM	5.7187	45.0339	Marly limestone	Toarcian	69	60	After	SS	40	8	138	45	122	-44	0.229	12	9	32
STNAZD1	5.2442	44.5206	Marl and limestone	Berriasian	212	32	Before	SS	85	7	68	-82	175	-2	0.358	10	5	15
STNAZD2	5.2431	44.5461	Marl and limestone	Barremian-Bedoulian	248	35	After	SS	84	-9	177	-13	140	73	0.202	11	18	35
STROME	5.0066	44.6885	Limestone	Oligocene	8	18	Before	SS	111	0	17	-89	21	1	0.238	11	9	24
TON1	5.1816	44.5774	Limestone	Barremian-Bedoulian	251	16	Before	SS	79	3	139	-83	169	6	0.482	5	4	12
TOUVET	5.9363	45.3445	Marly limestone	Up. Oxfordian-Low. Kimmeridgian	286	22	Before	SS	104	7	136	-82	14	-4	0.715	18	11	23
VILLEPERDRIX1	5.2858	44.4324	Limestone	Up. Kimmeridgian-Tithonian	125	18	After	SS	67	1	156	-54	158	36	0.122	9	9	30
VILLEPERDRIX2	5.2838	44.433	Limestone	Up. Kimmeridgian-Tithonian	226	20	After	C	68	-9	159	-7	104	79	0.451	8	8	22
VROM1	5.076	44.2368	Limestone	Barremian-Bedoulian	134	20	After	SS	101	-4	5	-59	13	30	0.373	24	10	34
VROM2	5.0776	44.2382	Limestone	Neocomian	245	21	Before	SS	100	-7	104	83	10	0	0.418	13	5	19

Site	Lat.	Long.	Lithology	Age	Dip direction	Dip	Faulting/ tilt timing	Tectonic regime	σ_1 trend	σ_1 plunge	σ_2 trend	σ_2 plunge	σ_3 trend	σ_3 plunge	R	N	ANGLE	RUP
Quaternary Compression																		
30PAS1	5.21	44.4443	Calcarenite	Turonian-Low. Coniacian	120	34	After	SS	15	-13	131	-62	99	24	0.325	16	10	27
30PAS2	5.212	44.4538	Calcarenite	Turonian-Low. Coniacian	~183	20	After	SS	0	-1	87	76	91	-14	0.566	22	10	24
BEDIOIS	5.268	44.6692	Limestone	Low. Valaginian	225	22	After	SS	16	4	130	79	106	-10	0.46	10	8	28
BEZAUDUN1	5.1716	44.6007	Limestone	Barremian	198	26	During	SS	48	2	140	47	136	-42	0.057	12	13	39
BEZAUDUN2	5.1697	44.5968	Limestone	Barremian-Bedoulian	221	19	During	SS	40	-21	3	64	125	14	0.172	4	9	40
CHAV1	5.2144	44.7443	Marly limestone	Low. Valaginian			?	SS	43	5	116	-72	135	17	0.553	7	12	51
FELINES1	5.0355	44.5808	Limestone	Barremian	190	36	Before	SS	50	4	154	75	139	-15	0.185	9	10	36
FELINES3	5.0388	44.5823	Marl and limestone	Barremian	214	19	After	SS	54	24	156	-66	144	1	0.761	12	8	33
JONCHER2	5.4075	44.5705	Limestone	Tithonian	129	32	?	SS	149	16	104	-67	55	15	0.206	10	13	38
MGAUTHIE	5.1824	44.2587	Calcarenite	Burdigalian	232	33	After	SS	45	23	77	-64	141	13	0.042	9	7	36
MOLLANS	5.195	44.2392	Calcarenite	Burdigalian	138	31	After	C	35	1	125	13	122	-77	0.413	15	10	26
MONTJOUX	5.09	44.501	Limestone	Turonian	227	32	During	SS	58	18	119	-56	158	28	0.065	7	7	29
MOUL	5.0769	44.37	Conglomerates	Pliocene			?	SS	21	-2	98	80	111	-10	0.715	7	6	27
NYONS2	5.1229	44.3469	Conglomerates	Mid.-Up. Helvetian	271	39	After	C	63	-12	150	14	11	72	0.349	15	8	28
RICOU	5.1405	44.3212	Marl and limestone	Barremian-Bedoulian	223	35	After	SS	33	-8	153	-75	121	13	0.758	7	9	36
ROUSSET	5.068	44.4162	Sandstone	Low. Helvetian	224	47	After	C	48	-11	137	4	27	79	0.537	7	8	29
VEAUX	5.2131	44.2218	Limestone	Urgonian	197	22	After	C	54	-4	145	-9	121	80	0.277	13	11	36

Tableau II.1: Results of fault-slip data inversion. R: $(\sigma_2-\sigma_3)/(\sigma_1-\sigma_3)$, N: number of fault observations, Low.: Lower, Mid.: Middle, Up. Upper, C: compressional, TP: transpressional, SS: strike-slip, TT: transtensional and T: extensional

Jurassic extension

Cretaceous extension

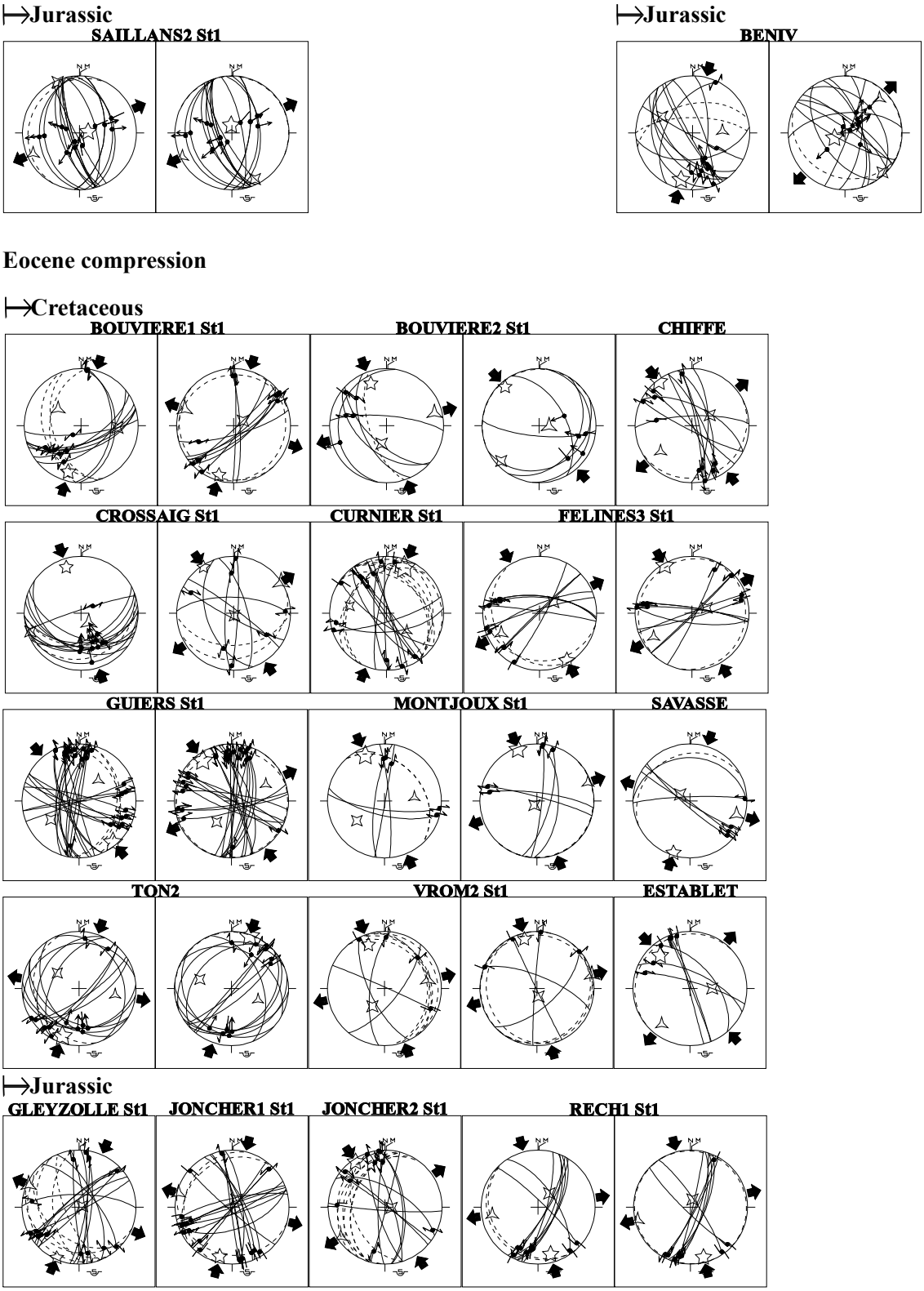

Figure II.3: Schmidt's diagrams with computed stress tensors of all measurement sites sorted by deformation stage and rocks age. Same legend than fig. II.1. St# indicates the local stress state chronology.

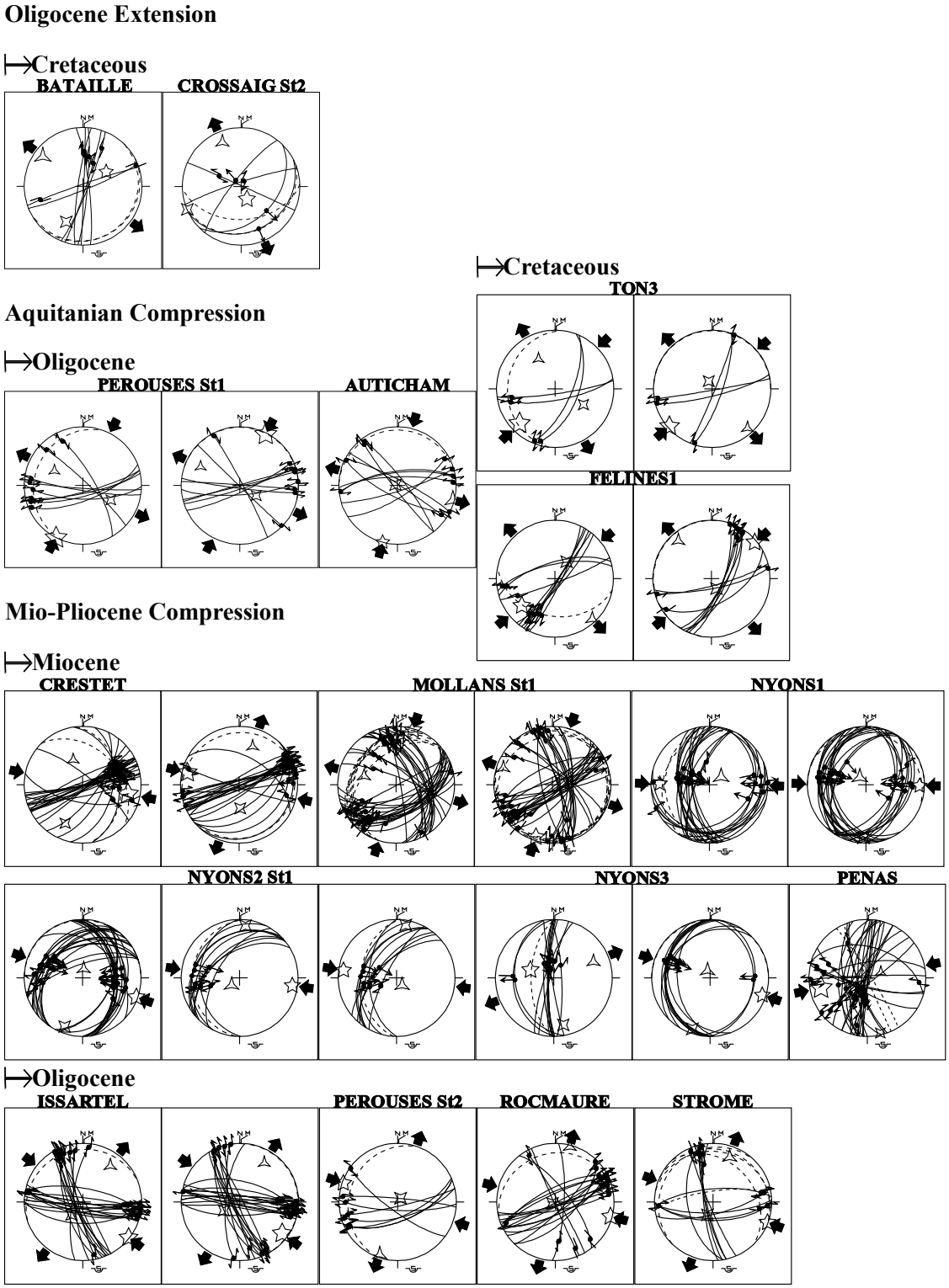

Figure II.3 (continuation)

Mio-Pliocene Compression (continuation)

⊢→Cretaceous

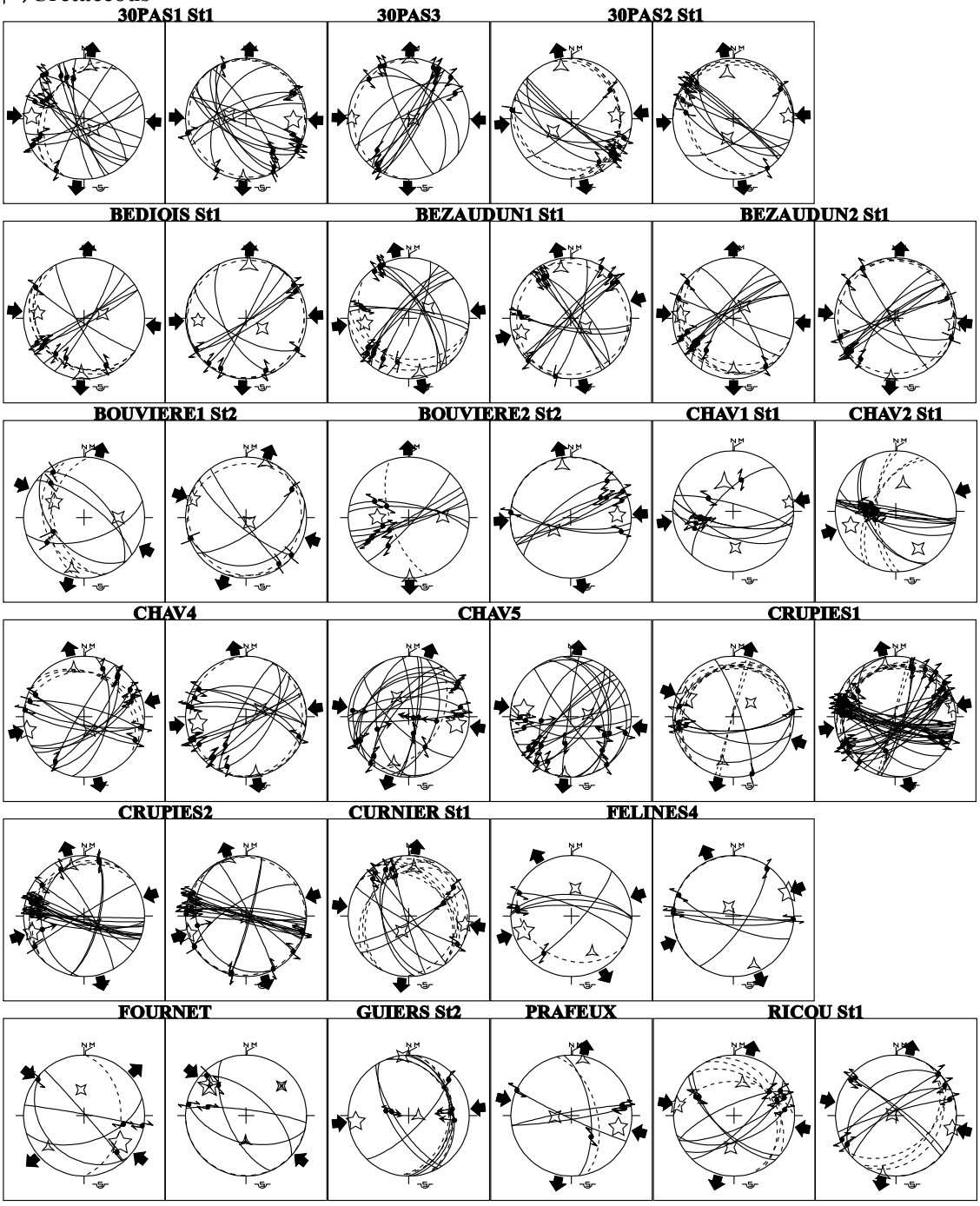

Figure II.3 (continuation)

Mio-Pliocene Compression (continuation)

⟼Cretaceous (continuation)

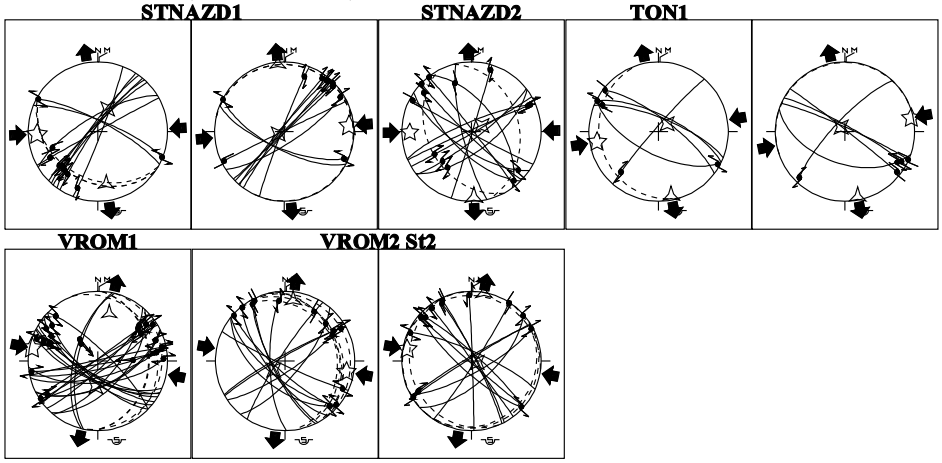

⟼Jurassic

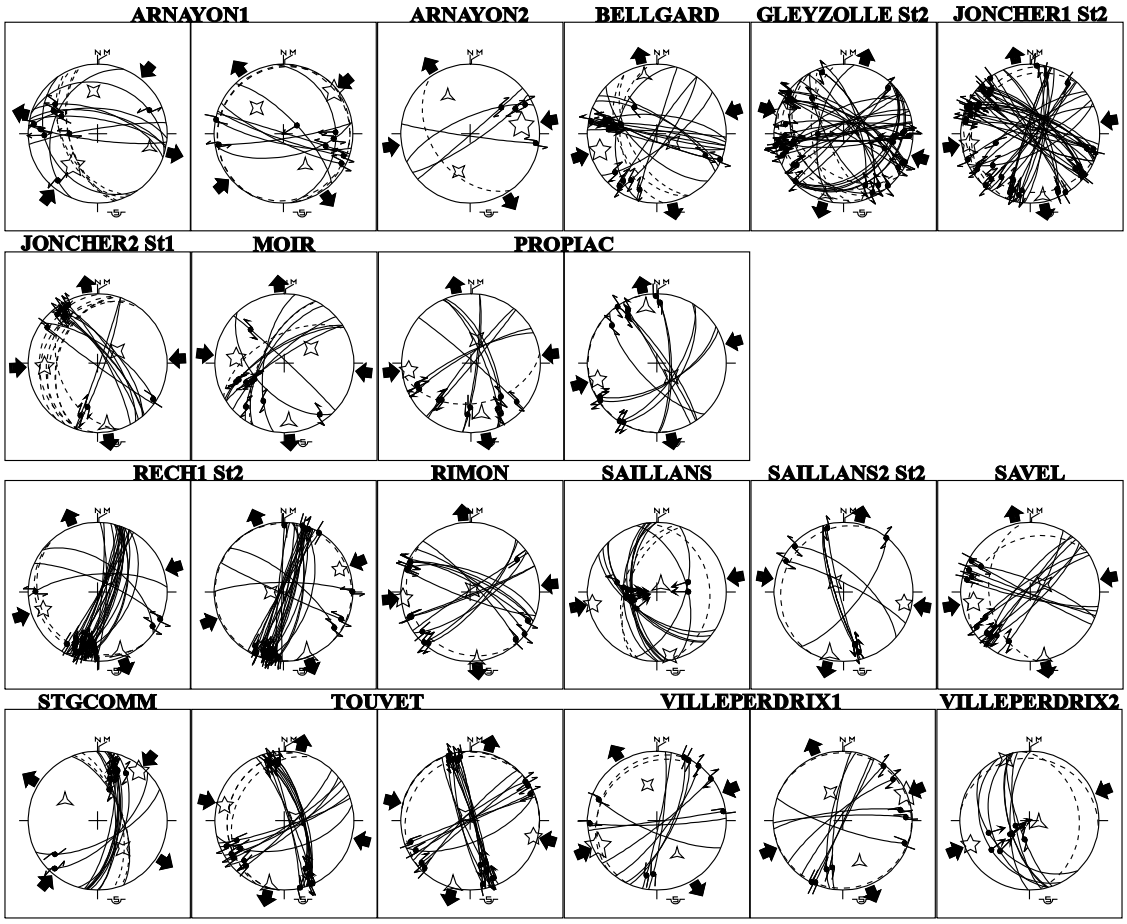

Figure II.3 (continuation)

Quaternary Compression

↦Upper Pliocene

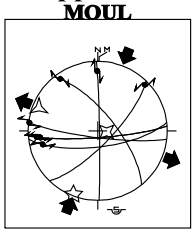

↦Miocene

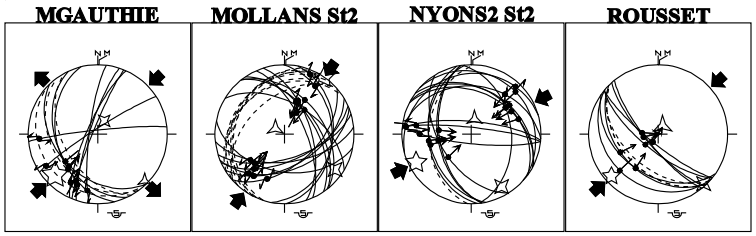

↦Cretaceous

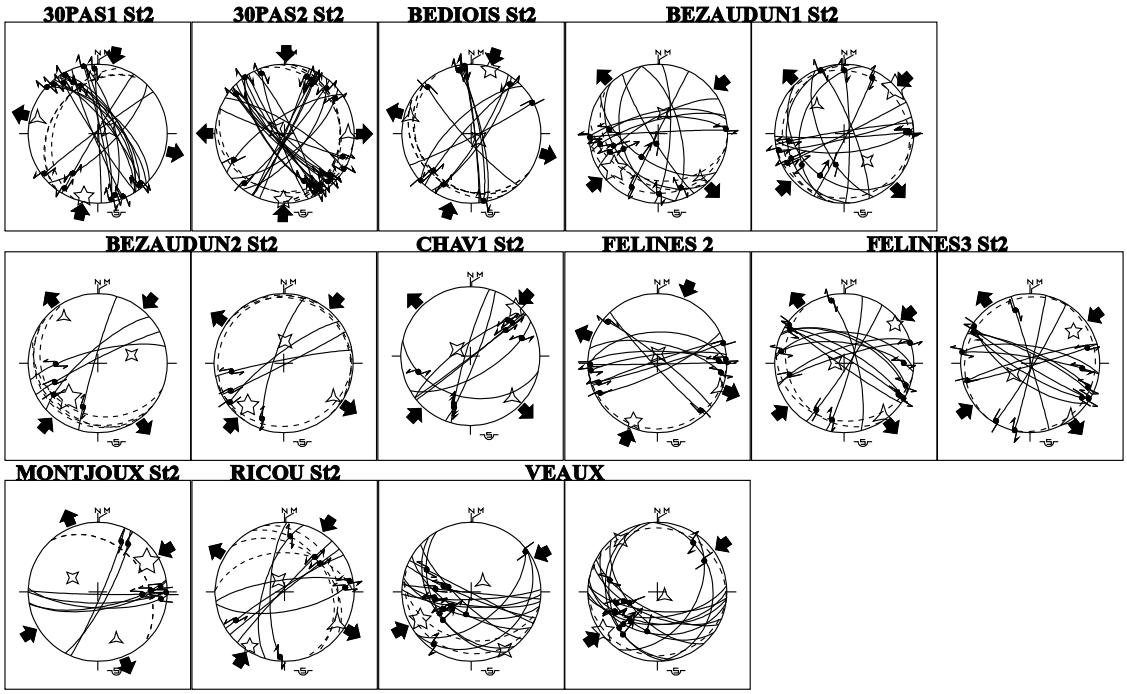

Figure II.3 (continuation)

II.4.1.1 - Average trends of the stress axis

A first sort of the stress tensors dataset was made according to the stress trend to segregate different regionally significant stress states. We did not find enough transtensional nor extensional stress tensors to sort characteristic extensional trends (Fig. II.4A). However, compressional and transpressional stress tensors display two σ_1 characteristic trends, the first ranged between N065°E and N085°E and the second between N095°E and N100°E (Fig. II.4B). Similar σ_1 characteristic trends exist for the strike-slip stress tensors which in addition display N015°E-N025°E and N040°E-N050°E trends (Fig. II.4C). Closed values are found when considering compressional to strike-slip stress regimes although N070°E-N075°E, N080°E-N090°E and N095°E-N105°E σ_1 characteristic trends appear more distinct. Nevertheless, it does not mean that each σ_1 characteristic trends correspond to an individual stage of stress state and stress trends can vary geographically or be deviated along major fault zone (e.g. Homberg et al., 1997). Geographic distribution of the measurement sites must so be taken into account in the sort process.

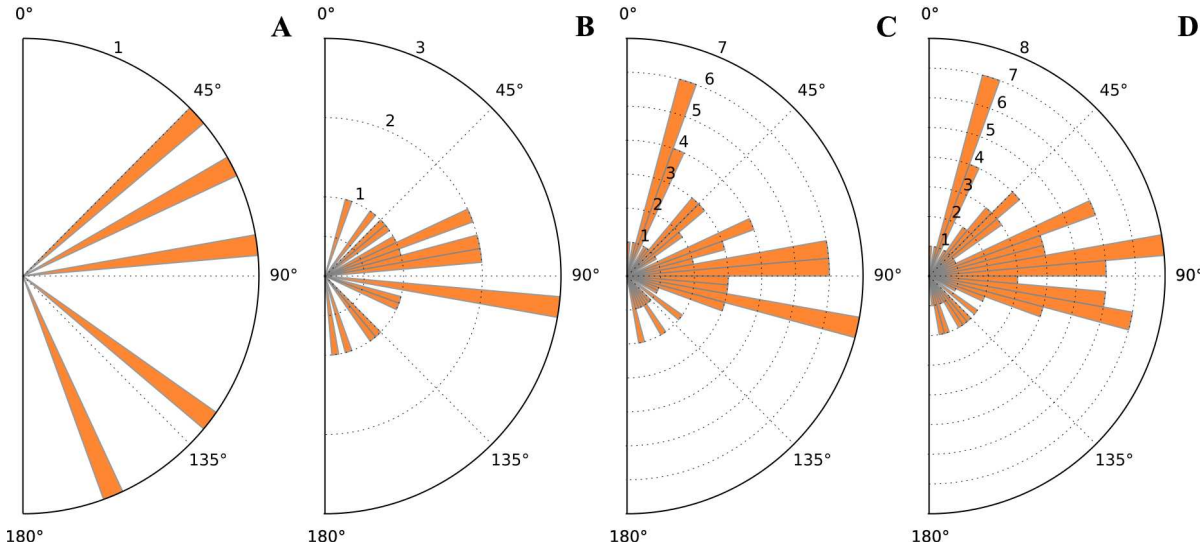

Figure II.4: Rose diagram histogram of A) trend of σ_3 for transtensional and extensional regimes, B) trend of $\sigma_1$for compressional and transpressional and C) σ_1 trend of σ_1 for strike-slip stress regimes. D summarizes B and C.

II.4.1.2 - Chronology of the stress states inferred from cross-cutting relationship, bedding attitudes and depositional ages.

We present thereafter the sites that allowed the determination of relative chronologies between stress states as well as their age.

The Tithonian limestone of the SAILLANS2 site (Fig. II.2) displays NNW trending normal faults, NNW to NW trending left-lateral and SE right lateral strike-slip faults. Normal faults are related to an extensional tectonic regime with an ENE trending σ_3 axis whereas strike slip faults are related to a strike-slip tectonic regime with an ~E trending σ_1 axis. Normal faulting is attested by the presence of corrugation, calcite steps and striae. Reactivation of normal faults as strike-slip faults is attested by the occurrence of calcite steps on one side of the corrugations and striating on the opposite side (Fig. II.2). Moreover, in agreement with this chronology, despite the low number of fault planes, if we compare to the plunges of the stress axis with the bedding attitude, it seems that normal faulting occurred before bed tilting and that strike-slip faulting occurred after this tilting. Moreover, some normal faults appears to have formed when the sediment was not consolidated and so are related to synsedimentary tectonics. Further south, the Berriasian deposits are affected by E trending and S dipping normal faults and display slumps which moved southward (Fig. II.5). These E trending normal faults are not consistent with the NNE trending extensional stress regime of site SAILLANS2 (Fig. II.2). Superposition of striation and comparison of stress axes with bedding planes imply that the extensional tectonic regime occurred before the strike-slip one and ended between Tithonian and Berriasian.

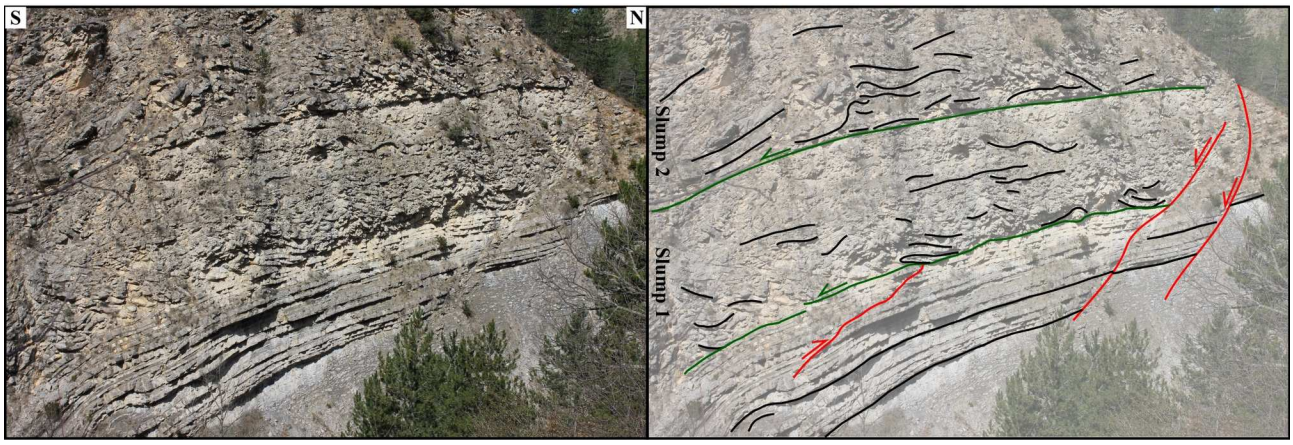

Figure II.5: Normal faults (in red) and slumps (bottom in green) in the Berriasian marls and limestones south of the SAILLANS2 site. Black lines underline beds.

Near the Cévennes fault, the CROSSAIG site was affected by a compressional to strike-slip tectonic regime defined by a NNW trending σ_1 axis after the southward tilt of the Bedoulian limestones. It was also affected, after the folding, by an extensional tectonic regime defined by a NNW trending σ_3 axis. Because fold trends in this area is mainly E-W, we can assume that the compressional to strike-slip tectonic regime corresponds to the folding event. So, the NNW trending extensional tectonic regime occurred after the NNW trending compression.

The upper Tithonian limestone of the GLEYZOLLE site was affected by two strike-slip tectonic regimes, one with a NNE trending σ_1 axis and the other with an ESE trending σ_1 axis (Fig. II.6). The site is located on the southern limit of a narrow E-W syncline interfering with a broad N trending syncline. One NE trending fault plane displays slightly tilted grooves and striae consistent with left lateral kinematics. Similar to the SAILLANS2 site, calcite steps indicating right-lateral kinematics have grown from side of the grooves. It indicates that the strike-slip tectonic regime with a NNE trending σ_1 axis was followed by the strike-slip tectonic regime with ESE trending σ_1 axis. The attitude of the bedding planes are not homogeneous enough in this site to confirm the chronology by tilting.

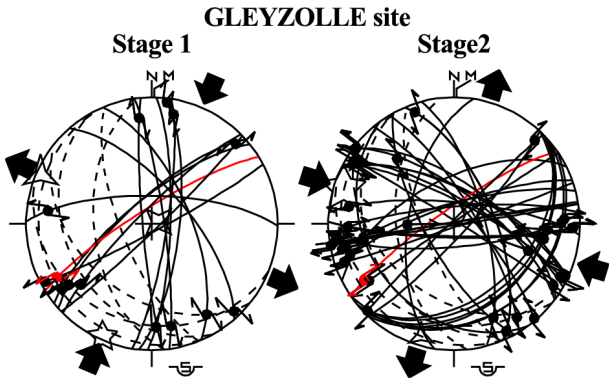

Figure II.6: Schmidt's diagrams with computed stress tensors of the GLEYZOLLE site. Same legend than fig. II.1. Red fault shows left and then right lateral strike slip kinematics.

The PEROUSES site is located in the Oligocene lacustrine limestones. This site is affected by ENE trending and SE trending faults both showing left- and right-lateral slips in response to two strike-slip tectonic regimes with NNE and ESE trending σ_1 axis (Fig. II.7). An ENE trending fault displayed striae and shelter zones consistent with left-lateral kinematics. Some of these shelter zones display stylolite indicating that this fault slips then with a right-lateral kinematics. It indicates that the strike-slip tectonic regime with a NNE trending σ_1 axis occurred first. Moreover, this first regime appears to predate the tilting whereas the strike-slip tectonic regime with a ESE trending σ_1 axis occurred after the tilting, which is consistent with the fault chronology.

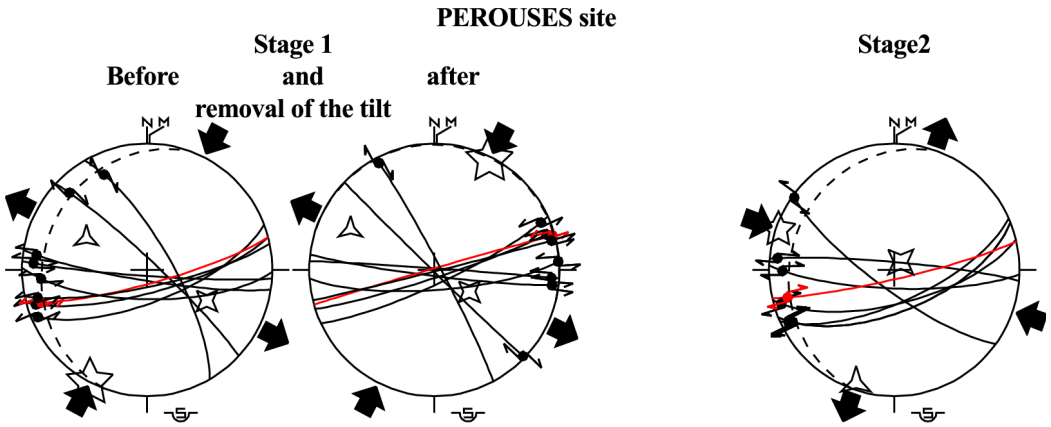

Figure II.7: Schmidt's diagrams with computed stress tensors of the PEROUSES site. Same legend than fig. II.1. Red fault shows left and then right lateral strike slip kinematics.

Other sites allowing the determination of a relative stress states chronology based on the relationship between the strata tilt and faulting are presented in figure II.8. The VROM2, BOUVIERE1, BOUVIERE2, GUIERS and CURNIER site display strata dip consistent a folding resulting from an ~E trending compression. They were affected before the folding by compressional or strike-slip tectonic regimes with a NW to N trending σ_1 axis. All were then affected by a strike-slip tectonic regime with an ~E trending σ_1 axis consistent with the dip direction of the strata. These 5 sites confirm that an ~E trending compression postdates an NNW trending compression.

The strike-slip tectonic regimes defined by an ~E trending σ_1 axis were also found at the BEZAUDUN1, BEZAUDUN2, BEDIOIS, 30PAS1, 30PAS2 and RICOU sites (Fig. II.8). At these sites the E-W compression occurred prior to the tilting of the rocks to the east or the west, in agreement with the E trending compression (except 30PAS1 site where both could be contemporaneous). All these sites display another strike-slip tectonic regime, defined by a N to NE trending σ_1 axis subsequent to the folding (except BEZAUDUN2 site where both could be contemporaneous). These are the same σ_1 axis trends found at the NYONS2 site (see below).

We propose thanks to our observations that the studied area has known at least three successive compressional to strike-slip tectonic regimes, the first under a NW to NNE trending compression, the second under an ~E trending compression and the last under a N to NE trending compression.

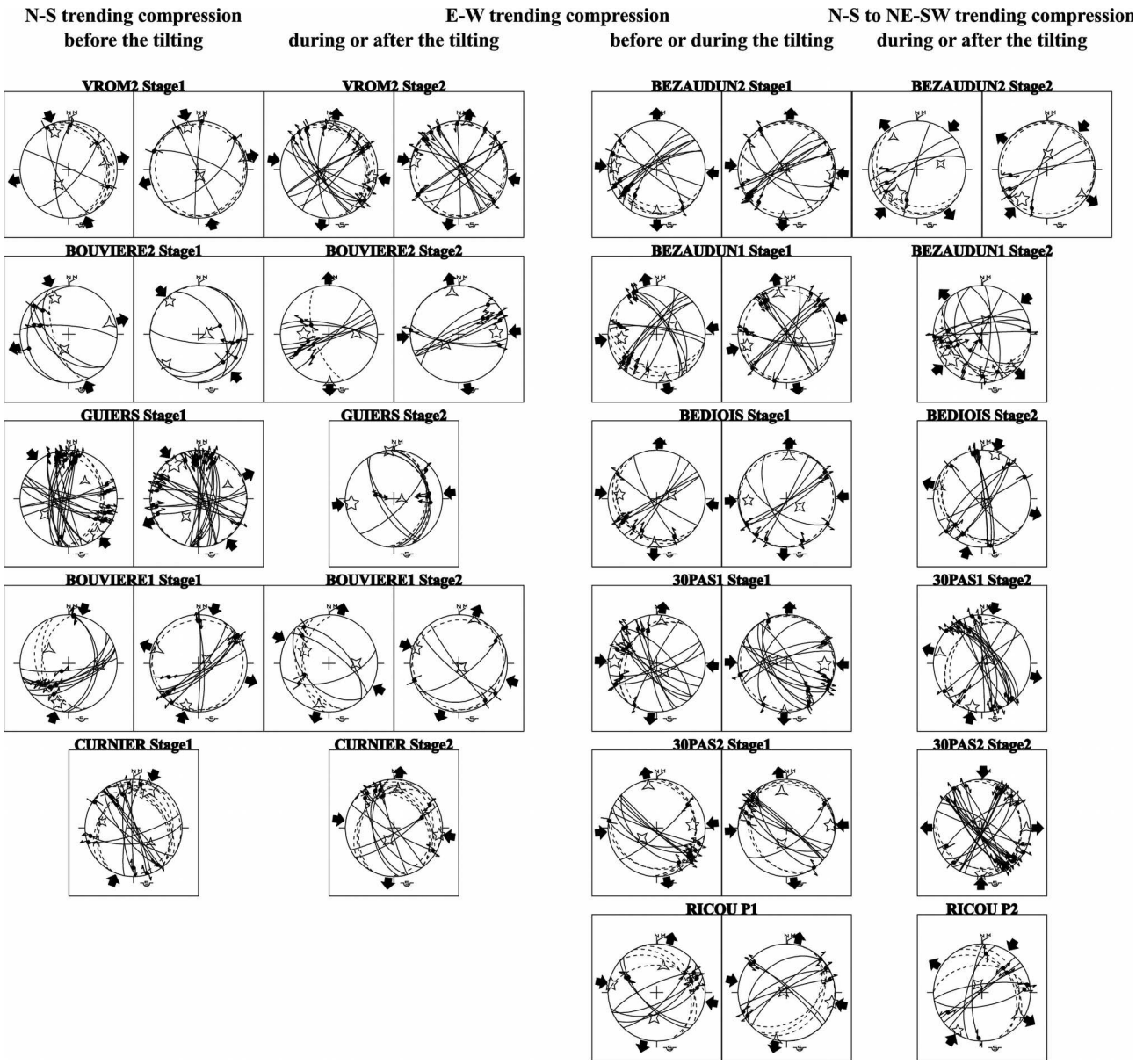

Figure II.8: Schmidt's diagrams with computed stress tensors of the sites displaying several stress state which relative chronology is constrained using relations with folding. Same legend as fig. II.1.

The NYONS2 site is located in middle to upper Helvetian 39° W dipping conglomerates. These deposits, as the Tortonian ones, showing progressive unconformity, were folded during their emplacement (Casagrande Fioretti, 1985). A complex striation pattern with horizontal to vertical tilted thrusts and E trending strike-slip faults was observed at the measurements site (Fig. II.9). After the sorting of the dataset, it appears that an ESE trending compression happened before, during and after the folding and so during Helvetian as attested by the successive stress states following Andersonian condition for different dip values (Fig. II.9). A second NE trending compression occurred only after the tilting and it is so the last stress state recorded in this site (Fig. II.9).

A similar NE trending compression was found further north in the upper Pliocene conglomerates at the MOUL site (Fig. II.3). ESE to E trending compression was found further north in the same upper Pliocene conglomerates (Billant et al., in prep, chapter V). It suggests that the change from an ~E trending compression to a N to NNE trending compression occurred during or after the upper Pliocene.

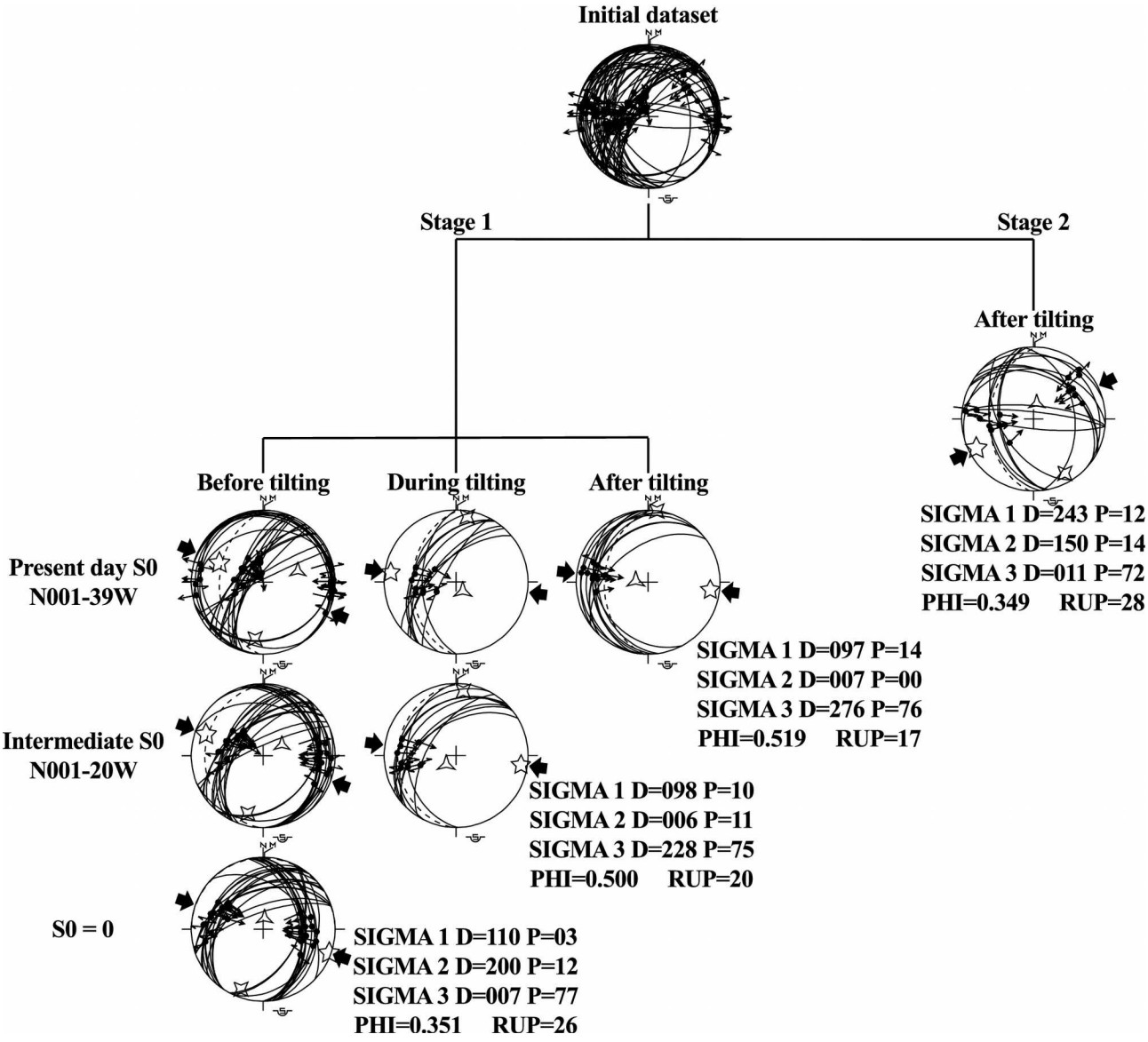

Figure II.9: Schmidt's diagrams with computed stress tensors of the NYONS2 site. Same legend than fig. II.1. Fault formed before and during the folding of the deposits were progressively tilted with them.

II.5 - Present-day stress state

We calculated a regionaly significant stress state by inversion of the focal mechanisms presented in Thouvenot et al. (2003). Using the method previously described (section II.2.2), we first performed the inversion on the whole dataset, i.e. including the focal mechanisms related to the Belledonne Border fault, the Laffrey fault and thus scattered in the area. This inversion allows the determination of an uniaxial compressional stress state with a subhorizontal N104°E trending σ_1 axis (Fig II.10A). Nevertheless, for this solution, the slip deviation is high (mean=19.7°, max value=57.8°) and the fault planes displaying the highest slip deviation are those associated to the Belledonne Border fault. Moreover, R ratio closed to 0 or 1 can indicate that different stress states are grouped in this synthetic stress-state (Ritz and Taboada, 1993). The dataset could so correspond to the combination of two domains submit to different stress state (i.e. the subalpine massifs domain and the Belledonne border fault domain).

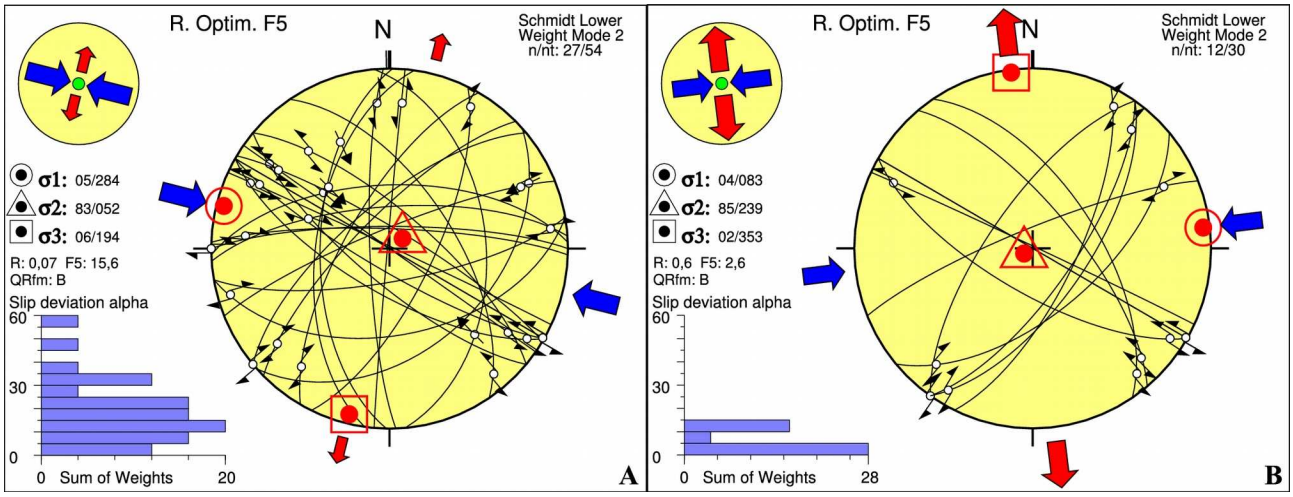

Figure II.10: Stress inversion of A) the whole dataset of focal mechanism (Klinger et al., 2011) and B) the focal mechanisms associated to the Belledonne Border fault (using the TENSOR program by Delvaux and Sperner (2003)).

We so performed a second inversion including only the focal mechanisms related to the Belledonne Border fault and the Laffrey fault. Three focal mechanisms were excluded using the counting deviation method. This inversion allows the determination of a strike-slip stress state with a subhorizontal N83°E trending σ_1 axis and subhorizontal N173°E trending σ_3 axis (Fig II.10B). In this case, mean slip deviation is only of 5.8° and is not higher than 14.4° implying that this solution is very consistent and more reliable than the first one.

II.6 - Summary of our observations and comparison with previous works in the Mediterranean geodynamic frame

II.6.1 - The Mesozoic extensions

At the end of the Paleozoic, erosion and crustal thinning of the Hercynian belt (Ménard and Molnar, 1988) formed a large peneplaine on which Triassic deposits from the erosion of the belt settled. The late Hercynian structures, which formed between 310 and 270 Ma, were mainly NE trending strike-slip fault in the eastern France. These faults found in the whole basement (Arthaud and Matte, 1975; von Raumer and Ménot, 1989) localized the deformations during the Jurassic extension and the alpine compression (Lemoine et al., 1986, 1981).

In the western Alps realm, Tethysian extension started during upper Triassic (Barféty and Gidon, 1990; Dumont, 1988). The NW trending extension (Grand et al., 1987) formed half-grabens and tilted blocks mainly along north and north-west trending crustal normal faults (Barféty et al., 1979; Claudel and Dumont, 1999; Dardeau et al., 1988; Dumont et al., 2008).

The oldest tectonic regime that we found (SAILLANS2 site) is extensional, defined by an ENE trending σ_3 axis and occurred until late Tithonian or early Berriasian. It was followed after or during Berriasian by ~N trending extension of which we supposed to have found the related stress state at the BENIV site (Fig. II.3). It corroborates the observations of previous works and the age of the transition between the two tectonic regimes (Blés et al., 1989; Homberg et al., 2013).

Regionally, the late Jurassic extension was ~WNW trending (Fig. II.11) and is related to the Alpine Tethys opening and/or then to North Atlantic opening (Grand et al., 1987; Homberg et al., 2013). The Cretaceous extension was N to ENE trending (Fig. II.12) and can be related to the opening of the bay of Biscay and/or Valais rift (Homberg et al., 2013). During the Cretaceous extension, NE trending as well as ESE trending normal faults were still active (Arnaud, 1981; De Graciansky and Lemoine, 1988). This extension has stopped before Cenomanian (De Graciansky et al., 1987).

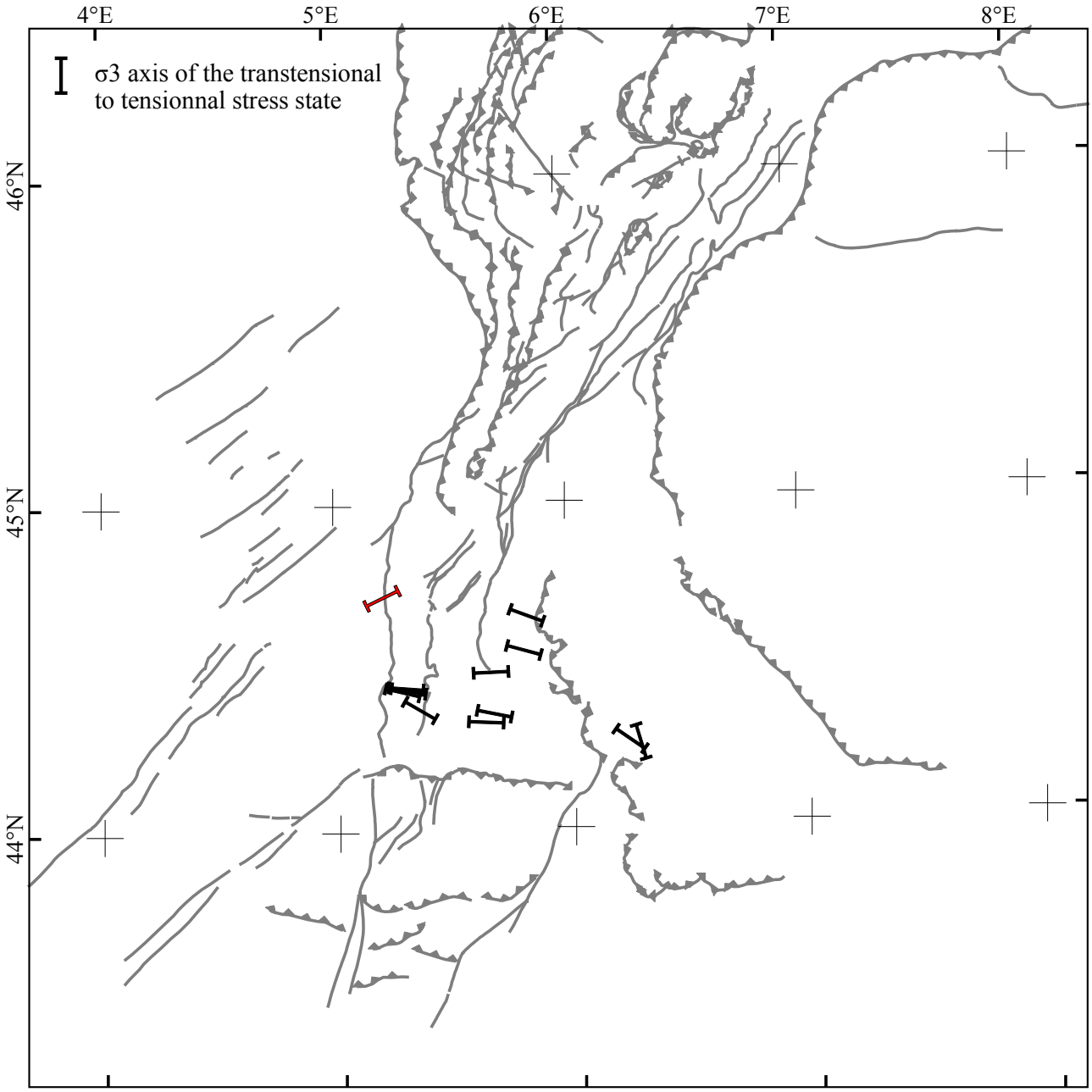

Figure II.11: Stress orientations during the Jurassic extension (in red, this work).

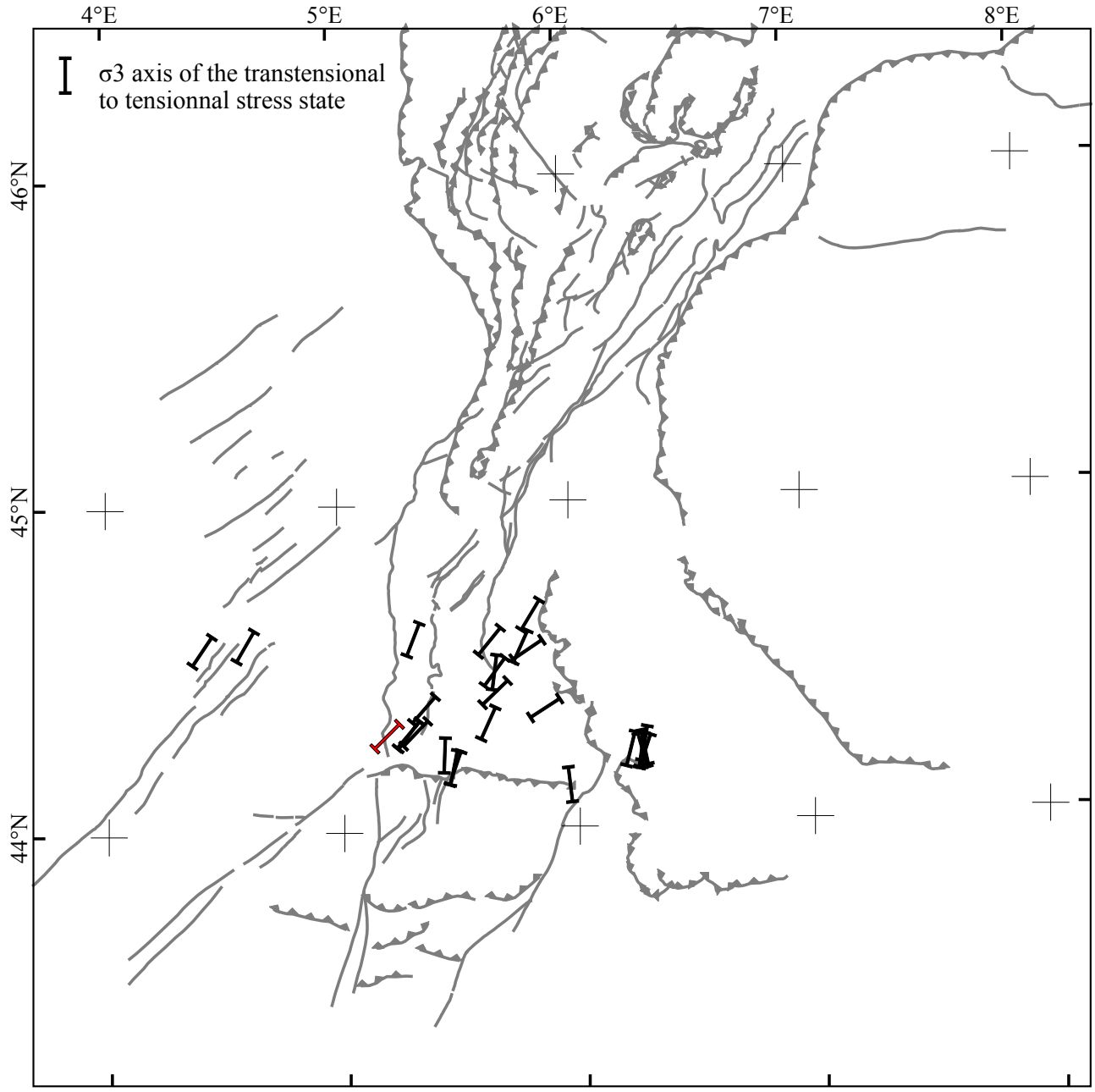

Figure II.12: Stress orientations during the Cretaceous extension (in red, this work).

II.6.2 - The late Cretaceous to Eocene compression

The first compression, that we observed at 17 sites, defines a strike-slip tectonic regime characterized by a NW to NNE σ_1 axis (Fig. II.13). We do not observed this tectonic regime in rocks younger than Turonian and it is older than the ESE to E trending compression Mio-Pliocene in age. We can so assume that this compression corresponds to the Late Cretaceous to Eocene compression revealed by Bergerat (1981) in the Rhône valley.

This compression corresponds to the Pyrenean tectonics and was related to the anticlokwise rotation of the Iberian and African plates during the Atlantic opening, leading first to the stop of the Ligurian Téthys spreading and later to the collision of the Iberian plate and Corsica-Sardinia microplate with the European plate (Lacombe and Jolivet, 2005). In the Provence realm, this compression led to the formation of the ~E trending folds and trusts (e.g. Espurt et al., 2012) and NE to NNE trending left lateral strike-slip faults (inherited from Hercynian structures (Arthaud and Matte, 1975)). The ~E trending folds and trusts of the Diois and Baronnies massifs were formed during this compression (Flandrin, 1966) as it is clear for the southern structures displaying growth strata in the Eocene deposits (Montenat et al., 2005). Nevertheless, the northern extension of this deformation in the sedimentary cover is poorly constrained. Indeed, whereas in the Alps it affected the southern external crystalline massifs (Dumont et al., 2012; Ford, 1996), in the Devoluy massif, some folds previously attributed to this compression appear to be only “mega-slump” structures coming from the northern border of the Vocontian basin (Michard et al., 2010).

Further south, the Ligurian Tethys was subducting beneath the Corsica-Sardinia microplate and the Iberian plate whereas the Alpine Tethys as well as the Briançonnais terrane were subducting beneath the Apulian plate (Lacombe and Jolivet, 2005; Stampfli et al., 2002). The sediments of the flexural basin (the flysch nappes) at the front of the accretionary prism of the Penninic frontal thrust were deformed since the late Eocene and were moved northward and then north-westward (Dewey et al., 1989; Dumont et al., 2012; Merle and Brun, 1984).

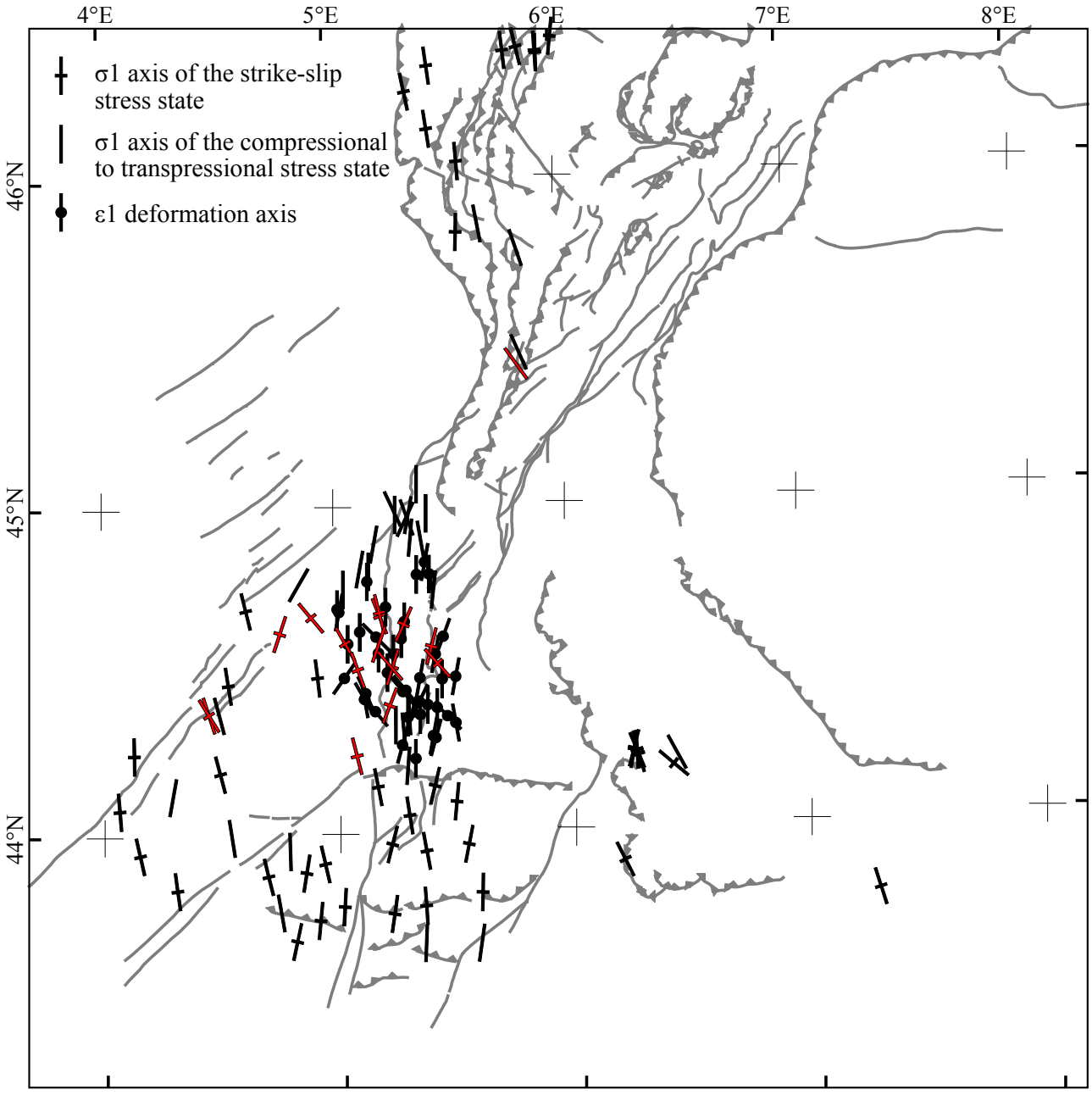

Figure II.13: Stress state orientations during the Eocene compression (in red, this work).

II.6.3 - The Oligocene stress states

The Eocene compression was followed by the E to SE trending Oligocene extension which we observed at only 2 sites (BATAILLE and CROSSAIG, Tab. II.1, Fig. II.14) without finding clear chronological clues except that they occurred after Aptian and so the Jurassic extension displaying a close extension trend. Age of this stress state has been inferred from correlation with previous works (Bergerat, 1981a; Blés et al., 1989; Hippolyte et al., 1993; Séranne, 1999).

In the Alpine foreland, a first E to SE trending extensional tectonics occurred during Oligocene time up to the Chattian and is related to the western European rifting (Bergerat, 1981a; Séranne, 1999; Villeger and Andrieux, 1987). This extension could have been caused by slab pull (Merle and Michon, 2001) or interaction between pyrenean and alpine compressions (Dèzes et al., 2004). In Provence, a second SSE-trending extensional event begun in the Late Rupelian and resulted in the opening of the Liguro-Provençal basin (Hippolyte et al., 1993). The Liguro-Provençal basin is the backarc basin of the southeastward retreating western Mediterranean subduction zone. It opened at the rear of the counter-clockwise rotating Corsica-Sardinia microplate (Bache et al., 2010; Gattacceca et al., 2007; Gueguen et al., 1998; Rollet et al., 2002; Speranza et al., 2002). The drifting of the Liguro-Provençal ocean occurred at least during Burdigalian as attested by 17.5 Ma old (Aguilar et al., 1996) Beaulieu basalts (exposed about 40 km to the north of Marseille) which contain numerous peridotite xenolith and maybe until 16 Ma as suggested by paleomagnetic data (Speranza et al., 2002).

In the western Inner Alps, the collisional thickening started in the early Oligocene. The internal units thrust north-westward the flysch nappes as well as the Oligocene molasse (Burkhard and Sommaruga, 1998) and reach the subalpine realm (Préapes and Sulens klippe) (Bellahsen et al., 2014). In the south-western Alps, the flysch nappes (Embrunais-Ubaye nappe) thrusted south-westward in front of the Penninic front thrust (Ford et al., 2006; Merle and Brun, 1984) which is consistent with the NE trending compression recorded in the Nice nappe (Ritz, 1991).

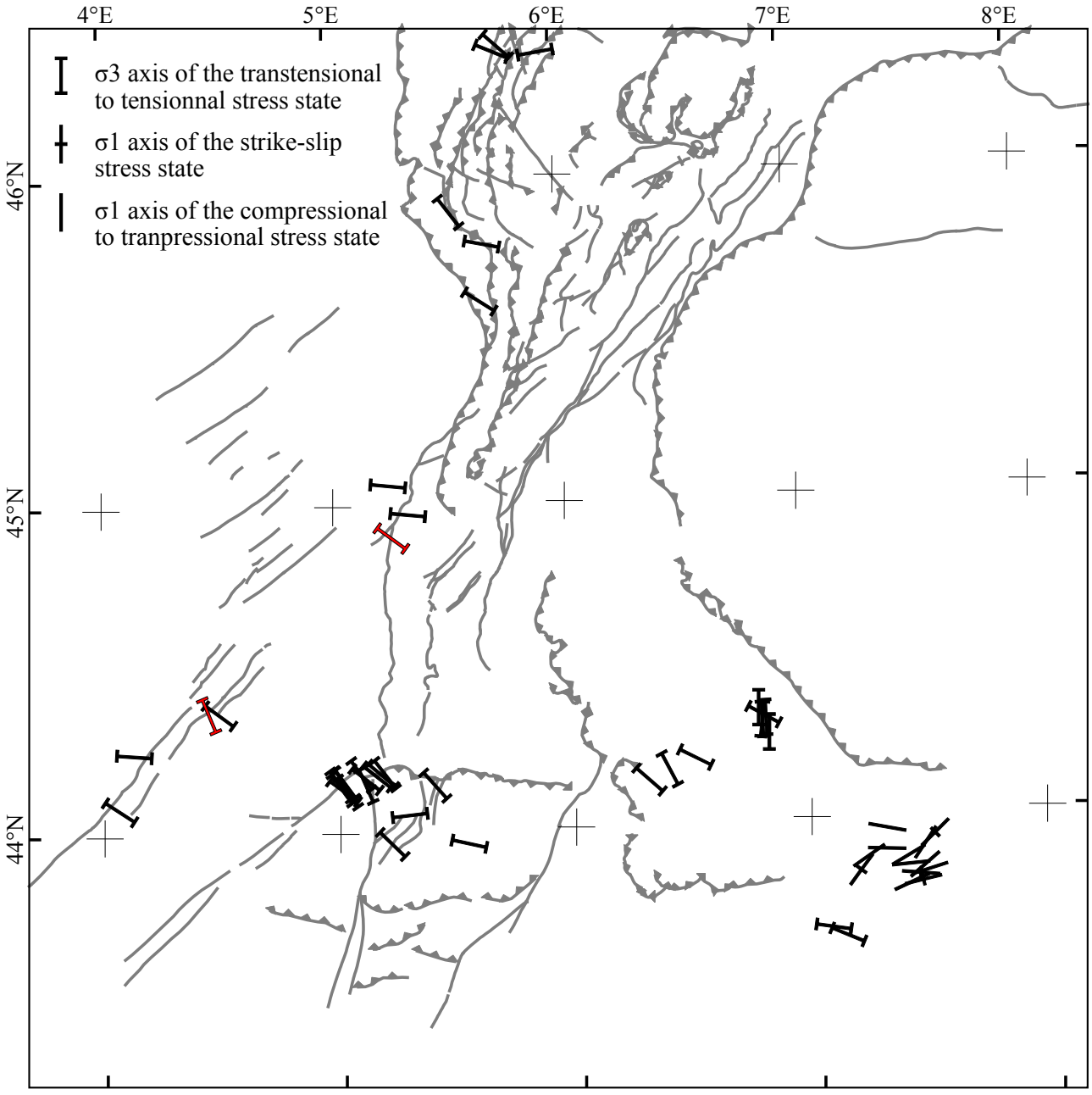

Figure II.14: Stress orientations during the Oligocene extension (in red, this work).

II.6.4 - The Aquitanian stress state

We found a strike-slip tectonic regime characterized by a NNE to NE trending σ_1 axis in two sites with Oligocene rocks (fig. II.15). A similar strike-slip regime characterized by ENE trending σ_1 axis (~N70°E) was also determined at 9 sites in the Oligocene rocks of the Marseille Basin (Hippolyte et al., 1993). In the studied area, this tectonic regime occurred before the E trending compression and after the Oligocene. It is therefore Aquitanian (to Burdigalian?) in age. It probably corresponds to the Savique stage already described by Bergerat (1981) in the Rhône valley.

No large structure appears contemporaneous nor reactivated during this deformation stage and it is difficult to link this strike-slip tectonic regime, at the Valence latitude, to the compression generate by Apulian collision. Bergerat (1985) proposed that this stress state is related to the expression again of the African plate convergence (which moved approximately north-eastward since ~80Ma (Schettino and Turco, 2011)) after the stop of the Oligocene extension. On the other hand, Oligocene extension is caracterized during late Chattian by a ~N155 trending σ_3 axis (Hippolyte et al., 1993) which is close to the σ_3 axis of this Aquitanian stress state. This stress state could so result of both source, the Liguro-Provençal rifting and the Africa-Eurasia convergence.

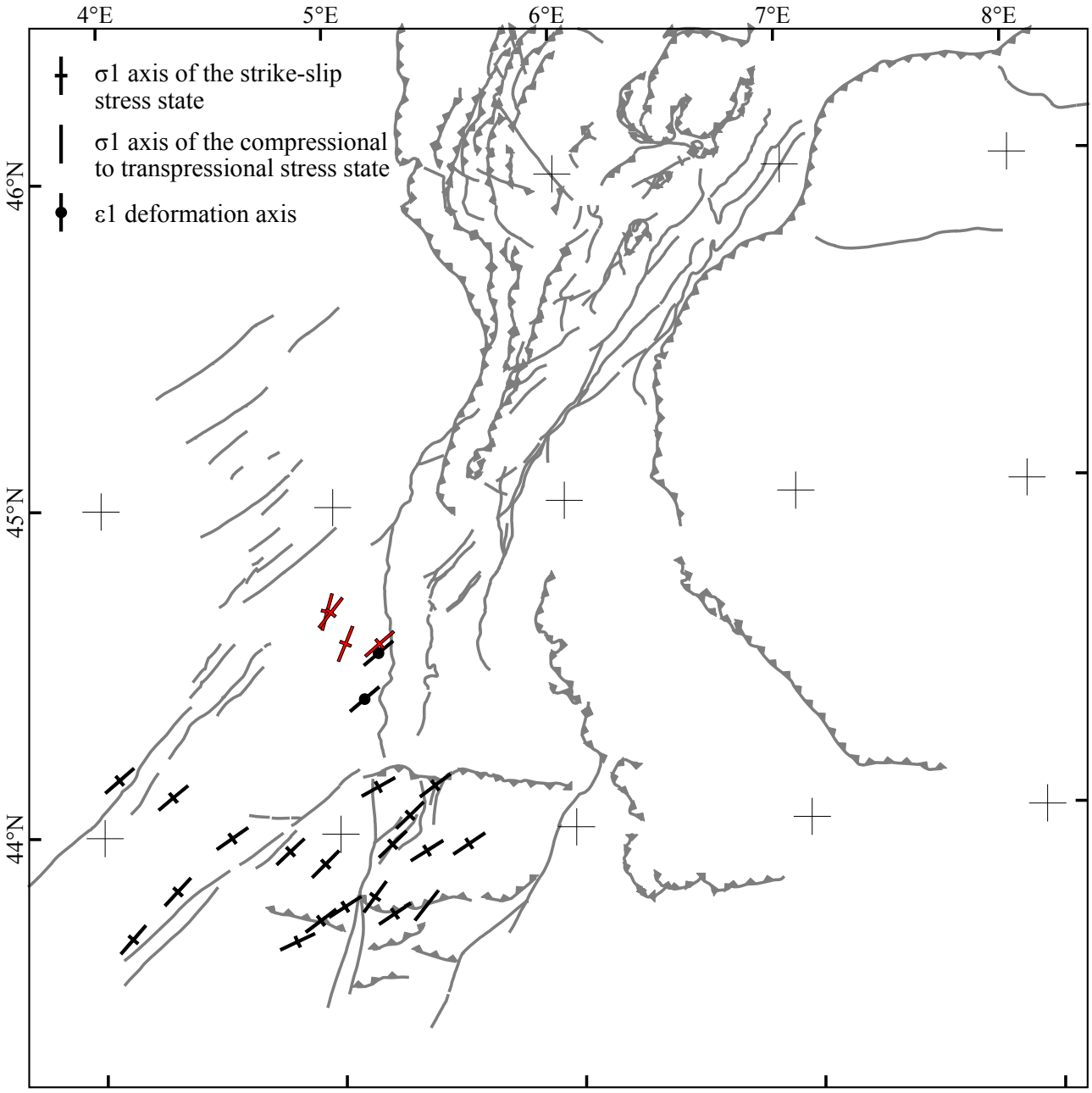

Figure II.15: Stress orientations during the Aquitanian compression (in red, this work).

II.6.5 - The Mio-Pliocene stress states

We defined 55 stress tensors that we attribute, according both to our observations and previous works (Bergerat, 1981a; Casagrande Fioretti, 1985; Philippe, 1994; Philippe et al., 1998) to the Mio-Pliocene compression (Fig. II.16) that started during Burdigalian or Langhian and occurred until upper Pliocene (Billant et al., in prep (Ch. Erreur : source de la référence non trouvée); Casagrande Fioretti, 1985). In the Jura and subalpine massifs, tectonic regimes are compressionnal to strike-slip with a σ_1 axis nearly normal to the folds and thrusts, i.e. ~NNE trending in the southern Jura, ESE trending in the Bornes, Chartreuse massifs, ~ESE to ENE trending in the Vercors, Diois and Baronnies, ~N trending in Provence and ~NE to ~N trending in the Digne nappe. Note that in the southern termination of the Mérindol-Condorcet-Saillans fault system, stress state can display a ~N trending σ_1 axis. These site are all included in or close to the fault zone, and their trend is probably deviated by stress perturbations at fault tips (e.g. Homberg et al., 1997). Similarly, the σ_1 axis trends are less homogeneous in the Valréas basin and range from NW-SE to NE-SW which is also caused by stress perturbations near strike-slip faults (Casagrande Fioretti, 1985).

This compression, normal to the arcuate shape of the Alpine belt, led to the southward Digne nappe emplacement thrusting over the Miocene deposits of the Valensole basin (Ford et al., 2006; Haccard et al., 1989). In the subalpine massifs, it produced N to N20°E trending folds and thin-skin style westward thrusting with a basal thrust lying within the basal units (Liassic or Triassic series) of the sedimentary cover (Arpin, 1988; Burkhard and Sommaruga, 1998; Deville and Chauvière, 2000; Philippe et al., 1998). Folding and thrusting occurred in two stages (Bellahsen et al., 2014). Until 20-15 Ma (Burdigalian), the sedimentary cover was deformed without implying thrusting at the base of the external crystalline massifs, leading to the formation of the most internal folds and thrust of the Chartreuse and Bauges massifs. After 20-15 Ma, thrusts at the base of the external crystalline massifs were activated leading to their uplift and to the formation of the most external folds and thrusts of the subalpine massifs and then of the Jura.

In the Vercors, Diois and Baronnies massifs, the NE trending mesozoic normal faults were reactivated as right-lateral strike-slip faults (Arnaud, 1981). The N trending ones were also reactivated as right-lateral strike-slip faults and do not show strong vertical thrusting component (Flandrin et al., 1974), the strain being mainly accommodated on a basal thrust lying down the liassic and triassic series and outcropping at the border of the Valence basin (Philippe et al., 1998). South of the Baronnies, the Ventoux-Lure Thrust was reactivated as attested by the angular unconformity between the different units of the Miocene deposits (Montenat et al., 2000).

However, whereas the external domain is subject to a compression, the internal Alps are under an extensional tectonic regime defined by a σ_3 axis parallel to the belt (Bistacchi et al., 2000a; Champagnac et al., 2004; Grosjean et al., 2004; Sue and Tricart, 2003; Sue et al., 2007b; Tricart et al., 2007) probably caused by the lateral extrusion resulting of the Adriatic plate indentation and/or rotation (Champagnac et al., 2004; Collombet et al., 2002).

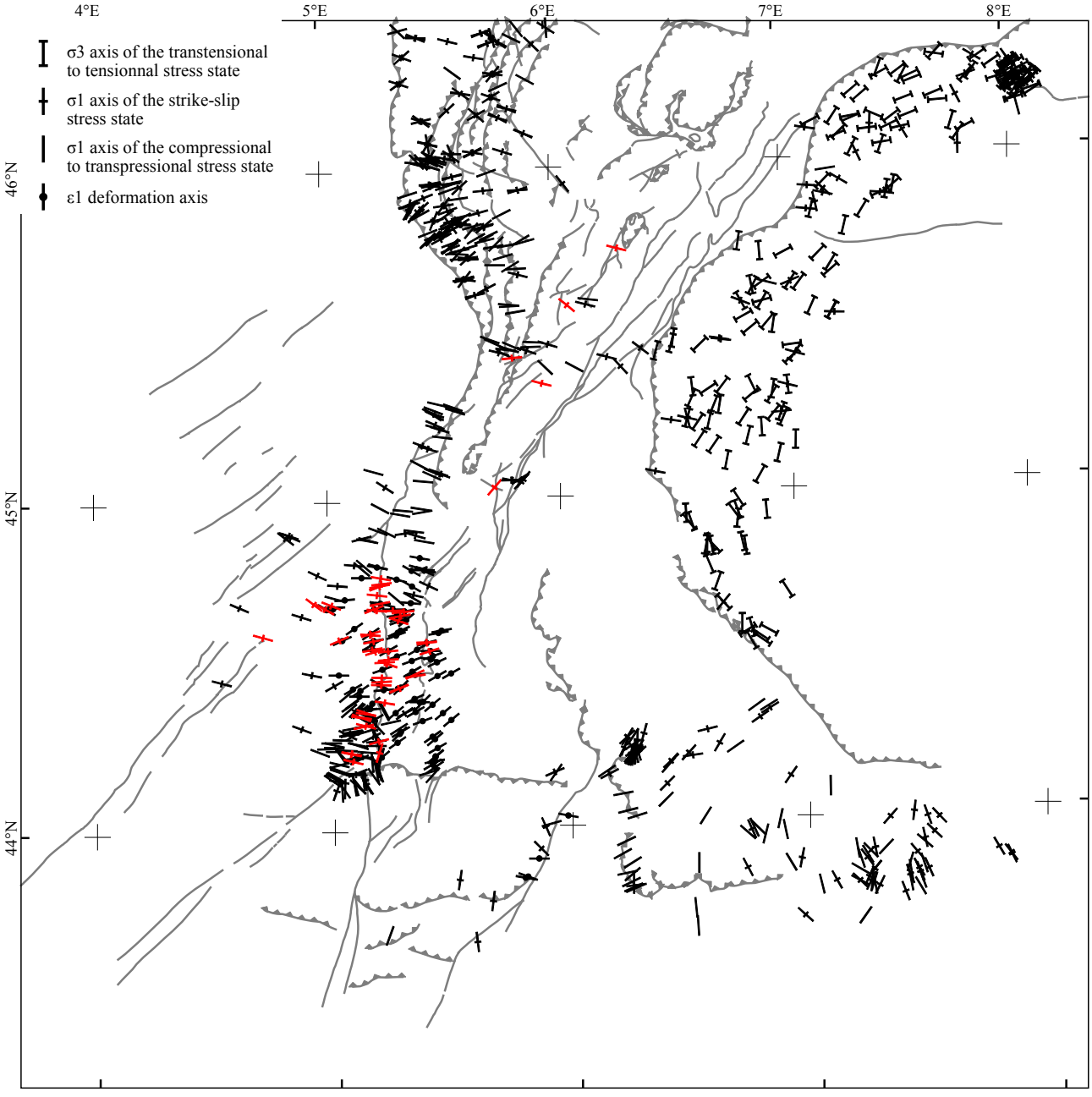

Figure II.16: Stress orientations during the middle Miocene to upper Pliocene (in red, this work).

II.6.6 - The Quaternary Stress states

We defined 17 stress tensors that we attribute, according to our observations and previous works, to the Quaternary stress field. These determined stress states correspond to strike-slip and compressional tectonic regimes. In the "Balcon de Belledonne" (Billant et al., 2015), the Vercors (Billant et al., submit (Ch. IV)), Diois and Baronnies massifs, it corresponds to a 30° to 45° counter-clockwise rotation of the Mio-Pliocene σ_1 axis trend whereas in the southern Jura, it is related to a clokwise rotation of about 45° of the Mio-Pliocene stress state, i.e. the whole stress field in the Jura became normal to the external crystalline massifs (Homberg et al., 1999). In the Inner Alps, the extension became normal to the belt (Champagnac et al., 2004).

It has been show that this late stress state is similar to the one deduced from focal mechanisms in the Inner Alps (Champagnac et al., 2004; Delacou et al., 2004) and locally in the outer Alps (Hippolyte, 2001) and Provence (Baroux, 2000). In the same way, the inversion of the focal mechanism of the southern Jura and northern Chartreuse (Delacou et al., 2004) yields a stress state similar to the late stress state defined in the southern Jura (Homberg et al., 2002). Moreover, the focal mechanism inversion from seismic events associated with the Belledonne border fault (see II.5) yields a stress tensor similar to the tectonically determined in the "Balcon de Belledonne" (Billant et al., 2015). Finally, the strike slip tectonic regime characterized by a NNE to NE σ_1 axis that we defined along the Mérindol-Condorcet-Saillans fault system is in agreement with the only focal mechanism defined along the Mérindol-Condorcet-Saillans fault system (Ménard, 1988).

Moreover, this stress state is coherent with the few well constrained present day fault kinematics in the western Alps and Provence. Indeed, in the Jura, the N120 trending compression is consitent with the left lateral strike-slip faulting along the NW trending Vuache, Culoz and Col du Chat faults (Baize et al., 2011; De La Taille et al., 2015; Thouvenot et al., 1998) whereas in the Provence, the N trending compression is consistent with the S verging thrusting of the E trending Trevaresse fault (Baroux et al., 2003; Chardon and Bellier, 2003; Lacassin et al., 2001) and left-lateral strike-slip faulting along the NNE trending middle Durance fault (Cushing et al., 2007).

Ongoing of this late stress state is well constrained thanks to the literature. Indeed, the trend change occurred during or after the late Miocene in the Jura (Homberg et al., 2002), after the Messinian in the "balcon de Belledonne" (Billant et al., 2015) and along the Middle Durance fault (Baroux, 2000) and after the Pliocene in the Valreas basin (Casagrande Fioretti, 1985). It is found in late Pleistocene deposits in the Inner Alps (Champagnac, 2006) whereas the previous stress state is

found in upper Pliocene deposits Billant et al. (in prep (Ch. V)). It so implies that ongoing of the modern stress state appended during the Pleistocene.

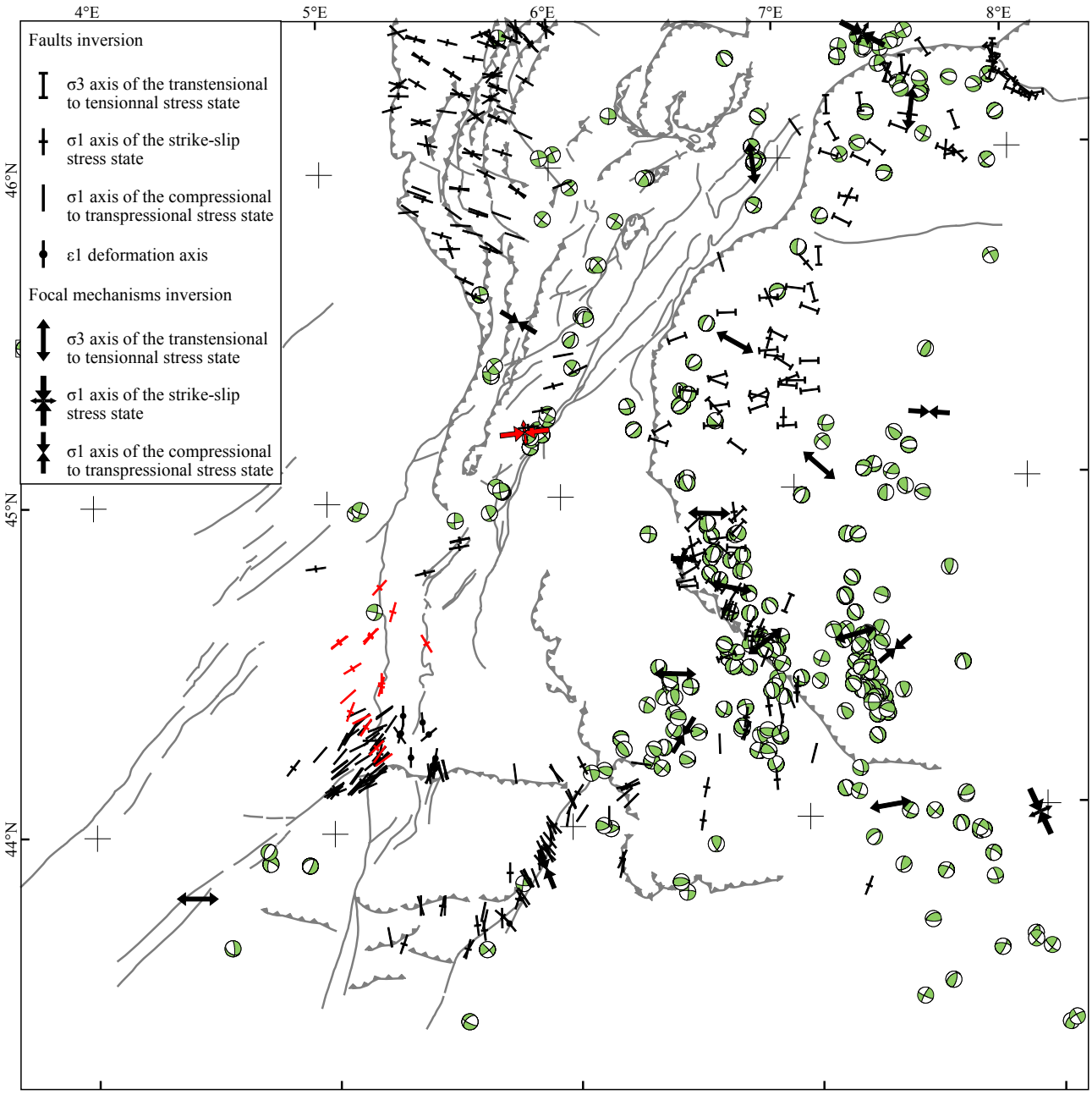

Figure II.17: Focal mechanisms and stress orientations during the Quaternary (in red, this work).

II.7 - Conclusion

This work allowed a better constrain of the stress state evolution in the foreland of the Western Alps. Even if the stress states related to the past were already well know, we provide new evidences about the time span of some stage and new data in the Diois and Baronies areas. To resume, the Western Alps and is foreland have been subjected to:

- a NW to NNW trending extension since late Triassic until Tithonian
- a N to ENE trending extension since Berriasian ending before Cenomanian
- a NNW to NNE trending strike-slip compression since late Cretaceous (~ 80Ma) until Priabonian
- an E trending extension during early Oligocene
- a SSE trending extension in Southern Provence during the rifting of the Provençal basin between late Rupelian and late Chattian
- a strike-slip tectonic regime characterized by a NE trending σ_1 axis during Aquitanian
- an ESE trending (in the north, except in the southern Jura where it is ENE trending) to N trending (in the south) compression in the external Alps associate to an extension parallel to the Belt in the western inner Alps since Burdigalian-Langhian until upper Pliocene
- since Pleistocene, an ESE trending compression in the Jura, ENE trending in the "balcon de Belledonne" and Vercors Massif, NE trending in the Diois and Baronnies massifs, N trending in the Provence associate to an extension normal to the belt in the western inner Alps.

We conclude that a reorganization of the stress field occurred at the scale of the whole western Alps during the Pleistocene. The late stress state is consistent with the present day stress state deduced from focal mechanisms.

The strike slip tectonic regime caracterized by the N80°E trending σ_1 axis implies that faults in the prolongation of the Belledonne border fault, i.e. the Arcalod fault north-eastward and the Cléry and Jasneuf fault south-westward must be right lateral strike-slip fault too. However, slightly north-eastward in the Jura and Chartreuse massifs, the tectonic regime is caracterized by a uniaxial compression caracterized by a N120°E trending σ_1 axis (Delacou et al., 2004) which is consistent with the both strike-slip and compressional tectonic regime in the Jura (Homberg et al.,

2002). We remind here that we favour the strike slip tectonic regime caracterized by the N80°E trending σ_1 axis along the Belledonne border fault because of the high misfit parameters and of the fact that the less compatible focal mechanisms with the solutions yielding a N120°E trending compression were those along the Belledonne border fault.

We so propose the existence of two tectonic regime in the western Alps. The first is the strike slip tectonic regime caracterized by the N80°E trending σ_1 axis and could be limited to a narrow zone along the Belledonne border fault and its extensions. The second affect the rest of the subalpine massifs and is a uniaxial compression caracterized by a N120°E trending σ_1 axis.

South-westward, according with the present-day stress state, the Mérindol-Condorcet-Saillans fault system must act as a right-lateral strike-slip fault. As already suggest by Le Pichon et al. (2011) this fault could allow the transfer of the deformation from the western Alps to the Provencal domain.

III - TECTONIC AND GEOMORPHIC ANALYSIS OF THE BELLEDONNE BORDER FAULT AND ITS EXTENSIONS, WESTERN ALPS

Nous présentons dans ce chapitre, publié dans la revue Tectonophysics, les résultats de l'analyse morphostructurale de la portion du système de failles de Belledonne comprenant du nord-est au sud-ouest : la faille de l'Arcalod, la faille bordière de Belledonne et sa faille antithétique, la faille du Brion.

Les états de contrainte déduits de l'inversion des plans de failles striés le long des failles de l'Arcalod et dans les marnes jurassiques surplombant la faille bordière de Belledonne sont cohérents avec l'état de contrainte déduit des mécanismes au foyer et sont en accord avec une cinématique en décrochement dextre de ces failles. Ce régime de contrainte en décrochement caractérisé par un axe σ_1 orienté ENE-WSW (~N080°) est post-messinien et succède à l'état de contrainte compressif à décrochant miocène caractérisé par un axe σ_1 de direction WNW-ESE (~N120°)

L'anomalie résiduelle de Bouguer dans la vallée du glacier de l'Isère présente des valeurs faibles caractéristiques du remplissage fluvio-lacustre des vallées glaciaires qui avait suivi leur fort creusement, excepté dans la zone de relais entre la faille d'Arcalod et la faille bordière de Belledonne où les anomalies résiduelles de Bouguer deviennent positives. Nous interprétons cette variation comme résultant d'un régime tectonique local en compression dans un relais transpressif entre ces deux failles. Cette compression induit localement soit une remontée du socle, soit une remontée du fond de la vallée glaciaire (« horst transpressif »).

Cette zone d'étude a été fortement marquée morphologiquement par les glaciations quaternaires rendant l'analyse morphologique difficile. Ainsi, aucun indice de déformation récente n'a pu être observé le long de la faille bordière de Belledonne et nous démontrons que la morphologie du flanc sud-est de la vallée inférieure de l'Isère (vallée du Grésivaudan) en face du massif de la Chartreuse, précédemment interprétée comme résultant du jeu d'une faille normale bordant ce flanc, peut être expliquée en terme de modelé glaciaire.

Nous avons tout de même pu identifier d'autres anomalies morphologiques que nous attribuons à une réactivation récente de certaines failles. Ainsi, la faille d'Arcalod est associée à un escarpement et les cours d'eau qui la recoupeent présentent un tracé sigmoïdal (baïonnettes) pouvant indiquer un décalage dextre d'environ 200 mètres. La faille antithétique du Brion semble décaler pour sa part de manière sénestre et d'une valeur comprise entre 430 mètres et 200 mètres la vallée du glacier de l'Isère. Ces morphologies décalées sont ambiguës et de plus d'âge incertain. Les taux de glissement que l'on peut en déduire sont discutés dans le texte.

TECTONIC AND GEOMORPHIC ANALYSIS OF THE BELLEDONNE BORDER FAULT AND ITS EXTENSIONS, WESTERN ALPS

Billant Jérémy[a], Hippolyte Jean-Claude[a], Bellier Olivier[a]

[a] Aix-Marseille Université, CNRS, IRD, CEREGE UM34, 13545 Aix-en-Provence, France

Keywords:

Alps; Cenozoic fault kinematics; Morphotectonic; Active tectonics; Belledonne fault system

Abstract

In the western Alps, the NE trending Belledonne fault system extends from the Mont Blanc massifs in the NE to the Vercors massif in the SW. It includes the Belledonne border fault, defined by an alignment of micro earthquakes (ML≤3.5). Focal mechanisms and their respective depths indicate a crustal scale NE trending dextral strike-slip faulting.

This study aims at better constrain the geometry, the fault kinematics and slip rate of the faults of the Belledonne fault system by using a multidisciplinary approach that includes tectonics, geomorphology and geophysics.

New clues of potential Quaternary deformations are observed: 1- the right-lateral offsets of morphologic markers (talwegs) along the NE trending Arcalod fault at the north-eastern termination of the Belledonne border fault; 2- the left-lateral offset of the valley carved by the Isère glacier along the NW trending Brion fault, which is consistent with the fault kinematics deduced from the focal mechanisms.

Stream network anomalies along the Belledonne border fault are related to glacial erosion processes rather than faulting. However, fault kinematics analysis along the Belledonne border fault allows us to determine a strike-slip tectonic regime characterized by horizontal ENE trending $\sigma 1$ stress axis. It is consistent with the mean trend of the P and T axes deduced from the focal mechanisms. We display evidences that this stress state is Messinian to Quaternary in age and

occurred after an Oligocene to Messinian strike-slip tectonic regime characterized by horizontal WNW trending σ1.

Fault slip rates can not be assessed because of the lack of morphologic features with constrained ages. However, it is likely that the presented geomorphic markers are older than Würm.

III.1 - Introduction

Although continental interiors are generally characterized by low strain rates, they can be struck by destructive earthquakes (e.g., the 1356 Basel Earthquake, Switzerland (Fäh et al., 2009), the 1811-1812 New Madrid earthquakes, United States (Tuttle et al., 2002), the 1909 Lambesc earthquake, France (Baroux et al., 2003; Chardon et al., 2005; Lacassin et al., 2001), the 2001 Gujarat earthquake, India (Rastogi, 2004)). A direct consequence of these low strain rates is that the recurrence intervals between destructive earthquakes can reach up to several millennia and thus historical seismicity can not document an entire earthquake cycle. Moreover, climatic conditions may not favour surface preservation of active fault traces. Generally, classic approaches developed for highly seismic regions, i.e. historical seismicity investigations and paleoseismology, are strongly limited and may not be suitable to assess seismic hazard in low strain rate areas.

This study takes place in an area as described above and is focused on the central part of a NE trending fault system that we name the Belledonne fault system. It is an alignment of NE-SW striking faults extending from the Aiguilles Rouges and Mont Blanc massifs, in the north-east (alpine external crystalline massifs), to the Vercors massif, in the south-west.

Based on microseismicity, Thouvenot et al., (2003) proposed that a dextral strike-slip fault, the Belledonne border fault, is an active fault bordering the Belledonne massif to the west. Indeed, a NE trending alignment of low magnitude seismic events with a mean focal depth of about 7 km testifies that an active fault affects the crystalline basement (Thouvenot et al., 2003). Until now, no geologic or morphotectonic study allowed mapping this fault on the surface. The aim of this study is to constrain the geometry, kinematics and fault slip rate of the Belledonne fault system, including the active strike-slip fault segment identified at depth by (Thouvenot et al., 2003). For this purpose, because of the moderate crustal deformation and high erosion rates prevailing in the study area, a multidisciplinary approach (morphotectonics, faults kinematics, structural analysis and geophysics) is needed in order to constrain fault geometry and kinematics and find offsets of inherited morphologies (e.g., Baize et al., 2011; Cushing et al., 2008; Le Roux et al., 2008; Molliex et al., 2011; Schlupp, 2001).

III.2 - Structural framework

The study area is located at the junction of two alpine domains: the external crystalline massifs and the subalpine massifs. They respectively represent the pre-Triassic crystalline basement and its Mesozoic cover. From north to south, the external crystalline massifs are the Aiguilles Rouges, Mont Blanc, Belledonne and Pelvoux Massifs and the subalpine massifs are the Bornes, Aravis, Bauges, Chartreuse and Vercors Massifs (Fig. III.1A). Bauges and Chartreuse massifs are separated from the Belledonne massif by the large Grésivaudan valley where the Isère river flows.

The main faults of the area are NE trending faults cutting the external crystalline massifs (e.g. synclinal median fault, Fig. III.1A) (Bodelle and Goguel, 1980). They formed during the Variscan tectonic event as dextral strike-slip faults (Guillot and Ménot, 2009). Injection of magma from lithospheric mantle within some of these fault zones confirms that they cut the entire crust (Guillot and Ménot, 2009). This crustal weakness zone was reactivated during the following tectonic phases, first by normal faulting during the Tethysian extension (Guillot and Ménot, 2009; Lemoine et al., 1981) and later by right-lateral strike-slip or reverse faulting during alpine collision (Debelmas and Kerckhove, 1980; Lemoine et al., 1981).

Tethysian extension, that occurred from late Triassic (Barféty and Gidon, 1990) to Dogger, created half-grabens and tilted blocks, mainly along east dipping crustal normal faults (Barféty et al., 1979; Lemoine et al., 1986, 1981).

From Oligocene to late Miocene (Beck et al., 1998; Bellahsen et al., 2014; Dumont et al., 2008), the alpine collision affected the external alpine domains (external crystalline massifs and subalpine massifs). This led to the verticalization of normal faults in the external crystalline massifs (Gidon, 2001; Lemoine et al., 1981) and to the westward thrusting and uplift of the external crystalline massifs. Beneath the crystalline massifs, some Tethysian crustal normal faults have been re-activated as thrusts (Ménard and Thouvenot, 1987). Gravimetric and seismic waves velocity anomalies (Ménard, 1979) and seismic profile (Deville and Chauvière, 2000) provided evidences of a sedimentary wedge and a basal thrust beneath the Belledonne massif. However, seismic data are of poor quality for the sedimentary wedge area and its interpretation is rather speculative. Moreover, this basal thrust was not imaged on the ECORS-CROP profile (Nicolas et al., 1990).

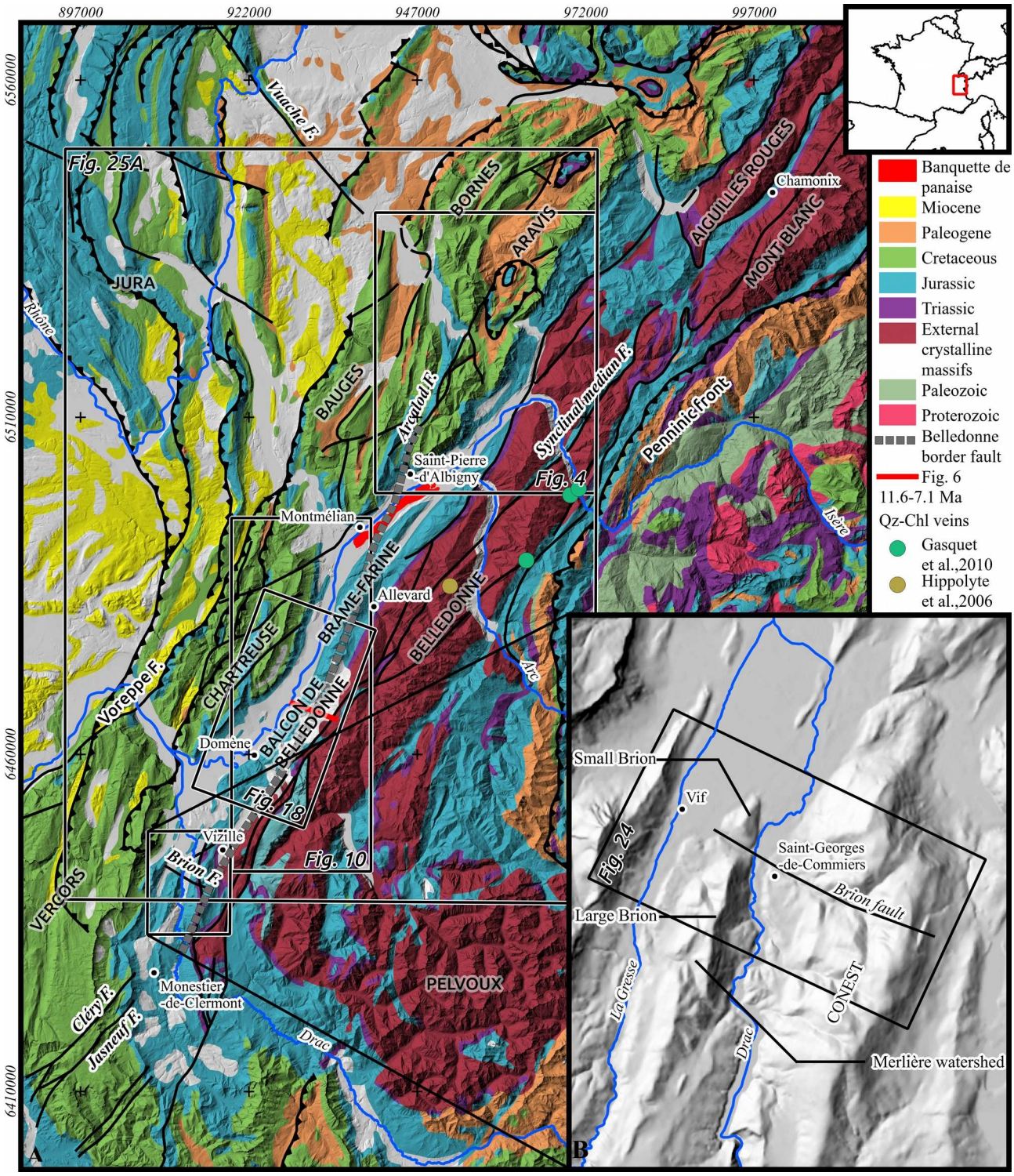

Figure III.1: A: Simplified geological map of the studied area (modified from Bodelle and Goguel (1980), Location in fig. I.1). B: Shaded DEM of the Brion fault area.

In the Subalpine massifs, the alpine collision led to the formation of N to N20°E trending folds and thin-skin style westward thrusting with a basal thrust lying within the basal units (Liassic or Triassic series) of the sedimentary cover (Arpin, 1988; Deville and Chauvière, 2000; Philippe et al., 1998). Formation of the folds and thrusts occurred in two stages (Bellahsen et al., 2014): until 20 Ma, the sedimentary cover was deformed without implying thrusting at the base of the external crystalline massifs, leading to the formation of the most internal folds and thrust faults of the Chartreuse and Bauges massifs. After 20-15 Ma, thrusts at the base of the external crystalline massifs were activated leading to the uplift and formation of the most external folds and thrusts of the subalpine massifs.

N45°E oriented dextral strike-slip faults laterally offset these folds and thrust belts (Gidon, 1999, 1996, 1990, 1981; Kerckhove and Antoine, 1964). These dextral faults are confined to the subalpine massifs and do not extend west of the frontal thrusts nor east in the external crystalline massif. Some of these dextral faults are connected to the thrust. These dextral strike-slip faults may result from a dextral shear of the whole subalpine massif between its frontal thrust and the external crystalline massif which occurred after the nappes emplacement (Gidon, 1990).

III.3 - Alpine active deformation

III.3.1 - Seismicity of the Western Alps

Several historical earthquakes are referenced in the SISFRANCE catalog (EDF-IRSN-BRGM) in the subalpine and Belledonne massifs (Fig. III.2). Historical earthquakes are diffuse and most of the events have a MSK epicentral intensity inferior to V and could not be firmly associated with a particular fault. However, some earthquakes exhibit higher epicentral intensities in this area like the two Chamonix earthquakes (March 11th 1817, MSK intensity = VII and August 13th 1905, MSK intensity = VII) in the Mont Blanc massif. One of the most destructive earthquake referenced is the Corrençon-en-vercors earthquake (April 25th 1962, MSK intensity = VII-VIII) which occured in the Vercors massif. This earthquake was felt over 140 km north and caused strong damages in the city of Corrençon-en-Vercors (http://fresques.ina.fr/rhone-alpes/fiche-media/Rhonal00357/un-tremblement-de-terre-a-correncon-en-vercors.html).

Seismic monitoring of the Western Alps (from the Si-Hex catalog, Cara et al., 2015) shows a relatively high micro seismicity density compared to other areas in France. In the study area, the external crystalline massifs seem to separate two seismic regions (Thouvenot, 1996):

- First, east of the external crystalline massifs a high seismic density area corresponds to the Briançonnais zone with the Penninic frontal thrust as western limit (Fig. III.2). Most of the earthquakes occur in the upper 10 km with a $M_L < 4$. Focal mechanisms of these events indicate mainly normal faulting (Fig. III.2) with T axis nearly normal to the trend of alpine belt (Delacou et al., 2004; Eva and Solarino, 1998; Sue et al., 1999).

-Second, an external seismic arc is located between the western limit of the external crystalline massifs and the subalpine frontal thrust (Thouvenot, 1996). It shows a less dense seismicity (Fig. III.2). Most of these earthquakes also occur in the first 10 km depth and have a $M_L < 4$. Available focal mechanisms within this domain indicate reverse and strike-slip faulting with a P axis nearly normal to the trend of the alpine belt (Fig. III.2) and therefore oriented E-W in the Grenoble area (Delacou et al., 2004; Sue et al., 1999) and N-S in the northern alpine foreland in Switzerland (Kastrup et al., 2004; Maurer et al., 1997).

Although the seismicity is generally diffuse in the subalpine massifs, a denser seismicity area along the Grésivaudan valley is attributed to a NNE trending fault zone called the Belledonne border fault (Thouvenot et al., 2003). It is defined by a N30°E trending alignment of earthquakes ($ML \leq 3.5$) covering an elongated ~50 km long and ~7 km wide area (Fig. III.2). With a mean focal depth of 7±3km, it implies that earthquakes are located in the basement (in this area, the top of the basement is less than 6 km deep (Barféty et al., 2000; Deville and Chauvière, 2000)).

This earthquake alignment runs from Monestier-de-Clermont to Montmélian (location on Fig. III.1A). The southern part of the Belledonne border fault follows on map the contact between the Belledonne massif and its Mesozoic cover. In its middle part, the Belledonne border fault is covered by the Mesozoic sequence and on its northern end it cuts the Isère valley to join the Bauges Massif. The Belledonne border fault does not match with any of the faults mapped at the surface.

Between Vizille and Allevard (location on Fig. III.1A), seven focal mechanisms indicate strike-slip faulting (Fig. III.2; Thouvenot et al., 2003). Focal planes are subvertical and trend about N36°E and N126°E. The N36°E trend is consistent with the N°30E orientation of the seismic alignment of the Belledonne border fault, which suggests a dextral strike-slip faulting along this fault strike (Thouvenot et al., 2003).

At the southern termination of the Belledonne border fault (Fig. III.2), focal mechanisms deduced from the seismic survey of the Laffrey earthquake (January 11th 1999, M_L 3.5, 4.3 km depth) and its aftershock sequence are consistent with sinistral strike-slip faulting along the N120° trending antithetic Brion fault (see III.6.3) (Thouvenot et al., 2003).

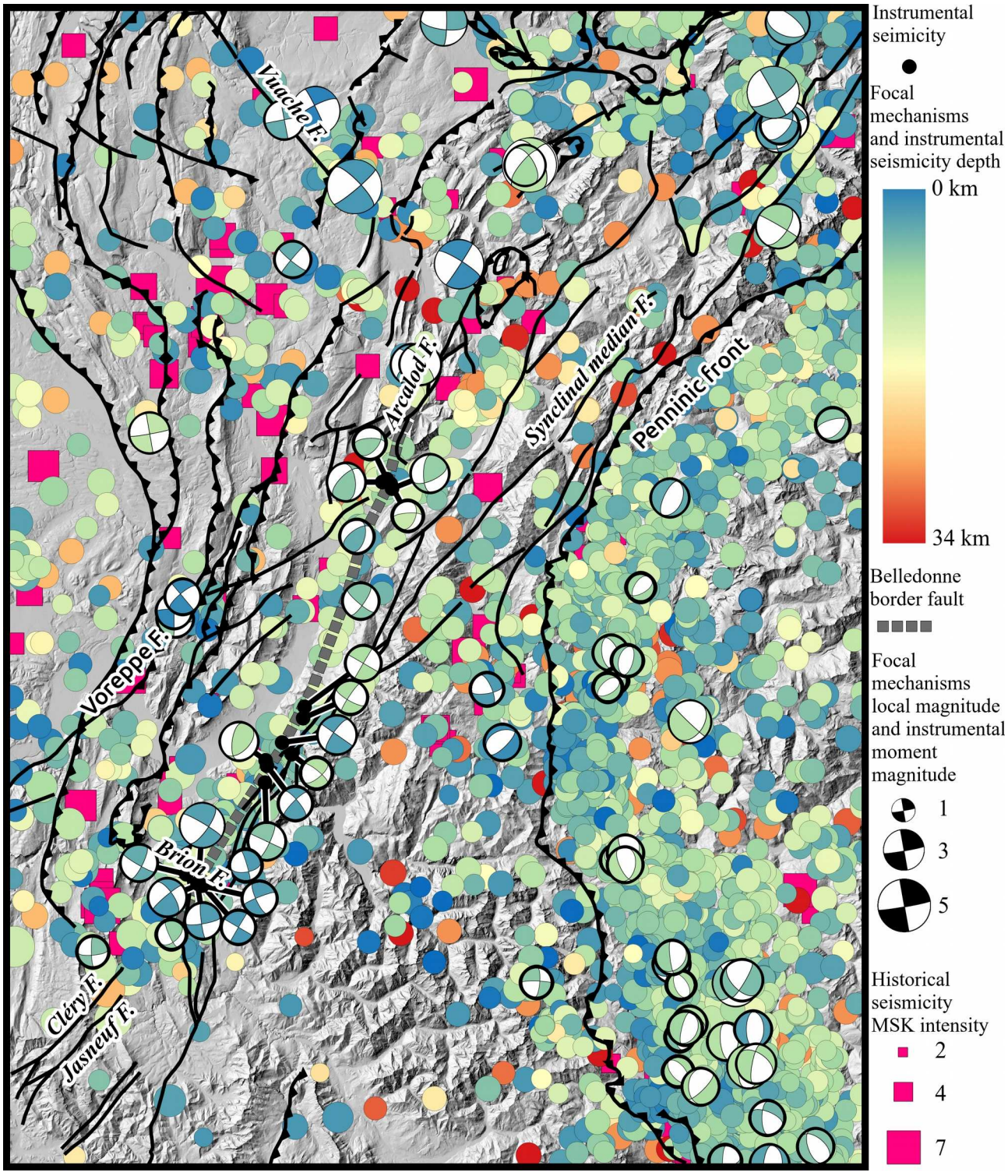

Figure III.2: Seismicity of the studied area. Historical seismicity from SISFRANCE catalog, instrumental seismicity form the Si-Hex catalog (Cara et al., 2015), focal mechanisms from(Eva and Solarino, 1998; Fréchet et al., 2010, 1996; Kastrup et al., 2004; Sue et al., 1999; Thouvenot, 1996; Thouvenot et al., 2003, 1998). Same coverage as figure III.1A.

III.3.2 - Geodesy and deformation rate

In the western Alps, GPS measurements were performed mainly during the GeoFrance 3D program (Calais et al., 2000). However, because of the slow deformation rate in the Alps (lower than 1 mm.yr^{-1}) and due to the low density of benchmarks, results can't be considered significants (rarely exceed the 2σ confidence level). It is hence difficult to attribute a deformation rate to a single fault (Calais et al., 2000).

At regional scale, permanent GPS measurements show an anticlockwise rotation of the Apulian plate, with a rotation pole located in the Po plain (Calais et al., 2002; Caporali and Martin, 2000; D'Agostino et al., 2008) or in the western Alps (Battaglia et al., 2004; Serpelloni et al., 2005; Ward, 1994). It suggests that this plate rotation is accommodated by dextral strike-slip faults in the Western Alps (Calais et al., 2002; Caporali and Martin, 2000). Deformation axes deduced from displacement measured with GPS (Calais et al., 2000; Nocquet, 2002) show that the central part of the Western Alps is affected by an E-W stretching (lower than 1 mm. yr^{-1}; Nocquet, 2002). This result is also confirmed by permanent GPS measurements over a 5 year period (Vigny et al., 2002). The reviewed and harmonized GPS measurements (Nocquet, 2002) have shown that the Belledonne and Mont Blanc faults are probable dextral strike-slip fault system that separates two domains: the subalpine and Jura massifs, characterized by a NW-SE to NNW-SSE shortening and the inner Alps characterized by a E-W stretching in its central zone and N-S stretching in its northern domain (Delacou et al., 2008).

GPS survey of the southern end of the Jura shows a sinistral displacement of the Vuache fault (Fig. III.1A), the north-eastern block moving at 1 mm.yr^{-1} toward the NW relatively to the south-western block (Walpersdorf et al., 2006). Moreover, GPS measurements show variable rates along the Belledonne massif, the benchmark in the north-western block being relatively stable compared to the south-eastern one moving southward at 0.7 ± 0.2mm.yr^{-1} (Walpersdorf et al., 2006).

In the Chartreuse, Grésivaudan and Belledonne Massifs, compared triangulation measurements from 1950, 1993 and 1999 indicate an E-W trending shortening of about 5 ± 2,5 mm.yr^{-1} (Martinod et al., 2001). Strain rates of this study are probably overestimated because they are of the same order as the maximum displacement rate of the Pô plain relative to Europe (e.g. Caporali and Martin, 2000) and largely exceed the strain rate measured by GPS in the Western Alps (Calais et al., 2002; Nocquet, 2002; Vigny et al., 2002).

In the Bas-Dauphiné, Jura, Subalpine Massifs of Vercors, Chartreuse and Bauges, vertical displacement rates are estimated through comparison of two campaigns of levelling measurements

(NGF between 1887 and 1907, and IGN69 between 1965 and 1979) (Jouanne et al., 1998). Uplift rates are comprised between 0.5 $mm.yr^{-1}$ and 2 $mm.yr^{-1}$. According to the authors, post-glacial rebound does not seem to be responsible for this uplift. They attribute this deformation to tectonics because the highest values of uplift match with ramp anticlines at the Jura and Chartreuse fronts.

III.3.3 - Summary of the present day deformation from seismicity and geodesy

The strain orientations derived from the GPS velocity field are consistent with the active tectonic regime deduced from the seismicity (Delacou et al., 2004). According to the faults identified by the seismicity studies and the strain orientations deduced from geodetic surveys, subalpine massifs are affected by strike-slip faulting and thrusting caused by an E-W trending compression. But, the strain rates derived from seismicity are five times less than those derived from the GPS velocity which suggests that 80-90% of the deformation could be accommodated by elastic loading, creeping or ductile deformation (Sue et al., 2007b). In fact, part of the deformation accommodated by aseismic deformation may be largely overestimated; indeed geodetic deformation measurements in the Alps rarely exceed the 95% confident level.

III.4 - Geomorphic characteristics of the Alps

III.4.1 - Geomorphological inheritance

In the studied area, the first geomorphological signal mainly results from the alpine collision that built most of the present day regional scale relief. Ridge and plateau are armed by hard rocks (crystalline rocks for the external crystalline massif and limestones for the subalpine massifs) and depressions correspond frequently to softer rocks (e.g. the Grésivaudan valley in the Bajocian marls). This leads to reliefs and morphologic frame modelled on alpine structures following the main folds and faults orientations.

The second morphological signal is the glacial imprint. During the Quaternary, the Alps were affected by several glaciations and largely covered by glaciers (Fig. III.3). Palaeogeographical reconstitutions (Buoncristiani and Campy, 2011; Coutterand, 2010) show that the top of the Würmian Isère glacier reached 1200 m elevation near Grenoble and up to 2400 m elevation near the northern termination of the Aiguilles Rouges massif. Crest of the Belledonne, Mont Blanc, Aiguilles Rouges, Bornes, Aravis and Bauges Massifs, above the main glaciers were nunataks. The Chartreuse massif and the northern part of the Vercors massif were not completely covered by ice, but several glaciers have locally been present in the wider topographic depressions. As attested by

Rissian end moraines deposits downstream of the Würmian ones, Rissian glaciers were more developed than the Würmian ones.

These glaciers were powerful erosion agents. For example, the Isère glacier eroded and shaped the large Grésivaudan valley whose bottom is at 535 m below the present Isère river (Nicoud et al., 2002). Consequently, the present morphology was largely acquired prior to 34,300 B.P., age of the glacial recession in the studied area (Nicoud et al., 2002).

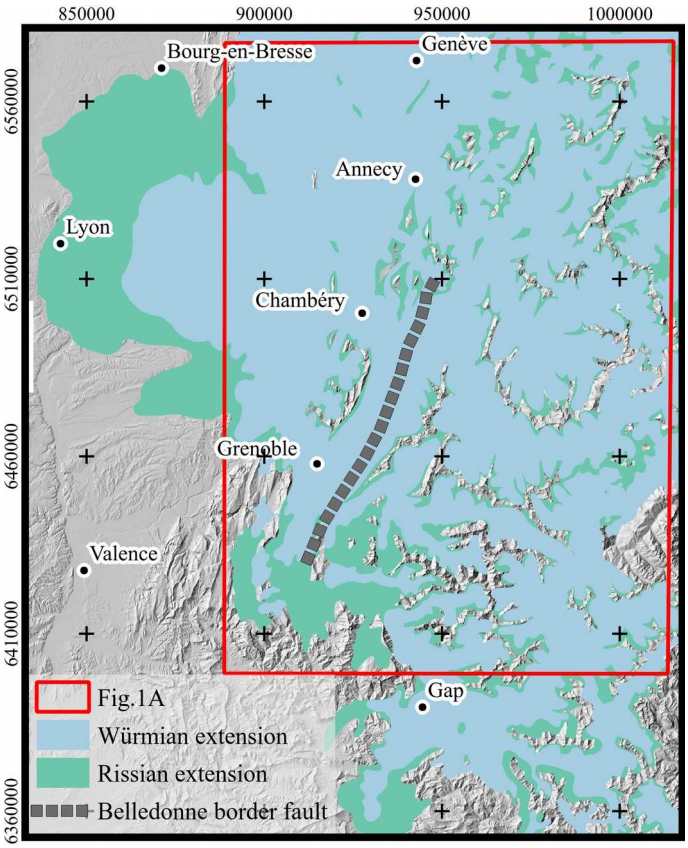

Figure III.3: Maximum glacial extension during Riss and Würm after Buoncristiani and Campy (2011).

III.4.2 - Sackungs

In high relief domains, slow (< 5 mm.yr^{-1}), deep (hectometric) and large (range scale) gravitational deformations may occur. They are named Deep seated gravitational slope deformation, or sackung. This deformation process is present in the Alps (e.g. Hippolyte et al., 2009, 2006a, 2006b; Jaurand and Kaiser, 1999). These large gravitational deformations are linked to the glacial retreat which triggers valley flank decompression. Their main expression are linear normal fault scarps and open tension fractures that reactivate inherited structural planes (faults, fractures, schistosity or bedding planes). Typical structures in a sackung are ridge-top troughs, double-crested ridges, uphill-facing fault scarps and open cracks (McCalpin and Irvine, 1995). They frequently

deform glacial morphology (i.e. polished glacial surfaces) and Quaternary screes can be cut and offset by the sackung faults. In mountain areas that contain active faults, it is difficult to discriminate the seismogenic faults from these large scale gravitational structures.

In the French Alps, these large gravitational faults with clear recent evidences of slip were often considered as tectonic faults (e.g., Baize et al., 2002; Bordet, 1970). 10Be dating of alpine sackung scarps showed that some sackungs were formed rapidly and are presently inactive (between 12,573±1482 yr BP and 8462±432 yr BP; Hippolyte et al., 2009); or active over a large period and still moving (>12 ka; Hippolyte et al., 2012b) which does not allow distinguishing them from active tectonics. Detailed mapping and morphologic analysis are necessary to distinguish the surface effects of these large gravitational faults from active tectonic faults.

III.5 - Morphotectonics in the studied zone: state of the art

Several works were performed in order to identify potential clues of active tectonics along the Belledonne fault system.

Through a geomorphological study, Darmendrail et al., 1994 suggested the existence of NW dipping normal fault along the Grésivaudan valley. The authors interpret the eastern flank of the valley as triangular facets attesting the presence of normal faults. They noticed that fans of the eastern flank of the valley are always smaller than those of the western flank. They interpreted this dissymmetry as resulting from the south-westward tilt of the Grésivaudan valley related from the normal faulting. This tilting allowed the burial of the eastern fans beneath interglacial deposits. Furthermore, they distinguished knick-points in the eastern Isère tributaries that would indicate a recent change in their base level. The older base level would be 150 meters higher than the present-day base level. This apparent base level fall would result from the uplift of the “Balcon de Belledonne” relative to the Grésivaudan valley because of normal faulting. However, the triangular facets could be related to the erosional expression of the Isère glacier and thus underline the escarpment of the eastern flank of the Würmian Isère glacier valley (Nicoud et al., 2002). Consequently, the difference of fan size could result from the difference of eroded rocks on each side of the valley.

Schwartz et al. (2005) looked for a geomorphological signature of the Belledonne border fault along the Grésivaudan valley. They showed that the Belledonne border fault is associated with a flat and counter-slope morphology (south-westward facing). Several changes in stream orientation were distinguished along the Belledonne border fault, but they could not be firmly linked to dextral

strike-slip fault. The authors could not clearly conclude that these morphological anomalies resulted from erosional processes or from recent tectonic deformation.

Nicoud (1984) mapped Pleistocene deposits forming the “Banquette de Planaise” bench in the Isère valley, between Montmélian and St-Pierre-d'Albigny (location on Fig. III.1A). A 15 km long geological cross-section shows that deposits of the north-eastern part of the bench dip 0.06° south-westward whereas its south-western part dip 0.3° also south-westward. Because of the constant thickness of the fluvio-lacustrine deposits, Nicoud (1984) proposed that this dip variation could result from tectonic deformation associated with a transtensionnal tectonic regime along the Arcalod fault that would downthrow the north-eastern part of the Isère valley. This dip variation could then only result from the initial geometry of the deposits. Moreover, the focal mechanism solutions deduced from microseimicity in this area (Thouvenot et al., 2003) rather indicate transpressional deformation along the Arcalod fault (Fig. III.2).

These few studies providing ambiguous results, our study aims to provide new evidences for present day faulting and to re-assess previous works thanks to new field observations, geophysical data and more accurate topographic analysis.

III.6 - Studied faults

III.6.1 - The Arcalod fault zone

The Arcalod fault zone (north-eastern extension of the Belledonne border fault, Fig. III.4) is 35 km long and extends from South to North from Saint-Pierre-d'Albigny to the Sulens klippe (internal units) (Doudoux et al., 1999, 1992). It is a N30°E trending subvertical normal component dextral fault (Doudoux, 1973). The strike-slip component would explain the about 7 km lateral displacement of the Arclosan syncline relatively to the Arcalod syncline (Fig. III.4), both synclines corresponding to the same laterally offset structure (Doudoux, 1973; Gidon, 1996). The normal fault component is suggested by the several hundred meters collapse of the Sulens klippe. Consequently, this faulting postdates the nappes emplacement.

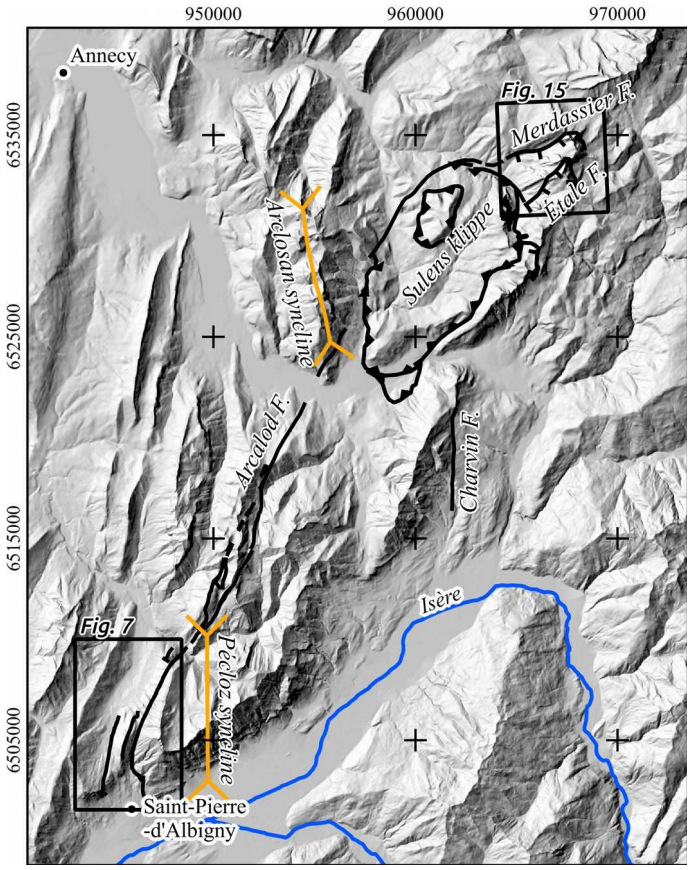

Figure III.4: The Arcalod fault system (location in Fig. III.1A).

On its northern termination, the Arcalod fault is connected to normal listric faults (Fig. III.4 and III.5) (e.g. Etale and Merdassier faults), dipping to the south and connecting on a decollement within the Bathonian Oxfordian black-shale, or at the contact with the Sulens klippe basal thrust (Doudoux et al., 1992). The SSW extension on these normal faults would be transferred south-westward by the Arcalod strike-slip fault.

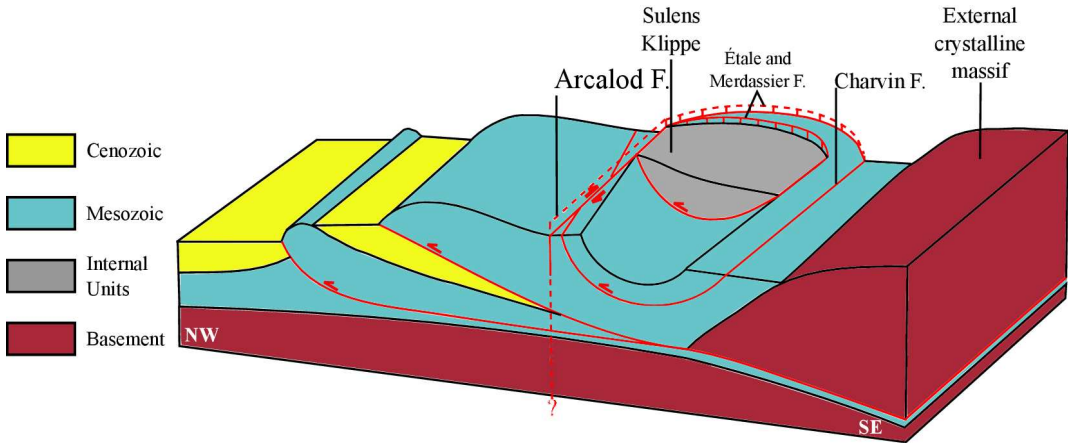

Figure III.5: Schematic block diagram of the Arcalod fault system and surrounding area.

Gidon (1996) suggests that the Arcalod fault is also connected to the Charvin fault at the east of the Aravis Massif (Fig. III.5). These two faults would correspond to an ancient thrust that marked the base of the Aravis Massif. The Arcalod fault and Charvin faults associated with the Étale and Merdassier normal listric faults would delimit a piggy back isolated by the uplift of the External Crystalline massif (Fig. III.5). Eastward, these faults were connected to the synclinal median (Gidon, 1996) or to a decollement within the Liassic series above the external crystalline massifs (Bellahsen et al., 2014). (Doudoux et al., 1982) propose that the Arcalod fault cross-cuts the thrusts and roots in the basement (Fig. III.5).

In this area, thrusts were formed during early deformations, dating back from late Oligocene to early Miocene (Beck et al., 1998; Bellahsen et al., 2014). Then, thrusting of the external crystalline massifs and their uplift led to the formation of the piggy back structure. So, right-lateral kinematics along the Arcalod fault occurred during or after the thrusting of the external crystalline massifs.

III.6.2 - The “Balcon de Belledonne” and Border hills of Grésivaudan.

The border hills of the Grésivaudan are reliefs reaching a maximum elevation of 1200 m on the eastern flank of the Isère valley. To the east of the border hills of Grésivaudan, the “Balcon de Belledonne” bench extends up to the Belledonne massif (location on Fig. III.1A).

These two domains are mainly made of Jurassic black-shales and marly limestones (from Hettangian to Bajocian) (Barféty et al., 2000). Underlying the Jurassic series, Triassic deposits crop out at the eastern border of the “Balcon de Belledonne” and consist of arkose, sandstone, dolomite, gypsum, cellular dolomite and basaltic lava levels (Barféty et al., 2000). They overlay the basement and the Permian sandstones, the Allevard sandstones, which constitute the tegument associated with the Belledonne Massif basement (Barféty and Gidon, 1996).

Structural mapping of this area shows folds with bedding generally dipping to the NW (Fig. III.6) (Barféty and Gidon, 1996; Barféty et al., 1972b). This trend is consistent with those of the schistosity planes mainly dipping to the SE and that are probably coeval with the folding (Barféty and Gidon, 1996; Barféty et al., 1972b). West vergent thrust faults cut Bajocian series in the upper limit of the border hills of Grésivaudan (Barféty and Gidon, 1996). To the west, a major west vergent thrust that duplicates the Bajocian series is presently dipping westward because it was tilted by the Belledonne massif uplift (Fig. III.6). This thrust is the counterpart of the Charvin fault (Fig. III.5), it was formed during the early deformation stage (late Oligocene to early Miocene in age) and then deformed by the external crystalline massifs uplift.

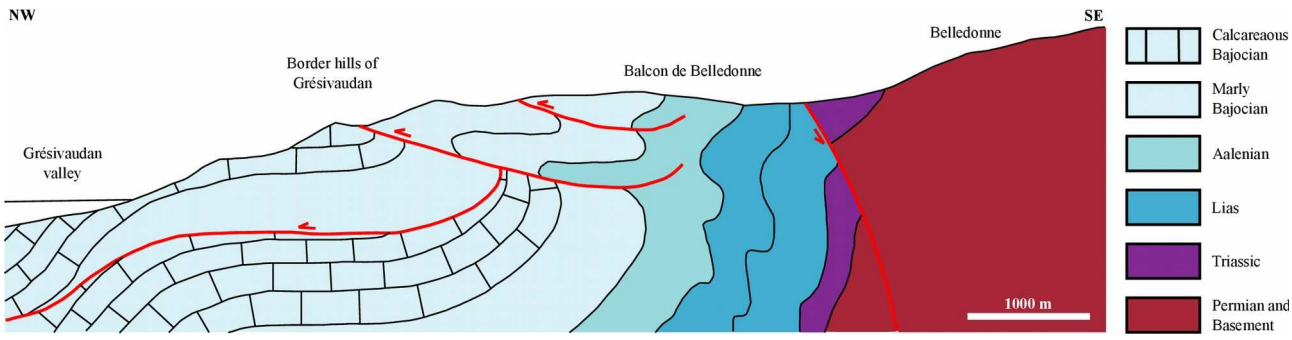

Figure III.6: Simplified geological cross-section (location in Fig. III.1A) of the Grésivaudan border hill and "Balcon de Belledonne" (modified from Barféty and Gidon, 1996).

III.6.3 - Brion fault

The Brion fault is an approximately N120°E trending fault (Fig. III.1B) (Barféty et al., 1972a; Debelmas et al., 1967b). It cuts the Liassic marly limestones of the Conest massif (Fig. III.1B). Senestrial strike-slip kinematics of the fault is attested by offsets of small amplitude folds in Triassic rocks (Debelmas et al., 1967b). The Brion massif (Fig. III.1B) consists of Middle Jurassic marly limestone tilted of about 45° westward (Debelmas et al., 1967b). The Brion fault cuts this massif into two parts: the Small and Large Brion, located north and south of the fault respectively.

III.7 - Fault kinematics analysis

The kinematics of a fault population is defined using the striations measured on fault planes at several sites. By measuring numerous striated fault planes at individual sites, we can characterize successive faulting events, tectonic regimes and related stress states. This methodology of fault kinematics studies to determine paleostress fields and to demonstrate temporal and spatial changes in the late Cenozoic stress states has been applied in many active tectonic areas around the world over the past thirty years (e.g., Bellier and Zoback, 1995; Champagnac et al., 2004; Hippolyte et al., 1993; Homberg et al., 2002, 1999; Mercier et al., 1991; Shabanian et al., 2010).

We used striae measured on both major (crustal scale) and minor (centimetric to metric scale) faults to determine the state of stress responsible for the deformation in the studied area. We realized quantitative inversion of distinct families of slip data measured at each individual site using the INVD method proposed by Angelier (1990). The results of the stress inversion include the orientation (azimuth and plunge) of the three principal stress axes σ_1, σ_2 and σ_3 (maximum, intermediate and minimum compressional stress axes) of a stress tensor and the stress ratio ($\varphi=(\sigma_2-\sigma_3)/(\sigma_1-\sigma_3)$)

In this study, we aim at characterizing the late Cenozoic deformation. Unfortunately, for fault striations, it is difficult to constrain the absolute age of fault slips more precisely than younger than the age of the rocks affected by the faults. In the study area, the analysed striations are observed on faults affecting rocks of Oxfordian to Tithonian age. Owning to outcrop conditions (weathering and abundant vegetation cover) the measurement sites are mainly located in the south of the studied area.

III.7.1 - Field observations and stress states

III.7.1.1 - The Arcalod fault area

At the Routhennes site (GPS: 45.599778°N-6.143417°E, Fig. III.7), Tithonian limestones are affected by a N020°E trending ~80°E dipping fault plane. The fault dip is very close to the bedding planes. Riedel fractures (as attested by their orientations, Fig. III.8A), corrugation grooves (Fig. III.8C), wide tearing lunates (convex tension cracks) as well as mechanical striations (Fig. III.8B) are observed. These pervasive brittle deformations clearly indicate a dextral strike-slip kinematics along this major fault plane. The Gratteloup site (GPS: 45.62233°N-6,16431°E, Fig. III.7) displays one metric right-lateral strike-slip fault plane with similar geometry.

Further south, at the Frêne pass site (GPS: 45.57982°N 6.13764°E, Fig. III.7), measurements were also done in the Tithonian limestones. Fracturing analysis shows two distinct striated antithetic fault trends. Kinematics was given by calcite steps associated with striae affecting the fault planes. The ENE trending subvertical planes show dextral strike-slip kinematics while a SE trending fault plane population shows left-lateral slips. The inversion of the complete data set allows to define a strike-slip stress regime characterized by N104°E and N194°E trending, sub-horizontal σ_1 and σ_3 axes, respectively (Fig. III.7).

At the “Crête de la Via” site, Tithonian limestones are affected by foliations defining sigmoid lenticulation within the fault zone (Fig. III.7 and III.9). The N150°E trending and 40°NE dipping fault planes exhibit oblique sinistral-reverse striations. A second family of about N trending antithetic fault planes show reverse faulting kinematics. Inversion of the fault slips yields a sinistral-reverse faulting tectonic regime characterized by an about N100°E sub-horizontal compressional (σ_1) axis.

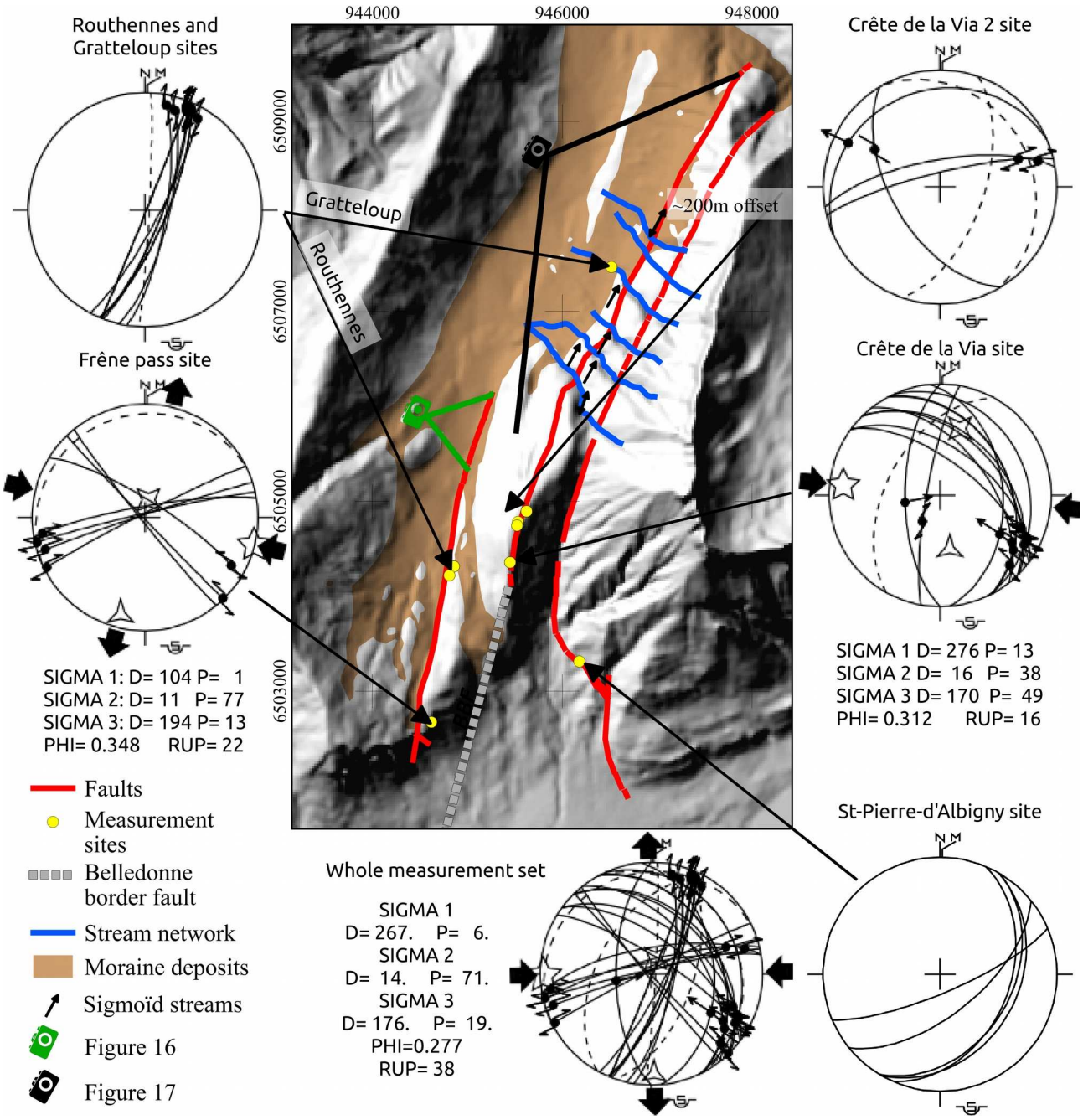

Figure III.7: Location of the sites of fault measurements and Schmidt's diagrams with computed stress tensors (location in Fig. III.4). Schmidt's diagrams: solid lines for fault planes, dashed lines for bedding planes. σ1, σ2, and σ3 as five branches, four branches and three branches stars respectively. PHI is the stress ratio and RUP a quality estimator (cf. Angelier (1990)). Stream network extracted from 1:25000 topographic map and 25m resolution DEM. Faults and moraine extension modified from the Albertville 1:50000 geological map (Doudoux et al., 1999).

Further north a few outcrops show scattered minor fault planes affecting Tithonian limestones. These data have been grouped in the Crête de la Via 2 site. The southernmost is a N65°E trending 18°NW dipping fault plane with mechanical and stylolitic striations indicating a normal component left-lateral oblique slip faulting. However, it is not possible to discriminate this deformation from bedding slip because the stratification was not clearly observed. ENE trending 75°N dipping fault planes exhibit dextral striations. Moreover, the strike, dip and kinematics of these fractures are similar to those of the Frêne Pass site suggesting that they are contemporaneous.

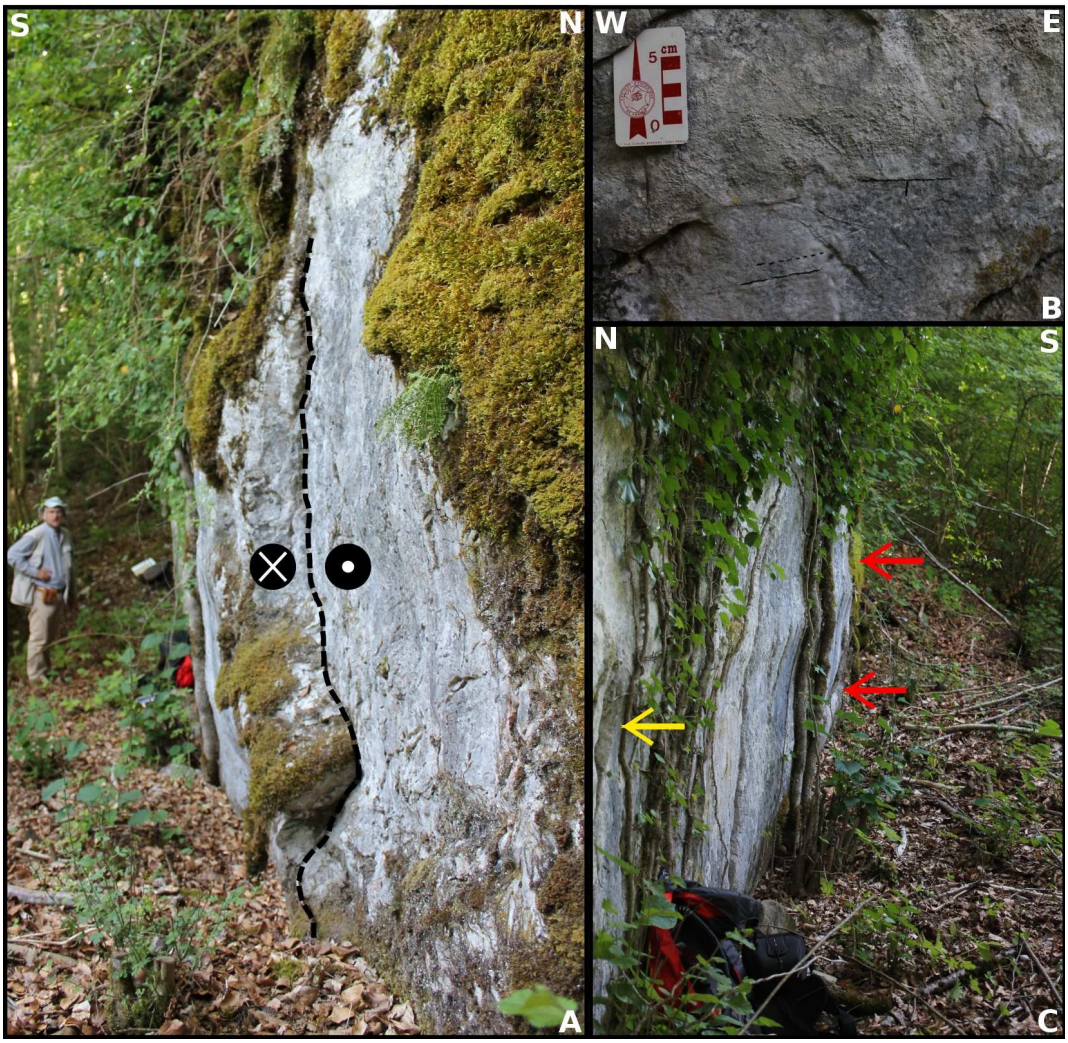

Figure III.8: Kinematics indicators along the Arcalod fault at the Routhennes site (location in Fig. III.7). A) Dextral strike-slip fault of the Routhennes site. Dashed line is a Riedel fracture indicating a right-lateral movement. B) striae indicating a right-lateral movement. C) Grooves and wide tearing lunate (red and yellow arrows respectively).

Finally, the St-Pierre-d'Albigny site exhibits a NE trending 35°SE dipping fault plane. The Jurassic black shales are affected by fracturing foliation underlying sigmoid lenticulation consistent with reverse faulting (Fig. III.7).

To constrain the regionally significance of the tectonic regime we did an inversion with all the measurements along the Arcalod fault (except the normal fault and the faults with unclear kinematics). The calculated stress tensor is well constrained and corresponds to a strike-slip tectonic regime with an about E trending horizontal compressional stress axis (Fig. III.7).

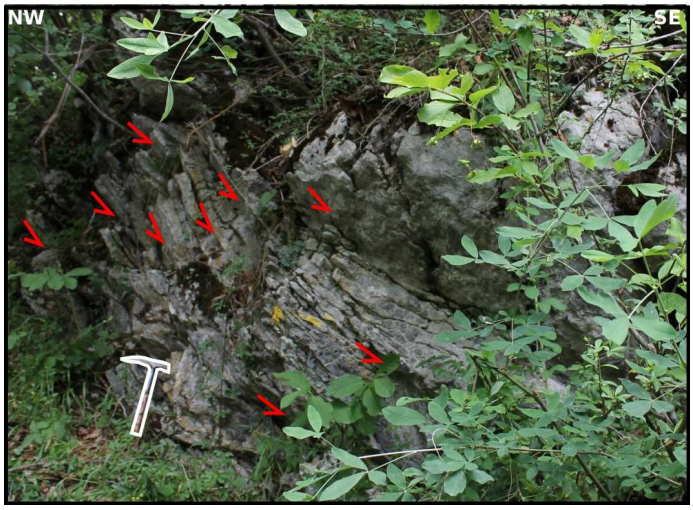

Figure III.9: Sigmoid lenticulation within the Arcalod fault zone at the Crête de la Via site (location in Fig. III.7). Red arrows indicate sense of slip.

III.7.1.2 - Balcon de Belledonne

Inside the border hills of Grésivaudan, between Allevard to the North and Domène to the South, we realised measures in the Bajocian deposits (Fig. III.10). Most of the measured bedding planes have dip directions ranged between N300°E and N325°E (Fig. III.11A). Most of the schistosity measurements provide dip directions ranged between N110°E and N125°E.

The Bajocian marls is affected by a fault set of three major orientations (Fig. III.10). One of this fault family has orientations close to N030°E and dip ranged between 50° and 80°SE whereas the two others are subvertical and trend about N105°E and N135°E (Fig. III.10 et III.11B). Fault planes display striated calcitic infill, fibrous calcite steps and/or stylolites indicating that the N030°E oriented fracture are dextral strike-slip faults and the N105°E and N135°E oriented fractures moved as sinistral strike-slip faults (Fig. III.10 et III.12). One site (THEYS3) exhibits N105°E trending dextral strike-slip faults (Fig. III.10). Difference in pitches of the striae on the

same fault plane and cross-cutting striae show that faults are affected by both pre-tilt and post-tilt faulting. Furthermore, pitches of the striae are variable, ranging between 0° and 35°.

In contact with the major faults, schistosity is sometimes deformed as drag folds, providing evidence for a major fault kinematics in agreement with the microtectonic markers. Some N120°E trending fractures show plumose structures.

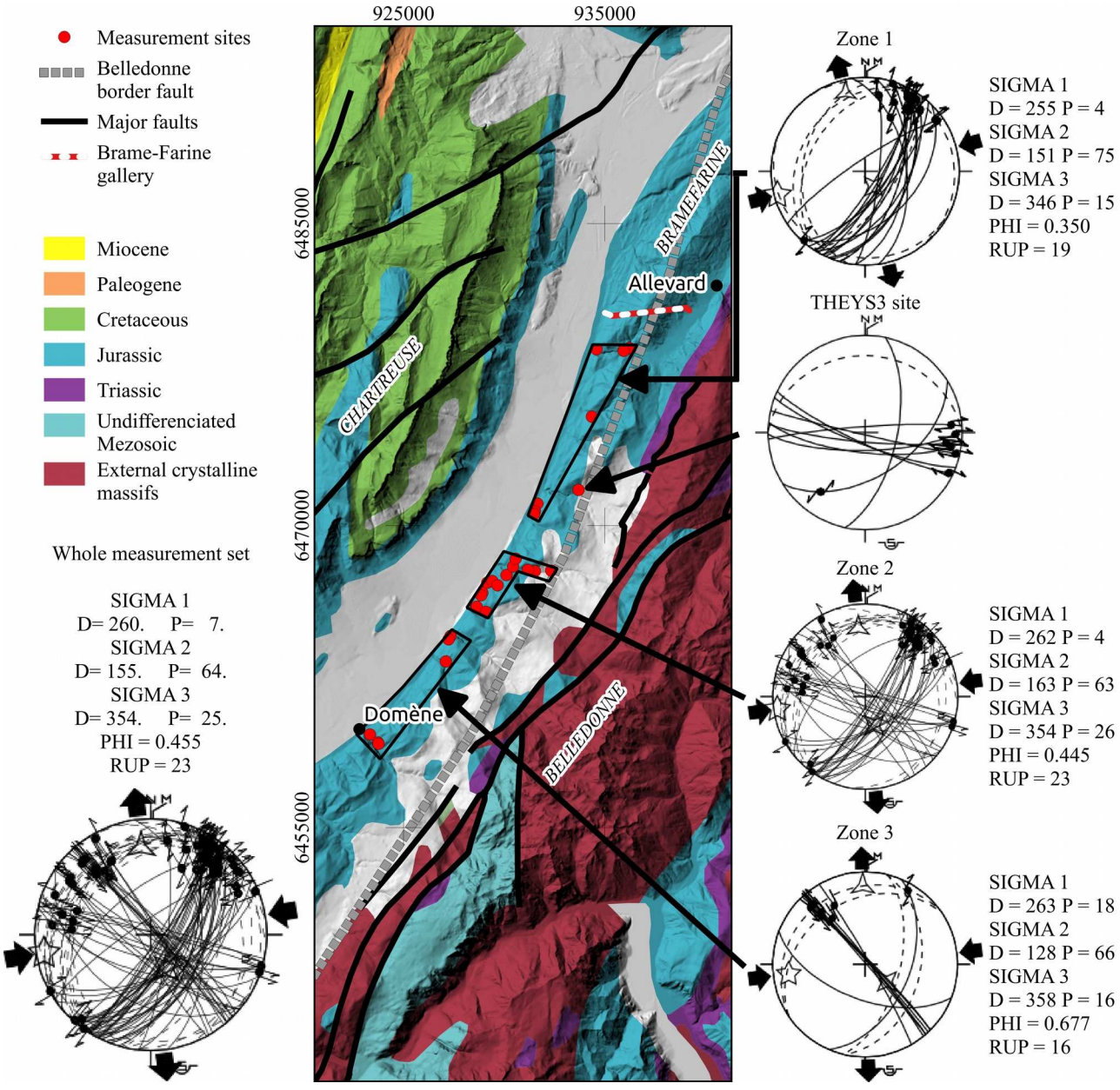

Figure III.10: Location of the sites of fault measurements in the "Balcon de Belledonne" and computed stress tensors (location in Fig. III.1A). Same legend of diagrams as in Fig. III.7.

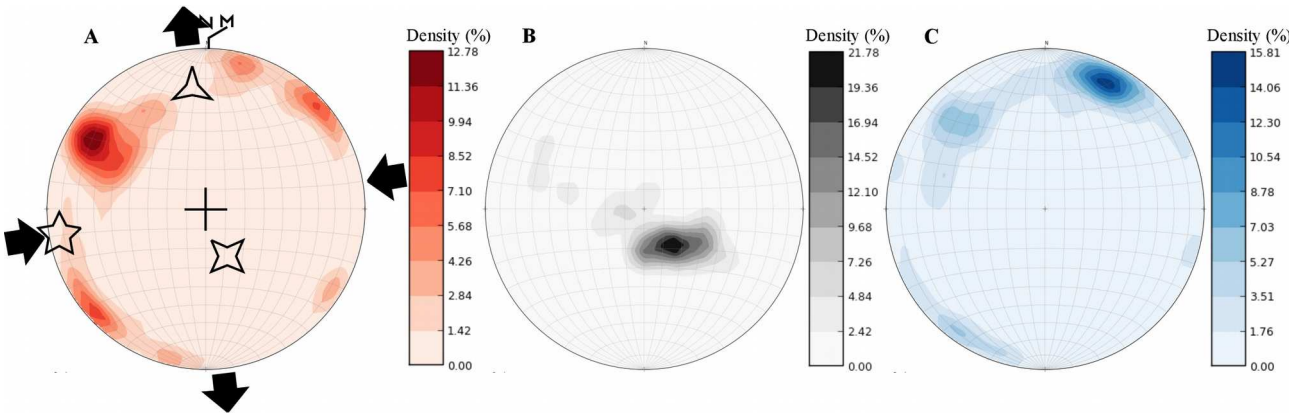

Figure III.11: Wulf density diagram (computed with OpenStereo (Grohmann and Campanha, 2010)) of A) poles of fault planes (89 measurements), B) poles of bedding planes (24 measurements) and C) striae for the 27 sites of measurement along the Belledonne border fault.

Figure III.12: N030°E trending fault plane in the Bajocian marls (GPS: 45.26564°N 5.92261°E). Striation with calcite steps indicate a dextral slip.

No similar fault deformations were observed, neither westward nor eastward because of the lack of outcrops nor northward in the Brame-Farine massif, although faults of close orientations (N030°E, N105°E and N135°E trending faults) are described in the Brame-Farine gallery survey (location on Fig. III.10). Unfortunately, fault kinematics is not provided.

The different measurement sites were grouped into three geographic areas in order to make the calculation of paleostress tensors. Inversion was done for the fault plane sets of different areas and the whole data set, except for the THEYS3 site. Computed stress tensors show a strike-slip tectonic regime with almost horizontal ENE trending σ1 axes, and about NNW trending σ3 axes (Fig. III.10). Determined paleostresses are consistent throughout the three geographic areas (Fig. III.10) indicating that the determined stress regime is regionally significant.

In order to determine if the observed strike-slip faulting predates or postdates the folding of the Jurassic series of the "Balcon de Belledonne", measurement sites were grouped according to the bedding dip direction (westward, northward and eastward). Despite these differences in bedding attitude, computed paleostress tensors are similar (Fig. III.13), indicating that this strike-slip faulting occurred after the folding.

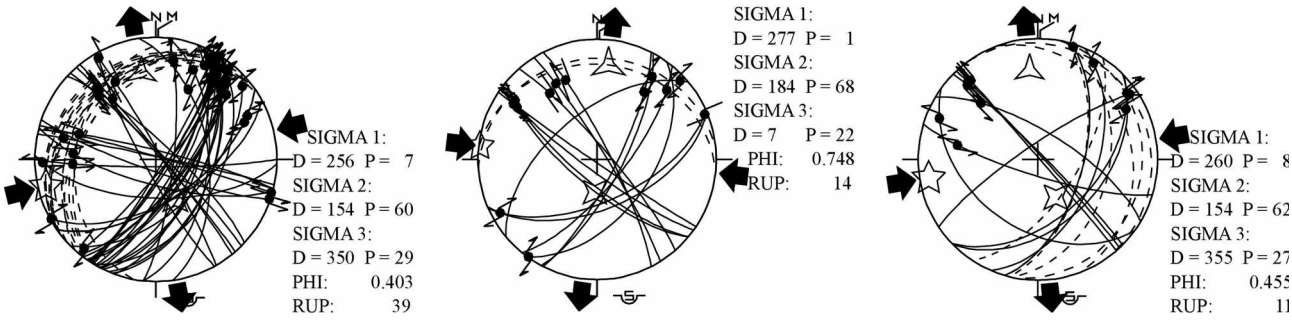

Figure III.13: Synthetic faults and stress diagrams. Fault planes are grouped according the three types of observed bedding attitudes. Same legend of diagrams as in Fig. III.7.

Finally, in agreement with striae pitch plunges distributed between 0° and 35°, it seems that these faults moved during the tilting induced by the Belledonne massif uplift. A backtilting of the fault planes of 23° to the SE along a NE-SW axis (close to the external crystalline massif ridge orientation) allows restoring to a near vertical attitude the N30°E trending fault planes (Fig. III.14A) and to restore to a near horizontal attitude the fold axis (Fig. III.14B), the striae of the three sets of fault planes (Fig. III.14C) and the σ1 and σ3 regional stress axis (Fig. III.14A).

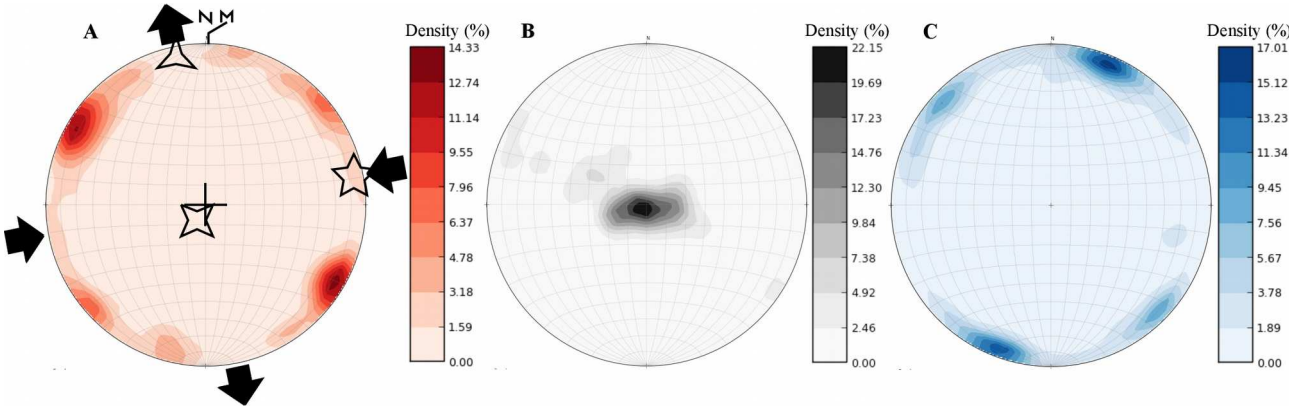

Figure III.14: A) Regional stress tensor (σ1: D=79 P=6, σ2: D=208 P=81, σ3: D=349 P=7) and Wulf density diagram of A) fault plane poles, B) bedding plane poles and C) striation after back rotation of 23,3° toward N135E (before the regional tilt).

III.8 - Geomorphologic analysis of the Belledonne fault system

III.8.1 - Geomorphic features and topographic anomalies in the Merdassier Étale faults area.

In the Aravis mountain, the Merdassier and Étale faults are listric normal faults connected to the Arcalod fault at its northern end (Fig. III.4). Some subsidiary faults show markers of recent tectonic activity that we will introduce next. On the geological map (Doudoux et al., 1992), Quaternary slope screes are mapped in contact with the normal faults (Fig. III.15A). These faults are also observable on the aerial photographs, being underlined by a linear and steep scarp, suggesting a recent faulting (Fig. III.15B).

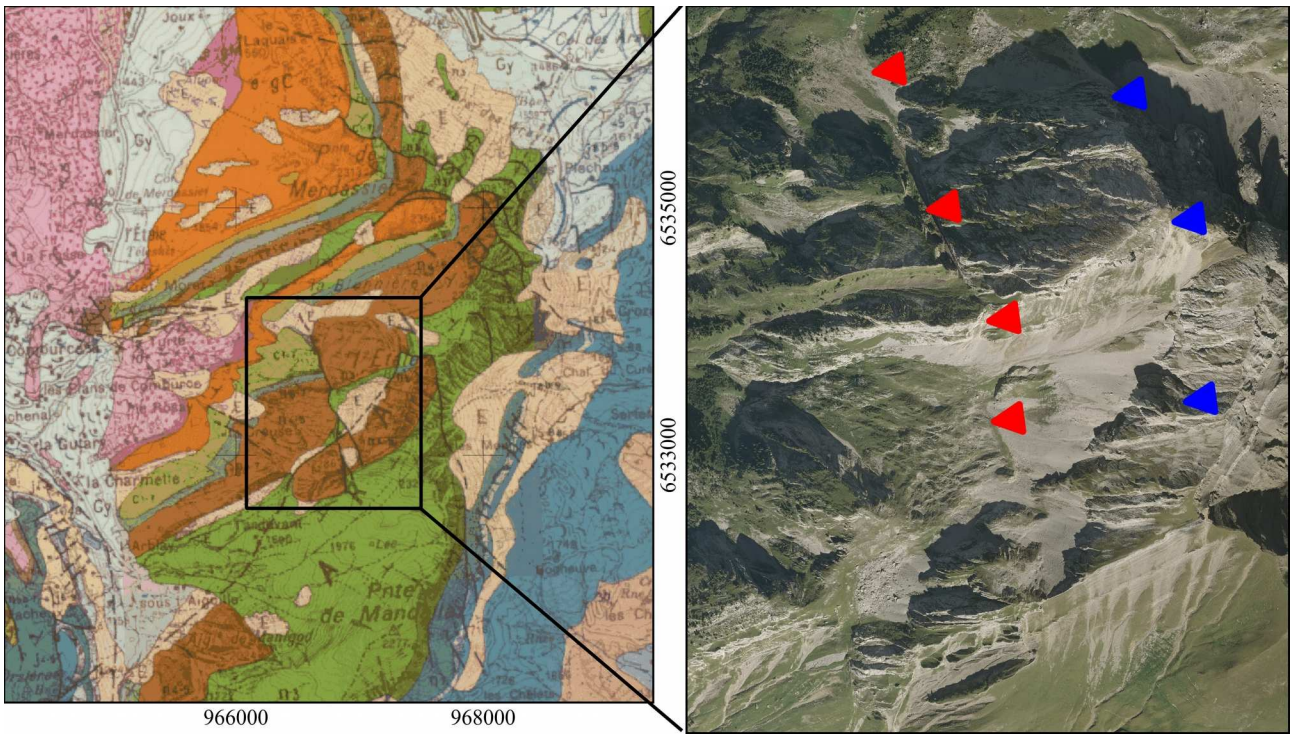

Figure III.15: 1:50000 Annecy-Ugine geological map (Doudoux et al., 1992) (location in Fig. III.4). Aerial photography of the Étale fault shows a sackung scarp along which screes are blocked (red arrows). To the northern termination of the fault, a creek allowed the deepening of the fault plane. A second large sackung showing is underlined by the blue arrows. Slope is toward the ESE.

Nevertheless, it is unlikely that these geomorphic anomalies could result from active plate tectonic deformations. The fault scarps are closely orthogonal to the greatest slope line and are more

probably linked to a gravitational movement due to the steepness of the valley flank. They are likely related to a sackung (see III.4.2).

However, the seismic event location suggests that the activity of Belledonne fault boundary (Thouvenot et al., 2003) continues along strike the Arcalod Fault within the Bauges domains (Fig. III.2). The dextral kinematics and the termination fault geometry could induce a local NE trending extension (parallel to the Arcalod fault) affecting the Aravis massifs and so facilitate this sackung type deformation.

III.8.2 - Geomorphic features and topographic anomalies as potential arguments for the Arcalod fault recent faulting

III.8.2.1 - Southern Arcalod Fault

At the southern end of the Arcalod fault, North of Saint Pierre d'Albigny, two geomorphic features could indicate a recent activity of this fault:

1- Along this fault, Würmian moraine deposits are in contact with the fault scarp. These deposits crop out at higher elevations east of this fault (close to the measurement site of Routhennes, Fig. III.7). Although this elevation difference can be the initial geometry of the moraine emplacement, it could alternatively result from an offset of these deposits caused by the vertical component displacement of the Arcalod fault.

2- In addition, we identified a sharp slope break similar to a scarp along the fault trace (Fig. III.16). This topographic anomaly can be due to differential erosion between the moraine and Jurassic limestone. However, a tectonic origin of this scarp related to a recent faulting of the Arcalod fault cannot be excluded.

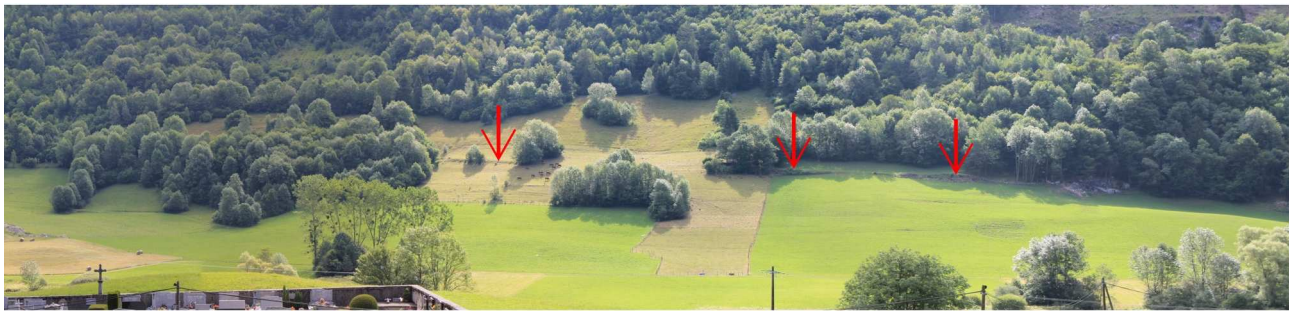

Figure III.16: Panoramic view of the Arcalod fault (from the cemetery south of Epernay, location in Fig. III.7). Red arrows indicate a scarp supposed linked to the Arcalod fault.

III.8.2.2 - Central Arcalod Fault

The stream network (Fig. III.7) extracted from both topographic maps and DEM (IGN BD ALTI, resolution 25 m) provides evidences for some anomalies along strike of the middle part of the Arcalod fault. In addition, along the fault trace, some streams present abrupt change of direction. Potential tectonic activity is attested by the sigmoid shape of the streams that suggests lateral 'en baïonnette' trace of the talwegs (Fig. III.17). These apparent baïonnettes are consistent with a dextral component lateral displacement along this fault, indicating a potential offset of about 200 ± 25 m.

These anomalies match with a mapped stratigraphic boundary (Doudoux et al., 1999). However, on both sides of this limit, the facies are similar lithographic limestone implying it is difficult to invoke the substrate lithology change as responsible for these geomorphic anomalies. It is also important to note that the stream offsets could also be due to the reused of an ancient lateral stream of the Würmian glacier flowing northward.

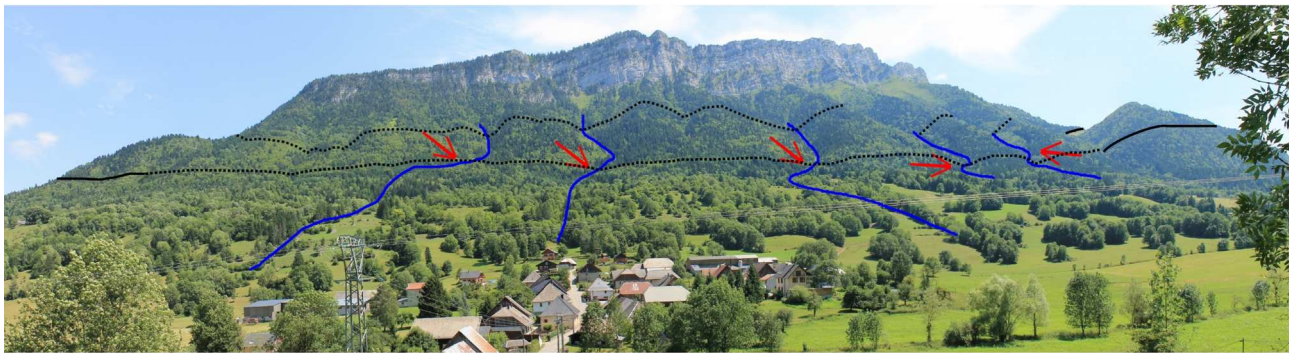

Figure III.17: Panoramic view of the Arcalod fault, west of the Arclusaz syncline (from le Villard location in Fig. III.7). Faults modified from 1:50000 Albertville geological map (Doudoux et al., 1999) in black. Streams in blue. Red arrows indicate right-lateral deviations of the streams.

III.8.3 - Geomorphic analysis of the "Balcon de Belledonne" and the Grésivaudan Border hills

At the regional scale the Grésivaudan valley presents a typical U-shape glacial valley profile formed by the Isère glacier (Fig. III.18, III.19A). The south-eastern shoulder of this glacial valley, where the Belledonne border fault lies, is less preserved than the north-western flank because it is strongly eroded by the streams running from the Belledonne massif to the Isère valley. Crest lines of the Grésivaudan border hills and of the "Balcon de Belledonne" correspond to the relics of this glacial shoulder (Fig. III.18, III.19A). Moreover, Würmian lateral moraines of the Isère glacier are described on these shoulders (Barféty et al., 2000), whereas the basal moraines are located 535 m beneath the present-day surface of the Isère valley, under lacustrine and fluvial deposits, as observed in the Montbonnot borehole sedimentary log (Nicoud et al., 2002).

Going into more details, the south-eastern flank of the Grésivaudan valley is marked by several benches (Fig. III.19B) corresponding - in most cases - to fluvio-glacial and/or moraines deposits (Barféty et al., 2000). It is suggested that these benches were formed by lateral streams running along the Isère glacier during the deglaciation and testify for the different glacier retreat stages.

The low resolution of the available topographic data and the dense vegetational cover unfortunately do not allow observing the Belledone border fault trace by using either DEM, topographic maps, aerial photographies or by field survey. We thus performed a morphometric analysis of the stream network.

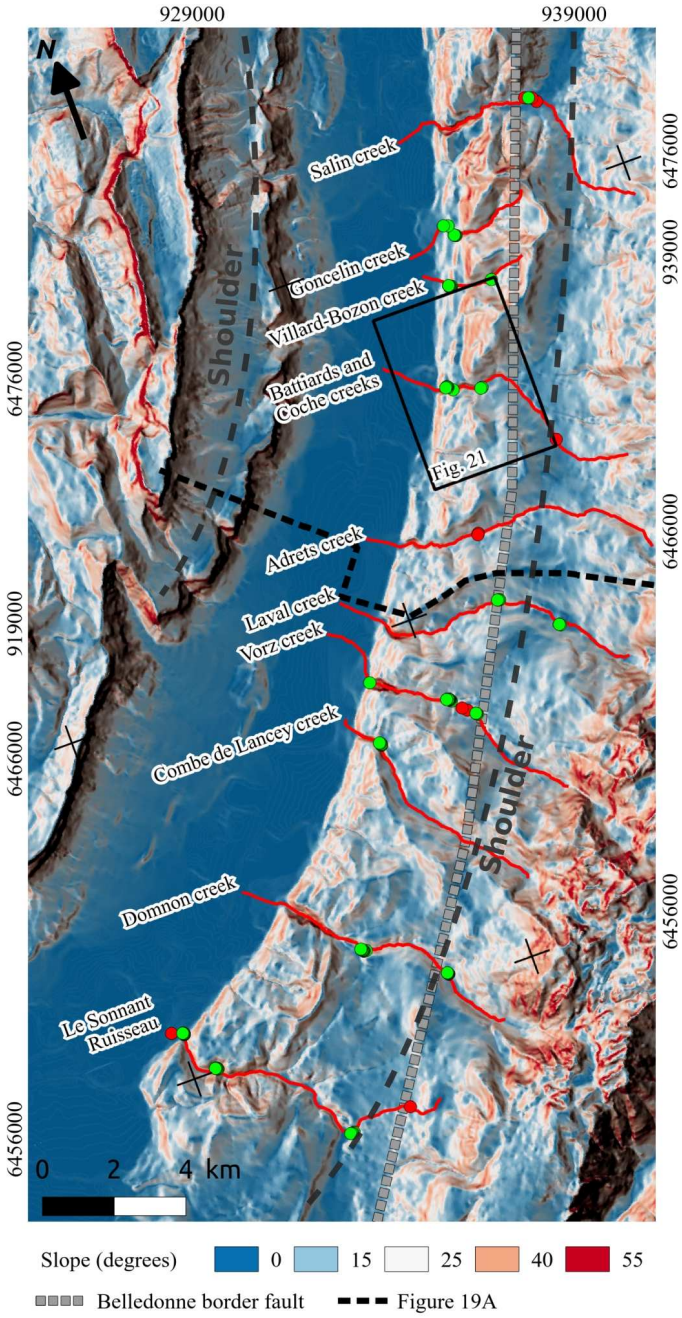

Figure III.18: Slope map of the Grésivaudan valley derived from the 25m DEM BD TOPO and analysed stream network along the Belledonne border fault (location in Fig. III.1A). Red and green dots are local and mean (200m) lateral drainage anomalies respectively.

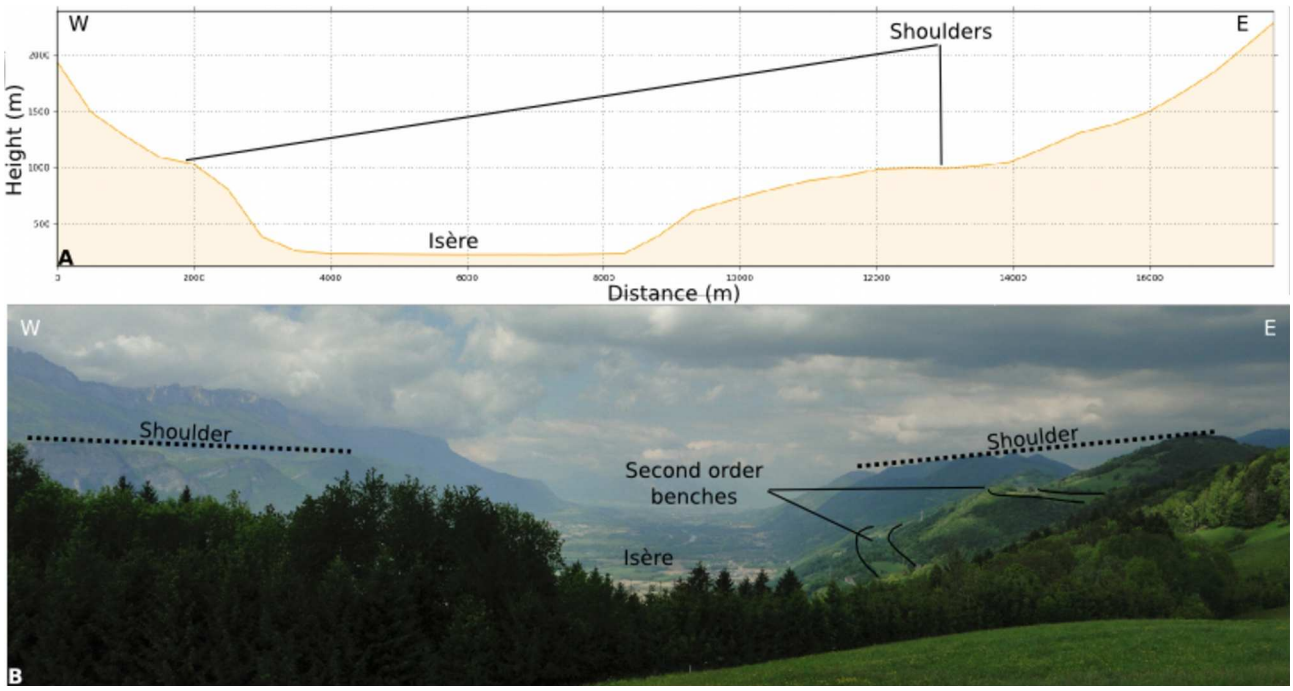

Figure III.19: A: Topographic profile (location in Fig. III.18) and B: view of the Grésivaudan valley.

III.8.3.1 - Stream network analysis

In order to analyse activity of the Belledonne border fault, we analysed the geometry of the different streams crossing the "Balcon de Belledonne" and border hills of Grésivaudan. Longitudinal bed profiles were extracted (annexe 2) using the hydrographic network from the BD TOPO database (IGN) (longitudinal and latitudinal precision lower than 10 meters) combined with the 25 meters resolution DEM BD ALTI (IGN).

For each stream, slopes, slope variations, flow directions and flow direction variations (as well as an average over 200 meters of these parameters, Fig. III.20) were computed in order to provide evidences for potential vertical and lateral offsets, respectively.

Figure III.20: Longitudinal bed profiles of the Goncelin and Battiards and Coche Creeks (see Fig. III.18 for location). Mean slopes and flow directions are calculated along a 200 meters interval. Green triangles: affluents, black lines: lithographic changes, red line: assumed intersection with the Belledonne border fault. Grey boxes highlight the knick points.►

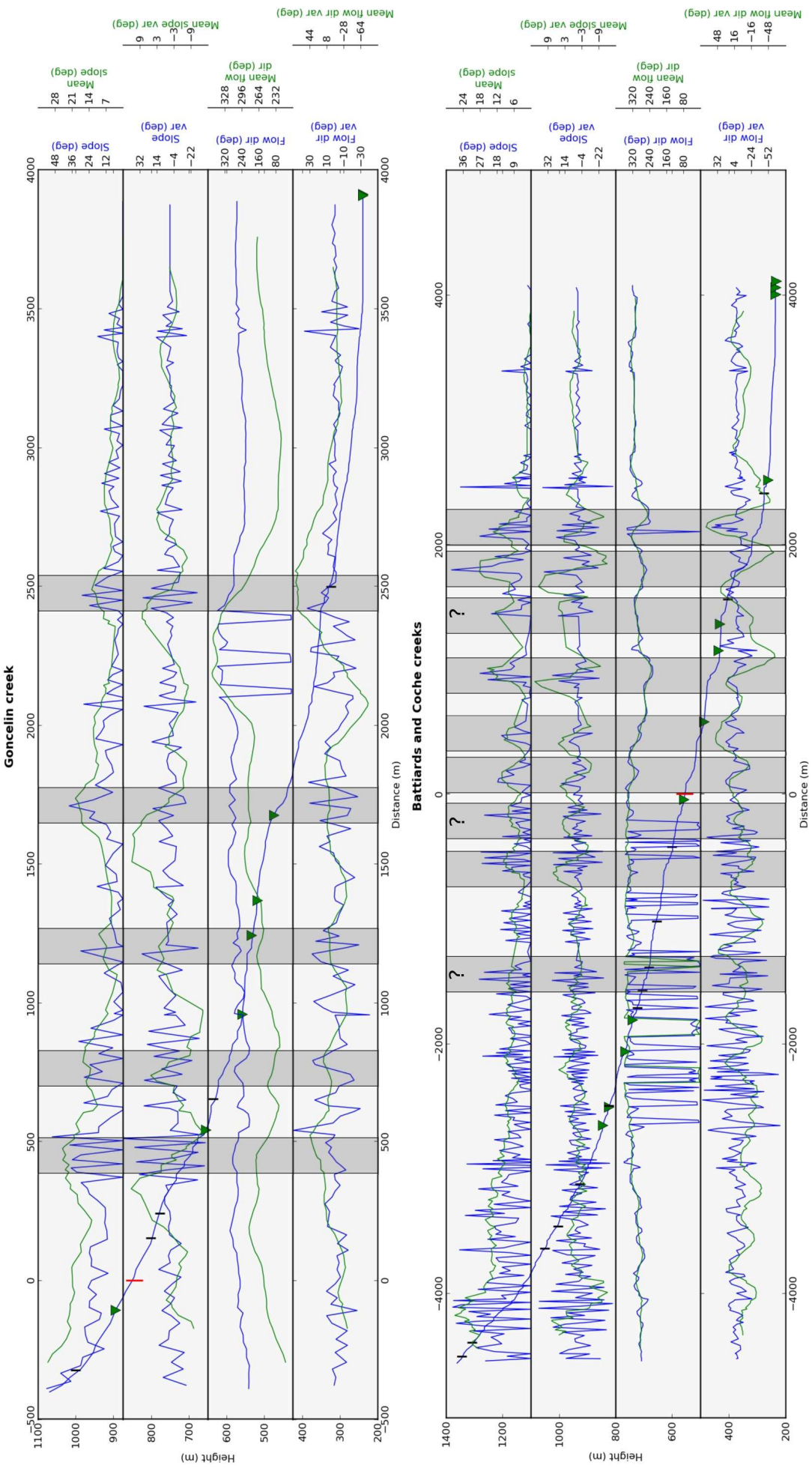
Goncelin creek
Battiards and Coche creeks
Slope (deg)
Slope var (deg)
Flow dir (deg)
Flow dir var (deg)
Mean slope (deg)
Mean slope var (deg)
Mean flow dir (deg)
Mean flow dir var (deg)
Distance (m)
Height (m)
?

III.8.3.1.1 - Vertical anomalies

All the extracted longitudinal bed profiles display several slope increases (Fig. III.20) interpreted as knick points. Elevation of the slope breaks were extracted. In most cases, slope breaks are not well expressed and most of the knick point elevations were obtained by extracting the elevation of the local maximum mean slope variation. Knick points can be grouped into 15 different levels of mean elevations : 258 m, 314 m, 349 m, 379 m, 412 m, 471m, 512 m, 550 m, 586 m, 612 m, 708 m, 751 m, 780 m, 821 m and 866 m (Fig. III.21). Some of these profiles show knick points that are not expressed in the other streams. These discrepancies may result from artifacts in the DEM or erosion of these minor topographic anomalies. For these reasons, these slope breaks, not regionally significant, are not considered as being representative for knick points caused by base level changes.

Darmendrail et al. (1994) reported major knick points along the border of the "Balcon de Belledonne". They proposed that these morphologic anomalies resulted from displacement along a west dipping normal fault located at the base of the border hills. However, they did not describe the minor knick points nor did they notice that the elevation of the knick point is close to the elevation of the fluvio-glacial benches observed along the border hills (Fig. III.22).

In order to ascertain if the glacier level changes allowed the formation of the knick points along the streams, we mapped the benches of the both sides of the Grésivaudan valley by extracting areas with a slope lower than 15° from a slope raster derived from the DEM. This method does not allow mapping narrow benches (<50m large), thus we complemented this first approach by using the 1:25000 topographic map. Each cell value of the DEM included in these areas were extracted (Fig. III.21 A1 and B1). Dataset was then demodulated using the Gaussian Mixture Modeling (GMM) algorithm developed by Muratov and Gnedin (2010) (Fig. III.21 A2 and B2).

We identify 13 bench levels on each sides of the Grésivaudan valley. The western flank (Fig. III.21 A2) shows benches at the mean elevations of 266±14 m, 319±31 m, 375±18 m, 414±23 m, 453±14 m, 481±22 m, 524±19 m, 570±15 m, 604±18 m, 632±14 m, 696±57 m, 737±14 m and 795±26 m and the eastern flank (Fig. III.21 B2) at 286±40 m, 339±32 m, 382±27 m, 417±16 m, 454±34 m, 479±10 m, 503±24 m, 535±17 m, 567±39 m, 613±26 m, 659±30 m, 695±13 m and 745±36 m. Note that the uncertainties, given at a 2σ confidence level, are very large. This is probably due either to the low raster resolution which did not allow well constraining elevation of the low amplitude benches and/or to the probable meridian variation of the bench elevations related to the 0.3° slope of the Isère glacier (Coutterand, 2010).

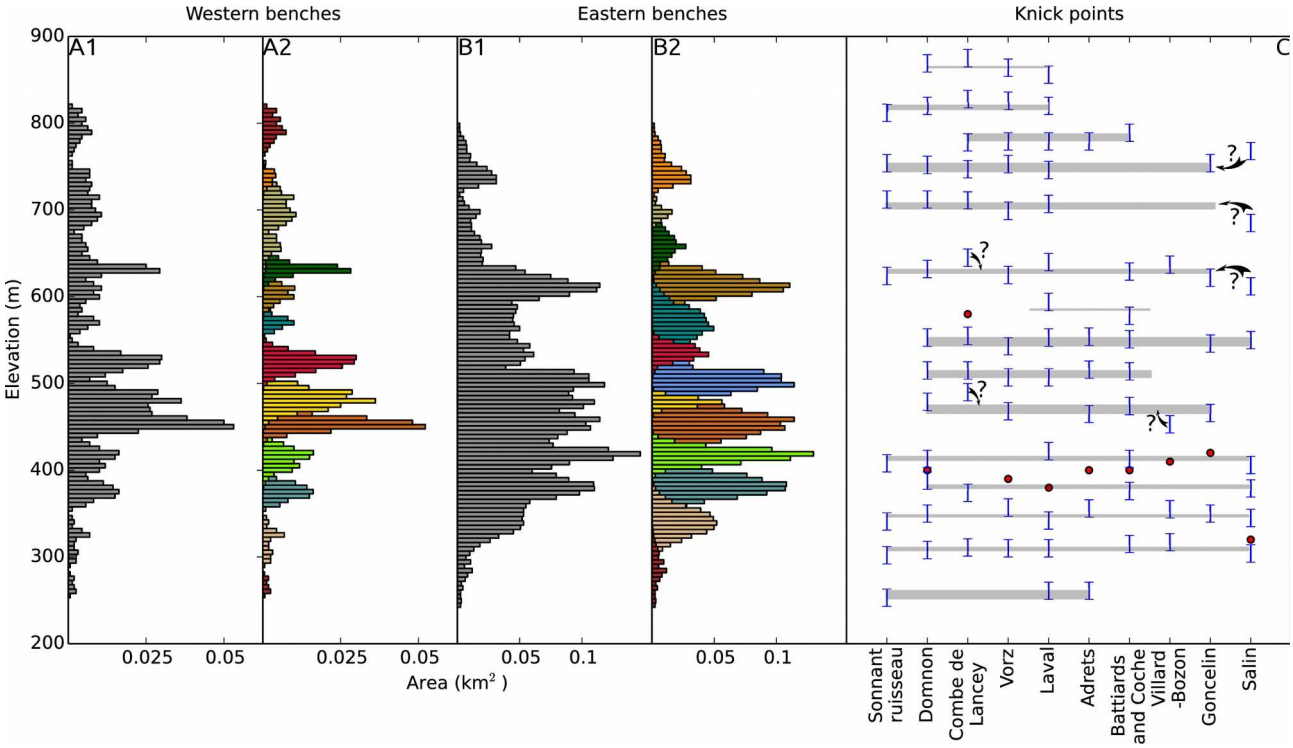

Figure III.21: Elevation of the western (A1 and A2) and eastern (B1 and B2) benches before and after the demodulation respectively, and knick point elevations of the ten analysed streams (C). Red dots are knick-point elevations proposed by Darmendrail et al. (1994).

Benches on both sides of the Grésivaudan valley are of close elevations. Two linear regressions have been made using the York equations (York et al., 2004) 1-between western and eastern bench elevations (Fig. III.23A) and 2-between knick points and eastern bench elevations (Fig. III.23B). Both show a slope close to 1. The coordinate origin of the linear regression between benches elevation of the two sides of the Grésivaudan valley is -32.76 ± 5.8 (Fig. III.23A). This indicates that eastern benches are apparently higher than the western ones and that the area of the Grésivaudan valley have been tilted westward. However, this average difference of elevations could alternately be an artifact resulting from the elevation uncertainties. The coordinate origin of the linear regression between eastern benches and knick points elevations is equal to -14.97 ± 14.39 which is clearly not significant (Fig. III.23B). However, knick points elevations must be higher than the benches, and it could also result from the elevation uncertainties.

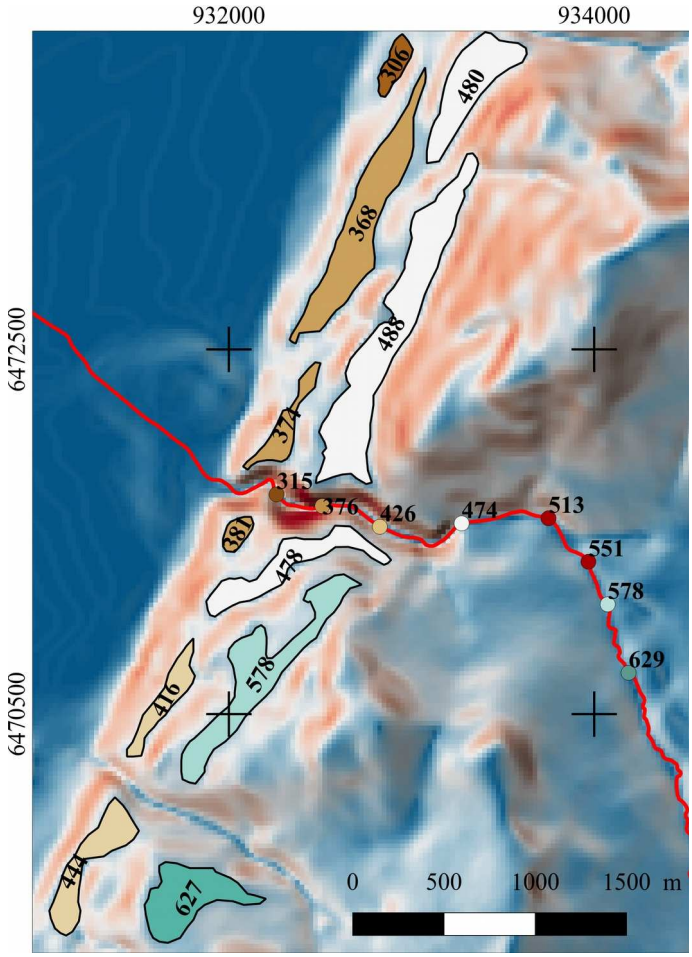

Figure III.22: Slope raster (same scale as Fig. III.18), mean elevation (in meters) of the major fluvio-glacial benches (coloured surfaces) along the border hills and elevation (in meters) of the knick points (dots) along the Battiards and Coche creeks (red line, location in Fig. III.18). Knick points and benches with close elevations are in the same color.

We conclude that knick points along the streams cutting the east flank of the Grésivaudan valley are linked to different stages of glacial retreat, each stage allowing the development of different base levels that produced knick points along the streams. Consequently, these topographic anomalies do not result from active faulting.

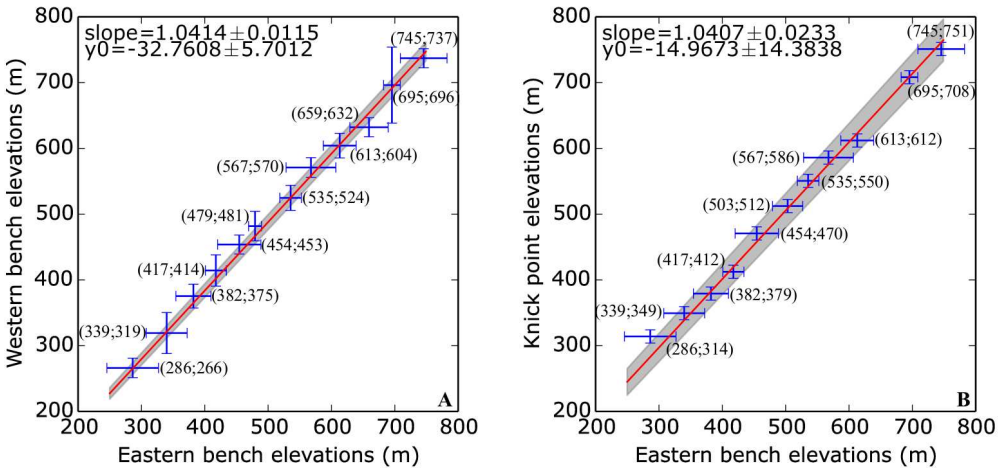

Figure III.23: Relation between A: western and eastern bench elevations B: average knick points elevations and eastern benches elevations given with a 2 sigma confidence level. Red line is the regression line and grey infill the uncertainty, both were obtained using the York's equations with a correlation coefficient fixed to 1. Note that for A, the slope is almost constant whereas coordinate origin become closer to 0 when correlation coefficient varies from 1 to 0.9 whereas for B the slope and coordinate origin remain almost constant.

III.8.3.1.2 - Lateral anomalies

In order to identify possible lateral offsets of the streams related to recent faulting along the Belledonne border fault, a statistical analysis was applied to the drainage direction values. Drainage direction and average drainage direction (average value calculated for 200 m interval) were computed from the hydrographic network of the BD TOPO database using the Vincenty formula (Vincenty, 1975). Drainage anomalies are considered as the outliers of the drainage direction variation, and average drainage direction variation calculated values. Outliers were identified by using the following equation (Tukey, 1977):

$$|O| > Q3 + 1.5(Q3 - Q1) \quad \text{(III.1)}$$

where O is the outlier, and Q1 and Q3 are, respectively, the first and third quartile of the absolute values of the drainage direction variation set or mean drainage direction variation set.

The identified drainage anomalies located at a distance: 1- less than 25 m of a lithological change extracted of the geological map (because of the uncertainty of its location) and 2- less than

10 m from a confluence, 10 m corresponding to the uncertainty of the BD TOPO database, are considered as non reliable and consequently removed from the analysed series.

The deduced drainage anomalies (Fig. III.18) can hardly be assigned to the activity of the Belledonne border fault, although several of them are close to the proposed fault location. Indeed, streams do not display evidence of typical sigmoid shape at any scale. Moreover, we noticed that the lateral drainage anomalies are located on each side of the main bench or at the foot of the knick points. Thus, the change of drainage direction can be considered as resulting from the slope variations and consequently can not be unambiguously attributed to active faulting.

In conclusion, because of the strong glacial imprints, the highly erodible substratum (mainly marls) and the low deformation rate, morphological features of deformation associated with the Belledonne border fault has not been clearly displayed in this area.

III.8.4 - Geomorphic analyses of the Brion fault

The Grenoble Gorge corresponds to a diffluence of the Würmian Isere glacier, flowing from north to south. Part of the glacier flowed westward toward Voreppe and other flowed southward toward Monestier-de-Clermont (Monjuvent, 1973). Basal moraines are mapped on the eastern flank beneath the Saint-Georges-de-Commiers town (Debelmas et al., 1967b). The Drac and Gresse valleys display the characteristical U-shape formed by glacial erosion (Fig. III.24). On both sides of these valleys, we can observe surfaces with relatively constant slope which correspond to ancient flanks of glacier valleys.

The flanks of these two glacial valleys were mapped using topographic maps at 1:25,000 scale, a 25 m resolution DEM as well as orthophotos by selecting surfaces with constant slope values (between 30° and 45°). The Quaternary slope screes deposits mapped on the geological map were excluded from these surfaces.

A first surface (Surface 1, Fig. III.24), west of Vif, is continuous in this area from north to south. East of Vif, the different parts of the eastern side of the glacial valley (area 2, Fig. III.24) are not observed aligned on both sides of the Brion fault. Similarly, the ridge separating the surfaces 2 and 3 (Fig. III.24) is not linearly observed across the fault. Conversely, the slope of glacial valley west of Saint-Georges-de-Commiers (area 3, Fig. III.24) is characterized by surfaces that are aligned on both sides of the Brion fault. But the flank of glacial valley, east of Saint-Georges-de-Commiers (surface 4, Fig. III.24), is also apparently offset by the Brion fault. In addition, at the eastern termination of the Brion fault, the flank of a watershed basin (area 5, Fig. III.24) seems also displaced left-laterally by the Brion fault.

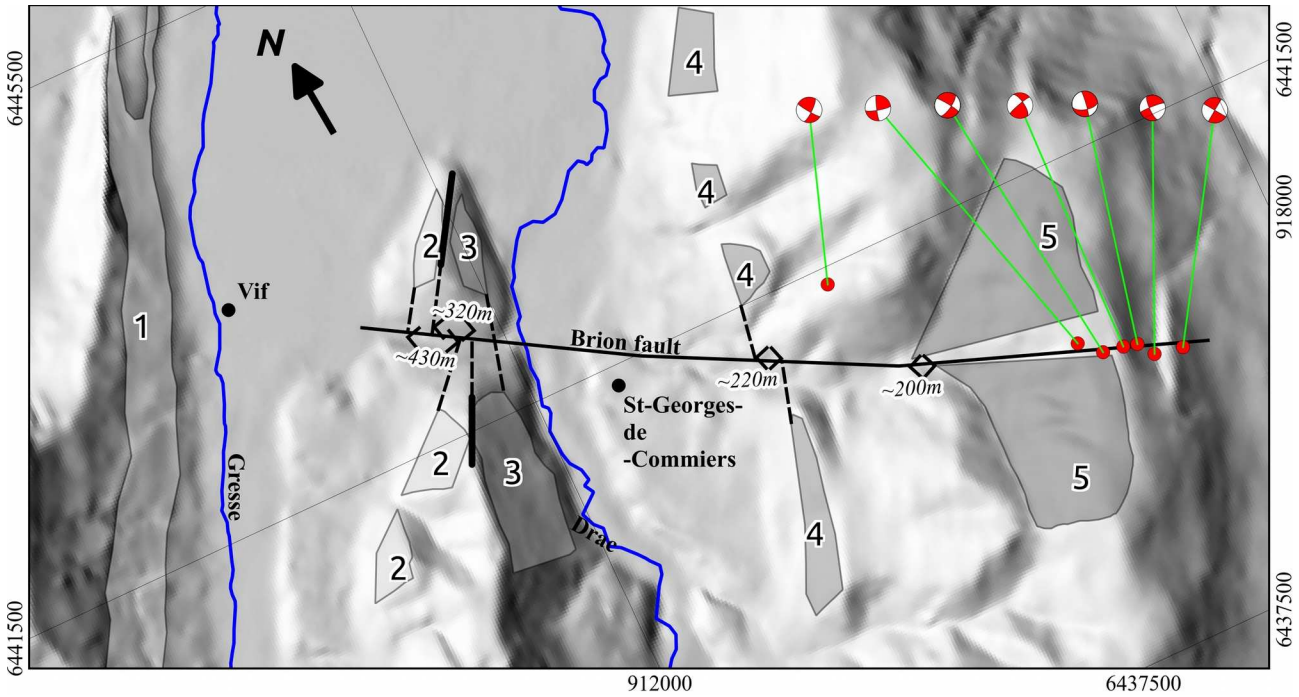

Figure III.24: Shaded DEM and morphological interpretation (location in Fig. III.1B). Brion fault (solid line) according to earthquakes localisation provided by Thouvenot et al. (2003) and morphological offsets. Surfaces 1 to 4 are glacier valley flanks, surface 5 is watershed flank. Bold solid lines are ridges. Dotted lines are projection of the proposed piercing points on the Brion fault.

The observed morphological apparent offsets are approximately of 430 m for surface 2, 320 m for the ridge of the Brion massif and 200 m for the surfaces 4 and 5. These offset estimates are determined with high uncertainties because the piercing points are not well constrained (at least 25 m, the DEM resolution). In addition, the presented morphologic features could have been eroded since their initial formation. However, all these apparent offsets are of the same order of magnitude (of some hundred meters) and indicate a potential displacement, consistent with a recent left-lateral slip along the Brion fault.

III.9 - Gravity data analysis

We used gravity data in order to identify possible subsurface deformations (Guineberteau et al., 1987; Molliex et al., 2011b) associated to the Belledonne fault system. 2769 field gravity measurements (Fig. III.25A) are available for the area covering the Arcalod and Belledonne border faults from the International Gravimetric Bureau (BGI) (Bonvalot, 2012). Measurements, provided by the BGI, are corrected of latitude, topography as well as tidal effects. The Bouguer anomaly is also computed for each point of the dataset using a mean density of 2670 $kg.m^{-3}$.

Bouguer anomalies of the measurement sites range from -57 to -195 mgals and decrease eastward (Fig. III.25A). The first order signal in the Bouguer anomaly being caused by the variation of the MOHO depth implies that the anomaly decreases eastward as the Alpine root deepens (Ménard, 1979; Vouillamoz et al., 2012; Waldhauser et al., 1998). This first order signal was removed by interpolating a third degree polynomial trending surface (consistent with the MOHO geometry constrained by Ménard (1979) in this area, Fig. III.25A) from the Bouguer anomalies of the measurement points and then remove to them in order to obtain the residual Bouguer anomaly (Fig. III.25B).

In the Bauges massif, residual Bouguer anomaly variations follow the main structural framework despite the fact that negative ones correspond to the main thrust in the sedimentary cover. It could result from: 1-west vergent thrust plunging into the crust backward of their outcrops in the sedimentary cover (Doudoux et al., 1982; Ménard and Thouvenot, 1987) or 2- to under cover tethysian half-grabens (Arpin, 1988; Thouvenot and Ménard, 1990).

The Isère and Arc valleys, before their confluence, show a negative residual Bouguer anomaly (range between -3.1 and 0 mgals, Fig. III.25B) which is caused by the glacial erosion and the low density Quaternary infill as described in other alpine glacial valleys (Finckh and Klingele, 1991; Masson et al., 2002). The residual anomaly increases south-eastward to reach 5 mgals west of the Brame-Farine massif and decreases southward reaching values between 0 and -2 mgals. The area where the residual Bouguer anomaly increase corresponds to the area where the Belledonne border fault connects to the Arcalod fault. This positive residual Bouguer anomaly implies that, in this part of the glacial valley, there is a lack of low density materials compared to the north and south. We consequently interpreted this positive anomaly as a bulge of the crust and/or the bottom of the glacier valley resulting from specific location within a restraining step-over (i.e., relay between two fault segments) that induces local transpressional stress regime. This interpretation is

consistent with the flexure deformation of the “Banquette de Panaise” bench as proposed by Nicoud (1984).

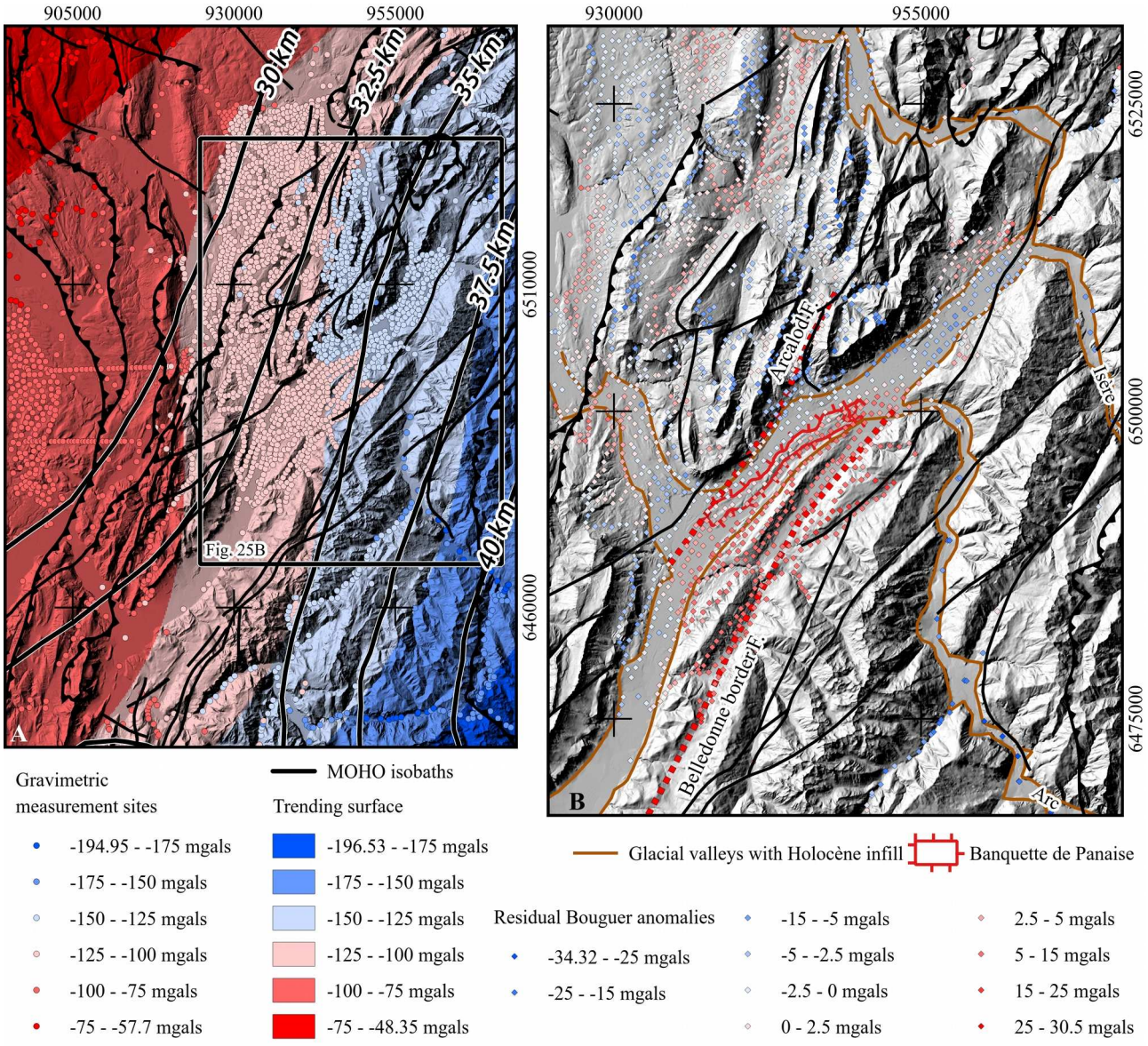

Figure III.25: A: Locations of gravimetric measurements and third order polynomial surface derived from these values (location in Fig. III.1A). MOHO isobaths from Ménard (1979). B: Residual Bouguer anomalies and major glacial valley infilled by Holocene sediments. These valleys show a low residual Bouguer anomaly except at the transition between the Arcalod and Belledonne border faults.

III.10 - Discussion

III.10.1 - Chronology and ages of the stress states

At the southern termination of the Arcalod fault, the stress state deduced from the inversion of the whole fault measurement set (Fig. III.7) is well constrained and consistent with the present kinematics at the southern end of the Arcalod fault deduced from focal plane mechanisms (Fig. III.2) and with the dextral component of the Belledonne border fault. The microseismicity alignment (Fig. III.2) suggests that we have a potential activity of the Belledonne border fault transferred to the Bauges through the Arcalod fault.

However, we can note that the computed stress tensors on the "Crête de la Via" and "Frêne pass" sites have a σ1 axis (N096°E and N104°E respectively) almost normal to the N020°E trending faults observed at the Routhennes and Gratteloup sites (Fig. III.7). Strike-slip faulting along fault with a strike normal to the compressional axis is possible (weak fault, e.g., Zoback et al., 1987), but here, strike-slip faulting along the Arcalod fault seems more consistent with the N080°E trending compression found in the "Balcon de Belledonne" (Fig. III.10).

In the "Balcon de Belledonne", the N30°E trending right-lateral strike-slip faults and N105°E and N135°E trending left-lateral strike-slip faults correspond to a strike-slip tectonic regime with a N080°E trending σ1 axis (Fig. III.10). It occurred after the folding of the Liassic series (Fig. III.13) as well as, during and after the tilting induced by the Belledonne massif uplift as suggested by the distribution of the pitch of the striae.

The average N030°E trend of folds and schistosity in the Liassic series are consistent with the ESE trending compression which built the folds and thrusts of the Jura, Vercors and Chartreuse massifs (Butler, 1992; Homberg et al., 2002; Philippe et al., 1998). The same ESE trending σ1 compressional tectonic regime is described in the Belledonne massif (Gasquet et al., 2010; Hippolyte et al., 2006b).

We can note that the right-lateral kinematics measured along the N105°E trending faults on the site THEYS3 (Fig. III.10) and the N120°E trending tension cracks with plumose structures are not compatible with the regionally significant paleo-stress orientation (N80°E trending σ1 axis).

Therefore, we propose that the two trends of faults sets N105°E and N135°E were first conjugate strike-slip faults contemporaneous with the folding; the N105°E trending faults

corresponding to dextral strike-slip faults (THEYS3 site, Fig. III.10) and the N135°E trending faults being sinistral strike-slip faults. N30°E trending folds, N105°E trending dextral strike-slip faults and N135°E trending sinistral strike-slip faults being consistent with the WNW trending compression.

The N080°E trending compression occurred during the Belledonne massif uplift. However, faults consistent with this compression were tilted only of 23° north-westward (Fig. III.14) whereas the Liassic series of the "Balcon de Belledonne" dip between ~45° and ~80° north-westward (Barféty and Gidon, 1996; Philippe et al., 1998) (Fig. III.6). It implies that the N80°E trending compression took place while the Belledonne massif uplift was already occurring.

Because the observed deformation only affects Mesozoic rocks, we can not determine the age of the stress state. However, several time constraints can be proposed:

- First, fault kinematics measurements made in the hanging wall of the Voreppe fault show that the formation of the fold and thrust belt of the Chartreuse massifs results from a mean N106°E trending compression (Butler, 1992). The Voreppe fault thrusts the upper marine molasses which are Burdigalian to Serravalian in age (Beck et al., 1998).

- Second, in the Belledonne massif, en échelon vertical veins infilled by sigmoidal near horizontal quartz-chloritic fibers, consistent with strike-slip kinematics, were formed during two hydrothermal events dated at 11.6 ± 0.2 Ma and 7.1 ± 0.4 Ma using the Th-Pb dating method on monazite (location on Fig.III.1A; Gasquet et al., 2010). Quartz-chloritic fibers show an average N30°E direction consistent with a ~N120°E trending compression. This quartz-chloritic paragenesis is affected by a N104°E trending compression (location on Fig.III.1A; Hippolyte et al., 2006b). This implies that the WNW trending compression occurred at least until 7.1 ± 0.4 Ma.

The ENE trending compression associated to strike slip tectonic regime is the last stress state recorded in the sedimentary cover. This strike-slip tectonic regime is characterized by about N80°E and N174°E trending horizontal σ1 and σ3 axes, respectively. The average P and T axes (ENE-WSW and NNW-SSE respectively) of the focal mechanisms beneath the "Balcon de Belledonne" are also consistent with the determined stress states. It implies that the ENE trending compression is Messinian to Quaternary in age.

Therefore, the following scenario can be proposed (Fig. III.26):

- A first deformation stage, before and during the beginning of the Belledonne massif uplift, under a WNW trending compression generated the N030°E trending folds, N105°E

trending dextral strike-slips faults, N135°E trending sinistral strike-slip faults and the N120°E oriented tension cracks associated with plumose structures. This deformation stage is late Oligocene to Messinian in age.

- A second deformation stage, under a N080°E trending compression (Fig. III.10), is contemporaneous of the ending of the massif uplift. It reactivated the dextral N105°E and sinistral N135°E trending faults as left-lateral strike-slip faults and generated the N030°E trending right-lateral strike-slip faults. This deformation stage is Messinian to Quaternary in age. Onset of right-lateral strike-slip faulting along the Arcalod is probably contemporaneous of this deformation stage.

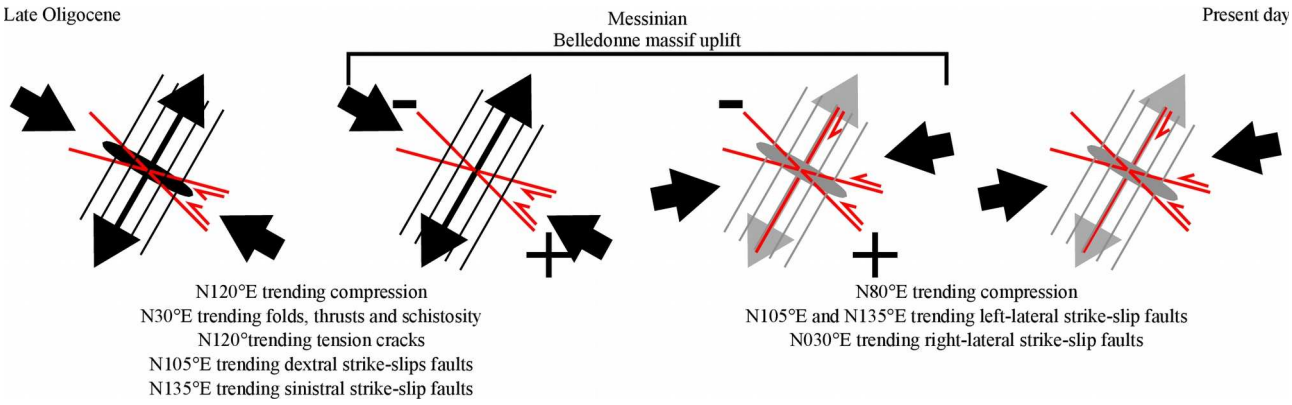

Figure III.26: Summary sketch of the Cenozoic deformation in the "Balcon de Belledonne".

III.10.2 - Age of the offset geomorphic features and slip rate estimates

In a first assumption, we can consider that the studied geomorphic features correspond to glacial landforms resulting from the Würmian glaciation. In this case, deglaciation and therefore the abandonment of these surfaces have started at about 34,300 years ago (Nicoud et al., 2002).

Sigmoid shape of the streams along the Arcalod fault agrees with a potential offset of about 200 ± 25 m. According to a deglaciation starting at 34,300 yr BP, the deduced fault slip rate would be of 5.8 ± 0.1 mm.y^{-1}. For the Brion fault, considering the smallest measured offset of 200 m, the calculated fault slip rate is of about 5.8 mm.yr^{-1}. This is higher than the expected faulting rates, comparing with slip rates determined by studies in the surrounding areas that are generally no higher that 1 mm.yr^{-1} (Baize et al., 2011; G. Sanchez et al., 2010). In addition, the surfaces 1 and 3 in the Brion massif area (Fig. III.24) do not display any evidence of visible offset. This is apparently in contradiction with the hypothesis that the Brion fault activity affected the glacial landforms.

The above presented arguments imply that it is difficult to attribute the offsets of markers resulting from the Würmian glaciation to the activity of the Arcalod and Brion faults. Consequently, we explored others environmental/climatic events that could be responsible for the studied morphologies.

In the Drac valley, Rissian end moraines are described to the south of the Würmian ones (Monjuvent, 1973) implying that the Drac valley, filled by the Isère glacier, also existed during the Riss. Moreover, the watershed of the Merlière stream (Fig. III.1B), running through the western flank of the Brion massif, is filled by Würmian moraines (Debelmas et al., 1967b). This implies that formation of the watershed, and therefore of the Brion massif, occurred before the Würmian glaciation. According to the flow direction, the current Small Brion was a rock spur where the base of the glacier splits (Fig. III.27A) inducing the incision of two nearly parallel glacial valleys on both sides of the massif. During the interglacial stage (Fig. III.27B), a less severe erosion and the left-lateral motion of the Brion fault induced the offset of the glacial landform. Then a new southward advance of the glacier (Fig. III.27C) eroded again both sides of the incised valleys. However, the offset caused by the Brion fault displacement allowed the preservation of the previous eastern flank of the two glacial valleys. Conversely, western flanks were not protected and have been eroded. The result is that only the eastern flank of the valleys presents preserved offset of the glacial morphology.

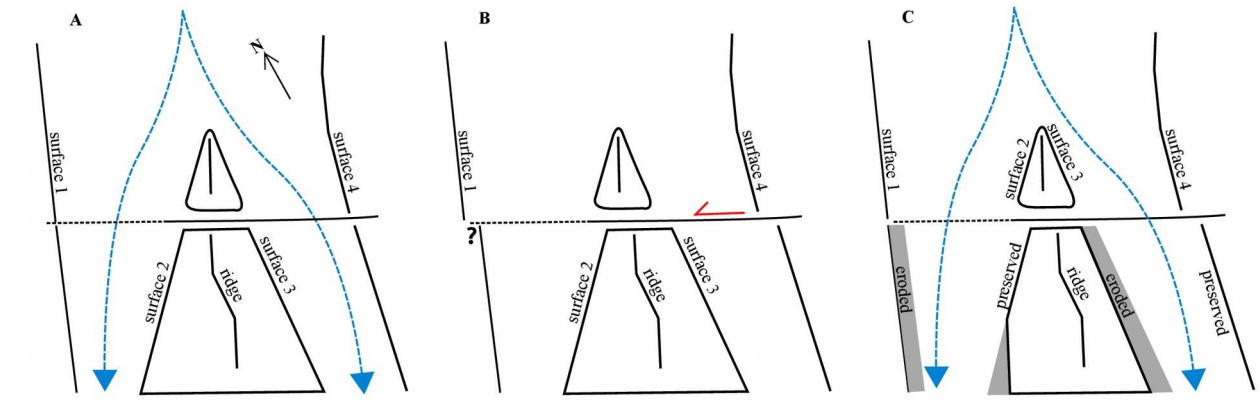

Figure III.27: Schematic reconstruction of the morphological history of the Drac valley. A) Morphology formation (Riss?). B) Offset of the morphology during interglacial. C) Glacial erosion resumption (Würm?)

Considering the surface and ridge line offsets inherited from the Rissian last glacial maximum, a Brion fault maximum slip rate can be calculated from the maximum 430 m offset of the surface 2 (Fig. III.24). The deduced slip rate of about 3 $mm.yr^{-1}$ is still very high for the studied area. However, the scenario may have taken place several times for each glacial and interglacial periods and/or for each stage and each inter-stages glacial periods, especially since the area is close to the termination of the glaciers. Calculated fault slip rate becomes realistic (~ 1 $mm.yr^{-1}$) if we consider that these surfaces are inherited at least from the first Rissian glacial stage (~ 400 ka).

We proposed that morphology along strike the Brion and Arcalod fault was not totally rejuvenated during the last glaciation and the offset geomorphic features are so older than Würm.

III.10.3 - Reliability of the geomorphic analysis

The morphological evidences of deformations are ambiguous and can be explained by inherited structural and/or glacial landforms. Thus, along the Arcalod fault, stream offsets could be due to the reuse of an ancient lateral stream of the Würmian glacier flowing northward, the slope break associated to the fault could be due to differential erosion and difference in elevation of the Würmian moraine deposits on both side of the fault could be the initial geometry of the moraine emplacement. Along the Brion fault, the offset eastern flanks of the glacial valleys corresponds to topographic surfaces that are very close to the strata dip, thus the morphology could simply be the result of the geological structure of the area, although it is difficult to deny the strong control of the present morphology by Quaternary glaciations. Finally, no morphological anomalies associated with faulting were found in the “Balcon de Belledonne” and fault scarps associated to the Merdassier and Étale normal faults are probably related to sackung type deformations.

However, these observations are all consistent with the strike-slip tectonic regime that has started during the Messinian and supports the interpretation that these faults are part of the same fault system:

- The observed right-lateral offsets of streams along strike of the Arcalod fault are consistent with a dextral strike-slip faulting. This is consistent with the late stress state we determined by fault slip data measurements as well as the Belledonne border fault kinematics deduced from focal mechanisms (Thouvenot et al., 2003). Gravitational origin of the fault scarps along the Merdassier and Étale fault is not questioned. However, south-westward movement of the block delimited north-westward by the Arcalod fault could have facilitated the decompression of the massif along a NE trending axis perpendicular to these normal faults.

- In the relay area between the Arcalod and Belledonne Border faults, gravity anomalies provide evidence for a structural bulge compatible with the flexure deformation of the Pleistocene deposits reported by Nicoud (1984). Both observations are consistent with compressional deformation within a restraining relay fault zone that induce local transpressional tectonic regime.

- No geomorphic marker of deformation was found along the Belledonne border fault and the vertical anomalies in the stream network result from different stages of glacial retreat. The regional stress state deduced from inversion of the fault kinematics measurements in the "Balcon de Belledonne" displays evidences for a late strike-slip tectonic regime characterized by about N80°E and N174°E trending horizontal σ1 and σ3 axes, respectively. The average P and T axes of the focal mechanisms beneath the "Balcon de Belledonne" are also almost horizontal and compatible in direction (ENE-WSW and NNW-SSE) with our determined stress states. The consistency between the stress states deduced from fault slip analysis, the focal mechanisms and the strain derived from geodetic measurements, suggests that the fault slips results from Messinian to present day deformation. Faults in this area were observed along a 3 km wide elongated domain. No similar fault deformation was observed westward or eastward because of the lack of outcrops, but the fault zone could be wider. The basement strike-slip faulting could be accommodated in the Jurassic marls by a wide distributed fracturing zone as it is the case for the Cléry fault (Gratier et al., 2013) which is the south-western prolongation of the Belledonne border fault in the Vercors massif. This could explain the lack of preserved geomorphic evidence for recent faulting as fault trace (scarp) and geomorphic feature offsets in the Jurassic marls.

- The lateral offset of the glacial morphology along the antithetic Brion fault is in agreement with the present-day left-lateral slip deduced from the focal plane mechanisms (Thouvenot et al., 2003). The lack of offset along western flanks of the glacial valley can be explained by successive progress and retreat of the Isère glacier.

We propose that the morphologic markers of deformation were not totally refreshed during the last glacial maximum and were inherited from a prior glaciation, at least the Rissian one. However, assuming that, the surfaces were probably rejuvenated by erosion related to glacial process. This implies that it is difficult to use these surfaces as markers to determine a fault slip rate, especially since the age of these surfaces can not be determined with certainty.

III.11 - Conclusion

We provide evidences for two successive strike-slip tectonic regimes within the Belledonne border fault domain during the middle to late Cenozoic alpine deformation. The first one, Oligocene to Messinian in age, is characterized by a WNW-trending compressional axis. The second one is a strike-slip tectonic regime characterized by ENE-trending compressional axis. It occurred after the Messinian and is consistent with the present-day deformation.

A positive gravimetric anomaly suggests the existence of a structural bulge, probably resulting from transpressional deformation, within a restraining relay fault zone between the Arcalod and Belledonne Border faults.

Stream network analysis do not show recent deformation associated to the Belledonne border fault in the “Balcon de Belledonne” area. It demonstrates that the vertical stream anomalies (knick points) previously interpreted as resulting from vertical movement along normal faults are in fact related to the retreat of the Isère glacier. Nevertheless, stream offsets along strike of the Arcalod fault, and glacial valley offsets along strike of the Brion fault, are consistent with the late stress state and with the fault kinematics indicated by focal plane mechanisms. The age of these offset morphologies has to be determined in order to better assess seismic hazard in this area.

Acknowledgements

Jeremy Billant benefits of a PhD allocation granted by EDF (Electricité De France) through the SIGMA research program (SeIsmic Ground Motion Assessment). This work is also a contribution to the Labex OT-Med (n ANR-11-LABX-0061) funded by the French Government «Investissements d’Avenir» program of the French National Research Agency (ANR) through the A*MIDEX project (n ANR-11-IDEX-0001-02). We acknowledge K. Manchuel, Ch. Durouchoux, F. Hollender, N. Espurt, L. Bollinger and V. Godard for discussions. We acknowledge G. Cher for the correction of the English language. We acknowledge Dr C. V. Hagke and an anonymous reviewer for comments and critical reviews that significantly improved the manuscript. We acknowledge the BGI (Bureau Gravimétrique International - http://bgi.obs-mip.fr) for providing gravimetric data and IGN (Institut national de l'information géographique et forestière) for providing geodata (BD ALTI®, BD ORTHO® and BD TOPO®).

IV - CONSTRAIN FAULT OFFSET USING STATISTICAL AND GEOMETRICAL METHODS. EXAMPLES FROM THE JASNEUF FAULT, WESTERN ALPS, FRANCE.

Ce chapitre, sous forme d'un article soumis à la revue Tectonophysics, se concentre sur la faille d'orientation NE-SW du Jasneuf qui se trouve, avec la faille de la Cléry, dans le prolongement sud-ouest de la faille bordière de Belledonne dans le massif du Vercors.

L'analyse des cinématiques de failles et les états de contrainte déduits de l'inversion de plans de faille striés révèlent la même succession de régimes tectoniques que celle déterminée le long de la faille bordière de Belledonne. Un premier régime tectonique compressif à décrochant caractérisé par un axe σ_1 orientéWNW-ESE suivi d'un régime tectonique en décrochement caractérisé par un axe σ_1 orienté ENE-WSW. Ceci atteste donc d'une cinématique en décrochement dextre récente le long des failles de la Cléry et du Jasneuf.

L'analyse morphologique, facilitée par la création d'un modèle numérique de surface à haute résolution par photogrammétrie, a été menée sur la bordure occidentale des Hauts Plateaux du Vercors, où la faille du Jasneuf se distribue en quatre segments. Ces segments sont associés à anomalies géomorphologiques et à des décalages de marqueurs morphologiques (décalage de la falaise bordant le plateau, escarpements, anomalies de drainage) suggérant une activité récente de cette zone de faille.

L'étude des morphologies décalées nous a permis de mettre en lumière deux points méthodologiques. Le premier provient de l'analyse des décalages latéraux du réseau hydrographique le long d'un des segments. L'étude statistique de ces décalages fait apparaître que des distances caractéristiques entre des cours d'eau peuvent être interprétées comme des décalages. Des exemples issus de la littérature sont présentés pour appuyer notre démonstration.

Le deuxième point méthodologique est dû au fait que les autres segments de faille ne présentent pas de marqueur morphologique décalé, excepté la topographie elle-même. Dans ce cas où seulement des décalages apparents peuvent être mesurés du fait de l'absence de « piercing points », nous proposons une méthode permettant de déterminer la cinématique de la faille et de mesurer de manière précise les valeurs respectives des rejets verticaux et horizontaux.

En utilisant ces méthodes, nous déterminons les décalages sur trois des segments de faille. L'âge des objets morphologiques décalés n'est pas contraint mais argumentés dans le texte, ce qui nous permet de proposer une magnitude maximum (Mw 5,7) et un temps de retour des séismes (~500 ans) pour la faille du Jasneuf qui ne tient toutefois pas compte du fait qu'une partie de la déformation puisse être accommodée de manière asismique de façon asismique (par creeping ou fluage asismique).

CONSTRAIN FAULT OFFSET USING STATISTICAL AND GEOMETRICAL METHODS. EXAMPLES FROM THE JASNEUF FAULT, WESTERN ALPS, FRANCE.

Billant Jérémy[a], Bellier Olivier[a], Godard Vincent[a], Hippolyte Jean-Claude[a]

[a] Aix-Marseille Université, CNRS, IRD, CEREGE UM34, 13545 Aix-en-Provence, France

Keywords:

Morphotectonic; Active tectonics; Offset measurements; Alps; Jasneuf fault

Highlights:

The new SSV method allows fault offset measurements without piercing point/line.

Stream spacing can generate wrong fault offset measurements.

Jasneuf fault slip rate is of 0.13±0.03 $mm.yr^{-1}$.

Jasneuf fault could generate at least a 5.7 Mw earthquake each ~500 years.

Abstract

The NE trending dextral strike-slip Jasneuf fault is the south-western prolongation of the Belledonne Fault system in the Vercors massif. This fault does not show strong associated seismicity but displays morphological anomalies (right-lateral offset of Messinian cliffs and recent talwegs, post Günz scarps) related to recent faulting. In order to quantify the seismogenic potential of the Jasneuf fault, we constrain its slip using morphological anomalies. Through this analysis, we highlight two methodological points.

First, a stream network can display characteristic distances between streams that does not coincide necessarily to the mean interfluve distance nor a multiple of it. We show that this characteristic spacing can be interpreted as fault offset. So when fault slip measurements are made using offset streams, it is necessary to test if the result does not match with spacing, especially when measured offset is higher than the mean interfluve distance and when genetic relation between upstream and downstream streams can not be ascertain.

Second, to counter the lack of morphologic features allowing the determination of piercing points or lines, we propose a new method that allows the determination of fault offset using recursive measurements of topographic apparent offsets. The application of this method along the Jasneuf fault provides consistent results.

By applying these methodologies, we determine the Jasneuf fault cumulated slip since the Messinian which corresponds to an average slip rate of 0.13±0.03 $mm.yr^{-1}$. Extension of the fault is poorly constrained and we can not ascertain the prolongation of the Jasneuf fault outside of the Vercors plateau nor in depth. Nevertheless, if this fault is limited to the sedimentary cover and do not extend outside of the Vercors plateau, using the Wells and Coppersmith's scale laws, we deduced that it could generate Mw 5.7 earthquakes each ~500 years.

IV.1 - Introduction

Although continental interiors are generally characterized by low strain rates, they can be struck by destructive earthquakes (e.g., the 1356 Basel Earthquake, Switzerland (e.g. Fäh et al., 2009), the 1811-1812 New Madrid earthquakes, United States (e.g. Tuttle et al., 2002), the 1909 Lambesc earthquake, France (e.g. Baroux et al., 2003; Chardon et al., 2005; Lacassin et al., 2001), the 2001 Gujarat earthquake, India (e.g. Rastogi, 2004)). A direct consequence of these low strain rates is that the recurrence intervals between destructive earthquakes can reach up to several millennia and thus historical seismicity can not document an entire earthquake cycle. Moreover, combination of these low strain rates and unfavourable climatic condition leave few offset markers lead to a complicated morphological analysis.

This study is focused on the NE trending Jasneuf fault in the French western Alps, which presents the characteristics mentioned above, and whose seismogenic potential is unconstrained. The Cléry and Jasneuf fault zones are located at the south-western end of the right-lateral strike-slip "Belledonne border fault" (Fig. IV.1) seismically defined by Thouvenot et al. (2003). These fault zones are included within the Belledonne fault system.

High resolution topographic data reveal a fault trace well expressed in the morphology but classical morphologic markers used to constrain fault offset are poorly preserved or absent, leading to a challenging offset quantification. In order to alleviate this lack of markers we constrain the talweg offset measurements by cross-cutting them with recursive measurements of the talweg spacing. In the case of a lack of usual morphologic markers (e.g., stream, fan, moraine) used to determine piercing point, only apparent offsets could be measured until now. We demonstrate that by recursively measuring these apparent offsets, we can determine the true fault offset and present the method to perform a such analysis.

IV.2 - Geological framework

The Vercors massif is a thin skinned fold-and-thrusts belt whose formation started during Miocene time with the thrusting of the external crystalline massif (Butler, 1987; Philippe et al., 1998). The Cléry and Jasneuf fault zones, cutting the southern highlands of the Vercors massif, are underlined by about 6 km long linear step escarpments (Fig. IV.1). Both fault zones affect the wide and flat Glandasse plateau. The geology headed by this plateau consists in approximately 200 m

thick Barremian limestones overlapping about 1000 m thick Barremian marl series (Arnaud, 1966; Arnaud et al., 1974). In this area, the sedimentary cover is 6-7 km thick (Bellahsen et al., 2014; Le Pichon et al., 2011; Philippe et al., 1998), the MOHO depth is 37-38 km (Ménard, 1979) and lower and upper crusts are ~10km and 27-28 km thick respectively (Ménard and Thouvenot, 1984).

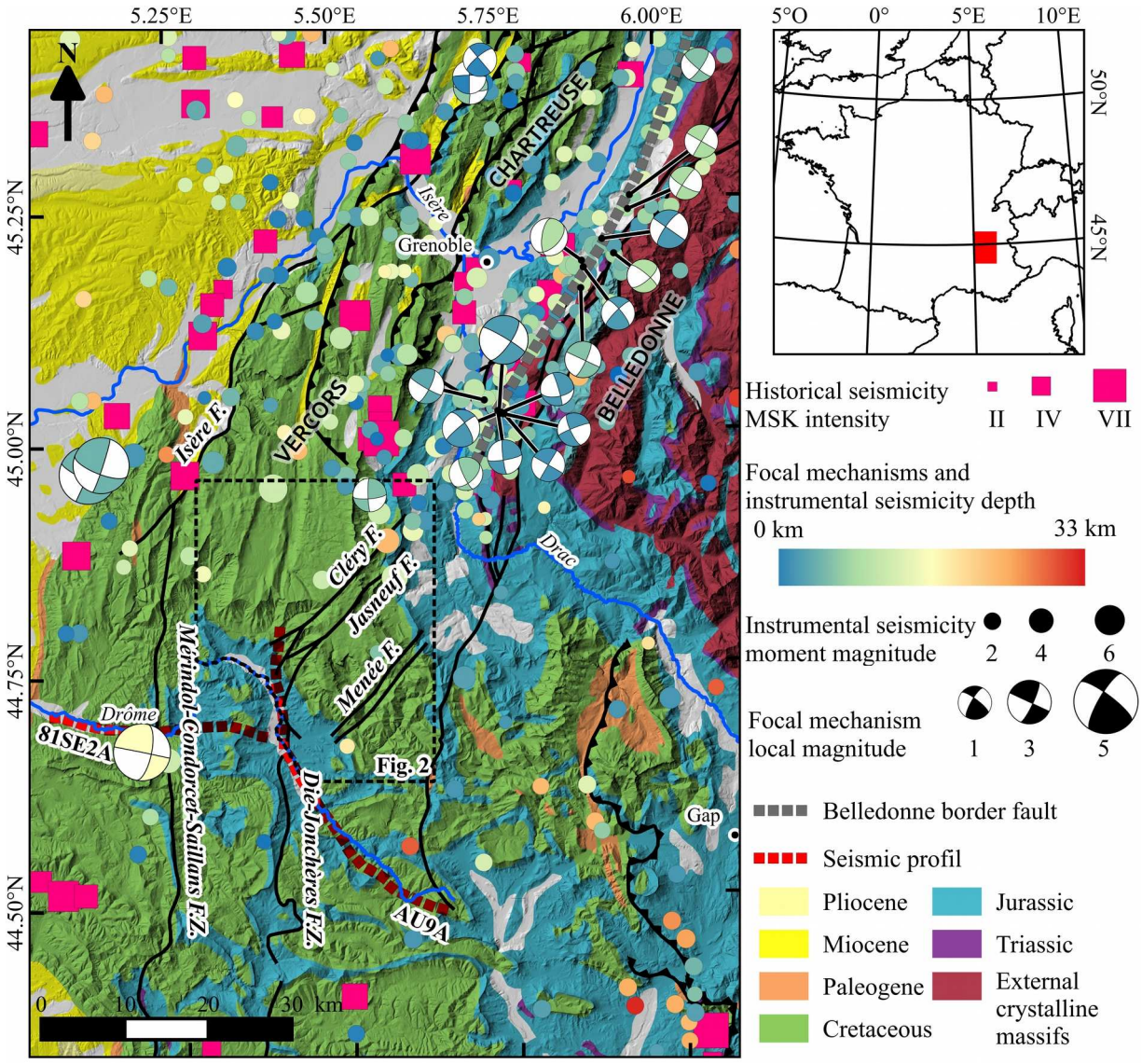

Figure IV.1: Simplified geological map (Bodelle and Goguel, 1980) and seismicity of the surrounding area (location in fig. I.1). Historical seismicity from SISFRANCE catalog, instrumental seismicity from the Si-Hex catalog (Cara et al., 2015) and focal mechanisms from Ménard (1988), Nicolas et al. (1990) and Thouvenot et al. (2003).

Arnaud et al., (1974) proposed that the Clery and Jasneuf faults extend north-eastward up the to Belledonne massif. According to the same authors, the Clery fault could connect south-westward to the Mérindol-Condorcet-Saillans fault system whereas the Jasneuf fault could connect to the Die-Joncheres fault system (Fig. IV.1). Therefore, the Clery and Jasneuf fault systems could reach ~52 km and ~34 km respectively. In fact, outside of the calcareous Vercors, both faults affect marly rocks (Debelmas et al., 1967a; Flandrin et al., 1974) which implies that their morphologies are not well expressed in such highly erodible deposits. At the south-western termination of the Glandasse plateau, both faults split in multiple segments (Fig. IV.1 And IV.2).

The total right-lateral offsets along the Clery and Jasneuf faults are of 3.5 km and 3 km respectively as suggested by the lateral offset of the southern limit of the lower Barremian detrital limestones (Arnaud, 1981; Robert, 1976) and by the difference in shortening between two parallel finite geological sections on both sides of the Cléry fault (Thibaut et al., 1996).

Studies of the fault network by aerial photographs (Arnaud, 1971; Robert, 1976) diplay evidences for a fracturing model arrangement organized into a Riedel system with an average direction of the dextral strike-slip faults ranging between N030°E and N080°E. Normal dip slip and/or low lateral component slip faults have directions ranging between N080°E and N105°E and sinistral strike-slip faults trend between N105°E and N160°E. Finally, reverse and thrust faults trend NNW to NNE (from N160°E to N210°E). Along the Cléry fault, clear markers of brittle deformation (fault planes with polished surface, cataclastic rocks) in limestone and markers of pressure-dissolution ductile deformation in the underlying marl have been described (Gratier et al., 2013; Thibaut et al., 1996).

The Jasneuf and Cléry faults are located at the south-western end of the right-lateral strike-slip “Belledonne border fault” (Fig. IV.1) seismically defined by Thouvenot et al. (2003). Unlike the “Belledonne border fault”, the Cléry and Jasneuf faults do not display associated seismic activity except in their north-eastern termination (Fig. IV.1) where earthquakes occurred, one of them reaching a 4.6 Mw (Cara et al., 2015). Present day accuracy of GPS measurements does not allow a strong constraint of the strain rate in the western Alps (Nocquet, 2012) but the shortening and extensional rates for a 50 km long baseline does not exceed 3 $mm.yr^{-1}$ (Delacou et al., 2008). Different models agreed with a counter-clockwise rotation of Adria (Calais et al., 2002; D’Agostino et al., 2008; Serpelloni et al., 2005).

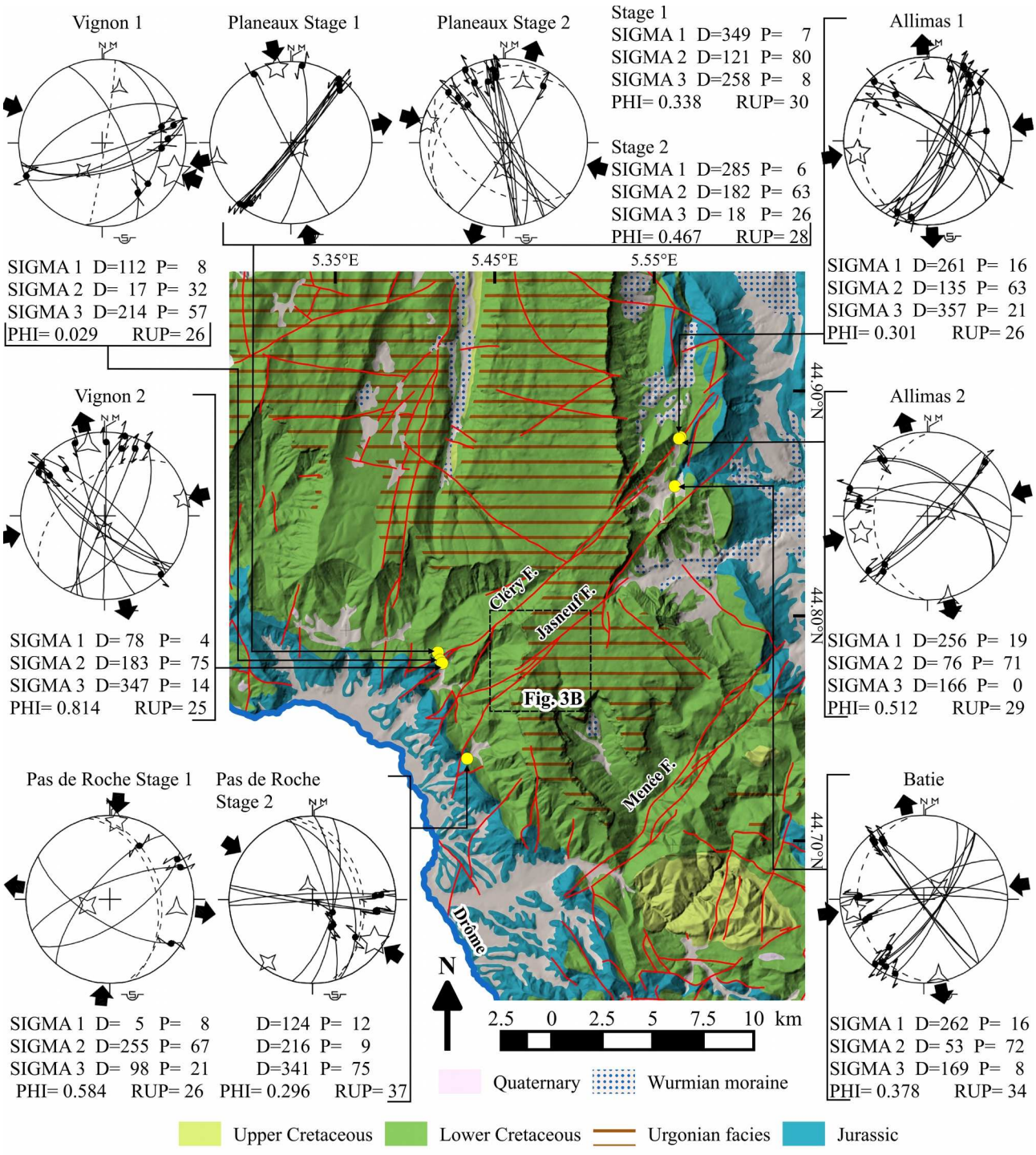

Figure IV.2: Geological map (location on Fig. IV.1) of the study area (modified from Rouire et al. (1980)), location of the sites of fault measurements and Schmidt's diagrams with computed stress tensors. Schmidt's diagrams: solid lines for fault planes, dashed lines for bedding planes. σ1, σ2, and σ3 as five branches, four branches and three branches stars respectively. PHI is the stress ratio and RUP a quality estimator (cf. Angelier (1990)). The stage 1 of the Planeaux site is presented after the backtilting.

IV.3 - Fault kinematics analysis and stress state determination

The kinematics of a fault population is defined using the striations measured on fault planes at several sites. By measuring numerous striated fault planes at individual sites, we can characterize successive faulting events, tectonic regimes and related stress states. This methodology of fault kinematics studies to determine paleostress fields and to demonstrate temporal and spatial changes in the late Cenozoic stress states has been applied in many active tectonic areas around the world over the past thirty years (e.g., Bellier and Zoback, 1995; Champagnac et al., 2004; Hippolyte et al., 2012, 1993; Homberg et al., 2002; Mercier et al., 1991; Shabanian et al., 2010).

We measured striae on both major (sedimentary cover scale) and minor (centimetric to metric scale) faults, at seven different sites, to determine the state of stress responsible for the deformation in the studied area (Fig. IV.2, Tab. IV.1). We realized quantitative inversions of distinct families of slip data measured at each individual site using the INVD method proposed by Angelier (1990) (Fig. IV.2). The results of the stress inversion include the orientation (azimuth and plunge) of the three principal stress axes σ_1, σ_2 and σ_3 (maximum, intermediate and minimum compressional stress axes) of the stress tensor and the stress ratio ($\varphi=(\sigma_2-\sigma_3)/(\sigma_1-\sigma_3)$)

The chronology between several fault kinematics (and indirectly several stress states) is deduced from the observations of cross-cutting relationship between kinematics markers (e.g. cross-cutting striae, fault offsetting another fault). Because stress axes are supposed to follow Andersonian orientations (i.e. two horizontal and one vertical), their dip are considered in light of the strata dip of the measurements site to determine chronology between faulting and strata tiliting.

In this study, we aim at characterizing the late Cenozoic deformations. Unfortunately, for fault striations, it is difficult to constrain the absolute age of fault slips more precisely than younger than the age of the rocks affected by the faults. In the study area, striations are measured on faults affecting Oxfordian to Hauterivian rocks (Fig. IV.2, Tab. IV.1) but are likely to be much more recent and related to Alpine deformations.

Site	Stage	GPS coordinates	Facies and dips	Faults			Kinematics markers	Tectonic regime	σ_1 trend
				Trend	Dip	Kinematics			
Planeaux	1	44.78901°N 5.40708°E	Tithonian limestones N037°E-15°N N051°E-30°W N125°E-43°S	~N30°E	SE	sinistral	Grooves Striae Tension cracks Stylolites	Strike-slip	N169°E
				~N150°E	~vertical	dextral			
	2			~N30°E	~vertical	dextral			N105°E
				~N150°E	~vertical	sinistral			
Pas de Roche	1	44.74136°N 5.42335°E	Kimmeridgian marl and limestone N164°E-44°E N168°E-39°E	~N45°E	NW and SE	sinistral	Striae Calcite steps	Strike-slip	N005°E
				N120°E	SW	dextral			
	2			~N0°E	E	reverse-sinistral		Reverse	N124°E
				~N90°E	~vertical	dextral			
Vignon 1	2	44.78559°N 5.40824°E	Oxfordian limestone N008°E-87°E	~N70°E	S	dextral		Tranpressional	N112°E
				N11°E	E	reverse			
				N155°E	E	sinistral			
Vignon 2	3	44.77176°N 5.40025°E	Kimmeridgian marl and limestone N051°E-51°N	~N20°E	E and W	dextral		Strike-slip	N078°E
				~N130°E	NE and SW	sinistral			
Allimas 1	3	44.88129°N 5.56319°E	Hauterivian limestones N005°E-20°W	~N30°E	SE	dextral	Calcite steps Stylolites Striae		N081°E
				~N120°E	NE	sinistral			
Allimas 2	3	44.88069°N 5.56221°E	Hauterivian limestones N001°E-36°W	~N40°E	~vertical	dextral			N076°E
				N86°E to N129°E	N to NE	sinistral			
Batie	3	44.85958°N 5.55859°E	Tithonian limestones N172°E-22°W	~N30°E and ~N70°E	~vertical	dextral	Grooves Striae Calcite steps Stylolites		N082°E
				~N90°E and ~N140°E		sinistral			

Table IV.1: Description of fault measurement sites and associated tectonic regime deduced from inversion.

At the Planeaux site (Fig. IV.2, Tab. IV.1), fault planes can be grouped into two sets of average orientations of N150°E and N30°E. Both trends show right-lateral and left-lateral kinematics of which we clearly determined the chronology. On a N151°E trending near vertical fault plane, a striation plunging 2° north-westward is consistent with left-lateral kinematics (as attested by styloliths and shelter zones) and cross-cuts another stria consistent with right-lateral kinematics (as attested by calcite steps) and plunge 34° north-westward. According to the dip of the strata (N51°E trending 30° north-westward) and to the cross-cutting relationship, N30°E and N150°E trending faults were first left-lateral and right-lateral strike-slip faults respectively, then they were tilted during the folding and finally they have been reactivated as right-lateral and left-lateral strike-slip faults, respectively. This last strike-slip kinematics probably occurred during and after the strata tilting as suggested by some striae showing this second kinematics closed to the strata dip. We backtilted the faults according to the strata dip before the stress inversion. Inversion allows the definition of a strike-slip tectonic regime for the both deformation stages, characterized by N169°E and N78°E trending, near horizontal σ_1 and σ_3 axes for the first and characterized by N105°E and N18°E trending, near horizontal σ_1 and σ_3 axes for the second.

At the “Pas de Roche” site (Fig. IV.2, Tab. IV.1), we observed ~N trending sinistral-reverse faults and E trending dextral strike-slip faults consistent with a SE trending compression, and SE trending dextral strike-slip faults and NE trending sinistral faults related with a N trending compression. No cross-cutting chronology has been observed. Inversion of the dataset allows defining a compressional tectonic regime characterized by N124°E and N36°E trending, near horizontal σ_1 and σ_2 axes, respectively. Inversion was also done for the second fault set even if the low number of data leads to a poorly constrained stress axes. In addition, inversions of the dataset with or without the backtilting provide similar solutions. Both are consistent with a strike-slip tectonic regime characterized by N5°E and N98°E trending, near horizontal σ_1 and σ_3 axes, respectively. However, trend of the σ_1 axis is close to the one of the first tectonic regime observed at the Planeaux site suggesting that both are probably coeval.

At the Vignon 1 site (Fig. IV.2, Tab. IV.1), the N8°E trending strata dips 87° eastward. Inversion of the dataset allows defining a transpressional tectonic regime characterized by N112°E trending near horizontal σ_1 axis and a N17°E trending 32° dipping northward σ_2 axis which is consistent with the dip of bedding. However, the near horizontal attitude of the striae indicates that faulting mainly occurred after the folding.

Inversion of the dataset of the Vignon 2 site allows the definition of a strike-slip tectonic regime characterized by N78°E and N167°E trending, near horizontal σ_1 and σ_3 axes, respectively (Fig. IV.2, Tab. IV.1). The strata dips of 51° toward 321°E is not consistent with the compression direction. The horizontal attitude of the striae indicates that faulting occurred after the folding.

Inversion of the seven sites shows three main tectonic regimes (Fig. IV.2, Tab. IV.1): a strike-slip tectonic regime with a N trending compressional axis (stage 1 of the Planeaux and Pas de Roche sites), a compressional to strike-slip tectonic regime with a WNW trending compressional axis (Vignon1 site and stage 2 of the Planeaux and Pas de Roche sites) and a strike-slip tectonic regime with an ENE trending compressional axis (Allimas1, Allimas2, Batie and Vignon2 sites).

The Planeaux site displays clear evidences to attribute at the N trending compression an age prior to the WNW trending compression. On the Pas de Roche site, relative chronology between these two stress states can not be ascertain but the N trending compression could predate the folding. We did not find clear evidence of relative chronology between the WNW and the ENE trending compression. However, as suggest by our observations at the Planeaux site and Vignon 1 site the WNW trending compression occurred during and after the folding and is consistent with the bedding deformation whereas at the Vignon2 site faulting occurred after the folding (consistent with the WNW trending compression).

Moreover, this three compression directions were already described in the surrounding areas:

- the N trending compression in the Rhône valley (Bergerat, 1981a) and in the Vercors massif (Philippe, 1995) is attributed to the Pyrenean stage, late Cretaceous to Eocene in age.

- the WNW trending compression in the Rhône valley (Bergerat, 1981a) and Vercors, Chartreuse, Belledonne and Jura massifs (Butler, 1987, 1992; Hippolyte et al., 2006b; Homberg et al., 2002; Philippe, 1994; Philippe et al., 1998) is the Miocene tectonic regime which leads to folding and thrusting in the Subalpine Massifs

- the ENE trending compression, Messinian to Quaternary in age, occurred during and after the thrusting of the Belledonne massif (Billant et al., 2015) and is consistent with focal plane mechanisms of earthquakes occurring along the Belledonne border fault (Thouvenot et al., 2003).

This is consistent with the chronology we propose and it agrees with a Jasneuf fault right-lateral strike-slip faulting recent kinematics.

IV.4 - Geomorphic analysis

The faults mapped on the geological map (Arnaud et al., 1974) were draped on the 1:25000 topographic map. We found that several topographic anomalies appear associated with the Jasneuf fault trace. To better constrain detailed fault pattern and to identify potential morphological faulting features (offset, scarp…) we have performed a field survey combined with the production and analysis of a high resolution digital surface model of the area.

IV.4.1 - High resolution Digital Surface Model (DSM) and orthophotograph generation

The low density vegetation cover of the area permits us to use photogrammetry. We used the software Agisoft Photoscan Professional for the orthophotograph and DSM generation.

We used 12 scans of not orthorectified aerial photographs from a 1972 survey campaign, available from the IGN website (http://www.geoportail.gouv.fr). The resolution of these aerial photographs is unknown but can be estimated as less than a meter. Photographs are arranged along two ~N trending lines. Between two photographs, meridian and longitudinal overlaps are approximately of 50 % and 10 % respectively. Initially, the software computes the position of the photographs and generates a first 3D model in an orthonormal Cartesian coordinate system.

In order to georeference the 3D model, ground control points are needed. We extracted 200 spot heights from the 1:25000 topographic map and reported them on the georeferenced orthorectified aerial photographs from a 2001 campaign produced by IGN. We identified 78 spot heights on both the 1972 and the 2001 aerial photographs and used them as ground control points. Error on the coordinates of this ground control points was set at 5 m which is the spot height diameter on the 1:25000 topographic raster map.

The software then computes a 30 cm resolution DSM (Fig. IV.3) and orthophotography, both georeferenced. Effective DSM resolution is less than meter, but it may spatially vary because of the roughness differences of the ground surface across the studied area.

IV.4.2 - Fault mapping

The fault mapping of the area (Fig. IV.3) was made based on geomorphic anomalies observed on the DSM, the 1:25000 topographic map (scarps and contour lines lateral offsets) the orthophotography (stratigraphy shift, lineaments, alignment of plants) and field survey.

Fault segments ranged between 60 m and 6 km in length and can be separated into two majors sets oriented approximately NE-SW and WNW-ESE (Fig. IV.3), the former including dextral strike-slip faults and the latter corresponding to the antithetic sinistral strike-slip faults. The NE trending faults locally delimit several shuttle ridges. The south-western termination of the fault zone is composed of four segments (numbered from 1 to 4, Fig. IV.4). The fault segment No. 1 is 1.8 km long and splits into two fault segments, one being connected north-eastward to the fault segment No. 3. The fault segment No. 2 is 1.7 km long and is connected north-eastward to the fault segment No. 3. The main fault segment is the No. 3. It runs trough the whole plateau and reaches ~6

km in length. The fault segment No. 4 is 1.9 km long and connects to the fault segment No. 3 north-eastward.

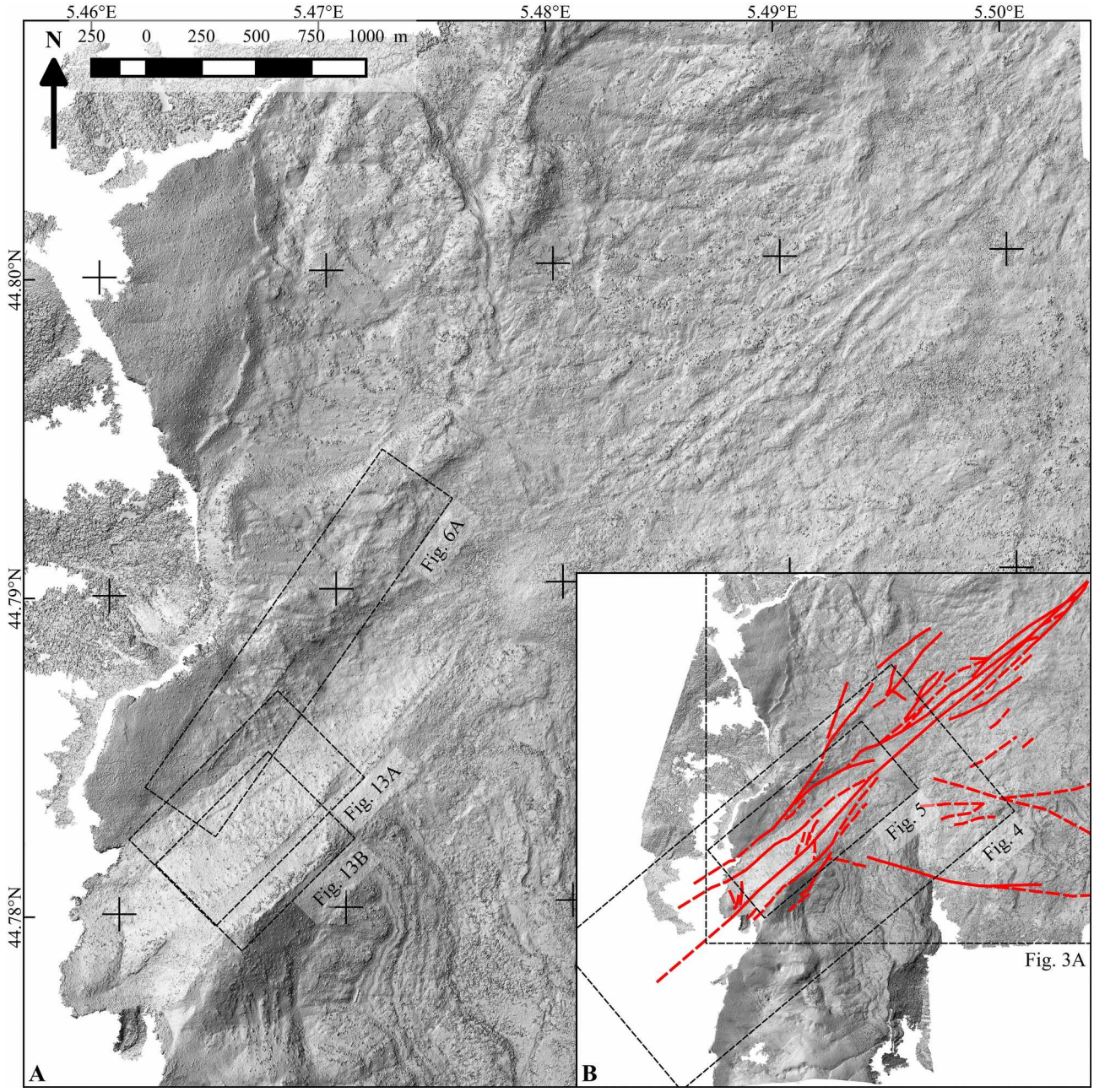

Figure IV.3: Shaded DSM and Jasneuf fault zone (location on Fig. IV.2). Solid red lines are faults with a strong signal (scarps and/or stratigraphic offsets) and dotted red lines are supposed faults (topography anomalies and/or lineaments).

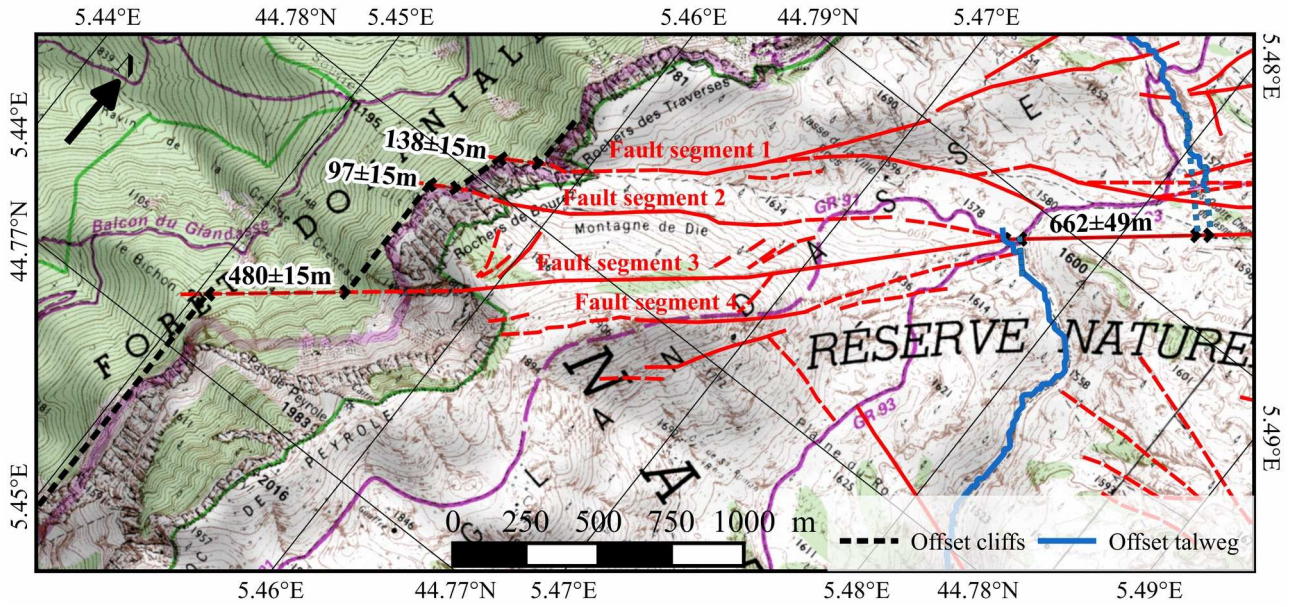

Figure IV.4: Topographic map of the south-western termination of the Jasneuf fault (location on Fig. IV.3) with offset values for a talweg and the cliffs bordering the plateau. The stream flows from north to south.

IV.4.3 - Morphological markers of recent deformation

Field survey and topographic analysis provide evidences for morphological anomalies (offset of morphological markers and scarps) interpreted as related to recent faulting. These anomalies can be grouped in two scale order, some showing hectometric offsets and others decametric offsets.

IV.4.3.1 - Small scale morphological anomalies

A stream crosscutting the fault zone seems to be right-lateraly offset of 662±49 m although we can not exclude that it was drained and deviated by the fault zone (Fig. IV.4). Cliffs on both sides of the different fault segments of this fault zone are not continues and display systematic right-lateral offsets (Fig. IV.4) :

- 138±15 m offset for the cliffs on both sides of the fault segment No. 1,
- 97±15 m offset for the cliffs on both sides of the fault segment No. 2 and
- 480±15 m offset for the cliffs on both sides of the fault segment No. 3 and No. 4.

Sum of the cliffs offset for the four fault segments is 715±45 m which is in close consistency with the 662±49 m stream offset.

IV.4.3.2 - Large scale morphological anomalies

Fault No.1 shows a scarp which may be locally up to 3 meters height. Along the south-western fault segment, field survey has revealed that talwegs are not continuous on both sides of the fault and display a vertical step (knick-point like morphology) when they cross-cut the fault scarp (Fig. IV.5A). Moreover, some talwegs on the downstream side of the fault plane appear beheaded (03a,05a,07a,09a,10a,11a,17a,19a, Fig. IV.5A and IV.6A). Field survey revealed that talweg 08 is characterized by a wineglass-like geomorphic features through the fault scarp suggesting a resume of the erosion after a relative vertical offset (Fig. IV.5C). Along the north-eastern segment, talwegs 20b, 21b and 22b terminated in a doline limited by the fault (Fig. IV.6A). This could result from a local uplift consistent with compressional deformation within a restraining relay fault zone that induce local transpressional tectonic regime. Finally, the upstream talweg 24b is clearly captured by the downstream talmweg 24a. It produces an apparent left-lateral “en baïonette” talweg (Fig. IV.6A). A windgap is present at the head of the talweg 24b, probably caused by regressive erosion of the talweg 24c running north-westward on the other flank of the relief (Fig. IV.6A).

Field observations of several fault scarps are presented on the Fig. IV.5. Along strike of faults No. 2, 3 and 4, decimeter to 2 m high scarps are visible on the DSM. The counterslope scarp related to the fault No. 3 which can reach 2 m in height in some place (Fig. IV.5B). Although the fault plane is very eroded and show lapiaz-like erosional forms, cataclasyte is visible in some place. Unfortunately, the fault planes observed one the plateau do not display kinematics markers like striations.

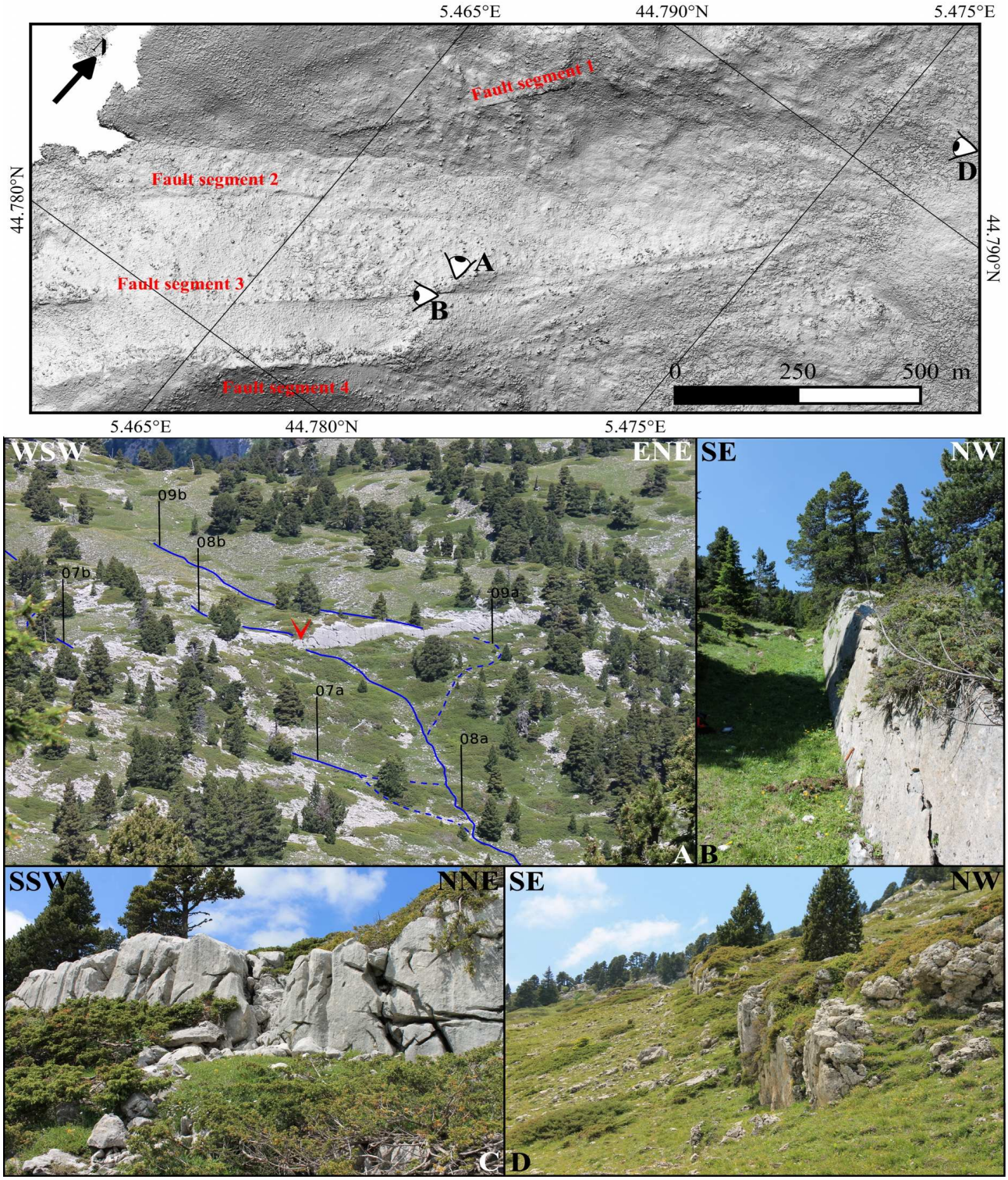

Figure IV.5: Shaded DSM of the fault scarps and field photographies: A) view of a part of fault No.1, red arrow indicates the location of the C) small wineglass structure. B) Scarp of the fault No. 3. D) Scarp of the fault No. 1 before its connection with fault No. 3.

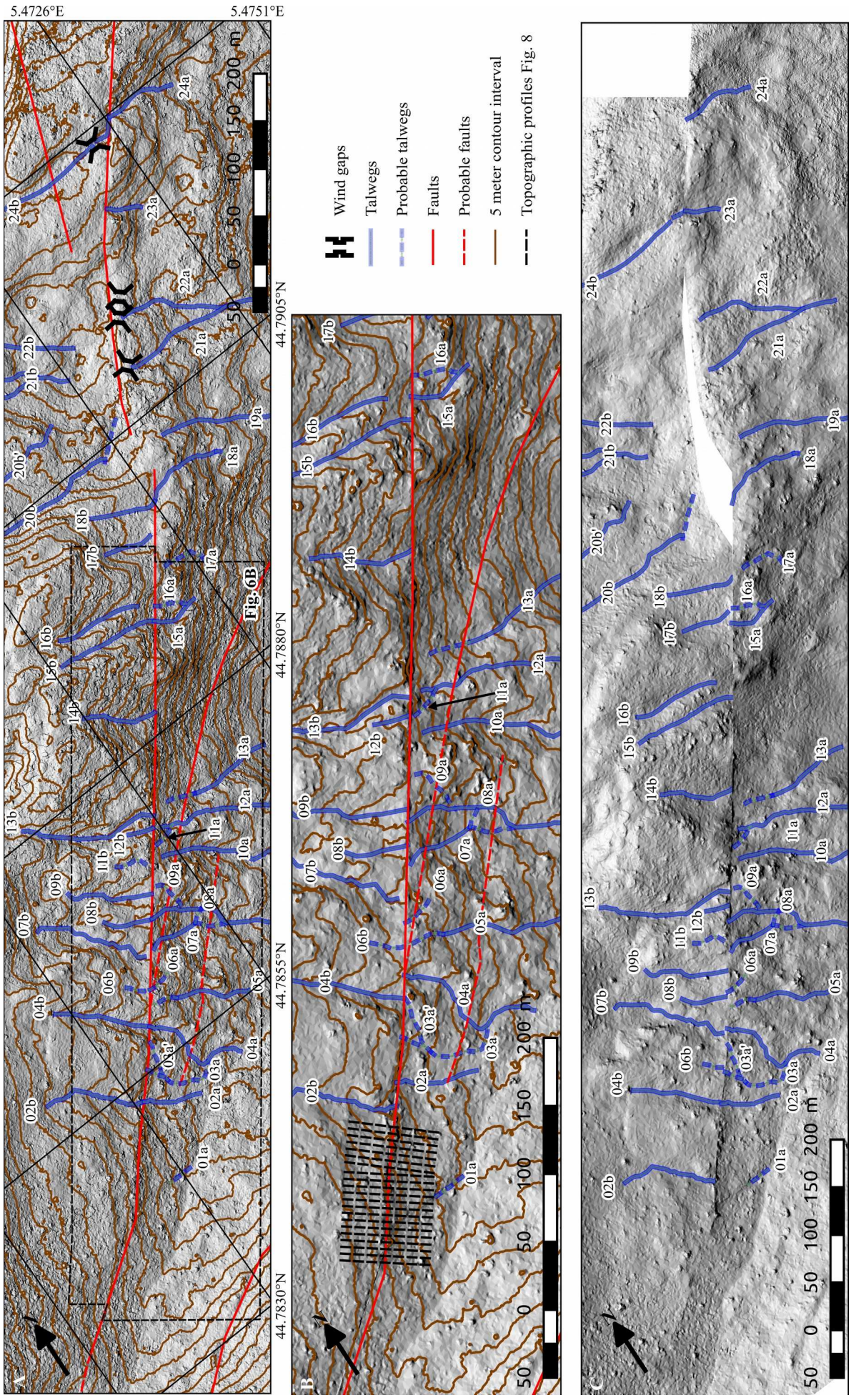
5.4726°E
5.4751°E
44.7905°N
44.7880°N
44.7855°N
44.7830°N
Fig. 6B
Wind gaps
Talwegs
Probable talwegs
Faults
Probable faults
5 meter contour interval
Topographic profiles Fig. 8
0 50 100 150 200 m
A
B
C

IV.5 - Offsets quantification

IV.5.1 - Constraining the reliability of lateral stream offsets along the fault No.1 using statistical analysis

Drainage network was mapped manually using orthophotography, contour lines derived from the DSM and field observations in order to avoid drainage network errors caused by the presence of vegetation cover in the DSM. We notwithstanding use a least-cost search algorithm (Ehlschlaeger, 1989) to extract stream network from the DSM to compare result with our mapping and both are in good agreement.

The removals of about 17 m and 77 m values of right-lateral displacement along the fault allow realigning several talwegs on both sides of the fault scarp (Fig. IV.6B and C). These talwegs do not display initially clear right-lateral “en baïonette” shapes and because we can not assess genetic relations between upstream and downstream talwegs thanks to there morphology, we perform a statistical analysis in order to constrain the reliability of the offset values. In this purpose, we map the intersection between each talwegs and the faults. When a talweg does not cross-cut the fault, we project it on the fault considering its mean direction and morphology of its watershed. This projection is also done for the talwegs 07a and 08a which display a direction change near the fault probably caused by there captures by the upstream talwegs. For both fault segments, we extract all the distances along the fault trace between downstream and upstream talweg intersections with the fault assuming a right-lateral kinematics. The kernel density estimation resulting from the determined offset dataset displays high probability density for offset values of about 17 m, 78 m and 120 m (Fig. IV.7A and B), the two first values being in good agreement with the offset values found previously. It also displays periodical increases of the probability density centered at ~216 m, ~320 m, ~418 m and ~514 m (Fig. IV.7A).

◀*Figure IV.6: Present day (A) and retrodeformed topography after the removal of a 16.9 m (B) and 78 m (C) right-lateral offset respectively.*

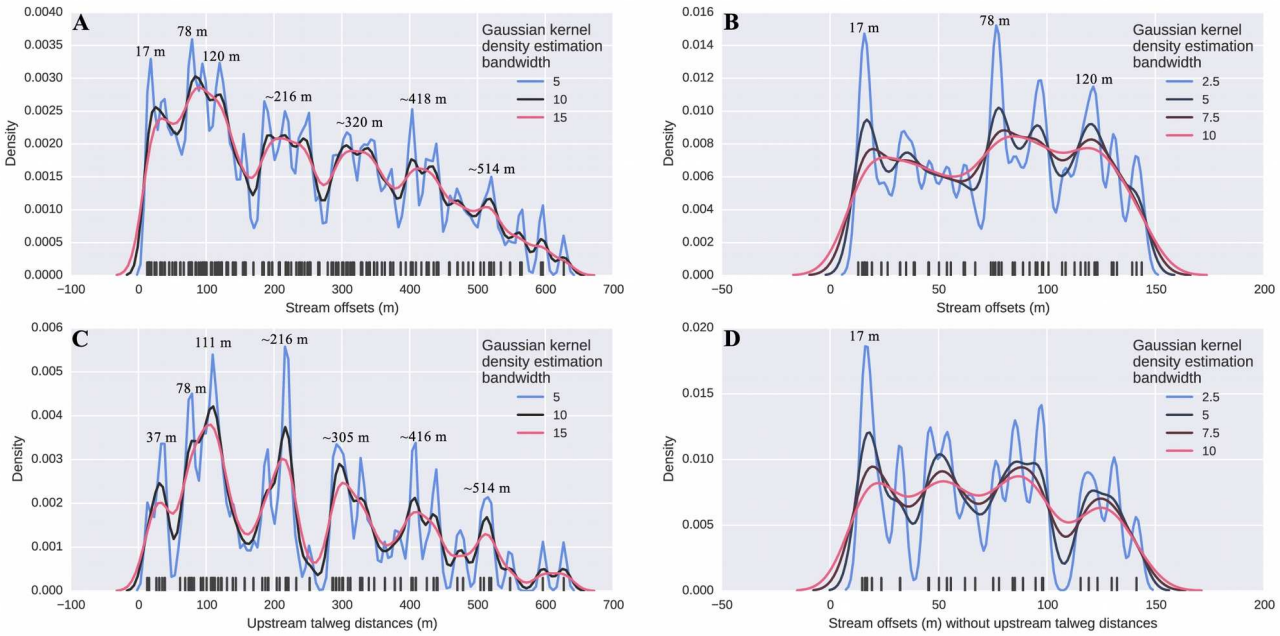

Figure IV.7: Probability density functions of measurements along the fault No.1 of A) the distance between each downstream and upstream talwegs (possible offset values), B) idem but limited to values lower than 150 m, C) the spacing between each upstream talwegs and D) the distances between downstream and upstream talwegs which do not correspond to a spacing distance (right offset value).

Because of this periodical increase of the probability density function, we suspect a possible influence of the stream spacing on our measurements. We perform the same analysis on the distance separating each pair combination of upstream talwegs (i.e. between streams 02b and 04b, 02b and 06b, etc. and idem then from streams 04b, 06b, etc., Fig. IV.6) and we find high probability density at 37 m, 78 m, 111 m and 216 m and increases of the probability density centered at ~305 m, ~416 m and ~514 m (Fig. IV.7C). Most of these values correspond to the high probability density determined for the stream offset values. It implies that the stream network spacing has a strong influence on the measured offsets. Therefore, we correct the offset dataset by removing offset values equal to a distance between two upstream talwegs (e.g. offset measured using distance between 04a and 07b is equal to the distance between 04b and 07b). The kernel density estimation made on the resulting dataset displays only one high probability density at ~17m (Fig. IV.7D).

We so conserved only distances between talwegs 3a' and 4b, 5a and 6b, 7a' and 8b, 8a' and 9b, 9a and 11b, 11a and 12b, and 12a and 13b.The mean offset of these right-laterally offset talwegs is of 16.9±2.9 m.

IV.5.2 - Vertical offset quantification along fault No.1

In order to constrain the vertical movement component along the fault segment, we first remove the 17 meters lateral offset on the DSM by cutting it along the fault trace and moving left-laterally its north-western part (Fig. IV.6). 21 topographic profiles were made in the south-western part of the fault segment (Fig. IV.8) which was less affected by stream erosion. We then measure vertical offset between profile trends on both sides of the fault and deduced a mean vertical offset of 3.2±0.6 meters.

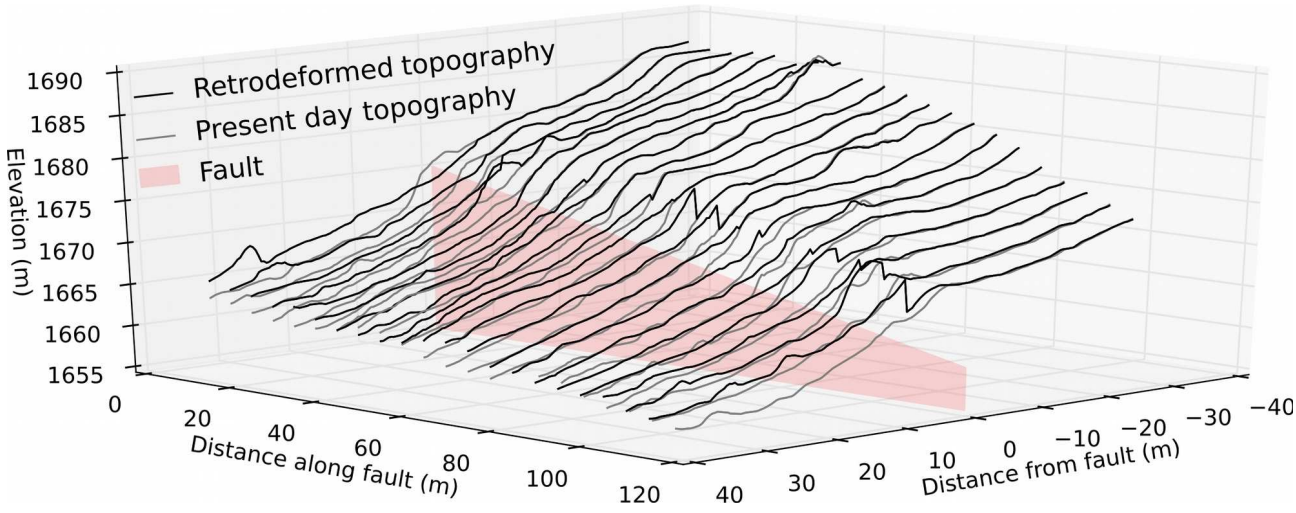

Figure IV.8: Topographic profiles across fault No.1 before and after the removal of a 16.9 m right-lateral offset (location on Fig. IV.6B). Retrodeformed topographic profiles were used to measured vertical offset along fault No.1.

IV.5.3 - Constraining fault No.2 and No.3 offsets without morphologic markers

Faults No.2 and No.3 do not display offset morphologic markers defining piercing points or lines. We propose thereafter a method that we called Search of the Shared Vector (SSV) which allows the determination of the fault kinematics and slip thanks to the recursive measurements of apparent lateral and vertical offsets.

IV.5.3.1 - Principle

Considering the following equation of a line l :

$$(l): y = ax+b \quad \text{(IV.1)}$$

Considering the line l' the translate of l by the vector $\vec{u}(x_u, y_u)$, $p'(x_{p'}, y_{p'})$ a point of the line l' and $\vec{v}_m(x_{v,m}, y_{v,m})$ the m vectors allowing the translation of every points $p_m(x, y)$ of the line l on the point p' (Fig. IV.9A and B), we can write:

$$x_{v,m} = x_{p'} - x \tag{IV.2}$$

and

$$y_{v,m} = y_{p'} - y \tag{IV.3}$$

Using IV.1, equation IV.3 can be written as:

$$y_{v,m} = y_{p'} - a\,x - b \tag{IV.4}$$

Using IV.2, equation IV.4 can be written as:

$$y_{v,m} = y_{p'} - b - a\left(-x_{v,m} + x_{p'}\right) \tag{IV.5}$$

Then equation IV.5 can be written as:

$$y_{v,m} = a\,x_{v,m} + y_{p'} - b - a\,x_{p'} \tag{IV.6}$$

Because l and l' are parallel, they share the same slope a. The term $y_{p'} - b - a\,x_{p'}$ in equation IV.6 is equal to $b' - b$, with b' the intercept of the line l'. Equation IV.6 can be written as:

$$y_{v,m} = a\,x_{v,m} + b' - b \tag{IV.7}$$

The equation IV.7 is linear and describes every possible translation vectors which allow obtaining l' from l. It so includes $\vec{u}(x_u, y_u)$ but also $\vec{v}_{lat}(x_{v,lat}, 0)$ and $\vec{v}_{vert}(0, y_{v,vert})$ (Fig. IV.9A and B).

So, for n lines $l_1, l_2, \ldots, l_n$ translated by $\vec{u}$, if $a_1 \neq a_2 \neq \ldots \neq a_n \neq 0$, the system of linear equations (Eq. IV.8,Fig. IV.9C)

$$\begin{cases} y_{v,m,1} = a_1\,x_{v,m,1} + b'_1 - b_1 \\ y_{v,m,2} = a_2\,x_{v,m,2} + b'_2 - b_2 \\ \quad\quad \ldots \\ y_{v,m,n} = a_n\,x_{v,m,n} + b'_n - b_n \end{cases} \tag{IV.8}$$

has an unique solution which is $x_{v,m} = x_u$ and $y_{v,m} = y_u$ (Fig. IV.9C).

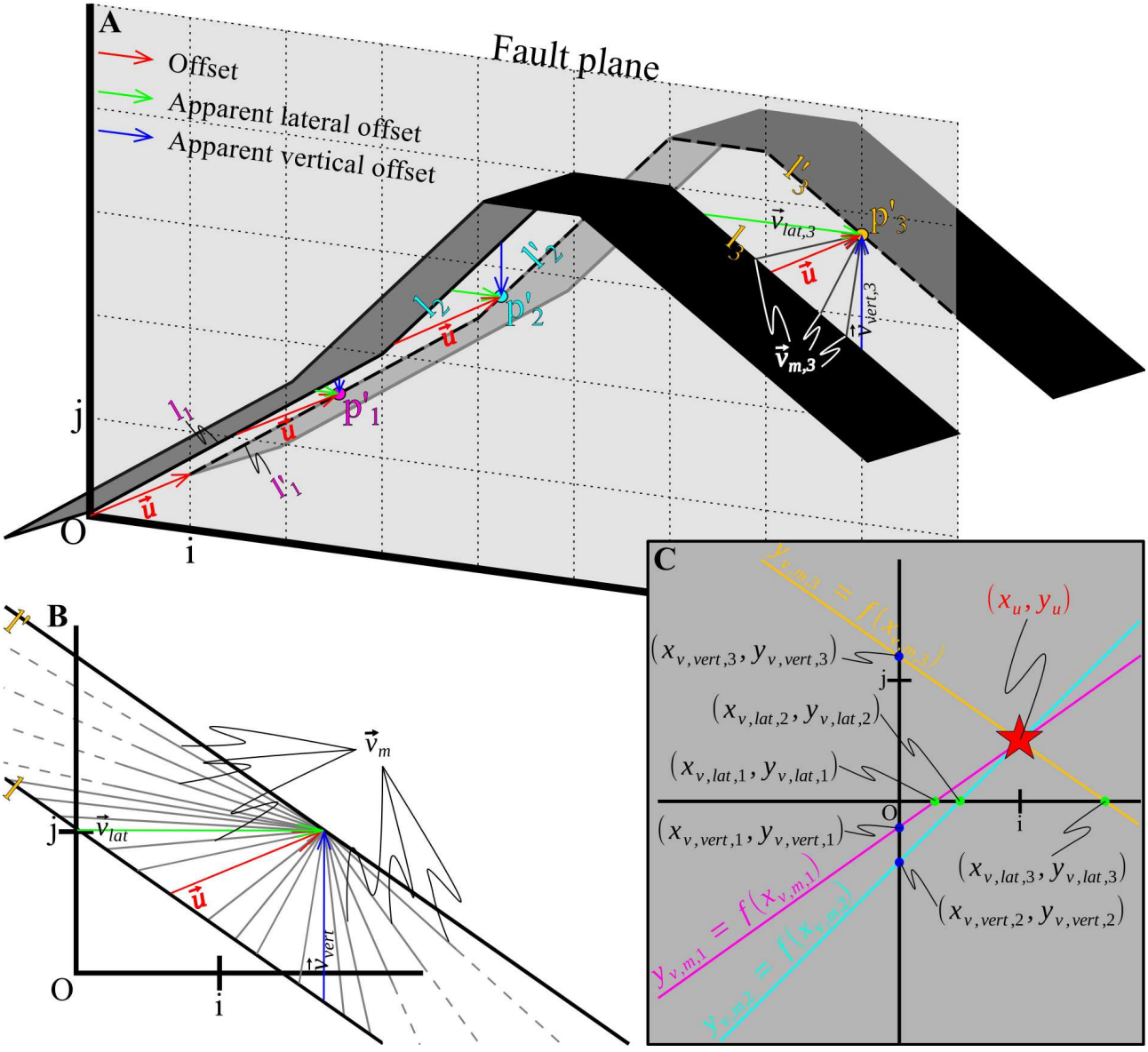

Figure IV.9: A) Schematic diagram of a topography offset by a fault and example of vectors allowing the translation of each surfaces. $\vec{u}$ *is the real offset,* $\vec{v}_{lat,n}$ *and* $\vec{v}_{vert,n}$ *the apparent lateral and vertical offsets respectively and* $\vec{v}_{m,3}$ *other possible offsets explaining translation of* l_3 *to* l'_3*. B) Example of a large span of vector allowing the translation of the line* l *to* l'*. Note that because the line* l *has the same slope than* l_3*, the same linear equations describing possible translation vectors is true for both. C) Plot of the apparent lateral and vertical offsets of A and the resulting system of linear equations. Intersections of the lines is the unique solution of the system of linear equations and is equal to the coordinates of* $\vec{u}$*.*

IV.5.3.2 - Method

Our aim is to determine lateral (x_u) and vertical (y_u) fault offset values. For a fault, we can measure at different points (p'_n) apparent lateral ($\vec{v}_{lat,n}$) and vertical ($\vec{v}_{vert,n}$) offsets (Fig. IV.9A and IV.10A). These pairs of values are then used to determine the n linear equations (Eq. IV.7) describing every possible offsets (Fig. IV.9C, IV.10B and IV.10C). In natural circumstance a problem is that the projection of the offset surfaces on the fault plane does not define lines but curves (Fig. IV.10A), implying that measured apparent lateral and vertical offsets are distorted (Fig. IV.10A1). This bias implies that each systems of linear equations composed of two linear equations provide different solutions. We so obtain a distribution of offsets scattered around the actual value (Fig. IV.10B) which is the mean of this distribution (Fig. IV.10B and C).

Figure IV.10: A) Synthetic test models A1) of a cylinder normal to the fault plane offset of 5 m vertically and 2.5 m laterally by a normal left-lateral fault and A2) of a topographic surface offset of 1 m vertically and 1 m laterally by an inverse right-lateral fault. Topographic profiles are the projection on the fault plane of the surfaces on both sides of it. Pink, cyan and yellow lines are couples of apparent lateral and vertical offsets measured each 3° for A1 and each 1 m for A2. B) Graphic representation of the system of linear equations for the synthetic test model of B1) the cylinder and B2) the topographic surface zoomed closed to the mean. Dots are the intersections between two lines, i.e. the solutions of system of linear equations composed by two equations. Green stars are the right offset values, red stars and ellipses the computed offsets and its error at a 99.99% confidence level present in C. C) Results of the SSV method applied to the synthetic test model of C1) the cylinder and C2) the topographic surfaces. 1D and 2D histograms are the solutions of all the systems of linear equations (i.e. offset $\vec{u}$) composed by two linear equations (green dashed lines). The mean of the dataset and its uncertainty include the initial offset.►

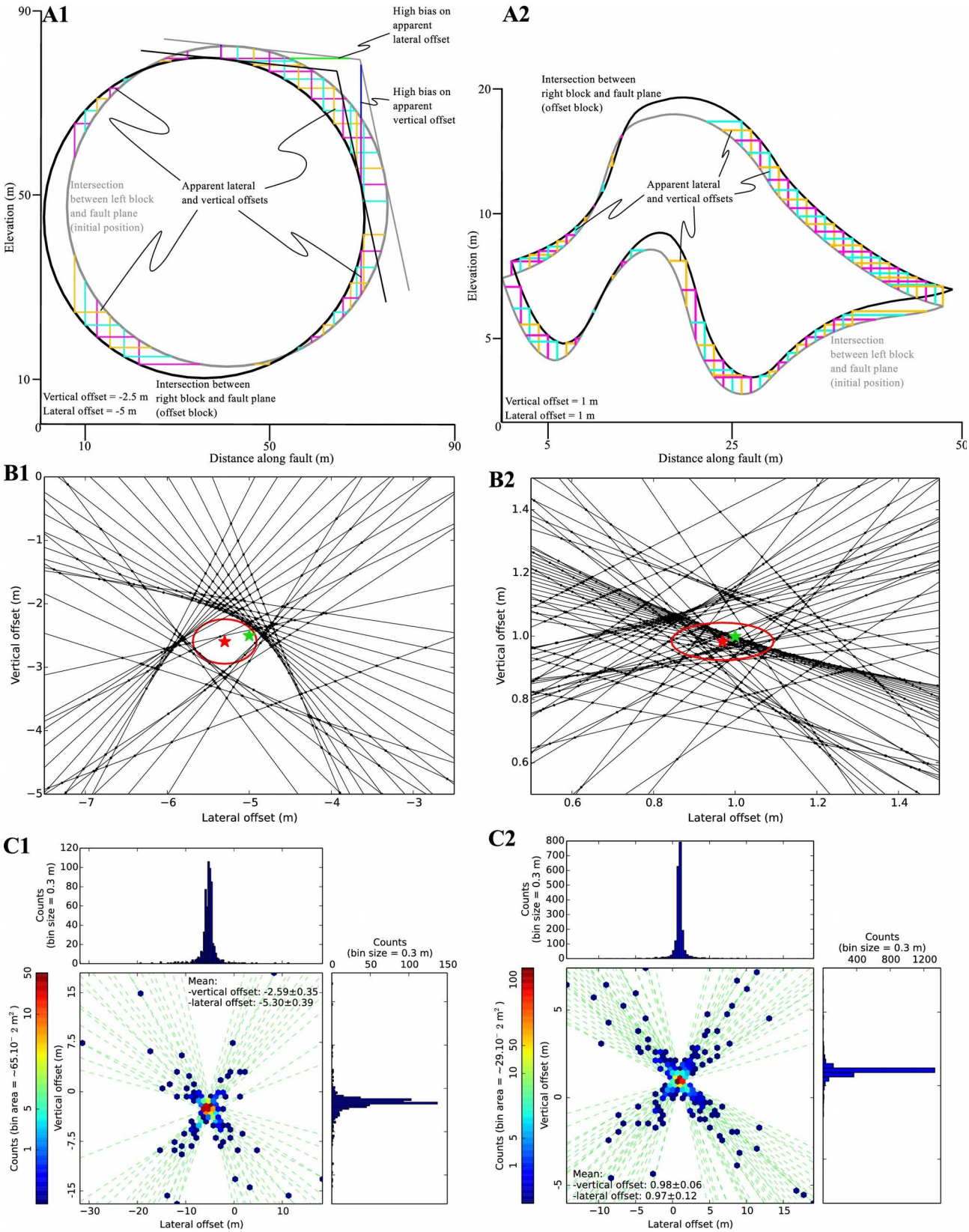
A1
High bias on apparent lateral offset
High bias on apparent vertical offset
Intersection between left block and fault plane (initial position)
Apparent lateral and vertical offsets
Intersection between right block and fault plane (offset block)
Vertical offset = -2.5 m
Lateral offset = -5 m
Elevation (m)
Distance along fault (m)
A2
Intersection between right block and fault plane (offset block)
Apparent lateral and vertical offsets
Intersection between left block and fault plane (initial position)
Vertical offset = 1 m
Lateral offset = 1 m
Elevation (m)
Distance along fault (m)
B1
Vertical offset (m)
Lateral offset (m)
B2
Vertical offset (m)
Lateral offset (m)
C1
Counts (bin size = 0.3 m)
Mean:
-vertical offset: -2.59±0.35
-lateral offset: -5.30±0.39
Counts (bin area = ~65.10⁻² m²)
Vertical offset (m)
Lateral offset (m)
C2
Counts (bin size = 0.3 m)
Mean:
-vertical offset: 0.98±0.06
-lateral offset: 0.97±0.12
Counts (bin area = ~29.10⁻² m²)
Vertical offset (m)
Lateral offset (m)

We develop a batch process in order to perform extensive offset measurements along a fault. In input, the batch process need a Digital Elevation Model (DEM) or a Digital Surface Model (DSM) and a GIS vectors for the fault trace, the contour lines and the areas of mistrust. The fault must be vectorized assuming it plunges on is right side, e.g., for a N trending E dipping fault, first vertex of the fault line must be the southern one and the last one the northern one (Fig. IV.11). Later in the process, it allows measurements of positive values for apparent right-lateral and reverse component faulting and of negative value for apparent left-lateral and normal component faulting. Areas of mistrust are zones that will not be considered during the process because they deform (or are not part of) the offset surfaces (e.g. vegetation, talwegs, roads, Fig. IV.11).

In order to well constrain the measurement of the offsets, we extract along the faults the elevation and the associated contour lines at a distance equal to the size of the diagonal of the DSM resolution. This method allows a regular lateral spacing between each contour lines and so a regular sampling of the measured apparent offsets. Indeed, using contour levels with a regular vertical spacing would imply that surfaces with high slopes would be oversampled in comparison to surfaces with lower slopes.

For every linear segments of the fault line, each contour line is cut when it cross-cut the fault (e.g. each contour lines except the 510 m one in Fig. IV.11). In the resulting contour lines, if the two longer ones are respectively on the right and left side of the fault (e.g. each contour lines except the 520 m one in Fig. IV.11), vertex are added at an interval equal to the maximum resolution (i.e. the diagonal of the pixel size of the DEM or DSM). For both contour lines each vertex is then extract and if they are not in an area of mistrust are used to interpolate a regression line intersecting the fault segment (small green dots in Fig. IV.11, note that in some case, a polynomial regression may be more relevant). Distance between the two intersections (large green dots in Fig. IV.11) gives the lateral offset, positive when it is right-lateral and negative when it is left-lateral.

From the intersection between the fault segment and the linear regression of the contour line on its left side, a segment of fixed length, normal to the fault segment, is generated on both sides of the fault in order to make topographic profiles (Fig. IV.11). Along these topographic profiles, elevation is extracted at an interval equal to the maximum resolution, except if the point is in an area of mistrust (Fig. IV.11). The two topographic profiles are then used to interpolate two regression lines intersecting the fault segment. Elevation difference between the two intersections (i.e. the intercept of both regression lines, large blue dots in Fig. IV.11) gives the vertical offset, positive and negative for reverse and normal faulting, respectively.

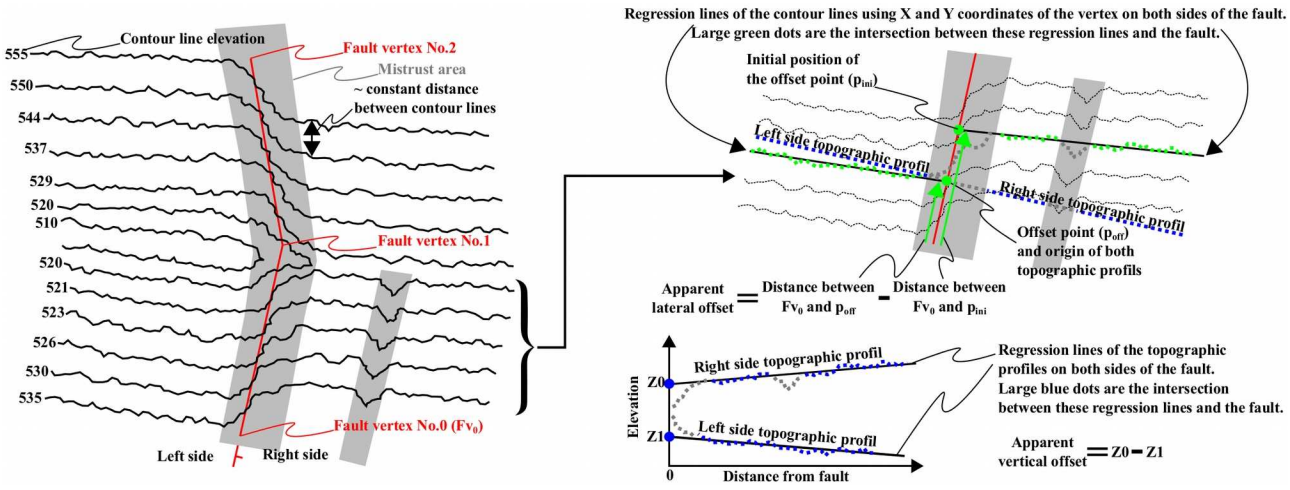

Figure IV.11: Apparent lateral and vertical offset measurement method. See text for further details.

At the end of this first step of the process, we obtain for each offset point an apparent vertical and an apparent lateral offset and so we can compute the associated linear equation IV.7 (Fig. IV.10B and C). We compute the solution for each pair of linear equations which yield a dataset of offsets (assuming they all have a different slope, n linear equations give $n\times(n-1)/2$ offsets). We remove from this dataset the percentile outliers using the Mahalanobis distance (calculated according to Gallego et al., 2013). This step is necessary when the method is applied on a natural topography because noise and uncertainty can generate nearly co-linear equations whose solution corresponds to very large offsets, over 10^9 m and far away from the mean value of the distribution. The problem is that these outliers are not necessary symmetric on both sides of the mean and have a strong influence on it. We so remove these outliers and then compute the mean of the measured fault offsets dataset which is the real fault offset. The standard error of the mean at a chosen confidence level is finally computed to obtain uncertainty on the measured fault offset (Fig. IV.10B and C).

IV.5.3.3 - Test of the SSV method on a constrained surface rupture

In order to perform a first test of the reliability of the SSV method, we apply it to determine the coseismic slip along one fault segment of the eastern California shear zone related to the Mw 7.1 Hector Mine earthquake (16 October 1999). This fault segment presents several advantages to test the SSV method. First, high resolution topographic data (airborne lidar) are freely available (http://www.opentopography.org). Second, because it is a recent coseismic slip, surfaces

used in the method would be slightly eroded since their offset. Third, two studies performed in the chose area constrained coseismic fault slip using different methods. Hudnut et al. (2002) measured it using the method proposed by Peltzer et al. (1988) which consists to project the topography along two profiles (location on fig. IV.12) on both sides of the fault and to realign then the recognized piercing points. They measured a 4.2 ± 0.5 m right-lateral slip and 0.9 ± 0.1 m vertical slip (uplift of northeastern side). Chen et al. (2015) performed measurements (Fig. IV.12) of laterally offset morphologic features and constrained vertical offsets using topographic Swath profiles (which implies that they are mostly apparent offsets). They measured a 3.55 ± 1.15 m mean right-lateral slip and -0.4 ± 0.3 m mean vertical slip (subsidence of the southwestern side).

We apply the SSV method along the surface rupture at two locality where we identify sufficiently homogeneous surfaces and use both to compute the fault slip (Fig. IV.12). We digitize fault from north to south which implies that soutwestern side is its right side (here the fault is near vertical). We exclude from the analysis the areas close to the faults which display contour level deflections and areas affected by stream erosion (Fig. IV.12). We measured 73 apparent vertical and lateral offsets. By computing each possible solutions and after removing the percentile outliers values, this apparent offset dataset allows the determination of 2531 offset measurements yielding a 3.73 ± 0.82 m mean right-lateral slip and -1.08 ± 0.07 m mean vertical slip (subsidence of the southwestern side).

We see here that the SSV method allows the determination of the right fault kinematics (right-lateral strike-slip indicated by a positive lateral offset value and subsidence of the southwestern side indicated by a negative vertical offset value) and provides lateral and vertical offset consistent with those measured using other methods considering uncertainties (it is worth recalling that vertical offset measured by Chen et al. (2015) are apparent).

IV.5.3.4 - Application

We apply the SSV method on the part of the faults No. 2 and No. 3 where we identify sufficiently homogeneous surfaces on both sides of the faults (Fig. IV.13). We exclude from the analysis the areas close to the faults which display contour level deflections, areas affected by stream erosion and vegetation. Topographic profiles constraining the apparent vertical offsets are extracted along the longest possible distance (more than 70 m except for the topographic profiles on the left side of fault No. 2 which are extracted over ~30 m).

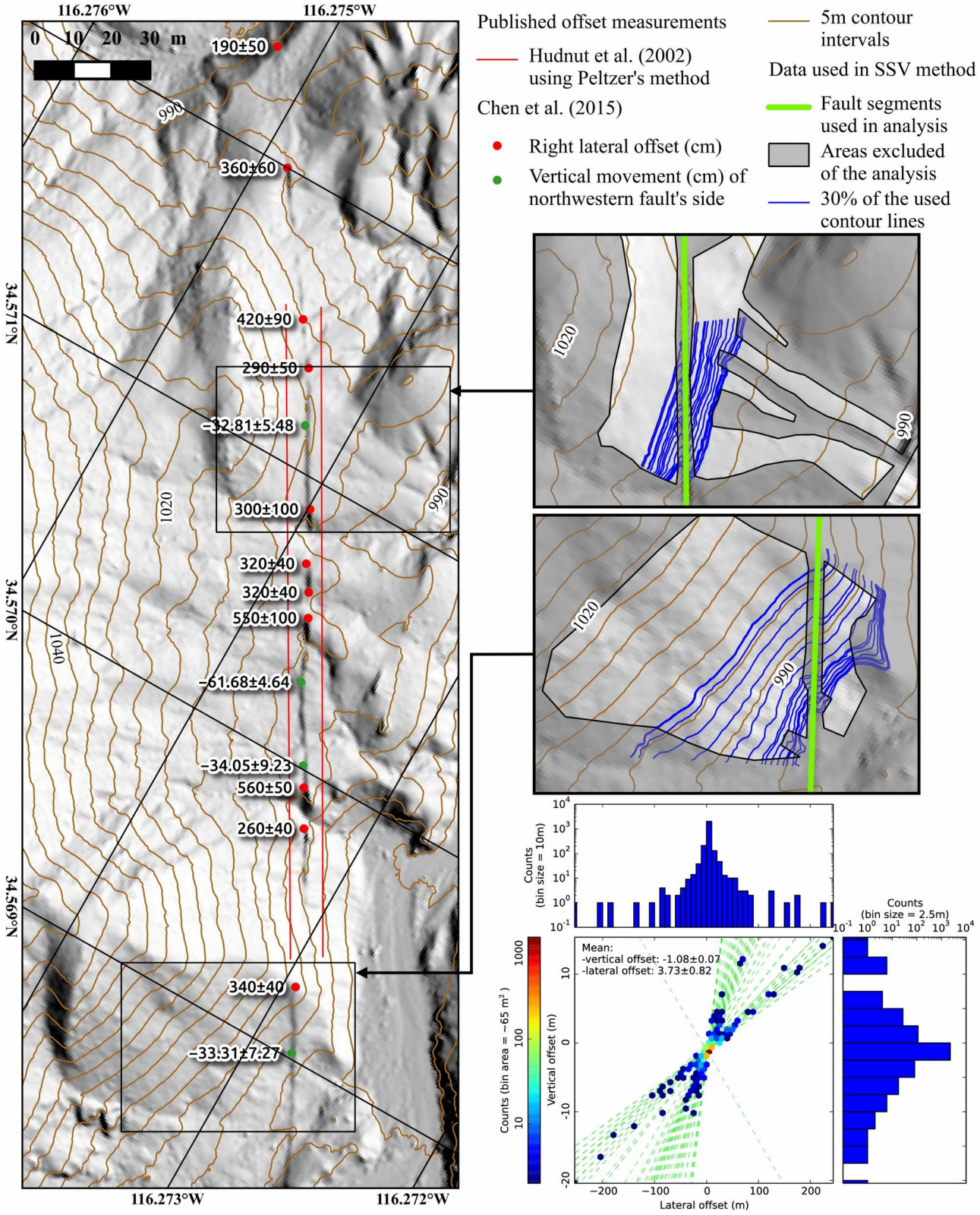

Figure IV.12: Shaded DEM, location of topographic profiles (Hudnut et al., 2002), measurements of offset topographic features (Chen et al., 2015) and surfaces on which we applied the SSV method along a part of the Hector Mine earthquake coseismic rupture. 1D and 2D histograms display results of the SSV method (uncertainty at a 99% confidence interval). Same legend as Fig. IV.10C. Counts axes of 1D histograms in logarithmic scale.

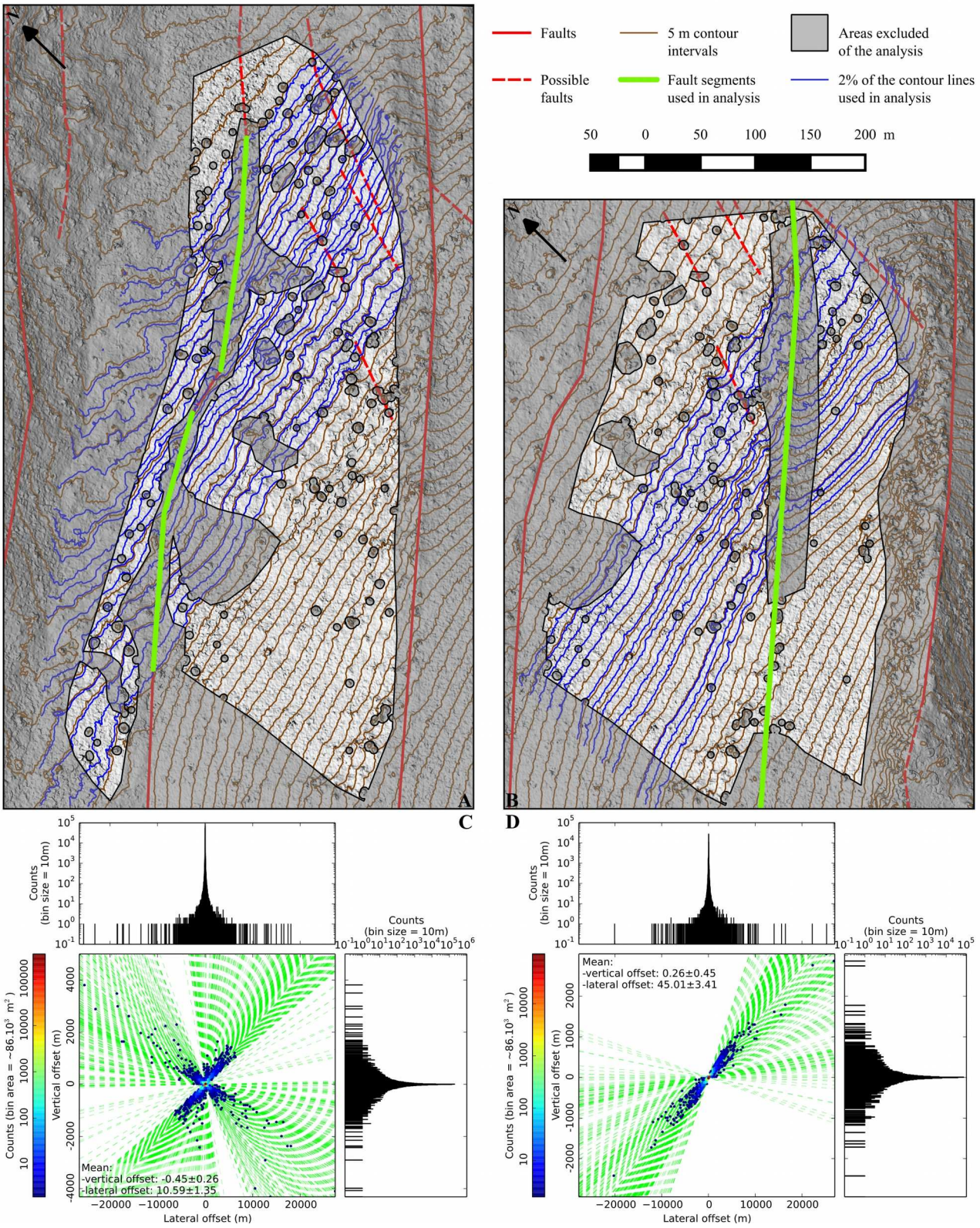

Figure IV.13: SSV method analysis applied on faults No.2 and No.3. A) and B) display the input parameters for faults No.2 and No.3 respectively (location on Fig. IV.3). DSM displayed in shaded version for readability. C) and D): results of the SSV method analysis for faults No.2 and No.3 respectively. Uncertainty given at a 99.99% confidence interval. Same legend as Fig. IV.10C. Counts axes of 1D histograms in logarithmic scale.

We measured 891 apparent vertical and lateral offsets for the fault No.2 and 511 for the fault No.3. By computing each possible solutions and after removing the percentile outliers values, these apparent offset datasets allow the determination of 395390 and 129651 offset measurements for fault No.2 and 3 respectively on which means are computed. Results show that both faults are right-lateral strike slip faults. Lateral offsets are 10.59±1.35 meters and 45.01±3.41 meters and vertical offsets are -0.45±0.26 meters and 0.26±0.45 meters for the faults No. 2 and No. 3, respectively (Fig. IV.13).

IV.6 - Fault geometry, slip rate and seimogenic potential

Fault offsets being constrained, we try to determine thereafter the seimogenic potential of the Jasneuf fault.

Fault segment No. 3 is 6 km long. However, we can not ascertain it is not longer because fault trace is not expressed in the marly border domain of the plateau. A seismic profile (AU9A) was acquired along the south-western limit of the Glandasse plateau (Fig. IV.14, location on Fig. IV.1). On this seismic profile, only one clear seismic reflector can be observed between 4500 s and 4000 s (Two-Way Time). To the west, another seismic profile (81SE2A, location on Fig. IV.1) also provides evidences for a seismic reflector at the same Two-Way Time interpreted as the top of the basement (Rangin et al., 2011b). Despite the low quality of the AU9A seismic profile, the Jasneuf fault does not seem to cut the basement. For the Jasneuf fault area, height of the plateau is of about 1600 m and top of the basement is at ~7 km depth south-westward and ~6 km depth north-eastward (Le Pichon et al., 2011). Fault segment No. 3 dip of 86° SE. It implies that fault surface is of about 48.7 km².

No datable geological nor geomorphic features has been observed during field surveys. Indeed, there is no deposit associated to the talwegs and fault planes display lapiaz like forms, which indicates significant erosion and makes exposure dating uncertain. However, according to the right-lateral offset of the southern limit of the lower Barremian detrital limestone, total offset of the Jasneuf fault is of about 3 km (Arnaud, 1981; Robert, 1976). Assuming an ongoing of the deformation between Burdigalian and Serravalian (Beck et al., 1998; Bellahsen et al., 2012), long term fault slip rate ranges between 0.15 and 0.26 $mm.yr^{-1}$.

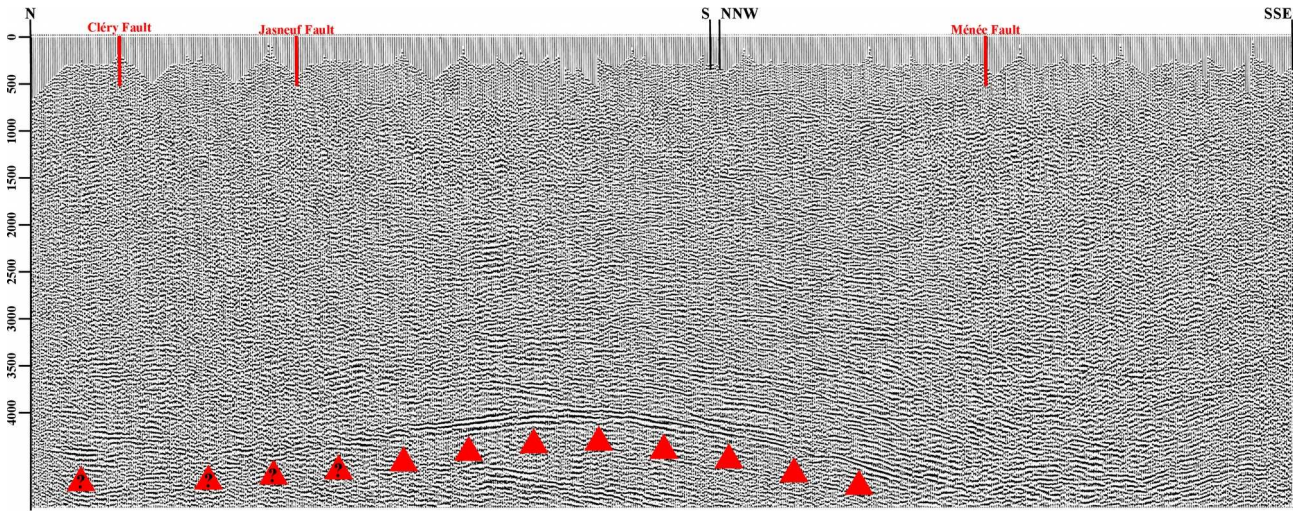

Figure IV.14: 23.5 first km from North of the AU9A seismic profile (location in Fig. IV.1). Red triangles underlines top of the basement.

Moreover, the total offset of the cliffs is larger than the offset of the talwegs along the fault No. 1 and of the topographic surface along the fault No. 2 and 3. It implies that the cliffs are older than the plateau morphology and have recorded fault slip over a longer time span. Assuming a constant fault slip rate, the ratio of the offset of both morphologies is equal to the ratio of their ages ($Offset_{cliffs}/Offset_{plateau\ morphology}=Age_{cliffs}/Age_{plateau\ morphology}$). Because the fault offset determination along the fault segment No. 4 is not constrained we avoid the comparison between the offsets of the cliffs on both sides of the faults No. 3 and 4. Thus, we will only consider fault segments No. 1 and No. 2 thereafter. For both faults, offsets of the older and younger morphologies are of 235±30 m and 27.5±4.2 m respectively and the ratio between the offset values is equal to 8.56±2.41. We assume that both morphologies are inherited from more erosive time and so related to interstadial stages (ages from Lisiecki and Raymo, 2005) or to the Messinian salinity crisis (age from Gautier et al., 1994); indeed, formation of the cliffs can be related to the Drôme incision which displays a Messinian canyon in its downstream part (Bodelle and Goguel, 1980). Ratios $Age_{cliffs}/Age_{plateau\ morphology}$ include in the 8.56±2.41 interval are found assuming the age pairs presented in Tab. IV.2.

Using the difference of fault slip rate calculated for both morphologies of different ages as a confidence factor, the best solution is for a formation of the cliff related to the Messinian salinity crisis and for a formation of the morphology of the plateau after the MIS 22, 16 or 14 (Tab. IV.2). Unlike other areas in the western Alps, Rissian and Würmian glacier were not present in this area (Buoncristiani and Campy, 2011). Therefore, we assume that in the study area, the morphologies within the plateau were not rejuvenated during this period. Moreover, fault slip rate calculated from the cliff offsets, assuming they are Messinian in age, is of 0.13±0.03 $mm.yr^{-1}$. It is of the same order

than the long term (since Burdigalian-Serravalian) slip rate calculated from the offset of the southern limit of the lower Barremian detrital limestone.

Age of the cliffs	**Age of the plateau morphology**	**Absolute difference between cumulative slip rates for both age of faults No.1 and N0.2**	**Cumulative slip rate of all faults according with cliffs offsets**	**M5.7 recurrence interval calculated from Wells and Coppersmith's laws**
~5.6 ± 0.3 Ma Messinian salinity crisis	0.86 Ma MIS 22 Termination Post Gunz Glaciation	1.10^{-2} mm.yr^{-1}	0.13±0.03 mm.yr^{-1}	507^{+113}_{-78} yr
	0.621 Ma Termination VII MIS 16 Termination	2.10^{-3} mm.yr^{-1}		
	0.533 Ma Termination VI MIS 14 Termination	1.10^{-2} mm.yr^{-1}		
0.86 Ma MIS 22 Termination Post Gunz Glaciation	0.13 Ma Termination II Post Riss Glaciation	6.10^{-2} mm.yr^{-1}	0.8±0.2 mm.yr^{-1}	77^{+12}_{-8} yr
0.13 Ma Termination II Post Riss Glaciation	0.014 Ma Termination I Post Würn Glaciation	15.10^{-2} mm.yr^{-1}	5.5±0.8 mm.yr^{-1}	12^{+2}_{-2} yr

Table IV.2: Possible ages of the morphological markers, slip rates and M5.7 recurrence interval assuming a constant fault slip rate since the ongoing of the offset of the cliffs.

Using the Wells and Coppersmith's scale laws (1994), assuming a 48.7 km² fault plane and a 0.13±0.03 mm.yr^{-1} fault slip rate, we calculate that the Jasneuf fault could potentially generate an earthquake of Mw 5.7 with recurrence interval of about 500 years. Note that because we used the cliff offset values to calculate fault slip rate, we did not take into account the vertical component of the movement which implies that the calculated recurrence interval could be slightly lower. However, as proposed by Gratier et al. (2013) for the Clery fault, a large part of the deformation could be accommodated by pressure solution creeping in the underlying marls which could imply a partially (or complet) aseismic fault behavior and explain the gap of seismic activity along these faults.

IV.7 - Discussion

IV.7.1 - Impact of the geometry of the stream network on recursive stream offset measurements

We measured talweg offsets along fault No. 1. by manually reconstructing offset and realigning talwegs on both sides of the faults, we first found two characteristic offset values close to 17 and 77 meters. These values where both found again during recursive measurements of talweg offsets along with other characteristic offset values displaying a periodical signal (every ~100 meters between offset values of 120 to 520 meters, Fig. IV.7B). However, it appears that offset values generating this signal, as well as the highest density increase associated to the 77 meters apparent offset, correspond in fact to a characteristic spacing distance between talwegs (Fig. IV.7C). A such statement could appear trivial, but we present thereafter examples where offset values correspond to characteristic spacing and for different offset order (kilometer to decameter).

In situations where morphological markers are not well preserved, recursive offset measurements are useful in order to find statistically significant offset values. For example, Replumaz et al. (2001) tried to constrain long term offset of the Red River fault by using an equivalent method consisting in measuring the distance between an upstream channel and the closest downstream channel at different increment of removal of the fault offset. Then, they computed the root mean square (RMS) of the distance values for each iteration (Fig. IV.15A1). A decrease of their RMS is equivalent to an increase of the probability density using our method (Fig. IV.15A1 and B1). However, these values are also found by measuring the distance between each upstream talwegs (Fig. IV.15C1). By removing these distances from the offset values dataset (Fig. IV.15C1), it appears that no offset value is more significant than another, all displaying closed probability density. The 25 km offset initially proposed as significant because showing the lowest RMS values is so finally not significant. Replumaz et al. (2001) noted the periodical signal of their RMS and proposed it was related to the stream spacing but they limit their control to interfluve distances.

Figure IV.15: Stream offset measurements along the Red River fault (Replumaz et al., 2001), the Middle Durance fault (Peulvast et al., 1999) and the Kunlun fault (Klinger et al., 2011) compared to characteristic stream spacing.►

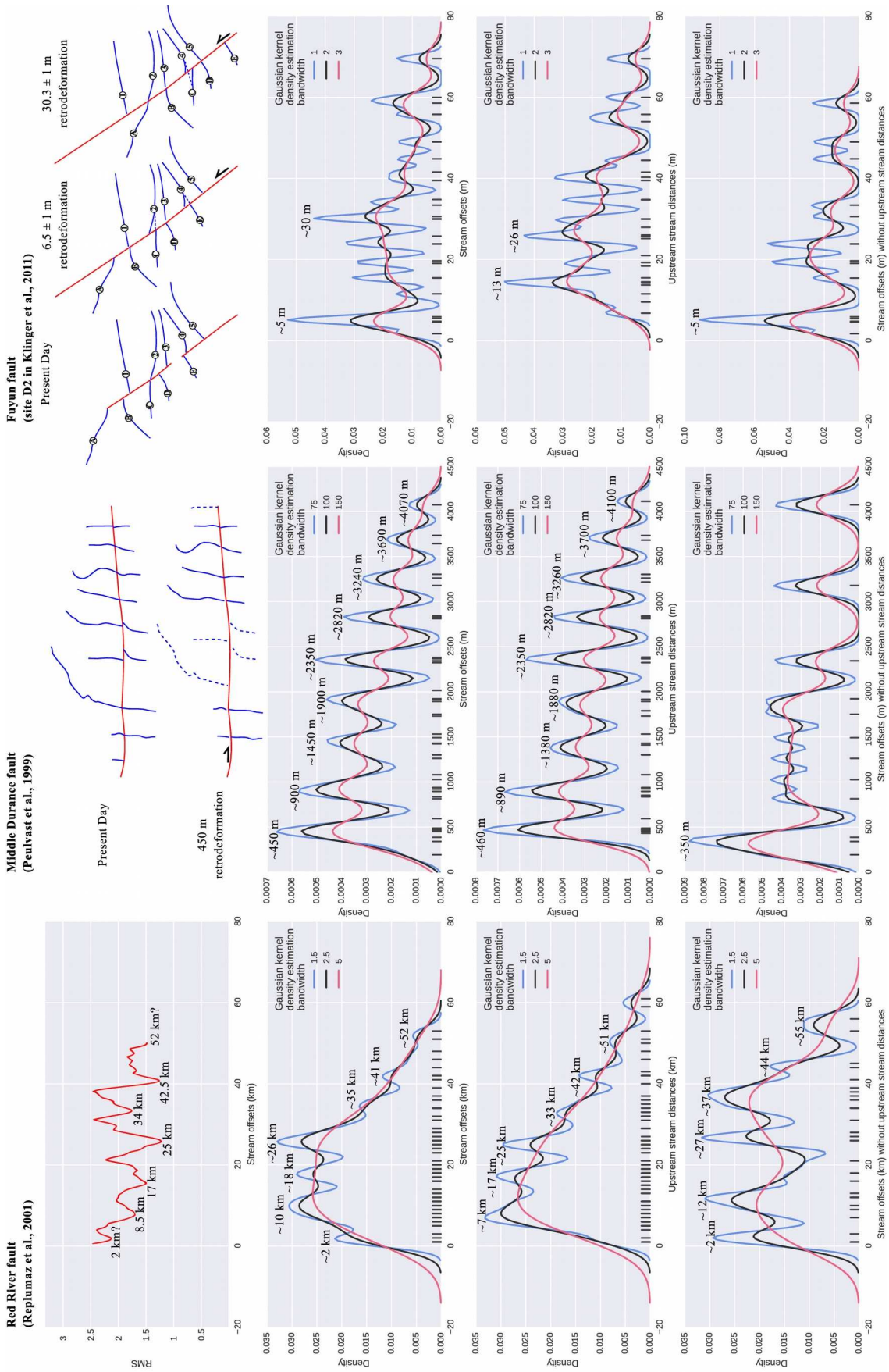
Red River fault
(Replumaz et al., 2001)
Middle Durance fault
(Peulvast et al., 1999)
Fuyun fault
(site D2 in Klinger et al., 2011)
Present Day
6.5 ± 1 m
retrodeformation
30.3 ± 1 m
retrodeformation
450 m
retrodeformation
Original measurements
RMS
2 km?
8.5 km
17 km
25 km
34 km
42.5 km
52 km?
Distance between each downstream and upstream streams along the fault
Spacing between each upstream streams
Distance between each downstream and upstream streams not corresponding to a spacing distance
Gaussian kernel density estimation bandwidth
Density
Stream offsets (km)
Stream offsets (m)
Upstream stream distances (km)
Upstream stream distances (m)
Stream offsets (km) without upstream stream distances
Stream offsets (m) without upstream stream distances

The same problem could occur even when no recursive measurement is performed or in the case of well expressed stream offset. Peulvast et al. (1999) proposed a possible 450 m offset of the stream along the Moyenne Durance fault, a value that we found by making the systematic measurement of possible offset values. After comparing the offset values with the stream spacing, it appears that no offset values can not be explain by the measurements of the spacing (350m peak is only composed of two offset). Klinger et al. (2011) present a stream offset measurements site (D2 site of their study) where they identify two characteristic offset values of 6.5±1 m and 30.3±1 m (Fig. IV.15A2). By the systematic measurement of possible offset values like previously, we find the closed characteristic offset values (Fig. IV.15B2). Nevertheless, after comparing the offset values with the stream spacing (Fig. IV.15C2), it appears that only the 6.5 m offset correspond only to a faulting displacement (Fig. IV.15D2).

It appears that measurements of fault offset using stream networks must be constrained by the analysis of the spacing between the whole stream sets and not limited to an interfluve distance, especially when measured offset is higher than the mean interfluve distance and when no genetic relation between the streams (e.g. according to the morphology of the stream like Zielke et al. (2010)) on both sides of the fault can be established. It does not necessary means that measured offset are wrong and stream can be offset of one spacing distance (Gaudemer et al., 1989) but it is a fact that must be argue.

IV.7.2 - Reliability of the SSV method

We used the SSV method along the fault No. 2 and 3 to quantify the fault offset. The method works well on the synthetic test models and the test performed on the coseismic rupture of the Hector Mine earthquake, allowing finding the right fault kinematics and offset (Fig. IV.10), but has several limitations when applied in natural conditions. The first one is that resolution of the topographic data, as in every geomorphic analysis, must be sufficient to measure the offset. Second, the surfaces on both sides of the fault must be sufficiently extensive and unaltered in order to perform significant linear or polynomial regression of the topographic profiles and contour lines. Third, the fault should not be normal to the topographic slope (i.e. the fault strike has to be oblique to the higher slope line), because in this situation we can only constrain an apparent vertical offset. Nevertheless, tilting the topography before using the SSV method could be a solution to counter this limitation. Fourth, we assume that no significant relative rotation has occurred between blocks on both sides of the faults, otherwise the mean will be poorly constrained. Finally, we must assume that erosion rates are the same on both sides of the faults or that the difference is insignificant (considering the time span), otherwise apparent offset measurement will not be reliable.

All these conditions are fulfilled for faults No. 2 and 3: we used a sub-metric resolution DSM, most of the topographic interpolations are made on a distance higher than 70 m (except for topographic profiles of the left side of fault No. 2 made mainly on a distance of 30 m), faults are not normal to the slope, there is no clue of rotation at the scale of the scarps and limestones are sub-outcropping over the whole area suggesting a homogeneous ground and consequently a homogeneous weathering rate over the analyzed area. Unfortunately, we can not apply the SSV method on fault No. 1 which does not display sufficient unaltered surfaces and on fault No. 4 which does not display sufficiently extensive offset surfaces (a large part being cover by vegetation).

The SSV method allows determining a right-lateral strike-slip kinematics along faults No. 2 and 3. The last tectonics regime recorded in the area is strike-slip with an ENE trending σ_1 axis (Fig. IV.2) and at the north-eastern end of the Jasneuf fault, the Belledonne Border fault kinematics, is testified by strike-slip focal mechanisms (Fig. IV.1) in agreement with our fault kinematics analysis (Billant et al., 2015). Both observations are consistent with a right-lateral strike-slip kinematics for the Jasneuf fault and with the right-lateral offset of both the border plateau cliffs (Fig. IV.4) and the streams along fault No.1 (Fig. IV.6) as well as with the southern limit of the lower Barremian detrital limestone apparent displacement.

It is difficult to assess the reliability of the offset values. However, we can compute the ratio between the offsets of the morphological features of the plateau and the offsets of the cliffs. Assuming a constant fault slip repartition between the faults since the onset of the offset of the cliff, these ratios would be equal for fault No. 1 and 2 and higher than the ratios between the offsets of the cliff by faults No. 3 and 4 and the topographic offsets measured for the fault No. 3. These ratios are 0.12±0.04 for fault No. 1, 0.11±0.03 for fault No. 2 and 0.09±0.01 for faults No. 3 and 4. This tends to confirm that offsets measured using the SSV method are trustworthy.

For the synthetic test models, uncertainties for both vertical and lateral offsets are of the same order (Fig. IV.10) whereas when applied on natural faults, uncertainties on lateral offsets are higher than uncertainties on vertical offsets (Figs. IV.12 and IV.13). This difference is due to the fact that for the synthetic test models, we make measurements on surfaces displaying a larger slope range than along the faults (Fig. IV.13A and B). It leads in this case to minimize the dispersion of the vertical offset measurements (Fig. IV.13C and D), so, the maximum uncertainty should be considered for the two offset directions.

Finally, the robustness of the SSV method needs to be tested in other situations and contexts. It is difficult to test its robustness in an area where long term fault offsets are constrained

using erosive geomorphic features like talwegs because in order to allow a meaningful comparison, the topographic surface used by the SSV method has to be of the same age as the stream network. Ideal cases are fresh coseismic rupture, where erosion not has time to strongly affect the morphology and several feature offsets (including anthropologic ones) can be used to compare with results provided by the SSV method.

IV.7.3 - Reliability on the determination of the seismogenic potential of the Jasneuf fault

Using Wells and Coppersmith's scale laws (1994), we proposed that the Jasneuf fault could generate earthquakes with a Mw 5.7 with a recurrence interval of about 500 years. However, assuming reliable fault offset measurements, there are still several sources of uncertainties related to the seismogenic potential of the Jasneuf fault, including a potential aseismic behaviour.

First, because of the lack of dated morphological features, fault slip rates are poorly constrained. However, thanks to the difference between the offsets of the plateau border cliffs and offsets of the morphological features on the plateau, we see that assuming a constant fault slip rate it is likely that the cliffs were formed during the Drôme incision in response to the base level fall caused by the Messinian salinity crisis. An alternative hypothesis could be that cliffs are younger than Gunz (Tab. IV.2). However, the Drôme valley displays its highest terrace at 130 m above the present day Drôme river (Chenevoy et al., 1976; Flandrin et al., 1974) which would be 0.7-1.2 Ma in age (Brocard, 2002). It implies that the Drôme valley was already formed during Gunz and it tends to confirm a Messinian age for the cliffs and a fault slip rate of 0.13±0.03 $mm.yr^{-1}$. Moreover, this slip rate is of the same order than the one calculated from the offset of the southern limit of the lower Barremian detrital limestone (since Burdigalian-Serravalian) and consistent with the present day strain rates proposed thanks to GPS measurements and seismicity (Delacou et al., 2008; Sue et al., 2007a).

Second, on the seismic profile, basement does not seem offset by the Cléry and Jasneuf faults. Moreover, whereas the Ménée and Isère faults (location in Fig. IV.1) display a thickening of the Cretaceous series on their south-eastern edge interpreted as depocenters related to normal crustal faults taking root in the basement, the Cléry and Jasneuf faults are not associated with such deposits thickening (Arnaud, 1981). On the other hand, the Cléry and Jasneuf faults show the same strike as the crustal faults in the surrounding area (Alps and Massif Central), which is inherited from the hercynian crustal fault emplacement. Moreover, although not well constrained, hypocenter depths of the strongest earthquakes at the north-eastern termination of the Cléry and Jasneuf faults are ranged between 12 and 24 km (Fig. IV.1, Cara et al., 2015), suggesting that these events

occurred in the basement, the upper crust reaching a 27-28 km depth. In such case, seismic fault could potentially reach this depth. We can also suspect that Cléry and Jasneuf faults extent north-eastward and south-eastward of the Vercors plateau. A such geometry would imply possible stronger earthquakes.

IV.8 - Conclusion

The Clery and Jasneuf faults are the south-western prolongation of the Belledonne border fault. We argue trough fault kinematics analysis and stress state inversion that these faults were under a strike-slip tectonic regime during Neogene and Quaternary, both implying right-lateral kinematics along them. The former strike-slip tectonic regime was characterized by an ESE trending σ_1 axis and is related to the Subalpine Massifs formation. The latter is characterized by an ENE trending σ_1 axis. It is similar to the post-Messinian tectonic regime and consistent with the focal mechanisms along the Belledonne border fault.

The Jasneuf fault zone, composed of four major segments, displays numerous fault scarps that we interpret as related to recent faulting. The stream network analysis along one of the segments allows us to show that misinterpretation can be done when measuring stream offsets. We demonstrate that it is possible to measure an offset which only correspond to a mean distance between the talweg. According to this, it is a necessary check that must be done when fault offsets are measured using stream offsets especially when deduced fault offset exceed the mean interfluve distance and when no genetic relation can be done between upstream and downstream streams. Indeed, this test allows the discrimination between the apparent offsets and the true offsets corresponding to displacement. By applying this test on our dataset of measured offsets, we have ascertained that the streams along the analysed fault segment display a 16.9±2.9 m right-lateral offset.

The SSV method allows determining offsets along two fault segments (10.59±1.35 m and 45.01±3.41 m right-lateral offsets) which do not display any morphological marker offset except the topography itself. The robustness of the method need to be further tested, but our measurements are in good agreement with long term morphological offsets (cliffs). It is a promising method which could find applications in other Earth Sciences fields (e.g., submarine geomorphology or structural geology).

According to the 715±45 m offset of the cliffs bordering the Vercors plateau and assuming these cliffs are related to the Messinian salinity crisis incision, we calculate a Messinian to present

day Jasneuf fault slip rate of 0.13±0.03 mm.yr^{-1}. The Jasneuf fault does not seem to root in the basement and we can not ascertain its extension beyond both sides of the plateau. If the fault plane does not extend over these limits, the fault could generate earthquakes of a 5.7 Moment Magnitude with recurrence interval of about 500 years. However, the geometry of the fault is poorly constrained and we can not exclude that the fault could generate stronger earthquakes. In return, because of the mostly marly sedimentary cover, a large part of the deformation could be accommodated by aseismic creeping.

Acknowledgements

Jeremy Billant benefits of a PhD allocation granted by EDF (Electricité De France) through the SIGMA research program (SeIsmic Ground Motion Assessment). This work is also a contribution to the Labex OT-Med (n ANR-11-LABX-0061) funded by the French Government «Investissements d'Avenir» program of the French National Research Agency (ANR) through the A*MIDEX project (n ANR-11-IDEX-0001-02). We acknowledge K. Manchuel, Ch. Durouchoux, F. Hollender, N. Espurt, L. Bollinger for discussions. We acknowledge the IGN (Institut national de l'information géographique et forestière) for providing geodata (BD TOPO®). Use of the seismic profile with the kind permission of VERMILLON REP, *November 2013*.

V - POST-MESSINIAN FAULTING ASSESSMENT FROM SALINITY CRISIS GEOMORPHIC MARKERS: THE EXAMPLE OF TOULAUD (RHÔNE-ALPES, FRANCE)

Un des objectifs de ce travail est d'étudier la possible relation du système de faille de Belledonne avec le système de faille des Cévennes. Des travaux préliminaires, engagés durant le stage de recherche de Master 2 de Sébastien Baixas, nous ont permis de remarquer certaines anomalies morphologiques possiblement liées à un jeu récent de l'accident tardi-hercynien orienté NE-SW que nous appellerons faille de Toulaud dans ce manuscrit.

Cette faille serait le prolongement d'une faille de socle affectant le Massif Central, au sud-ouest de Valence. L'analyse de la déformation récente intégrée sur le Plio-Quaternaire de cet accident de socle a été facilité du fait qu'il recoupe le canyon Messinien du Rhône dont le lit se trouvait ici plus à l'Ouest du cours actuel.

Les cinématiques de failles observées dans le socle, le Trias et le Pliocène supérieur et les états de contrainte déduits de nos mesures indiquent un régime tectonique récent en décrochement, caractérisé par un axe σ_1 orienté WNW-ESE. Ce régime est compatible avec une cinématique en décrochement dextre du Miocène au Pliocene supérieur le long de la faille de Toulaud. Un autre site d'observations dans le Pliocene supérieur nous a permis de définir un régime de déformation en décrochement caractérisé par un axe σ_1 orienté ENE-WSW suggérant toujours un glissement dextre de la faille de Toulaud, mais probablement accompagné d'une composante normale plus importante.

Une analyse morphologique, bénéficiant ici aussi de la création d'un modèle numérique de surface à haute résolution par photogrammétrie, a été réalisée durant le stage de Master 2 de Franck Thomas. Des prospections géophysiques (H/V et tomographie électrique) ont été engagées en vue d'imager la géométrie du canyon en profondeur et d'en déduire d'éventuelles anomalies morphologiques pouvant être attribuées à de la déformation plio-quaternaire.

POST-MESSINIAN FAULTING ASSESSMENT FROM SALINITY CRISIS GEOMORPHIC MARKERS: THE EXAMPLE OF TOULAUD (RHÔNE-ALPES, FRANCE)

Billant Jérémy[a], Thomas Franck[a], Bellier Olivier[a], Dusouillez Philippe[a]

[a] Aix-Marseille Université, CNRS, IRD, CEREGE UM34, 13545 Aix-en-Provence, France

V.1 - Introduction

Although continental interiors are generally characterized by low strain rates, they can be struck by destructive earthquakes (e.g., the 1356 Basel Earthquake, Switzerland (Fäh et al., 2009) or the 1811-1812 New Madrid earthquakes, United States (Tuttle et al., 2002). A direct consequence of these low strain rates is that the recurrence intervals between destructive earthquakes can reach up to several millennia and thus historical seismicity can not document an entire earthquake cycle. On a global scale, France is a relatively quiet country in terms of seismicity, with very few major historical earthquakes ($M_W > 5$) because faulting is characterized by very low slip rate. However, on a national scale, some territories and regions are subject to substantial seismic activity. In particular, the South Eastern quarter, including Provence and the Rhône valley, has a non-negligible historic and instrumental earthquake record.

This study aims at understanding and evaluating the recent (post-Messinian, last 5.3 Ma) tectonic activity of the Toulaud fault, located in the vicinity of Valence and northeastern termination of the Cévennes fault system, thus providing information on the seismic hazard in a densely populated region.

The slow fault slip rate (between 0.1 and 0.01 $mm.yr^{-1}$ e.g., Chardon and Bellier, 2003; Chardon et al., 2005; Hippolyte and Dumont, 2000; Schlupp et al., 2001)) and high regional erosion rate (close to 0.02 $mm.yr^{-1}$ (Siame et al., 2004)) prevailing in the area do not favor the preservation of offset morphological features testifying for active faulting and so limit the classical morphotectonic analysis. A multidisciplinary approach (geomorphic, tectonics, faults kinematics and geophysics) is needed in order to constrain fault geometry and kinematics and to find possible offsets of inherited morphologies for characterized active faulting (e.g., Baize et al., 2011; Baroux, 2000; Cushing et al., 2008).

V.2 - Geological framework

The city of Toulaud is located on the Eastern edge of the Massif Central, 5 kilometers South-West of the city of Valence and the Rhône river (Fig. V.1). Toulaud lies in a N trending and relatively narrow valley (ranging from 1 km at its narrowest in the Toulaud area up to more than 2 km). The flanks of the Toulaud valley are composed of Paleozoic basement and its Mesozoic sedimentary cover (Fig. V.1) (Bornand et al., 1974). The Toulaud valley is cross-cut by the near vertical N062°E trending Toulaud fault (Fig. V.1) (Mandier, 1974) which is a late Hercynian strike-slip fault (Arthaud and Matte, 1975).

The Toulaud valley is separated of the Valence basin by the Crussol hill displaying a near linear N trending cliff as its eastern edge (Fig. V.1). Normal faults in the Crussol hill also show N trends (Bornand et al., 1974) as other normal faults bordering the Valence trough to the west (Blés et al., 1989; Germain and Demaison, 1958). These normal faults are the western limit of an Oligocene graben (Blés et al., 1989; Busson et al., 1992). The Miocene sea reached the western border of the Crussols hills during the lower Helvetian as attested by the transgressive marine molasse attributed to this age (Debelmas and Demarcq, 1980; Demarcq, 1960a; Germain and Demaison, 1958). Slightly southward of the Toulaud valley, the top of the Helvetian marine molasse reaches an elevation of ~300 m. They were covered by at least 90 m thick Tortonian continental deposits (Chenevoy et al., 1976).

In the context of the Africa-Europe tectonic plate convergence, the Mediterranean sea got separated from the world ocean ~6 My ago (Gautier et al., 1994; Hsü et al., 1973; Krijgsman et al., 1999) following the closure of straits linking it to the Atlantic ocean (Denizot, 1952; Hsü et al., 1977; Krijgsman et al., 1999). The combination of arid climate and sparse precipitations triggered a major Mediterranean sea level drop in what had become a deep dessicated bassin (Hsü et al., 1973). This event is called the Messinian Salinity Crisis (MSC) (e.g., Clauzon et al., 1996; Hsü et al., 1977; Krijgsman et al., 1999). This crisis ended around 5.32 My ago (Gautier et al., 1994; Hilgen and Langereis, 1993) when the Atlantic ocean and the Mediterranean sea were connected again.

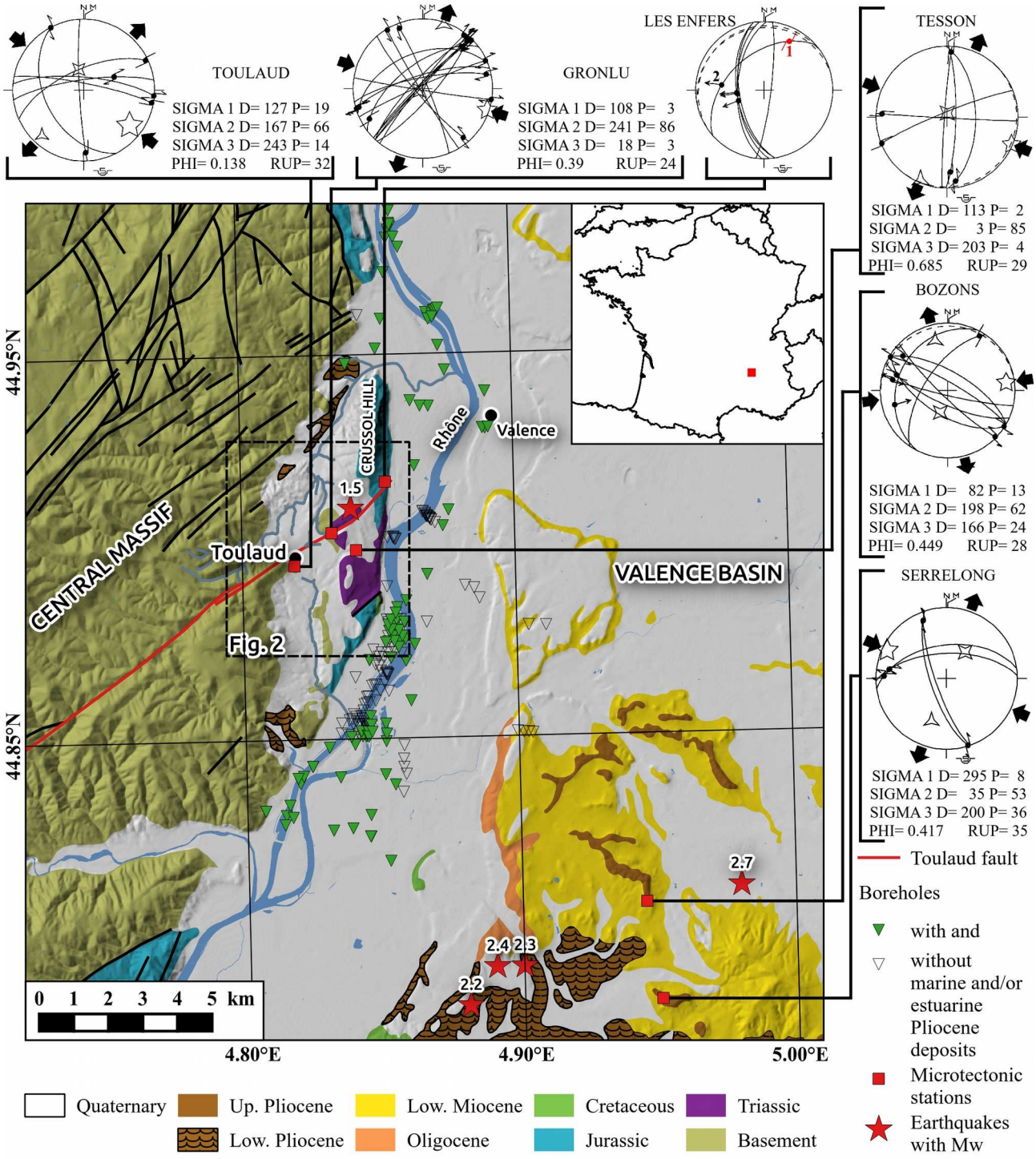

Figure V.1: Simplified geological map (modified from Rouire et al. (1980)) boreholes (from BSS, BRGM), instrumental seismicity (Cara et al., 2015) and locations of the sites of fault kinematics measurements in the study area (location in fig. I.1). Schmidt's diagrams with computed stress tensors: solid lines for fault planes, dashed lines for bedding planes. σ1, σ2, and σ3 as five branches, four branches and three branches stars respectively. PHI is the stress ratio and RUP a quality estimator (cf. Angelier (1990))

During the MSC, evaporation in the Mediterranean sea caused the lowering of the base level, estimate at approximately 1500 meters (Clauzon, 1982; Hsü et al., 1973; Rehault et al., 1984; Ryan, 1976). To reach equilibrium, all river systems flowing into the Mediterranean sea eroded their beds at an increased pace, digging deep valley and canyons (Bourcart and Glangeaud, 1954; Clauzon, 1982, 1974). The end of the MSC was accompanied by a sudden increase in sea level. The previously dug canyons were filled by sea water far inland and became rias (Clauzon, 1982; Debelmas and Demarcq, 1980). They were then progressively filled by marine and then continental sediments (blue marls, sands and conglomerates from basement to top) thanks to the progradation of Gilbert type fan delta until the end of the Pliocene (Clauzon, 1996).

The digging and subsequent sedimentary filling of the Messinian valleys led to the formation of several sedimentary and morphologic markers described by Clauzon (1996). The first is the pre-evaporitic abandonment surface which corresponds to the top surface before the MSC (prior to 5.95 Ma (Gautier et al., 1994; Krijgsman et al., 1999)). The second is the Messinian erosional surface which corresponds to the flanks and bed of the canyons that was observed on outcrops, in boreholes or in seismic profiles (Clauzon, 1982; Schlupp et al., 2001). This surface is 5.95 Ma to 5.32 Ma old (Gautier et al., 1994; Krijgsman et al., 1999). The third surface is found in the canyon's fill and corresponds to the transition between marine and continental sediments. This surface is diachronic along the canyon (older upstream), is younger than 5.32 Ma (Gautier et al., 1994; Krijgsman et al., 1999) and has a constant height corresponding to the Pliocene sea level. The last surface is the upper Pliocene abandonment surface which corresponds to the morphology before river incision resumed during the Quaternary. The height of this surface is lower than the one of the pre-evaporitic abandonment surface and higher than the one of Quaternary fluvial terraces.

Some of these surfaces have been identified ~39 km northward of the Toulaud valley in the abandoned Saint-Désirat meander (Clauzon, 1996), the pre-evaporitic abandonment surface being at a 360 m height, the Messinian erosional surface at a ~-140 m height and the marine/continental transition at a 200 m height. Moreover, ~52 km northward (located at le Péage-de-Roussillon), a borehole revealed Pliocene marine marls until a ~-110 m height without reaching the Messinian erosional surface (Ballesio, 1972) whereas ~50 km southward, canyon's bed was found at a -236 m height (Demarcq, 1960b).

The presence of lower Pliocene marine to tidal deposits underlying the basement on both sides of the Toulaud valley (Fig. V.1) (Bornand et al., 1974; Mandier, 1974) attests that it was once a canyon dug by the Rhône during the MSC. In the Toulaud valley, the outcropping lower Pliocene marine deposits are not found higher that ~200 m and the upper one are clayey yellow fine sand

with plant fragment remains attesting for tidal depositional environment (Bornand et al., 1974). This ~200 m height corresponds to the contact between Helvetian marine molasse and upper Pliocene continental conglomerates eastward in the Valence trough (Bornand et al., 1974). The lower Pliocene marine marls were also found in several boreholes dug in the modern Rhône valley (Fig. V.1) which implies that the Crussols hills already existed during Messinian.

Finally, the Toulaud valley displays several old (late Neogene to early Quaternary) benches and deposits associated to continental depositional environment. Thus, scattered quartzitic pebbles attributed to upper Pliocene are found at the top of the Crussol hill (Bornand et al., 1974) which range between 350 m and 400 m height. We have to underline that the Tortonian continental deposits could have reach this altitude. A second fluvial terrace is found at a ~275 m height and is attributed to Tortonian (Mandier, 1988) or "Villafranchian" (Bornand et al., 1974; Mandier, 1974). Then, at a ~220 m height appears the pre-Günz fluvial sands and pebbles and at a ~200 m height the Günz fluvial sands and pebbles attributed to the Rhône river (Bornand et al., 1974; Mandier, 1974). The other Quaternary deposits in the Toulaud valley are constituted by post-Günz fluvial terraces, alluvial fans and loess (Bornand et al., 1974; Mandier, 1974).

Numerous Plio-Quaternary formations being cross-cut by the Toulaud fault, the study of the valley morphology is an opportunity to evaluate and understand late Cenozoic fault activity in the Valence area.

V.3 - Seismicity and modern deformation

The Toulaud fault does not display associated seismicity except one 1.5 M_W earthquakes (May 10Th 2004) around the fault in the Crussol hill (Fig. V.1) (Cara et al., 2015). Regionally, seismic events in the Central massif within a distance of 50 km of the Toulaud valley do not exceed 2.8 M_W (Cara et al., 2015) whereas known historical earthquakes do not exceed a 5 MSK intensity (SISFRANCE catalog).

Although poorly constrained because of the few stations in western France and few earthquakes in the study area, the strain rates deduced from geodetic measurements and seismicity are close or lower to 1 nanostrain per year (Tesauro et al., 2006). According with the same study, around the Toulaud fault, compressional and tensional strain axis are of the same order and trend ESE to SE and NNE to NE respectively. On the other hand, although poorly constrained too in the area because of the few seismic events, the compressional axis interpolated from earthquakes focal mechanisms (Delacou et al., 2004) displays an E to ENE trend. Both studies slightly differ about

trend of the compressional axis but both imply a potential modern right lateral kinematics along the Toulaud fault.

V.4 - Methodology

In order to better constrain a potential activity of the Toulaud fault during Plio-Quaternary, we performed a multidisplinary study including fault kinematics analysis, stress state determination, morphological analysis as well as geophysical survey that we describe thereafter.

V.4.1 - Fault kinematics analysis and stress state determination

The kinematics of a fault population is defined using the striations measured on fault planes at several sites. By measuring numerous striated fault planes at individual sites, we can characterize successive faulting events, tectonic regimes and related stress states. This methodology of fault kinematics studies to determine paleostress fields and to demonstrate temporal and spatial changes in the late Cenozoic stress states has been applied in many active tectonic areas around the world over the past thirty years (e.g., Bellier and Zoback, 1995; Hippolyte et al., 2012a; Mercier et al., 1991; Shabanian et al., 2010).

We measured striae on both major (crustal scale) and minor (centimetric to metric scale) faults, at seven different sites, to determine the state of stress responsible for the deformation in the studied area. We realized quantitative inversion of distinct families of slip data measured at each individual site using the INVD method proposed by Angelier (1990). The results of the stress inversion include the orientation (azimuth and plunge) of the three principal stress axes σ_1, σ_2 and σ_3 (maximum, intermediate and minimum compressional stress axes) of the stress tensor and the stress ratio ($\varphi=(\sigma_2-\sigma_3)/(\sigma_1-\sigma_3)$)

In this study, we aim at characterizing the late Cenozoic deformation. For fault striations, it is difficult to constrain the absolute age of fault slips more precisely than younger than the age of the rocks affected by the faults. In the study area, striations are measured on faults affecting Paleozoic basement, Triassic sandstone and upper Pliocene conglomerates.

V.4.2 - High resolution Digital Surface Model

In order to identify and well constrain potential morphological offsets, we generated a high resolution digital surface model (DSM). The low density vegetation cover of the area allows us to use photogrammetry. We used the software Agisoft Photoscan Professional for the orthophotograph and DSM generation.

We used 13 scanned non orthorectified aerial photographs from a 1969 campaign, available from the geoportail (http://www.geoportail.gouv.fr, IGN). We chose this campaign since it was the best compromise between aerial pictures resolution, sparse vegetation and negligible human impact on the land. Resolution of the aerial photographs is unknown but can be estimated as less than one meter. Photographs are arranged under three ~N trending lines. Between two photographs, meridian and longitudinal overlaps are approximately of 70% and 25% respectively. Initially, the software computes the position of the photographs and generates a first 3D model in an orthonormal Cartesian coordinate system.

In order to georeference the 3D model, ground control points are needed. We extracted 80 spot heights from the 1:25000 topographic map and reported them on the georeferenced orthorectified aerial photographs from a 2001 campaign produced by IGN. We identified 32 spot heights on both the 1969 and the 2001 aerial photographs and used them as ground control points. Error on the coordinates of this ground control points was set at 5 m which is the spot height diameter on the 1:25000 topographic raster map.

The software then computed a 60 cm resolution georeferenced DSM (Fig. V.2). Effective DSM resolution is less than meter, but it may spatially vary because of the roughness differences of the ground.

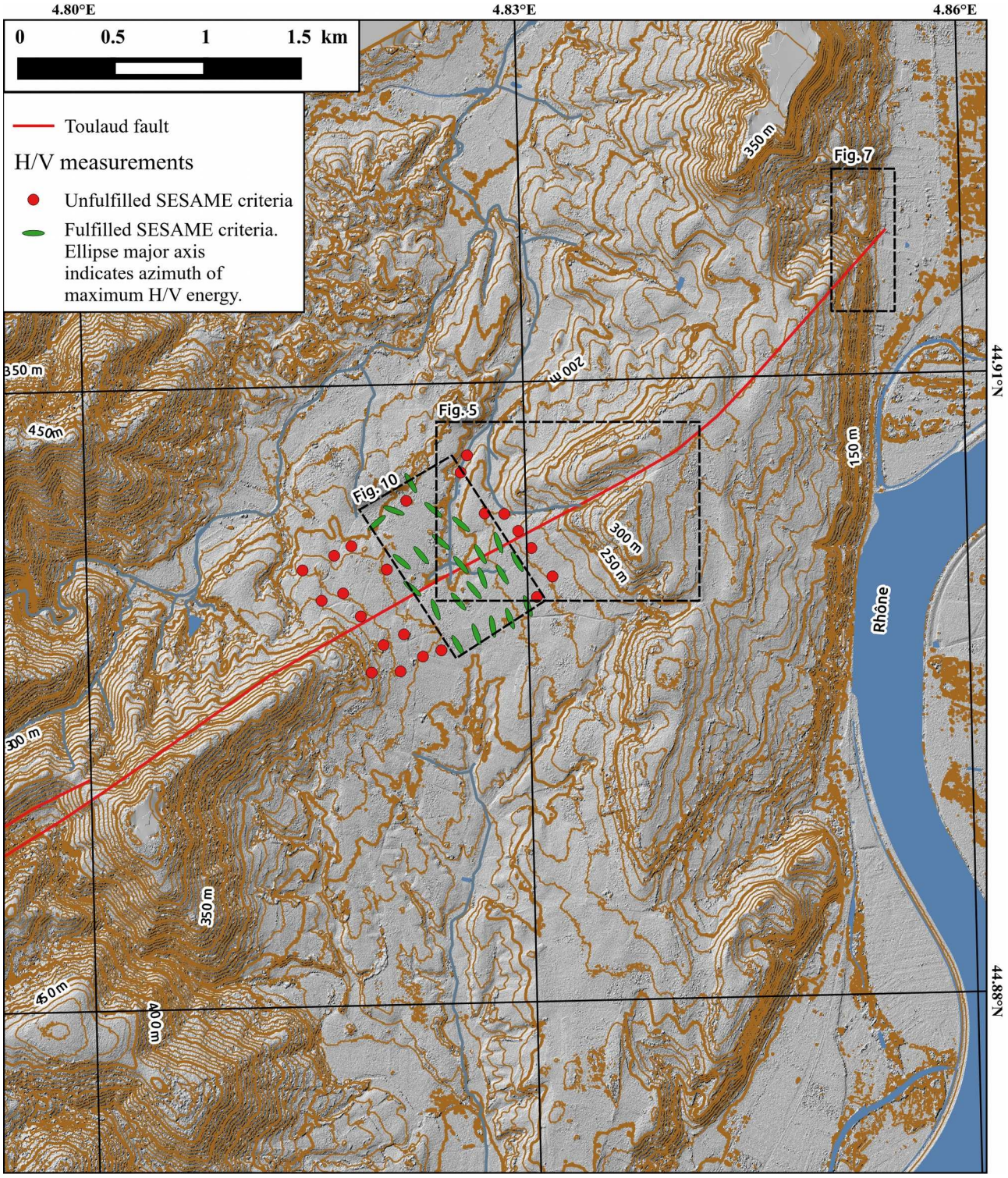

Figure V.2: 0.6 m resolution DSM of the Toulaud valley (location on Fig. V.1) and H/V measurements emplacements with azimuth of maximum energy for stations following SESAME report standards (SESAME European research project, 2005).

V.4.3 - Geophysical prospecting

V.4.3.1 - H/V method

The H/V method (Nakamura, 1989) can be used to measure a sediment thickness at one given station where substratum can be approximated as a two-layer model. Several studies provide evidences that it is an efficient method to determine the thickness of soft sediment infilling basin or valley (Guéguen et al., 2007; Hollender et al., 2015; Le Roux et al., 2010; Schlupp et al., 2001; Seht and Wohlenberg, 1999). It consists in estimating the ratio $R_{H/V}$ between the Fourier amplitude spectra of the horizontal (H) to vertical (V) components of the ambient noise vibrations. If a substratum is composed of two layers displaying sufficient impedance contrasts, the $R_{H/V}$=f(f) curve will display a peak corresponding to the seismic resonance fundamental frequency (f_0 in hertz) related to the interface depth (H in meter). The applied function is (Bard and Bouchon, 1985):

$$f_0 = V_S / 4H \quad \text{(V.1)}$$

where V_S is the average shear-wave velocity in meter per second of the upper layer. It should be noted that we can deduce from this formula only a first approximation of the depth interface (Bard and Bouchon, 1985). Moreover, the method gives low reliable results when applied on sloping interface (Guéguen et al., 2007; Guillier et al., 2006).

Measurements were done using buried seismometers at 45 sites spaced of ~150 m (Fig. V.2). The three components (north, east and vertical) were recorded during ~1 hour at each sites. From these records, using the Geopsy software, we selected the most stationary 60 seconds long time windows in order to avoid transient noise. For each components and time windows, a smooth Fourier amplitude spectra is computed. In the case of filled valley, seismic waves can be polarized (normal and parallel to the valley (Bard and Bouchon, 1985; Roten et al., 2006)). In such a case, H/V ratio displays a higher energy when horizontal components are projected along these trends (Barazza et al., 2009; Hollender et al., 2015). The “H/V rotate” tool allows the identification of the azimuth of maximum energy which here is of ~N145°E (Fig. V.2) which is closed to the trend of the canyon in this area (Mandier, 1974). Horizontal components were projected on N145°E and N55°E azimuth in order to identify clearer H/V peaks. After averaging the two projected horizontal components using a quadratic mean, a H/V ratio curve is computed for each time window. Finally, a mean H/V ratio curve is computed from all the time windows (Annexe 3). Data points have been examined and only points respecting the SESAME report standards (SESAME European research project, 2005) (except one displaying a consistent result with surrounding measurements, see V.5.3.1) were kept for further interpretation and interpolation.

V.4.3.2 - Electrical resistivity tomography

The electrical resistivity tomography (ERT) allows the determination of a section of the repartition of rock resistivity in the underground. The analysis of the measured data allows the identification of geological formations displaying sufficient resistivity contrast as well as their geometry. The ERT has been successfully applied in numerous studies to constrain underground geological geometries (e.g., Gélis et al., 2010; Le Roux et al., 2010; Nguyen et al., 2007; Rizzo et al., 2004; Suzuki et al., 2000). The method consists in injecting an electric current in the ground along a cable that has previously been set along the section of interest. The measured apparent resistivity of a material is function of the intensity I of the current, the potential difference ΔV between two measurement points and of a K factor that depends on the geometric configuration of the acquisition device (Telford et al., 1990).

The profiles presented in this study have been generated with an ABEM-Terrameter SAS4000 using 64 electrodes (10 m spaced) and a Wenner-Schlumberger protocol. Such a device allows the acquisition of 900 independent measurements of apparent resistivity (Griffiths et al., 1990) along 640 meters long and 80 meters deep profiles. Inversion to determine true resistivity at each point, interpolation and topographic correction were performed using the RES2DINV software (Loke, 2003).

ERT does not allow the determination of an unique interpretation, e.g., several rocks can have similar resistivity properties or water content of the substratum can influence the resistivity. The interpretation of ERT data requires a good knowledge of the geological context in order to match geological formations and resistivity values.

V.5 - Observations, results and interpretations

V.5.1 - Fault kinematics and stress state

Near the eastern edge of the Crussol hills, at the “Les Enfers” locality (LES ENFERS site, Fig. V.1), we observed a N trending W dipping normal fault between Rhaetian-Hettangian dolomitic sandstone (hangingwall) and Muschelkalk-lower Keuper black shale (footwall) (Fig. V.3). A N048°E trending fault plane displays striae consistent with left-lateral and normal kinematics (Fig. V.1) without a clear observable chronological relationship.

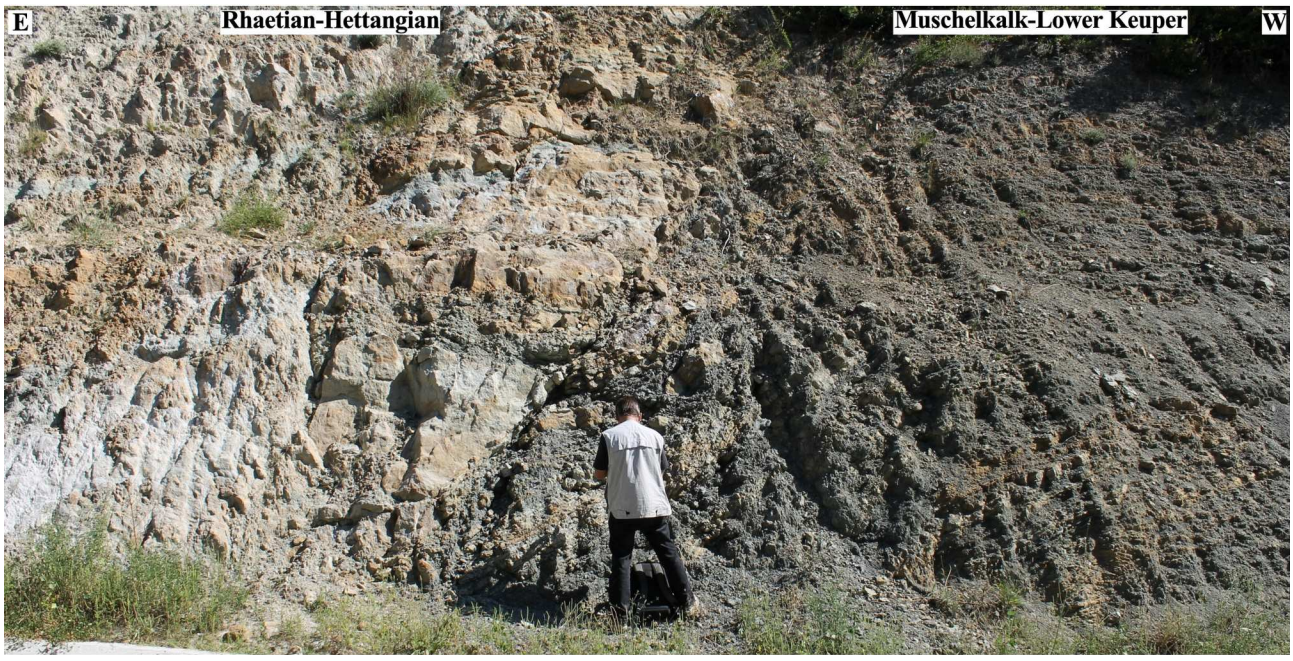

Figure V.3: Normal fault within middle Triassic - lower Jurassic deposits at the "Les Enfers" locality.

We observed on the eastern flank of the Toulaud Valley (GRONLU site, Fig. V.1) a major NE trending near-vertical fault affecting the granite basement that corresponds to the Toulaud fault trace (Fig. V.4). Along the fault plane, striae, shelter zones as well as Riedel fractures attest of a right-lateral kinematics and brittle faulting. This outcrop also displays NW trending left-lateral strike-slip faults whose kinematics is inferred from the observation of striae. The stress inversion from measured striae allows the determination of a well constrained strike-slip tectonic regime characterized by near horizontal σ_1 and σ_3 axis trending ESE and NNE respectively (Fig. V.1).

Two other oudrops displaying striated fault planes were found on both sides of the Toulaud valley, one in the granite (TOULAUD site, Fig. V.1) and the other in the Triassic sandstones (TESSON site, Fig. V.1). Stress inversion on both sites yields strike-slip tectonic regime characterized by near horizontal σ_1 and σ_3 axis trending ESE and NNE respectively at the TESSON site and by near horizontal σ_1 and σ_3 axis trending SE and NE respectively at the TOULAUD site (Fig. V.1).

Finally, two measurements sites were found in the continental Pliocene deposits of the Valence basin. The SERRELG site (Fig. V.1) displays pitted but slightly striated pebbles. We performed a stress inversion even if the few data implies that the inversion is poorly constrained. It yields a transpressive tectonic regime defined by a near-horizontal ESE trending σ_1 axis and a NNE trending 36° SSE dipping σ_3 axis (Fig. V.1). The BOZONS site also shows striated pebbles (Fig. II.1) whose stress inversion allows the determination of a strike-slip tectonic regime characterized by near horizontal σ_1 and σ_3 axis trending N082°E and N166°E respectively (Fig. V.1).

We can not strongly ascertain the age of faulting observed on the Toulaud fault but we present thereafter some arguments. For the LES ENFERS site, the N048°E trending left-lateral strike-slip fault is consistent with a ~N trending compression whereas normal faults are consistent with an ~E trending extension. According with previous works performed in the surrounding area (Bellier and Vergely, 1987; Bergerat, 1981a, 1981b; Blés et al., 1989), these fault kinematics could correspond to the N trending Eocene compression and the E trending Oligocene extension.

Figure V.4: The Toulaud fault at the Gronlu site.

The Central Massif was affected only twice, during the late Carboniferous and the late Miocene, by tectonic regime with an E to SE trending σ_1 axis (Blés et al., 1989). The late Miocene strike-slip to compressive tectonic regime characterized by a NE to ESE trending σ_1 axis was already described further East in the Rhône valley (Bergerat, 1981a) and the Vercors massif (Philippe et al., 1998) and further South in the Valréas basin (Casagrande Fioretti, 1985), along the Cévennes fault (Bergerat, 1981b) and in the Ardèche plateau (Bellier and Vergely, 1987). The measurements sites in the granite, the Triassic sandstones and upper Pliocene deposits all display close tectonic regimes (strike slip to transpressive) characterized by a near horizontal SE to ESE trending σ_1 axis compatible with a right-lateral kinematics along the Toulaud fault. Sedimentary rocks affected by faulting are all younger than Paleozoic. It leads us to propose that observed right-lateral strike-slip faulting along the Toulaud fault is late Miocene to (at least) upper Pliocene in age.

The tectonic regime found at the BOZONS site slightly differs but is still compatible with a right-lateral kinematics along the Toulaud fault. It should be noted, however, that the difference of the σ_1 axis trend (ENE) could be related to the late Neogene counter-clockwise rotation of the alpine stress state reported north-eastward in the Belledonne Massif (Billant et al., 2015) and southward in the Valréas basin (Casagrande Fioretti, 1985).

V.5.2 - Morphological analysis

In and around the Toulaud valley, the study of the high resolution DSM allowed the identification of several geomorphic attributes and anomalies. The first is the fact that the modern watershed divide corresponds to the Toulaud fault (Figs. V.1 and V.2), i.e. the streams to the north of the fault flow northward whereas streams to the south of it flow southward. The set up of this watershed divide occurred after Günz (Mandier, 1974). Although it could have been caused by the filling of the Toulaud valley by the post-Günz alluvial fans which could have obstructed it, we can not exclude that it was caused by a vertical slip along the Toulaud fault which would generate uplift of the southeastern side.

The second is located on the eastern flank of the Toulaud valley, near the GRONLU station (Fig. V.5). The ~N140°E trending flank of the valley (same trend as H/V maximum energy) is composed of Paleozoic basement and Triassic rocks outcropping at altitudes ranging between 200 m and 300 meters (Bornand et al., 1974). We propose that this modern flank corresponds to a flank of the Messinian canyon. This flank is cross-cut by the Toulaud fault and is not continuous on both sides of it (Fig. V.5) suggesting that the Messinian canyon was offset after is formation. We projected topographic profiles of the flank on the fault (Figs. V.5 and V.6). Topographic profiles displaying both an almost constant slope, we performed linear regressions of them in order to measure apparent offsets (Fig. V.6, note that we forced both linear regression to share the same slope). Apparent right-lateral (given by difference between x intercept of both linear equations) and vertical offsets (given by difference between y intercept of both linear equations) of the flank are of 99 m and 31 m respectively (Fig. V.6). Although we can constrain what is the real offset, it implies that the relation between vertical ($offset_Z$) and lateral ($offset_X$) offset must be:

$$offset_Z = -0.313 * offset_X - 31 \quad \text{(V.2)}$$

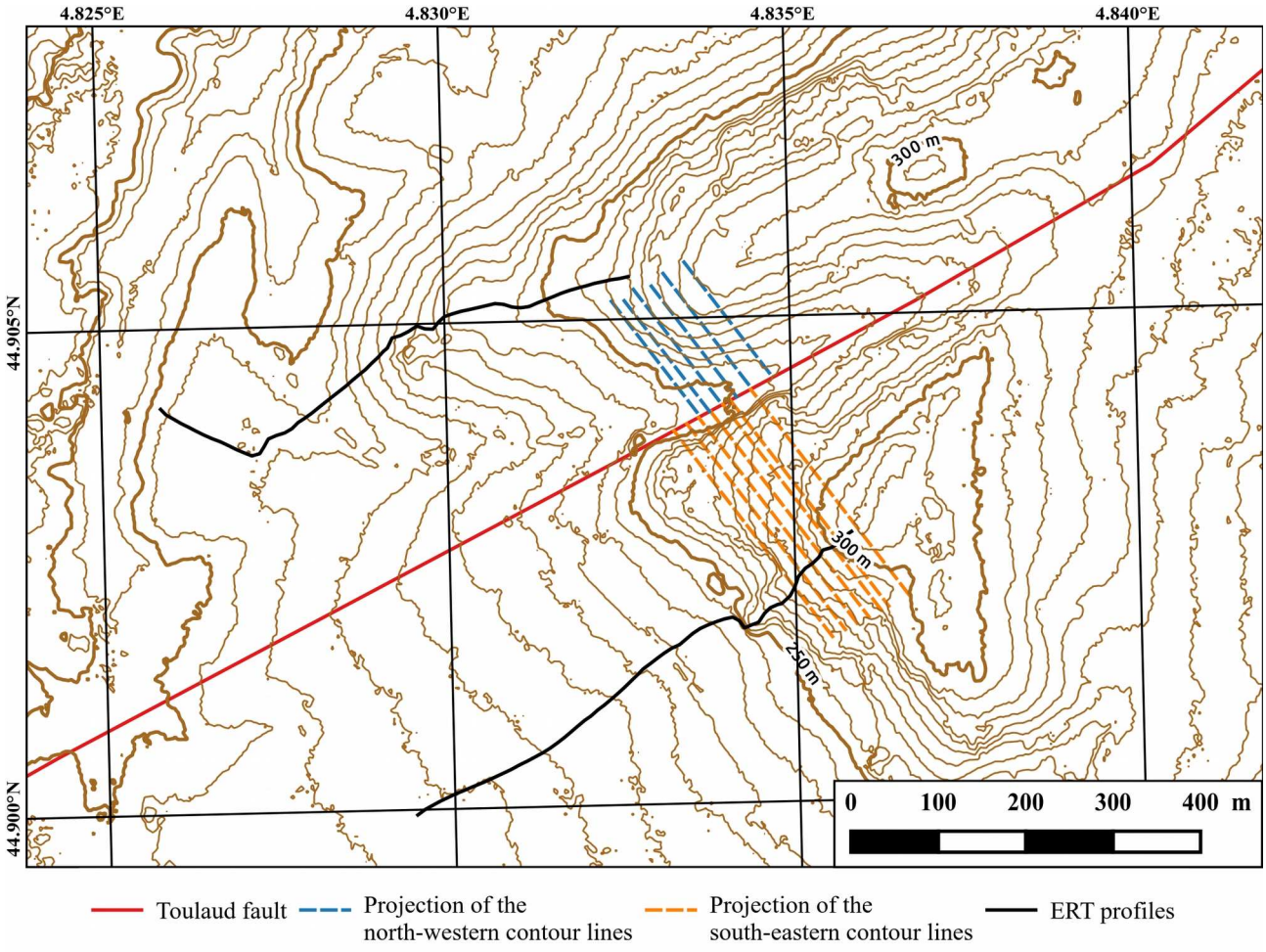

Figure V.5: Offset of the eastern flank of the Toulaud valley. Location on Fig. V.2.

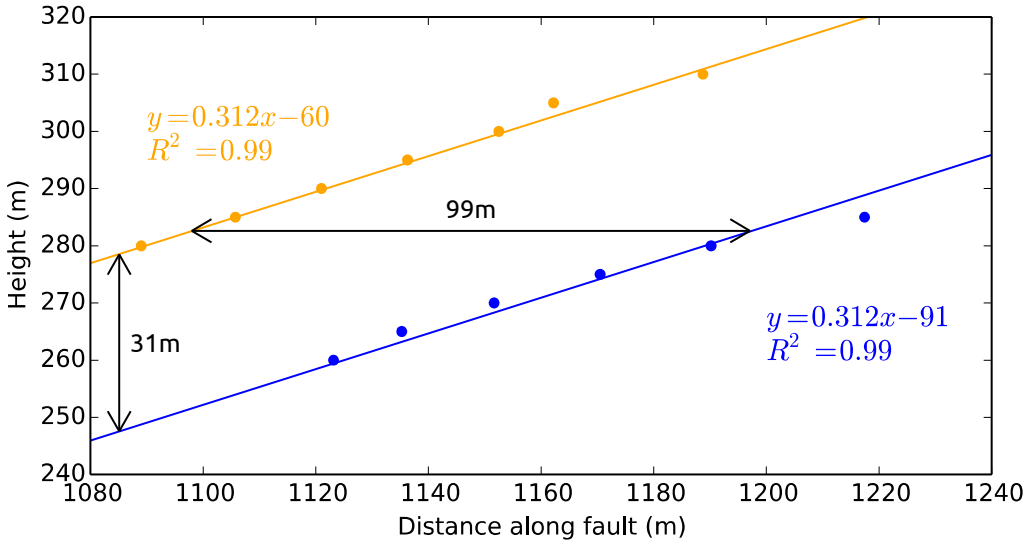

Figure V.6: Topographic profiles projected on the fault plane and associated linear regression at the Gronlu site. Blue and orange profiles are northwestern and southeastern flank relatively to the Toulaud fault respectively.

The third is located north-eastward, near the locality “Les Enfers”, at the intersection between the Toulaud fault and the north trending eastern edge of the Crussol hill (Fig. V.7). Here, this near linear edge is not continuous on both sides of the fault and displays an apparent right-lateral offset (Fig. V.7). As previously, we projected the topography on the fault plane and performed linear regression of the topographic profiles. In this case, topographic profiles display very different slopes (24° and 38°, Fig. V.8). Assuming that they were previously aligned, it would imply that a rotation occurred along the fault. In this case, because we can not ascertain the location of the rotation pole, we can not measure reliable apparent offsets as in the Gronlu area.

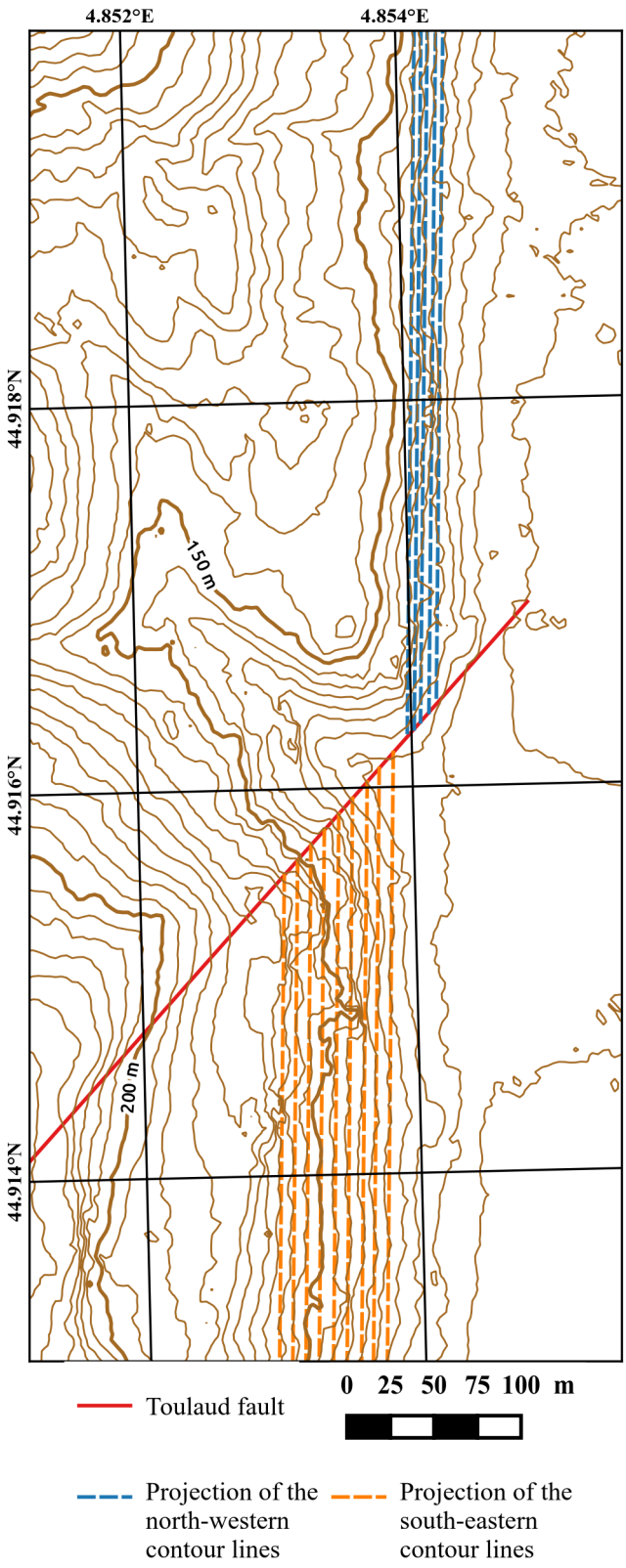

Figure V.7: Offset of the eastern edge of the Crussol hills. Location on Fig. V.2.

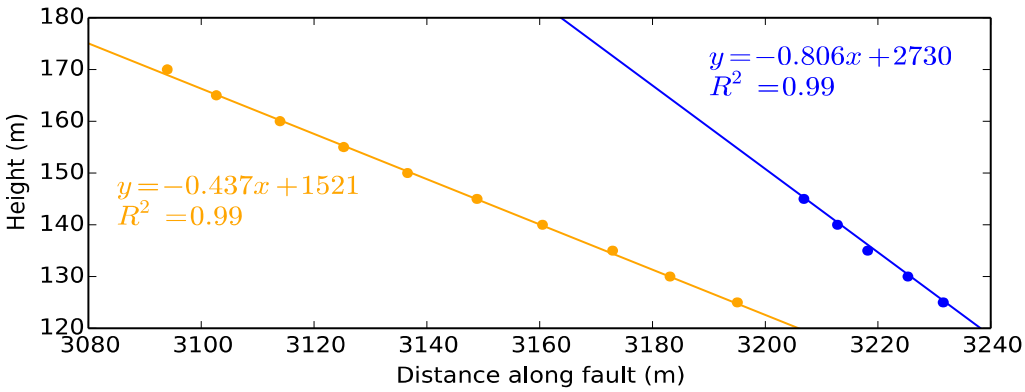

Figure V.8: Topographic profiles projected on the fault plane and associated linear regression of the eastern edge of the Crussol hills. Blue and orange profiles are northwestern and southeastern edge relatively to the Toulaud fault respectively.

V.5.3 - Underground imagery

V.5.3.1 - Canyon's bed depth

H/V measurements provide reliable points, i.e. distinct peak values for the H/V ratio at low frequencies, mainly in the center of the Toulaud valley. Measurement points located closer to the flanks display high frequencies peak values or noisy results attesting that they were measured at the top of the flank of the Messinian canyon or out of it. For the 23 stations located in the center of the valley, H/V ratio curves display peaks for fundamental resonance frequencies ranging between 0.662 Hz and 0.768 Hz with a mean value of 0.72±0.01 Hz for the whole dataset. Without considering points at the top of the Toulaud fault that could have recorded a signal related from each sides of it, the mean values of fundamental resonance frequencies are 0.71±0.02 Hz and 0.74±0.02 Hz for stations located northwestward and southeastward of the fault respectively.

To constrain the depth of the interface, the mean shear wave velocity (V_S) of the sedimentary filling is needed. We do not constrain it in the Toulaud valley, but mean V_S of the Pliocene marine sediments (and its Quaternary cover) were already measured at other locations further south in the canyon (Bailly et al., 2013a, 2013b; Schlupp et al., 2001). We so consider here that these values can be used and that there is no significant variations of the physical properties of the Pliocene marine filling along the Rhône canyon.

V_S of ~800 m.s^{-1} (Bailly et al., 2013a; Schlupp et al., 2001) and 1300±100 m.s^{-1} (Bailly et al., 2013b; Schlupp et al., 2001) were measured for the Pliocene marine sediments (it should be noted that in Schlupp et al. (2001) the mean V_S of ~800 m.s^{-1} was measured for Miocene molasse

and extrapolated to the Pliocene marine sediments). According with the 0.72±0.01 Hz mean fundamental resonance frequency, using equation V.1, it implies a canyon's bed at a -67±5 m mean height (for V_S = 800 m.s^{-1}) or at a -241±42 m mean height (for V_S = 1300±100 m.s^{-1}) (Fig. V.9). The facts that the Rhône river was already flowing southward during the MSC and that the canyon height is lower than -110 m 52 km northward (Fig. V.9) imply that a canyon's bed at a -67±5 m mean height under the Toulaud valley is highly improbable. The V_S = 1300±100 m.s^{-1} allows the determination of a more consistent canyon's bed height with other known bed's height along the canyon (Fig. V.9), so we kept it for further depth computation.

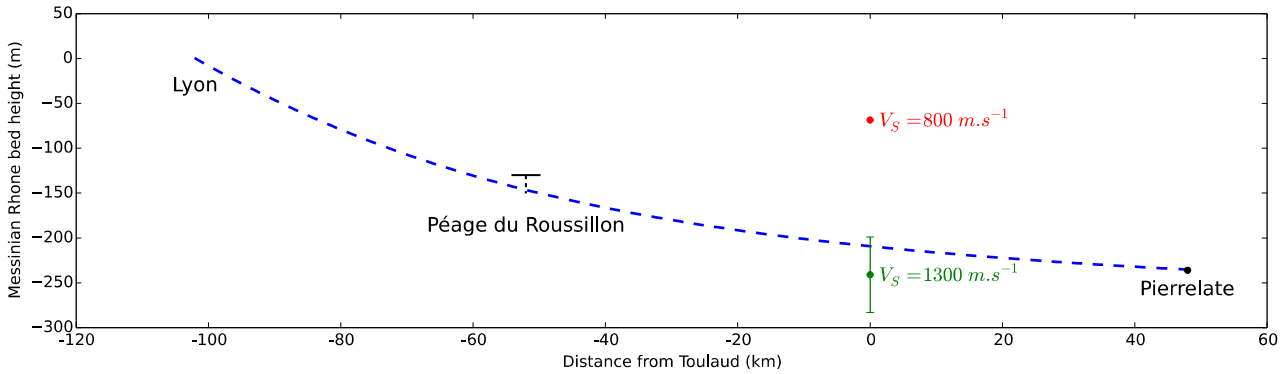

Figure V.9: Messinian canyon's bed height computed for different shear waves velocity (V_S) in Toulaud valley using H/V method compare to height measured from boreholes.

Height of the canyon's bed was computed for each measurement site using equation V.1 with a V_S of 1300 m.s^{-1} and resulting datasets was interpolated using a spline method (Fig. V.10). Because of the low sampling density and precision of height, we consider that small topographic variations are few reliable. It should be note that the fact that highest heights are found in the middle of the canyon's bed and not along the flank is an artifact, H/V frequency being overestimated in the center of a valley and underestimated near its edges (Guillier et al., 2006). Considering the large wavelength morphology, it appears that the canyon's bed is relatively flat and large (>550 m) (Fig. V.10). The lowest heights are found upstream of the fault which is inconsistent with the southward course of the Rhône river's (Fig. V.10). We interpret this geometry as an apparent vertical offset of the canyon caused by faulting along the Toulaud fault.

Measuring the apparent vertical offset using topographic profiles remains risky because of the low density of points used for the interpolation. Therefore, we consider mean elevation on both sides of the fault. Considering V_S included between 1200 m.s^{-1} and 1400 m.s^{-1}, the minimum mean heights northwestward and southeastward of the faults are of -219 m and -202 m respectively whereas maximum mean heights are of -289 m and -270 m respectively. Disregarding the Messinian canyon slope along it course (ranging only between 0.1% and 0.15% (Beaudoin et al.,

1997)), it implies that the downstream part of the canyon was uplifted of 18 ± 1 m relatively to the upstream part.

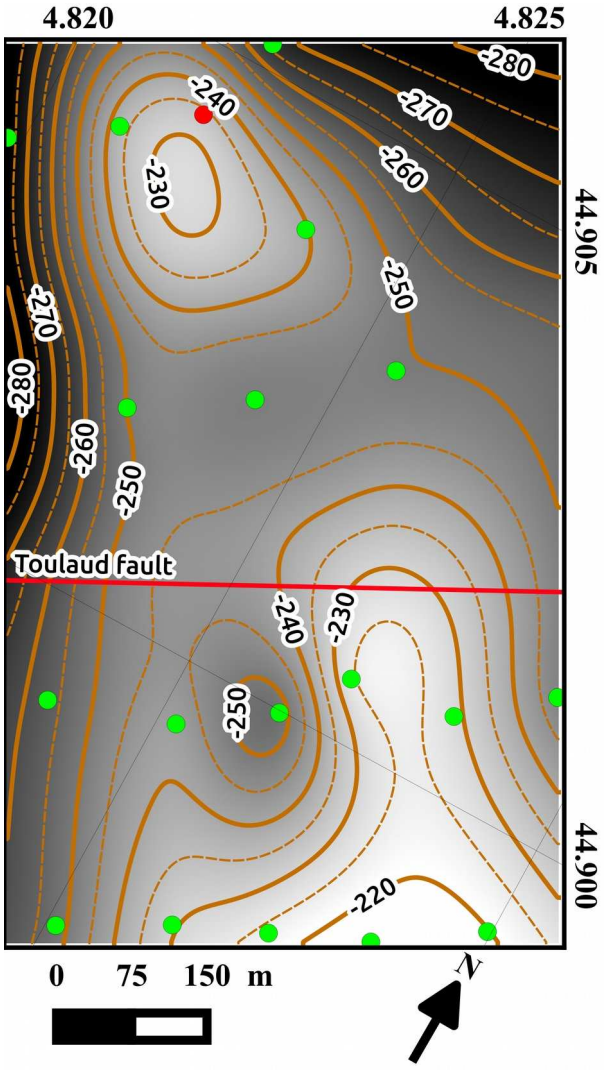

Figure V.10: Canyon's bed interpolated from H/V measurements (points). Red points is a measurement station whose result does not follow the SESAME criterion but was kept because it was showing close fundamental resonance frequency to neighboring stations. Location on Fig. V.2.

V.5.3.2 - Constraining the canyon's flank geometry

In order to assess, constrain in depth and confirm the observed morphological right lateral offset, we realized two ERT profiles (Fig. V.11) on the western slope of Gronlu relief on both sides of the Toulaud fault. Both profiles display high resistivity values (>1000 Ω.m) northeastward which correspond to the outcropping basement and which is a resistivity consistent with granite (Palacky, 1988). Within this highly resistive basement appears highly conductive zones which we interpret as resulting from water content within a fractured zone. Southwestward of this highly resistive materials appear two more conductive layers. The bottom one displays resistivity ranging between

~100 Ω.m and ~770 Ω.m and lies on the basement. A such resistivity is too high to correspond to the Pliocene marine marls (e.g. Molliex, 2009; Palacky, 1988) but it could correspond to sand or unconsolidated conglomerates (Palacky, 1988). This layer could be the tidal upper Pliocene sands. The top layer presents low resistivity (<50 Ω.m), is 0 to 40 m thick, lies on the two other formations and probably corresponds to Quaternary loess and alluvial deposits.

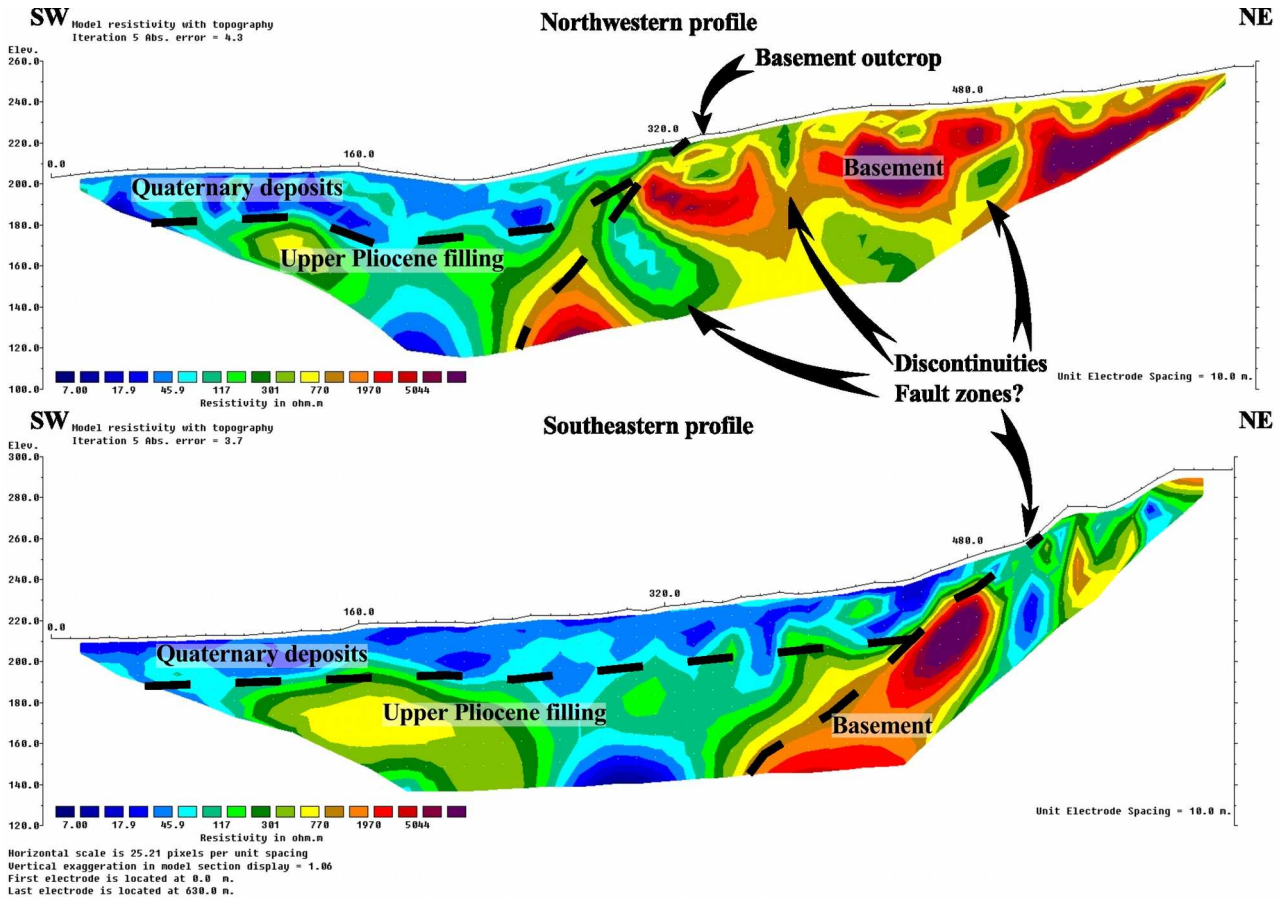

Figure V.11: ERT profiles on both sides of the Toulaud fault with interpretation. Location on Fig. V.5.

The canyon's flank is assumed to be at the transition between the highly resistive basement and a ~100 Ω.m to ~770 Ω.m layer. We used arbitrarily a resistivity of about 1000 Ω.m as the limit between the two layer and so corresponding to the canyon's flank. The canyon's flank profiles were then projected on the fault plane (Fig. V.12) assuming that the canyon's flank has the same trend (~N140°E, see V.5.2) in depth than the one observed in the Gronlu area. It appears that for the southeastern profile, the canyon's flank inferred from the ERT profile is almost in the continuation of the modern valley flank seen in the topography whereas the northwestern profile presents a ~240m bench between the modern flank and the one defined using ERT profile (Fig. V.12). So,

considering only the ERT profiles, the flank of the canyon on both sides of the Toulaud fault displays an apparent left-lateral offset of ~140 m which is not in agreement with the apparent right-lateral offset observed with the modern flanks of the Toulaud valley (Fig. V.12).

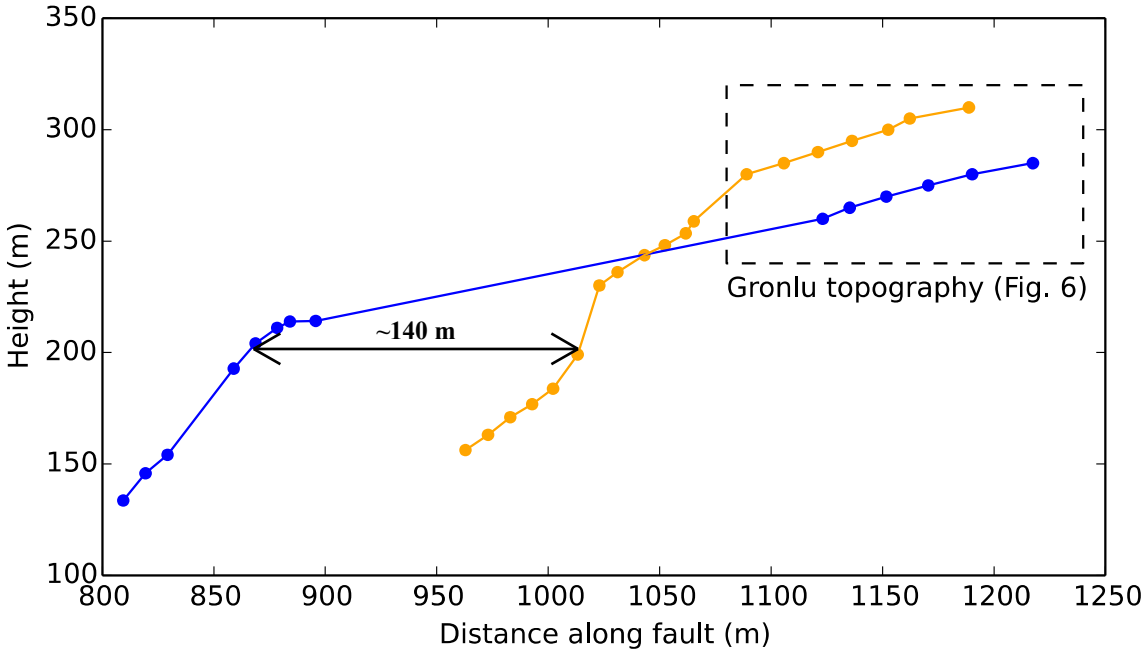

Figure V.12: ERT and topographic profiles projected on the fault plane. Blue and orange profiles are northwestern and southeastern flank relatively to the Toulaud fault respectively.

V.6 - Discussion and preliminary conclusion

V.6.1 - Cenozoic fault kinematics and tectonic regime

Fault kinematics measurements and stress-state inversions revealed that several tectonic regimes affected the Toulaud fault domain during the Cenozoic. Correlation with other studies (Bellier and Vergely, 1987; Bergerat, 1981a, 1981b; Blés et al., 1989) permits proposing that the ~E trending extension (LES ENFERS site) corresponds to the Oligocene extension responsible for the formation of the ~2000 m depth half-graben beneath the Valence basin (Blés et al., 1989; Germain and Demaison, 1958). The foot of the eastern edge of the Crussol hill displays Triassic and basement outcrops (Bornand et al., 1974) whereas a few hundred meters eastward boreholes made in the Rhône's plain reach Jurassic or Oligocene rocks (sometimes covered by Miocene molasse or Pliocene marls) (BSS, BRGM) and a borehole reaching the basement at a 3650 m depth beneath the Valence city reveals at least 800 m thick Oligocene deposits (http://ficheinfoterre.brgm.fr/InfoterreFiche/ficheBss.action?id=08183X0172/GVA1). It agrees with

the existence of N trending normal fault at the western border of the Valence basin and suggests that the N trending linear escarpment marking the eastern edge of the Crussol hill is one of them. It would explain the geometrical change of this edge on both sides of the Toulaud fault. Indeed, if we assumed that the edge is an Oligocene normal fault or that the morphology of the edge evolved from an Oligocene fault scarp, then the Toulaud fault could have behaved like a transfer fault between two normal fault segments during the Oligocene. In such a case, it does not exclude post-Oligocene offset of these two normal fault segments, but it implies that this landform was probably never continuous on both sides of the Toulaud fault and so that it can not be used to measure offset along the Toulaud fault.

Other fault kinematics measurements sites and stress-state inversions yield a strike-slip to transpressional tectonic regime characterized by a SSE trending σ_1 axis which occurred until the upper Pliocene. The defined stress-state is consistent with right-lateral kinematics of the Toulaud fault. A measurement site (BOZONS) shows faulting in the upper Pliocene conglomerates consistent with a strike-slip tectonic regime characterized by a ENE trending σ_1 axis. According with previous works (Billant et al., 2015; Casagrande Fioretti, 1985), this stress state could be Pleistocene in age. Such a tectonic regime would still imply an oblique right-lateral strike-slip faulting with a minor normal component along the Toulaud fault.

V.6.2 - Post-Messinian slip of the Toulaud fault

H/V measurements in the center of the Toulaud valley revealed that the downstream part of the Messinian canyon, southeastward of the Toulaud fault is higher than the upstream part located northwestward of the fault. The fact that we do not constrained the shear-wave velocity (V_S) in the study area implies that the canyon's bed depth deduced from our measurements is poorly constrained. However, the computed depth using mean V_S measured in other part of the canyon yields consistent results compared to depth constrained upstream and downstream using boreholes. The deduced 18±1 meters offset of the canyon's bed appears reliable. Anyway, using any other shear-wave velocity will still imply that the canyon's bed downstream of the fault is higher than its upstream part. The existence of a post-Messinian vertical offset along the Toulaud fault can thus be assessed.

The main remaining problem is about the quantification of the lateral offset, topography at the Gronlu location (assumed to correspond to the flank of the Messinian canyon) displaying an apparent right-lateral offset whereas underground part of the flank observed on ERT profiles shows an apparent left-lateral offset (Fig. V.13A). No fault slip scenario, including successive different

fault kinematics and/or rotation allows the realignment of canyon's bed, underground flank and the Gronlu topography and two hypotheses are still possible.

The first hypothesis assumes that the Gronlu topography corresponds to the canyon's flank. The fact that ERT profiles projected on the fault display an apparent left-lateral offset could be explained by a more complex geometry in depth that we can observe using only two profiles, i.e. the underground canyon flank does not have a constant N140°E trend. According with the 18±1 m vertical offset and using it in equation V.2, we can deduce a 41.5±0.2 m right-lateral offset along the Toulaud fault (Fig. V.13B) for a total slip of 45.2±1.2 m. Assuming a formation of the canyon between 5.95 Ma and 5.32 Ma, such an offset will imply a Toulaud fault slip rate of $0.8*10^{-3}$ ± $0.1*10^{-3}$ $mm.an^{-1}$ integrated for the Plio-Quaternary period.

The second hypothesis is that the Gronlu topography does not correspond to the canyon's flank and was strongly eroded. Indeed, a stream currently flows along the Toulaud fault and then immediately northward after crossing the modern flank of the Toulaud valley (Fig. V.2). It is then possible that this stream eroded the modern flank on the north-western side of the Toulaud fault which would have been previously in the continuation of the flank determined using ERT. In such a case, the removal of 18±1 m vertical offset and 150±10 m left-lateral offset allows the realignment of the canyon sections of both sides of the Toulaud fault. It yields a total slip of 151±11 m and assuming same the time span than previously, the slip rate integrated for Plio-Quaternary period would be of 0.027 ± 0.001 $mm.an^{-1}$.

Our observations revealed that surface and underground morphologies are not continuous on both sides of the Toulaud fault, especially the canyon's bed, which testify for post-Messinian faulting along the Toulaud fault. However, we can not strongly assess value of the Messinian canyon offset, because two possible explanations (or a combination of both) of our observations remain, although the first hypothesis has the advantage of being consistent with the observed fault kinematics. More prospection of the underground geometry of the canyon's flank must be performed in order to better constrain its offset and finally well determine the Plio-Quaternary slip of the Toulaud fault.

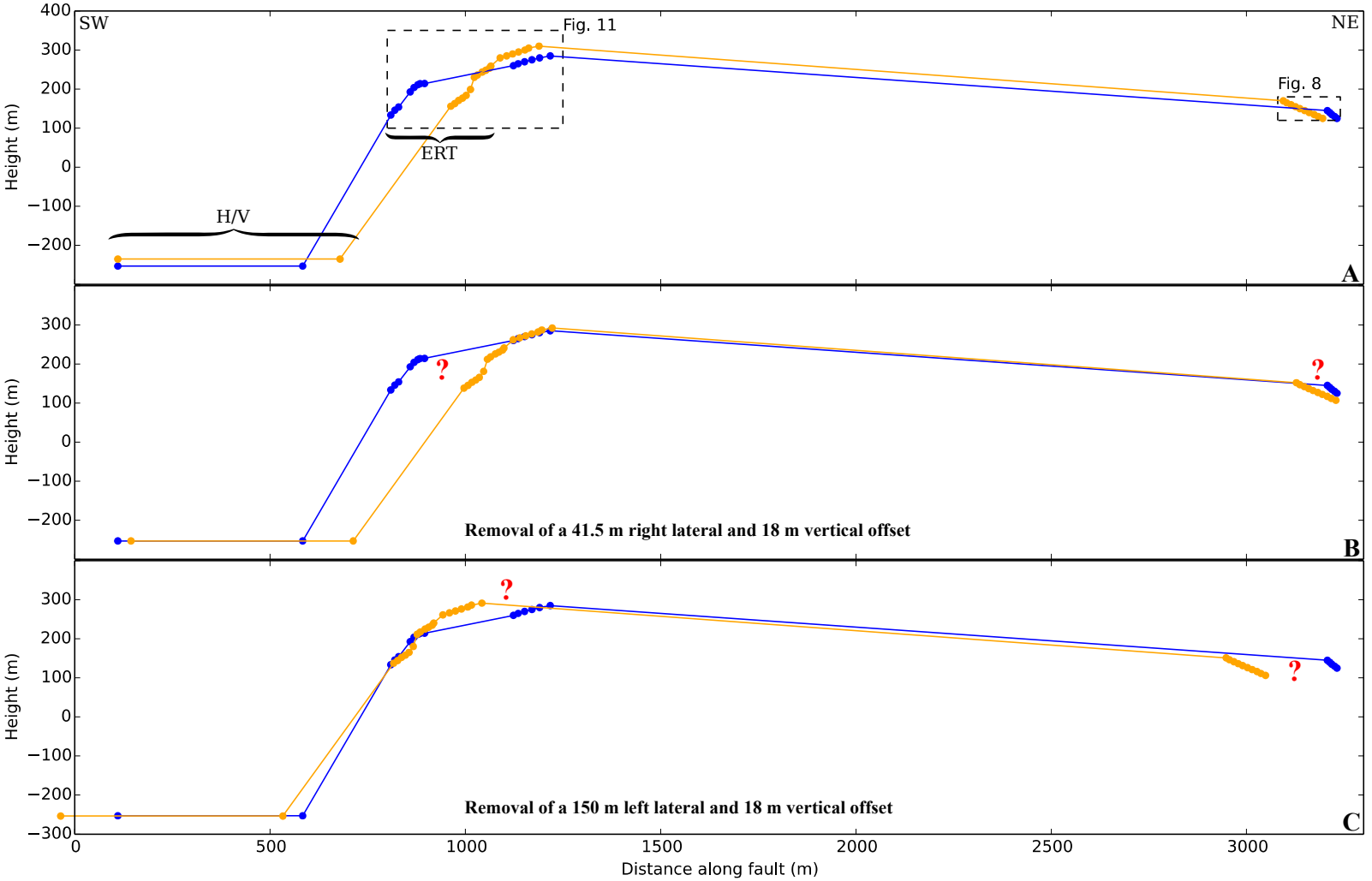

Figure V.13: Offset Messinian topographic markers projected on the Toulaud fault plane and proposed offset values.

VI - DISCUSSION ET CONCLUSION

VI.1 - Discussion et conclusions

VI.1.1 - Résumé des observations et résultats

VI.1.1.1 - Cinématique de failles et états de contraintes

La compréhension de la tectonique active d'une région repose sur la connaissance de l'évolution dans le temps des cinématiques de faille et régimes tectoniques afin de bien remettre dans leur contexte géodynamique les failles étudiées. Bien que nos travaux aient permis de confirmer et préciser certaines cinématiques de faille et états de contrainte anté-Neogene, nous ne discuterons ici que des résultats portant sur le Néogène et le Quaternaire.

Nous avons identifié dans notre zone d'étude deux régimes de déformation successifs tardi-cénozoïques. Le long du système de faille de Belledonne (faille de l'Arcalod, balcon de Belledonne et failles de la Cléry et du Jasneuf) le premier régime est compressif à décrochant et caractérisé par un axe σ_1 orienté WNW-ESE, perpendiculaire aux plis et chevauchements des massifs subalpins. Dans le Diois et les Baronnies ainsi qu'en rive gauche de la vallée du Rhône, ce premier régime de déformation présente un axe σ_1 perpendiculaire aux plis et chevauchements. Ilest orienté E-W à NE-SW. En rive droite de la vallée du Rhône et dans le Massif Central, le régime de déformation est principalement décrochant et caractérisé à nouveau par un axe σ_1 orienté WNW-ESE. Ce premier régime de déformation est contemporain des plis synsédimentaires helvétiens du bassin de Valréas et a été retrouvé dans les dépôts continentaux du Pliocène supérieur.

Le second régime de déformation que nous avons mis en évidence le long du système de faille de Belledonne à partir de l'inversion de plans de faille striés et des mécanismes au foyer (et donc correspondant au régime actuel) est principalement décrochant et caractérisé par un axe σ_1 orienté ENE-WSW. En rive gauche du Rhône et bordure ouest du Diois et des Baronnies, le régime de déformation est chevauchant à décrochant et présente un axe σ_1 orienté NE-SW cohérent avec le seul mécanisme au foyer existant le long de la faille de Mérindol-Condorcet-Saillans. Ce régime de déformation a également été retrouvé dans les dépôts continentaux du Pliocène supérieur indiquant que la transition entre les deux régimes de déformation s'est produite durant ou après le Pliocène supérieur.

VI.1.1.2 - Indice de déformation récente

Les analyses morphologiques et géophysiques de notre zone d'étude nous ont permis d'identifier plusieurs anomalies des morphologies plio-quaternaires que nous attribuons, pour certaines, à des déformations récentes. Ainsi, du nord-est au sud-ouest de la zone étudiée, nous avons mis en évidence :

- Des cours d'eau sigmoïdes le long de la faille d'Arcalod indiquant un probable décalage dextre de ~200 m ainsi qu'une rupture de pente topographique interprétée comme l'escarpement de la faille. L'âge de ces cours d'eau n'est pas connu mais supposé anté-Würmien. Notons tout de même que l'érosion glaciaire pourrait expliquer ces morphologies. La faille de l'Arcalod se connecte à sa terminaison nord-orientale sur un système de faille normale dont les escarpements bloquent des éboulis, suggérant un jeu récent. Ici, c'est une origine gravitaire à cette déformation qui ne peut être exclue pour ces mouvements récents, ces failles normales à contre-pente étant sub-parallèles et en bordure d'une vallée très encaissée comme dans le cas des sackungs.

- La zone de transition entre la faille de l'Arcalod et la faille bordière de Belledonne présente une anomalie résiduelle de Bouguer positive en accord avec l'existence probable d'un relais en transpression entre ces deux segments de failles dextres.

- Aucun indice de déformation de surface lié au jeu dextre de la faille bordière de Belledonne n'a été mis en évidence. Le fait qu'à l'affleurement seules des failles secondaires témoignent du mouvement dextre cette faille sismique, suggère que la déformation pourrait être accommodée en surface par une large bande de cisaillement dans les marnes du balcon de Belledonne. La morphologie du balcon de Belledonne et les anomalies de profil en long des rivières sont expliquées par l'érosion et le retrait du glacier de l'Isère. Ceci nous permet de rejeter l'hypothèse que ces anomalies morphologiques seraient dues au jeu d'une faille normale bordant le balcon de Belledonne.

- La faille senestre antithétique du Brion semble décaler la vallée glaciaire qu'elle recoupe d'une valeur comprise entre 430 m et 200 m. L'âge des surfaces décalées n'est pas connu mais supposé anté-Würmien

- La faille du Jasneuf décale de manière dextre des falaises supposées d'âge messinien de 715±45 m et des marqueurs morphologiques ante-rissiens (entre 0,86 et 0,533 Ma) de plus

de 73 m. La vitesse de glissement intégrée depuis le Messinien que l'on peut en déduire serait de 0,13±0,03 mm.yr^{-1}.

- Les mesures de bruits de fond sismique (méthode H/V) indiquent que la faille de Toulaud a décalé verticalement le canyon messinien du Rhône de 18±1 m. La composante latérale du mouvement de la faille n'est pour l'instant pas contrainte.

VI.1.2 - Discussion

Le champ de contrainte dans le quart sud est de la France au Miocène et début du Pliocene, responsable notamment de la formation des massifs subalpins et cristallins et lié à la collision entre les plaques apulienne et européenne, était déjà connu du fait de nombreux travaux (Bergerat, 1981a, 1981b; Blés et al., 1989; Casagrande Fioretti, 1985; Homberg et al., 1999; Philippe et al., 1998; Ritz, 1991). Notre étude confirme et complète les précédentes analyses. Les états de contrainte mio-pliocènes sont compressifs à décrochants et caractérisés par un axe σ_1 approximativement perpendiculaire aux plis et chevauchements des massifs subalpins et du Jura. Ce champ de contrainte résulte de la compression engendrée par la collision des plaques adriatique et européenne. Dans le même temps, les zones internes, en arrière du front pennique, étaient elles caractérisées par un régime en extension avec un axe σ_3 approximativement parallèle à la chaîne (Bistacchi and Massironi, 2000; Champagnac et al., 2004; Sue and Tricart, 2003; Sue et al., 2007b). Ce régime de déformation extensif était lié à l'extrusion latérale d'un bloc limité au nord par la faille de Simplon (Bistacchi et al., 2000b). Cette extrusion aurait été facilitée au début du Miocène par la poursuite de l'ouverture de la mer Ligure (Sue et al., 2007b) et pourrait avoir été causée par l'indentation de la plaque adriatique et/ou de la rotation anti-horaire de cette dernière (Champagnac et al., 2004; Collombet et al., 2002).

L'ensemble du champ de contrainte se réorganise ensuite durant ou après le Pliocène supérieur (Casagrande Fioretti, 1985; ce travail). Cette réorganisation est contemporaine de la baisse de la vitesse de convergence entre les plaques africaine et européenne ainsi que de la mise en place d'une convergence plus oblique à la limite de plaque qui se serait produite il y a ~3Ma (Calais et al., 2003), mais il est difficile d'affirmer en l'état que les deux phénomènes soient effectivement liés.

Durant cette période, les zones internes, en arrière du front pennique, sont cette fois caractérisées par un régime extensif à transtensif présentant un axe σ_3 approximativement perpendiculaire à la chaîne (Champagnac et al., 2004; Delacou et al., 2004), confirmé (du moins dans le Briançonnais) par les mesures géodésiques indiquant des taux d'extension de l'ordre de

plusieurs dixièmes de mm par an (Walpersdorf et al., 2015). Le Jura est affecté par un régime tectonique, compressif à décrochant, caractérisé par un axe σ_1 désormais homogène orienté NNW-SSE (Homberg et al., 1999). Dans la nappe de Digne (Ritz, 1991), une partie du bassin de Valréas (Casagrande Fioretti, 1985) et d'après nos observations dans la vallée du Rhône, le Diois, les Baronnies et le long du système de faille de Belledonne, le champ de contrainte subit une rotation anti-horaire de 30° à 45° et il est toujours compressif à décrochant. Il est devenu essentiellement décrochant le long du système de faille de Belledonne, en accord avec la cinématique dextre des failles constitutives de ce dernier. Ces états de contrainte tardifs sont comparables à ceux déterminés par l'inversion des mécanismes au foyer (Baroux, 2000; Delacou et al., 2004; ce travail). Enfin, plus au Sud, le massif de l'Argentera est soumis à une transpression, avec une contrainte σ_1 subméridienne impliquant une cinématique dextre des failles orientées NW-SE (Bauve et al., 2014; Guillaume Sanchez et al., 2010). L'extension mise en évidence dans cette zone (Larroque et al., 2009; Guillaume Sanchez et al., 2010) pourrait n'être que local et liée à un système en pull-appart (Bauve et al., 2014; Guillaume Sanchez et al., 2010). Au sud du massif de l'Argentera, la marge de la mer Ligure est pour sa part caractérisée par un régime décrochant caractérisé par un axe σ_1 orienté NNW-SSE et la partie Nord de la mer Ligure par un régime compressif caractérisé par un axe σ_1 orienté WNW-ESE (Baroux et al., 2001).

La déformation plio-quaternaire est donc complexe et il faut ajouter à cela le fait que les Alpes, depuis les unités externes vers les unités internes, présentent actuellement des taux de surrection de 0,5 à 3 $mm.an^{-1}$ (Serpelloni et al., 2013; Walpersdorf et al., 2015), ce qui est cohérent avec le basculement vers l'extérieur de la chaîne des plateaux conglomératiques plio-quaternaires de Chambaran et de Valensole (Champagnac et al., 2008). Plusieurs modèles et processus peuvent être proposés en vue de l'expliquer.

La convergence entre les plaques africaine et européenne (de 3 $mm.an^{-1}$ à l'ouest (Gibraltar) à 7 $mm.an^{-1}$ à l'est (Tunisie)) selon une direction NW-SE à NNW-SSE (Argus et al., 1989; Calais et al., 2003) ne permet pas d'expliquer la cinématique dextre du système de faille de Belledonne. De plus, la croûte très amincie et fracturée du bassin liguro-provençal (Carminati et al., 2004; Roca and Guimerá, 1992) ne présente presque aucune sismicité, cette dernière étant concentrée sur les marges (Vannucci et al., 2004) suggérant que l'essentiel de la déformation liée à la remontée de la plaque africaine soit accommodée le long des côtes méditerranéennes du Maroc, de l'Algérie et de la Tunisie. Une partie de la convergence pourrait cependant être transmise au travers du bloc corso-sarde (Billi et al., 2011), ce dernier convergeant vers l'Europe à ~0,3 $mm.an^{-1}$ selon une direction NW-SE (Nocquet, 2012) ce qui est cohérent avec la compression orientée WNW-ESE rencontrée dans le Nord de la mer Ligure (Baroux et al., 2001).

L'indentation d'un coin de lithosphère mantellique de la plaque apulienne, du fait de la poursuite d'une partie de la convergence, permettrait d'expliquer le champ de contrainte actuel (Lardeaux et al., 2006). Cette hypothèse est basée sur le fait que la topographie calculée à partir d'un modèle à l'équilibre isostatique cohérent avec la coupe géologique d'échelle crustale ne correspond pas à celle observée et lui est inférieure, impliquant que des forces tectoniques sont nécessaires pour compenser la gravité. Un tel modèle est cohérent avec la compression observée dans le Jura et la Chartreuse mais ne pourrait être confirmé que par la mise en évidence par mesures géodésiques de la poursuite de la convergence entre les plaques apulienne et européenne ce qui n'a toujours pas été confirmé aujourd'hui (Nocquet, 2012). Enfin, les calculs ayant conduit à cette hypothèse devraient être à nouveau effectués sur le modèle géologique d'échelle crustale produit récemment par Zhao et al. (2015) qui est notamment en désaccord avec le précédent modèle sur la géométrie du corps d'Ivrée (le coin mantellique de la plaque apulienne).

Les mesures géodésiques indiquent que la plaque apulienne subit une rotation anti-horaire à une vitesse inférieure à 1°/Ma (Battaglia et al., 2004; Calais et al., 2002; Serpelloni et al., 2005). Cette seule rotation permet d'expliquer la cinématique dextre le long du système de faille de Belledonne, du système de faille de Mérindol-Condorcet-Saillans, de la bordure orientale de la nappe de Digne (Hippolyte et al., 2011), mais également le long des failles NW-SE du massif de l'Argentera. Cette rotation impliquerait ~1 $mm.an^{-1}$ de glissement cumulés le long de l'ensemble des décrochements dextres des Alpes de l'ouest accommodant cette rotation (Nocquet and Calais, 2004), la vitesse proposée pour la faille du Jasneuf (0,13±0,03 $mm.yr^{-1}$) semble donc réaliste. La compression en Provence peut dans ce contexte être expliquée par un transfert de la déformation du domaine alpin le long du système de faille de Mérindol-Condorcet-Saillans de même que la compression en mer Ligure résulterait du transfert de la déformation le long des accidents NO-SE du massif de l'Argentera. Un modèle semblable de déformation avait déjà été proposé par Gidon (1974) pour expliquer la forme arquée des Alpes et les modélisations analogiques (Collombet, 2001) produisent des résultats comparables aux systèmes de failles énumérés précédemment (Fig. VI.1). Néanmoins, un tel modèle ne permet pas de retrouver un analogue au Jura est ses failles actives senestres orientées NW-SE (Baize et al., 2011; De La Taille et al., 2015). De plus l'extension radiale dans la chaîne interne ne peut être expliquée dans un contexte géodynamique gouverné uniquement par la rotation de la plaque apulienne. Les modèles numériques ne prenant en compte que la rotation de la plaque apulienne ne parviennent d'ailleurs pas à recréer le champ de contrainte actuel (Delacou et al., 2005; Jiménez-Munt et al., 2005).

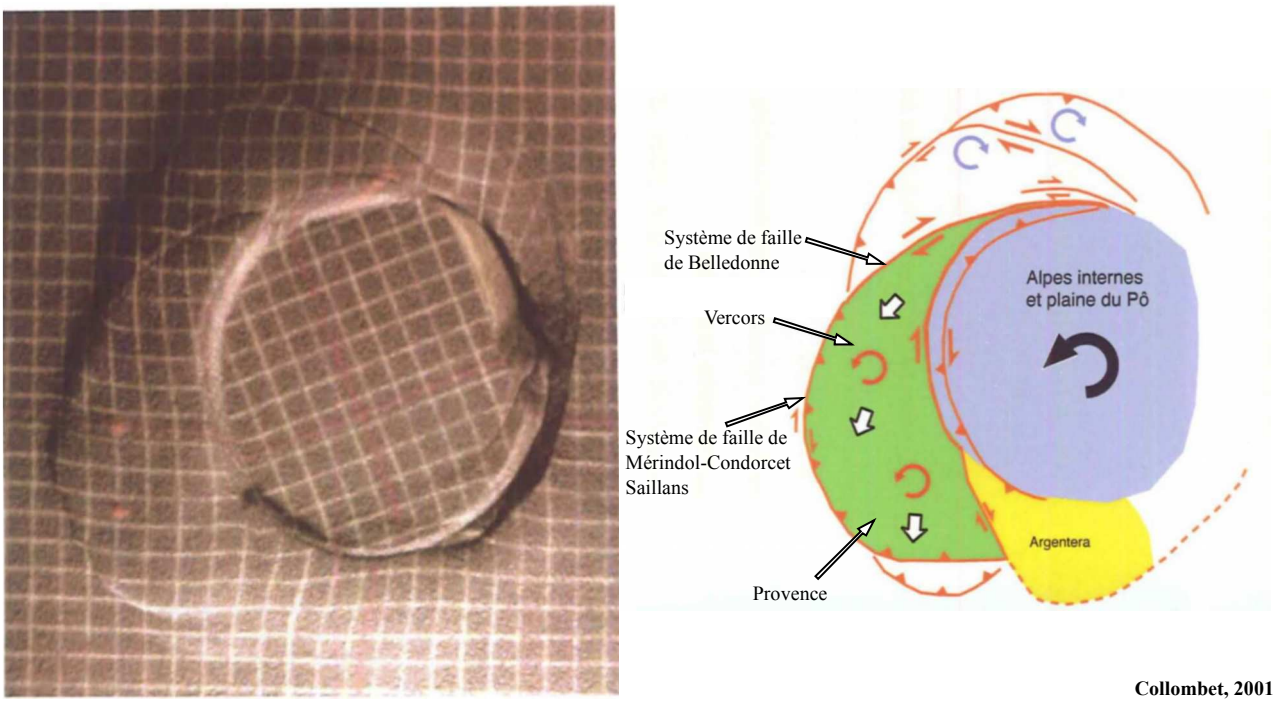

Figure VI.1: Résultats d'une modélisation analogique des Alpes par une plaque tournant sous du sable (Collombet, 2001). On peut noter l'analogie avec les failles actives actuelles du quart SE de la france. Les failles sénestres du Jura sont en revanche manquantes.

La modélisation numérique du champ de contrainte généré uniquement par l'énergie potentielle gravitationnelle permet de déterminer des champs proches de l'actuel (Delacou et al., 2005; Jiménez-Munt et al., 2005) avec une extension perpendiculaire à la chaîne dans les zones internes et une compression perpendiculaire à la chaîne dans les zones externes. Il reste cependant nécessaire d'inclure la rotation de la plaque apulienne dans les modèles afin de recréer le cisaillement dextre le long du système de Belledonne (Delacou et al., 2005; Jiménez-Munt et al., 2005). Cependant, un étalement gravitaire implique un amincissement de la croûte (par exemple, Ménard and Molnar (1988)) et donc un affaissement des zones internes en contradiction avec les mesures géodésiques récentes (Serpelloni et al., 2013; Walpersdorf et al., 2015).

La convergence étant nulle d'après la géodésie, il convient donc de chercher la cause de l'élévation de la chaîne par un potentiel réajustement isostatique. Les vitesses de surrection liées au rebond glaciaire modélisées à l'échelle des Alpes sont de ~0,2 $mm.an^{-1}$ (Barletta et al., 2006; Stocchi et al., 2005) et peuvent localement atteindre ~0,9 $mm.an^{-1}$ (Barletta et al., 2006) ce qui ne suffit pas à expliquer les ~2 $mm.an^{-1}$ de surrection dans les Alpes internes. De plus, à l'échelle européenne et en prenant en compte le retrait de l'inlandsis eurasiatique, la modélisation du réajustement isostatique prédit une subsidence de ~0,4 $mm.an^{-1}$ (Serpelloni et al., 2013).

Molnar and England (1990) avaient proposé que l'érosion puisse favoriser l'élévation des reliefs par réajustement isostatique. Des travaux de modélisation numérique ont permis de démontrer que l'érosion peut induire à la fois de l'extension et de la surrectione dans les parties hautes d'une chaîne de montagnes accommodant peu voir aucune convergence (Vernant et al., 2013). La modélisation du rebond isostatique lié à l'érosion pour les Alpes prévoit des vitesses d'élévation de 0,4 à 0,5 $mm.an^{-1}$ (Champagnac et al., 2007) ce qui reste insuffisant.

Il convient donc d'invoquer une source plus profonde. La rupture du slab de la plaque européenne, observée par tomographie télésismique (Lippitsch et al., 2003) pour les Alpes de l'ouest, impliquerait un soulèvement par réajustement isostatique qui pourrait expliquer la part manquante du soulèvement (Sue et al., 1999).

La dynamique actuelle des Alpes de l'Ouest résulte donc de multiple facteurs (Fig. VI.2) :

- La rotation de la plaque apulienne est accommodée notamment le long du système de faille de Belledonne et le long des failles NO-SE du massif de l'Argentera. Cette déformation pourrait être transférée en Provence le long du système de faille de Mérindol-Condorcet-Saillans et dans le nord de la mer Ligure via les failles NW-SE du massif de l'Argentera.

- La convergence des plaques africaine et européenne pourrait participer à la compression du nord de la mer Ligure par transfert au travers du bloc corso-sarde.

- L'étalement gravitaire est à l'origine d'une partie de l'extension des zones internes. L'énergie potentielle gravitationnelle de ces zones hautes est transférée vers le Jura et la marge ouest de la plaine du Pô permettant leur compression mais pourrait aussi être à l'origine d'une partie des déformations de la nappe de Digne, du Diois, des Baronnies et de la Provence.

- Le soulèvement de l'ensemble de la chaîne est lié au réajustement isostatique causé par la rupture du slab, l'érosion de la chaîne et peut être à la déglaciation. Ce soulèvement pourrait d'ailleurs entretenir l'étalement gravitaire en permettant à la chaîne de conserver de l'énergie potentielle gravitationnelle.

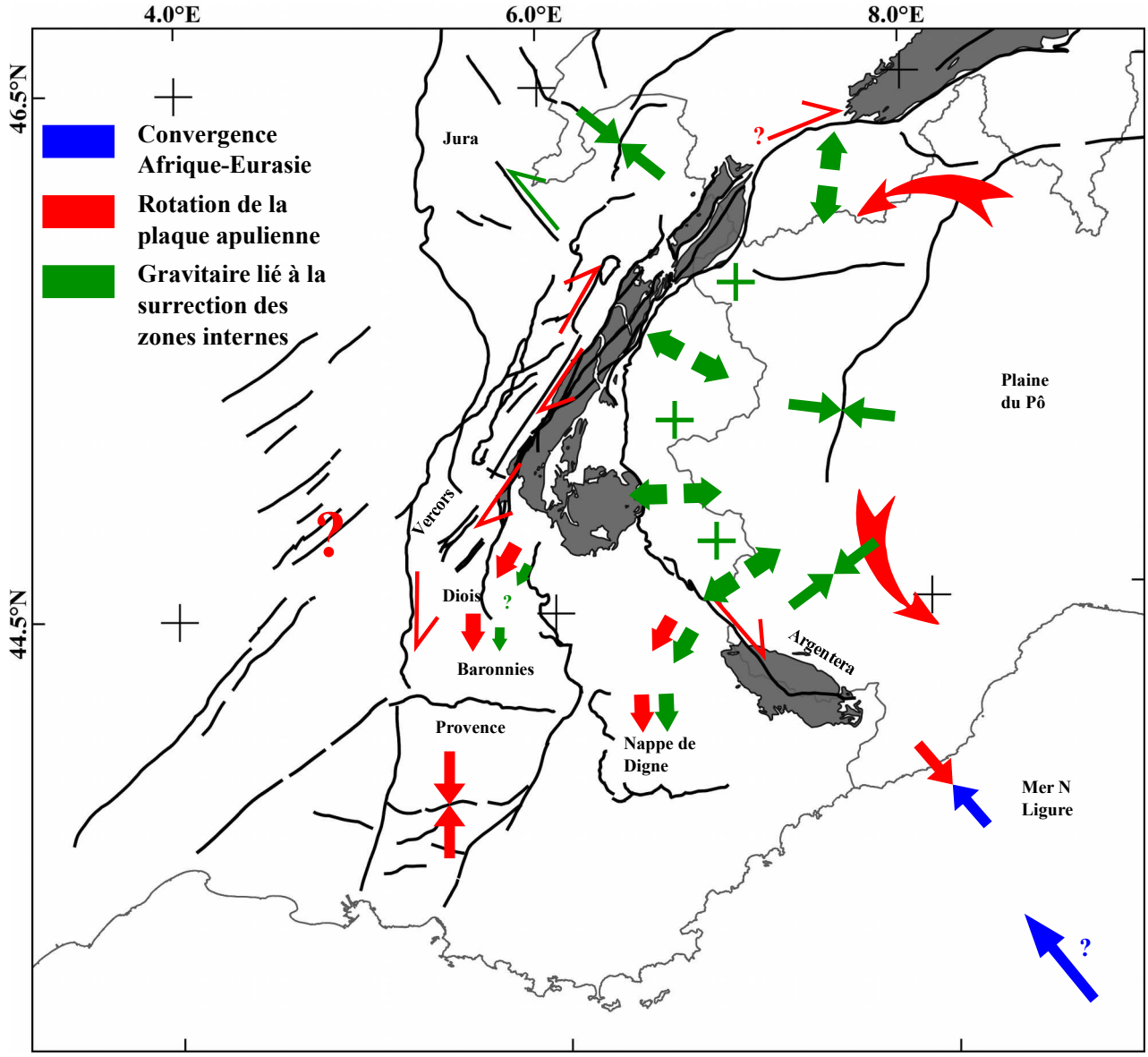

Figure VI.2: modèle géodynamique proposé pour le quart sud est de la France. Voir le texte pour les explications.

VI.1.3 - Conclusions et perspectives

VI.1.3.1 - Apports méthodologiques

L'étude des anomalies géomorphologiques liées à l'activité de la faille du Jasneuf nous a permis de mettre en évidence deux points méthodologiques importants pour de futures études de tectonique active suivant une approche morphotectonique.

Nous avons ainsi démontré que des décalages apparents de cours d'eau interprétés comme liés au jeu d'une faille peuvent en fait correspondre à des distances interfluves moyennes. Il nous semble donc que cette possibilité doit être systématiquement testée dès que les décalages de cours d'eau mesurés excèdent la distance interfluve. Il n'est pas exclu que le décalage enregistré par le réseau hydrographique le long d'une faille puisse être égal ou supérieur à une distance interfluve moyenne, mais il s'agit alors d'un fait à argumenter.

Nous proposons également une nouvelle méthode ne nécessitant pas la définition de « piercing point » pour contraindre les décalages de faille. Les premiers tests effectués indiquent que la méthode fonctionne mais de plus amples tests, notamment sur des failles normales et inverses, restent à effectuer. Cette méthode apparaît être également robuste lorsqu'elle est appliquée sur des données topographiques à haute résolution, notamment grâce au fait que de très nombreuses mesures peuvent être effectuées. Il conviendrait néanmoins d'effectuer des tests de reproductibilité, l'erreur liée à l'utilisateur pouvant être supérieure à celle intrinsèque à la méthode.

VI.1.3.2 - Apports sur la connaissance du système de faille active de Belledonne.

Nous avons pu démontrer que la faille bordière de Belledonne fait partie d'un système de faille active dextre d'environ 150 km de long comprenant la faille de l'Arcalod au nord-est et la faille du Jasneuf au sud-ouest. L'état de contrainte responsable de la cinématique actuelle de ces failles s'est mis en place durant ou après le Pliocène supérieur.

Les anomalies morphologiques associées à la faille d'Arcalod sont ambiguës mais peuvent tout de même indiquer une activité quaternaire de cette faille. Les failles normales en terminaison de la faille d'Arcalod présentent des escarpements récents mais fonctionnent possiblement aujourd'hui comme des sackungs dont le jeu serait facilité par une composante tectonique. Les sackungs sont fréquents dans les Alpes. Contraindre les vitesses de glissement de l'ensemble des sackungs alpins serait intéressant car cela pourrait potentiellement permettre de mettre en évidence des signaux liés à de la tectonique active. Les failles normales en terminaison de

la faille d'Arcalod pourraient par exemple présenter des vitesses de glissement supérieures par rapport aux sackungs uniquement « gravitaire » du fait qu'elles accommoderaient à la fois le jeu dextre de la faille d'Arcalod et une déformation gravitaire.

Aucune anomalie morphologique associée au jeu de la faille bordière de Belledonne n'a été mise en évidence. Nous proposons que la déformation puisse être accommodée par une large bande de déformation en cisaillement. Néanmoins, il n'est pas exclu que nous ayons échoué à identifier la trace de la faille en surface du fait de données topographiques de trop faible résolution ou du couvert végétal. Une analyse morphologique appuyée par des données topographiques plus fines (l'IGN est actuellement en train de doter le territoire français d'un modèle numérique de terrain d'une résolution de 1 à 5 m) pourrait être envisagée. Il est également nécessaire de contraindre la géométrie de cette faille. Cette faille recoupe l'ensemble des unités chevauchantes avant d'atteindre le socle (fig. I.2), impliquant que sur les dix premiers kilomètres de profondeur elle est recoupée par plusieurs chevauchements qui pourrait ainsi délimiter plusieurs segments et donc limiter l'aire de faille jouant durant une rupture. En revanche, il est possible qu'en profondeur, dans le socle chevauché, cette faille utilise une ancienne faille normale téthysienne crustale ce qui impliquerait un fort potentiel sismogénique (fig. I.2). Il semble donc nécessaire de contraindre la segmentation aussi bien latérale que verticale de cette faille. **L'analyse des replats glaciaires de part et d'autre de la vallée du Grésivaudan semble indiquer que les replats au sud-est de la vallée sont légèrement plus élevés que ceux au nord-ouest. De même, il est étonnant de constater que les knick-points des cours d'eau et les replats glaciaires le long du balcon de Belledonne aient une altitude constante et que l'on ne retrouve pas dans leur répartition altimétrique la pente du glacier de l'Isère. Cela pourrait indiquer un basculement de la zone selon un axe perpendiculaire à la vallée du Grésivaudan.** Une cartographie plus fine de ces replats ainsi que leur datation pourrait permettre de mettre en évidence et caractériser le basculement de la zone (ou la surrection des massifs cristallins externes en fonction des interprétations) durant les derniers 34ka.

La faille senestre du Brion décale la vallée formée par le glacier de l'Isère ce qui atteste de son activité durant le Quaternaire. L'âge des décalages n'est pas contraint et empêche la détermination de la vitesse de glissement. La vallée glaciaire a été comblée de sédiments lacustres après le retrait du glacier würmien. Contraindre le décalage de cette vallée enfouie grâce à des prospections géophysiques de subsurfaces pourrait permettre d'améliorer la détermination de la vitesse de la faille du Brion.

La faille dextre du Jasneuf présente des anomalies morphologiques d'origine tectonique. La vitesse de glissement intégrée depuis le Messinien que nous proposons est de

0,13±0,03 mm.yr^{-1}. En considérant que l'extension de cette faille est limitée latéralement aux Hauts Plateaux du Vercors et verticalement à la couverture sédimentaire et que l'accommodation de la déformation ne s'effectue pas par glissement asismique, cette faille pourrait générer des séismes de magnitude 5,7 tous les ~500 ans. Il convient donc maintenant de mieux contraindre le potentiel sismogénique de cette faille : 1- en précisant sa géométrie notamment en profondeur (faille de socle ou non), 2- en effectuant des tranchées pour attester de l'existence ou non de rupture en surface et donc d'accommodation sismique et 3- en tentant de mieux contraindre sa vitesse de glissement, potentiellement par datation des âges d'exposition des escarpements présents sur le plateau. De plus, les autres failles orientées NE-SW dans la région devraient être prospectées. Il n'y a en effet aucune raison que seule la faille du Jasneuf accommode le décrochement, la faille de la Cléry se trouvant à seulement 3 km au nord-ouest et la faille de Ménée à ~7,5 km au sud-est.

La relation entre le système de faille de Belledonne et les accidents cévenols n'est pas clairement établie même si un champ de contrainte homogène et cohérent avec celui du système de faille de Belledonne existe dans la vallée du Rhône au Plio-Quaternaire. La morphologie messinienne est discontinue de part et d'autre de la faille de Toulaud. Un jeu vertical plio-quaternaire de 18±1 m a pu être identifié mais le décalage latéral reste incertain. La densification des mesures géophysiques de subsurfaces à proximité de la faille est nécessaire en vue de mieux contraindre un possible décalage latéral.

RÉFÉRENCES BIBLIOGRAPHIQUES

Aguilar, J.-P., Clauzon, G., de Goer de Herve, A., Maluski, H., Michaux, J., Welcomme, J.-L., 1996. The MN3 fossil mammal-bearing locality of Beaulieu (France): Biochronology, Radiometric dating, and lower age limit of the Early Neogene renewal of the mammalian fauna in Europe. Newsletters Stratigr. 34, 177–191.

Angelier, J., 1975. Sur l'analyse de mesures recueillies dans des sites faillés: l'utilité d'une confrontation entre les méthodes dynamiques et cinématiques. Comptes rendus l'Académie des Sci. Série D, Sci. Nat. 281, 1805–1808.

Angelier, J., 1990. Inversion of field data in fault tectonics to obtain the regional stress-III. A new rapid direct inversion method by analytical means. Geophys. J. Int. 103, 363–376. doi:10.1111/j.1365-246X.1990.tb01777.x

Angelier, J., Mechler, P., 1977. Sur une methode graphique de recherche des contraintes principales egalement utilisables en tectonique et en seismologie : la methode des diedres droits. Bull. la Société Géologique Fr. S7-XIX, 1309–1318. doi:10.2113/gssgfbull.S7-XIX.6.1309

Argus, D.F., Gordon, R.G., Demets, C., Stein, S., 1989. Azores triple junction record a rate of 24 mm/yr, 4 mm/yr slower than used by prior models. 94, 5585–5602.

Arnaud, H., 1966. Contribution à l'étude du Diois nord-oriental. Trav. Lab. Géol. Grenoble 42, 17–31.

Arnaud, H., 1971. Le plateau de Glandasse: structure et place dans le cadre géologique régional. Géologie Alp. 47, 25–44.

Arnaud, H., 1981. De la plate-forme urgonienne au bassin vocontien: le Barrémo-Bédoulien des Alpes occidentales entre Isère et Buëch (Vercors méridional, Diois orental et Dévoluy). Géol. Alp. (Grenoble), Mém.

Arnaud, H., Montjuvent, G., Gonnard, R., 1974. Carte géologique de la france à 1/50 000 : Mens (feuille 844). Orléans.

Arpin, R., 1988. Déformations et déplacements des massifs subalpins de Vercors et Chartreuse. Université Joseph Fourier de Grenoble.

Arthaud, F., 1969. Methode de determination graphique des directions de raccourcissement, d'allongement et intermediaire d'une population de failles. Bull. la Société Géologique Fr. S7-XI, 729–737. doi:10.2113/gssgfbull.S7-XI.5.729

Arthaud, F., Laurent, P., 1995. Contraintes, déformation et déplacement dans l'avant-pays Nord-pyrénéen du Languedoc méditerranéen. Geodin. Acta 8, 142–157.

Arthaud, F., Matte, P., 1975. Les decrochements tardi-hercyniens du sud-ouest de l'europe. Geometrie et essai de reconstitution des conditions de la deformation. Tectonophysics 25, 139–171. doi:10.1016/0040-1951(75)90014-1

Bache, F., Olivet, J.L., Gorini, C., Aslanian, D., Labails, C., Rabineau, M., 2010. Evolution of rifted continental margins: The case of the Gulf of Lions (Western Mediterranean Basin). Earth Planet. Sci. Lett. 292, 345–356. doi:10.1016/j.epsl.2010.02.001

Bailly, T., Cushing, M., Nechtschein, S., Dussoulliez, P., Gonzales, A., Aymard, B., Bellier, O., Hollender, F., Gaune, R., 2013a. Cartographie des fréquences fondamentales par mesures H/V – Fossé de Pujaut.

Bailly, T., Hollender, F., Dussoulliez, P., Cushing, M., Nechtschein, S., Bellier, O., 2013b. Profil de vitesse Vs obtenu par mesures de vibrations ambiantes dans le fossé de Pujaut.

Baize, S., Cushing, M., Lemeille, F., Gelis, C., Texier, D., Nicoud, G., Schwenninger, J.L., 2011. Contribution to the seismic hazard assessment of a slow active fault, the Vuache fault in the southern Molasse basin (France). Bull. la Soc. Geol. Fr. 182, 347–365. doi:10.2113/gssgfbull.182.4.347

Baize, S., Cushing, M., Lemeille, F., Granier, T., Grellet, B., Carbon, D., Combes, P., Hibsch, C., 2002. Inventaire des indices de rupture affectant le Quaternaire en relation avec les grandes structures connues en France métropolitaine et dans les régions limitrophes. Mémoire la société géologique Fr. H.S. 175, 142.

Ballesio, R., 1972. Étude stratigraphique du Pliocène rhodanien. Doc. des Lab. Géologie Lyon 55, 333.

Barazza, F., Malisan, P., Carniel, R., 2009. Improvement of H/V technique by rotation of the coordinate system. Commun. Nonlinear Sci. Numer. Simul. 14, 182–193. doi:10.1016/j.cnsns.2007.11.016

Bard, P.-Y., Bouchon, M., 1985. The Two-Dimensional Resonance of Sediment-Filled Valleys. Bull. Seismol. Soc. Am. 75, 519–541.

Barféty, J.C., Bordet, P., Carme, F., Debelmas, J., Meloux, M., Monjuvent, G., Mouterde, R., Sarrot-reynauld, J., 1972a. Carte géologique de la france à 1/50 000 : Vizille (feuille 797). Orléans.

Barféty, J.C., Debelmas, J., Mouterde, R., 1972b. Caractères stratigraphiques, paléontologiques et structuraux du Jurassique inférieur et moyen des bordures W et SE du massif de Belledonne (Isère). Géologie Alp. 48, 61–86.

Barféty, J.C., Gidon, M., 1990. La tectonique alpine du massif cristallin du Taillefer (Alpes occidentales françaises) : découverte de chevauchements vers le Nord. Géologie Alp. 66, 1–9.

Barféty, J.C., Gidon, M., 1996. La structure des Collines bordières du Grésivaudan et des secteurs adjacents, à l'est de Grenoble (Isère, France), (cartes géologiques à 1/50000 Domène et Vizille). Géologie Alp. 72, 5–22.

Barféty, J.C., Gidon, M., Lemoine, M., Mouterde, R., 1979. Tectonique synsédimentaire liassique dans les massifs cristallins de la zone externe des Alpes occidentales françaises : la faille du col d'Ornon. Comptes rendus Hebd. des séances l'Académie des Sci. Série D, Sci. Nat. 289, 1207–1210.

Barféty, J.C., Gidon, M., Ménot, R.-P., Debon, F., 2000. Carte géologique de la france à 1/50 000 : Domène (feuille 773)., 2ème ed. Orléans.

Barletta, V.R., Ferrari, C., Diolaiuti, G., Carnielli, T., Sabadini, R., Smiraglia, C., 2006. Glacier shrinkage and modeled uplift of the Alps. Geophys. Res. Lett. 33, L14307. doi:10.1029/2006GL026490

Baroux, E., 2000. Tectonique active en région à sismicité modérée : le cas de la provence (France). Apport d'une approche pluridisciplinaire. Université de Paris 11, Orsay, France.

Baroux, E., Béthoux, N., Bellier, O., 2001. Analyses of the stress field in southeastern France from earthquake focal mechanisms. Geophys. J. Int. 145, 336–348. doi:10.1046/j.1365-246x.2001.01362.x

Baroux, E., Pino, N.A., Valensise, G., Scotti, O., Cushing, E.M., 2003. Source parameters of the 11 June 1909, Lambesc (Provence, southeastern France) earthquake: A reappraisal based on macroseismic, seismological, and geodetic observations. J. Geophys. Res. doi:10.1029/2002JB002348

Battaglia, M., Murray, M.H., Serpelloni, E., Bürgmann, R., 2004. The Adriatic region: An independent microplate within the Africa-Eurasia collision zone. Geophys. Res. Lett. 31, L09605. doi:10.1029/2004GL019723

Bauve, V., Plateaux, R., Rolland, Y., Sanchez, G., Bethoux, N., Delouis, B., Darnault, R., 2014. Long-lasting transcurrent tectonics in SW Alps evidenced by Neogene to present-day stress fields. Tectonophysics 621, 85–100. doi:10.1016/j.tecto.2014.02.006

Beaudoin, B., Accarie, H., Berger, E., Brulhet, J., Cojan, I., Haccard, D., Mercier, D., Mouroux, B., Clauzon, G., 1997. Caractérisation de la "crise messinienne" et de la réinondation pliocène, in: Journées Scientifiques de l'ANDRA. p. 77.

Beck, C., Deville, E., Blanc, E., Philippe, Y., Tardy, M., 1998. Horizontal shortening control of Middle Miocene marine siliciclastic accumulation (Upper Marine Molasse) in the southern termination of the Savoy Molasse Basin (northwestern Alps/southern Jura). Geol. Soc. London, Spec. Publ. 134, 263–278. doi:10.1144/GSL.SP.1998.134.01.12

Bellahsen, N., Jolivet, L., Lacombe, O., Bellanger, M., Boutoux, a., Garcia, S., Mouthereau, F., Le Pourhiet, L., Gumiaux, C., 2012. Mechanisms of margin inversion in the external Western Alps: Implications for crustal rheology. Tectonophysics 560-561, 62–83. doi:10.1016/j.tecto.2012.06.022

Bellahsen, N., Mouthereau, F., Boutoux, A., Bellanger, M., Lacombe, O., Jolivet, L., Rolland, Y., 2014. Collision kinematics in the western external Alps. Tectonics 33, 1055–1088. doi:10.1002/2013TC003453

Bellier, O., Vergely, P., 1987. États de contraintes et tectogenèse cénozoïque du plateau calcaire de Basse Ardèche (France). Comptes Rendus l'Académie des Sci. - Ser. II 305, 1379–1382.

Bellier, O., Zoback, M. Lou, 1995. Recent state of stress change in the Walker Lane zone, western Basin and Range province, United States. Tectonics 14, 564–593. doi:10.1029/94TC00596

Bergerat, F., 1981a. Le couloir rhodanien au Paléogène: analyse de la fracturation et interprétation cinématique régionale. Rev. Géogr. Phys. Géol. Dyn. 23, 329–343.

Bergerat, F., 1981b. Dynamique des accidents cévenols au cours du Tertiaire. Comptes Rendus l'Academie des Sci. Paris Série II 292, 1049–1052.

Bergerat, F., 1985. Déformations cassantes et champs de contrainte tertiaires dans la plate-forme européenne. Université Pierre et Marie Curie.

Billant, J., Hippolyte, J.-C., Bellier, O., 2015. Tectonic and geomorphic analysis of the Belledonne border fault and its extensions, Western Alps. Tectonophysics 659, 31–52. doi:10.1016/j.tecto.2015.07.025

Billi, A., Faccenna, C., Bellier, O., Minelli, L., Neri, G., Piromallo, C., Presti, D., Scrocca, D., Serpelloni, E., 2011. Recent tectonic reorganization of the Nubia-Eurasia convergent boundary heading for the closure of the western Mediterranean. Bull. la Soc. Geol. Fr. 182, 279–303.

Bistacchi, A., Eva, E., Massironi, M., Solarino, S., 2000a. Miocene to Present kinematics of the NW-Alps: evidences from remote sensing, structural analysis, seismotectonics and thermochronology. J. Geodyn. 30, 205–228.

Bistacchi, A., Eva, E., Massironi, M., Solarino, S., 2000b. Miocene to Present kinematics of the NW-Alps: evidences from remote sensing, structural analysis, seismotectonics and thermochronology. J. Geodyn. 30, 205–228.

Bistacchi, A., Massironi, M., 2000. Post-nappe brittle tectonics and kinematic evolution of the north-western Alps: an integrated approach. Tectonophysics 327, 267–292. doi:10.1016/S0040-1951(00)00206-7

Blés, J.L., Bonijoly, D., Castaing, C., Gros, Y., 1989. Successive post-Variscan stress fields in the French Massif Central and its borders (Western European plate): comparison with geodynamic data. Tectonophysics 169, 79–111. doi:10.1016/0040-1951(89)90185-6

Bodelle, J., Goguel, J., 1980. Carte géologique de la France et de la marge continentale (1/1 500 000). Orléans.

Bonvalot, S., 2012. “The International Gravimetric Bureau”. In: IAG Geodesist’s Handbook. J. Geod. 86, 946–949.

Bordet, P., 1970. Les failles vivantes du massif des Grands Moulins (Massif cristallin externe de Belledonne). Géologie Alp. 46, 43–47.

Bornand, M., Mandier, P., Montjuvent, G., Chenevoy, M., Horon, O., Combier, J., 1974. Carte géologique de la france à 1/50 000 : Valence (feuille 818). Orléans.

Bott, M.H.P., 1959. The Mechanics of Oblique Slip Faulting. Geol. Mag. 96, 109. doi:10.1017/S0016756800059987

Bourcart, J., Glangeaud, L., 1954. Morphotectonique de la marge continentale nord-africaine. Bull. la Société géologique Fr. 6, 751–772.

Brocard, G., 2002. Origine, variabilité spatio-temporelle et signature morphologique de l’incision fluvial dans les Alpes dauphinoises (SE France). Géologie Alp. Université Joseph Fourier, Grenoble.

Buoncristiani, J.-F., Campy, M., 2011. Quaternary Glaciations in the French Alps and Jura, in: Ehlers, J., Gibbard, P.L., Hughes, P.D. (Eds.), Quaternary Glaciations - Extent and Chronology - A Closer Look, Developments in Quaternary Sciences. Elsevier, pp. 117–125. doi:10.1016/B978-0-444-53447-7.00010-6

Burkhard, M., Sommaruga, A., 1998. Evolution of the western Swiss Molasse basin: structural relations with the Alps and the Jura belt. Geol. Soc. London, Spec. Publ. 134, 279–298. doi:10.1144/GSL.SP.1998.134.01.13

Busson, G., Blanc-Valleron, M.-M., Cornée, A., Curial, A., Dromart, G., Dumas, D., Moretto, R., Rouchy, J.-M., Schreber, C., 1992. Bassins paléogènes salifères de l'Est de la France (Valence, Bresse et Haute-Alsace). Géologie la Fr. 1, 15–64.

Butler, R., 1987. Thrust evolution within previously rifted regions: an example from the Vercors, French Subalpine chains. Mem. della Soc. Geol. Ital. 38, 5–18.

Butler, R.W.H., 1992. Structural evolution of the western Chartreuse fold and thrust system, NW French Subalpine chains, in: McClay, K.R. (Ed.), Thrust Tectonics. Springer Netherlands, Dordrecht, pp. 287–298.

Calais, É., Bayer, R., Chéry, J., Cotton, F., Doerflinger, E., Flouzat, M., Jouanne, F., Kasser, M., Laplanche, M., Maillard, D., Martinod, J., Mathieu, F., Nicolon, P., Nocquet, J.-M., Scotti, O., Serrurier, L., Tardy, M., Vigny, C., 2000. Regal : réseau GPS permanent dans les Alpes occidentales. Configuration et premiers résultats. Comptes Rendus l'Académie des Sci. - Ser. IIA - Earth Planet. Sci. 331, 435–442. doi:10.1016/S1251-8050(00)01441-5

Calais, E., DeMets, C., Nocquet, J.-M., 2003. Evidence for a post-3.16-Ma change in Nubia–Eurasia–North America plate motions? Earth Planet. Sci. Lett. 216, 81–92. doi:10.1016/S0012-821X(03)00482-5

Calais, E., Nocquet, J., Jouanne, F., Tardy, M., 2002. Current strain regime in the Western Alps from continuous Global Positioning System measurements, 1996–2001. Geology 30, 651–654. doi:10.1130/0091-7613(2002)030<0651:CSRITW>2.0.CO;2

Caporali, A., Martin, S., 2000. First results from GPS measurements on present day alpine kinematics. J. Geodyn. 30, 275–283. doi:10.1016/S0264-3707(99)00037-X

Cara, M., Cansi, Y., Schlupp, A., Arroucau, P., Bethoux, N., Beucler, E., Bruno, S., Calvet, M., Chevrot, S., Deboissy, A., Delouis, B., Denieul, M., Deschamps, A., Doubre, C., Frechet, J., Godey, S., Golle, O., Grunberg, M., Guilbert, J., Haugmard, M., Jenatton, L., Lambotte, S., Leobal, D., Maron, C., Mendel, V., Merrer, S., Macquet, M., Mignan, A., Mocquet, A., Nicolas, M., Perrot, J., Potin, B., Sanchez, O., Santoire, J.-P., Sebe, O., Sylvander, M., Thouvenot, F., Van Der Woerd, J., Van Der Woerd, K., 2015. SI-Hex: a new catalogue of instrumental seismicity for metropolitan France. Bull. la Société Géologique Fr. 186, 3–19. doi:10.2113/gssgfbull.186.1.3

Carey, E., Brunier, B., 1974. Analyse théorique et numérique d'un modèle mécanique élémentaire appliqué à l'étude d'une population de failles. Comptes rendus l'Académie des Sci. Série D, Sci. Nat. 279, 891–894.

Carey-Gailhardis, E., Mercier, J.L., 1987. A numerical method for determining the state of stress using focal mechanisms of earthquake populations: application to Tibetan teleseisms and microseismicity of Southern Peru. Earth Planet. Sci. Lett. 82, 165–179. doi:10.1016/0012-821X(87)90117-8

Carminati, E., Doglioni, C., Argnani, A., Carrara, G., Dabovski, C., Dumurdzhanov, N., Gaetani, M., Georgiev, G., Mauffret, A., Nazai, S., Sartori, R., Scionti, V., Scrocca, D., Séranne, M., Torelli, L., Zagorchev, I., 2004. TRANSMED - TRANSECT III: a description of the section and of the data sources, in: Cavazza, P., Roure, W., Spakman, F., Stampfli, W., Ziegler, G.M., P.A. Transmed Project Working Group (Eds.), The TRANSMED Atlas - The Mediterranean Region From Crust to Mantle. Springer Berlin Heidelberg, p. 141.

Casagrande Fioretti, L., 1985. Évolution tectonosedimentaire post-Eocene de la bordure ouest des Baronnies et du massif de Suzette (Chaînes subalpines des Baronnies). Paris Sud.

Champagnac, J.-D., 2006. Regional brittle extension in Quaternary sediments of Lanslebourg (Haute-Maurienne valley, western Alps). Bull. la Société Géologique Fr. 177, 215–223. doi:10.2113/gssgfbull.177.4.215

Champagnac, J.-D., Sue, C., Delacou, B., Burkhard, M., 2004. Brittle deformation in the inner NW Alps: from early orogen-parallel extrusion to late orogen-perpendicular collapse. Terra Nov. 16, 232–242. doi:10.1111/j.1365-3121.2004.00555.x

Champagnac, J.D., Molnar, P., Anderson, R.S., Sue, C., Delacou, B., 2007. Quaternary erosion-induced isostatic rebound in the western Alps. Geology 35, 195. doi:10.1130/G23053A.1

Champagnac, J.D., Van Der Beek, P., Diraison, G., Dauphin, S., 2008. Flexural isostatic response of the Alps to increased Quaternary erosion recorded by foreland basin remnants, SE France. Terra Nov. 20, 213–220. doi:10.1111/j.1365-3121.2008.00809.x

Chardon, D., Bellier, O., 2003. Geological boundary conditions of the 1909 Lambesc (Provence, France) earthquake : structure and evolution of the Trevaresse ridge anticline. Bull. la Société géologique Fr. 174, 497–510. doi:10.2113/174.5.497

Chardon, D., Hermitte, D., Nguyen, F., Bellier, O., 2005. First paleoseismological constraints on the strongest earthquake in France (Provence) in the twentieth century. Geology 33, 901. doi:10.1130/G21713.1

Chen, T., Akciz, S.O., Hudnut, K.W., Zhang, D.Z., Stock, J.M., 2015. Fault-Slip Distribution of the 1999 M w 7.1 Hector Mine Earthquake, California, Estimated from Postearthquake Airborne LiDAR Data. Bull. Seismol. Soc. Am. 105, 776–790. doi:10.1785/0120130108

Chenevoy, M., Elmi, S., Lorenchet de Monjamont, M., Combier, J., Michel, R., Gros, J.-J., Ballesio, R., Truc, G., 1976. Carte géologique de la france à 1/50 000 : Crest (feuille 842). Orléans.

Chiron, J.-C., Kerrien, Y., 1980. Carte géologique de la france à 1/250 000 : Lyon (feuille 29). Orléans.

Claudel, M., Dumont, T., 1999. A record of multistage continental break-up on the Briançonnais marginal plateau (Western Alps): Early and Middle-Late Jurassic rifting. Eclogae Geol. Helv. 92, 45–61.

Clauzon, G., 1974. L'hypothèse eustatique et le creusement prépliocène de la vallée du Rhône. Ann. Georgr. 83, 129–140. doi:10.3406/geo.1974.18930

Clauzon, G., 1982. Le canyon messinien du Rhone; une preuve decive du “desiccated deep-basin model” (Hsue, Cita and Ryan, 1973). Bull. la Société Géologique Fr. S7-XXIV, 597–610. doi:10.2113/gssgfbull.S7-XXIV.3.597

Clauzon, G., 1996. Limites de séquences et évolution géodynamique/Sequence boundaries and geodynamic evolution. Géomorphologie Reli. Process. Environ. 2, 3–21. doi:10.3406/morfo.1996.867

Clauzon, G., Fleury, T.J., Bellier, O., Molliex, S., Mocochain, L., Aguilar, J.P., 2011. Morphostructural evolution of the Luberon since the Miocene (SE France). Bull. la Soc. Geol. Fr. 182, 95–110.

Clauzon, G., Suc, J.-P., Gautier, F., Berger, A., Loutre, M.-F., 1996. Alternate interpretation of the Messinian salinity crisis: Controversy resolved? Geology 24, 363. doi:10.1130/0091-7613(1996)024<0363:AIOTMS>2.3.CO;2

Collombet, M., 2001. Cinématique et rotation des Alpes occidentales. Approche paléomagnétique et modélisation analogique. Université Joseph Fourier - Grenoble 1.

Collombet, M., Thomas, J.C., Chauvin, A., Tricart, P., Bouillin, J.P., Gratier, J.P., 2002. Counterclockwise rotation of the western Alps since the Oligocene: New insights from paleomagnetic data 21.

Combes, P., 1984. La tectonique récente de la Provence occidentale : microtectonique, caractéristiques dynamiques et cinématiques. Méthodologie de zonation tectonique et relations avec la sismicité. Université de Strasbourg.

Coutterand, S., 2010. Étude géomorphologique des flux glaciaires dans les Alpes Nord-Occidentales au Pléistocène Récent. Du maximum de la dernière glaciation aux premières étapes de la déglaciation. Université de Savoie.

Cushing, E.M., Bellier, O., Nechtschein, S., Lomax, A., Dervin, P., Guignard, P., Bove, L., 2007. A multidisciplinary study of a slow-slipping fault for seismic hazard assessment: the example of the Middle Durance Fault (SE France). Geophys. J. Int. doi:10.1111/j.1365-246X.2007.03683.x

Cushing, E.M., Bellier, O., Nechtschein, S., Sébrier, M., Lomax, A., Volant, P., Dervin, P., Guignard, P., Bove, L., 2008. A multidisciplinary study of a slow-slipping fault for seismic hazard assessment: the example of the Middle Durance Fault (SE France). Geophys. J. Int. 172, 1163–1178. doi:10.1111/j.1365-246X.2007.03683.x

D’Agostino, N., Avallone, A., Cheloni, D., D’Anastasio, E., Mantenuto, S., Selvaggi, G., 2008. Active tectonics of the Adriatic region from GPS and earthquake slip vectors. J. Geophys. Res. 113, B12413. doi:10.1029/2008JB005860

Dardeau, G., Atrops, F., Fortwengler, D., de Graciansky, P.-C., Marchand, D., 1988. Jeu de blocs et tectonique distensive au Callovien et à l’Oxfordian dans le bassin du Sud-Est de la France. Bull. la Société Géologique Fr. 4, 771–777.

Darmendrail, X., Menard, G., Tardy, M., 1994. Interprétation néotectonique d'anomalies géomorphologiques dans une grande vallée des Alpes nord-occidentales : le Grésivaudan. Comptes rendus l'Académie des Sci. Série 2. Sci. la terre des planètes.

De Graciansky, P.-C., Arnaud, H., Busnardo, R., Dardeau, G., Gerlier, A., Lemoine, M., Mascle, G., Philip, J., 1987. « Rifting » et basculement de blocs au Crétacé inférieur dans les Alpes occidentales : un écho à l'ouverture du Golfe de Gascogne. Comptes Rendus l'Academie des Sci. Paris Série II 305, 711–713.

De Graciansky, P.C., Lemoine, M., 1988. Early Cretaceous extensional tectonics in the southwestern French Alps : A consequence of North-Atlantic rifting during Tethyan spreading. Bull Soc Géol Fr. 8 ème sériel 4, 733–737. doi:10.2113/gssgfbull.IV.5.733

De La Taille, C., Jouanne, F., Crouzet, C., Beck, C., Jomard, H., de Rycker, K., Van Daele, M., 2015. Impact of active faulting on the post LGM infill of Le Bourget Lake (western Alps, France). Tectonophysics 664, 31–49. doi:10.1016/j.tecto.2015.08.024

Debelmas, J., Arnaud, H., Audebaud, E., Sarrot-reynauld, J., Montjuvent, G., 1967a. Carte géologique de la france à 1/50 000 : La Chapelle-en-Vercors (feuille 820). Orléans.

Debelmas, J., Barféty, J.C., Antoine, P., Girod, J.P., Bellamy, J., Chabod, J.C., Boullud, C., Bullière, J., Sarrot-reynauld, J., 1967b. Carte géologique de la france à 1/50 000 : Vif (feuille 796). Orléans.

Debelmas, J., Demarcq, G., 1980. LE BASSIN RHODANIEN (de Lyon à la Méditerranée). Géologie Alp. 56, 59–62.

Debelmas, J., Desmons, J., Carraro, F., Giraud, P., Montjuvent, G., Sacchi, R., 1979. Carte géologique de la france à 1/250 000 : Annecy (feuille 30). Orléans.

Debelmas, J., Kerckhove, C., 1980. II. Les alpes franco-italiennes. Géologie Alp. 56, 21–58.

Delacou, B., Sue, C., Champagnac, J.-D., Burkhard, M., 2004. Present-day geodynamics in the bend of the western and central Alps as constrained by earthquake analysis. Geophys. J. Int. 158, 753–774. doi:10.1111/j.1365-246X.2004.02320.x

Delacou, B., Sue, C., Champagnac, J.-D., Burkhard, M., 2005. Origin of the current stress field in the western/central Alps: role of gravitational re-equilibration constrained by numerical modelling. Geol. Soc. London, Spec. Publ. 243, 295–310. doi:10.1144/GSL.SP.2005.243.01.19

Delacou, B., Sue, C., Nocquet, J.-M., Champagnac, J.-D., Allanic, C., Burkhard, M., 2008. Quantification of strain rate in the Western Alps using geodesy: comparisons with seismotectonics. Swiss J. Geosci. 101, 377–385. doi:10.1007/s00015-008-1271-3

Delvaux, D., Sperner, B., 2003. New aspects of tectonic stress inversion with reference to the TENSOR program. Geol. Soc. London, Spec. Publ. 212, 75–100. doi:10.1144/GSL.SP.2003.212.01.06

Demarcq, G., 1960a. Contribution à l'Etude des Facies du Miocene de la Vallee du Rhone. Mitteilungen der Geol. Gesellschaft Wien 52, 93–104.

Demarcq, G., 1960b. Observations à propos de la série Pliocène du sondage de Pierrelate (Drôme). Comptes rendus Hebd. des séances l'Académie des Sci. 250, 4013–4015.

Denizot, G., 1952. Le Pliocène dans la vallée du Rhône. Rev. géographie Lyon 27, 327–357. doi:10.3406/geoca.1952.1144

Deville, É., Chauvière, A., 2000. Thrust tectonics at the front of the western Alps: constraints provided by the processing of seismic reflection data along the Chambéry transect. Comptes Rendus l'Académie des Sci. - Ser. IIA - Earth Planet. Sci. 331, 725–732. doi:10.1016/S1251-8050(00)01463-4

Dewey, J.F., Helman, M.L., Knott, S.D., Turco, E., Hutton, D.H.W., 1989. Kinematics of the western Mediterranean. Geol. Soc. London, Spec. Publ. 45, 265–283. doi:10.1144/GSL.SP.1989.045.01.15

Dèzes, P., Schmid, S.M., Ziegler, P. a., 2004. Evolution of the European Cenozoic Rift System: interaction of the Alpine and Pyrenean orogens with their foreland lithosphere. Tectonophysics 389, 1–33. doi:10.1016/j.tecto.2004.06.011

Doudoux, B., 1973. Nouvelles données tectoniques sur le massif des Bauges (Savoie). Ann. du Cent. Univ. Savoie 1, 125–139.

Doudoux, B., Barféty, J.C., Vivier, G., Carfantan, J.C., Nicoud, G., Colleta, B., Tardy, M., Montjuvent, G., Debon, F., Menot, R.-P., Aprahamian, J., 1999. Carte géologique de la france à 1/50 000 : Albertville (feuille 726). Orléans.

Doudoux, B., Mercier de Lepinay, B., Tardy, M., 1982. Une interprétation nouvelle de la structure des massifs subalpins savoyards (Alpes occidentales) : nappes de charriage oligocènes et déformations superposées. Comptes Rendus l'Académie des Sci. - Ser. II 295, 63–68.

Doudoux, B., Rosset, J., Barféty, J.C., Carfantan, J.C., Pairis, J.-L., 1992. Carte géologique de la france à 1/50 000 : Annecy-Ugine (feuille 702). Orléans.

Dumont, T., 1988. Late Triassic-early Jurassic evolution of the western Alps and of their European foreland - Initiation of the Tethyan rifting. Bull. la Sociéte Geol. Fr. 4, 601–611.

Dumont, T., Champagnac, J.-D., Crouzet, C., Rochat, P., 2008. Multistage shortening in the Dauphiné zone (French Alps): the record of Alpine collision and implications for pre-Alpine restoration. Swiss J. Geosci. 101, 89–110. doi:10.1007/s00015-008-1280-2

Dumont, T., Schwartz, S., Guillot, S., Simon-Labric, T., Tricart, P., Jourdan, S., 2012. Structural and sedimentary records of the Oligocene revolution in the Western Alpine arc. J. Geodyn. 56-57, 18–38. doi:10.1016/j.jog.2011.11.006

Ehlschlaeger, C., 1989. Using the {A^T} Search Algorithm to Develop Hydrologic Models from Digital Elevation Data. Proc. Int. Geogr. Inf. Syst. Symp. 275–281.

Espurt, N., Hippolyte, J.-C., Saillard, M., Bellier, O., 2012. Geometry and kinematic evolution of a long-living foreland structure inferred from field data and cross section balancing, the Sainte-Victoire System, Provence, France. Tectonics 31, n/a–n/a. doi:10.1029/2011TC002988

Eva, E., Solarino, S., 1998. Variations of stress directions in the western Alpine arc. Geophys. J. Int. 135, 438–448. doi:10.1046/j.1365-246X.1998.00649.x

Fäh, D., Gisler, M., Jaggi, B., Kästli, P., Lutz, T., Masciadri, V., Matt, C., Mayer-Rosa, D., Rippmann, D., Schwarz-Zanetti, G., Tauber, J., Wenk, T., 2009. The 1356 Basel earthquake: an interdisciplinary revision. Geophys. J. Int. 178, 351–374. doi:10.1111/j.1365-246X.2009.04130.x

Finckh, P., Klingele, E., 1991. Seismic reflection profiling in the Swiss Rhone valley. Part 2, Gravimetric and geological interpretation of the Roche-Vouvry line. Eclogae Geol. Helv. 84, 359–368.

Flandrin, J., 1966. Sur l'âge des principaux traits structuraux du Diois et des Baronnies. Bull. la Société Géologique Fr. 7, 376–386.

Flandrin, J., Rueff, S., Auclair, D., Tillement, B., Alliot, C., Bitot, P., Porthault, B., Belleville, J.M., Berthon, M., Ruandel, M., 1974. Carte géologique de la france à 1/50 000 : Die (feuille 843). Orléans.

Ford, M., 1996. Kinematics and geometry of early Alpine, basement-involved folds, SW Pelvoux Massif, SE France. Eclogae Geol. Helv. 89, 269–295. doi:10.5169/seals-167902

Ford, M., Duchene, S., Gasquet, D., Vanderhaeghe, O., 2006. Two-phase orogenic convergence in the external and internal SW Alps. J. Geol. Soc. London. 163, 815–826. doi:10.1144/0016-76492005-034

Fournier, M., Agard, P., Petit, C., 2008. Micro-tectonic constraints on the evolution of the Barles half-window (Digne nappe, southern Alps). Implications for the timing of folding in the Valensole foreland basin. Bull. la Soc. Geol. Fr. 179, 551–568. doi:10.2113/gssgfbull.179.6.551

François, D., 1981. Étude des accidents méridiens de Saillans-Mérindol et de Die-La Motte Chalançon (Diois-Baronnies).

Fréchet, J., Thouvenot, F., Frogneux, M., Deichmann, N., Cara, M., 2010. The MW 4.5 Vallorcine (French Alps) earthquake of 8 September 2005 and its complex aftershock sequence. J. Seismol. 15, 43–58. doi:10.1007/s10950-010-9205-8

Fréchet, J., Thouvenot, F., Jenatton, L., Hoang-Trong, P., Frogneux, M., 1996. Le séisme du Grand-Bornand (Haute-Savoie) du 14 décembre 1994 : un coulissage dextre dans le socle subalpin. Comptes Rendus l'Académie des Sci. - Ser. IIA - Earth Planet. Sci. 323, 517–524.

Gallego, G., Cuevas, C., Mohedano, R., García, N., 2013. On the mahalanobis distance classification criterion for multidimensional normal distributions. IEEE Trans. Signal Process. 61, 4387–4396. doi:10.1109/TSP.2013.2269047

Gasquet, D., Bertrand, J.-M., Paquette, J.-L., Lehmann, J., Ratzov, G., De Ascencao Guedes, R., Tiepolo, M., Boullier, A.-M., Scaillet, S., Nomade, S., 2010. Miocene to Messinian deformation and hydrothermal activity in a pre-Alpine basement massif of the French western Alps: new U-Th-Pb and argon ages from the Lauziere massif. Bull. la Soc. Geol. Fr. 181, 227–241. doi:10.2113/gssgfbull.181.3.227

Gattacceca, J., Deino, A., Rizzo, R., Jones, D.S., Henry, B., Beaudoin, B., Vadeboin, F., 2007. Miocene rotation of Sardinia: New paleomagnetic and geochronological constraints and geodynamic implications. Earth Planet. Sci. Lett. 258, 359–377. doi:10.1016/j.epsl.2007.02.003

Gaudemer, Y., Tapponier, P., Turcotte, D., 1989. River offsets across active strike-slip faults. Ann. Tectonicae 3, 55–76.

Gautier, F., Clauzon, G., Suc, J.-P., Cravatte, J., Violanti, D., 1994. Age et durée de la crise de salinité messinienne/Age and duration of the Messinian salinity crisis. Comptes rendus l'Académie des Sci. Série 2. Sci. la terre des planètes 318, 1103–1109.

Gélis, C., Revil, A., Cushing, M.E., Jougnot, D., Lemeille, F., Cabrera, J., De Hoyos, A., Rocher, M., 2010. Potential of Electrical Resistivity Tomography to Detect Fault Zones in Limestone and Argillaceous Formations in the Experimental Platform of Tournemire, France. Pure Appl. Geophys. 167, 1405–1418. doi:10.1007/s00024-010-0097-x

Gephart, J.W., Forsyth, D.W., 1984. An improved method for determining the regional stress tensor using earthquake focal mechanism data: Application to the San Fernando Earthquake Sequence. J. Geophys. Res. 89, 9305. doi:10.1029/JB089iB11p09305

Germain, C., Demaison, G., 1958. Contribution a l'histoire géologique du bassin de valence. Trav. du Lab. Géologie Grenoble 34, 49–82.

Gidon, M., 1974. L'arc alpin a-t-il une origine tourbillonnaire? Comptes rendus Hebd. des séances l'Académie des Sci. Série D, Sci. Nat. 278, 21–24.

Gidon, M., 1981. La structure de l'extrémité méridionale du massif de la Chartreuse aux abords de Grenoble et son prolongement en Vercors. Géologie Alp. 57, 93–107.

Gidon, M., 1990. Les décrochements et leur place dans la structuration du massif de la Chartreuse (Alpes occidentales françaises). Géologie Alp. 66, 39–55.

Gidon, M., 1996. Vues nouvelles sur la structure des massifs des Bornes et des Bauges orientales. Géologie Alp. 72, 35–59.

Gidon, M., 1999. Tectoniques superposées dans le synclinal des Aillons et ses abords (massif des Bauges, Savoie, France). Géologie Alp. 75, 91–102.

Gidon, M., 2001. Les massifs cristallins externes des Alpes occidentales françaises sont-ils charriés ? Géologie Alp. 77, 23–38.

Grand, T., Dumont, T., Pinto-Bull, F., 1987. Distension liées au rifting téthysien et paléochamps de contrainte associés dans le bassin liasique de Bourg d'Oisans (Alpes occidentales). Bull. la Société Géologique Fr. 3, 699–704.

Gratier, J.-P., Thouvenot, F., Jenatton, L., Tourette, A., Doan, M.-L., Renard, F., 2013. Geological control of the partitioning between seismic and aseismic sliding behaviours in active faults: Evidence from the Western Alps, France. Tectonophysics 600, 226–242. doi:10.1016/j.tecto.2013.02.013

Griffiths, D.H., Turnbull, J., Olayinka, A.I., 1990. Two-dimensional resistivity mapping with a computer-controlled array. First Break 8, 121–129. doi:10.3997/1365-2397.1990008

Grohmann, C., Campanha, G., 2010. OpenStereo: open source, cross-platform software for structural geology analysis. AGU Fall Meet. Abstr.

Grosjean, G., Sue, C., Burkhard, M., 2004. Late Neogene extension in the vicinity of the Simplon fault zone (central Alps, Switzerland). Eclogae Geol. Helv. 97, 33–46. doi:10.1007/s00015-004-1114-9

Gueguen, E., Doglioni, C., Fernandez, M., 1998. On the post-25 Ma geodynamic evolution of the western Mediterranean. Tectonophysics 298, 259–269. doi:10.1016/S0040-1951(98)00189-9

Guéguen, P., Cornou, C., Garambois, S., Banton, J., 2007. On the Limitation of the H/V Spectral Ratio Using Seismic Noise as an Exploration Tool: Application to the Grenoble Valley (France), a Small Apex Ratio Basin. Pure Appl. Geophys. 164, 115–134. doi:10.1007/s00024-006-0151-x

Guillier, B., Cornou, J., Kristek, C.., Moczo, P., Bonnefoy-Claudet, S., Bard, P.-Y., Fäh, D., 2006. Simulation of seismic ambient vibrations : does the H/V Provide quantitative information in 2D-3D structures ?, in: Third International Symposium on the Effects of Surface Geology on Seismic Motion. Grenoble, p. 9.

Guillot, S., Ménot, R.-P., 1999. Nappe stacking and first evidence of Late Variscan extension in the Belledonne Massif (External Crystalline Massifs, French Alps). Geodin. Acta 12, 97–111.

Guillot, S., Ménot, R.-P., 2009. Paleozoic evolution of the External Crystalline Massifs of the Western Alps. Comptes Rendus Geosci. 341, 253–265. doi:10.1016/j.crte.2008.11.010

Guineberteau, B., Bouchez, J.-L., Vigneresse, J.-L., 1987. The Mortagne granite pluton (France) emplaced by pull-apart along a shear zone: Structural and gravimetric arguments and regional implication. Geol. Soc. Am. Bull. 99, 763. doi:10.1130/0016-7606(1987)99<763:TMGPFE>2.0.CO;2

Haccard, D., Beaudoin, B., Gigot, P., Jorda, M., 1989. Carte géologique de la France à 1/50 000 : La Javie (feuille 918). Orléans.

Hilgen, F.J., Langereis, C.G., 1993. A critical re-evaluation of the Miocene/Pliocene boundary as defined in the Mediterranean. Earth Planet. Sci. Lett. 118, 167–179. doi:10.1016/0012-821X(93)90166-7

Hippolyte, J.-C., 2001. Palaeostress and neotectonic analysis of sheared conglomerates: Southwest Alps and Southern Apennines. J. Struct. Geol. 23, 421–429. doi:10.1016/S0191-8141(00)00120-6

Hippolyte, J.-C., Angelier, J., Bergerat, F., Nury, D., Guieu, G., 1993. Tectonic-stratigraphic record of paleostress time changes in the Oligocene basins of the Provence, southern France. Tectonophysics 226, 15–35. doi:10.1016/0040-1951(93)90108-V

Hippolyte, J.-C., Bellier, O., Espurt, N., 2012a. Quaternary deformation and stress perturbations along the Digne thrust front, Southwestern Alps. Comptes Rendus Geosci. 344, 205–213. doi:10.1016/j.crte.2012.03.002

Hippolyte, J.-C., Bergerat, F., Gordon, M.B., Bellier, O., Espurt, N., 2012b. Keys and pitfalls in mesoscale fault analysis and paleostress reconstructions, the use of Angelier's methods. Tectonophysics 581, 144–162. doi:10.1016/j.tecto.2012.01.012

Hippolyte, J.-C., Bourlès, D., Braucher, R., Carcaillet, J., Léanni, L., Arnold, M., Aumaitre, G., 2009. Cosmogenic 10Be dating of a sackung and its faulted rock glaciers, in the Alps of Savoy (France). Geomorphology 108, 312–320. doi:10.1016/j.geomorph.2009.02.024

Hippolyte, J.-C., Bourlès, D., Léanni, L., Braucher, R., Chauvet, F., Lebatard, A.E., 2012c. 10Be ages reveal >12ka of gravitational movement in a major sackung of the Western Alps (France). Geomorphology 171-172, 139–153. doi:10.1016/j.geomorph.2012.05.013

Hippolyte, J.-C., Brocard, G., Tardy, M., Nicoud, G., Bourlès, D., Braucher, R., Ménard, G., Souffaché, B., 2006a. The recent fault scarps of the Western Alps (France): Tectonic surface ruptures or gravitational sackung scarps? A combined mapping, geomorphic, levelling, and 10Be dating approach. Tectonophysics 418, 255–276. doi:10.1016/j.tecto.2006.02.009

Hippolyte, J.-C., Clauzon, G., Suc, J.-P., 2011. Messinian-Zanclean canyons in the Digne nappe (southwestern Alps): tectonic implications. Bull. la Soc. Geol. Fr. 182, 111–132. doi:10.2113/gssgfbull.182.2.111

Hippolyte, J.-C., Tardy, M., Nicoud, G., 2006b. Les failles récentes des Grands-Moulins (Savoie) : un Sackung (tassement gravitaire) majeur dans les Alpes françaises. Comptes Rendus Geosci. 338, 734–741. doi:10.1016/j.crte.2006.04.002

Hippolyte, J.C., Dumont, T., 2000. Identification of Quaternary thrusts, folds and faults in a low seismicity area: examples in the Southern Alps (France). Terra Nov. 12, 156–162. doi:10.1046/j.1365-3121.2000.00287.x

Hollender, F., Cushing, M.E., Gélis, C., Dussouillez, P., Bailly, T., Nechtschein, S., Guyonnet-Benaize, C., Delavaud, E., Bellier, O., Cornou, C., Perron, V., 2015. Apport des méthodes de mesure de vibration ambiante pour la caractérisation des paléo-canyons messiniens dans le sud-est de la France, in: 9ème Colloque National AFPS 2015 – IFSTTAR. p. 10.

Homberg, C., Bergerat, F., Philippe, Y., Lacombe, O., Angelier, J., 2002. Structural inheritance and cenozoic stress fields in the Jura fold-and-thrust belt (France). Tectonophysics 357, 137–158. doi:10.1016/S0040-1951(02)00366-9

Homberg, C., Hu, J.C., Angelier, J., Bergerat, F., Lacombe, O., 1997. Characterization of stress perturbations near major fault zones: insights from 2-D distinct-element numerical modelling and field studies (Jura mountains). J. Struct. Geol. 19, 703–718. doi:10.1016/S0191-8141(96)00104-6

Homberg, C., Lacombe, O., Angelier, J., Bergerat, F., 1999. New constraints for indentation mechanisms in arcuate belts from the Jura Mountains, France. Geology 27, 827. doi:10.1130/0091-7613(1999)027<0827:NCFIMI>2.3.CO;2

Homberg, C., Schnyder, J., Benzaggagh, M., 2013. Late Jurassic-Early Cretaceous faulting in the Southeastern French basin: does it reflect a tectonic reorganization? Bull. la Soc. Geol. Fr. 184, 501–514. doi:10.2113/gssgfbull.184.4-5.501

Hsü, K.J., Montadert, L., Bernoulli, D., Cita, M.B., Erickson, A., Garrison, R.E., Kidd, R.B., Mèlierés, F., Müller, C., Wright, R., 1977. History of the Mediterranean salinity crisis. Nature 267, 399–403. doi:10.1038/267399a0

Hsü, K.J., Ryan, W.B.F., Cita, M.B., 1973. Late Miocene Desiccation of the Mediterranean. Nature 242, 240–244. doi:10.1038/242240a0

Hudnut, K.W., Borsa, A., Glennie, C., Minster, J.-B., 2002. High-Resolution Topography along Surface Rupture of the 16 October 1999 Hector Mine, California, Earthquake (Mw 7.1) from Airborne Laser Swath Mapping. Bull. Seismol. Soc. Am. 92, 1570–1576. doi:10.1785/0120000934

Jaurand, E., Kaiser, B., 1999. Accidents cassants dans des glaciers rocheux du Beaufortin (Alpes françaises du Nord) : origine gravitaire ou néotectonique ?/Scarps in rock glaciers of Beaufortin (Northern French Alps): a gravity or neotectonic origin? Géomorphologie Reli. Process. Environ. 5, 305–325. doi:10.3406/morfo.1999.997

Jiménez-Munt, I., Garcia-Castellanos, D., Negredo, a. M., Platt, J.P., 2005. Gravitational and tectonic forces controlling postcollisional deformation and the present-day stress field of the Alps: Constraints from numerical modeling. Tectonics 24, n/a–n/a. doi:10.1029/2004TC001754

Jouanne, F., Genaudeau, N., Ménard, G., Darmendrail, X., 1998. Estimating present-day displacement fields and tectonic deformation in active mountain belts: an example from the Chartreuse Massif and the southern Jura Mountains, western Alps. Tectonophysics 296, 403–419. doi:10.1016/S0040-1951(98)00156-5

Jouanne, F., Ménard, G., Jault, D., 1994. Present-day deformation of the French northwestern Alps/southern Jura mountains: comparison between historical triangulations. Geophys. J. … 119, 151–165.

Kastrup, U., Zoback, M. Lou, Deichmann, N., Evans, K.F., Giardini, D., Michael, A.J., 2004. Stress field variations in the Swiss Alps and the northern Alpine foreland derived from inversion of fault plane solutions. J. Geophys. Res. 109, B01402. doi:10.1029/2003JB002550

Kerckhove, C., Antoine, P., 1964. Sur l'existence de failles de décrochement dans le massif des Bauges (zone subalpine, Savoie). Trav. du Lab. Géologie Grenoble 40, 81–89.

Klinger, Y., Etchebes, M., Tapponnier, P., Narteau, C., 2011. Characteristic slip for five great earthquakes along the Fuyun fault in China. Nat. Geosci. 4, 389–392. doi:10.1038/ngeo1158

Krijgsman, W., Hilgen, F.J., Raffi, I., Sierro, F.J., Wilson, D.S., 1999. Chronology, causes and progression of the Messinian salinity crisis. Nature 400, 652–655. doi:10.1038/23231

Lacassin, R., Tapponnier, P., Meyer, B., Armijo, R., 2001. Was the Trévaresse thrust the source of the 1909 Lambesc (Provence, France) earthquake? Historical and geomorphic evidence. Comptes Rendus l'Académie des Sci. - Ser. IIA - Earth Planet. Sci. 333, 571–581. doi:10.1016/S1251-8050(01)01646-9

Lacombe, O., Jolivet, L., 2005. Structural and kinematic relationships between Corsica and the Pyrenees-Provence domain at the time of the Pyrenean orogeny. Tectonics 24, n/a–n/a. doi:10.1029/2004TC001673

Lardeaux, J.M., Schwartz, S., Tricart, P., Paul, A., Guillot, S., Béthoux, N., Masson, F., 2006. A crustal-scale cross-section of the south-western Alps combining geophysical and geological imagery. Terra Nov. 18, 412–422. doi:10.1111/j.1365-3121.2006.00706.x

Larroque, C., Delouis, B., Godel, B., Nocquet, J.-M., 2009. Active deformation at the southwestern Alps–Ligurian basin junction (France–Italy boundary): Evidence for recent change from compression to extension in the Argentera massif. Tectonophysics 467, 22–34. doi:10.1016/j.tecto.2008.12.013

Larroque, C., Delouis, B., Hippolyte, J.C., Deschamps, A., Lebourg, T., Courboulex, F., Bellier, O., 2011. Joint multidisciplinary study of the Saint-Sauveur-Donareo fault (lower Var valley, French Riviera): a contribution to seismic hazard assessment in the urban area of Nice. Bull. la Soc. Geol. Fr. 182, 323–336. doi:10.2113/gssgfbull.182.4.323

Le Pichon, X., Rangin, C., Hamon, Y., Loget, N., Lin, J.Y., Andreani, L., Flotte, N., 2011. Geodynamics of the France Southeast Basin. Bull. la Soc. Geol. Fr. 181, 477–501. doi:10.2113/gssgfbull.181.6.477

Le Roux, O., Schwartz, S., Gamond, J.F., Jongmans, D., Tricart, P., Sebrier, M., 2010. Interaction between tectonic and erosion processes on the morphogenesis of an Alpine valley: geological and geophysical investigations in the lower Romanche valley (Belledonne massif, western Alps). Int. J. Earth Sci. 99, 427–441. doi:10.1007/s00531-008-0393-1

Lemoine, M., Bas, T., Arnaud-Vanneau, A., Arnaud, H., Dumont, T., Gidon, M., Bourbon, M., de Graciansky, P.-C., Rudkiewicz, J.-L., Megard-Galli, J., Tricart, P., 1986. The continental margin of the Mesozoic Tethys in the Western Alps. Mar. Pet. Geol. 3, 179–199. doi:10.1016/0264-8172(86)90044-9

Lemoine, M., Gidon, M., Barféty, J., 1981. Les massifs cristallins externes des Alpes occidentales: d'anciens blocs basculés nés au Lias lors du rifting téthysien. Comptes rendus des séances l'Académie des Sci. Série II, Mécanique-physique, Chim. Sci. l'univers. 292, 917–920.

Lippitsch, R., Kissling, E., Ansorge, J., 2003. Upper mantle structure beneath the Alpine orogen from high-resolution teleseismic tomography. J. Geophys. Res. 108, 2376. doi:10.1029/2002JB002016

Lisiecki, L.E., Raymo, M.E., 2005. A Pliocene-Pleistocene stack of 57 globally distributed benthic $\delta^{18}O$ records. Paleoceanography 20, 1–17. doi:10.1029/2004PA001071

Loke, M.H., 2003. RES2DINV, Rapid 2-D Resistivity and IP Inversion Using the Least –Square Method. Geotomo Softw. user's Man. 123.

Mandier, P., 1974. Les passages du Rhône dans la dépression de Saint-Péray. Rev. géographie Lyon 49, 139–154. doi:10.3406/geoca.1974.1644

Mandier, P., 1988. Le relief de la moyenne vallée du Rhône au Tertiaire et au Quaternaire, essai de synthèse paléogéographique.

Martinod, J., Roux, L., Gamond, J.-F., Glot, J.-P., 2001. Deformation actuelle de la chaine de Belledonne (massifs cristallins externes alpins, France); comparaison triangulation historique-GPS. Bull. la Société géologique Fr. 172, 713–721. doi:10.2113/172.6.713

Masson, F., Gal, F., Leloup, P.-H., 2002. Une carte gravimétrique haute résolution du massif du Mont-Blanc : implications structurales. Comptes Rendus Geosci. 334, 1011–1019. doi:10.1016/S1631-0713(02)01846-1

Maurer, H.R., Burkhard, M., Deichmann, N., Green, A.G., 1997. Active tectonism in the central Alps: contrasting stress regimes north and south of the Rhone Valley. Terra Nov. 9, 91–94. doi:10.1111/j.1365-3121.1997.tb00010.x

McCalpin, J., Irvine, J., 1995. Sackungen at the Aspen Highlands Ski Area, Pitkin County, Colorado. Environ. Eng. Geosci. 1, 277–290.

Ménard, G., 1979. Relations entre structures profondes et structures superficielles dans le Sud-Est de la France. Essai d'utilisation de données géophysiques. Université Scientifique et Médicale de Grenoble.

Ménard, G., 1988. Structure et cinematique d'une chaine de collision : les alpes occidentales et centrales. Université Joseph-Fourier - Grenoble I.

Ménard, G., Molnar, P., 1988. Collapse of a Hercynian Tibetan Plateau into a late Palaeozoic European Basin and Range province. Nature 334, 235–237. doi:10.1038/334235a0

Ménard, G., Thouvenot, F., 1984. Écaillage de la lithosphere europeenne sous les Alpes Occidentales; arguments gravimétriques et sismiques liés à l'anomalie d'Ivrea. Bull. la Société Géologique Fr. S7-XXVI, 875–884. doi:10.2113/gssgfbull.S7-XXVI.5.875

Ménard, G., Thouvenot, F., 1987. Coupes équilibrées crustales : méthodologie et application aux Alpes occidentales. Geodin. Acta 1, 35–45.

Mercier, J.L., Carey-Gailhardis, E., Sebrier, M., Stein, S., Hancock, P., England, P., 1991. Palaeostress Determinations from Fault Kinematics: Application to the Neotectonics of the Himalayas-Tibet and the Central Andes [and Discussion]. Philos. Trans. R. Soc. A Math. Phys. Eng. Sci. 337, 41–52. doi:10.1098/rsta.1991.0105

Merle, O., Brun, J.-P., 1984. The curved translation path of the Parpaillon Nappe (French Alps). J. Struct. Geol. 6, 711–719. doi:10.1016/0191-8141(84)90010-5

Merle, O., Michon, L., 2001. The formation of the West European Rift; a new model as exemplified by the Massif Central area. Bull. la Société Géologique Fr. 172, 213–221. doi:10.2113/172.2.213

Michard, A., Dumont, T., Andreani, L., Loget, N., 2010. Cretaceous folding in the Devoluy mountains (Subalpine Chains, France): gravity-driven detachment at the European paleomargin versus compressional event. Bull. la Soc. Geol. Fr. 181, 565–581. doi:10.2113/gssgfbull.181.6.565

Molliex, S., 2009. Caractérisation de la déformation tectonique récente en Provence (Sud-Est France). Cent. Eur. Rech. d'Enseignement en Géosciences l'Environnement. Université Paul Cézanne.

Molliex, S., Bellier, O., Terrier, M., Lamarche, J., Martelet, G., Espurt, N., 2011a. Tectonic and sedimentary inheritance on the structural framework of Provence (SE France): Importance of the Salon-Cavaillon fault. Tectonophysics 501, 1–16. doi:10.1016/j.tecto.2010.09.008

Molliex, S., Fabbri, O., Bichet, V., Madritsch, H., 2011b. Possible Quaternary growth of a hidden anticline at the front of the Jura fold-and-thrust belt: geomorphological constraints from the Foret de Chaux area, France. Bull. la Soc. Geol. Fr. 182, 337–346. doi:10.2113/gssgfbull.182.4.337

Molnar, P., England, P., 1990. Late Cenozoic uplift of mountain ranges and global climate change: chicken or egg? Nature 346, 29–34. doi:10.1038/346029a0

Monjuvent, G., 1973. La transfluence Durance-Isère Essai de synthèse du Quaternaire du bassin du Drac (Alpes françaises). Géologie Alp. 49, 57–118.

Montenat, C., Barrier, P., Garnier, L., 2000. La sédimentation miocène au nord des massifs de Ventoux-Lure (chaînes subalpines méridionales). Géologie la Fr. 3, 3–32.

Montenat, C., Barrier, P., Hibsch, C., 2005. Enregistrement des événements pyrénéo-provençaux dans les chaînes subalpines méridionales (Baronnies, France). Géologie la Fr. 1, 22–73.

Muratov, A., Gnedin, O., 2010. Modeling the metallicity distribution of globular clusters. Astrophys. J. 1266–1288. doi:10.1088/0004-637X/718/2/1266

Nakamura, Y., 1989. A method for dynamic characteristics estimation of subsurface using microtremor on the ground surface. Quaterly Reports Railw. Tech. Res. Inst. 30, 25–33.

Nguyen, F., Garambois, S., Chardon, D., Hermitte, D., Bellier, O., Jongmans, D., 2007. Subsurface electrical imaging of anisotropic formations affected by a slow active reverse fault, Provence, France. J. Appl. Geophys. 62, 338–353. doi:10.1016/j.jappgeo.2007.03.003

Nicolas, A., Hirn, A., Nicolich, R., Polino, R., 1990. Lithospheric wedging in the western Alps inferred from the ECORS-CROP traverse. Geology 18, 587. doi:10.1130/0091-7613(1990)018<0587:LWITWA>2.3.CO;2

Nicolas, M., Santoire, J.P., Delpech, P.Y., 1990. Intraplate seismicity: new seismotectonic data in Western Europe. Tectonophysics 179, 27–53. doi:10.1016/0040-1951(90)90354-B

Nicoud, G., 1984. Incidences de la fracturation récente sur la répartition des dépôts pléistocènes dans l'avant-pays savoyard et la Combe de Savoie. Ann. la Société Géologique du Nord CIII, 247–252.

Nicoud, G., Royer, G., Corbin, J., Lemeille, F., Paillet, A., 2002. Creusement et remplissage de la vallée de l'Isère au Quaternaire récent. Apports nouveaux du forage GMB1 (1999) dans la région de Grenoble (France). Géologie la Fr. 4, 39–49.

Nocquet, J., 2002. Mesure de la deformation crustale en europe occidentale par geodesie spatiale. Université de Nice-Sophia Antipolis.

Nocquet, J.-M., 2012. Present-day kinematics of the Mediterranean: A comprehensive overview of GPS results. Tectonophysics 579, 220–242. doi:10.1016/j.tecto.2012.03.037

Nocquet, J.-M., Calais, E., 2004. Geodetic Measurements of Crustal Deformation in the Western Mediterranean and Europe. Pure Appl. Geophys. 161, 661–681. doi:10.1007/s00024-003-2468-z

Palacky, G.J., 1988. 3. Resistivity Characteristics of Geologic Targets, in: Electromagnetic Methods in Applied Geophysics. Society of Exploration Geophysicists, pp. 52–129. doi:10.1190/1.9781560802631.ch3

Peltzer, G., Tapponnier, P., Gaudemer, Y., Meyer, B., Guo, S., Yin, K., Chen, Z., Dai, H., 1988. Offsets of Late Quaternary morphology, rate of slip, and recurrence of large earthquakes on the Chang Ma Fault (Gansu, China). J. Geophys. Res. 93, 7793. doi:10.1029/JB093iB07p07793

Petit, J.P., 1987. Criteria for the sense of movement on fault surfaces in brittle rocks. J. Struct. Geol. 9, 597–608. doi:10.1016/0191-8141(87)90145-3

Petit, J.P., Proust, F., Tapponnier, P., 1983. Criteres de sens de mouvement sur les miroirs de failles en roches non calcaires. Bull. la Société Géologique Fr. S7-XXV, 589–608. doi:10.2113/gssgfbull.S7-XXV.4.589

Peulvast, J.-P., Baroux, E., Bellier, O., Sébrier, M., 1999. The problem of tectonic activity along the Nimes, Salon-Cavaillon and Moyenne Durance fault zones: evidence from structural geomorphology. Géomorphologie Reli. Process. Environ. 5, 327–358.

Philippe, Y., 1994. Transfer Zone in the Southern Jura Thrust Belt (Eastern France): Geometry, Development, and Comparison with Analogue Modeling Experiments, in: Mascle, A. (Ed.), Hydrocarbon and Petroleum Geology of France. Springer Berlin Heidelberg, Berlin, Heidelberg, pp. 327–346. doi:10.1007/978-3-642-78849-9_23

Philippe, Y., 1995. Rampes latérales et zones de transfert dans les chaînes plissées : géométrie, conditions de formation et pièges structuraux associés. Université de Savoie.

Philippe, Y., Deville, E., Mascle, A., 1998. Thin-skinned inversion tectonics at oblique basin margins: example of the western Vercors and Chartreuse Subalpine massifs (SE France), in: Mascle, A., Puigdefabre-Gas, C., Luterbacher, H.P., Fernandez, M. (Eds.), Cenozoic Foreland Basins of Western Europe. Geological Society Special Publications, pp. 239–262. doi:10.1144/GSL.SP.1998.134.01.11

Pothérat, P., Effendiantz, L., 2009. Néotectonique et grands mouvements de versant. Le cas de Séchilienne (Isère, France). Bull. Eng. Geol. Environ. 68, 567–577. doi:10.1007/s10064-009-0221-2

Rangin, C., Le Pichon, X., Hamon, Y., Loget, N., Crespy, a., 2011a. Gravity tectonics in the SE Basin (Provence, France) imaged from seismic reflection data. Bull. la Soc. Geol. Fr. 181, 503–530. doi:10.2113/gssgfbull.181.6.503

Rangin, C., Le Pichon, X., Hamon, Y., Loget, N., Crespy, A., 2011b. Gravity tectonics in the SE Basin (Provence, France) imaged from seismic reflection data. Bull. la Soc. Geol. Fr. 181, 503–530. doi:10.2113/gssgfbull.181.6.503

Rastogi, B.K., 2004. Damage due to the Mw 7.7 Kutch, India earthquake of 2001. Tectonophysics 390, 85–103. doi:10.1016/j.tecto.2004.03.030

Rebaï, S., 1988. (1) Le champ de contraintes actuel en Europe et dans les régions méditerranéennes. (2) Étude du décrochement sénestreplio-quaternaire de Laghet-Peille (Nice) et signification des failles normales dans un contexte compressif.

Rehault, J.-P., Boillot, G., Mauffret, A., 1984. The Western Mediterranean Basin geological evolution. Mar. Geol. 55, 447–477. doi:10.1016/0025-3227(84)90081-1

Replumaz, A., Lacassin, R., Tapponnier, P., Leloup, P.H., 2001. Large river offsets and Plio-Quaternary dextral slip rate on the Red River fault (Yunnan, China). J. Geophys. Res. doi:10.1029/2000JB900135

Ritz, J.-F., 1991. Évolution du champ de contraintes dans les Alpes du sud depuis la fin de l'Oligocene. Implications sismotectoniques. Université Montpellier II.

Ritz, J.-F., Taboada, A., 1993. Revolution stress ellipsoids in brittle tectonics resulting from an uncritical use of inverse methods. Bull. la Soc. Geol. Fr.

Rizzo, E., Colella, A., Lapenna, V., Piscitelli, S., 2004. High-resolution images of the fault-controlled High Agri Valley basin (Southern Italy) with deep and shallow electrical resistivity tomographies. Phys. Chem. Earth, Parts A/B/C 29, 321–327. doi:10.1016/j.pce.2003.12.002

Robert, J., 1976. Les décrochements, fracturations et mouvements de blocs associés. Exemples des massifs subalpins dauphinois.

Roca, E., Guimerá, J., 1992. The Neogene structure of the eastern Iberian margin: Structural constraints on the crustal evolution of the Valencia trough (western Mediterranean). Tectonophysics 203, 203–218. doi:10.1016/0040-1951(92)90224-T

Rollet, N., Déverchère, J., Beslier, M.-O., Guennoc, P., Réhault, J.-P., Sosson, M., Truffert, C., 2002. Back arc extension, tectonic inheritance, and volcanism in the Ligurian Sea, Western Mediterranean. Tectonics 21, 6–1–6–23. doi:10.1029/2001TC900027

Roten, D., Fäh, D., Cornou, C., Giardini, D., 2006. Two-dimensional resonances in Alpine valleys identified from ambient vibration wavefields. Geophys. J. Int. 165, 889–905. doi:10.1111/j.1365-246X.2006.02935.x

Rouire, J., Chiron, J.-C., Camus, G., Kieffer, G., Masse, J.-P., Mergoil, J., Montjuvent, G., Rousset, C., GIDON, M., 1980. Carte géologique de la france à 1/250 000 : Valence (feuille 34).

Ryan, W.B.F., 1976. Quantitative evaluation of the depth of the western Mediterranean before, during and after the Late Miocene salinity crisis. Sedimentology 23, 791–813. doi:10.1111/j.1365-3091.1976.tb00109.x

Sanchez, G., Rolland, Y., Corsini, M., Braucher, R., Bourlès, D., Arnold, M., Aumaître, G., 2010. Relationships between tectonics, slope instability and climate change: Cosmic ray exposure dating of active faults, landslides and glacial surfaces in the SW Alps. Geomorphology 117, 1–13. doi:10.1016/j.geomorph.2009.10.019

Sanchez, G., Rolland, Y., Schreiber, D., Giannerini, G., Corsini, M., Lardeaux, J.-M., 2010. The active fault system of SW Alps. J. Geodyn. 49, 296–302. doi:10.1016/j.jog.2009.11.009

Sanchis, E., Séranne, M., 2000. Structural style and tectonic evolution of a polyphase extensional basin of the Gulf of Lion passive margin: the Tertiary Alès Basin, southern France. Tectonophysics 322, 219–242.

Schettino, A., Turco, E., 2011. Tectonic history of the western Tethys since the Late Triassic. Geol. Soc. Am. Bull. 123, 89–105. doi:10.1130/B30064.1

Schlupp, A., Clauzon, G., Avouac, J.-P., 2001. Mouvement post-messinien sur la faille de Nimes; implications pour la sismotectonique de la Provence. Bull. la Société Géologique Fr. 172, 697–711. doi:10.2113/172.6.697

Schwartz, S., Jongmans, D., Gamond, J.-F., Le Roux, O., Delacourt, C., Allemand, P., 2005. Recherche morphologique, géologique et géophysique d'indices de surface confirmant le risque lié au fonctionnement d'une faille active dans le massif de Belledonne.

Seht, M.I. V, Wohlenberg, J., 1999. Microtremor Measurements Used to Map Thickness of Soft Sediments. Bull. Seismol. Soc. Am. 89, 250–259.

Séranne, M., 1999. The Gulf of Lion continental margin (NW Mediterranean) revisited by IBS: an overview, in: Durand, B., Jolivet, L., Horvath, F., Séranne, M. (Eds.), The Mediterranean Basins: Tertiary Extension within the Alpine Orogen. pp. 15–36.

Serpelloni, E., Anzidei, M., Baldi, P., Casula, G., Galvani, a., 2005. Crustal velocity and strain-rate fields in Italy and surrounding regions: new results from the analysis of permanent and non-permanent GPS networks. Geophys. J. Int. 161, 861–880. doi:10.1111/j.1365-246X.2005.02618.x

Serpelloni, E., Faccenna, C., Spada, G., Dong, D., Williams, S.D.P., 2013. Vertical GPS ground motion rates in the Euro-Mediterranean region: New evidence of velocity gradients at different spatial scales along the Nubia-Eurasia plate boundary. J. Geophys. Res. Solid Earth 118, 6003–6024. doi:10.1002/2013JB010102

SESAME European research project, 2005. Guidelines for the implementation of the H/V spectral ratio technique on ambient vibrations. Deliv. D23.12.

Shabanian, E., Bellier, O., Abbassi, M., Siame, L., Farbod, Y., 2010. Plio-Quaternary stress states in NE Iran: Kopeh Dagh and Allah Dagh-Binalud mountain ranges. Tectonophysics 480, 280–304. doi:10.1016/j.tecto.2009.10.022

Siame, L., Bellier, O., Braucher, R., Sébrier, M., Cushing, M., Bourlès, D., Hamelin, B., Baroux, E., de Voogd, B., Raisbeck, G., Yiou, F., 2004. Local erosion rates versus active tectonics: cosmic ray exposure modelling in Provence (south-east France). Earth Planet. Sci. Lett. 220, 345–364. doi:10.1016/S0012-821X(04)00061-5

Speranza, F., Villa, I.M., Sagnotti, L., Florindo, F., Cosentino, D., Cipollari, P., Mattei, M., 2002. Age of the Corsica–Sardinia rotation and Liguro–Provençal Basin spreading: new paleomagnetic and Ar/Ar evidence. Tectonophysics 347, 231–251. doi:10.1016/S0040-1951(02)00031-8

Stampfli, G.M., Borel, G.D., Marchant, R., Mosar, J., 2002. Western Alps geological constraints on western Tethyan reconstructions. J. Virtual Explor. 08, 75–104. doi:10.3809/jvirtex.2002.00057

Stocchi, P., Spada, G., Cianetti, S., 2005. Isostatic rebound following the Alpine deglaciation: impact on the sea level variations and vertical movements in the Mediterranean region. Geophys. J. Int. 162, 137–147. doi:10.1111/j.1365-246X.2005.02653.x

Sue, C., Delacou, B., Champagnac, J.-D., Allanic, C., Burkhard, M., 2007a. Aseismic deformation in the Alps: GPS vs. seismic strain quantification. Terra Nov. 19, 182–188. doi:10.1111/j.1365-3121.2007.00732.x

Sue, C., Delacou, B., Champagnac, J.-D., Allanic, C., Tricart, P., Burkhard, M., 2007b. Extensional neotectonics around the bend of the Western/Central Alps: an overview. Int. J. Earth Sci. 96, 1101–1129. doi:10.1007/s00531-007-0181-3

Sue, C., Martinod, J., Tricart, P., Thouvenot, F., Gamond, J.-F., Fréchet, J., Marinier, D., Glot, J.-P., Grasso, J.-R., 2000. Active deformation in the inner western Alps inferred from comparison between 1972-classical and 1996-GPS geodetic surveys. Tectonophysics 320, 17–29.

Sue, C., Thouvenot, F., Fréchet, J., Tricart, P., 1999. Widespread extension in the core of the western Alps revealed by earthquake analysis. J. Geophys. Res. 104, 25611. doi:10.1029/1999JB900249

Sue, C., Tricart, P., 2003. Neogene to ongoing normal faulting in the inner western Alps: A major evolution of the late alpine tectonics. Tectonics 22, n/a–n/a. doi:10.1029/2002TC001426

Suzuki, K., Toda, S., Kusunoki, K., Fujimitsu, Y., Mogi, T., Jomori, A., 2000. Case studies of electrical and electromagnetic methods applied to mapping active faults beneath the thick quaternary, in: Developments in Geotechnical Engineering. pp. 29–45. doi:10.1016/S0165-1250(00)80005-X

Telford, W.M., Geldart, L.P., Sheriff, R.E., 1990. Applied Geophysics, 2nd ed. Cambridge University press.

Tesauro, M., Hollenstein, C., Egli, R., Geiger, a, Kahle, H., 2006. Analysis of central western Europe deformation using GPS and seismic data. J. Geodyn. 42, 194–209. doi:10.1016/j.jog.2006.08.001

Thibaut, M., Gratier, J., Léger, M., Morvan, J., 1996. An inverse method for determining three-dimensional fault geometry with thread criterion: application to strike-slip and thrust faults (Western Alps and California). J. Struct. Geol. 18, 1127–1138.

Thouvenot, F., 1996. Aspects géophysiques et structuraux des Alpes occidentales et des trois autres orogènes (Atlas, Pyrennées, Oural). Université Joseph-Fourier de Grenoble.

Thouvenot, F., Fréchet, J., Jenatton, L., Gamond, J.-F., 2003. The Belledonne Border Fault: identification of an active seismic strike-slip fault in the western Alps. Geophys. J. Int. 155, 174–192. doi:10.1046/j.1365-246X.2003.02033.x

Thouvenot, F., Fréchet, J., Tapponnier, P., Thomas, J.-C., Le Brun, B., Ménard, G., Lacassin, R., Jenatton, L., Grasso, J.-R., Coutant, O., Paul, A., Hatzfeld, D., 1998. The M L 5.3 Épagny

(French Alps) earthquake of 1996 July 15: a long-awaited event on the Vuache Fault. Geophys. J. Int. 135, 876–892. doi:10.1046/j.1365-246X.1998.00662.x

Thouvenot, F., Ménard, G., 1990. Allochthony of the Chartreuse Subalpine massif: explosion-seismology constraints. J. Struct. Geol. 12, 113–121. doi:10.1016/0191-8141(90)90052-Z

Tricart, P., Lardeaux, J.-M., Schwartz, S., Sue, C., 2007. The late extension in the inner western Alps: a synthesis along the south-Pelvoux transect. Bull. la Société Géologique Fr. 299–310.

Tukey, J.W., 1977. Exploratory Data Analysis.

Tuttle, M.P., Schweig, E.S., Sims, J.D., Lafferty, R.H., Wolf, L.W., Haynes, M.L., 2002. The earthquake potential of the New Madrid seismic zone. Bull. Seismol. Soc. Am. 92, 2080–2089. doi:10.1785/0120010227

Vannucci, G., Pondrelli, S., Argnani, A., Morelli, A., Gasperini, P., Boschi, E., 2004. An atlas of mediterranean seismicity. Ann. Geophys. 47, 247–306. doi:10.4401/ag-3276

Vernant, P., Hivert, F., Chery, J., Steer, P., Cattin, R., Rigo, a., 2013. Erosion-induced isostatic rebound triggers extension in low convergent mountain ranges. Geology 41, 467–470. doi:10.1130/G33942.1

Vigny, C., Chéry, J., Duquesnoy, T., Jouanne, F., Ammann, J., Anzidei, M., Avouac, J.-P., Barlier, F., Bayer, R., Briole, P., Calais, E., Cotton, F., Duquenne, F., Feigl, K.L., Ferhat, G., Flouzat, M., Gamond, J.-F., Geiger, a., Harmel, a., Kasser, M., Laplanche, M., Le Pape, M., Martinod, J., Ménard, G., Meyer, B., Ruegg, J.-C., Scheubel, J.-M., Scotti, O., Vidal, G., 2002. GPS network monitors the Western Alps' deformation over a five-year period: 1993-1998. J. Geod. 76, 63–76. doi:10.1007/s00190-001-0231-8

Villeger, M., Andrieux, J., 1987. Phases tectoniques post-eocenes et structuration polyphasee du panneau de couverture nord provencal (Alpes externes meridionales). Bull. la Société Géologique Fr. 8, 147–156. doi:10.2113/gssgfbull.III.1.147

Vincenty, T., 1975. Direct and Inverse Solutions of Geodesics on the Ellipsoid with application of nested equations. Surv. Rev. 23, 88–93. doi:10.1179/sre.1975.23.176.88

von Raumer, J.F., Ménot, R.-P., 1989. Evolution paléozoïque du socle ouest-alpin et place des Massifs cristallins externes dans l'orogène varisque. Comptes Rendus l'Academie des Sci. Paris Série II 309, 397–402.

Vouillamoz, N., Sue, C., Champagnac, J.-D., Calcagno, P., 2012. 3D cartographic modeling of the Alpine arc. Tectonophysics 579, 131–143. doi:10.1016/j.tecto.2012.06.012

Waldhauser, F., Kissling, E., Ansorge, J., Mueller, S., 1998. Three-dimensional interface modelling with two-dimensional seismic data: the Alpine crust-mantle boundary. Geophys. J. Int. 135, 264–278. doi:10.1046/j.1365-246X.1998.00647.x

Wallace, R.E., 1951. Geometry of Shearing Stress and Relation to Faulting. J. Geol. 59, 118–130.

Walpersdorf, A., Baize, S., Calais, E., Tregoning, P., Nocquet, J.-M., 2006. Deformation in the Jura Mountains (France): First results from semi-permanent GPS measurements. Earth Planet. Sci. Lett. 245, 365–372. doi:10.1016/j.epsl.2006.02.037

Walpersdorf, A., Sue, C., Baize, S., Cotte, N., Bascou, P., Beauval, C., Collard, P., Daniel, G., Dyer, H., Grasso, J.-R., Hautecoeur, O., Helmstetter, A., Hok, S., Langlais, M., Menard, G., Mousavi, Z., Ponton, F., Rizza, M., Rolland, L., Souami, D., Thirard, L., Vaudey, P., Voisin, C., Martinod, J., 2015. Coherence between geodetic and seismic deformation in a context of slow tectonic activity (SW Alps, France). J. Geodyn. 85, 58–65. doi:10.1016/j.jog.2015.02.001

Ward, S.N., 1994. Constraints On the Seismotectonics of the Central Mediterranean From Very Long Baseline Interferometry. Geophys. J. Int. 117, 441–452. doi:10.1111/j.1365-246X.1994.tb03943.x

Wells, D.L., Coppersmith, K.J., 1994. New Empirical Relationships among Magnitude, Rupture Length, Rupture Width, Rupture Area, and Surface Displacement. Bull. Seismol. Soc. Am. 84, 974–1002.

York, D., Evensen, N.M., Martínez, M.L., De Basabe Delgado, J., 2004. Unified equations for the slope, intercept, and standard errors of the best straight line. Am. J. Phys. 72, 367–371. doi:10.1119/1.1632486

Zhao, L., Paul, A., Guillot, S., Solarino, S., Malusà, M.G., Zheng, T., Aubert, C., Salimbeni, S., Dumont, T., Schwartz, S., Zhu, R., Wang, Q., 2015. First seismic evidence for continental subduction beneath the Western Alps. Geology 43, 815–818. doi:10.1130/G36833.1

Zielke, O., Arrowsmith, J.R., Ludwig, L.G., Akciz, S.O., 2010. Slip in the 1857 and Earlier Large Earthquakes Along the Carrizo Plain, San Andreas Fault. Science (80-.). 327, 1119–1122. doi:10.1126/science.1182781

Zoback, M.D., Zoback, M.L., Mount, V.S., Suppe, J., Eaton, J.P., Healy, J.H., Oppenheimer, D., Reasenberg, P., Jones, L., Raleigh, C.B., Wong, I.G., Scotti, O., Wentworth, C., 1987. New evidence on the state of stress of the san andreas fault system. Science 238, 1105–1111. doi:10.1126/science.238.4830.1105

INDEX DES FIGURES

INDEX DES TABLEAUX

INDEX DES TABLEAUX

ANNEXES

ANNEXE 1: STRESS TENSOR DATABASE

We present thereafter the stress tensor database built from literature and used in chapter II. We do not present the whole of the field (e.g. relative chronology with folding, inversion method used, dip) due to the lack of space but the dataset is available in shapefile format. We hope to develop in the future an online searchable database first focused on the French southern quarter and progressively extent to the France, Pyrenees and Alps.

Long.: longitude in degree

Lat.: latitude in degree

Tectonic regime: C: compressional, TP: transpressional, SS: strike-slip, TT: transtensional and T: extensional

R: shape ratio $=(\sigma_2-\sigma_3)/(\sigma_1-\sigma_3)$

N: number of fault observations

F, α and RUP: misfit parameters, see Carey and Brunier (1974) and Angelier (1990)

REF: 1: Baroux (2000), 2: Bergerat (1985), 3: Billant et al. (2015), 4: Billant et al. (in prep.), 5: Billant et al. (submit), 6: Casagrande Fioretti (1985), 7: Champagnac et al. (2004), 8: Combes (1984), 9: Fournier et al. (2008), 10: François (1981), 11: Grosjean et al. (2004), 12: Hippolyte et al. (2006b), 13: Hippolyte et al. (2012a), 14: Homberg et al. (2002), 15: Homberg et al. (2013), 16: Larroque et al. (2011),17: Le Roux et al. (2010), 18: Philippe (1995), 19: Rebaï (1988), 20: Ritz (1991) and 21: Sue and Tricart (2003)

Site	Long.	Lat.	Age	Tectonic regime	σ_1 trend	σ_1 plunge	σ_2 trend	σ_2 plunge	σ_3 trend	σ_3 plunge	R	N	F	α	RUP	REF
			Jurassic													
L2A	*6.2883*	*44.2533*	*Hettangien*	*T*	*133*	*-79*	*72*	*6*	*163*	*10*	*0.42*	*42*				*9*
L6A	*6.2433*	*44.2633*	*Hettangien*	*T*	*155*	*-62*	*40*	*-12*	*124*	*24*	*0.28*	*8*				*9*
Baume	*5.8189*	*44.6524*	*Upper Oxfordian*	*T*	*291*	*81*	*200*	*0*	*110*	*9*	*0.52*	*10*		*19*	*41*	*15*
La Piarre 1	*5.6586*	*44.4814*	*Tithonian*	*T*	*44*	*83*	*177*	*4*	*267*	*5*	*0.17*	*12*		*14*	*32*	*15*
Sahune	*5.279*	*44.4271*	*Lower Kimmeridgian*	*T*	*284*	*72*	*194*	*0*	*103*	*18*	*0.31*	*11*		*7*	*29*	*15*
Soubeyran	*5.3514*	*44.3716*	*Middle Oxfordian*	*T*					*120*			*6*				*15*
St May	*5.3045*	*44.4309*	*Tithonian*	*T*	*23*	*72*	*188*	*17*	*279*	*4*	*0.62*	*11*		*16*	*38*	*15*
Trescléoux	*5.6681*	*44.3547*	*Middle Oxfordian*	*T*	*103*	*74*	*11*	*1*	*281*	*16*	*0.3*	*11*		*6*	*23*	*15*
Veynes	*5.8026*	*44.5462*	*Upper Oxfordian*	*T*	*298*	*79*	*195*	*2*	*105*	*11*	*0.42*	*6*		*7*	*18*	*15*
Villebois	*5.632*	*44.3289*	*Tithonian*	*T*	*343*	*72*	*179*	*14*	*272*	*11*	*0.27*	*8*		*10*	*27*	*15*
Villeperdrix	*5.2935*	*44.4382*	*Tithonian*	*T*					*94*			*10*				*15*
			Cretaceous													
K11	*6.228*	*44.2313*	*Berriasien-Valanginian*	*T*	*169*	*83*	*103*	*-3*	*14*	*6*	*0.47*	*4*				*9*
K12	*6.2883*	*44.2233*	*Berriasien-Valanginian*	*T*	*105*	*-64*	*109*	*26*	*18*	*2*	*0.49*	*5*				*9*
L8	*6.2867*	*44.2467*	*Hettangien*	*T*	*10*	*73*	*100*	*0*	*10*	*-17*	*0.26*	*12*				*9*
M4	*6.2758*	*44.2255*	*Oxfordian-Tithonian*	*T*	*18*	*-70*	*92*	*6*	*0*	*19*	*0.4*	*10*				*9*
M5	*6.2777*	*44.2253*	*Tithonian*	*T*	*3*	*-75*	*75*	*5*	*164*	*-14*	*0.24*	*5*				*9*
M6	*6.2738*	*44.2257*	*Tithonian*	*T*	*82*	*-75*	*99*	*14*	*8*	*4*	*0.5*	*6*				*9*
T15	*6.2872*	*44.2347*	*Late Eocene-Early Oligocene*	*T*	*12*	*-71*	*81*	*7*	*168*	*-18*	*0.18*	*30*				*9*
Agnielles	*5.7728*	*44.5569*	*Tithonian*	*T*					*24*			*23*				*15*
Aulan	*5.4346*	*44.2302*	*Valanginian*	*T*					*2*			*28*				*15*
Autanne	*5.3131*	*44.2995*	*Tithonian*	*T*					*44*			*8*				*15*
Baume	*5.8189*	*44.6524*	*Upper Oxfordian*	*T*					*31*			*6*				*15*
Brette	*5.3135*	*44.5879*	*Middle Oxfordian*	*T*	*227*	*72*	*113*	*7*	*21*	*16*	*0.21*	*19*		*19*	*46*	*15*
Buis	*5.2844*	*44.2959*	*Berriasien*	*T*					*36*			*2*				*15*
Creyers	*5.6407*	*44.5758*	*Berriasien*	*T*	*34*	*72*	*128*	*1*	*219*	*18*	*0.27*	*6*		*5*	*26*	*15*
Estève	*5.6242*	*44.3248*	*Valanginian*	*T*	*78*	*84*	*294*	*5*	*204*	*3*	*0.57*	*5*		*7*	*20*	*15*
Jalle	*5.2821*	*44.2962*	*Berriasien – Valanginian*	*T*	*207*	*66*	*308*	*5*	*40*	*24*	*0.23*	*5*		*11*	*24*	*15*
La Piarre 1	*5.6586*	*44.4814*	*Tithonian*	*T*	*92*	*74*	*308*	*13*	*216*	*9*	*0.59*	*6*		*9*	*39*	*15*
La Piarre 2	*5.6578*	*44.4799*	*Middle Oxfordian*	*T*	*55*	*80*	*278*	*0*	*187*	*7*	*0.5*	*6*		*1*	*23*	*15*

Site	Long.	Lat.	Age	Tectonic regime	σ_1 trend	σ_1 plunge	σ_2 trend	σ_2 plunge	σ_3 trend	σ_3 plunge	R	N	F	α	RUP	REF
Lazer	*5.8689*	*44.3655*	*Upper Bathonian – Lower Oxfordian*	*T*	*76*	*79*	*327*	*3*	*237*	*10*	*0.4*	*16*		*5*	*18*	*15*
Moulin 1	*5.4722*	*44.1915*	*Berriasien*	*T*	*235*	*74*	*103*	*11*	*11*	*12*	*0.47*	*12*		*12*	*32*	*15*
Moulin 2	*5.4779*	*44.1909*	*Tithonian*	*T*	*112*	*76*	*289*	*14*	*19*	*1*	*0.26*	*42*		*15*	*38*	*15*
Peipin	*5.9651*	*44.1288*	*Aptian*	*T*	*210*	*68*	*87*	*13*	*353*	*18*	*0.31*	*13*		*8*	*29*	*15*
Sceautres	*4.5936*	*44.578*	*Hauterivian*	*T*					*30*			*9*				*15*
Soubeyran	*5.3514*	*44.3716*	*Middle Oxfordian*	*T*					*41*			*10*				*15*
Terrus	*5.6577*	*44.4179*	*Barremian*	*T*	*5*	*85*	*135*	*3*	*226*	*4*	*0.14*	*23*		*14*	*30*	*15*
Veynes	*5.8026*	*44.5462*	*Upper Oxfordian*	*T*					*56*			*23*				*15*
Vogué	*4.4083*	*44.5655*	*Middle Oxfordian*	*T*	*283*	*83*	*124*	*6*	*34*	*2*	*0.38*	*21*		*6*	*16*	*15*
				Eocene												
Alpilles-Centre	*4.7419*	*43.763*		*TP*	*170*	*-8*	*86*	*35*	*69*	*-53*						*2*
Alpilles-Nord	*5.0106*	*43.7777*		*SS*	*3*	*5*	*60*	*-81*	*94*	*8*						*2*
Alpilles-Sud	*4.9066*	*43.737*		*SS*	*5*	*3*	*124*	*83*	*95*	*-6*						*2*
Ardeche Nord	*4.4941*	*44.3696*		*TP*	*165*	*-2*	*78*	*50*	*73*	*-40*						*2*
Ardeche Sud	*4.4942*	*44.1896*		*SS*	*165*	*-1*	*83*	*79*	*75*	*-10*						*2*
Bord Est Fosse d Ales	*4.292*	*44.1218*		*TP*	*10*	*-5*	*95*	*48*	*104*	*-41*						*2*
Bordure cevenole N	*4.129*	*44.2482*		*SS*	*179*	*7*	*108*	*69*	*86*	*-20*						*2*
Bordure cevenole S	*4.0647*	*44.0796*		*SS*	*175*	*1*	*149*	*88*	*85*	*-1*						*2*
Champ de fractures de Banon	*5.5427*	*43.9605*		*SS*	*11*	*5*	*122*	*76*	*99*	*-13*						*2*
Collines d Avignon	*4.7846*	*43.9503*		*TP*	*178*	*0*	*88*	*31*	*87*	*-59*						*2*
Collines de Chateaurenard	*4.8517*	*43.883*		*SS*	*9*	*3*	*92*	*-67*	*100*	*23*						*2*
Collines de Gaumont	*4.9321*	*43.9096*		*SS*	*167*	*4*	*18*	*85*	*77*	*-3*						*2*
Collines de Vacquieres	*4.8062*	*43.6744*		*SS*	*12*	*-11*	*132*	*-70*	*99*	*17*						*2*
G. Nesque	*5.2951*	*44.0524*		*SS*	*171*	*3*	*48*	*84*	*81*	*-5*						*2*
Garrigues d Uzes	*4.5396*	*43.9941*		*TP*	*171*	*-1*	*80*	*-36*	*82*	*54*						*2*
Garrigues de Nimes	*4.3047*	*43.8339*		*SS*	*172*	*-8*	*17*	*-81*	*83*	*4*						*2*
Grand Luberon	*5.5944*	*43.8117*		*SS*	*1*	*-5*	*15*	*85*	*91*	*-1*						*2*
La Montagnette	*4.6908*	*43.8742*		*SS*	*166*	*-5*	*88*	*75*	*74*	*-24*						*2*
Les Costes	*5.3499*	*43.6612*		*P*	*2*	*17*	*95*	*10*	*34*	*-70*						*2*
Luberon-Centre	*5.3545*	*43.7752*		*SS*	*176*	*4*	*78*	*64*	*88*	*-26*						*2*
Luberon-Sud	*5.2196*	*43.7526*		*SS*	*8*	*-17*	*32*	*72*	*100*	*-7*						*2*

Site	Long.	Lat.	Age	Tectonic regime	σ_1 trend	σ_1 plunge	σ_2 trend	σ_2 plunge	σ_3 trend	σ_3 plunge	R	N	F	α	RUP	REF
Murs	*5.2181*	*43.9652*		*SS*	*14*	*1*	*94*	*-86*	*104*	*4*						*2*
Pertuis	*5.5836*	*43.6568*		*TP*	*8*	*-2*	*96*	*42*	*99*	*-48*						*2*
Revest du Bion	*5.4964*	*44.0913*		*SS*	*5*	*3*	*49*	*-85*	*95*	*3*						*2*
Sault	*5.4058*	*44.1416*		*SS*	*13*	*1*	*105*	*60*	*102*	*-30*						*2*
St-Saturnin d-Apt	*5.3626*	*43.9428*		*SS*	*169*	*-10*	*30*	*76*	*81*	*9*						*2*
Valdaine	*4.9171*	*44.4789*		*SS*	*173*	*2*	*72*	*-77*	*83*	*12*						*2*
Vaunage	*4.1488*	*43.9425*		*SS*	*167*	*6*	*55*	*75*	*78*	*-14*						*2*
Ventoux-Nord	*5.294*	*44.2044*		*P*	*4*	*3*	*94*	*5*	*64*	*-84*						*2*
Ventoux-Sud	*5.1642*	*44.1417*		*SS*	*169*	*1*	*167*	*-88*	*79*	*1*						*2*
Vivarais Nord	*4.6154*	*44.6874*		*SS*	*166*	*-10*	*88*	*52*	*69*	*-37*						*2*
Vivarais Sud	*4.5345*	*44.4598*		*SS*	*171*	*5*	*9*	*65*	*83*	*-24*						*2*
PAS2ROCH	*5.4234*	*44.7414*	*Tithonique*	*P*	*6*	*-6*	*82*	*68*	*98*	*-21*	*0.584*	*4*		*10*	*26*	*5*
PLANEAUX	*5.4071*	*44.789*	*Tithonique*	*SS*	*169*	*-7*	*121*	*80*	*78*	*-8*	*0.338*	*8*		*7*	*20*	*5*
COL D EY	*5.2797*	*44.3098*	*Barremien-Bedoulien*	*P*	*354.5*	*28*	*89.3*	*8.7*	*196*	*50.4*	*0.76*	*19*	*18.25*			*6*
FERME CURNIER	*5.3052*	*44.3564*	*Barremien sup.*	*SS*	*176.8*	*11.7*	*354.4*	*78*	*86.7*	*0.49*	*0.92*	*14*	*10*			*6*
FERME DES PLATES	*5.2462*	*44.33*	*Barremian*	*P*	*359.7*	*15.34*	*265.6*	*14.9*	*133.5*	*68.4*	*0.97*	*24*	*23*			*6*
FERME DES PRES	*5.3135*	*44.3593*	*Bedoulien*	*TP*	*15*	*0.23*	*285*	*49*	*105.5*	*41*	*0.99*	*20*	*18.36*			*6*
P43a	*6.2017*	*43.8967*	*L. Cretaceous*	*SS*	*153*	*-2*	*61*	*-49*	*65*	*41*	*0.72*					*8*
K10	*6.27*	*44.23*	*Berriasien*	*SS*	*177*	*4*	*55*	*83*	*88*	*-6*	*0.6*	*12*				*9*
K1A	*6.2763*	*44.2168*	*Berriasien*	*SS*	*163*	*7*	*114*	*-80*	*72*	*8*	*0.6*	*17*				*9*
K2	*6.257*	*44.2315*	*Valanginian*	*SS*	*9*	*-11*	*62*	*72*	*102*	*-14*	*0.4*	*20*				*9*
K4B	*6.27*	*44.2283*	*Hauterivian*	*SS*	*157*	*26*	*151*	*-64*	*66*	*2*	*0.89*	*10*				*9*
K9	*6.268*	*44.2305*	*Berriasien*	*SS*	*170*	*1*	*140*	*-88*	*80*	*1*	*0.49*	*9*				*9*
M1A	*6.2572*	*44.235*	*Tithonian*	*SS*	*14*	*-3*	*115*	*-77*	*103*	*13*	*0.37*	*24*				*9*
9	*5.0077*	*44.6883*	*Stampien sup.*		*0*											*10*
65	*5.2988*	*44.3534*	*Barrémien*		*0*											*10*
72	*5.3269*	*44.2261*	*Barrémien*		*0*											*10*
74	*5.4153*	*44.2886*	*Barrémien*		*15*											*10*
11a	*5.0149*	*44.6791*	*Barrémien*		*10*											*10*
13a	*5.2155*	*44.6919*	*Kimméridgien*		*0*											*10*
18a	*5.2946*	*44.6457*	*Oxfordien sup.*		*0*											*10*

Site	Long.	Lat.	Age	Tectonic regime	σ_1 trend	σ_1 plunge	σ_2 trend	σ_2 plunge	σ_3 trend	σ_3 plunge	R	N	F	α	RUP	REF
1a	*5.3892*	*44.8265*	*Hautériven*		*10*											*10*
22a	*5.4592*	*44.5977*	*Berriasien*		*20*											*10*
25a	*5.423*	*44.5438*	*Tithonique-Hauterivien*		*10*											*10*
2a	*5.4068*	*44.7896*	*Tithonique-Berriasien*		*0*											*10*
31a	*5.2788*	*44.5935*	*Berriasien*		*0*											*10*
33a	*5.2444*	*44.5484*	*Hautériven*		*0*											*10*
34a	*5.1803*	*44.5509*	*Barrémien*		*0*											*10*
38a	*5.1714*	*44.6007*	*Barrémien*		*135*											*10*
3a	*5.3524*	*44.7888*	*Kimméridgien*		*0*											*10*
40a	*5.1022*	*44.6172*	*Barrémien*		*0*											*10*
41a	*5.0495*	*44.5815*	*Barrémien*		*0*											*10*
42a	*5.0315*	*44.477*	*Barrémien*		*35*											*10*
44a	*5.121*	*44.4285*	*Berriasien*		*155*											*10*
45a	*5.1158*	*44.4116*	*Hautériven-Berriasien*		*150*											*10*
45d	*5.1158*	*44.4116*	*Hautériven-Berriasien*		*170*											*10*
47a	*5.1604*	*44.3731*	*Turonien*		*140*											*10*
48a	*5.2164*	*44.491*	*Bédoulien*		*0*											*10*
51a	*5.2801*	*44.4322*	*Tithonique*		*140*											*10*
52a	*5.2929*	*44.4355*	*Tithonique*		*140*											*10*
54a	*5.3545*	*44.4726*	*Berriasien*		*10*											*10*
55a	*5.4492*	*44.4674*	*Barrémien*		*0*											*10*
56a	*5.5074*	*44.4739*	*Barrémien*		*10*											*10*
57a	*5.5023*	*44.3326*	*Hautériven*		*170*											*10*
58a	*5.4677*	*44.3543*	*Bédoulien*		*135*											*10*
59a	*5.4245*	*44.3807*	*Bédoulien*		*0*											*10*
60a	*5.3848*	*44.3899*	*Berriasien*		*0*											*10*
62a	*5.3495*	*44.3998*	*Oxfordien*		*25*											*10*
64a	*5.3519*	*44.3601*	*Barrémien*		*0*											*10*
70a	*5.272*	*44.2685*	*Berriasien*		*15*											*10*
73a	*5.405*	*44.2948*	*Bédoulien*		*10*											*10*
7a	*5.1385*	*44.7707*	*Barrémien*		*0*											*10*

Site	Long.	Lat.	Age	Tectonic regime	σ_1 trend	σ_1 plunge	σ_2 trend	σ_2 plunge	σ_3 trend	σ_3 plunge	R	N	F	α	RUP	REF
Bellefontaine	*6.0867*	*46.5533*	*Sequan. Argov.*	*SS*	*178*	*-5*	*36*	*-84*	*88*	*4*	*0.59*	*18*		*11*	*21*	*14*
Bonlieu	*5.8483*	*46.5983*	*Kimmeridgian*	*SS*	*168*	*-8*	*28*	*-79*	*79*	*7*	*0.36*	*6*		*5*	*13*	*14*
Boulu	*6.0117*	*46.4233*	*Valanginian*	*SS*	*5*	*4*	*50*	*-85*	*95*	*4*	*0.21*	*4*		*11*	*23*	*14*
Brenod	*5.5783*	*46.05*	*Mid.-Up. Oxfordian*	*SS*	*175*	*9*	*10*	*81*	*85*	*-2*	*0.61*	*5*		*7*	*23*	*14*
Buvilly	*5.7317*	*46.855*	*Bathonian*	*SS*	*4*	*0*	*95*	*77*	*94*	*-13*	*0.56*	*10*		*16*	*37*	*14*
Cernois	*6.19*	*46.6867*	*Up. Kimmeridgian*	*SS*	*171*	*10*	*165*	*-80*	*80*	*1*	*0.43*	*15*		*10*	*26*	*14*
Cery	*6.0117*	*47.14*	*Bathonian*		*10*											*14*
Chaffois	*6.28*	*46.92*	*Port. -Up. Kimme.*	*SS*	*175*	*-11*	*130*	*75*	*82*	*-10*	*0.46*	*22*		*8*	*21*	*14*
Chaille	*6.0533*	*46.465*	*Purbeckian*	*SS*	*167*	*5*	*37*	*82*	*78*	*-6*	*0.36*	*7*		*15*	*35*	*14*
Champagnole	*5.9183*	*46.7533*	*Argovian*	*SS*	*165*	*-1*	*88*	*84*	*75*	*-6*	*0.43*	*16*		*5*	*13*	*14*
Châtelneuf	*5.93*	*46.66*	*Sequanian*	*TP*	*162*	*2*	*69*	*60*	*73*	*-30*	*0.16*	*7*		*3*	*14*	*14*
Chaumusse	*5.925*	*46.5867*	*Portlandian*	*SS*	*175*	*6*	*105*	*-74*	*83*	*15*	*0.42*	*13*		*7*	*13*	*14*
Cht Prés	*5.9017*	*46.515*	*Portland. Kimmeridg.*	*SS*	*161*	*-14*	*100*	*63*	*65*	*-23*	*0.18*	*15*		*21*	*41*	*14*
Cize	*5.92*	*46.72*	*Low. Call.-Bath.*	*SS*	*173*	*2*	*60*	*85*	*83*	*-4*	*0.45*	*4*		*2*	*13*	*14*
Cuisia	*5.4117*	*46.535*	*Bathonian*	*SS*	*168*	*-6*	*62*	*-71*	*80*	*18*	*0.46*	*7*		*18*	*37*	*14*
Cuvier	*5.035*	*46.83*	*Kimmeridgian*	*SS*	*178*	*-7*	*111*	*72*	*85*	*-17*	*0.25*	*9*		*3*	*26*	*14*
Epeugney	*6.0033*	*47.0983*	*Callovian*	*SS*	*171*	*14*	*69*	*72*	*82*	*-18*	*0.64*	*4*		*2*	*17*	*14*
Forges	*5.94*	*46.72*	*Bathonian*	*SS*	*15*	*-4*	*63*	*85*	*105*	*-4*	*0.16*	*16*		*4*	*10*	*14*
Frasne	*6.14*	*46.87*	*Low. Kimme.*	*SS*	*8*	*-3*	*121*	*-83*	*97*	*7*	*0.45*	*18*		*5*	*16*	*14*
Golisse	*6.25*	*46.625*	*Port. -Up. Kimme.*	*SS*	*178*	*19*	*32*	*67*	*92*	*-12*	*0.08*	*4*		*3*	*17*	*14*
Gouland	*6.0317*	*46.4917*	*Sequanian*	*SS*	*163*	*-24*	*28*	*-58*	*82*	*20*	*0.38*	*7*		*16*	*41*	*14*
Grusse	*5.5083*	*46.6*	*Oxfordian Bathonian*	*SS*	*175*	*5*	*150*	*-84*	*85*	*2*	*0.57*	*7*		*10*	*22*	*14*
Hôpithaux	*6.3633*	*46.795*	*Port. -Up. Kimme.*	*SS*	*168*	*-4*	*125*	*84*	*78*	*-4*	*0.74*	*7*		*9*	*20*	*14*
Jougne E1	*6.385*	*46.7567*	*Port. -Up. Kimme.*	*SS*	*163*	*14*	*4*	*75*	*74*	*-5*	*0.34*	*8*		*9*	*27*	*14*
Lajoux	*5.945*	*46.375*	*Rauracian*	*SS*	*178*	*-19*	*158*	*70*	*86*	*-7*	*0.52*	*17*		*8*	*21*	*14*
Lamoura	*5.9417*	*46.3817*	*Barrem. Hauteriv.*	*SS*	*176*	*10*	*54*	*72*	*89*	*-15*	*0.61*	*11*		*9*	*22*	*14*
Lavans	*5.7983*	*46.385*	*Purbeckian*	*SS*	*173*	*7*	*134*	*-81*	*83*	*6*	*0.56*	*8*		*5*	*13*	*14*
Lods	*6.2433*	*47.045*	*Sequanian*		*170*											*14*
Longchaumois	*5.94*	*46.46*	*Barrem. to Valangin.*	*SS*	*172*	*8*	*112*	*-74*	*80*	*14*	*0.43*	*14*		*11*	*24*	*14*
Maissières	*6.1*	*47.1083*	*Bathonian*	*SS*	*179*	*-10*	*144*	*78*	*88*	*-7*	*0.44*	*7*		*6*	*15*	*14*
Mirebel	*5.7333*	*46.7*	*Argovian*	*SS*	*2*	*20*	*44*	*-63*	*98*	*16*	*0.67*	*6*		*14*	*29*	*14*

Site	Long.	Lat.	Age	Tectonic regime	σ_1 trend	σ_1 plunge	σ_2 trend	σ_2 plunge	σ_3 trend	σ_3 plunge	R	N	F	α	RUP	REF
Montagna	*5.46*	*46.345*	*Sequanian*	*SS*	*172*	*-3*	*68*	*-76*	*83*	*14*	*0.28*	*19*		*13*	*27*	*14*
Montrond	*5.84*	*46.79*	*Bathonian*	*SS*	*167*	*-5*	*56*	*-77*	*78*	*12*	*0.42*	*11*		*7*	*19*	*14*
Mouthe S	*6.1717*	*46.7*	*Port. -Up. Kimme.*	*SS*	*168*	*-13*	*117*	*70*	*75*	*-15*	*0.36*	*12*		*11*	*30*	*14*
Mouthe-N	*6.1833*	*46.7167*	*Rauracian*	*SS*	*168*	*-2*	*62*	*-83*	*78*	*7*	*0.48*	*10*		*8*	*25*	*14*
Ney	*5.83*	*46.79*	*Sequanian*		*10*											*14*
Ordonnaz	*5.5667*	*45.8333*	*Kimmeridg. Oxford.*	*SS*	*1*	*4*	*120*	*83*	*90*	*-6*	*0.44*	*7*		*11*	*25*	*14*
Pannessières	*5.6083*	*46.7*	*Bathonian*	*SS*	*177*	*-6*	*26*	*-83*	*87*	*4*	*0.41*	*9*		*12*	*29*	*14*
Piards	*5.8283*	*46.505*	*Kimmeridg. Bathon.*	*SS*	*168*	*-3*	*69*	*-73*	*79*	*17*	*0.31*	*22*		*17*	*37*	*14*
Poligny est	*5.7417*	*46.82*	*Low.- Mid. Baj.*	*SS*	*15*	*19*	*179*	*71*	*103*	*-5*	*0.51*	*5*		*4*	*32*	*14*
Poncets	*5.945*	*46.5583*	*Barremian*	*SS*	*175*	*-10*	*138*	*77*	*83*	*-8*	*0.57*	*11*		*7*	*16*	*14*
Prénovel	*5.85*	*46.52*	*Kimmeridgian*	*SS*	*170*	*-4*	*57*	*-80*	*80*	*9*	*0.21*	*11*		*8*	*22*	*14*
Repentys	*5.9767*	*46.475*	*Hauterivian*	*SS*	*174*	*-6*	*122*	*80*	*83*	*-8*	*0.46*	*7*		*10*	*20*	*14*
Risol	*6.2067*	*46.6533*	*Low. Kimmeridgian*	*SS*	*176*	*-3*	*49*	*-85*	*86*	*4*	*0.44*	*8*		*5*	*9*	*14*
Rixouse	*5.865*	*46.45*	*Portlandian*	*SS*	*174*	*0*	*78*	*-85*	*84*	*5*	*0.60*	*6*		*4*	*8*	*14*
Ronchaux	*5.7867*	*46.4917*	*Portland. Kimmeridg.*	*SS*	*177*	*6*	*51*	*80*	*88*	*-8*	*0.22*	*11*		*11*	*26*	*14*
Rousses	*6.0617*	*46.4817*	*Valangin. Portland.*	*SS*	*13*	*-18*	*175*	*-71*	*101*	*6*	*0.81*	*14*		*12*	*31*	*14*
Séchey	*6.2967*	*46.665*	*Port. -Up. Kimme.*	*SS*	*174*	*-20*	*14*	*-69*	*86*	*7*	*0.58*	*5*		*3*	*10*	*14*
Serrières	*5.4517*	*46.1517*	*Rauracian*	*SS*	*171*	*-5*	*94*	*70*	*80*	*-19*	*0.18*	*7*		*8*	*27*	*14*
Silley	*6.14*	*47.0317*	*Sequanian*	*SS*	*177*	*10*	*17*	*79*	*87*	*-4*	*0.51*	*16*		*4*	*20*	*14*
Sirod	*5.9783*	*46.7217*	*Portlandian*	*SS*	*167*	*-4*	*129*	*85*	*77*	*-3*	*0.33*	*4*		*3*	*11*	*14*
Sirod	*5.9783*	*46.7217*	*Portlandian*		*15*											*14*
St Claude	*5.8583*	*46.395*	*Portlandian*	*SS*	*166*	*3*	*130*	*-87*	*75*	*2*	*0.67*	*21*		*17*	*32*	*14*
Thévenins	*5.995*	*46.605*	*Barremian*	*SS*	*7*	*5*	*85*	*-68*	*99*	*21*	*0.37*	*7*		*9*	*23*	*14*
Titi	*6.3317*	*46.8383*	*Hauterivian*	*SS*	*0*	*6*	*27*	*-84*	*91*	*3*	*0.31*	*9*		*6*	*20*	*14*
Treffort	*5.3583*	*46.2667*	*Argovian*	*SS*	*168*	*-7*	*105*	*74*	*76*	*-15*	*0.51*	*13*		*4*	*18*	*14*
Vallorbe	*6.3433*	*46.7*	*Sequan. Raurac.*	*SS*	*168*	*-1*	*152*	*89*	*78*	*0*	*0.42*	*20*		*5*	*12*	*14*
Vaulion S	*6.3483*	*46.6567*	*Low. Kimmeridgian*	*SS*	*172*	*-3*	*107*	*84*	*82*	*-6*	*0.58*	*6*		*5*	*13*	*14*
Villeneuve	*5.98*	*46.92*	*Low. Bathonian*	*SS*	*172*	*-10*	*141*	*78*	*81*	*-6*	*0.43*	*5*		*11*	*24*	*14*
jura chartreuse 056	*5.6609*	*45.8573*		*P*	*169*	*-1*	*78*	*-30*	*81*	*60*	*0.79*	*4*				*18*
jura chartreuse 079	*5.8268*	*45.7792*		*P*	*161*	*-7*	*68*	*-22*	*87*	*67*	*0.87*	*4*				*18*
jura chartreuse 102	*5.8254*	*45.4597*		*P*	*156*	*-16*	*65*	*-2*	*150*	*74*	*0.91*	*6*				*18*

Site	Long.	Lat.	Age	Tectonic regime	σ_1 trend	σ_1 plunge	σ_2 trend	σ_2 plunge	σ_3 trend	σ_3 plunge	R	N	F	α	RUP	REF
vercors22	*5.3625*	*45.065*		*P*	*0*											*18*
vercors27	*5.4003*	*44.9752*		*P*	*0*											*18*
vercors28	*5.3227*	*44.9714*		*P*	*10*											*18*
vercors29	*5.3175*	*44.9642*		*P*	*160*											*18*
vercors30	*5.311*	*44.959*		*P*	*25*											*18*
vercors31	*5.2659*	*44.9732*		*P*	*0*											*18*
vercors32	*5.2571*	*44.9917*		*P*	*155*											*18*
vercors35	*5.3746*	*44.8951*		*P*	*170*											*18*
vercors37	*5.3297*	*44.9023*		*P*	*5*											*18*
vercors40	*5.1715*	*44.8841*		*P*	*10*											*18*
vercors47	*5.1456*	*44.8011*		*P*	*0*											*18*
vercors49	*5.1087*	*44.809*		*P*	*10*											*18*
vercors55	*4.8451*	*44.7654*		*P*	*30*											*18*
vercors56	*5.0351*	*44.748*		*P*	*0*											*18*
D10	*6.4394*	*44.2178*	*U. Cretaceous*	*P*	*151*	*-17*	*60*	*-2*	*143*	*72*	*0.86*					*20*
D3a1	*6.4236*	*44.1842*	*U. Jurassic*	*SS*	*130*	*-6*	*32*	*-51*	*45*	*39*	*0.76*					*20*
N19a	*7.2758*	*43.7781*	*U. Cretaceous*	*SS*	*162*	*16*	*14*	*53*	*162*	*33*	*0.26*					*20*
			Oligocene													
Ardeche Nord	*4.4941*	*44.3696*		*T*	*9*	*66*	*41*	*-21*	*126*	*12*						*2*
Bordure cevenole N	*4.129*	*44.2482*		*T*	*110*	*82*	*5*	*2*	*94*	*-8*						*2*
Bordure cevenole S	*4.0647*	*44.0796*		*T*	*163*	*86*	*33*	*2*	*123*	*3*						*2*
Champ de fractures de Banon	*5.5427*	*43.9605*		*T*	*120*	*-86*	*12*	*-1*	*102*	*4*						*2*
G. Nesque	*5.2951*	*44.0524*		*T*	*123*	*-78*	*175*	*8*	*83*	*9*						*2*
Murs	*5.2181*	*43.9652*		*T*	*174*	*-79*	*45*	*-7*	*134*	*9*						*2*
Sault	*5.4058*	*44.1416*		*T*	*36*	*-80*	*48*	*9*	*138*	*-2*						*2*
BARROUX	*5.1121*	*44.1462*	*oligocene*	*T*	*314*	*86*	*67*	*1.4*	*156*	*3.6*	*0.97*	*20*	*18.9*			*6*
CLAIRIER	*5.113*	*44.1653*	*oligocene*	*T*	*nan*	*nan*	*nan*	*nan*	*128*	*nan*	*nan*	*nan*	*nan*			*6*
COL D ALSAU	*5.0218*	*44.154*	*Callovien-oxfordien*	*T*	*nan*	*nan*	*nan*	*nan*	*143*	*nan*	*nan*	*nan*	*nan*			*6*
COL D ALSAU	*5.0248*	*44.1526*	*valanginien*	*T*	*nan*	*nan*	*nan*	*nan*	*144*	*nan*	*nan*	*nan*	*nan*			*6*
DARDEL	*5.0028*	*44.1499*	*oligocene*	*T*	*nan*	*nan*	*nan*	*nan*	*144*	*nan*	*nan*	*nan*	*nan*			*6*
FERINGUANDE	*5.1799*	*44.1772*	*oligocene*	*T*	*nan*	*nan*	*nan*	*nan*	*130*	*nan*	*nan*	*nan*	*nan*			*6*

Site	Long.	Lat.	Age	Tectonic regime	σ_1 trend	σ_1 plunge	σ_2 trend	σ_2 plunge	σ_3 trend	σ_3 plunge	R	N	F	α	RUP	REF
FERME D URBAN	*5.0176*	*44.1307*	*oligocene*	*T*	*nan*	*nan*	*nan*	*nan*	*126*	*nan*	*nan*	*nan*	*nan*			*6*
GIPIERE	*5.1594*	*44.1732*	*oligocene*	*T*	*nan*	*nan*	*nan*	*nan*	*128*	*nan*	*nan*	*nan*	*nan*			*6*
GRANGIER	*5.035*	*44.1276*	*oligocene*	*T*	*125*	*89*	*235*	*0.3*	*325*	*0.8*	*0.67*	*21*	*17.6*			*6*
LA VILLASSE	*5.195*	*44.1795*	*oligocene*	*T*	*nan*	*nan*	*nan*	*nan*	*142*	*nan*	*nan*	*nan*	*nan*			*6*
MONTMIRAIL	*5.0085*	*44.1379*	*oligocene*	*T*	*nan*	*nan*	*nan*	*nan*	*144*	*nan*	*nan*	*nan*	*nan*			*6*
VALLAT DE LA CHAINE	*5.0933*	*44.18*	*oligocene*	*T*	*109*	*71.4*	*231*	*10*	*324*	*15*	*0.57*	*29*	*21*			*6*
Abergement	*5.95*	*46.92*	*Bajocian*						*130*							*14*
Buvilly	*5.7317*	*46.855*	*Bathonian*	*T*	*37*	*81*	*44*	*-9*	*134*	*1*	*0.43*	*12*		*13*	*40*	*14*
Champagnole	*5.9183*	*46.7533*	*Argovian*						*127*							*14*
Chatelneuf	*5.93*	*46.66*	*Sequanian*						*125*							*14*
Cht Chalon	*5.66*	*46.76*	*Low. Baj.-Aalen.*						*112*							*14*
Cize	*5.92*	*46.72*	*Low. Call.-Bath.*						*115*							*14*
Condon	*5.68*	*45.7933*	*Aptian Barremian*	*T*	*69*	*-70*	*7*	*10*	*100*	*17*	*0.28*	*14*		*6*	*18*	*14*
Cuisia	*5.4117*	*46.535*	*Bathonian*	*T*	*112*	*-71*	*177*	*8*	*85*	*17*	*0.39*	*25*		*10*	*27*	*14*
Dompierre	*5.63*	*46.5817*	*Bathonian*	*T*	*59*	*75*	*171*	*6*	*83*	*-14*	*0.37*	*7*		*4*	*11*	*14*
Doucier	*5.79*	*46.66*	*Sequanian*						*120*							*14*
Fay	*5.6617*	*45.6183*	*Portlandian*	*T*	*162*	*77*	*33*	*9*	*122*	*-10*	*0.25*	*4*		*9*	*30*	*14*
Grusse	*5.5083*	*46.6*	*Oxfordian Bathonian*	*T*	*166*	*-82*	*31*	*-6*	*121*	*6*	*0.37*	*8*		*11*	*30*	*14*
Hérisson	*5.8683*	*46.6*	*Valangin. Purbeck.*	*T*	*80*	*-66*	*167*	*1*	*76*	*24*	*0.21*	*5*		*4*	*33*	*14*
Hostias	*5.5383*	*45.8933*	*Oxfordian*	*T*	*56*	*-73*	*51*	*16*	*142*	*1*	*0.40*	*8*		*8*	*27*	*14*
Lajoux	*5.945*	*46.375*	*Rauracian*	*T*	*172*	*-76*	*169*	*14*	*80*	*-1*	*0.37*	*10*		*8*	*27*	*14*
Lemuy	*5.96*	*46.9*	*Callovian*						*125*							*14*
Lods	*6.2433*	*47.045*	*Sequanian*	*T*	*163*	*72*	*21*	*15*	*108*	*-11*	*0.33*	*8*		*14*	*43*	*14*
Longchaumois	*5.94*	*46.46*	*Barrem. to Valangin.*	*T*	*174*	*63*	*42*	*19*	*126*	*-19*	*0.48*	*5*		*10*	*45*	*14*
Maisières	*6.1*	*47.1083*	*Bathonian*						*110*							*14*
Mirebel	*5.7333*	*46.7*	*Argovian*	*T*	*59*	*80*	*31*	*-8*	*121*	*-4*	*0.47*	*16*		*11*	*34*	*14*
Montrond	*5.84*	*46.79*	*Bathonian*	*T*	*59*	*-80*	*29*	*9*	*120*	*5*	*0.43*	*7*		*13*	*52*	*14*
Mortes	*6.0817*	*46.5683*	*Raurac. Argov.*	*T*	*101*	*-71*	*20*	*3*	*111*	*19*	*0.59*	*7*		*5*	*27*	*14*
Mouille	*5.9867*	*46.5133*	*Portlandian*	*T*	*8*	*75*	*51*	*-11*	*139*	*10*	*0.34*	*11*		*12*	*38*	*14*
Ney	*5.83*	*46.79*	*Sequanian*						*122*							*14*
Piards	*5.8283*	*46.505*	*Kimmeridg. Bathon.*	*T*	*118*	*88*	*9*	*1*	*99*	*-2*	*0.33*	*15*		*18*	*39*	*14*

Site	Long.	Lat.	Age	Tectonic regime	σ_1 trend	σ_1 plunge	σ_2 trend	σ_2 plunge	σ_3 trend	σ_3 plunge	R	N	F	α	RUP	REF
Poligny est	*5.7417*	*46.82*	*Low.- Mid. Baj.*						*118*							*14*
Pont-d'Héry	*5.9*	*47.0267*	*Argovian*						*125*							*14*
Pratz	*5.7517*	*46.3817*	*Bathonian*	*T*	*158*	*74*	*24*	*11*	*112*	*-11*	*0.38*	*6*		*11*	*37*	*14*
Prénovel	*5.8517*	*46.52*	*Kimmeridgian*	*T*	*115*	*72*	*175*	*-9*	*82*	*-16*	*0.17*	*12*		*6*	*20*	*14*
Raviolle	*5.7733*	*46.3983*	*Portland. Kimmeridg.*	*T*	*13*	*-83*	*42*	*6*	*131*	*-3*	*0.49*	*7*		*10*	*35*	*14*
Rixouse	*5.865*	*46.45*	*Portlandian*	*T*	*70*	*-72*	*28*	*13*	*120*	*11*	*0.37*	*4*		*10*	*57*	*14*
Ronchaux	*5.7867*	*46.4917*	*Portland. Kimmeridg.*	*T*	*150*	*79*	*23*	*7*	*112*	*-9*	*0.27*	*7*		*13*	*35*	*14*
Valempoulières	*5.8617*	*46.83*	*Argovian*	*T*	*150*	*80*	*52*	*3*	*141*	*-10*	*0.42*	*24*		*10*	*40*	*14*
Vaux	*6.2367*	*46.82*	*Low. Kimmeridgian*						*121*							*14*
Villleneuve	*5.98*	*46.92*	*Bathonian*						*122*							*14*
vercors24	*5.2402*	*45.061*		*T*					*95*							*18*
vercors28	*5.3227*	*44.9714*		*T*	*100*	*74*	*2*	*5*	*95*	*-16*	*0.168*	*8*				*18*
S10a	*7.4072*	*43.7856*	*L. Cretaceous*	*P*	*65*	*32*					*0*					*19*
S4a	*7.4078*	*43.8428*	*U. Cretaceous*	*P*	*84*	*10*					*0.07*					*19*
S8a	*7.4475*	*43.8125*	*U. Cretaceous*	*SS*	*94*	*9*	*172*	*-52*	*11*	*-37*	*0.34*					*19*
C21a	*7.0683*	*43.6614*	*U. Jurassic*	*T*	*29*	*-79*	*7*	*10*	*98*	*4*	*0.4*					*20*
C22	*7.1264*	*43.6344*	*U. Oligocene*	*T*	*132*	*-71*	*24*	*-6*	*112*	*18*	*0.17*					*20*
D11	*6.3172*	*44.1364*	*M. Jurassic*	*T*	*132*	*69*	*41*	*0*	*131*	*-21*	*0.17*					*20*
D25	*6.815*	*44.3203*	*L. Oligocene*	*T*	*132*	*75*	*29*	*4*	*118*	*-14*	*0.12*					*20*
D26a	*6.8242*	*44.3114*	*U. Eocene/L. Oligocene*	*T*			*87*	*-10*	*177*	*1*	*0.23*					*20*
D28a1	*6.8083*	*44.3064*	*U. Eocene/L. Oligocene*	*T*	*156*	*72*	*92*	*-8*	*5*	*16*	*0.3*					*20*
D28b	*6.8083*	*44.3064*	*U. Eocene/L. Oligocene*	*T*	*13*	*61*	*90*	*-7*	*176*	*28*	*0.58*					*20*
D30a	*6.7953*	*44.3428*	*U. Eocene/L. Oligocene*	*T*							*0.01*					*20*
D49	*6.8356*	*44.2667*	*U. Jurassic*	*T*							*0.03*					*20*
D5	*6.405*	*44.1664*	*U. Jurassic*	*T*	*134*	*-71*	*60*	*5*	*152*	*18*	*0.53*					*20*
D7a	*6.5167*	*44.1989*	*M.U. Eocene*	*T*	*45*	*-34*	*178*	*-46*	*116*	*25*	*0.86*					*20*
N11b	*7.3158*	*43.9564*	*U. Cretaceous*	*P*	*100*	*15*	*25*	*-45*	*176*	*-41*	*0.12*					*20*
N18a	*7.31*	*43.8925*	*U. Cretaceous*	*P*	*91*	*-18*	*173*	*58*	*33*	*58*	*0.36*					*20*
N24a1	*7.4739*	*43.9039*	*U. Cretaceous*	*P*	*33*	*23*	*121*	*-7*	*16*	*-66*	*0.27*					*20*
N25a	*7.4667*	*43.8369*	*U. Cretaceous*	*P*	*49*	*0*	*139*	*0*			*0.33*					*20*
N26a	*7.5167*	*43.9331*	*U. Cretaceous*	*SS*	*45*	*9*	*122*	*-54*	*141*	*35*	*0.62*					*20*

Site	Long.	Lat.	Age	Tectonic regime	σ_1 trend	σ_1 plunge	σ_2 trend	σ_2 plunge	σ_3 trend	σ_3 plunge	R	N	F	α	RUP	REF
N27a	*7.4561*	*43.7906*	*U. Jurassic*	*SS*	*76*	*-3*					*0.02*					*20*
N32a	*7.4853*	*43.8233*	*U. Cretaceous*	*P*	*72*	*-15*					*0*					*20*
N33	*7.3997*	*43.8683*	*M. Eocene*	*P*	*59*	*-11*	*150*	*-5*	*82*	*78*	*0.43*					*20*
N6a	*7.1969*	*43.8308*	*M. Jurassic*	*SS*	*36*	*-20*	*18*	*69*	*124*	*6*	*0.12*					*20*
N8a	*7.2325*	*43.8731*	*L. Cretaceous*	*P*	*55*	*-44*	*162*	*-17*	*88*	*41*	*0.47*					*20*
D26b	*6.8242*	*44.3114*	*U. Eocene/L. Oligocene*	*T*	*46*	*66*					*0.07*					*20*
D28a3	*6.8083*	*44.3064*	*U. Eocene/L. Oligocene*	*T*	*46*	*-75*	*128*	*2*	*37*	*15*	*0.25*					*20*
			Aquitanian													
Alpilles-Nord	*5.0106*	*43.7777*		*SS*	*57*	*-5*	*167*	*74*	*146*	*15*						*2*
Alpilles-Sud	*4.9066*	*43.737*		*SS*	*53*	*1*	*151*	*79*	*143*	*-11*						*2*
Bord Est Fosse d Ales	*4.292*	*44.1218*		*SS*	*50*	*3*	*146*	*65*	*139*	*-24*						*2*
Bordure Cevenole	*4.0651*	*44.1766*		*SS*	*49*	*5*	*157*	*75*	*138*	*-14*						*2*
Champ de fractures de Banon	*5.5427*	*43.9605*		*SS*	*56*	*-9*	*8*	*77*	*144*	*10*						*2*
Collines d Avignon	*4.7846*	*43.9503*		*SS*	*47*	*-8*	*118*	*66*	*140*	*-22*						*2*
Collines de Gaumont	*4.9321*	*43.9096*		*SS*	*45*	*11*	*70*	*-78*	*136*	*5*						*2*
Collines de Vacquieres	*4.8062*	*43.6744*		*SS*	*65*	*-30*	*41*	*58*	*149*	*11*						*2*
G. Nesque	*5.2951*	*44.0524*		*SS*	*46*	*17*	*177*	*-65*	*131*	*18*						*2*
Garrigues d Uzes	*4.5396*	*43.9941*		*SS*	*55*	*-1*	*38*	*89*	*145*	*0*						*2*
Garrigues de Lunel	*4.1136*	*43.6897*		*SS*	*41*	*-9*	*83*	*78*	*132*	*-8*						*2*
Garrigues de Nimes	*4.3047*	*43.8339*		*SS*	*43*	*6*	*82*	*-83*	*134*	*5*						*2*
Luberon-Centre	*5.3545*	*43.7752*		*TP*	*38*	*-5*	*125*	*34*	*36*	*55*						*2*
Luberon-Ouest	*5.1376*	*43.8059*		*SS*	*36*	*-11*	*52*	*-79*	*127*	*-3*						*2*
Luberon-Sud	*5.2196*	*43.7526*		*SS*	*56*	*-16*	*106*	*66*	*157*	*-17*						*2*
Murs	*5.2181*	*43.9652*		*SS*	*46*	*1*	*129*	*-81*	*147*	*5*						*2*
Sault	*5.4058*	*44.1416*		*SS*	*53*	*-9*	*68*	*-81*	*143*	*-2*						*2*
St-Saturnin d-Apt	*5.3626*	*43.9428*		*SS*	*58*	*-10*	*32*	*79*	*147*	*5*						*2*
Ventoux-Sud	*5.1642*	*44.1417*		*SS*	*61*	*-14*	*167*	*-49*	*140*	*38*						*2*
34b	*5.1803*	*44.5509*	*Barrémien*		*50*											*10*
45b	*5.1158*	*44.4116*	*Hautériven-Berriasien*		*50*											*10*
			Mio-Pliocene													
S12b	*5.8528*	*43.9033*	*Up. Oligocene*		*90*											*1*

Site	Long.	Lat.	Age	Tectonic regime	σ_1 trend	σ_1 plunge	σ_2 trend	σ_2 plunge	σ_3 trend	σ_3 plunge	R	N	F	α	RUP	REF
S12b	*5.8528*	*43.9033*	*Up. Oligocene*		*90*											*1*
S13b	*5.8036*	*43.85*	*Tortonien*		*110*											*1*
S13b	*5.8036*	*43.85*	*Tortonien*		*110*											*1*
S15b	*5.7933*	*43.8464*	*Vindobonian*		*100*											*1*
S15b	*5.7933*	*43.8464*	*Vindobonian*		*100*											*1*
S4b	*5.9817*	*44.0308*	*Tortonien*		*100*											*1*
S4b	*5.9817*	*44.0308*	*Tortonien*		*100*											*1*
S5b	*5.91*	*44.0081*	*Oligcene*	*P*	*74*	*0*	*164*	*0*	*330*	*90*	*0.55*					*1*
S5b	*5.91*	*44.0081*	*Oligocene*	*P*	*74*	*0*	*164*	*0*	*330*	*90*	*0.55*					*1*
S9b	*5.8639*	*43.9336*	*Oligcene*	*SS*	*135*	*3*	*237*	*77*	*45*	*12*	*0.69*					*1*
S9b	*5.8639*	*43.9336*	*Oligocene*	*SS*	*135*	*3*	*237*	*77*	*45*	*12*	*0.69*					*1*
Apt	*5.5183*	*43.8462*		*SS*	*8*	*3*	*136*	*86*	*98*	*-3*						*2*
Forcalquier	*5.8861*	*43.999*		*SS*	*156*	*3*	*71*	*-59*	*65*	*31*						*2*
Manosque	*5.6547*	*43.7791*		*SS*	*7*	*-6*	*128*	*-78*	*96*	*10*						*2*
Pertuis	*5.5836*	*43.6568*		*SS*	*173*	*2*	*24*	*87*	*83*	*-1*						*2*
Sud-Crest	*4.8789*	*44.656*		*SS*	*107*	*-5*	*171*	*79*	*18*	*10*						*2*
Tricastin	*4.8693*	*44.3155*		*SS*	*110*	*-9*	*60*	*76*	*18*	*-11*						*2*
Valdaine	*4.9171*	*44.4789*		*SS*	*101*	*9*	*76*	*-81*	*10*	*4*						*2*
Vivarais Nord	*4.6154*	*44.6874*		*SS*	*113*	*0*	*24*	*-76*	*23*	*14*						*2*
Vivarais Sud	*4.5345*	*44.4598*		*SS*	*104*	*-10*	*92*	*80*	*13*	*-2*						*2*
COL FREN	*6.1376*	*45.5798*	*Kimmeridgien sup ? Tithonien*	*SS*	*104*	*1*	*11*	*77*	*14*	*-13*	*0.348*	*7*		*5*	*22*	*3*
CRETEVIA	*6.1491*	*45.5947*	*Oxfordien moy-Tithonien*	*TP*	*96*	*-13*	*16*	*38*	*170*	*49*	*0.312*	*11*		*5*	*16*	*3*
GRONLU	*4.8329*	*44.9037*	*Paleozoic*	*SS*	*108*	*3*	*61*	*-86*	*18*	*3*	*0.39*	*16*		*5*	*24*	*4*
SERRELG	*4.9503*	*44.7806*	*Pliocene sup*	*SS*	*115*	*-8*	*35*	*53*	*20*	*-36*	*0.417*	*4*		*6*	*35*	*4*
TESSON	*4.8417*	*44.8991*	*Trias*	*SS*	*113*	*2*	*3*	*85*	*23*	*-4*	*0.685*	*5*		*7*	*29*	*4*
TOULAUD	*4.819*	*44.8953*	*Paleozoic*	*SS*	*127*	*19*	*43*	*-14*	*167*	*-66*	*0.138*	*6*		*14*	*32*	*4*
PAS2ROCH	*5.4234*	*44.7414*	*Tithonique*	*SS*	*115*	*-19*	*0*	*-51*	*38*	*33*	*0.498*	*5*		*6*	*35*	*5*
PLANEAUX	*5.4071*	*44.789*	*Tithonique*	*SS*	*104*	*18*	*65*	*-68*	*10*	*13*	*0.354*	*11*		*11*	*30*	*5*
VIGNON1	*5.4082*	*44.7856*	*Tithonique*	*TP*	*112*	*8*	*17*	*32*	*34*	*-57*	*0.029*	*7*		*7*	*26*	*5*
ASTAUDS	*5.1639*	*44.2105*	*Miocene sup.*	*P*	*355*	*9.7*	*242.5*	*67*	*89.8*	*20.6*	*0.997*	*11*	*10.5*			*6*
BEAUMETTES	*5.1447*	*44.2411*	*Burdigalien*	*TP*	*94.8*	*2.2*	*2.6*	*44*	*187*	*46*	*0.91*	*30*	*20.3*			*6*

Site	Long.	Lat.	Age	Tectonic regime	σ_1 trend	σ_1 plunge	σ_2 trend	σ_2 plunge	σ_3 trend	σ_3 plunge	R	N	F	α	RUP REF
BOIS DES ABRIGEAUX	*5.0055*	*44.2656*	*Tortonien sup.*	*P*	*283*	*5.2*	*192*	*5.3*	*57*	*82.6*	*0.9*	*21*	*19.8*		*6*
BRIGUIERE	*5.0227*	*44.1879*	*Miocene sup.*	*P*	*110*	*nan*	*nan*	*nan*	*nan*	*nan*	*nan*	*nan*	*nan*		*6*
BUISSON	*4.9939*	*44.2717*	*Tortonien inf.*	*TP*	*269.5*	*0.6*	*179*	*21*	*1.2*	*69*	*0.92*	*16*	*15.4*		*6*
BUTTE DE SEGURET	*5.139*	*44.2259*	*Serravalien sup.*	*P*	*109.6*	*0.7*	*19.4*	*19.5*	*201.7*	*70.5*	*0.77*	*21*	*20*		*6*
BUTTE MARODY	*5.0592*	*44.2477*	*Serravalien sup.*	*P*	*272*	*1.5*	*182*	*6.5*	*14*	*83*	*0.88*	*15*	*14.15*		*6*
BUTTE ST MARC	*5.1859*	*44.2772*	*Burdigalien*	*P*	*156.8*	*11.2*	*66.5*	*1.6*	*328.3*	*78.6*	*0.9*	*36*	*31.5*		*6*
CARREFOUR D938-D15	*5.0864*	*44.2267*	*Burdigalien*	*TP*	*64*	*17*	*291*	*65.6*	*159*	*17*	*0.84*	*14*	*13.9*		*6*
CARRIERE DE BEAUME	*5.0426*	*44.1299*	*Burdigalien*	*TP*	*145*	*16*	*245*	*31*	*31*	*54.5*	*0.91*	*16*	*15.75*		*6*
CASCADE	*5.0458*	*44.1323*	*Burdigalien*	*TP*	*1.46*	*14.6*	*100.5*	*31*	*250*	*55*	*0.43*	*13*	*12.8*		*6*
CHAMP LONG	*5.1039*	*44.2646*	*Serravalien sup.*	*P*	*101*	*nan*	*nan*	*nan*	*nan*	*nan*	*nan*	*nan*	*nan*		*6*
CHAMP PAGA	*5.0868*	*44.1401*	*oligocene*	*P*	*169.6*	*11.5*	*77*	*12*	*301*	*73*	*0.9*	*15*	*8.6*		*6*
CHANTEDUC	*5.0627*	*44.2953*	*Pliocene sup.*	*P*	*117*	*nan*	*nan*	*nan*	*nan*	*nan*	*nan*	*nan*	*nan*		*6*
CHAPELLE D AUBUNE	*5.0111*	*44.1261*	*Burdigalien*	*SS*	*199*	*28*	*13*	*61.5*	*107*	*2.5*	*0.82*	*25*	*24.25*		*6*
CHAPELLE-ST-JEAN	*5.1891*	*44.3177*	*Barremian*	*P*	*137*	*5.3*	*45.5*	*14.7*	*246*	*74.3*	*0.6*	*29*	*26.1*		*6*
CHATEAU DE GIGONDAS	*5.0041*	*44.1643*	*Burdigalien*	*P*	*124.5*	*nan*	*nan*	*nan*	*nan*	*nan*	*nan*	*nan*	*nan*		*6*
CHENES VERTS	*5.0762*	*44.3832*	*Tortonien moy.*	*P*	*55.5*	*0.6*	*325*	*10*	*149*	*80*	*0.944*	*26*	*20.7*		*6*
CIMETIERE DE GIGONDAS	*5.0041*	*44.1634*	*Burdigalien*	*P*	*115*	*nan*	*nan*	*nan*	*nan*	*nan*	*nan*	*nan*	*nan*		*6*
CIMETIERE DE SAINTE MARGUERITE	*5.1921*	*44.1841*	*Burdigalien*	*P*	*168*	*nan*	*nan*	*nan*	*nan*	*nan*	*nan*	*nan*	*nan*		*6*
CIMETIERE DE VILLEDIEU	*5.0413*	*44.2796*	*Plaisancien*	*P*	*92*	*nan*	*nan*	*nan*	*nan*	*nan*	*nan*	*nan*	*nan*		*6*
CLAUX	*5.1329*	*44.1567*	*Burdigalien*	*SS*	*174*	*nan*	*nan*	*nan*	*nan*	*nan*	*nan*	*nan*	*nan*		*6*
COL D ALSAU	*5.0218*	*44.154*	*Callovien-oxfordien*	*SS*	*99*	*nan*	*nan*	*nan*	*nan*	*nan*	*nan*	*nan*	*nan*		*6*
COL D EY	*5.2797*	*44.3098*	*Barremien-Bedoulien*	*P*	*57*	*nan*	*nan*	*nan*	*nan*	*nan*	*nan*	*nan*	*nan*		*6*
COL DE LA CHAINE	*5.0986*	*44.1747*	*oligocene*	*P*	*94.5*	*2.5*	*4*	*11*	*197*	*78.8*	*0.25*	*11*	*10.67*		*6*
COL DE PROPIAC	*5.1826*	*44.2739*	*Burdigalien*	*TP*	*83.5*	*4.6*	*345*	*61*	*176*	*28.6*	*0.86*	*10*	*9.7*		*6*
COMBE GIBOUSE	*5.1251*	*44.156*	*Burdigalien*	*P*	*355*	*5*	*264.3*	*6*	*128*	*81.7*	*0.87*	*10*	*7.4*		*6*
COMBES	*5.074*	*44.2968*	*Plaisancien*	*P*	*255*	*2.4*	*165*	*0.13*	*72*	*87.6*	*0.89*	*21*	*18.5*		*6*
COMBES-CORIANCON	*5.0754*	*44.2991*	*Pliocene conti. inf.*	*SS*	*74.2*	*3.5*	*276*	*86*	*164*	*1.4*	*0.995*	*24*	*18.5*		*6*
CONGLOMERATS DE CRESTET	*5.0843*	*44.2209*	*nan*	*P*	*86.5*	*11*	*356.6*	*1*	*261.7*	*79*	*0.92*	*18*	*15.9*		*6*
COTE 265m	*5.0341*	*44.1226*	*Burdigalien*	*P*	*176*	*nan*	*nan*	*nan*	*nan*	*nan*	*nan*	*nan*	*nan*		*6*
COTE 268m	*5.1426*	*44.3537*	*Burdigalien*	*P*	*116*	*nan*	*nan*	*nan*	*nan*	*nan*	*nan*	*nan*	*nan*		*6*
COTE 322m	*4.9762*	*44.2541*	*Tortonien sup.*	*P*	*89*	*nan*	*nan*	*nan*	*nan*	*nan*	*nan*	*nan*	*nan*		*6*

Site	Long.	Lat.	Age	Tectonic regime	σ_1 trend	σ_1 plunge	σ_2 trend	σ_2 plunge	σ_3 trend	σ_3 plunge	R	N	F	α	RUP	REF
COTE 330m	*5.1221*	*44.3583*	*Serravalien sup.*	*P*	*114*	*1.6*	*204*	*4*	*2.6*	*85.5*	*0.33*	*31*	*23.8*			*6*
COTE 380m	*5.1081*	*44.3681*	*Tortonien inf.*	*P*	*46*	*4.3*	*136.4*	*2.3*	*254*	*85*	*0.29*	*22*	*18*			*6*
COTE 383m	*5.0908*	*44.2937*	*Serravalien sup.*	*P*	*239*	*9.6*	*329*	*0*	*60*	*80*	*0.98*	*15*	*14.3*			*6*
COTE 519m	*5.1884*	*44.2702*	*Burdigalien*	*P*	*156.6*	*11*	*66*	*3*	*321.6*	*75.4*	*0.9*	*16*	*14.95*			*6*
COTE CHAUDE	*5.2183*	*44.3631*	*Burdigalien*	*P*	*151*	*nan*	*nan*	*nan*	*nan*	*nan*	*nan*	*nan*	*nan*			*6*
D938	*5.1062*	*44.1396*	*oligocene*	*P*	*321.3*	*9.4*	*230.5*	*4.4*	*115.8*	*79.8*	*0.83*	*18*	*15.13*			*6*
ESPINIAUX	*5.1402*	*44.3042*	*Serravalien sup.*	*P*	*73*	*nan*	*nan*	*nan*	*nan*	*nan*	*nan*	*nan*	*nan*			*6*
ESSARTS DU PONT	*5.1271*	*44.2253*	*Burdigalien*	*P*	*88*	*nan*	*nan*	*nan*	*nan*	*nan*	*nan*	*nan*	*nan*			*6*
FADES	*5.0249*	*44.1821*	*Burdigalien*	*P*	*108*	*nan*	*nan*	*nan*	*nan*	*nan*	*nan*	*nan*	*nan*			*6*
FERME CURNIER	*5.3052*	*44.3564*	*Barremien sup.*	*SS*	*235.4*	*6*	*59.7*	*84*	*325.4*	*0.5*	*0.92*	*25*	*22*			*6*
FERME DE CHAMP PAGA	*5.0899*	*44.14*	*oligocene*	*P*	*163*	*nan*	*nan*	*nan*	*nan*	*nan*	*nan*	*nan*	*nan*			*6*
FERME DES PLATES	*5.2462*	*44.33*	*Barremian*	*P*	*77.5*	*nan*	*nan*	*nan*	*nan*	*nan*	*nan*	*nan*	*nan*			*6*
FERME DES PRES	*5.3135*	*44.3593*	*Bedoulien*	*P*	*63*	*nan*	*nan*	*nan*	*nan*	*nan*	*nan*	*nan*	*nan*			*6*
FERME VELOUZE	*5.1753*	*44.3029*	*Burdigalien*	*TP*	*327.5*	*21.6*	*76*	*39*	*215*	*43.7*	*0.61*	*10*	*9.3*			*6*
FLORETS	*5.0115*	*44.1677*	*Burdigalien*	*P*	*119*	*nan*	*nan*	*nan*	*nan*	*nan*	*nan*	*nan*	*nan*			*6*
FONT DE MERLE	*5.2214*	*44.3675*	*Burdigalien*	*P*	*152*	*20*	*54.8*	*19*	*284.5*	*61.5*	*0.95*	*17*	*12*			*6*
GARRIGUE DE ST ANDEOL	*4.9444*	*44.2425*	*Tortonien sup.*	*P*	*111*	*nan*	*nan*	*nan*	*nan*	*nan*	*nan*	*nan*	*nan*			*6*
GIPPIERE	*5.1694*	*44.1673*	*oligocene*	*P*	*144.4*	*14.7*	*237.4*	*11.4*	*3.8*	*71*	*0.46*	*14*	*12.23*			*6*
HAUT FABRANCHE	*5.0819*	*44.3043*	*Pliocene sup.*	*P*	*80*	*4.5*	*171*	*11.5*	*330*	*77.5*	*0.9*	*30*	*28*			*6*
HAUTIMAGNE	*5.0689*	*44.2947*	*Pliocene sup.*	*P*	*84*	*1*	*354*	*16*	*178*	*73.6*	*0.997*	*18*	*16.8*			*6*
JAS CREMAD	*5.0992*	*44.1386*	*oligocene*	*P*	*131*	*nan*	*nan*	*nan*	*nan*	*nan*	*nan*	*nan*	*nan*			*6*
LE JAS	*5.0121*	*44.2452*	*Tortonien sup.*	*P*	*90*	*nan*	*nan*	*nan*	*nan*	*nan*	*nan*	*nan*	*nan*			*6*
LOGIS DE FRANCE	*5.1856*	*44.2761*	*Miocene moyen*	*P*	*156.8*	*11.2*	*66.5*	*1.6*	*328.3*	*78.6*	*0.9*	*36*	*31.5*			*6*
LOZIEU	*5.1081*	*44.2618*	*Miocene moyen*	*P*	*108*	*nan*	*nan*	*nan*	*nan*	*nan*	*nan*	*nan*	*nan*			*6*
MIOCENE DU COL DE LA CHAINE	*5.1011*	*44.1791*	*Burdigalien*	*P*	*68.3*	*13.7*	*158.3*	*0.18*	*249*	*76*	*0.53*	*24*	*20.6*			*6*
MOLLANS SUR OUVEZE	*5.1935*	*44.2399*	*Burdigalien*	*P*	*180.5*	*2*	*89.4*	*29.6*	*274*	*60.3*	*0.75*	*24*	*22.6*			*6*
MONTBRISON	*5.0111*	*44.4446*	*Burdigalien*	*SS*	*60*	*nan*	*nan*	*nan*	*nan*	*nan*	*nan*	*nan*	*nan*			*6*
MOULIERES	*5.0708*	*44.369*	*Pliocene*	*TP*	*49*	*nan*	*nan*	*nan*	*nan*	*nan*	*nan*	*nan*	*nan*			*6*
MOULIN GAUTHIER	*5.1826*	*44.2604*	*Burdigalien*	*P*	*90*	*nan*	*nan*	*nan*	*nan*	*nan*	*nan*	*nan*	*nan*			*6*
MOULINS	*5.0651*	*44.415*	*Miocene moyen*	*P*	*50*	*nan*	*nan*	*nan*	*nan*	*nan*	*nan*	*nan*	*nan*			*6*
NORD DE CRESTET	*5.0827*	*44.2232*	*Burdigalien*	*TP*	*82.9*	*27*	*302.6*	*56.6*	*182.65*	*18.3*	*0.91*	*12*	*11*			*6*

Site	Long.	Lat.	Age	Tectonic regime	σ_1 trend	σ_1 plunge	σ_2 trend	σ_2 plunge	σ_3 trend	σ_3 plunge	R	N	F	α	RUP	REF
OSIERES	*5.0045*	*44.2571*	*Tortonien moy.*	*P*	*91*	*3.6*	*181*	*5.3*	*327*	*83.6*	*0.78*	*22*	*21.2*			*6*
PAS DE BEYNET	*5.1625*	*44.2857*	*Burdigalien*	*TP*	*243*	*7.4*	*149*	*28.4*	*346*	*60.5*	*0.75*	*28*	*20.5*			*6*
PAS DE CHAUVET	*5.178*	*44.2954*	*Burdigalien*	*P*	*161*	*nan*	*nan*	*nan*	*nan*	*nan*	*nan*	*nan*	*nan*			*6*
PAS DE MANEYROL	*5.1778*	*44.3096*	*Burdigalien*	*SS*	*12.9*	*1.5*	*106*	*64*	*282*	*25*	*0.89*	*24*	*18.56*			*6*
PAS DU ROCHER	*5.1347*	*44.321*	*Burdigalien*	*P*	*259.5*	*16.4*	*350*	*1.3*	*84.5*	*73.5*	*0.91*	*47*	*42.9*			*6*
PATY-CRILLON	*5.1412*	*44.1399*	*oligocene*	*P*	*147*	*nan*	*nan*	*nan*	*nan*	*nan*	*nan*	*nan*	*nan*			*6*
PEYROL EST	*5.0311*	*44.2362*	*Miocene sup.*	*P*	*137*	*12*	*43*	*18*	*259*	*68*	*0.9*	*30*	*26*			*6*
PEYROL OUEST	*5.0286*	*44.2349*	*Miocene sup.*	*P*	*325*	*12.5*	*57*	*6.6*	*174*	*75.8*	*0.74*	*29*	*22.3*			*6*
PEYROUSE	*5.0824*	*44.3147*	*Pliocene*	*P*	*259.5*	*0.6*	*349*	*7.3*	*165*	*82.6*	*0.47*	*14*	*13*			*6*
PLAN DE LA VACHE	*5.1193*	*44.3651*	*Serravalien sup.*	*P*	*229.5*	*9.2*	*139.5*	*0.29*	*49*	*80.8*	*0.84*	*15*	*15.5*			*6*
RAVIN DE FERINGUANDE	*5.1818*	*44.1771*	*oligocene*	*P*	*169*	*nan*	*nan*	*nan*	*nan*	*nan*	*nan*	*nan*	*nan*			*6*
RICHARDS BURDIGALIEN	*5.2019*	*44.2244*	*Burdigalien*	*NAN*	*8*	*nan*	*nan*	*nan*	*nan*	*nan*	*nan*	*nan*	*nan*			*6*
RICHARDS URGONIEN	*5.2022*	*44.2244*	*Barremian*	*P*	*14*	*nan*	*nan*	*nan*	*nan*	*nan*	*nan*	*nan*	*nan*			*6*
ROCHE GALLIERE	*5.1093*	*44.2194*	*Serravalien sup.*	*TP*	*63*	*5*	*157*	*38.7*	*326.7*	*51*	*0.96*	*22*	*19.3*			*6*
SERRE LAUZIERE	*5.1245*	*44.3429*	*Serravalien sup.*	*P*	*121*	*1.8*	*31*	*4.3*	*234*	*85.3*	*0.17*	*36*	*32*			*6*
SERRE LONGUE	*5.091*	*44.3928*	*Serravalien sup.*	*P*	*234*	*9.6*	*324*	*0.9*	*59.5*	*80*	*0.895*	*18*	*16.7*			*6*
SOUVESTRES	*5.1013*	*44.3705*	*nan*	*P*	*44*	*nan*	*nan*	*nan*	*nan*	*nan*	*nan*	*nan*	*nan*			*6*
ST AMAND	*5.0854*	*44.1772*	*oligocene*	*TP*	*89*	*1*	*180.5*	*50*	*358*	*40*	*0.98*	*20*	*19*			*6*
SUD DE SEGURET	*5.0253*	*44.2043*	*Burdigalien*	*TP*	*255.7*	*4.5*	*353*	*59*	*163*	*30.7*	*0.86*	*18*	*17.15*			*6*
TAULEIGNE	*4.9938*	*44.1573*	*Burdigalien*	*P*	*304*	*1.8*	*34*	*1*	*153*	*88*	*0.57*	*28*	*26.6*			*6*
TROIS THERMES	*5.1369*	*44.1422*	*oligocene*	*SS*	*148.3*	*18*	*335*	*72*	*239*	*2*	*0.94*	*23*	*21*			*6*
TROU DU PONTIAS	*5.1482*	*44.3666*	*Burdigalien*	*P*	*75*	*9.3*	*345*	*1.8*	*244*	*80.5*	*0.12*	*25*	*21.7*			*6*
TUNNEL DE NYONS	*5.1363*	*44.3611*	*Burdigalien*	*P*	*113*	*nan*	*nan*	*nan*	*nan*	*nan*	*nan*	*nan*	*nan*			*6*
VALETTES	*5.1806*	*44.1929*	*Burdigalien*	*P*	*341*	*5.4*	*249*	*14.8*	*90*	*74.3*	*0.72*	*22*	*20.3*			*6*
VALLAT DE LA CHAINE	*5.0931*	*44.1748*	*oligocene*	*SS*	*269*	*11.6*	*134*	*73.7*	*1.25*	*11.3*	*0.91*	*27*	*21.9*			*6*
VILLAGE DE SEGURET	*5.0251*	*44.2059*	*Burdigalien*	*P*	*103.5*	*7*	*12.4*	*9*	*230*	*78.6*	*0.27*	*13*	*12.7*			*6*
VILLASSE	*5.1937*	*44.1786*	*oligocene*	*P*	*160*	*nan*	*nan*	*nan*	*nan*	*nan*	*nan*	*nan*	*nan*			*6*
AMBIN	*6.8738*	*45.1858*		*T*	*67*	*70*	*89*	*-19*	*176*	*7*	*0.12*	*75*		*10.5*		*7*
ARPON2	*6.7123*	*45.3169*		*TT*	*131*	*59*	*126*	*-31*	*37*	*2*	*0.55*	*34*		*9.3*		*7*
artsin	*7.4279*	*46.1166*		*T*	*8*	*61*	*27*	*-27*	*113*	*8*	*0.47*	*18*		*11.5*		*7*
AVISE	*7.1526*	*45.7059*		*T*	*5*	*63*	*128*	*16*	*44*	*-22*	*0.05*	*17*		*7.3*		*7*

Site	Long.	Lat.	Age	Tectonic regime	σ_1 trend	σ_1 plunge	σ_2 trend	σ_2 plunge	σ_3 trend	σ_3 plunge	R	N	F	α	RUP	REF
BARDO	*6.7172*	*45.0895*		*T*	*57*	*-75*	*103*	*10*	*11*	*10*	*0.06*	*31*		*13.5*		*7*
BOZEL	*6.6236*	*45.4446*		*TT*	*135*	*53*	*137*	*-37*	*46*	*-1*	*0.55*	*31*		*14.9*		*7*
BUTHIER	*7.2713*	*45.7845*		*TT*	*93*	*-49*	*111*	*40*	*13*	*9*	*0.323*	*16*		*5.1*		*7*
cargn	*7.5589*	*46.2326*		*T*	*105*	*-73*	*118*	*17*	*27*	*4*	*0.08*	*18*		*6.5*		*7*
CARLO	*7.003*	*45.7136*		*T*	*50*	*65*	*150*	*5*	*62*	*-24*	*0.89*	*20*		*8.1*		*7*
CELS	*6.9431*	*45.1048*		*TT*	*122*	*-33*	*72*	*45*	*13*	*-27*	*0.51*	*14*		*10.9*		*7*
CENIS1	*6.9271*	*45.2269*		*T*	*145*	*-79*	*129*	*10*	*39*	*-3*	*0.21*	*31*		*10.9*		*7*
CENIS2(1)	*6.9614*	*45.2292*		*SS*	*84*	*-68*	*87*	*22*	*177*	*-1*	*0.23*	*17*		*11.2*		*7*
CENIS2(2)	*6.9614*	*45.2292*		*T*	*107*	*6*	*4*	*66*	*19*	*-23*	*0.63*	*18*		*7.4*		*7*
CENIS3	*6.9243*	*45.2831*		*T*	*134*	*-65*	*107*	*22*	*30*	*-10*	*0.67*	*16*		*8.8*		*7*
CENIS6(1)	*6.9695*	*45.2137*		*T*	*1*	*74*	*111*	*6*	*23*	*-15*	*0.19*	*32*		*8.3*		*7*
CHAMB	*6.2788*	*45.3873*		*SS*	*137*	*-24*	*133*	*65*	*46*	*-1*	*0.49*	*18*		*11.5*		*7*
CHAMPA	*6.7087*	*45.4599*		*SS*	*98*	*-7*	*171*	*68*	*10*	*21*	*0.35*	*26*		*11.7*		*7*
CHAMPA2	*6.7167*	*45.4566*		*SS*	*96*	*-8*	*40*	*75*	*4*	*-12*	*0.54*	*17*		*12.8*		*7*
CHAT1	*6.858*	*45.6178*		*T*	*3*	*-72*	*79*	*5*	*168*	*-17*	*0.264*	*15*		*7.8*		*7*
CHAT2	*6.8628*	*45.6148*		*T*	*38*	*-61*	*119*	*5*	*27*	*28*	*0.008*	*18*		*1.8*		*7*
cleus1	*7.3219*	*46.1148*		*T*	*135*	*-69*	*172*	*17*	*79*	*12*	*0.06*	*12*		*2.9*		*7*
cleus2	*7.327*	*46.1094*		*T*	*175*	*-53*	*148*	*33*	*67*	*-13*	*0.32*	*11*		*3.2*		*7*
couta	*7.4913*	*46.0824*		*T*	*26*	*87*	*154*	*2*	*64*	*-2*	*0.22*	*22*		*9.4*		*7*
danger	*7.3227*	*46.0212*		*TT*	*140*	*-48*	*101*	*35*	*26*	*-20*	*0.95*	*16*		*6.7*		*7*
dix	*7.4073*	*46.0887*		*SS*	*2*	*-9*	*69*	*67*	*91*	*-21*	*0.97*	*33*		*7.3*		*7*
emdd (1)	*7.8388*	*46.223*		*T*	*30*	*-71*	*129*	*-3*	*40*	*19*	*0.06*	*22*		*4.8*		*7*
emdd (2)	*7.8388*	*46.223*		*SS*	*70*	*-12*	*88*	*78*	*161*	*-3*	*0.24*	*13*		*7.8*		*7*
emmd2	*7.8609*	*46.2319*		*T*	*22*	*-81*	*123*	*-2*	*33*	*8*	*0.07*	*16*		*7.6*		*7*
ergi1	*7.7082*	*46.2959*		*T*	*70*	*-74*	*134*	*7*	*42*	*14*	*0.4*	*11*		*5.3*		*7*
ergi2	*7.7062*	*46.2898*		*T*	*46*	*-64*	*2*	*19*	*98*	*17*	*0.93*	*9*		*9.8*		*7*
ETACHE	*6.8136*	*45.1613*		*T*	*9*	*73*	*104*	*1*	*14*	*-16*	*0.05*	*35*		*4.7*		*7*
evole	*7.5043*	*46.1085*		*T*	*2*	*53*	*131*	*25*	*53*	*-25*	*0.26*	*28*		*4.3*		*7*
EXTRA	*6.7986*	*45.2186*		*T*	*145*	*66*	*119*	*-22*	*33*	*10*	*0.26*	*10*		*3.5*		*7*
FERRE	*7.1212*	*45.911*		*SS*	*93*	*-28*	*149*	*47*	*21*	*30*	*0.06*	*12*				*7*
findel	*7.7856*	*46.0126*		*SS*	*179*	*36*	*146*	*-49*	*76*	*17*	*0.77*	*21*		*9.7*		*7*

Site	Long.	Lat.	Age	Tectonic regime	σ_1 trend	σ_1 plunge	σ_2 trend	σ_2 plunge	σ_3 trend	σ_3 plunge	R	N	F	α	RUP	REF
FONDS	*6.6524*	*45.3089*		*T*	*10*	*69*	*142*	*14*	*56*	*-15*	*0.17*	*43*		*11.5*		*7*
FONT	*6.5006*	*45.4514*		*T*	*116*	*-59*	*100*	*30*	*14*	*-7*	*#*	*24*				*7*
forcl	*7.4563*	*46.0302*		*T*	*20*	*64*	*164*	*21*	*80*	*-14*	*0.45*	*15*		*7.7*		*7*
FOUR	*7.0167*	*45.3945*		*T*	*101*	*78*	*138*	*-10*	*46*	*-7*	*0.29*	*28*		*8.5*		*7*
FREJUS	*6.665*	*45.1386*		*T*	*74*	*-85*	*124*	*3*	*34*	*4*	*0.21*	*26*		*14.9*		*7*
FRETE (1)	*6.8085*	*45.5709*		*T*	*88*	*-55*	*51*	*29*	*151*	*17*	*0.068*	*17*		*4*		*7*
FRETE (2)	*6.8085*	*45.5709*		*SS*	*111*	*-8*	*147*	*80*	*22*	*6*	*0.565*	*8*		*10.2*		*7*
GALIB	*6.4096*	*45.065*		*SS*	*101*	*-12*	*30*	*57*	*4*	*-30*	*0.13*	*35*		*14.1*		*7*
gallen	*7.7891*	*46.0486*		*T*	*53*	*59*	*129*	*-8*	*35*	*-30*	*0.79*	*9*		*4.3*		*7*
GIAGLI	*7.0171*	*45.143*		*T*	*7*	*79*	*91*	*-1*	*1*	*-10*	*0.56*	*17*		*15.5*		*7*
grime	*7.5604*	*46.1609*		*T*	*129*	*82*	*160*	*-7*	*69*	*-4*	*0.32*	*29*		*8.6*		*7*
GSB1	*7.1877*	*45.8865*		*SS*	*101*	*11*	*35*	*-65*	*7*	*22*	*0.91*	*21*		*7.7*		*7*
GSB2	*7.1896*	*45.8995*		*SS*	*133*	*-24*	*159*	*64*	*47*	*10*	*0.577*	*19*		*16.9*		*7*
GSBIT	*7.1512*	*45.8598*		*SS*	*167*	*-25*	*108*	*48*	*61*	*-32*	*0.37*	*15*		*4.6*		*7*
GURRAZ	*6.9033*	*45.6249*		*T*	*179*	*-75*	*142*	*12*	*54*	*-9*	*0.234*	*24*		*6.1*		*7*
ISERAN	*7.021*	*45.4317*		*T*	*84*	*84*	*172*	*0*	*82*	*-6*	*0.2*	*34*		*9.4*		*7*
LACPLAG	*6.845*	*45.488*		*T*	*139*	*-65*	*141*	*25*	*51*	*1*	*0.07*	*14*		*3.7*		*7*
LANSLEV	*6.9287*	*45.2998*		*T*	*155*	*82*	*98*	*-4*	*9*	*7*	*0.26*	*19*		*11*		*7*
MAD	*6.368*	*45.4403*		*SS*	*127*	*27*	*140*	*-62*	*39*	*-5*	*0.46*	*26*		*13.3*		*7*
MALAT	*7.1313*	*45.8409*		*TT*	*91*	*-32*	*129*	*52*	*13*	*19*	*0.18*	*15*		*4.7*		*7*
MALAT2	*7.1113*	*45.8408*		*SS*	*95*	*-21*	*117*	*67*	*8*	*8*	*0.252*	*14*		*4.3*		*7*
MASSE2	*6.6974*	*45.2598*		*T*	*127*	*75*	*97*	*-13*	*9*	*7*	*0.56*	*19*		*7.9*		*7*
MENU	*6.5822*	*45.3168*		*T*	*110*	*-82*	*83*	*7*	*173*	*4*	*0.46*	*17*		*5.4*		*7*
MICHE	*6.4865*	*45.2184*		*SS*	*98*	*-29*	*54*	*52*	*175*	*22*	*0.57*	*27*		*17.8*		*7*
MICOEUR	*7.2449*	*46.1183*		*T*	*136*	*73*	*122*	*-16*	*33*	*4*	*0.55*	*10*		*6.8*		*7*
MODAN	*6.6004*	*45.2091*		*T*	*155*	*68*	*120*	*-18*	*34*	*12*	*0.53*	*24*		*12.3*		*7*
moiry (1)	*7.5769*	*46.1122*		*T*	*2*	*32*	*124*	*40*	*68*	*-34*	*0.45*	*28*		*10.3*		*7*
MONAL (1)	*6.9009*	*45.5687*		*T*	*48*	*85*	*165*	*2*	*75*	*-4*	*0.25*	*20*		*11.8*		*7*
MONAL (2)	*6.9009*	*45.5687*		*TT*	*119*	*36*	*118*	*-54*	*29*	*0*	*0.539*	*11*		*6.2*		*7*
monv2	*7.3415*	*46.005*		*SS*	*154*	*-13*	*16*	*-72*	*64*	*11*	*0.49*	*25*		*9.6*		*7*
nax	*7.4597*	*46.2412*		*T*	*138*	*-82*	*151*	*8*	*61*	*2*	*0.22*	*9*		*6.1*		*7*

Site	Long.	Lat.	Age	Tectonic regime	σ_1 trend	σ_1 plunge	σ_2 trend	σ_2 plunge	σ_3 trend	σ_3 plunge	R	N	F	α	RUP	REF
NEIGE(1)	*7.0328*	*45.4064*		*T*	*174*	*82*	*123*	*-5*	*34*	*6*	*0.13*	*39*		*12.7*		*7*
NEIGE(2)	*7.0328*	*45.4064*		*SS*	*105*	*-9*	*92*	*81*	*15*	*-2*	*0.3*	*14*		*14.4*		*7*
nikla	*7.7879*	*46.1638*		*SS*	*152*	*5*	*34*	*79*	*63*	*-10*	*0.49*	*22*		*12.5*		*7*
NIORD	*7.2035*	*45.9589*		*TP*	*81*	*-2*	*168*	*59*	*172*	*-31*	*0.57*	*16*		*9.2*		*7*
OREL(1)	*6.5565*	*45.2223*		*SS*	*102*	*78*	*136*	*-10*	*45*	*-6*	*0.15*	*12*		*8.8*		*7*
OREL(2)	*6.5565*	*45.2223*		*SS*	*165*	*9*	*93*	*-63*	*70*	*25*	*0.06*	*9*		*5.9*		*7*
OREL(3)	*6.5565*	*45.2223*		*T*	*105*	*5*	*115*	*-85*	*15*	*-1*	*0.47*	*12*		*18.9*		*7*
ORGIE	*6.65*	*45.2135*		*T*	*125*	*-72*	*100*	*17*	*12*	*-7*	*0.36*	*10*		*7.9*		*7*
OULX	*6.8577*	*45.0425*		*T*	*43*	*76*	*120*	*-3*	*29*	*-14*	*0.67*	*17*		*13.5*		*7*
PARTIE(1)	*6.6722*	*45.2584*		*T*	*108*	*36*	*120*	*-54*	*22*	*-6*	*0.46*	*19*		*8.9*		*7*
PEIPOU	*6.818*	*45.5253*		*TT*	*142*	*76*	*142*	*76*	*61*	*-2*	*0.25*	*22*		*13*		*7*
PLAN	*6.9258*	*45.6244*		*TP*	*104*	*-16*	*39*	*55*	*5*	*-30*	*0.603*	*14*		*9*		*7*
PUIT	*6.5093*	*45.4674*		*T*	*103*	*-68*	*97*	*22*	*8*	*-2*	*#*	*34*				*7*
randa2	*7.7615*	*46.0847*		*T*	*107*	*73*	*107*	*-17*	*17*	*0*	*0.13*	*27*		*7.5*		*7*
RIBON(1)	*6.9941*	*45.3104*		*T*	*22*	*-68*	*87*	*10*	*173*	*-20*	*0.13*	*21*		*7.2*		*7*
RIBON(3)	*6.9941*	*45.3104*		*SS*	*104*	*1*	*12*	*77*	*15*	*-13*	*0.16*	*20*		*7.2*		*7*
rotba	*7.8215*	*46.0656*		*TT*	*170*	*-46*	*138*	*39*	*62*	*-16*	*0.04*	*14*		*2.4*		*7*
SAPIN	*7.1486*	*46.1063*		*T*	*172*	*-73*	*151*	*16*	*63*	*-6*	*0.77*	*15*		*7.8*		*7*
SARRA	*6.6038*	*45.158*		*T*	*131*	*80*	*123*	*-9*	*33*	*1*	*0.26*	*28*		*21.6*		*7*
sarray	*7.2593*	*46.0606*		*TT*	*173*	*-51*	*148*	*37*	*67*	*-12*	*0.87*	*16*		*4.8*		*7*
schler	*7.2715*	*46.0697*		*TT*	*59*	*-65*	*137*	*5*	*45*	*24*	*0.16*	*8*		*3.8*		*7*
SEIGNE	*6.8091*	*45.7528*		*TT*	*128*	*-48*	*82*	*32*	*8*	*-24*	*0.779*	*17*		*7.1*		*7*
solay1	*7.5481*	*46.0653*		*SS*	*149*	*-22*	*15*	*-60*	*67*	*19*	*0.06*	*8*		*6.2*		*7*
solay2	*7.5385*	*46.0743*		*T*	*150*	*71*	*169*	*-18*	*77*	*-6*	*0.17*	*16*		*8.6*		*7*
stlu1	*7.5939*	*46.2312*		*T*	*178*	*67*	*151*	*-21*	*65*	*10*	*0.23*	*13*		*3.3*		*7*
stlu2	*7.6029*	*46.2182*		*TT*	*151*	*37*	*173*	*-51*	*69*	*-11*	*0.6*	*15*		*6.3*		*7*
TERMI	*6.8373*	*45.2859*		*T*	*120*	*-67*	*143*	*21*	*50*	*8*	*0.01*	*20*		*9.1*		*7*
TERMI2	*6.8407*	*45.3164*		*T*	*21*	*70*	*67*	*-14*	*154*	*14*	*0.02*	*24*		*4.8*		*7*
THUIL	*6.8991*	*45.7203*		*T*	*88*	*71*	*85*	*-19*	*175*	*-1*	*0.53*	*10*		*4*		*7*
thyon	*7.3709*	*46.1787*		*T*	*82*	*-70*	*142*	*10*	*49*	*17*	*0.29*	*14*		*6.3*		*7*
TIGNES1	*6.9199*	*45.5054*		*T*	*32*	*73*	*129*	*2*	*40*	*-17*	*0.127*	*17*		*5.1*		*7*

Site	Long.	Lat.	Age	Tectonic regime	σ_1 trend	σ_1 plunge	σ_2 trend	σ_2 plunge	σ_3 trend	σ_3 plunge	R	N	F	α	RUP	REF
TIGNES3	*6.9442*	*45.4977*		*T*	*65*	*75*	*100*	*-12*	*8*	*-8*	*0.812*	*11*		*4.3*		*7*
TOULJE	*7.1882*	*45.922*		*TT*	*120*	*-47*	*145*	*40*	*44*	*13*	*0.87*	*24*		*6.5*		*7*
trift	*7.4505*	*46.0245*		*T*	*123*	*81*	*108*	*-9*	*18*	*2*	*0.33*	*35*		*8.7*		*7*
turgl	*7.7096*	*46.1496*		*T*	*49*	*89*	*175*	*1*	*85*	*-1*	*0.83*	*15*		*10.4*		*7*
turtm	*7.6913*	*46.1714*		*T*	*22*	*57*	*147*	*21*	*67*	*-25*	*0.24*	*27*		*7.5*		*7*
VALDER2	*7.1119*	*45.546*		*T*	*92*	*-78*	*115*	*11*	*24*	*5*	*0.33*	*13*		*6.6*		*7*
VALDER4 (1)	*7.0259*	*45.6242*		*T*	*79*	*79*	*123*	*-8*	*32*	*-8*	*0.05*	*10*		*14.7*		*7*
VALDER4 (2)	*7.0259*	*45.6242*		*SS*	*67*	*-3*	*163*	*-63*	*155*	*26*	*0.65*	*12*		*2.9*		*7*
VALGR3	*7.0632*	*45.6206*		*T*	*48*	*-87*	*126*	*1*	*36*	*3*	*0.5*	*12*		*5.1*		*7*
VALMO	*6.4333*	*45.4306*		*TT*	*120*	*-51*	*94*	*36*	*14*	*-13*	*0.11*	*19*		*2.1*		*7*
VALP2 (1)	*7.4924*	*45.9007*		*T*	*161*	*57*	*132*	*-30*	*49*	*13*	*0.345*	*12*		*11.4*		*7*
VALP2 (2)	*7.4924*	*45.9007*		*TT*	*98*	*31*	*8*	*-59*	*10*	*-4*	*0.949*	*11*		*5.1*		*7*
VALP3	*7.4628*	*45.8881*		*T*	*16*	*-85*	*99*	*1*	*9*	*5*	*0.707*	*13*		*6.1*		*7*
VALP4 (1)	*7.437*	*45.8782*		*SS*	*94*	*4*	*114*	*-86*	*4*	*-1*	*0.256*	*14*		*6.8*		*7*
VALP4 (2)	*7.437*	*45.8782*		*T*	*179*	*-75*	*155*	*13*	*66*	*-6*	*0.07*	*17*		*8*		*7*
VALP5	*7.3534*	*45.8323*		*TT*	*121*	*-38*	*122*	*55*	*31*	*0*	*0.548*	*17*		*7*		*7*
VALSA1 (1)	*7.2008*	*45.5295*		*TT*	*88*	*45*	*139*	*-32*	*30*	*-27*	*0.13*	*11*		*3*		*7*
VALSA1 (2)	*7.2008*	*45.5295*		*TT*	*101*	*35*	*142*	*-47*	*27*	*-21*	*0.511*	*10*		*8.6*		*7*
VALSA2	*7.2115*	*45.5228*		*SS*	*91*	*36*	*147*	*-38*	*28*	*-32*	*0.48*	*11*		*4.1*		*7*
VALSA3	*7.2032*	*45.6525*		*T*	*28*	*79*	*139*	*4*	*49*	*-11*	*0.16*	*10*		*4.2*		*7*
VALSA4	*7.2051*	*45.6742*		*T*	*93*	*70*	*124*	*-17*	*31*	*-10*	*0.773*	*16*		*14.4*		*7*
VALTHO1	*6.5781*	*45.2825*		*T*	*53*	*-80*	*115*	*5*	*24*	*9*	*0.59*	*22*		*18.7*		*7*
VELAN	*7.2591*	*45.9267*		*SS*	*120*	*-1*	*21*	*-85*	*30*	*5*	*0.499*	*16*		*8*		*7*
VENS	*7.1241*	*46.0865*		*SS*	*98*	*-8*	*165*	*70*	*11*	*19*	*0.635*	*26*		*19.9*		*7*
verc1	*7.4558*	*46.2582*		*T*	*147*	*73*	*107*	*-13*	*20*	*11*	*0.01*	*19*		*11.4*		*7*
verc2	*7.5433*	*46.2479*		*T*	*122*	*73*	*145*	*-16*	*53*	*-6*	*0.3*	*18*		*10.6*		*7*
veyso	*7.3321*	*46.194*		*T*	*118*	*65*	*143*	*-23*	*49*	*-9*	*0.14*	*9*		*3.8*		*7*
vingt	*7.3956*	*46.0752*		*T*	*91*	*-81*	*173*	*1*	*83*	*9*	*0.57*	*16*		*3.8*		*7*
zeneg	*7.871*	*46.2795*		*SS*	*120*	*-19*	*82*	*67*	*26*	*-13*	*0.59*	*20*		*6.2*		*7*
P33	*6.1617*	*44.1528*	*Mio-Pliocene*	*SS*	*62*	*13*					*0.03*					*8*
P34	*6.1508*	*44.1608*	*Mio-Pliocene*	*P*	*56*	*-9*	*147*	*-2*			*0.12*					*8*

Site	Long.	Lat.	Age	Tectonic regime	σ_1 trend	σ_1 plunge	σ_2 trend	σ_2 plunge	σ_3 trend	σ_3 plunge	R	N	F	α	RUP	REF
P35	*6.2167*	*44.0911*	*Mio-Pliocene*	*P*	*79*	*3*	*169*	*1*			*0.11*					*8*
P36	*6.2339*	*44.0392*	*Mio-Pliocene*	*P*	*76*	*3*	*166*	*-3*			*0.27*					*8*
P38	*6.2722*	*44.0222*	*Mio-Pliocene*	*P*	*73*	*9*	*166*	*19*	*138*	*-69*	*0.58*					*8*
P3b	*5.2181*	*43.6833*	*L. Oligocene*	*P*	*20*	*8*	*110*	*2*			*0.56*					*8*
P41	*6.2217*	*43.9464*	*Mio-Pliocene*	*P*	*64*	*-9*	*155*	*-7*	*101*	*78*	*0.57*					*8*
P42	*6.2042*	*43.9083*	*Mio-Pliocene*	*P*	*61*	*-14*	*155*	*-15*	*109*	*69*	*0.16*					*8*
P46	*6.2444*	*43.8808*	*Pliocene*	*P*	*58*	*-5*					*0.01*					*8*
P47	*6.2417*	*43.845*	*Mio-Pliocene*	*P*	*49*	*-3*	*139*	*0*			*0.51*					*8*
P48	*6.2203*	*43.85*	*Mio-Pliocene*	*P*	*78*	*-34*	*151*	*24*	*33*	*46*	*0.33*					*8*
P49	*6.2353*	*43.8214*	*Mio-Pliocene*	*P*	*64*	*-19*					*0*					*8*
P50	*6.2439*	*43.805*	*U. Miocene*	*P*	*66*	*-9*					*0.09*					*8*
P51	*6.2456*	*43.8164*		*P*					*9*	*-74*	*0.99*					*8*
P52	*6.2558*	*43.8114*		*P*	*83*	*-1*	*175*	*0*			*0.36*					*8*
P53	*6.2511*	*43.8025*		*P*	*67*	*-18*					*0.01*					*8*
P8a	*5.4167*	*44.1667*	*L. Miocene*	*P*	*42*	*0*	*132*	*0*			*0.85*					*8*
K13	*6.285*	*44.2183*	*Berriasien*	*P*	*163*	*-6*	*74*	*1*	*177*	*84*	*0.56*	*19*				*9*
K1B	*6.2763*	*44.2168*	*Berriasien*	*SS*	*33*	*-5*	*167*	*-83*	*122*	*5*	*0.86*	*9*				*9*
K6	*6.2867*	*44.2267*	*Valanginian*	*SS*	*32*	*0*	*120*	*-86*	*122*	*4*	*0.06*	*11*				*9*
K8	*6.2317*	*44.235*	*Berriasien*	*TP*	*20*	*-16*	*101*	*29*	*136*	*-56*	*0.16*	*9*				*9*
L1A	*6.266*	*44.2617*	*Hettangien*	*P*	*34*	*2*	*125*	*6*	*108*	*-83*	*0.5*	*10*				*9*
L2B	*6.285*	*44.2517*	*Hettangien*	*SS*	*2*	*-21*	*32*	*66*	*96*	*-11*	*0.45*	*9*				*9*
L3	*6.2422*	*44.2618*	*Carixian-Domerian*	*SS*	*48*	*-10*	*167*	*-70*	*135*	*17*	*0.24*	*13*				*9*
L4	*6.2433*	*44.2633*	*Carixian-Domerian*	*SS*	*32*	*19*	*11*	*-70*	*120*	*-7*	*0.4*	*12*				*9*
M1B	*6.2572*	*44.235*	*Tithonian*	*SS*	*58*	*24*	*76*	*-65*	*151*	*7*	*0.78*	*11*				*9*
T1	*6.2633*	*44.205*	*Late Miocene – Pliocene*	*P*	*8*	*4*	*97*	*-15*	*112*	*74*	*0.11*	*4*				*9*
T14	*6.2763*	*44.2168*	*Late Eocene-Early Oligocene*	*P*	*32*	*-11*	*123*	*-6*	*60*	*77*	*0.39*	*7*				*9*
T18	*6.26*	*44.21*	*Late Miocene – Pliocene*	*SS*	*38*	*7*	*147*	*69*	*126*	*-20*	*0.19*	*6*				*9*
T19	*6.2542*	*44.2083*	*Late Miocene – Pliocene*	*SS*	*40*	*-9*	*165*	*-74*	*128*	*13*	*0.34*	*6*				*9*
T21	*6.27*	*44.2183*	*Late Eocene-Early Oligocene*	*P*	*60*	*-8*	*147*	*18*	*173*	*-70*	*0.57*	*4*				*9*
T22	*6.255*	*44.205*	*Late Miocene – Pliocene*	*SS*	*34*	*2*	*104*	*-83*	*125*	*6*	*0.18*	*15*				*9*
T23	*6.2542*	*44.2067*	*Late Miocene – Pliocene*	*SS*	*10*	*-14*	*59*	*69*	*104*	*-15*	*0.68*	*7*				*9*

Site	Long.	Lat.	Age	Tectonic regime	σ_1 trend	σ_1 plunge	σ_2 trend	σ_2 plunge	σ_3 trend	σ_3 plunge	R	N	F	α	RUP	REF
T24A	*6.2687*	*44.2022*	*Burdigalian*	*P*	*26*	*1*	*116*	*25*	*115*	*-65*	*0.32*	*14*				*9*
T24B	*6.2687*	*44.2022*	*Burdigalian*	*SS*	*52*	*9*	*86*	*-79*	*143*	*6*	*0.21*	*14*				*9*
T25	*6.275*	*44.2258*	*Late Eocene-Early Oligocene*	*P*	*177*	*-3*	*88*	*13*	*76*	*-77*	*0.71*	*7*				*9*
T26	*6.2773*	*44.2148*	*Stampian*	*P*	*41*	*-5*	*130*	*12*	*154*	*-77*	*0.41*	*13*				*9*
T27	*6.2872*	*44.2117*	*Late Eocene-Early Oligocene*	*P*	*48*	*-6*	*138*	*12*	*151*	*-78*	*0.54*	*14*				*9*
T28	*6.2745*	*44.2117*	*Stampian*	*SS*	*163*	*6*	*177*	*-84*	*73*	*-1*	*0.51*	*12*				*9*
T29	*6.2745*	*44.2117*	*Stampian*	*SS*	*45*	*45*	*33*	*-45*	*129*	*-6*	*0.71*	*7*				*9*
T2A	*6.2637*	*44.2028*	*Langhian-Tortonian*	*P*	*28*	*-4*	*115*	*15*	*132*	*-75*	*0.35*	*7*				*9*
T2B	*6.2637*	*44.2028*	*Langhian-Tortonian*	*SS*	*33*	*14*	*157*	*66*	*118*	*-19*	*0.44*	*14*				*9*
*T31***	*6.279*	*44.2075*	*Aquitanian-Burdigalian*	*P*	*29*	*-5*	*119*	*2*	*13*	*84*	*0.39*	*12*				*9*
T32	*6.2718*	*44.208*	*Aquitanian-Burdigalian*	*P*	*17*	*3*	*107*	*9*	*91*	*-81*	*0.42*	*10*				*9*
T33A	*6.2615*	*44.2092*	*Langhian-Tortonian*	*P*	*21*	*8*	*109*	*-13*	*143*	*75*	*0.42*	*12*				*9*
T33B	*6.2615*	*44.2092*	*Langhian-Tortonian*	*SS*	*6*	*10*	*7*	*-80*	*96*	*0*	*0.42*	*10*				*9*
T36	*6.2277*	*44.2295*	*Stampian*	*SS*	*26*	*-21*	*66*	*63*	*122*	*-16*	*0.49*	*14*				*9*
T4A	*6.273*	*44.2087*	*Langhian-Tortonian*	*P*	*2*	*2*	*91*	*-1*	*148*	*88*	*0.09*	*19*				*9*
T4B	*6.273*	*44.2087*	*Aquitanian-Burdigalian*	*SS*	*51*	*2*	*157*	*82*	*140*	*-8*	*0.43*	*26*				*9*
TR1	*6.3138*	*44.2713*	*Buntsandstein*	*SS*	*15*	*-9*	*150*	*-77*	*103*	*9*	*0.51*	*8*				*9*
4	*5.3525*	*44.741*	*Berriasien*		*120*											*10*
5	*5.2879*	*44.7634*	*Kimméridgien*		*105*											*10*
6	*5.2058*	*44.802*	*Barrémien*		*100*											*10*
8	*5.0647*	*44.705*	*Barrémien*		*85*											*10*
10	*4.987*	*44.6766*	*Stampien sup.*		*120*											*10*
12	*5.1888*	*44.675*	*Tithonique*		*80*											*10*
14	*5.2676*	*44.673*	*Berriasien*		*90*											*10*
15	*5.2837*	*44.6537*	*Tithonique*		*85*											*10*
16	*5.2942*	*44.6372*	*Tithonique*		*70*											*10*
17	*5.324*	*44.64*	*Berriasien*		*50*											*10*
19	*5.3171*	*44.6663*	*Kimméridgien*		*80*											*10*
20	*5.3449*	*44.6908*	*Berriasien*		*95*											*10*
21	*5.4728*	*44.6046*	*Tithonique*		*80*											*10*
23	*5.4488*	*44.5088*	*Berriasien*		*65*											*10*

Site	Long.	Lat.	Age	Tectonic regime	σ_1 trend	σ_1 plunge	σ_2 trend	σ_2 plunge	σ_3 trend	σ_3 plunge	R	N	F	α	RUP	REF
24	*5.4322*	*44.5282*	*Hautériven*		*70*											*10*
26	*5.4229*	*44.5181*	*Berriasien*		*100*											*10*
27	*5.4079*	*44.5685*	*Tithonique*		*75*											*10*
28	*5.366*	*44.5489*	*Berriasien*		*60*											*10*
29	*5.3422*	*44.5153*	*Berriasien*		*70*											*10*
30	*5.2861*	*44.6018*	*Berriasien*		*70*											*10*
32	*5.28*	*44.5304*	*Hautériven*		*70*											*10*
35	*5.1772*	*44.5514*	*Barrémien*		*90*											*10*
36	*5.1767*	*44.5672*	*Bédoulien*		*60*											*10*
37	*5.1829*	*44.5792*	*Barrémien*		*80*											*10*
39	*5.2984*	*44.6078*	*Hautériven*		*65*											*10*
43	*5.0898*	*44.4338*	*Barrémien*		*60*											*10*
46	*5.17*	*44.3886*	*Hautériven-Berriasien*		*50*											*10*
49	*5.2017*	*44.4468*	*Turonien*		*120*											*10*
50	*5.2197*	*44.4293*	*Barrémien*		*85*											*10*
53	*5.3431*	*44.4828*	*Hautériven*		*60*											*10*
61	*5.371*	*44.3893*	*Kimméridgien*		*90*											*10*
67	*5.2677*	*44.3587*	*Hautériven*		*50*											*10*
68	*5.1771*	*44.3403*	*Barrémien*		*60*											*10*
69	*5.2035*	*44.2248*	*Bédoulien-Burdigalien*		*50*											*10*
76	*5.431*	*44.276*	*Berriasien*		*50*											*10*
77	*5.4408*	*44.2488*	*Hautériven*		*60*											*10*
78	*5.4314*	*44.2238*	*Berriasien*		*50*											*10*
80	*5.4262*	*44.2086*	*Kimméridgien*		*80*											*10*
11b	*5.0149*	*44.6791*	*Barrémien*		*80*											*10*
13b	*5.2155*	*44.6919*	*Kimméridgien*		*90*											*10*
18b	*5.2946*	*44.6457*	*Oxfordien sup.*		*70*											*10*
1b	*5.3892*	*44.8265*	*Hautériven*		*100*											*10*
22b	*5.4592*	*44.5977*	*Berriasien*		*80*											*10*
25b	*5.423*	*44.5438*	*Tithonique-Hauterivien*		*90*											*10*
2b	*5.4068*	*44.7896*	*Tithonique-Berriasien*		*90*											*10*

Site	Long.	Lat.	Age	Tectonic regime	σ_1 trend	σ_1 plunge	σ_2 trend	σ_2 plunge	σ_3 trend	σ_3 plunge	R	N	F	α	RUP	REF
31b	*5.2788*	*44.5935*	*Berriasien*		*70*											*10*
33b	*5.2444*	*44.5484*	*Hautériven*		*60*											*10*
34c	*5.1803*	*44.5509*	*Barrémien*		*90*											*10*
38b	*5.1714*	*44.6007*	*Barrémien*		*55*											*10*
3b	*5.3524*	*44.7888*	*Kimméridgien*		*120*											*10*
40b	*5.1022*	*44.6172*	*Barrémien*		*55*											*10*
41b	*5.0495*	*44.5815*	*Barrémien*		*65*											*10*
42b	*5.0315*	*44.477*	*Barrémien*		*90*											*10*
44b	*5.121*	*44.4285*	*Berriasien*		*55*											*10*
45c	*5.1158*	*44.4116*	*Hautériven-Berriasien*		*90*											*10*
47b	*5.1604*	*44.3731*	*Turonien*		*90*											*10*
48b	*5.2164*	*44.491*	*Bédoulien*		*70*											*10*
51b	*5.2801*	*44.4322*	*Tithonique*		*60*											*10*
52b	*5.2929*	*44.4355*	*Tithonique*		*45*											*10*
54b	*5.3545*	*44.4726*	*Berriasien*		*85*											*10*
55b	*5.4492*	*44.4674*	*Barrémien*		*60*											*10*
56b	*5.5074*	*44.4739*	*Barrémien*		*60*											*10*
57b	*5.5023*	*44.3326*	*Hautériven*		*50*											*10*
58b	*5.4677*	*44.3543*	*Bédoulien*		*50*											*10*
59b	*5.4245*	*44.3807*	*Bédoulien*		*50*											*10*
60b	*5.3848*	*44.3899*	*Berriasien*		*45*											*10*
62b	*5.3495*	*44.3998*	*Oxfordien*		*65*											*10*
63a	*5.3805*	*44.3319*	*Barrémien*		*70*											*10*
64b	*5.3519*	*44.3601*	*Barrémien*		*60*											*10*
66a	*5.2874*	*44.3005*	*Hautériven*		*60*											*10*
70b	*5.272*	*44.2685*	*Berriasien*		*55*											*10*
71a	*5.2821*	*44.2948*	*Tithonique-Berriasien*		*45*											*10*
75a	*5.4207*	*44.2835*	*Hautériven*		*55*											*10*
79a	*5.43*	*44.222*	*Berriasien*		*50*											*10*
7b	*5.1385*	*44.7707*	*Barrémien*		*90*											*10*
81a	*5.4169*	*44.1994*	*Hautériven*		*60*											*10*

Site	Long.	Lat.	Age	Tectonic regime	σ_1 trend	σ_1 plunge	σ_2 trend	σ_2 plunge	σ_3 trend	σ_3 plunge	R	N	F	α	RUP	REF
82a	*5.4271*	*44.1906*	*Hautériven-Barrémien*		*55*											*10*
S1	*8.107*	*46.2143*		*T*	*132*	*-69*	*125*	*21*	*36*	*-2*	*0.273*	*13*		*5.8*		*11*
S10	*8.0206*	*46.253*		*T*	*39*	*87*	*138*	*1*	*48*	*-3*	*0.767*	*15*		*7.2*		*11*
S11	*8.0203*	*46.2256*		*T*	*90*	*80*	*149*	*-5*	*58*	*-9*	*0.508*	*46*		*11.53*		*11*
S12	*8.0249*	*46.1956*		*T*	*10*	*80*	*134*	*6*	*44*	*-8*	*0.439*	*21*		*11.76*		*11*
S13	*8.0112*	*46.1919*		*T*	*60*	*-85*	*133*	*1*	*43*	*4*	*0.29*	*18*		*18.22*		*11*
S15	*8.0714*	*46.212*		*T*	*174*	*75*	*145*	*-13*	*56*	*7*	*0.625*	*21*		*8.476*		*11*
S16	*8.052*	*46.1923*		*T*	*39*	*-83*	*129*	*0*	*39*	*7*	*0.346*	*16*		*6*		*11*
S17	*8.0584*	*46.213*		*T*	*134*	*82*	*157*	*-7*	*66*	*-3*	*0.52*	*17*		*8.353*		*11*
S18	*8.0526*	*46.2171*		*T*	*128*	*67*	*172*	*-17*	*77*	*-15*	*0.192*	*13*		*5.692*		*11*
S19	*8.0374*	*46.2437*		*T*	*101*	*74*	*145*	*-12*	*52*	*-11*	*0.686*	*17*		*9.7*		*11*
S2	*8.1074*	*46.2174*		*T*	*124*	*72*	*171*	*-12*	*78*	*-13*	*0.296*	*13*		*10.25*		*11*
S20	*8.0703*	*46.1724*		*T*	*0*	*69*	*117*	*10*	*31*	*-18*	*0.16*	*42*		*10.79*		*11*
S21	*8.0904*	*46.1766*		*T*	*161*	*75*	*144*	*-15*	*56*	*4*	*0.655*	*9*		*13.56*		*11*
S23	*8.0413*	*46.1908*		*T*	*70*	*72*	*122*	*-12*	*29*	*-14*	*0.323*	*17*		*6.9*		*11*
S25	*8.0485*	*46.1951*		*T*	*54*	*73*	*6*	*-12*	*99*	*-14*	*0.113*	*43*		*10.28*		*11*
S26	*8.0397*	*46.1881*		*T*	*103*	*73*	*149*	*-12*	*57*	*-14*	*0.218*	*31*		*8.968*		*11*
S27	*8.0312*	*46.1839*		*T*	*85*	*75*	*140*	*-9*	*48*	*-14*	*0.283*	*27*		*9.37*		*11*
S28	*8.0445*	*46.1847*		*T*	*16*	*81*	*171*	*8*	*82*	*-4*	*0.187*	*12*		*14.5*		*11*
S29	*8.0902*	*46.1872*		*T*	*151*	*83*	*135*	*-7*	*45*	*2*	*0.513*	*26*		*9.76*		*11*
S3	*8.1041*	*46.2105*		*T*	*120*	*-80*	*129*	*10*	*38*	*2*	*0.591*	*10*		*6.9*		*11*
S30	*8.0559*	*46.249*		*T*	*81*	*76*	*153*	*-5*	*62*	*-14*	*0.343*	*47*		*9.447*		*11*
S31	*8.0345*	*46.252*		*T*	*106*	*77*	*145*	*-10*	*54*	*-8*	*0.519*	*12*		*6.167*		*11*
S33	*8.062*	*46.1824*		*T*	*93*	*77*	*168*	*-4*	*77*	*-12*	*0.337*	*30*		*13.97*		*11*
S34	*8.0515*	*46.1721*		*T*	*128*	*-79*	*125*	*11*	*35*	*-1*	*0.437*	*27*		*7.926*		*11*
S36	*8.0547*	*46.2256*		*T*	*67*	*73*	*152*	*-2*	*62*	*-17*	*0.192*	*34*		*8.559*		*11*
S37	*8.0781*	*46.2345*		*T*	*83*	*73*	*155*	*-5*	*63*	*-16*	*0.325*	*27*		*5.667*		*11*
S38	*8.0818*	*46.221*		*T*	*150*	*64*	*6*	*21*	*90*	*-14*	*0.388*	*15*		*8.9*		*11*
S39	*8.1149*	*46.1962*		*T*	*12*	*87*	*137*	*2*	*47*	*-3*	*0.482*	*17*		*7.2*		*11*
S41	*7.8937*	*46.2785*		*T*	*56*	*76*	*145*	*-1*	*55*	*-14*	*0.24*	*15*		*12.73*		*11*
S42	*8.0214*	*46.2055*		*T*	*166*	*76*	*136*	*-12*	*47*	*7*	*0.501*	*24*		*9.9*		*11*

Site	Long.	Lat.	Age	Tectonic regime	σ_1 trend	σ_1 plunge	σ_2 trend	σ_2 plunge	σ_3 trend	σ_3 plunge	R	N	F	α	RUP	REF
S43	*8.0127*	*46.2105*		*T*	*62*	*-73*	*154*	*-1*	*65*	*17*	*0.138*	*15*		*6.8*		*11*
S45	*8.0181*	*46.2022*		*T*	*58*	*-85*	*161*	*-1*	*71*	*5*	*0.28*	*9*		*9.556*		*11*
S46	*8.0535*	*46.2067*		*T*	*174*	*85*	*142*	*-5*	*52*	*3*	*0.396*	*26*		*8.3*		*11*
S47	*8.046*	*46.1487*		*T*	*148*	*76*	*152*	*-14*	*62*	*-1*	*0.311*	*27*		*11.2*		*11*
S48	*8.0408*	*46.1416*		*T*	*180*	*80*	*164*	*-9*	*74*	*2*	*0.253*	*19*		*7.6*		*11*
S49	*8.1245*	*46.1629*		*T*	*157*	*-74*	*147*	*15*	*57*	*-3*	*0.241*	*21*		*9.1*		*11*
S5	*7.9689*	*46.2085*		*T*	*177*	*-63*	*159*	*26*	*73*	*-7*	*0.589*	*10*		*7.9*		*11*
S51	*8.1219*	*46.171*		*T*	*5*	*80*	*160*	*10*	*70*	*-4*	*0.529*	*9*		*8*		*11*
S52	*8.1292*	*46.2007*		*T*	*30*	*76*	*134*	*4*	*44*	*-14*	*0.423*	*19*		*7.47*		*11*
S53	*8.0162*	*46.2337*		*T*	*121*	*73*	*142*	*-16*	*50*	*-6*	*0.166*	*27*		*9.963*		*11*
S54	*7.9548*	*46.2578*		*T*	*130*	*75*	*145*	*-15*	*55*	*-4*	*0.785*	*21*		*7.9*		*11*
S55	*8.0055*	*46.2333*		*T*	*9*	*75*	*140*	*0*	*52*	*-11*	*0.162*	*11*		*6.6*		*11*
S56	*8.0544*	*46.1174*		*TP*	*165*	*56*	*160*	*-34*	*71*	*3*	*0.227*	*10*		*12.2*		*11*
S6	*8.0967*	*46.1894*		*T*	*149*	*82*	*146*	*-8*	*56*	*1*	*0.401*	*17*		*5.8*		*11*
S7	*8.0242*	*46.2543*		*T*	*110*	*81*	*142*	*-7*	*52*	*-5*	*0.629*	*10*		*6.4*		*11*
S8	*8.0222*	*46.2546*		*T*	*128*	*70*	*156*	*-17*	*63*	*-9*	*0.9*	*13*		*6.154*		*11*
S9	*8.0213*	*46.2582*		*T*	*135*	*63*	*154*	*-26*	*60*	*-8*	*0.459*	*11*		*12*		*11*
SD	*8.0227*	*46.2645*		*SS*	*145*	*4*	*177*	*-85*	*55*	*-2*	*0.737*	*11*		*9.7*		*11*
GD MOULINS	*6.221*	*45.418*		*SS*	*104*	*4*	*29*	*-74*	*12*	*15*	*0.3*			*10*	*25*	*12*
Ambléon	*5.595*	*45.745*	*Portlandian*	*P*	*93*	*14*	*180*	*-12*	*49*	*-71*	*0.12*	*13*		*15*	*33*	*14*
Ambléon	*5.595*	*45.745*	*Portlandian*	*P*	*43*	*11*	*134*	*6*	*72*	*-78*	*0.55*	*17*		*9*	*31*	*14*
Arc.s Cion	*6.3533*	*47.05*	*Argov. to Raurac.*	*SS*	*172*	*23*	*161*	*-66*	*80*	*4*	*0.54*	*12*		*9*	*32*	*14*
Arcine	*5.895*	*46.105*	*Rauracian*	*SS*	*112*	*-5*	*76*	*84*	*22*	*-4*	*0.35*	*30*		*13*	*33*	*14*
Artemare	*5.6883*	*45.8683*	*Valangin. Berrias.*	*SS*	*74*	*-3*	*175*	*-74*	*164*	*13*	*0.43*	*28*		*5*	*15*	*14*
Belleydoux	*5.7917*	*46.2483*	*Valanginian*	*P*	*65*	*-9*	*158*	*-17*	*129*	*71*	*0.41*	*4*		*4*	*22*	*14*
Blanaz	*5.4517*	*45.9183*	*Up. Bathonian*	*SS*	*68*	*3*	*145*	*-78*	*159*	*12*	*0.39*	*31*		*9*	*25*	*14*
Bouis	*5.4233*	*45.8767*	*Bathonian*	*SS*	*43*	*-4*	*20*	*86*	*133*	*2*	*0.38*	*20*		*6*	*20*	*14*
Brenaz	*5.7117*	*45.935*	*Aptian Barremian*	*SS*	*84*	*-11*	*80*	*79*	*174*	*1*	*0.53*	*26*		*10*	*29*	*14*
Brenod	*5.5783*	*46.05*	*Mid.-Up. Oxfordian*	*SS*	*158*	*-15*	*148*	*75*	*67*	*-3*	*0.63*	*10*		*10*	*25*	*14*
Brenod	*5.5783*	*46.05*	*Mid.-Up. Oxfordian*	*SS*	*91*	*-5*	*166*	*71*	*33*	*19*	*0.48*	*38*		*13*	*28*	*14*
Cerdon	*5.4767*	*46.0817*	*Up. Oxfordian*	*SS*	*105*	*1*	*30*	*-85*	*15*	*5*	*0.44*	*56*		*15*	*35*	*14*

Site	Long.	Lat.	Age	Tectonic regime	σ_1 trend	σ_1 plunge	σ_2 trend	σ_2 plunge	σ_3 trend	σ_3 plunge	R	N	F	α	RUP	REF
Cerdon	*5.4767*	*46.0817*	*Up. Oxfordian*	*SS*	*28*	*7*	*77*	*-79*	*119*	*8*	*0.07*	*8*		*12*	*33*	*14*
Chaffois	*6.28*	*46.92*	*Port. -Up. Kimme.*	*SS*	*122*	*-20*	*127*	*70*	*33*	*1*	*0.79*	*13*		*10*	*28*	*14*
Chavoley	*5.71*	*45.8267*	*Portlandian*	*SS*	*75*	*12*	*41*	*-75*	*164*	*-8*	*0.49*	*40*		*13*	*33*	*14*
Chavoley	*5.71*	*45.8267*	*Portlandian*	*P*	*50*	*6*	*140*	*1*	*62*	*-84*	*0.36*	*13*		*24*	*45*	*14*
Cherezy	*5.8267*	*46.1817*	*Aptian Barremian*	*SS*	*103*	*8*	*66*	*-80*	*12*	*6*	*0.37*	*29*		*11*	*25*	*14*
Chosas	*5.52*	*45.7917*	*Bajocian*	*SS*	*61*	*2*	*178*	*85*	*151*	*-4*	*0.04*	*13*		*10*	*39*	*14*
Cht Près	*5.9017*	*46.515*	*Portland. Kimmeridg.*	*TP*	*113*	*-5*	*31*	*60*	*21*	*-30*	*0.19*	*14*		*21*	*43*	*14*
Colomieu	*5.6367*	*45.7317*	*Valangin. Portland.*	*P*	*82*	*9*	*173*	*6*	*116*	*-79*	*0.69*	*31*		*11*	*25*	*14*
Colomieu	*5.6367*	*45.7317*	*Valangin. Portland.*	*SS*	*94*	*23*	*75*	*-65*	*1*	*7*	*0.02*	*10*		*13*	*30*	*14*
Colomieu	*5.6367*	*45.7317*	*Valangin. Portland.*	*SS*	*48*	*-5*	*38*	*85*	*138*	*1*	*0.33*	*12*		*9*	*31*	*14*
Contrevoz	*5.61*	*45.835*	*Valanginian*	*SS*	*91*	*0*	*1*	*79*	*1*	*-11*	*0.25*	*8*		*13*	*27*	*14*
Contrevoz	*5.61*	*45.835*	*Valanginian*	*SS*	*58*	*0*	*147*	*-85*	*148*	*5*	*0.72*	*6*		*13*	*23*	*14*
Coramaranch.	*5.61*	*45.9467*	*Purbeckian*	*SS*	*47*	*-11*	*156*	*-59*	*131*	*29*	*0.03*	*10*		*13*	*42*	*14*
Corlier	*5.4817*	*46.0383*	*Rauracian*	*SS*	*133*	*-7*	*61*	*70*	*41*	*-19*	*0.28*	*23*		*10*	*25*	*14*
Corlier	*5.4817*	*46.0383*	*Rauracian*	*SS*	*87*	*-11*	*114*	*78*	*178*	*-5*	*0.43*	*34*		*6*	*17*	*14*
Corlier	*5.4817*	*46.0383*	*Rauracian*	*SS*	*33*	*-5*	*54*	*85*	*124*	*-2*	*0.55*	*44*		*11*	*30*	*14*
Coux	*5.4933*	*45.8483*	*Bathonian*	*SS*	*21*	*-29*	*1*	*60*	*106*	*8*	*0.54*	*4*		*3*	*26*	*14*
Coux	*5.4933*	*45.8483*	*Bathonian*	*SS*	*78*	*2*	*18*	*-85*	*168*	*-4*	*0.61*	*17*		*9*	*21*	*14*
Cuisia	*5.4117*	*46.535*	*Bathonian*	*P*	*64*	*14*	*159*	*21*	*123*	*-64*	*0.29*	*4*		*7*	*36*	*14*
Culoz	*5.7883*	*45.8617*	*Kimmeridgian*	*TP*	*63*	*6*	*158*	*39*	*146*	*-50*	*0.08*	*19*		*18*	*41*	*14*
Fay	*5.6617*	*45.6183*	*Portlandian*	*P*	*67*	*-3*	*156*	*6*	*165*	*-74*	*0.54*	*12*		*14*	*44*	*14*
Fay	*5.6617*	*45.6183*	*Portlandian*	*SS*	*78*	*3*	*146*	*-82*	*169*	*7*	*0.50*	*49*		*8*	*22*	*14*
Galaz	*6.4017*	*46.6933*	*Port. -Up. Kimme.*	*SS*	*170*	*-4*	*136*	*85*	*79*	*-3*	*0.44*	*14*		*7*	*27*	*14*
Galaz	*6.4017*	*46.6933*	*Port. -Up. Kimme.*	*SS*	*111*	*-1*	*7*	*-86*	*21*	*4*	*0.44*	*18*		*6*	*16*	*14*
Glandieu	*5.6183*	*45.6683*	*Kimmeridgian*	*P*	*73*	*0*	*163*	*-2*	*172*	*88*	*0.45*	*23*		*9*	*39*	*14*
Glandieu	*5.6183*	*45.6683*	*Kimmeridgian*	*SS*	*79*	*-1*	*165*	*73*	*169*	*-17*	*0.29*	*20*		*11*	*23*	*14*
Glandieu	*5.6183*	*45.6683*	*Kimmeridgian*	*SS*	*37*	*-2*	*122*	*66*	*128*	*-24*	*0.20*	*23*		*10*	*33*	*14*
Goux	*6.29*	*46.9733*	*Port. -Up. Kimme.*	*SS*	*140*	*12*	*72*	*-61*	*44*	*26*	*0.03*	*5*		*5*	*20*	*14*
Hauteville	*5.5783*	*45.98*	*Valangin. Berrias.*	*P*	*78*	*-9*	*167*	*7*	*41*	*79*	*0.38*	*6*		*11*	*31*	*14*
Hauteville	*5.5783*	*45.98*	*Valangin. Berrias.*	*SS*	*74*	*6*	*95*	*-84*	*165*	*2*	*0.47*	*42*		*10*	*37*	*14*
Hostias	*5.5383*	*45.8933*	*Oxfordian*	*SS*	*81*	*-13*	*67*	*76*	*170*	*3*	*0.40*	*10*		*11*	*25*	*14*

Site	Long.	Lat.	Age	Tectonic regime	σ_1 trend	σ_1 plunge	σ_2 trend	σ_2 plunge	σ_3 trend	σ_3 plunge	R	N	F	α	RUP	REF
Hostias	*5.5383*	*45.8933*	*Oxfordian*	*SS*	*36*	*-18*	*32*	*72*	*126*	*1*	*0.43*	*8*		*7*	*31*	*14*
Hotonne	*5.7283*	*45.9883*	*Portlandian*	*TP*	*70*	*-6*	*165*	*-41*	*152*	*49*	*0.22*	*4*		*8*	*34*	*14*
Ilay	*5.885*	*46.6167*	*Purbeck. Portland.*	*P*	*127*	*-3*	*37*	*-5*	*70*	*84*	*0.46*	*59*		*12*	*27*	*14*
Innimond	*5.56*	*45.765*	*Kimmeridg. Oxford.*	*P*	*52*	*-5*	*142*	*7*	*176*	*-82*	*0.53*	*13*		*13*	*34*	*14*
Innimond	*5.56*	*45.765*	*Kimmeridg. Oxford.*	*SS*	*57*	*-1*	*140*	*79*	*148*	*-11*	*0.14*	*24*		*10*	*35*	*14*
Jalinard	*5.6717*	*46.0517*	*Portlandian*	*P*	*67*	*-2*	*157*	*-5*	*132*	*85*	*0.48*	*12*		*10*	*23*	*14*
Jalinard	*5.6717*	*46.0517*	*Portlandian*	*SS*	*62*	*-2*	*137*	*82*	*152*	*-8*	*0.25*	*29*		*13*	*35*	*14*
Jougne E1	*6.385*	*46.7567*	*Port. -Up. Kimme.*	*SS*	*163*	*14*	*4*	*75*	*74*	*-5*	*0.34*	*8*		*9*	*27*	*14*
Lagnieu	*5.385*	*45.88*	*Up. Bajocian*	*SS*	*29*	*-6*	*3*	*83*	*118*	*3*	*0.46*	*35*		*12*	*29*	*14*
Lelex	*5.9117*	*46.2683*	*Barremian*	*P*	*118*	*9*	*26*	*11*	*67*	*-76*	*0.56*	*10*		*6*	*15*	*14*
Lompnas	*5.5267*	*45.8067*	*Up. Oxfordian*	*P*	*54*	*10*	*143*	*-6*	*23*	*-78*	*0.69*	*22*		*12*	*34*	*14*
Lompnas	*5.5267*	*45.8067*	*Up. Oxfordian*	*SS*	*66*	*17*	*92*	*-71*	*159*	*8*	*0.94*	*25*		*14*	*39*	*14*
Lompnas	*5.5267*	*45.8067*	*Up. Oxfordian*	*SS*	*57*	*-3*	*1*	*85*	*147*	*4*	*0.63*	*25*		*8*	*21*	*14*
Main	*6.3283*	*47.01*	*Sequanian*	*SS*	*112*	*5*	*84*	*-84*	*22*	*3*	*0.34*	*14*		*10*	*30*	*14*
Mandallaz	*6.0583*	*45.9483*	*Purbeckian*	*SS*	*142*	*1*	*61*	*-85*	*52*	*5*	*0.37*	*13*		*17*	*45*	*14*
Moirans	*5.7267*	*46.4133*	*Sequan. Raurac.*	*SS*	*74*	*-19*	*74*	*71*	*164*	*0*	*0.55*	*31*		*16*	*32*	*14*
Mollens	*6.3317*	*46.58*	*Portland. Kimmeridg.*	*SS*	*152*	*14*	*112*	*-71*	*59*	*11*	*0.85*	*11*		*12*	*26*	*14*
Monniot	*6.4017*	*47.0383*	*Rauracian*	*SS*	*111*	*3*	*3*	*82*	*21*	*-8*	*0.44*	*8*		*4*	*14*	*14*
Montarmeux	*6.445*	*47.1082*	*Sequanian*	*SS*	*145*	*10*	*87*	*-73*	*52*	*14*	*0.27*	*21*		*9*	*21*	*14*
Montréal	*5.565*	*46.1817*	*Low. Bajocian*	*SS*	*47*	*5*	*11*	*-84*	*137*	*-4*	*0.60*	*16*		*10*	*31*	*14*
Mt Noir	*6.0233*	*46.605*	*Sequanian*	*SS*	*108*	*14*	*148*	*-74*	*20*	*-11*	*0.40*	*16*		*10*	*29*	*14*
Mt Tendre	*6.34*	*46.6083*	*Portland. Kimmeridg.*	*SS*	*84*	*16*	*45*	*-70*	*171*	*-12*	*0.63*	*7*		*13*	*26*	*14*
Nods	*6.3517*	*47.0817*	*Up. Bajocian*	*SS*	*141*	*5*	*64*	*-71*	*50*	*19*	*0.28*	*27*		*2*	*34*	*14*
Nogna	*5.6667*	*46.5983*	*Bathon. Bajoc.*	*P*	*81*	*-9*	*171*	*4*	*58*	*80*	*0.50*	*11*		*11*	*25*	*14*
Nogna	*5.6667*	*46.5983*	*Bathon. Bajoc.*	*SS*	*84*	*8*	*123*	*-80*	*175*	*6*	*0.57*	*21*		*12*	*28*	*14*
Ordonnaz	*5.5667*	*45.8333*	*Kimmeridg. Oxford.*	*P*	*30*	*-13*	*120*	*2*	*20*	*77*	*0.59*	*6*		*11*	*29*	*14*
Ordonnaz	*5.5667*	*45.8333*	*Kimmeridg. Oxford.*	*SS*	*45*	*2*	*145*	*77*	*135*	*-13*	*0.28*	*32*		*14*	*33*	*14*
Ordonnaz	*5.5667*	*45.8333*	*Kimmeridg. Oxford.*	*P*	*144*	*0*	*54*	*-14*	*54*	*76*	*0.09*	*7*		*9*	*33*	*14*
Piards	*5.8283*	*46.505*	*Kimmeridg. Bathon.*	*P*	*160*	*0*	*70*	*-3*	*70*	*87*	*0.63*	*14*		*15*	*37*	*14*
Pratz	*5.7517*	*46.3817*	*Bathonian*	*P*	*65*	*-5*	*154*	*13*	*177*	*-76*	*0.64*	*19*		*12*	*38*	*14*
Pratz	*5.7517*	*46.3817*	*Bathonian*	*SS*	*72*	*-8*	*33*	*80*	*161*	*6*	*0.35*	*34*		*11*	*31*	*14*

Site	Long.	Lat.	Age	Tectonic regime	σ_1 trend	σ_1 plunge	σ_2 trend	σ_2 plunge	σ_3 trend	σ_3 plunge	R	N	F	α	RUP	REF
Prénovel	*5.8517*	*46.52*	*Kimmeridgian*	*SS*	*122*	*-4*	*7*	*-80*	*32*	*9*	*0.49*	*13*		*12*	*45*	*14*
Rochejean	*6.29*	*46.7333*	*Hauteriv. Kimmeridg.*	*SS*	*169*	*3*	*92*	*-75*	*78*	*14*	*0.20*	*12*		*7*	*29*	*14*
Rochejean	*6.29*	*46.7333*	*Hauteriv. Kimmeridg.*	*SS*	*125*	*0*	*37*	*-83*	*35*	*7*	*0.19*	*10*		*9*	*20*	*14*
Roissiat	*5.375*	*46.3467*	*Mid. Bajocian*	*SS*	*110*	*13*	*156*	*-72*	*23*	*-12*	*0.17*	*19*		*6*	*30*	*14*
Roissiat	*5.375*	*46.3467*	*Mid. Bajocian*	*SS*	*48*	*12*	*70*	*-77*	*139*	*5*	*0.29*	*29*		*10*	*45*	*14*
Rosnay	*5.6167*	*46.7*	*Low. Baj.-Aalen.*	*SS*	*127*	*7*	*9*	*76*	*38*	*-13*	*0.45*	*18*		*9*	*32*	*14*
Séchey	*6.2967*	*46.665*	*Port. -Up. Kimme.*	*SS*	*123*	*-1*	*45*	*87*	*33*	*-3*	*0.37*	*16*		*9*	*26*	*14*
Serrières	*5.4517*	*46.1517*	*Rauracian*	*SS*	*124*	*-21*	*160*	*64*	*39*	*14*	*0.31*	*30*		*14*	*45*	*14*
St Croix	*6.4967*	*46.8317*		*SS*	*98*	*1*	*0*	*79*	*8*	*-11*	*0.24*	*16*		*8*	*32*	*14*
St Julien	*5.4383*	*46.405*	*Bathonian Bajocian*	*SS*	*90*	*-10*	*35*	*73*	*177*	*13*	*0.40*	*41*		*16*	*36*	*14*
St Maurice	*5.8333*	*46.5517*	*Sequanian*	*SS*	*99*	*0*	*12*	*-83*	*9*	*7*	*0.38*	*19*		*13*	*30*	*14*
Tare	*5.555*	*45.8767*	*Up. Oxfordian*	*p*	*70*	*-7*	*161*	*-5*	*104*	*81*	*0.40*	*8*		*8*	*26*	*14*
Tare	*5.555*	*45.8767*	*Up. Oxfordian*	*SS*	*70*	*-12*	*86*	*78*	*160*	*-3*	*0.45*	*42*		*19*	*42*	*14*
Titi	*6.3317*	*46.8383*	*Hauterivian*	*SS*	*113*	*-2*	*29*	*71*	*23*	*-19*	*0.17*	*22*		*14*	*38*	*14*
Val du Fier	*5.8617*	*45.9333*	*Portland. to Oford.*	*P*	*86*	*-9*	*179*	*-18*	*150*	*70*	*0.60*	*4*		*1*	*11*	*14*
Val du Fier	*5.8617*	*45.9333*	*Portland. to Oford.*	*SS*	*72*	*-3*	*169*	*-70*	*161*	*20*	*0.36*	*30*		*9*	*27*	*14*
Vaulion S	*6.3483*	*46.6567*	*Low. Kimmeridgian*	*SS*	*138*	*-5*	*71*	*76*	*47*	*-12*	*0.29*	*46*		*17*	*35*	*14*
Les Rivoirands	*5.7923*	*45.0543*		*SS*	*88*	*-6*	*148*	*78*	*179*	*-10*		*31*				*17*
RN91 Est	*5.8437*	*45.0557*		*SS*	*39*	*-3*	*49*	*87*	*129*	*-1*		*16*				*17*
RN91 Ouest	*5.7951*	*45.0537*		*SS*	*101*	*-8*	*68*	*80*	*10*	*-5*		*15*				*17*
Saint Barthelemy	*5.8343*	*45.0486*		*SS*	*43*	*-16*	*88*	*68*	*137*	*-15*		*15*				*17*
Sechilienne Nord	*5.8298*	*45.0574*		*P*	*59*	*-3*	*150*	*-22*	*140*	*68*		*48*				*17*
jura chartreuse 001	*5.4197*	*46.0247*		*P*	*95*	*-7*	*5*	*-3*	*70*	*83*	*0.35*	*16*				*18*
jura chartreuse 002	*5.4269*	*46.0288*		*TP*	*135*	*-3*	*44*	*-21*	*52*	*68*	*0.4*	*4*				*18*
jura chartreuse 003	*5.447*	*46.0275*		*P*	*140*	*-4*	*49*	*-17*	*64*	*73*	*0.69*	*7*				*18*
jura chartreuse 004	*5.4435*	*46.0167*		*P*	*104*	*-4*	*14*	*1*	*121*	*85*	*0.59*	*10*				*18*
jura chartreuse 005	*5.4635*	*46.037*		*P*	*95*	*7*	*5*	*2*	*80*	*-83*	*0.54*	*14*				*18*
jura chartreuse 006	*5.4669*	*46.0342*		*P*	*96*	*-4*	*4*	*-16*	*80*	*-83*	*0.54*	*8*				*18*
jura chartreuse 007	*5.4892*	*46.0447*		*P*	*114*	*-18*	*16*	*-25*	*56*	*58*	*0.61*	*4*				*18*
jura chartreuse 008	*5.4802*	*46.0271*		*SS*	*115*	*-8*	*6*	*-66*	*28*	*23*	*0.03*	*6*				*18*
jura chartreuse 009	*5.486*	*46.0297*		*P*	*88*	*3*	*178*	*-11*	*12*	*-79*	*0.21*	*22*				*18*

Site	Long.	Lat.	Age	Tectonic regime	σ_1 trend	σ_1 plunge	σ_2 trend	σ_2 plunge	σ_3 trend	σ_3 plunge	R	N	F	α	RUP	REF
jura chartreuse 010	*5.4845*	*46.0116*		*TP*	*106*	*-11*	*8*	*-33*	*32*	*55*	*0.13*	*4*				*18*
jura chartreuse 011	*5.5024*	*46.0229*		*P*	*114*	*-18*	*15*	*-25*	*56*	*58*	*0.61*	*4*				*18*
jura chartreuse 012	*5.5132*	*46.0264*		*SS*	*106*	*6*	*0*	*69*	*18*	*-20*	*0.24*	*12*				*18*
jura chartreuse 013	*5.5151*	*46.0323*		*SS*	*106*	*6*	*0*	*69*	*18*	*-20*	*0.24*	*12*				*18*
jura chartreuse 014	*5.5484*	*46.0364*		*SS*	*101*	*4*	*161*	*-81*	*12*	*-8*	*0.31*	*10*				*18*
jura chartreuse 015	*5.5781*	*46.0416*		*SS*	*124*	*-2*	*33*	*-16*	*42*	*74*	*0.57*	*4*				*18*
jura chartreuse 016	*5.3821*	*45.929*		*P*	*72*	*-5*	*61*	*88*	*162*	*0*	*0.8*	*5*				*18*
jura chartreuse 019	*5.4783*	*45.9583*		*SS*	*87*	*0*	*178*	*80*	*177*	*-10*	*0.4*	*15*				*18*
jura chartreuse 020	*5.4835*	*45.9537*		*SS*	*92*	*-5*	*169*	*70*	*4*	*19*	*0.12*	*9*				*18*
jura chartreuse 021	*5.4852*	*45.9608*		*TP*	*79*	*-5*	*165*	*37*	*176*	*-52*	*0.11*	*6*				*18*
jura chartreuse 022	*5.4881*	*45.957*		*SS*	*75*	*-12*	*88*	*78*	*166*	*-3*	*0.14*	*9*				*18*
jura chartreuse 023	*5.491*	*45.9503*		*P*	*67*	*-4*	*157*	*-3*	*104*	*85*	*0.42*	*21*				*18*
jura chartreuse 024	*5.5475*	*45.9508*		*TP*	*71*	*20*	*149*	*-30*	*9*	*-53*	*0.52*	*4*				*18*
jura chartreuse 025	*5.5709*	*45.9591*		*P*	*86*	*12*	*2*	*-23*	*150*	*-64*	*0.31*	*10*				*18*
jura chartreuse 026	*5.5762*	*45.9608*		*P*	*78*	*5*	*166*	*-24*	*178*	*65*	*0.36*	*6*				*18*
jura chartreuse 027	*5.5605*	*45.9391*		*TP*	*70*	*-17*	*145*	*42*	*177*	*-43*	*0.43*	*4*				*18*
jura chartreuse 028	*5.6017*	*45.9128*		*P*	*82*	*-5*	*179*	*-24*	*142*	*61*	*0.11*	*4*				*18*
jura chartreuse 029	*5.3844*	*45.8967*		*P*	*74*	*0*	*164*	*-14*	*163*	*76*	*0.31*	*21*				*18*
jura chartreuse 030	*5.3862*	*45.8999*		*P*	*66*	*0*	*156*	*10*	*156*	*-80*	*0.56*	*23*				*18*
jura chartreuse 031	*5.394*	*45.8976*		*P*	*73*	*-9*	*162*	*9*	*28*	*77*	*0.39*	*4*				*18*
jura chartreuse 032	*5.3846*	*45.8863*		*TP*	*14*	*5*	*100*	*-33*	*111*	*36*	*0.54*	*7*				*18*
jura chartreuse 034	*5.3949*	*45.8806*		*P*	*31*	*1*	*121*	*-8*	*126*	*82*	*0.17*	*17*				*18*
jura chartreuse 035	*5.4132*	*45.8677*		*TP*	*41*	*-1*	*132*	*-42*	*130*	*48*	*0.17*	*5*				*18*
jura chartreuse 036	*5.4196*	*45.8674*		*P*	*51*	*-10*	*142*	*-7*	*88*	*78*	*0.74*	*10*				*18*
jura chartreuse 037	*5.4366*	*45.8676*		*P*	*61*	*11*	*155*	*18*	*121*	*-68*	*0.28*	*7*				*18*
jura chartreuse 038	*5.4402*	*45.8851*		*SS*	*47*	*-1*	*140*	*-79*	*137*	*11*	*0.01*	*6*				*18*
jura chartreuse 039	*5.4666*	*45.8107*		*P*	*68*	*-9*	*153*	*28*	*174*	*-61*	*0.22*	*4*				*18*
jura chartreuse 040	*5.4672*	*45.7909*		*P*	*45*	*-19*	*127*	*23*	*170*	*-59*	*0.15*	*5*				*18*
jura chartreuse 041	*5.4654*	*45.7857*		*P*	*49*	*-7*	*139*	*0*	*49*	*83*	*0.71*	*10*				*18*
jura chartreuse 042	*5.488*	*45.7945*		*P*	*44*	*-6*	*134*	*-1*	*55*	*84*	*0.52*	*6*				*18*
jura chartreuse 043	*5.491*	*45.8019*		*P*	*65*	*10*	*156*	*6*	*96*	*-78*	*0.65*	*9*				*18*

Site	Long.	Lat.	Age	Tectonic regime	σ_1 trend	σ_1 plunge	σ_2 trend	σ_2 plunge	σ_3 trend	σ_3 plunge	R	N	F	α	RUP	REF
jura chartreuse 044	*5.5269*	*45.8007*		*SS*	*73*	*3*	*155*	*-66*	*164*	*23*	*0.1*	*12*				*18*
jura chartreuse 045	*5.5228*	*45.8046*		*P*	*69*	*1*	*158*	*-16*	*163*	*74*	*0.14*	*29*				*18*
jura chartreuse 046	*5.5555*	*45.8325*		*P*	*67*	*-31*	*147*	*16*	*33*	*54*	*0.8*	*4*				*18*
jura chartreuse 047	*5.5649*	*45.8309*		*TP*	*69*	*-13*	*138*	*56*	*167*	*-31*	*0.45*	*6*				*18*
jura chartreuse 048	*5.5613*	*45.8429*		*TP*	*63*	*1*	*152*	*-41*	*155*	*49*	*0.19*	*6*				*18*
jura chartreuse 049	*5.5451*	*45.8619*		*P*	*55*	*-9*	*145*	*-1*	*58*	*81*	*0.64*	*5*				*18*
jura chartreuse 050	*5.5785*	*45.8474*		*P*	*75*	*3*	*165*	*2*	*116*	*-87*	*0.44*	*4*				*18*
jura chartreuse 051	*5.587*	*45.8382*		*P*	*54*	*-4*	*144*	*-1*	*69*	*86*	*0.56*	*7*				*18*
jura chartreuse 052	*5.5956*	*45.8281*		*P*	*63*	*-9*	*156*	*-16*	*126*	*71*	*0.04*	*9*				*18*
jura chartreuse 054	*5.6128*	*45.858*		*TP*	*76*	*-5*	*169*	*-33*	*158*	*57*	*0.22*	*11*				*18*
jura chartreuse 055	*5.6165*	*45.8539*		*P*	*60*	*6*	*152*	*22*	*136*	*-67*	*0.2*	*6*				*18*
jura chartreuse 058	*5.6596*	*45.8267*		*P*	*74*	*-1*	*164*	*30*	*166*	*-60*	*0.17*	*10*				*18*
jura chartreuse 059	*5.7077*	*45.8233*		*SS*	*73*	*-2*	*169*	*-75*	*163*	*15*	*0.18*	*17*				*18*
jura chartreuse 060	*5.6553*	*45.8148*		*P*	*40*	*19*	*121*	*2*	*47*	*-71*	*0.87*	*4*				*18*
jura chartreuse 062	*5.6751*	*45.7903*		*P*	*60*	*-1*	*150*	*-7*	*142*	*83*	*0.57*	*4*				*18*
jura chartreuse 063	*5.5661*	*45.7771*		*P*	*69*	*0*	*159*	*5*	*163*	*-85*	*0.34*	*7*				*18*
jura chartreuse 064	*5.566*	*45.7712*		*P*	*47*	*-11*	*139*	*-10*	*93*	*75*	*0.76*	*10*				*18*
jura chartreuse 065	*5.5624*	*45.7616*		*P*	*68*	*-3*	*157*	*1*	*47*	*87*	*0.21*	*10*				*18*
jura chartreuse 066	*5.5829*	*45.7524*		*TP*	*73*	*-3*	*160*	*49*	*165*	*-40*	*0.25*	*6*				*18*
jura chartreuse 067	*5.6008*	*45.7551*		*P*	*79*	*10*	*169*	*2*	*90*	*-79*	*0.61*	*5*				*18*
jura chartreuse 068	*5.6377*	*45.7628*		*P*	*73*	*-8*	*164*	*-13*	*130*	*75*	*0.58*	*11*				*18*
jura chartreuse 069	*5.6029*	*45.7293*		*P*	*88*	*-10*	*176*	*10*	*43*	*75*	*0.69*	*6*				*18*
jura chartreuse 070	*5.639*	*45.7277*		*P*	*88*	*-8*	*176*	*11*	*31*	*76*	*0.43*	*5*				*18*
jura chartreuse 071	*5.729*	*45.7977*		*P*	*64*	*2*	*155*	*35*	*152*	*-55*	*0.43*	*5*				*18*
jura chartreuse 072	*5.7107*	*45.7887*		*P*	*61*	*-4*	*151*	*-3*	*99*	*85*	*0.2*	*9*				*18*
jura chartreuse 073	*5.7109*	*45.7828*		*P*	*76*	*3*	*166*	*16*	*155*	*-74*	*0.41*	*9*				*18*
jura chartreuse 076a	*5.7493*	*45.7638*		*P*	*80*	*6*	*167*	*-29*	*180*	*60*	*0.23*	*14*				*18*
jura chartreuse 077	*5.7609*	*45.7724*		*P*	*45*	*-10*	*137*	*-9*	*89*	*76*	*0.63*	*6*				*18*
jura chartreuse 078	*5.8078*	*45.7663*		*TP*	*79*	*-7*	*0*	*58*	*164*	*31*	*0.23*	*5*				*18*
jura chartreuse 081	*5.8671*	*45.7803*		*P*	*59*	*5*	*147*	*-17*	*165*	*72*	*0.32*	*12*				*18*
jura chartreuse 082	*5.8841*	*45.776*		*TP*	*74*	*-9*	*178*	*-58*	*158*	*31*	*0.06*	*12*				*18*

Site	Long.	Lat.	Age	Tectonic regime	σ_1 trend	σ_1 plunge	σ_2 trend	σ_2 plunge	σ_3 trend	σ_3 plunge	R	N	F	α	RUP	REF
jura chartreuse 083	*5.6135*	*45.6641*		*TP*	*86*	*4*	*172*	*-44*	*180*	*46*	*0.08*	*19*				*18*
jura chartreuse 084	*5.6115*	*45.6692*		*P*	*78*	*12*	*169*	*2*	*90*	*-77*	*0.3*	*22*				*18*
jura chartreuse 085	*5.6236*	*45.6663*		*TP*	*97*	*-16*	*169*	*47*	*20*	*39*	*0.33*	*7*				*18*
jura chartreuse 086	*5.7519*	*45.7083*		*P*	*90*	*-10*	*2*	*13*	*142*	*74*	*0.24*	*19*				*18*
jura chartreuse 087	*5.7886*	*45.7324*		*P*	*73*	*14*	*163*	*1*	*76*	*-76*	*0.78*	*4*				*18*
jura chartreuse 088	*5.8187*	*45.702*		*P*	*58*	*-6*	*151*	*-28*	*138*	*62*	*0.43*	*5*				*18*
jura chartreuse 089	*5.8429*	*45.6947*		*P*	*87*	*-8*	*177*	*-5*	*120*	*81*	*0.6*	*8*				*18*
jura chartreuse 090	*5.85*	*45.6767*		*SS*	*104*	*22*	*92*	*-68*	*12*	*4*	*0.14*	*16*				*18*
jura chartreuse 091	*5.7129*	*45.6374*		*SS*	*62*	*-13*	*179*	*-63*	*147*	*23*	*0.34*	*6*				*18*
jura chartreuse 092	*5.8043*	*45.5864*		*P*	*95*	*12*	*5*	*1*	*88*	*-78*	*0.84*	*9*				*18*
jura chartreuse 093	*5.8086*	*45.5816*		*P*	*87*	*-11*	*176*	*5*	*62*	*78*	*0.68*	*5*				*18*
jura chartreuse 094	*5.8338*	*45.5636*		*TP*	*80*	*9*	*64*	*-30*	*5*	*-28*	*0.36*	*8*				*18*
jura chartreuse 095	*5.7195*	*45.4819*		*P*	*109*	*1*	*19*	*19*	*22*	*-71*	*0.2*	*17*				*18*
jura chartreuse 096	*5.7344*	*45.4713*		*P*	*114*	*-1*	*25*	*-11*	*20*	*-79*	*0.23*	*12*				*18*
jura chartreuse 097	*5.7569*	*45.4419*		*SS*	*104*	*21*	*130*	*-67*	*17*	*-9*	*0.13*	*5*				*18*
jura chartreuse 098	*5.7863*	*45.4503*		*P*	*96*	*-15*	*13*	*25*	*158*	*60*	*0.38*	*12*				*18*
jura chartreuse 099	*5.7858*	*45.4347*		*P*	*116*	*-15*	*26*	*3*	*129*	*75*	*0.7*	*6*				*18*
jura chartreuse 100	*5.8016*	*45.4509*		*P*	*106*	*-2*	*16*	*5*	*176*	*85*	*0.26*	*21*				*18*
jura chartreuse 101	*5.813*	*45.4603*		*P*	*113*	*12*	*22*	*2*	*58*	*-78*	*0.26*	*11*				*18*
jura chartreuse 103	*5.8769*	*45.445*		*SS*	*108*	*-1*	*14*	*-78*	*18*	*12*	*0.26*	*14*				*18*
jura chartreuse 104	*5.895*	*45.4559*		*P*	*88*	*20*	*169*	*-23*	*34*	*-59*	*0.18*	*5*				*18*
jura chartreuse 105	*5.9051*	*45.4702*		*TP*	*92*	*1*	*3*	*-36*	*1*	*54*	*0.35*	*6*				*18*
jura chartreuse 106	*5.9682*	*45.4624*		*SS*	*106*	*1*	*24*	*-83*	*16*	*7*	*0.15*	*12*				*18*
jura chartreuse 107	*5.9542*	*45.3923*		*P*	*134*	*-16*	*43*	*-7*	*87*	*81*	*0.53*	*6*				*18*
jura chartreuse 109	*6.0796*	*45.3907*		*P*	*118*	*0*	*28*	*-20*	*29*	*70*	*0.23*	*9*				*18*
vercors01	*5.4848*	*45.291*		*TP*	*103*	*-20*	*41*	*53*	*1*	*-30*	*0.291*	*31*				*18*
vercors02	*5.4663*	*45.2722*		*P*	*111*	*-4*	*40*	*12*	*40*	*77*	*0.093*	*18*				*18*
vercors03	*5.4592*	*45.2656*		*P*	*113*	*-2*	*24*	*26*	*20*	*-64*	*0.151*	*15*				*18*
vercors04	*5.4706*	*45.262*		*SS*	*109*	*15*	*75*	*-72*	*17*	*10*	*0.223*	*27*				*18*
vercors05	*5.464*	*45.2598*		*TP*	*124*	*-5*	*28*	*-50*	*38*	*40*	*0.368*	*7*				*18*
vercors06	*5.4712*	*45.2569*		*P*	*116*	*-4*	*25*	*-17*	*38*	*72*	*0.185*	*11*				*18*

Site	Long.	Lat.	Age	Tectonic regime	σ_1 trend	σ_1 plunge	σ_2 trend	σ_2 plunge	σ_3 trend	σ_3 plunge	R	N	F	α	RUP	REF
vercors07	*5.4719*	*45.229*		*SS*	*114*	*10*	*38*	*-54*	*17*	*34*	*0.393*	*19*				*18*
vercors08	*5.4732*	*45.2202*		*TP*	*105*	*-10*	*7*	*-37*	*28*	*51*	*0.253*	*8*				*18*
vercors09	*5.5508*	*45.2801*		*P*	*109*	*-4*	*39*	*-42*	*158*	*84*	*0.557*	*26*				*18*
vercors10	*5.5575*	*45.2723*		*P*	*110*											*18*
vercors11	*5.5604*	*45.2678*		*TP*	*107*	*22*	*39*	*-42*	*177*	*-39*	*0.374*	*8*				*18*
vercors12	*5.4914*	*45.2142*		*SS*	*107*	*-14*	*48*	*64*	*11*	*-21*	*0.064*	*36*				*18*
vercors13	*5.5012*	*45.1904*		*TP*	*97*	*-44*	*29*	*22*	*138*	*39*	*0.585*	*10*				*18*
vercors14	*5.4149*	*45.1665*		*SS*	*110*	*-10*	*98*	*80*	*20*	*-2*	*0.204*	*32*				*18*
vercors15	*5.4376*	*45.1567*		*SS*	*106*	*-13*	*38*	*58*	*8*	*-29*	*0.368*	*15*				*18*
vercors16	*5.3992*	*45.1088*		*P*	*118*	*-6*	*31*	*21*	*13*	*-68*	*0.082*	*15*				*18*
vercors17	*5.4612*	*45.0847*		*P*	*112*	*-12*	*22*	*3*	*126*	*75*	*0.806*	*19*				*18*
vercors18	*5.4799*	*45.0842*		*P*	*109*	*-9*	*18*	*-3*	*89*	*81*	*0.581*	*32*				*18*
vercors19	*5.489*	*45.0798*		*SS*	*111*	*14*	*64*	*-70*	*17*	*14*	*1.136*	*9*				*18*
vercors20	*5.4518*	*45.0755*		*P*	*114*	*-9*	*24*	*-1*	*109*	*81*	*0.1*	*12*				*18*
vercors21	*5.4129*	*45.0586*		*P*	*95*											*18*
vercors23	*5.2491*	*45.0434*		*SS*	*123*	*-12*	*6*	*-65*	*38*	*22*	*0.216*	*9*				*18*
vercors25	*5.2016*	*45.0908*		*P*	*105*											*18*
vercors26	*5.4065*	*44.9653*		*P*	*80*											*18*
vercors27	*5.4003*	*44.9752*		*P*	*99*	*9*	*8*	*4*	*72*	*-80*	*0.385*	*20*				*18*
vercors28	*5.3227*	*44.9714*		*P*	*95*											*18*
vercors30	*5.311*	*44.959*		*P*	*100*											*18*
vercors33	*5.2258*	*44.9799*		*P*	*118*	*-6*	*28*	*10*	*130*	*84*	*0.528*	*16*				*18*
vercors34	*5.4105*	*44.8761*		*P*	*100*	*15*	*7*	*14*	*57*	*-69*	*0.172*	*12*				*18*
vercors35	*5.3746*	*44.8951*		*SS*	*106*	*0*	*159*	*89*	*16*	*1*	*0.241*	*8*				*18*
vercors36	*5.3678*	*44.9079*		*P*	*97*	*15*	*7*	*0*	*97*	*-75*	*0.723*	*5*				*18*
vercors37	*5.3297*	*44.9023*		*SS*	*82*	*-13*	*100*	*76*	*173*	*-4*	*0.551*	*5*				*18*
vercors38	*5.2499*	*44.906*		*TP*	*116*	*-1*	*25*	*-57*	*27*	*33*	*0.073*	*4*				*18*
vercors39	*5.2142*	*44.9104*		*P*	*110*											*18*
vercors40	*5.1715*	*44.8841*		*P*	*105*											*18*
vercors41	*5.1639*	*44.8833*		*P*	*100*											*18*
vercors42	*5.1434*	*44.8895*		*P*	*75*											*18*

Site	Long.	Lat.	Age	Tectonic regime	σ_1 trend	σ_1 plunge	σ_2 trend	σ_2 plunge	σ_3 trend	σ_3 plunge	R	N	F	α	RUP	REF
vercors43	*5.4138*	*44.7911*		*SS*	*105*	*-33*	*119*	*56*	*19*	*6*	*0.617*	*7*				*18*
vercors44	*5.3844*	*44.7966*		*P*	*105*											*18*
vercors45	*5.21*	*44.8035*		*TP*	*105*	*-4*	*9*	*-41*	*17*	*48*	*0.127*	*4*				*18*
vercors46	*5.1511*	*44.805*		*P*	*130*											*18*
vercors48	*5.1409*	*44.7968*		*P*	*130*											*18*
vercors49	*5.1087*	*44.809*		*SS*	*95*	*35*	*118*	*-53*	*13*	*-11*	*0.563*	*16*				*18*
vercors50	*5.3578*	*44.7153*		*SS*	*103*	*-5*	*13*	*-2*	*83*	*14*	*0.321*	*7*				*18*
vercors51	*5.3529*	*44.7069*		*P*	*120*											*18*
vercors52	*5.2837*	*44.7046*		*P*	*130*											*18*
vercors53	*5.2359*	*44.6876*		*TP*	*103*	*-16*	*30*	*45*	*179*	*41*	*0.088*	*7*				*18*
vercors54	*5.2131*	*44.692*		*P*	*100*	*-11*	*13*	*15*	*157*	*71*	*0.238*	*24*				*18*
vercors56	*5.0351*	*44.748*		*SS*	*94*	*-2*	*155*	*85*	*7*	*4*	*0.503*	*5*				*18*
vercors57	*5.0214*	*44.7093*		*P*	*105*											*18*
vercors58	*5.022*	*44.6842*		*P*	*90*											*18*
S10b	*7.4072*	*43.7856*	*L. Cretaceous*	*P*	*169*	*28*	*93*	*-23*	*36*	*52*	*0.18*					*19*
S12	*7.4053*	*43.8064*	*L. Cretaceous*	*SS*	*158*	*-26*	*110*	*53*	*56*	*-24*	*0.35*					*19*
S3	*7.4078*	*43.8428*	*U. Cretaceous*	*P*	*17*	*-5*	*110*	*-27*	*97*	*62*	*0.71*					*19*
S5b	*7.4442*	*43.8253*	*U. Cretaceous*	*SS*	*149*	*-19*	*8*	*-66*	*64*	*14*	*0.22*					*19*
S8b	*7.4475*	*43.8125*	*U. Cretaceous*	*P*	*156*	*2*	*66*	*-9*			*0.42*					*19*
S8c	*7.4475*	*43.8125*	*U. Cretaceous*	*SS*	*161*	*-29*					*0.04*					*19*
S9	*7.4097*	*43.8194*	*U. Jurassic*	*P*	*170*	*-8*	*75*	*-32*	*93*	*57*	*0.18*					*19*
C1	*6.5081*	*43.6806*	*U. Jurassic*	*P*	*176*	*16*	*91*	*-17*	*45*	*66*	*0.37*					*20*
C10	*6.7339*	*43.9575*	*M.U. Eocene*	*P*	*131*	*-3*	*40*	*-17*	*50*	*72*	*0.68*	*0*				*20*
C12	*6.8922*	*43.9608*	*M.U. Eocene*	*P*	*168*	*12*					*0.03*					*20*
C13	*6.8722*	*43.9944*	*L. Jurassic*	*P*	*12*	*8*					*0*					*20*
C14b	*6.5231*	*43.8719*	*L. Cretaceous*	*P*					*86*	*70*	*0.9*					*20*
C16	*7.0906*	*44.0869*	*Trias*	*P*	*179*	*26*	*95*	*-12*	*28*	*61*	*0.5*					*20*
C18b	*6.9583*	*43.6992*	*M. Jurassic*	*SS*	*132*	*-3*			*42*	*0*	*0.19*					*20*
C19	*7.0969*	*43.8*	*U. Jurassic*	*SS*	*151*	*-21*	*5*	*-66*	*66*	*12*	*0.48*					*20*
C2	*6.5025*	*43.7364*	*M. Cretaceous*	*P*	*174*	*-12*					*0.04*					*20*
C20	*7.0333*	*43.79*	*U. Jurassic*	*P*	*166*	*-24*	*65*	*-23*	*117*	*56*	*0.29*					*20*

Site	Long.	Lat.	Age	Tectonic regime	σ_1 trend	σ_1 plunge	σ_2 trend	σ_2 plunge	σ_3 trend	σ_3 plunge	R	N	F	α	RUP	REF
C23a	*7.1942*	*43.795*	*Pliocene*	*SS*	*133*	*43*	*98*	*-41*	*24*	*18*	*0.18*					*20*
C23b	*7.1942*	*43.795*	*Pliocene*	*P*	*118*	*0*	*28*	*0*			*0.56*					*20*
C3	*6.7267*	*43.8514*	*U. Jurassic*	*SS*	*152*	*-11*	*157*	*79*	*63*	*1*	*0.34*					*20*
C4	*6.9097*	*43.8611*	*M. Jurassic*	*P*	*149*	*-11*	*62*	*15*	*23*	*-71*	*0.27*					*20*
C5	*6.9556*	*43.8728*	*L. Cretaceous*	*SS*	*11*	*-17*	*14*	*73*	*101*	*-1*	*0.55*					*20*
C6	*6.8078*	*43.9503*	*M.U. Eocene*	*P*	*14*	*3*	*104*	*-3*			*0.67*					*20*
C7	*6.7792*	*43.9697*	*M.U. Eocene*	*P*	*134*	*10*	*50*	*-20*	*14*	*64*	*0.34*					*20*
C8	*6.7619*	*43.9708*	*M.U. Eocene*	*P*	*155*	*1*					*0.01*					*20*
C9	*6.7508*	*43.9667*	*M.U. Eocene*	*SS*	*156*	*28*	*166*	*-61*	*68*	*-4*	*0.1*	*0*				*20*
D12	*6.4039*	*44.1167*	*U. Jurassic*	*SS*	*45*	*-19*	*15*	*68*	*131*	*10*	*0.66*					*20*
D13	*6.3953*	*44.0681*	*M. Cretaceous*	*P*	*45*	*6*					*0.09*					*20*
D17	*6.6978*	*44.2194*	*L. Oligocene*	*P*	*55*	*-12*	*151*	*-27*	*123*	*60*	*0.22*					*20*
D28a2	*6.8083*	*44.3064*	*U. Eocene/L. Oligocene*	*SS*	*55*	*3*	*52*	*-87*	*145*	*0*	*0.12*					*20*
D29b2	*6.8472*	*44.3406*	*Cretaceous*	*P*	*58*	*27*	*157*	*18*	*96*	*-57*	*0.68*					*20*
D30b	*6.7953*	*44.3428*	*U. Eocene/L. Oligocene*	*P*	*54*	*-11*	*150*	*-27*	*123*	*60*	*0.11*					*20*
D38	*6.5833*	*44.2761*	*M. Cretaceous*	*SS*	*76*	*54*	*59*	*-35*	*155*	*-8*	*0.43*					*20*
D39a	*6.6322*	*44.2333*	*M. Cretaceous*	*SS*	*30*	*-31*	*62*	*55*	*129*	*-15*	*0.2*					*20*
D3a2	*6.4236*	*44.1842*	*U. Jurassic*	*P*	*42*	*13*					*0.01*					*20*
D3b	*6.4236*	*44.1842*	*U. Jurassic*	*SS*	*48*	*4*	*152*	*72*	*137*	*-17*	*0.03*					*20*
D4	*6.4128*	*44.1719*	*U. Jurassic*	*P*	*41*	*5*					*0.01*					*20*
D43a	*6.8514*	*44.3322*	*Cretaceous*	*SS*	*58*	*-16*	*34*	*72*	*146*	*7*	*0.28*					*20*
D55	*6.5592*	*44.0136*	*M.U. Eocene*	*P*	*32*	*1*	*121*	*-30*	*125*	*60*	*0.31*					*20*
D57	*6.9258*	*44.1256*	*M. Jurassic*	*SS*	*35*	*-15*	*122*	*-43*	*111*	*43*	*0.19*					*20*
D7b	*6.5167*	*44.1989*	*M.U. Eocene*	*SS*	*82*	*26*	*70*	*-62*	*168*	*-6*	*0.84*					*20*
D8	*6.5003*	*44.2072*	*U. Cretaceous*	*SS*	*42*	*8*					*0.09*					*20*
N1	*7.2394*	*43.7919*	*U. Miocene*	*SS*	*25*	*-12*	*136*	*-60*	*109*	*27*	*0.19*					*20*
N12	*7.2453*	*43.8844*	*M.U. Jurassic*	*SS*	*135*	*7*					*0.02*					*20*
N13	*7.2647*	*43.8933*	*U. Cretaceous*	*SS*	*169*	*-25*	*29*	*-59*	*88*	*17*	*0.2*					*20*
N14	*7.2442*	*43.7942*	*U. Miocene*	*SS*	*3*	*-7*	*107*	*-64*	*89*	*24*	*0.27*					*20*
N15	*7.2514*	*43.7883*	*U. Miocene*	*SS*	*17*	*-4*	*118*	*-70*	*105*	*19*	*0.17*					*20*
N17	*7.2325*	*43.8056*	*Pliocene*	*SS*	*24*	*-15*	*46*	*74*	*116*	*-6*	*0.22*					*20*

Site	Long.	Lat.	Age	Tectonic regime	σ_1 trend	σ_1 plunge	σ_2 trend	σ_2 plunge	σ_3 trend	σ_3 plunge	R	N	F	α	RUP	REF
N18b	*7.31*	*43.8925*	*U. Cretaceous*	*P*	*43*	*-8*	*133*	*82*			*0.17*					*20*
N19b	*7.2758*	*43.7781*	*U. Cretaceous*	*SS*	*26*	*-29*	*47*	*59*	*121*	*-9*	*0.33*					*20*
N2	*7.2556*	*43.7817*	*Pliocene*	*P*	*168*	*-5*	*78*	*-4*			*0.78*					*20*
N20	*7.2583*	*43.8283*	*U. Cretaceous*	*SS*	*40*	*-2*	*133*	*-56*	*129*	*34*	*0.31*					*20*
N21	*7.2583*	*43.8283*	*U. Miocene*	*SS*	*38*	*7*					*0.09*					*20*
N22	*7.4461*	*43.7686*	*L. Miocene*	*P*	*149*	*17*					*0.01*					*20*
N23	*7.5408*	*43.9786*	*Jurassic*	*SS*	*136*	*10*	*60*	*-54*	*39*	*34*	*0.14*					*20*
N24a2	*7.4739*	*43.9039*	*U. Cretaceous*	*P*	*130*	*6*					*0.01*					*20*
N24b	*7.4758*	*43.9144*	*M. Eocene*	*SS*	*167*	*7*	*36*	*80*	*78*	*-8*	*0.12*					*20*
N25b	*7.4667*	*43.8369*	*U. Cretaceous*	*P*	*161*	*18*	*76*	*-14*	*23*	*67*	*0.29*					*20*
N26b	*7.5167*	*43.9331*	*U. Cretaceous*	*SS*	*133*	*4*					*0.04*					*20*
N27b	*7.4561*	*43.7906*	*U. Jurassic*	*P*	*160*	*15*					*0.01*					*20*
N28a	*7.8364*	*43.85*	*Pliocene*	*SS*	*154*	*9*	*33*	*73*	*67*	*-15*	*0.58*					*20*
N28b	*7.8333*	*43.8544*	*Pliocene*	*SS*	*142*	*-13*	*174*	*74*	*54*	*8*	*0.45*					*20*
N29	*7.3825*	*43.7553*	*Quaternary*	*SS*	*159*	*20*	*85*	*-37*	*47*	*46*	*0.42*					*20*
N30	*7.4408*	*43.8733*	*Quaternary*	*SS*	*139*	*-15*	*73*	*58*	*41*	*-28*	*0.39*					*20*
N31	*7.4922*	*43.9831*	*U. Cretaceous*	*SS*	*160*	*10*	*21*	*77*	*72*	*-8*	*0.78*					*20*
N32b	*7.4853*	*43.8233*	*U. Cretaceous*	*SS*	*156*	*-25*	*91*	*42*	*45*	*-38*	*0.35*					*20*
N34	*7.7836*	*43.8747*	*U. Cretaceous*	*SS*	*149*	*5*	*56*	*53*	*56*	*-37*	*0.28*					*20*
N35	*7.4364*	*43.9986*	*U. Cretaceous*	*SS*	*7*	*-29*	*46*	*55*	*108*	*-19*	*0.76*					*20*
N3b	*7.1911*	*43.8939*	*U. Jurassic*	*P*	*170*	*12*					*0.01*					*20*
N4	*7.2092*	*43.6883*	*L. Quaternary*	*P*	*35*	*-4*					*0.09*					*20*
N5	*7.2039*	*43.8617*	*M.U. Jurassic*	*P*	*161*	*5*	*74*	*-29*	*63*	*61*	*0.57*					*20*
N6b	*7.1969*	*43.8308*	*M. Jurassic*	*P*	*120*	*6*	*31*	*-3*			*0.61*					*20*
N7	*7.2289*	*43.8636*	*Pliocene*	*SS*	*142*	*16*	*0*	*70*	*55*	*-11*	*0.11*					*20*
N8b	*7.2325*	*43.8731*	*L. Cretaceous*	*P*	*148*	*-1*	*57*	*-13*	*64*	*77*	*0.3*					*20*
N9a	*7.335*	*43.9847*	*U. Cretaceous*	*SS*	*41*	*-5*			*2941*	*-4*	*0.59*					*20*
P25a	*5.4019*	*44.1753*	*Miocene*	*P*	*73*	*-8*	*163*	*3*			*0.38*					*20*
P29a	*5.9319*	*44.1644*	*L. Cretaceous*	*SS*	*67*	*-6*					*0.08*					*20*
P30a	*5.9372*	*44.1625*	*L. Cretaceous*	*P*	*34*	*15*	*123*	*-4*	*19*	*-75*	*0.41*					*20*
BARAI	*6.8263*	*44.5552*		*T*	*76*	*-83*	*33*	*5*	*123*	*5*	*0.4*	*15*				*21*

Site	Long.	Lat.	Age	Tectonic regime	σ_1 trend	σ_1 plunge	σ_2 trend	σ_2 plunge	σ_3 trend	σ_3 plunge	R	N	F	α	RUP	REF
BOUCH	*6.9492*	*44.6902*		*T*	*64*	*69*	*56*	*-21*	*147*	*-3*	*0.2*	*30*				*21*
CHABE	*6.759*	*44.973*		*T*	*13*	*-83*	*58*	*5*	*147*	*-5*	*0.4*	*21*				*21*
CHAMB	*6.8347*	*44.5413*		*T*	*32*	*67*	*34*	*-23*	*124*	*1*	*0.3*	*23*				*21*
CHESU	*6.7527*	*44.9123*		*T*	*81*	*-73*	*97*	*17*	*5*	*4*	*0.3*	*10*				*21*
COLRI	*6.5333*	*44.9342*		*T*	*54*	*-71*	*89*	*16*	*176*	*-1*	*0.3*	*19*				*21*
CPEYR	*6.6245*	*44.7763*		*T*	*84*	*82*	*67*	*-7*	*157*	*-3*	*0.2*	*30*				*21*
CROUS	*6.6552*	*44.7238*		*T*	*62*	*67*	*114*	*-15*	*19*	*-17*	*0.4*	*8*				*21*
GROOU	*6.6755*	*44.6593*		*T*	*38*	*-68*	*48*	*22*	*137*	*-4*	*0.2*	*27*				*21*
GROOU	*6.6755*	*44.6593*		*SS*	*39*	*-39*	*37*	*5*	*128*	*1*	*0.8*	*27*				*21*
JANES	*6.7385*	*44.9338*		*T*	*56*	*-70*	*53*	*19*	*143*	*1*	*0.5*	*11*				*21*
JANOU	*6.7535*	*44.9382*		*T*	*163*	*-81*	*70*	*0*	*160*	*9*	*0.4*	*13*				*21*
LAVAL	*6.8773*	*44.935*		*T*	*175*	*75*	*84*	*0*	*174*	*-15*	*0.4*	*22*				*21*
LCORD	*6.7688*	*44.841*		*T*	*24*	*-84*	*77*	*4*	*167*	*-5*	*0.4*	*13*				*21*
MLZOU	*6.6318*	*44.8422*		*T*	*91*	*52*	*52*	*-32*	*151*	*-14*	*0.2*	*30*				*21*
MLZSU	*6.6363*	*44.8327*		*T*	*97*	*62*	*78*	*-28*	*169*	*-28*	*0.1*	*12*				*21*
NEUFC	*6.7725*	*44.5713*		*T*	*101*	*-70*	*150*	*13*	*57*	*15*	*0.3*	*20*				*21*
PCHAT	*6.7878*	*44.54*		*T*	*30*	*-69*	*64*	*18*	*150*	*-11*	*0.1*	*29*				*21*
PSTRL	*6.7918*	*44.5793*		*T*	*38*	*-71*	*76*	*15*	*163*	*-11*	*0.2*	*14*				*21*
PTPUY	*6.6457*	*44.8325*		*T*	*118*	*-85*	*47*	*1*	*137*	*4*	*0.4*	*15*				*21*
RBLES	*6.5543*	*44.9083*		*T*	*101*	*72*	*67*	*-15*	*160*	*-9*	*0.5*	*45*				*21*
RBLOU	*6.5423*	*44.9083*		*T*	*132*	*-71*	*50*	*3*	*141*	*18*	*0.4*	*22*				*21*
RMOES	*6.6122*	*44.8347*		*T*	*72*	*-72*	*102*	*16*	*10*	*8*	*0.2*	*19*				*21*
RMOOU	*6.6175*	*44.84*		*T*	*65*	*-75*	*93*	*14*	*1*	*6*	*0.3*	*26*				*21*
TURGE	*6.7807*	*44.8288*		*T*	*1*	*-76*	*82*	*2*	*171*	*-14*	*0.5*	*25*				*21*
VLAUG	*6.7508*	*44.5945*		*T*	*145*	*-79*	*89*	*6*	*180*	*9*	*0.4*	*6*				*21*
VMARY	*6.8625*	*44.5702*		*T*	*50*	*73*	*26*	*-16*	*118*	*-7*	*0.4*	*17*				*21*
Undifferentiated Miocene to Quaternary																
Alex	*5.6283*	*46.2317*	*Valanginian*	*P*	*98*	*12*	*11*	*-15*	*149*	*-71*	*0.48*	*7*		*5*	*19*	*14*
Alex	*5.6283*	*46.2317*	*Valanginian*	*SS*	*125*	*-8*	*66*	*75*	*33*	*-13*	*0.08*	*33*		*7*	*40*	*14*
Arc.s Cion	*6.3533*	*47.05*	*Argov. to Raurac.*	*P*	*150*	*0*	*60*	*7*	*62*	*-83*	*0.51*	*6*		*23*	*45*	*14*
Arc.s Cion	*6.3533*	*47.05*	*Argov. to Raurac.*	*SS*	*174*	*10*	*21*	*79*	*85*	*-5*	*0.27*	*19*		*19*	*42*	*14*

Site	Long.	Lat.	Age	Tectonic regime	σ_1 trend	σ_1 plunge	σ_2 trend	σ_2 plunge	σ_3 trend	σ_3 plunge	R	N	F	α	RUP	REF
Arcine	*5.895*	*46.105*	*Rauracian*	*P*	*115*	*-16*	*28*	*10*	*150*	*71*	*0.77*	*4*		*5*	*18*	*14*
Arinthod	*5.5783*	*46.3917*	*Kimmeridg. Sequan.*	*SS*	*104*	*-7*	*95*	*83*	*14*	*-1*	*0.43*	*36*		*9*	*37*	*14*
Athose	*6.2967*	*47.0683*	*Portland. Kimmeridg.*	*SS*	*130*	*8*	*17*	*71*	*42*	*-18*	*0.10*	*9*		*13*	*36*	*14*
Bellefontaine	*6.0867*	*46.5533*	*Sequan. Argov.*	*SS*	*128*	*7*	*156*	*-82*	*39*	*-4*	*0.48*	*27*		*5*	*16*	*14*
Bessain	*5.83*	*46.7917*	*Bathonian*	*SS*	*118*	*38*	*111*	*-52*	*26*	*3*	*0.72*	*6*		*2*	*15*	*14*
Bessain	*5.83*	*46.7917*	*Bathonian*		*143*											*14*
Bois Amont	*6.1367*	*46.5417*	*Barrem. Kimmeridg.*	*P*	*131*	*0*	*41*	*-1*	*26*	*89*	*0.52*	*26*		*9*	*21*	*14*
Bois Amont	*6.1367*	*46.5417*	*Barrem. Kimmeridg.*	*SS*	*132*	*11*	*62*	*-61*	*36*	*27*	*0.14*	*17*		*17*	*44*	*14*
Boulu	*6.0117*	*46.4233*	*Valanginian*	*P*	*176*	*-24*	*84*	*-6*	*161*	*65*	*0.08*	*5*		*8*	*10*	*14*
Boulu	*6.0117*	*46.4233*	*Valanginian*	*P*	*122*	*13*	*32*	*1*	*117*	*-77*	*0.50*	*15*		*14*	*17*	*14*
Brey	*6.2567*	*46.75*	*Porland. Kimmeridg.*	*SS*	*164*	*2*	*50*	*85*	*74*	*-4*	*0.47*	*29*		*8*	*25*	*14*
Brey	*6.2567*	*46.75*	*Porland. Kimmeridg.*	*SS*	*104*	*2*	*1*	*80*	*15*	*-10*	*0.36*	*24*		*10*	*24*	*14*
Briod	*5.6333*	*46.655*	*Bathonian*	*SS*	*131*	*-14*	*129*	*76*	*41*	*-1*	*0.49*	*5*		*4*	*42*	*14*
Busy	*5.96*	*47.17*	*Rauracian*	*P*	*141*	*-12*	*50*	*-7*	*111*	*76*	*0.71*	*23*		*3*	*31*	*14*
Buvilly	*5.7317*	*46.855*	*Bathonian*	*SS*	*107*	*3*	*31*	*-79*	*16*	*10*	*0.31*	*6*		*17*	*41*	*14*
C. Crotenay	*5.9833*	*46.6567*	*Purbeck. Kimmeridg.*	*P*	*138*	*0*	*48*	*-7*	*52*	*83*	*0.47*	*11*		*8*	*23*	*14*
C. Crotenay	*5.9833*	*46.6567*	*Purbeck. Kimmeridg.*	*SS*	*127*	*-5*	*175*	*82*	*38*	*6*	*0.26*	*32*		*23*	*46*	*14*
C. Dombief	*5.9067*	*46.63*	*Kmmeridg. Bathon.*	*P*	*120*	*1*	*31*	*-12*	*24*	*78*	*0.34*	*6*		*8*	*27*	*14*
Cerdon	*5.4767*	*46.0817*	*Up. Oxfordian*	*SS*	*170*	*9*	*40*	*76*	*82*	*-11*	*0.67*	*6*		*12*	*28*	*14*
Cerdon	*5.4767*	*46.0817*	*Up. Oxfordian*	*P*	*101*	*-6*	*12*	*7*	*153*	*81*	*0.51*	*61*		*13*	*28*	*14*
Cernois	*6.19*	*46.6867*	*Up. Kimmeridgian*	*SS*	*138*	*5*	*38*	*63*	*50*	*-26*	*0.13*	*39*		*10*	*34*	*14*
Chaille	*6.0533*	*46.465*	*Purbeckian*	*P*	*120*	*0*	*30*	*12*	*30*	*-78*	*0.59*	*13*		*17*	*41*	*14*
Chaille	*6.0533*	*46.465*	*Purbeckian*	*SS*	*109*	*7*	*132*	*-83*	*20*	*-3*	*0.46*	*49*		*15*	*36*	*14*
Champagnole	*5.9183*	*46.7533*	*Argovian*	*P*	*128*	*-5*	*39*	*10*	*13*	*-79*	*0.11*	*9*		*9*	*21*	*14*
Charchilla	*5.7133*	*46.455*	*Up. Kimmeridgian*	*SS*	*107*	*1*	*22*	*-74*	*17*	*16*	*0.25*	*47*		*12*	*26*	*14*
Chasse	*5.6133*	*46.6183*	*Bathonian*	*SS*	*136*	*-11*	*91*	*74*	*44*	*-11*	*0.21*	*9*		*3*	*55*	*14*
Chasse	*5.6133*	*46.6183*	*Bathonian*		*146*											*14*
Châtel J.	*5.7967*	*46.525*	*Kimmeridgian*	*SS*	*123*	*9*	*96*	*-79*	*32*	*5*	*0.48*	*26*		*12*	*44*	*14*
Chaumusse	*5.925*	*46.5867*	*Portlandian*	*SS*	*120*	*7*	*2*	*75*	*31*	*-13*	*0.32*	*13*		*11*	*37*	*14*
Cherezy	*5.8267*	*46.1817*	*Aptian Barremian*	*P*	*112*	*-6*	*23*	*5*	*153*	*82*	*0.54*	*20*		*5*	*18*	*14*
Chevrotaine	*5.84*	*46.66*	*Sequanian*	*TP*	*161*	*-9*	*86*	*56*	*66*	*-32*	*0.36*	*20*		*9*	*29*	*14*

Site	Long.	Lat.	Age	Tectonic regime	σ_1 trend	σ_1 plunge	σ_2 trend	σ_2 plunge	σ_3 trend	σ_3 plunge	R	N	F	α	RUP	REF
Choux	*5.7717*	*46.2883*	*Sequanian*	*SS*	*97*	*5*	*167*	*-75*	*8*	*-14*	*0.18*	*26*		*10*	*36*	*14*
Choux	*5.7717*	*46.2883*	*Sequanian*	*SS*	*74*	*0*	*157*	*-89*	*164*	*1*	*0.29*	*25*		*11*	*24*	*14*
Choux	*5.7717*	*46.2883*	*Sequanian*	*SS*	*39*	*-6*	*102*	*77*	*130*	*-12*	*0.23*	*26*		*8*	*21*	*14*
Cht Joux	*6.3733*	*46.8717*	*Low. Kimmeridgian*	*P*	*125*	*14*	*37*	*-18*	*178*	*-67*	*0.64*	*6*		*6*	*25*	*14*
Cht Joux	*6.3733*	*46.8717*	*Low. Kimmeridgian*	*SS*	*124*	*0*	*35*	*84*	*34*	*-6*	*0.34*	*10*		*15*	*38*	*14*
Cht Près	*5.9017*	*46.515*	*Portland. Kimmeridg.*	*P*	*161*	*-15*	*72*	*3*	*173*	*75*	*0.47*	*9*		*8*	*25*	*14*
Cinquétral	*5.8817*	*46.4233*	*Valanginian*	*P*	*142*	*4*	*52*	*5*	*94*	*-83*	*0.51*	*43*		*16*	*35*	*14*
Cize	*5.92*	*46.72*	*Low. Call.-Bath.*		*137*											*14*
Clairvaux	*5.7617*	*46.5617*	*Sequanian*	*SS*	*111*	*-1*	*37*	*88*	*21*	*-2*	*0.33*	*25*		*7*	*26*	*14*
Clées	*6.4683*	*46.73*	*Hauteriv. Valangin.*	*P*	*151*	*-4*	*62*	*10*	*40*	*-79*	*0.39*	*7*		*13*	*29*	*14*
Cogna	*5.7683*	*46.5967*	*Kimmeridg. Sequan.*	*SS*	*146*	*1*	*48*	*86*	*56*	*-4*	*0.31*	*70*		*9*	*23*	*14*
Coiselet	*5.595*	*46.295*	*Rauracian*	*P*	*126*	*-1*	*36*	*-9*	*41*	*81*	*0.50*	*23*		*10*	*30*	*14*
Col Savine	*6.005*	*46.565*	*Kimmeridgian*	*P*	*134*	*6*	*42*	*11*	*73*	*-77*	*0.55*	*9*		*10*	*38*	*14*
Col Savine	*6.005*	*46.565*	*Kimmeridgian*	*SS*	*111*	*1*	*14*	*80*	*21*	*-9*	*0.46*	*46*		*10*	*34*	*14*
Contrevoz	*5.61*	*45.835*	*Valanginian*	*P*	*93*	*10*	*2*	*1*	*88*	*-80*	*0.84*	*13*		*14*	*39*	*14*
Crouzet	*6.01*	*46.9617*	*Low. Callovian*	*P*	*162*	*-7*	*74*	*17*	*50*	*-72*	*0.20*	*23*		*0*	*26*	*14*
Cuisia	*5.4117*	*46.535*	*Bathonian*	*TP*	*34*	*-9*	*114*	*49*	*132*	*-39*	*0.35*	*8*		*11*	*42*	*14*
Cuisia	*5.4117*	*46.535*	*Bathonian*	*P*	*116*	*-8*	*25*	*-8*	*71*	*79*	*0.43*	*20*		*12*	*29*	*14*
Cuisia	*5.4117*	*46.535*	*Bathonian*	*SS*	*111*	*6*	*64*	*-81*	*20*	*6*	*0.51*	*31*		*18*	*42*	*14*
Cuvier	*5.035*	*46.83*			*125*											*14*
Dortan	*5.69*	*46.34*	*Portland. Kimmeridg.*	*SS*	*99*	*2*	*175*	*-83*	*10*	*-7*	*0.34*	*57*		*11*	*32*	*14*
Ecrille	*5.6533*	*46.4983*	*Oxford. Kimmerid.*	*P*	*109*	*1*	*19*	*0*	*104*	*-89*	*0.51*	*18*		*9*	*17*	*14*
Etraches	*6.41*	*46.9283*	*Barremian*	*P*	*151*	*0*	*61*	*9*	*64*	*-81*	*0.35*	*20*		*14*	*33*	*14*
Etraches	*6.41*	*46.9283*	*Barremian*	*SS*	*148*	*-5*	*70*	*67*	*56*	*-22*	*0.32*	*44*		*12*	*28*	*14*
Fallerans	*6.2883*	*47.13*	*Kimmeridgian*	*SS*	*143*	*1*	*51*	*74*	*53*	*-16*	*0.27*	*9*		*6*	*26*	*14*
Foncine b	*6.025*	*46.6283*	*Valanginian*	*SS*	*126*	*19*	*163*	*-67*	*40*	*-13*	*0.09*	*24*		*5*	*33*	*14*
Foncine h	*6.0483*	*46.6667*	*Sequanian*	*SS*	*148*	*-19*	*157*	*71*	*59*	*3*	*0.65*	*13*		*10*	*32*	*14*
Forges	*5.94*	*46.72*	*Bathonian*		*145*											*14*
Fourgs	*6.4033*	*46.835*	*Port. -Up. Kimme.*	*TP*	*149*	*7*	*55*	*29*	*71*	*-60*	*0.22*	*10*		*9*	*34*	*14*
Gémissiat	*5.8017*	*46.0517*	*Aptian Barremian*	*SS*	*107*	*1*	*57*	*-88*	*17*	*2*	*0.23*	*30*		*13*	*35*	*14*
Giron	*5.76*	*46.2183*	*Kimmeridgian*	*SS*	*110*	*-5*	*6*	*-71*	*21*	*18*	*0.30*	*11*		*8*	*23*	*14*

Site	Long.	Lat.	Age	Tectonic regime	σ_1 trend	σ_1 plunge	σ_2 trend	σ_2 plunge	σ_3 trend	σ_3 plunge	R	N	F	α	RUP	REF
Giron	*5.76*	*46.2183*	*Kimmeridgian*	*SS*	*57*	*-3*	*176*	*-83*	*146*	*6*	*0.15*	*16*		*14*	*33*	*14*
Golisse	*6.25*	*46.625*	*Port. -Up. Kimme.*	*P*	*141*	*-2*	*50*	*-13*	*61*	*77*	*0.42*	*9*		*13*	*31*	*14*
Gouland	*6.0317*	*46.4917*	*Sequanian*	*SS*	*168*	*-3*	*72*	*-63*	*60*	*26*	*0.31*	*9*		*14*	*31*	*14*
Gouland	*6.0317*	*46.4917*	*Sequanian*	*TP*	*116*	*8*	*14*	*57*	*31*	*-32*	*0.15*	*17*		*20*	*48*	*14*
Goux	*6.29*	*46.9733*	*Port. -Up. Kimme.*	*P*	*125*	*-2*	*35*	*7*	*21*	*-82*	*0.53*	*13*		*8*	*22*	*14*
Goux	*6.29*	*46.9733*	*Port. -Up. Kimme.*	*SS*	*145*	*-2*	*74*	*82*	*55*	*-7*	*0.42*	*13*		*16*	*34*	*14*
Grusse	*5.5083*	*46.6*	*Oxfordian Bathonian*	*P*	*123*	*5*	*33*	*-3*	*156*	*-85*	*0.49*	*17*		*17*	*32*	*14*
Grusse	*5.5083*	*46.6*	*Oxfordian Bathonian*	*SS*	*106*	*-4*	*4*	*-72*	*17*	*17*	*0.44*	*20*		*16*	*35*	*14*
Hérisson	*5.8683*	*46.6*	*Valangin. Purbeck.*	*SS*	*126*	*2*	*137*	*-87*	*36*	*0*	*0.46*	*12*		*7*	*27*	*14*
Hôpithaux	*6.3633*	*46.795*	*Port. -Up. Kimme.*	*SS*	*111*	*-4*	*58*	*84*	*21*	*-5*	*0.54*	*34*		*14*	*34*	*14*
Hôpithaux	*6.3633*	*46.795*	*Port. -Up. Kimme.*	*SS*	*66*	*-14*	*8*	*65*	*151*	*20*	*0.21*	*5*		*7*	*23*	*14*
Jalinard	*5.6717*	*46.0517*	*Portlandian*	*SS*	*98*	*22*	*98*	*-68*	*8*	*0*	*0.41*	*11*		*13*	*28*	*14*
Jougne E1	*6.385*	*46.7567*	*Port. -Up. Kimme.*	*SS*	*104*	*24*	*77*	*-63*	*9*	*11*	*0.71*	*14*		*9*	*30*	*14*
Jougne E1	*6.385*	*46.7567*	*Port. -Up. Kimme.*	*P*	*161*	*-10*	*73*	*13*	*36*	*-74*	*0.33*	*14*		*15*	*34*	*14*
Jougne E1	*6.385*	*46.7567*	*Port. -Up. Kimme.*	*SS*	*169*	*-7*	*65*	*-65*	*82*	*24*	*0.35*	*8*		*10*	*33*	*14*
Jougne S	*6.375*	*46.74*	*Low. Kimmeridgian*	*SS*	*164*	*-6*	*62*	*-64*	*77*	*25*	*0.27*	*12*		*20*	*42*	*14*
Jougne S	*6.375*	*46.74*	*Low. Kimmeridgian*	*SS*	*129*	*3*	*44*	*-61*	*38*	*29*	*0.18*	*21*		*13*	*39*	*14*
Lajoux	*5.945*	*46.375*	*Rauracian*	*SS*	*134*	*-7*	*176*	*81*	*45*	*6*	*0.39*	*29*		*10*	*24*	*14*
Larmont	*6.3883*	*46.89*	*Sequanian*	*P*	*103*	*-5*	*13*	*-4*	*66*	*84*	*0.68*	*4*		*14*	*29*	*14*
Larmont	*6.3883*	*46.89*	*Sequanian*	*SS*	*148*	*2*	*63*	*-73*	*57*	*17*	*0.41*	*19*		*9*	*23*	*14*
Lavans	*5.7983*	*46.385*	*Purbeckian*	*P*	*125*	*4*	*34*	*8*	*59*	*-81*	*0.48*	*25*		*7*	*20*	*14*
Lavans	*5.7983*	*46.385*	*Purbeckian*	*SS*	*117*	*12*	*82*	*-87*	*27*	*1*	*0.34*	*49*		*9*	*37*	*14*
Lemme	*5.9567*	*46.625*	*Kimmeridgian*	*SS*	*99*	*-2*	*155*	*87*	*9*	*2*	*0.26*	*30*		*12*	*30*	*14*
Lemuy	*5.96*	*46.9*	*Callovian*		*140*											*14*
Lent	*5.9683*	*46.755*	*Kimmeridgian*	*P*	*153*	*3*	*63*	*-14*	*51*	*75*	*0.17*	*19*		*12*	*32*	*14*
Lessus	*6.4817*	*47.07*	*Rauracian*	*P*	*160*	*-9*	*66*	*-22*	*91*	*66*	*0.13*	*5*		*6*	*24*	*14*
Lessus	*6.4817*	*47.07*	*Rauracian*	*SS*	*127*	*3*	*165*	*-86*	*37*	*-2*	*0.29*	*26*		*7*	*26*	*14*
Levier	*6.14*	*46.96*	*Sequanian*	*SS*	*139*	*1*	*13*	*88*	*49*	*-1*	*0.44*	*8*		*6*	*35*	*14*
Longchaumois	*5.94*	*46.46*	*Barrem. to Valangin.*	*P*	*138*	*-6*	*49*	*4*	*171*	*83*	*0.51*	*14*		*10*	*24*	*14*
Luisans	*6.5233*	*47.0915*	*Kimmeridgian*	*P*	*156*	*-14*	*65*	*-8*	*127*	*74*	*0.65*	*5*		*4*	*31*	*14*
Main	*6.3283*	*47.01*	*Sequanian*	*P*	*119*	*-14*	*28*	*-3*	*106*	*76*	*0.71*	*7*		*8*	*261*	*14*

Site	Long.	Lat.	Age	Tectonic regime	σ_1 trend	σ_1 plunge	σ_2 trend	σ_2 plunge	σ_3 trend	σ_3 plunge	R	N	F	α	RUP	REF
Main	*6.3283*	*47.01*	*Sequanian*	*SS*	*109*	*-26*	*119*	*64*	*21*	*4*	*0.55*	*13*		*11*	*34*	*14*
Maisières	*6.1*	*47.1083*	*Bathonian*	*SS*	*119*	*-5*	*62*	*81*	*28*	*-8*	*0.72*	*6*		*1*	*45*	*14*
Marchairuz	*6.2767*	*46.545*	*Portland. Kimmeridg.*	*SS*	*166*	*8*	*146*	*-82*	*75*	*3*	*0.63*	*7*		*4*	*11*	*14*
Marchairuz	*6.2767*	*46.545*	*Portland. Kimmeridg.*	*SS*	*111*	*-2*	*27*	*73*	*21*	*-17*	*0.17*	*14*		*8*	*25*	*14*
Meix	*5.67*	*46.52*	*Up. Kimmeridg.*	*SS*	*120*	*-1*	*34*	*74*	*29*	*-16*	*0.11*	*12*		*9*	*32*	*14*
Meussia	*5.7267*	*46.4817*	*Low. Kimmeridgian*	*TP*	*109*	*-1*	*18*	*-42*	*20*	*48*	*0.14*	*8*		*7*	*21*	*14*
Moirans	*5.7267*	*46.4133*	*Sequan. Raurac.*	*P*	*72*	*3*	*162*	*-2*	*43*	*-87*	*0.47*	*27*		*15*	*36*	*14*
Moirans	*5.7267*	*46.4133*	*Sequan. Raurac.*	*SS*	*68*	*2*	*151*	*-77*	*159*	*12*	*0.44*	*22*		*16*	*38*	*14*
Mollendruz	*6.3533*	*46.6383*	*Purbeck. Valangin.*	*SS*	*111*	*10*	*50*	*-71*	*18*	*16*	*0.30*	*33*		*15*	*33*	*14*
Mont	*6.3817*	*46.6483*	*Valanginian.*	*P*	*147*	*-4*	*56*	*-10*	*79*	*79*	*0.56*	*14*		*9*	*23*	*14*
Mont	*6.3817*	*46.6483*	*Valanginian.*	*SS*	*137*	*11*	*171*	*-77*	*48*	*-7*	*0.09*	*21*		*12*	*37*	*14*
Montanges	*5.7867*	*46.155*	*Hauterivian*	*SS*	*118*	*14*	*81*	*-73*	*25*	*10*	*0.14*	*4*		*9*	*22*	*14*
Montanges	*5.7867*	*46.155*	*Hauterivian*	*P*	*108*	*10*	*16*	*10*	*62*	*-75*	*0.40*	*27*		*9*	*41*	*14*
Montront	*6.3433*	*46.745*	*Low. Kimmeridg.*	*SS*	*165*	*-13*	*30*	*-72*	*78*	*12*	*0.23*	*14*		*12*	*28*	*14*
Morbier	*6.01*	*46.5367*	*Portlandian*	*SS*	*120*	*24*	*119*	*-66*	*30*	*0*	*0.93*	*58*		*13*	*40*	*14*
Mortes	*6.0817*	*46.5683*	*Raurac. Argov.*	*P*	*130*	*-13*	*42*	*6*	*158*	*76*	*0.62*	*9*		*4*	*14*	*14*
Mortes	*6.0817*	*46.5683*	*Raurac. Argov.*	*SS*	*144*	*-6*	*111*	*83*	*54*	*-4*	*0.36*	*23*		*5*	*15*	*14*
Mouille	*5.9867*	*46.5133*	*Portlandian*	*SS*	*101*	*-6*	*68*	*83*	*11*	*-4*	*0.47*	*14*		*7*	*26*	*14*
Mouthe N	*6.1833*	*46.7167*	*Rauracian*	*P*	*134*	*11*	*42*	*10*	*27*	*75*	*0.51*	*19*		*14*	*35*	*14*
Mouthe S	*6.1717*	*46.7*	*Portland. Kimmeridg.*	*P*	*122*	*-10*	*32*	*-1*	*118*	*80*	*0.46*	*17*		*11*	*33*	*14*
Mouthier	*6.2833*	*47.0367*	*Low.- Mid. Baj.*	*SS*	*130*	*-2*	*37*	*-65*	*41*	*25*	*0.18*	*16*		*8*	*30*	*14*
Mt Noir	*6.0233*	*46.605*	*Sequanian*	*SS*	*173*	*10*	*144*	*-79*	*82*	*5*	*0.60*	*5*		*15*	*27*	*14*
Mt Noir	*6.0233*	*46.605*	*Sequanian*	*P*	*137*	*17*	*46*	*3*	*127*	*-73*	*0.54*	*6*		*4*	*15*	*14*
Nantua	*5.6933*	*46.165*	*Sequanian*	*SS*	*131*	*3*	*50*	*-73*	*40*	*16*	*0.28*	*26*		*12*	*43*	*14*
Nantua	*5.6933*	*46.165*	*Sequanian*	*SS*	*60*	*-18*	*79*	*71*	*151*	*-6*	*0.78*	*9*		*8*	*21*	*14*
Neuve	*6.39*	*47.0867*	*Sequanian*	*P*	*12*	*13*	*100*	*-9*	*155*	*74*	*0.52*	*5*		*7*	*21*	*14*
Neuve	*6.39*	*47.0867*	*Sequanian*	*SS*	*169*	*-7*	*60*	*-68*	*82*	*21*	*0.46*	*13*		*7*	*37*	*14*
Ney	*5.83*	*46.79*	*Sequanian*	*SS*	*136*	*10*	*168*	*-78*	*47*	*-6*	*0.75*	*13*		*9*	*22*	*14*
Nods	*6.3517*	*47.0817*	*Up. Bajocian*	*P*	*147*	*5*	*57*	*2*	*121*	*-85*	*0.50*	*10*		*6*	*31*	*14*
Nods	*6.3517*	*47.0817*	*Up. Bajocian*	*SS*	*132*	*-10*	*95*	*77*	*41*	*-7*	*0.21*	*22*		*1*	*35*	*14*
Pannessières	*5.6083*	*46.7*	*Bathonian*	*SS*	*112*	*3*	*150*	*-86*	*22*	*-3*	*0.29*	*8*		*12*	*25*	*14*

Site	Long.	Lat.	Age	Tectonic regime	σ_1 trend	σ_1 plunge	σ_2 trend	σ_2 plunge	σ_3 trend	σ_3 plunge	R	N	F	α	RUP	REF
Planches	*6.0133*	*46.6483*	*Kimmeridgian*	*P*	*154*	*7*	*64*	*-6*	*15*	*81*	*0.41*	*10*		*10*	*23*	*14*
Planches	*6.0133*	*46.6483*	*Kimmeridgian*	*SS*	*2*	*-32*	*24*	*56*	*98*	*-10*	*0.35*	*6*		*11*	*31*	*14*
Planches	*6.0133*	*46.6483*	*Kimmeridgian*	*SS*	*116*	*37*	*92*	*-51*	*17*	*12*	*0.44*	*11*		*16*	*50*	*14*
Poligny est	*5.7417*	*46.82*	*Low.- Mid. Baj.*		*141*											*14*
Poligny ouest	*5.72*	*46.83*	*Mid. Baj.-Aalen.*	*SS*	*145*	*-21*	*141*	*69*	*54*	*-1*	*0.72*	*5*		*10*	*43*	*14*
Poncets	*5.945*	*46.5583*	*Barremian*	*SS*	*114*	*8*	*38*	*-59*	*20*	*29*	*0.13*	*33*		*14*	*41*	*14*
Pontarlier	*6.3617*	*46.895*	*Low. Kimmeridgian*	*TP*	*160*	*-7*	*73*	*26*	*56*	*-63*	*0.06*	*20*		*14*	*40*	*14*
Pontarlier	*6.3617*	*46.895*	*Low. Kimmeridgian*	*SS*	*112*	*-13*	*98*	*76*	*21*	*-3*	*0.38*	*22*		*15*	*38*	*14*
Raviolle	*5.7733*	*46.3983*	*Portland. Kimmeridg.*	*SS*	*164*	*12*	*94*	*-59*	*68*	*29*	*0.14*	*9*		*12*	*30*	*14*
Raviolle	*5.7733*	*46.3983*	*Portland. Kimmeridg.*	*P*	*135*	*15*	*45*	*3*	*125*	*-75*	*0.61*	*35*		*9*	*24*	*14*
Raviolle	*5.7733*	*46.3983*	*Portland. Kimmeridg.*	*SS*	*124*	*15*	*97*	*-73*	*32*	*8*	*0.29*	*15*		*18*	*43*	*14*
Repentys	*5.9767*	*46.475*	*Hauterivian*	*P*	*134*	*11*	*43*	*2*	*124*	*-79*	*0.47*	*14*		*7*	*20*	*14*
Risol	*6.2067*	*46.6533*	*Low. Kimmeridgian*	*SS*	*134*	*-1*	*35*	*-82*	*44*	*8*	*0.33*	*17*		*5*	*11*	*14*
Rixouse	*5.865*	*46.45*	*Portlandian*	*SS*	*129*	*8*	*145*	*-82*	*39*	*-2*	*0.42*	*62*		*8*	*31*	*14*
Ronchaux	*5.7867*	*46.4917*	*Portland. Kimmeridg.*	*P*	*140*	*-6*	*50*	*7*	*8*	*-80*	*0.51*	*18*		*18*	*36*	*14*
Ronchaux	*5.7867*	*46.4917*	*Portland. Kimmeridg.*	*SS*	*123*	*3*	*72*	*-85*	*33*	*4*	*0.23*	*17*		*10*	*27*	*14*
Rousses	*6.0617*	*46.4817*	*Valangin. Portland.*	*P*	*136*	*3*	*47*	*-8*	*29*	*81*	*0.52*	*17*		*14*	*31*	*14*
Rousses	*6.0617*	*46.4817*	*Valangin. Portland.*	*SS*	*131*	*2*	*55*	*-82*	*41*	*8*	*0.43*	*52*		*15*	*36*	*14*
Scancia	*5.585*	*46.4833*	*Up. Oxfordian*	*SS*	*95*	*14*	*118*	*-75*	*7*	*-3*	*0.23*	*15*		*7*	*24*	*14*
Scey	*6.06*	*47.0967*	*Bathonian*	*SS*	*159*	*-5*	*19*	*-84*	*70*	*4*	*0.46*	*20*		*4*	*37*	*14*
Scey	*6.06*	*47.0967*	*Bathonian*	*SS*	*105*	*0*	*3*	*88*	*15*	*-2*	*0.39*	*7*		*4*	*36*	*14*
Serrières	*5.4517*	*46.1517*	*Rauracian*	*SS*	*76*	*15*	*29*	*-69*	*162*	*-15*	*0.48*	*13*		*15*	*35*	*14*
Serrières	*5.4517*	*46.1517*	*Rauracian*	*P*	*108*	*-13*	*16*	*-6*	*81*	*75*	*0.64*	*16*		*10*	*19*	*14*
Sirod	*5.9783*	*46.7217*	*Portlandian*	*SS*	*128*	*-7*	*170*	*81*	*38*	*6*	*0.28*	*12*		*3*	*11*	*14*
Soucia	*5.755*	*46.535*	*Up. Oxfordian*	*SS*	*118*	*-2*	*43*	*84*	*28*	*-6*	*0.25*	*17*		*7*	*22*	*14*
St Amour	*5.36*	*46.4267*	*Up. Bajocian*	*TP*	*134*	*10*	*36*	*41*	*55*	*-47*	*0.06*	*6*		*12*	*34*	*14*
St Amour	*5.36*	*46.4267*	*Up. Bajocian*	*TP*	*75*	*8*	*175*	*52*	*160*	*-37*	*0.22*	*25*		*13*	*34*	*14*
St Claude	*5.8583*	*46.395*	*Portlandian*	*P*	*116*	*7*	*25*	*1*	*103*	*-83*	*0.60*	*41*		*16*	*36*	*14*
St Croix	*6.4967*	*46.8317*		*SS*	*121*	*-13*	*146*	*76*	*33*	*5*	*0.29*	*20*		*16*	*40*	*14*
St Georges	*6.2733*	*46.525*	*Aptian Barremian*	*SS*	*110*	*5*	*2*	*73*	*21*	*-16*	*0.49*	*8*		*13*	*36*	*14*
St Julien	*5.4383*	*46.405*	*Bathonian Bajocian*	*SS*	*112*	*6*	*60*	*-80*	*21*	*8*	*0.37*	*12*		*11*	*38*	*14*

Site	Long.	Lat.	Age	Tectonic regime	σ_1 trend	σ_1 plunge	σ_2 trend	σ_2 plunge	σ_3 trend	σ_3 plunge	R	N	F	α	RUP	REF
St Julien	*5.4383*	*46.405*	*Bathonian Bajocian*	*P*	*99*	*-14*	*12*	*14*	*147*	*70*	*0.50*	*13*		*9*	*25*	*14*
St Maurice	*5.8333*	*46.5517*	*Sequanian*	*SS*	*168*	*-3*	*61*	*-80*	*78*	*9*	*0.58*	*11*		*17*	*32*	*14*
St Point	*6.28*	*46.79*	*Hauterivian*	*SS*	*107*	*-12*	*74*	*76*	*16*	*-8*	*0.43*	*30*		*15*	*33*	*14*
Suchet	*6.5083*	*46.8*	*Argov. Oxford.*	*SS*	*107*	*-3*	*32*	*77*	*17*	*-12*	*0.56*	*7*		*13*	*28*	*14*
Syam	*5.96*	*46.68*	*Kimmeridgian*	*SS*	*106*	*-2*	*177*	*84*	*16*	*6*	*0.51*	*10*		*5*	*22*	*14*
Tancua	*5.955*	*46.5067*	*Hauterivian*	*P*	*146*	*1*	*56*	*-5*	*45*	*85*	*0.49*	*23*		*7*	*22*	*14*
Thévenins	*5.995*	*46.605*	*Barremian*	*SS*	*122*	*-1*	*21*	*-86*	*32*	*4*	*0.40*	*18*		*10*	*41*	*14*
Treffort	*5.3583*	*46.2667*	*Argovian*	*SS*	*53*	*14*	*18*	*-73*	*140*	*-9*	*0.78*	*19*		*9*	*31*	*14*
Treffort	*5.3583*	*46.2667*	*Argovian*	*SS*	*108*	*-7*	*86*	*82*	*17*	*-3*	*0.45*	*33*		*6*	*22*	*14*
Valempoulières	*5.8617*	*46.83*	*Argovian*	*SS*	*150*	*1*	*71*	*-87*	*60*	*3*	*0.30*	*24*		*8*	*25*	*14*
Vallorbe	*6.3433*	*46.7*	*Sequan. Raurac.*	*SS*	*118*	*2*	*165*	*-88*	*28*	*-2*	*0.38*	*52*		*10*	*27*	*14*
Vaulion S	*6.3483*	*46.6567*	*Low. Kimmeridgian*	*SS*	*9*	*-11*	*129*	*-68*	*95*	*18*	*0.47*	*20*		*10*	*32*	*14*
Vaux	*6.2367*	*46.82*	*Low. Kimmeridgian*	*P*	*140*	*-3*	*50*	*-4*	*89*	*85*	*0.35*	*9*		*9*	*32*	*14*
Vaux	*6.2367*	*46.82*	*Low. Kimmeridgian*	*SS*	*145*	*2*	*65*	*-79*	*55*	*10*	*0.23*	*18*		*9*	*32*	*14*
Verrière	*6.4317*	*46.8867*	*Hauterivian*	*P*	*139*	*1*	*49*	*5*	*57*	*-85*	*0.50*	*31*		*9*	*22*	*14*
Verrière	*6.4317*	*46.8867*	*Hauterivian*	*SS*	*131*	*1*	*35*	*79*	*42*	*-11*	*0.13*	*18*		*17*	*38*	*14*
				Quaternary												
S1	*6*	*44.0861*	*Oligocene*	*P*	*157*	*0*	*67*	*0*	*256*	*90*	*0.93*					*1*
S1	*6*	*44.0861*	*Oligocene*	*P*	*157*	*0*	*67*	*0*	*256*	*90*	*0.93*					*1*
S10	*5.8911*	*43.9231*	*Tortonien*	*P*	*135*	*0*	*45*	*0*	*315*	*90*	*0.31*					*1*
S10	*5.8911*	*43.9231*	*Tortonien*	*P*	*135*	*0*	*45*	*0*	*315*	*90*	*0.31*					*1*
S11	*5.8908*	*43.9231*	*Rissian*	*P*	*332*	*18*	*242*	*2*	*147*	*72*	*0.46*					*1*
S11	*5.8908*	*43.9231*	*Rissian*	*P*	*332*	*18*	*242*	*2*	*147*	*72*	*0.46*					*1*
S12a	*5.8528*	*43.9033*	*Up. Oligocene*	*TP*	*358*	*5*	*91*	*39*	*262*	*51*	*0.53*					*1*
S12a	*5.8528*	*43.9033*	*Up. Oligocene*	*TP*	*358*	*5*	*91*	*39*	*262*	*51*	*0.53*					*1*
S13a	*5.8036*	*43.85*	*Tortonien*	*P*	*154*	*0*	*64*	*0*	*295*	*90*	*0.57*					*1*
S13a	*5.8036*	*43.85*	*Tortonien*	*P*	*154*	*0*	*64*	*0*	*295*	*90*	*0.57*					*1*
S14	*5.8333*	*43.8492*	*Wurmian*	*P*	*159*	*2*	*250*	*21*	*64*	*68*	*0.65*					*1*
S14	*5.8333*	*43.8492*	*Wurmian*	*P*	*159*	*2*	*250*	*21*	*64*	*68*	*0.65*					*1*
S15a	*5.7933*	*43.8464*	*Vindobonian*	*P*	*148*	*0*	*58*	*0*	*271*	*90*	*0.85*					*1*
S15a	*5.7933*	*43.8464*	*Vindobonian*	*P*	*148*	*0*	*58*	*0*	*271*	*90*	*0.85*					*1*

Site	Long.	Lat.	Age	Tectonic regime	σ_1 trend	σ_1 plunge	σ_2 trend	σ_2 plunge	σ_3 trend	σ_3 plunge	R	N	F	α	RUP	REF
S16	*5.7825*	*43.795*	*Pliocene*	*P*	*146*	*0*	*56*	*0*	*294*	*90*	*0.69*					*1*
S16	*5.7825*	*43.795*	*Pliocene*	*P*	*146*	*0*	*56*	*0*	*294*	*90*	*0.69*					*1*
S17	*5.7183*	*43.7139*	*Pliocene*		*140*	*0*										*1*
S17	*5.7183*	*43.7139*	*Pliocene*		*140*	*0*										*1*
S18	*5.5447*	*43.6414*	*Berriasian*	*P*	*210*	*10*	*118*	*14*	*335*	*73*	*0.41*					*1*
S18	*5.5447*	*43.6414*	*Berriasian*	*P*	*210*	*10*	*118*	*14*	*335*	*73*	*0.41*					*1*
S2	*5.9942*	*44.0817*	*Oligcene*	*P*	*151*	*0*	*241*	*9*	*64*	*81*	*0.8*					*1*
S2	*5.9942*	*44.0817*	*Oligocene*	*P*	*151*	*0*	*241*	*9*	*64*	*81*	*0.8*					*1*
S3	*5.9969*	*44.0667*	*Tortonien*	*P*	*26*	*0*	*116*	*0*	*299*	*90*	*0.85*					*1*
S3	*5.9969*	*44.0667*	*Tortonien*	*P*	*26*	*0*	*116*	*0*	*299*	*90*	*0.85*					*1*
S4a	*5.9817*	*44.0308*	*Tortonien*	*P*	*9*	*6*	*278*	*11*	*127*	*78*	*0.42*					*1*
S4a	*5.9817*	*44.0308*	*Tortonien*	*P*	*9*	*6*	*278*	*11*	*127*	*78*	*0.42*					*1*
S5a	*5.91*	*44.0081*	*Oligcene*	*P*	*153*	*0*	*63*	*0*	*301*	*90*	*0.47*					*1*
S5a	*5.91*	*44.0081*	*Oligocene*	*P*	*153*	*0*	*63*	*0*	*301*	*90*	*0.47*					*1*
S6	*5.9053*	*43.9892*	*Oligcene*	*TP*	*158*	*18*	*275*	*54*	*57*	*30*	*0.71*					*1*
S6	*5.9053*	*43.9892*	*Oligocene*	*TP*	*158*	*18*	*275*	*54*	*57*	*30*	*0.71*					*1*
S7	*5.9053*	*43.9781*	*Oligcene*	*P*	*176*	*13*	*86*	*1*	*349*	*77*	*0.74*					*1*
S7	*5.9053*	*43.9781*	*Oligocene*	*P*	*176*	*13*	*86*	*1*	*349*	*77*	*0.74*					*1*
S8	*5.88*	*43.9489*	*Pliocene*	*P*	*152*	*0*	*62*	*11*	*241*	*79*	*0.91*					*1*
S8	*5.88*	*43.9489*	*Pliocene*	*P*	*152*	*0*	*62*	*11*	*241*	*79*	*0.91*					*1*
S9a	*5.8639*	*43.9336*	*Oligcene*	*SS*	*334*	*4*	*76*	*70*	*243*	*19*	*0.80*					*1*
S9a	*5.8639*	*43.9336*	*Oligocene*	*SS*	*334*	*4*	*76*	*70*	*243*	*19*	*0.80*					*1*
BBZ1	*5.9863*	*45.3384*	*Middle Jurassique*	*SS*	*75*	*-4*	*151*	*75*	*166*	*-15*	*0.35*	*17*		*7*	*19*	*3*
BBZ2	*5.9344*	*45.2661*	*Middle Jurassique*	*SS*	*80*	*-4*	*163*	*63*	*172*	*-27*	*0.433*	*40*		*9*	*24*	*3*
BBZ3	*5.8723*	*45.2164*	*Middle Jurassique*	*SS*	*83*	*-18*	*128*	*66*	*178*	*-16*	*0.677*	*8*		*7*	*16*	*3*
BOZONS	*4.9453*	*44.806*	*Pliocene sup*	*SS*	*82*	*13*	*18*	*-62*	*166*	*24*	*0.449*	*8*		*8*	*28*	*4*
ALLIMAS1	*5.5632*	*44.8813*	*Hauterivien*	*SS*	*79*	*9*	*12*	*-68*	*166*	*-20*	*0.269*	*13*		*12*	*26*	*5*
ALLIMAS2	*5.5622*	*44.8807*	*Hauterivien*	*SS*	*76*	*-3*	*12*	*83*	*166*	*6*	*0.501*	*9*		*15*	*29*	*5*
BATIE	*5.5586*	*44.8596*	*Tithonique*	*SS*	*80*	*8*	*126*	*-78*	*171*	*8*	*0.401*	*13*		*10*	*34*	*5*
VIGNON2	*5.4096*	*44.7842*	*Tithonique*	*SS*	*76*	*-2*	*158*	*78*	*166*	*-12*	*0.85*	*10*		*7*	*19*	*5*
AMBROSIS	*5.119*	*44.1595*	*Burdigalien*	*SS*	*39.6*	*15.7*	*219.6*	*74.3*	*309.6*	*0.6*	*0.92*	*19*	*18.5*			*6*

Site	Long.	Lat.	Age	Tectonic regime	σ_1 trend	σ_1 plunge	σ_2 trend	σ_2 plunge	σ_3 trend	σ_3 plunge	R	N	F	α	RUP	REF
ASTAUDS	*5.1639*	*44.2105*	*Miocene sup.*	*P*	*50*	*nan*	*nan*	*nan*	*nan*	*nan*	*nan*	*nan*	*nan*			*6*
BRIGUIERE	*5.0227*	*44.1879*	*Miocene sup.*	*P*	*48*	*nan*	*nan*	*nan*	*nan*	*nan*	*nan*	*nan*	*nan*			*6*
BUTTE ST MARC	*5.1859*	*44.2772*	*Burdigalien*	*P*	*37.5*	*3*	*127.5*	*2*	*249*	*26*	*0.25*	*28*	*25*			*6*
CASTARLIERE	*5.1017*	*44.3664*	*Tortonien moy.*	*P*	*245.5*	*2.5*	*155.5*	*0.6*	*64.3*	*87.5*	*0.78*	*17*	*16.4*			*6*
CHAMP PAGA	*5.0868*	*44.1401*	*oligocene*	*TP*	*41.6*	*16.6*	*142*	*30*	*287*	*54*	*0.99*	*10*	*6.38*			*6*
CHANTEDUC	*5.0627*	*44.2953*	*Pliocene sup.*	*P*	*36*	*nan*	*nan*	*nan*	*nan*	*nan*	*nan*	*nan*	*nan*			*6*
CHAPELLE D AUBUNE	*5.0111*	*44.1261*	*Burdigalien*	*SS*	*248*	*13.8*	*114.4*	*70.4*	*341.5*	*13.6*	*0.87*	*14*	*13.6*			*6*
CHAPELLE-ST-JEAN	*5.1891*	*44.3177*	*Barremian*	*P*	*250*	*25*	*155*	*11*	*43.6*	*62.2*	*0.77*	*13*	*11.5*			*6*
CIMETIERE DE SAINTE MARGUERITE	*5.1921*	*44.1841*	*Burdigalien*	*P*	*47*	*nan*	*nan*	*nan*	*nan*	*nan*	*nan*	*nan*	*nan*			*6*
CIMETIERE DE VILLEDIEU	*5.0413*	*44.2796*	*Plaisancien*	*P*	*28*	*nan*	*nan*	*nan*	*nan*	*nan*	*nan*	*nan*	*nan*			*6*
CLAUX	*5.1329*	*44.1567*	*Burdigalien*	*SS*	*66*	*nan*	*nan*	*nan*	*nan*	*nan*	*nan*	*nan*	*nan*			*6*
COL DE LA CHAINE	*5.0986*	*44.1747*	*oligocene*	*P*	*36*	*nan*	*nan*	*nan*	*nan*	*nan*	*nan*	*nan*	*nan*			*6*
COMBE GIBOUSE	*5.1251*	*44.156*	*Burdigalien*	*P*	*53.7*	*6.4*	*145.5*	*14.5*	*300.6*	*74*	*0.87*	*20*	*15.1*			*6*
COMBES-CORIANCON	*5.0754*	*44.2991*	*Pliocene conti. inf.*	*TP*	*53.8*	*0.65*	*144*	*23.7*	*322*	*66*	*0.98*	*19*	*18.5*			*6*
COTE 519m	*5.1884*	*44.2702*	*Burdigalien*	*P*	*229*	*4*	*319*	*0.3*	*54*	*86*	*0.92*	*17*	*16*			*6*
COTE BELLE	*5.0018*	*44.1274*	*Miocene moyen*	*SS*	*53*	*nan*	*nan*	*nan*	*nan*	*nan*	*nan*	*nan*	*nan*			*6*
COTE CHAUDE	*5.2183*	*44.3631*	*Burdigalien*	*P*	*53.2*	*15.6*	*322.5*	*2.4*	*224*	*74.2*	*0.7*	*11*	*10.85*			*6*
CROTTE D AMBROSIS	*5.0008*	*44.1392*	*Burdigalien*	*SS*	*242.3*	*15.5*	*61.8*	*74.4*	*162*	*0.13*	*0.64*	*26*	*21.8*			*6*
D938	*5.1062*	*44.1396*	*oligocene*	*P*	*243.4*	*2.3*	*152.6*	*18*	*340.4*	*71.6*	*0.73*	*16*	*13.6*			*6*
ESSARTS DU PONT	*5.1271*	*44.2253*	*Burdigalien*	*P*	*58*	*nan*	*nan*	*nan*	*nan*	*nan*	*nan*	*nan*	*nan*			*6*
FADES	*5.0249*	*44.1821*	*Burdigalien*	*P*	*57*	*nan*	*nan*	*nan*	*nan*	*nan*	*nan*	*nan*	*nan*			*6*
FERME DE CHAMP PAGA	*5.0899*	*44.14*	*oligocene*	*P*	*47*	*nan*	*nan*	*nan*	*nan*	*nan*	*nan*	*nan*	*nan*			*6*
FERME DE LA BRIQUETTE	*5.012*	*44.1304*	*oligocene*	*P*	*39*	*nan*	*nan*	*nan*	*nan*	*nan*	*nan*	*nan*	*nan*			*6*
FERME DES PLATES	*5.2462*	*44.33*	*Barremian*	*P*	*34*	*nan*	*nan*	*nan*	*nan*	*nan*	*nan*	*nan*	*nan*			*6*
FERME VELOUZE	*5.1753*	*44.3029*	*Burdigalien*	*P*	*237*	*2.4*	*147*	*4.4*	*355.5*	*85*	*0.51*	*8*	*7.6*			*6*
FONT DE MERLE	*5.2214*	*44.3675*	*Burdigalien*	*P*	*55*	*nan*	*nan*	*nan*	*nan*	*nan*	*nan*	*nan*	*nan*			*6*
GARRIGUE DE ST ANDEOL	*4.9444*	*44.2425*	*Tortonien sup.*	*P*	*41*	*nan*	*nan*	*nan*	*nan*	*nan*	*nan*	*nan*	*nan*			*6*
GIPPIERE	*5.1694*	*44.1673*	*oligocene*	*P*	*41*	*nan*	*nan*	*nan*	*nan*	*nan*	*nan*	*nan*	*nan*			*6*
HAUTIMAGNE	*5.0689*	*44.2947*	*Pliocene sup.*	*P*	*31*	*nan*	*nan*	*nan*	*nan*	*nan*	*nan*	*nan*	*nan*			*6*
JAS CREMAD	*5.0992*	*44.1386*	*oligocene*	*P*	*44*	*nan*	*nan*	*nan*	*nan*	*nan*	*nan*	*nan*	*nan*			*6*
LA CASSE	*5.1686*	*44.281*	*Burdigalien*	*P*	*89*	*nan*	*nan*	*nan*	*nan*	*nan*	*nan*	*nan*	*nan*			*6*

Site	Long.	Lat.	Age	Tectonic regime	σ_1 trend	σ_1 plunge	σ_2 trend	σ_2 plunge	σ_3 trend	σ_3 plunge	R	N	F	α	RUP	REF
LOGIS DE FRANCE	*5.1856*	*44.2761*	*Miocene moyen*	*P*	*37.5*	*3*	*127.5*	*2*	*249*	*26*	*0.25*	*28*	*25*			*6*
LOZIEU	*5.1081*	*44.2618*	*Miocene moyen*	*P*	*64*	*nan*	*nan*	*nan*	*nan*	*nan*	*nan*	*nan*	*nan*			*6*
MOLLANS SUR OUVEZE	*5.1935*	*44.2399*	*Burdigalien*	*P*	*41.6*	*1.7*	*311*	*19.8*	*nan*	*nan*	*nan*	*22*	*20.68*			*6*
MONTBRUN ANARY	*5.4686*	*44.1865*	*Burdigalien*	*P*	*170*	*nan*	*nan*	*nan*	*nan*	*nan*	*nan*	*nan*	*nan*			*6*
MONTBRUN FLANC NORD	*5.4513*	*44.1821*	*Burdigalien*	*TP*	*346*	*40*	*112*	*35*	*226*	*30.6*	*nan*	*19*	*17.86*			*6*
MONTBRUN FLANC SUD	*5.4479*	*44.1791*	*Burdigalien*	*P*	*159.5*	*5.5*	*69.4*	*1.3*	*326*	*84.3*	*0.82*	*17*	*15.5*			*6*
MONTBRUN OLIVES	*5.4016*	*44.1757*	*Burdigalien*	*P*	*172*	*nan*	*nan*	*nan*	*nan*	*nan*	*nan*	*nan*	*nan*			*6*
MONTMIRAIL	*5.0085*	*44.1374*	*oligocene*	*P*	*50.5*	*nan*	*nan*	*nan*	*nan*	*nan*	*nan*	*nan*	*nan*			*6*
MOULIN GAUTHIER	*5.1826*	*44.2604*	*Burdigalien*	*P*	*228*	*11*	*320*	*8*	*86*	*76.5*	*0.7*	*17*	*16.25*			*6*
NORD DE CRESTET	*5.0827*	*44.2232*	*Burdigalien*	*P*	*228.5*	*3.6*	*137*	*17.2*	*330*	*72.3*	*0.96*	*12*	*9.8*			*6*
PAS DE BEYNET	*5.1625*	*44.2857*	*Burdigalien*	*P*	*231*	*5.6*	*321*	*0.2*	*53.4*	*84.4*	*0.53*	*18*	*17*			*6*
PAS DU ROCHER	*5.1347*	*44.321*	*Burdigalien*	*TP*	*42*	*nan*	*nan*	*nan*	*nan*	*nan*	*nan*	*nan*	*nan*			*6*
PASSAGE DES COMBETTES	*4.9926*	*44.1308*	*Burdigalien*	*SS*	*234*	*18.6*	*41*	*71*	*143*	*4*	*0.81*	*21*	*20.9*			*6*
PATY-CRILLON	*5.1412*	*44.1399*	*oligocene*	*P*	*66*	*nan*	*nan*	*nan*	*nan*	*nan*	*nan*	*nan*	*nan*			*6*
PEYROL OUEST	*5.0286*	*44.2349*	*Miocene sup.*	*P*	*40*	*nan*	*nan*	*nan*	*nan*	*nan*	*nan*	*nan*	*nan*			*6*
PEYROUSE	*5.0824*	*44.3147*	*Pliocene*	*P*	*31*	*nan*	*nan*	*nan*	*nan*	*nan*	*nan*	*nan*	*nan*			*6*
RAVIN DE FERINGUANDE	*5.1818*	*44.1771*	*oligocene*	*P*	*71*	*nan*	*nan*	*nan*	*nan*	*nan*	*nan*	*nan*	*nan*			*6*
RICHARDS BURDIGALIEN	*5.2019*	*44.2244*	*Burdigalien*	*SS*	*225*	*14.5*	*93*	*68.8*	*319*	*15*	*0.73*	*22*	*19.7*			*6*
RICHARDS URGONIEN	*5.2022*	*44.2244*	*Barremian*	*TP*	*232*	*24.8*	*351*	*46*	*124*	*33.5*	*0.95*	*20*	*18.8*			*6*
ROCHEGUDE	*4.83*	*44.2034*	*Burdigalien*	*SS*	*217.5*	*2.6*	*329*	*83*	*127*	*6.6*	*0.98*	*22*	*20.8*			*6*
SERRE LAUZIERE	*5.1245*	*44.3429*	*Serravalien sup.*	*P*	*48*	*nan*	*nan*	*nan*	*nan*	*nan*	*nan*	*nan*	*nan*			*6*
SUD DE SEGURET	*5.0253*	*44.2043*	*Burdigalien*	*P*	*233*	*1.3*	*143.3*	*0.3*	*39.3*	*86.6*	*0.46*	*13*	*12.9*			*6*
TROIS THERMES	*5.1369*	*44.1422*	*oligocene*	*P*	*51*	*nan*	*nan*	*nan*	*nan*	*nan*	*nan*	*nan*	*nan*			*6*
VALETTES	*5.1806*	*44.1929*	*Burdigalien*	*P*	*50*	*nan*	*nan*	*nan*	*nan*	*nan*	*nan*	*nan*	*nan*			*6*
VALLAT DE LA CHAINE	*5.0931*	*44.1748*	*oligocene*	*P*	*36*	*nan*	*nan*	*nan*	*nan*	*nan*	*nan*	*nan*	*nan*			*6*
VILLAGE DE SEGURET	*5.0251*	*44.2059*	*Burdigalien*	*P*	*53*	*nan*	*nan*	*nan*	*nan*	*nan*	*nan*	*nan*	*nan*			*6*
VILLASSE	*5.1937*	*44.1786*	*oligocene*	*P*	*49*	*nan*	*nan*	*nan*	*nan*	*nan*	*nan*	*nan*	*nan*			*6*
anniv (1)	*7.5641*	*46.2645*		*T*	*91*	*-71*	*82*	*17*	*174*	*9*	*0.52*	*12*		*6*		*7*
anniv (2)	*7.5641*	*46.2645*		*TT*	*103*	*-37*	*68*	*47*	*178*	*18*	*0.49*	*10*		*5.7*		*7*
ARPON1	*6.6961*	*45.3295*		*T*	*40*	*-73*	*18*	*16*	*110*	*6*	*0.21*	*14*		*7.2*		*7*
AVERO1	*7.0884*	*45.2918*		*T*	*155*	*-75*	*174*	*14*	*83*	*5*	*0.49*	*20*		*9.3*		*7*

Site	Long.	Lat.	Age	Tectonic regime	σ_1 trend	σ_1 plunge	σ_2 trend	σ_2 plunge	σ_3 trend	σ_3 plunge	R	N	F	α	RUP	REF
AVERO2	*7.0306*	*45.3236*		*T*	*29*	*85*	*179*	*4*	*89*	*-2*	*0.49*	*45*		*12.4*		*7*
BAUCHE	*6.7464*	*45.5394*		*T*	*9*	*75*	*177*	*15*	*88*	*-3*	*0.62*	*18*		*5.9*		*7*
BISELX	*7.2227*	*46.0058*		*T*	*38*	*-58*	*107*	*13*	*107*	*13*	*0.99*	*16*		*2.8*		*7*
CENIS4	*6.9822*	*45.1886*		*T*	*166*	*-83*	*178*	*6*	*87*	*1*	*0.52*	*19*		*10.3*		*7*
CENIS5	*6.8634*	*45.2473*		*T*	*153*	*-76*	*161*	*14*	*71*	*2*	*0.37*	*17*		*8.2*		*7*
CENIS6(2)	*6.9695*	*45.2137*		*SS*	*1*	*-11*	*157*	*-78*	*91*	*5*	*0.92*	*29*		*6.6*		*7*
CHAP	*6.7318*	*45.6937*		*TP*	*163*	*-8*	*69*	*-30*	*87*	*59*	*0.36*	*16*		*10.1*		*7*
chevre	*7.4318*	*46.0181*		*T*	*34*	*-69*	*38*	*21*	*127*	*-1*	*0.2*	*11*		*5.5*		*7*
ECHEV	*7.2638*	*45.8026*		*T*	*31*	*61*	*25*	*-29*	*116*	*-2*	*0.518*	*28*		*4*		*7*
ECOT	*7.0927*	*45.3807*		*T*	*160*	*-66*	*3*	*-22*	*89*	*8*	*0.16*	*23*		*4.2*		*7*
furi (1)	*7.7326*	*45.9992*		*T*	*178*	*63*	*26*	*25*	*111*	*-11*	*0.08*	*21*		*6.3*		*7*
furi (2)	*7.7326*	*45.9992*		*SS*	*5*	*1*	*107*	*83*	*95*	*-7*	*0.91*	*9*		*5*		*7*
GENEP	*6.9191*	*45.4192*		*T*	*45*	*-81*	*175*	*-6*	*86*	*7*	*0.47*	*24*		*9.1*		*7*
gorner	*7.7867*	*45.9847*		*T*	*130*	*75*	*47*	*-2*	*135*	*-15*	*0.04*	*16*		*10*		*7*
ires	*7.2418*	*46.0733*		*TT*	*81*	*-49*	*48*	*36*	*151*	*17*	*0.24*	*9*		*7.6*		*7*
leuker	*7.6603*	*46.3134*		*T*	*129*	*58*	*164*	*-27*	*146*	*16*	*0.23*	*18*		*7*		*7*
LLBOURG	*6.8697*	*45.2852*		*T*	*156*	*54*	*155*	*-36*	*65*	*1*	*#*	*30*				*7*
LLBOURG2	*6.8671*	*45.2829*		*T*	*121*	*-85*	*13*	*-2*	*103*	*5*	*0.38*	*22*		*10*		*7*
LORES	*6.9429*	*45.4013*		*T*	*155*	*-76*	*8*	*-12*	*96*	*8*	*0.43*	*17*		*8.5*		*7*
MARTI	*7.0814*	*46.0918*		*P*	*145*	*-22*	*51*	*-10*	*118*	*65*	*0.576*	*11*		*9.7*		*7*
MASSE	*6.6984*	*45.2596*		*TT*	*162*	*-38*	*7*	*-49*	*82*	*12*	*#*	*20*				*7*
MODAN2	*6.6658*	*45.198*		*TT*	*36*	*58*	*170*	*23*	*89*	*-21*	*0.98*	*17*		*8.4*		*7*
moiry (2)	*7.5769*	*46.1122*		*SS*	*97*	*-3*	*151*	*84*	*8*	*4*	*0.63*	*24*		*16.5*		*7*
monv1	*7.3596*	*45.9852*		*T*	*48*	*69*	*24*	*-19*	*116*	*-8*	*0.11*	*13*		*6.3*		*7*
PARTIE(2)	*6.6722*	*45.2584*		*TT*	*136*	*-85*	*48*	*0*	*138*	*5*	*0.44*	*10*		*10.8*		*7*
PRIOUX	*6.6941*	*45.348*		*T*	*142*	*78*	*165*	*-11*	*74*	*-5*	*0.15*	*11*		*25.7*		*7*
randa1	*7.7751*	*46.0878*		*T*	*105*	*59*	*61*	*-24*	*160*	*-19*	*0.78*	*13*		*13.6*		*7*
rech1 (1)	*7.4992*	*46.2461*		*SS*	*22*	*23*	*146*	*-62*	*118*	*14*	*0.78*	*9*		*2*		*7*
rech1 (2)	*7.4992*	*46.2461*		*T*	*29*	*-68*	*58*	*19*	*145*	*-10*	*0.13*	*13*		*5*		*7*
rech2	*7.4953*	*46.2416*		*T*	*173*	*76*	*96*	*-3*	*7*	*14*	*0.03*	*19*		*8.9*		*7*
RECUL	*6.9618*	*45.4669*		*T*	*171*	*69*	*31*	*17*	*117*	*-13*	*0.16*	*19*		*10.1*		*7*

Site	Long.	Lat.	Age	Tectonic regime	σ_1 trend	σ_1 plunge	σ_2 trend	σ_2 plunge	σ_3 trend	σ_3 plunge	R	N	F	α	RUP	REF
RIBON(2)	*6.9941*	*45.3104*		*T*	*56*	*70*	*2*	*-12*	*95*	*-16*	*0.64*	*31*		*8.9*		*7*
RIDD	*7.2233*	*46.1551*		*T*	*119*	*68*	*84*	*-19*	*178*	*-12*	*0.815*	*22*		*8.8*		*7*
ROCHEU	*6.9818*	*45.3804*		*T*	*79*	*73*	*31*	*-12*	*123*	*-12*	*0.48*	*15*		*7.6*		*7*
ROMOL	*6.7638*	*45.1324*		*T*	*52*	*71*	*34*	*-18*	*126*	*-5*	*0.27*	*22*		*14.4*		*7*
roten	*7.7674*	*45.9866*		*SS*	*78*	*-8*	*19*	*75*	*167*	*12*	*0.75*	*12*		*5.5*		*7*
SALIN	*6.528*	*45.4678*		*T*	*3*	*64*	*155*	*23*	*70*	*-11*	*0.93*	*15*		*8.6*		*7*
solay3	*7.534*	*46.0761*		*TT*	*0*	*50*	*32*	*-36*	*110*	*16*	*0.98*	*11*		*3.5*		*7*
STFOY (1)	*6.9313*	*45.5787*		*TT*	*91*	*56*	*179*	*-2*	*87*	*-34*	*0.701*	*16*		*4*		*7*
STFOY (2)	*6.9313*	*45.5787*		*SS*	*157*	*11*	*48*	*61*	*73*	*-27*	*0.492*	*14*		*7.1*		*7*
tdela	*7.3723*	*46.1571*		*T*	*58*	*-61*	*91*	*25*	*174*	*-14*	*0.08*	*16*		*3.9*		*7*
TELEG	*6.4442*	*45.1977*		*T*	*168*	*72*	*149*	*-18*	*61*	*6*	*0.57*	*14*		*10.2*		*7*
TIGNES2	*6.9254*	*45.4539*		*SS*	*15*	*-25*	*60*	*56*	*115*	*-21*	*0.418*	*13*		*7.3*		*7*
VALDER1	*7.1055*	*45.54*		*TT*	*136*	*-51*	*29*	*-13*	*110*	*36*	*0.07*	*12*		*3.6*		*7*
VALDER3	*7.122*	*45.5882*		*TT*	*83*	*50*	*68*	*-39*	*164*	*-7*	*0.922*	*11*		*6.5*		*7*
VALGR1	*7.1562*	*45.6978*		*T*	*36*	*73*	*91*	*-10*	*178*	*14*	*0.09*	*12*		*4.1*		*7*
VALGR25	*7.0482*	*45.6041*		*T*	*16*	*56*	*3*	*-33*	*97*	*-6*	*0.74*	*22*		*10.5*		*7*
VALGR4	*7.1008*	*45.679*		*SS*	*139*	*-39*	*24*	*-28*	*89*	*38*	*0.95*	*20*		*4.5*		*7*
VALLO	*6.4273*	*45.1594*		*T*	*118*	*-86*	*17*	*-1*	*107*	*4*	*0.14*	*25*		*11.6*		*7*
VALP1 (1)	*7.2974*	*45.8715*		*SS*	*26*	*5*	*168*	*84*	*116*	*-4*	*0.76*	*17*		*8.8*		*7*
VALP1 (2)	*7.2974*	*45.8715*		*T*	*117*	*78*	*9*	*4*	*99*	*-11*	*0.62*	*21*		*9.6*		*7*
VALTHO2	*6.5669*	*45.308*		*T*	*52*	*82*	*7*	*-6*	*97*	*-6*	#	*20*				*7*
VILLARO	*7.0023*	*45.3313*		*T*	*146*	*87*	*159*	*-3*	*69*	*-1*	*0.05*	*21*		*6.9*		*7*
visso	*7.5809*	*46.2344*		*SS*	*25*	*-8*	*91*	*71*	*118*	*-17*	*0.85*	*17*		*5.6*		*7*
P11	*5.6889*	*43.7311*	*M. Miocene*	*P*	*179*	*14*	*90*	*-4*	*15*	*75*	*0.21*					*8*
P12a	*5.9222*	*44.0061*	*Mio-Pliocene*	*SS*	*138*	*30*	*113*	*-57*	*41*	*11*	*0.67*					*8*
P14	*5.6111*	*43.7517*	*Miocene*	*P*	*12*	*8*	*100*	*-11*	*139*	*76*	*0.13*					*8*
P15	*5.6178*	*43.7289*	*Oligocene/Miocene*	*P*	*12*	*-37*	*100*	*3*	*6*	*53*	*0.4*					*8*
P16	*5.585*	*43.7114*	*Oligocene*	*SS*	*173*	*-2*	*88*	*68*	*82*	*-22*	*0.18*					*8*
P17	*5.6131*	*43.6956*	*Mio-Pliocene*	*SS*	*173*	*10*	*21*	*79*	*84*	*-5*	*0.21*					*8*
P18	*5.6925*	*43.7347*	*Miocene*	*SS*	*130*	*-22*					*0.02*					*8*
P19	*5.76*	*43.7853*	*Oligocene/Miocene*	*SS*	*18*	*8*	*90*	*-67*	*111*	*22*	*0.16*					*8*

Site	Long.	Lat.	Age	Tectonic regime	σ_1 trend	σ_1 plunge	σ_2 trend	σ_2 plunge	σ_3 trend	σ_3 plunge	R	N	F	α	RUP	REF
P2	*5.275*	*43.6611*	*L. Oligocene*	*SS*	*19*	*-2*					*0.08*					*8*
P20	*5.7736*	*43.7881*	*Mio-Pliocene*	*SS*	*149*	*10*	*82*	*-66*	*55*	*21*	*0.17*					*8*
P21	*5.8036*	*43.8481*	*Mio-Pliocene*	*P*	*147*	*12*					*0.07*					*8*
P22	*5.8606*	*43.8947*	*Mio-Pliocene*	*SS*	*138*	*-7*					*0.03*					*8*
P23	*5.9*	*43.9625*	*Mio-Pliocene*	*P*	*141*	*3*	*52*	*-10*	*33*	*79*	*0.37*					*8*
P24	*6.0406*	*44.04*	*Quaternary*	*P*	*34*	*-17*	*125*	*-3*	*46*	*73*	*0.54*					*8*
P3a	*5.2181*	*43.6833*	*L. Oligocene*	*P*	*169*	*-13*	*76*	*10*	*23*	*-73*	*0.12*					*8*
P4	*5.35*	*43.7764*	*Miocene*	*P*	*163*	*22*	*71*	*3*	*153*	*-67*	*0.15*					*8*
P5	*5.35*	*43.7764*	*L. Miocene*	*P*	*0*	*-19*					*0.04*					*8*
P6	*5.4514*	*43.775*	*U. Miocene*	*P*	*2*	*31*	*91*	*-3*	*177*	*59*	*0.28*					*8*
P7	*5.4411*	*43.7728*	*U. Miocene*	*SS*	*10*	*-2*					*0.06*					*8*
P9	*5.5422*	*43.6403*	*L. Oligocene*	*SS*	*13*	*-6*	*115*	*-64*	*101*	*25*	*0.2*					*8*
65	*5.2988*	*44.3534*	*Barrémien*		*0*											*10*
72	*5.3269*	*44.2261*	*Barrémien*		*0*											*10*
63b	*5.3805*	*44.3319*	*Barrémien*		*175*											*10*
66b	*5.2874*	*44.3005*	*Hautériven*		*15*											*10*
71b	*5.2821*	*44.2948*	*Tithonique-Berriasien*		*145*											*10*
73b	*5.405*	*44.2948*	*Bédoulien*		*50*											*10*
79b	*5.43*	*44.222*	*Berriasien*		*10*											*10*
81b	*5.4169*	*44.1994*	*Hautériven*		*10*											*10*
82b	*5.4271*	*44.1906*	*Hautériven-Barrémien*		*10*											*10*
S14	*8.0366*	*46.2034*		*T*	*123*	*-73*	*50*	*5*	*141*	*17*	*0.404*	*29*		*9.7*		*11*
S22	*8.0871*	*46.1696*		*T*	*176*	*-56*	*42*	*-18*	*126*	*17*	*0.048*	*14*		*8.786*		*11*
S24	*7.9523*	*46.2302*		*T*	*66*	*77*	*105*	*-10*	*14*	*-8*	*0.244*	*31*		*10*		*11*
S32	*7.9694*	*46.2528*		*T*	*66*	*86*	*108*	*-3*	*18*	*-3*	*0.365*	*15*		*5.1*		*11*
S35	*8.0452*	*46.1654*		*T*	*72*	*74*	*20*	*-10*	*112*	*-12*	*0.136*	*21*		*9.9*		*11*
S4	*7.9962*	*46.2151*		*T*	*168*	*-74*	*42*	*-10*	*129*	*13*	*0.159*	*9*		*5.8*		*11*
S40	*8.1328*	*46.153*		*T*	*77*	*-71*	*170*	*-1*	*81*	*19*	*0.266*	*34*		*12.72*		*11*
S44	*8.0179*	*46.2121*		*T*	*104*	*-70*	*24*	*4*	*116*	*20*	*0.361*	*12*		*9.5*		*11*
S50	*8.1082*	*46.154*		*T*	*10*	*-77*	*26*	*12*	*115*	*-3*	*0.589*	*10*		*7.2*		*11*
S57	*8.0778*	*46.151*		*T*	*24*	*72*	*23*	*-18*	*113*	*-1*	*0.253*	*19*		*7.9*		*11*

Site	Long.	Lat.	Age	Tectonic regime	σ_1 trend	σ_1 plunge	σ_2 trend	σ_2 plunge	σ_3 trend	σ_3 plunge	R	N	F	α	RUP	REF
S58	*7.963*	*46.2983*		*T*	*176*	*-69*	*91*	*2*	*1*	*-21*	*0.337*	*11*		*8.9*		*11*
S59	*7.9583*	*46.2838*		*T*	*12*	*75*	*101*	*-1*	*11*	*-15*	*0.114*	*18*		*11.3*		*11*
S60	*7.9568*	*46.2763*		*T*	*114*	*86*	*68*	*-3*	*158*	*-3*	*0.292*	*26*		*13.04*		*11*
S61	*7.959*	*46.2868*		*T*	*1*	*87*	*47*	*-2*	*137*	*2*	*0.163*	*13*		*15.77*		*11*
Armans	*5.44*	*46.2683*	*Rauracian*	*SS*	*121*	*-8*	*50*	*68*	*28*	*-21*	*0.15*	*9*		*13*	*29*	*14*
Artemare	*5.6883*	*45.8683*	*Valangin. Berrias.*	*SS*	*107*	*-1*	*18*	*64*	*16*	*-26*	*0.15*	*16*		*9*	*24*	*14*
Belleydoux	*5.7917*	*46.2483*	*Valanginian*	*P*	*122*	*-5*	*33*	*11*	*9*	*-78*	*0.42*	*8*		*10*	*31*	*14*
Belleydoux	*5.7917*	*46.2483*	*Valanginian*	*SS*	*105*	*-14*	*75*	*74*	*13*	*-8*	*0.35*	*26*		*18*	*41*	*14*
Blanaz	*5.4517*	*45.9183*	*Up. Bathonian*	*SS*	*108*	*0*	*18*	*-80*	*18*	*10*	*0.42*	*8*		*3*	*17*	*14*
Boulu	*6.0117*	*46.4233*	*Valanginian*	*SS*	*127*	*-3*	*103*	*86*	*37*	*-2*	*0.38*	*44*		*13*	*33*	*14*
C. Dombief	*5.9067*	*46.63*	*Kmmeridg. Bathon.*	*SS*	*172*	*-6*	*157*	*84*	*82*	*-1*	*0.57*	*5*		*17*	*30*	*14*
C. Dombief	*5.9067*	*46.63*	*Kmmeridg. Bathon.*	*SS*	*126*	*5*	*137*	*-85*	*36*	*-1*	*0.38*	*5*		*6*	*33*	*14*
Cezeriat	*5.3267*	*46.1933*	*Low. Baj.-Up. Aalen.*	*SS*	*74*	*-1*	*76*	*89*	*164*	*0*	*0.23*	*13*		*12*	*36*	*14*
Chevrotaine	*5.84*	*46.66*	*Sequanian*	*SS*	*105*	*-9*	*133*	*80*	*15*	*5*	*0.54*	*5*		*6*	*17*	*14*
Cinquétral	*5.8817*	*46.4233*	*Valanginian*	*SS*	*175*	*-5*	*130*	*83*	*84*	*-5*	*0.42*	*34*		*14*	*31*	*14*
Cinquétral	*5.8817*	*46.4233*	*Valanginian*	*SS*	*122*	*-4*	*16*	*-76*	*33*	*13*	*0.25*	*57*		*18*	*40*	*14*
Clées	*6.4683*	*46.73*	*Hauteriv. Valangin.*	*SS*	*160*	*8*	*15*	*81*	*70*	*-5*	*0.27*	*25*		*10*	*30*	*14*
Coiselet	*5.595*	*46.295*	*Rauracian*	*SS*	*120*	*11*	*61*	*-69*	*27*	*18*	*0.57*	*12*		*11*	*33*	*14*
Col de France	*5.3567*	*46.2333*	*Bathonian*	*SS*	*91*	*-9*	*151*	*73*	*3*	*15*	*0.38*	*23*		*7*	*19*	*14*
Coramaranch.	*5.61*	*45.9467*	*Purbeckian*	*P*	*91*	*-7*	*1*	*3*	*112*	*82*	*0.72*	*17*		*11*	*25*	*14*
Coramaranch.	*5.61*	*45.9467*	*Purbeckian*	*SS*	*100*	*-43*	*109*	*47*	*14*	*5*	*0.63*	*6*		*17*	*31*	*14*
Culoz	*5.7883*	*45.8617*	*Kimmeridgian*	*P*	*110*	*8*	*20*	*4*	*84*	*-81*	*0.49*	*7*		*9*	*25*	*14*
Ecrille	*5.6533*	*46.4983*	*Oxford. Kimmerid.*	*SS*	*113*	*15*	*89*	*-73*	*21*	*6*	*0.44*	*4*		*10*	*32*	*14*
Fay	*5.6617*	*45.6183*	*Portlandian*	*SS*	*115*	*13*	*149*	*-75*	*27*	*-8*	*0.64*	*9*		*3*	*118*	*14*
Glandieu	*5.6183*	*45.6683*	*Kimmeridgian*	*P*	*116*	*-1*	*26*	*6*	*18*	*-84*	*0.38*	*6*		*10*	*24*	*14*
Glandieu	*5.6183*	*45.6683*	*Kimmeridgian*	*SS*	*113*	*5*	*134*	*-84*	*23*	*-2*	*0.51*	*30*		*12*	*30*	*14*
Golisse	*6.25*	*46.625*	*Port. -Up. Kimme.*	*SS*	*114*	*10*	*82*	*-78*	*23*	*6*	*0.64*	*10*		*19*	*38*	*14*
Grosjean	*6.275*	*46.62*	*Hauterivian*	*SS*	*114*	*2*	*164*	*-87*	*24*	*-2*	*0.27*	*10*		*10*	*29*	*14*
Hotonne	*5.7283*	*45.9883*	*Portlandian*	*SS*	*117*	*-27*	*108*	*63*	*25*	*-4*	*0.76*	*10*		*12*	*25*	*14*
Ilay	*5.885*	*46.6167*	*Purbeck. Portland.*	*SS*	*4*	*-4*	*104*	*-68*	*92*	*22*	*0.27*	*6*		*4*	*20*	*14*
Ilay	*5.885*	*46.6167*	*Purbeck. Portland.*	*SS*	*126*	*0*	*35*	*65*	*36*	*-25*	*0.19*	*63*		*11*	*31*	*14*

Site	Long.	Lat.	Age	Tectonic regime	σ_1 trend	σ_1 plunge	σ_2 trend	σ_2 plunge	σ_3 trend	σ_3 plunge	R	N	F	α	RUP	REF
Innimond	*5.56*	*45.765*	*Kimmeridg. Oxford.*	*SS*	*162*	*-5*	*116*	*82*	*71*	*-5*	*0.28*	*7*		*4*	*17*	*14*
Innimond	*5.56*	*45.765*	*Kimmeridg. Oxford.*	*SS*	*89*	*10*	*20*	*-63*	*174*	*-25*	*0.12*	*17*		*12*	*32*	*14*
Jalinard	*5.6717*	*46.0517*	*Portlandian*	*SS*	*124*	*4*	*62*	*-81*	*34*	*8*	*0.07*	*10*		*8*	*25*	*14*
Lagnieu	*5.385*	*45.88*	*Up. Bajocian*	*P*	*85*	*-6*	*175*	*-11*	*174*	*79*	*0.08*	*8*		*19*	*45*	*14*
Lamoura	*5.9417*	*46.3817*	*Barrem. Hauteriv.*	*SS*	*142*	*-13*	*167*	*76*	*54*	*6*	*0.78*	*33*		*18*	*39*	*14*
Lelex	*5.9117*	*46.2683*	*Barremian*	*SS*	*121*	*-20*	*90*	*67*	*27*	*-11*	*0.55*	*18*		*18*	*43*	*14*
Lemme	*5.9567*	*46.625*	*Kimmeridgian*	*SS*	*161*	*0*	*70*	*-82*	*71*	*8*	*0.52*	*9*		*6*	*19*	*14*
Lompnas	*5.5267*	*45.8067*	*Up. Oxfordian*	*SS*	*106*	*8*	*2*	*60*	*20*	*-29*	*0.16*	*21*		*12*	*28*	*14*
Longchaumois	*5.94*	*46.46*	*Barrem. to Valangin.*	*SS*	*124*	*1*	*25*	*85*	*34*	*-5*	*0.46*	*45*		*14*	*37*	*14*
Mandallaz	*6.0583*	*45.9483*	*Purbeckian*	*TP*	*69*	*6*	*166*	*50*	*154*	*-39*	*0.48*	*12*		*7*	*23*	*14*
Mirebel	*5.7333*	*46.7*	*Argovian*	*SS*	*105*	*21*	*71*	*-65*	*10*	*12*	*0.27*	*5*		*14*	*34*	*14*
Montagna	*5.46*	*46.345*	*Sequanian*	*P*	*129*	*3*	*38*	*16*	*48*	*-74*	*0.78*	*9*		*8*	*27*	*14*
Montagna	*5.46*	*46.345*	*Sequanian*	*SS*	*117*	*37*	*128*	*-53*	*31*	*-6*	*0.34*	*9*		*12*	*50*	*14*
Montréal	*5.565*	*46.1817*	*Low. Bajocian*	*TP*	*97*	*18*	*21*	*-38*	*167*	*-46*	*0.21*	*7*		*15*	*37*	*14*
Mouthe N	*6.1833*	*46.7167*	*Rauracian*	*SS*	*7*	*18*	*61*	*-60*	*104*	*22*	*0.55*	*9*		*10*	*26*	*14*
Mouthe N	*6.1833*	*46.7167*	*Rauracian*	*SS*	*124*	*-3*	*95*	*87*	*34*	*-1*	*0.23*	*33*		*17*	*38*	*14*
Mouthe S	*6.1717*	*46.7*	*Portland. Kimmeridg.*	*SS*	*104*	*9*	*153*	*-77*	*16*	*-10*	*0.51*	*40*		*13*	*28*	*14*
Nogna	*5.6667*	*46.5983*	*Bathon. Bajoc.*	*SS*	*124*	*19*	*76*	*-63*	*27*	*19*	*0.48*	*27*		*13*	*30*	*14*
Piards	*5.8283*	*46.505*	*Kimmeridg. Bathon.*	*SS*	*106*	*4*	*179*	*-77*	*17*	*-13*	*0.52*	*36*		*16*	*34*	*14*
Pratz	*5.7517*	*46.3817*	*Bathonian*	*SS*	*109*	*7*	*155*	*-80*	*20*	*-7*	*0.30*	*47*		*14*	*38*	*14*
Repentys	*5.9767*	*46.475*	*Hauterivian*	*SS*	*148*	*4*	*125*	*-85*	*58*	*2*	*0.35*	*10*		*17*	*42*	*14*
St Claude	*5.8583*	*46.395*	*Portlandian*	*SS*	*111*	*10*	*71*	*-77*	*19*	*9*	*0.55*	*94*		*15*	*37*	*14*
Tancua	*5.955*	*46.5067*	*Hauterivian*	*SS*	*137*	*2*	*63*	*-83*	*47*	*7*	*0.20*	*25*		*10*	*26*	*14*
Val du Fier	*5.8617*	*45.9333*	*Portland. to Oford.*	*P*	*133*	*9*	*41*	*14*	*74*	*-73*	*0.72*	*5*		*7*	*17*	*14*
Val du Fier	*5.8617*	*45.9333*	*Portland. to Oford.*	*SS*	*119*	*-2*	*47*	*84*	*29*	*-6*	*0.76*	*36*		*13*	*31*	*14*
Donareo	*7.23*	*43.782*	*Pliocene*	*SS*	*21*	*7*	*145*	*78*	*110*	*-10*	*0.58*	*15*		*7*		*16*
jura chartreuse 017	*5.4234*	*45.9341*		*P*	*109*	*5*	*165*	*-82*	*20*	*-7*	*0.3*	*4*				*18*
jura chartreuse 018	*5.4439*	*45.9464*		*TP*	*111*	*-13*	*11*	*-39*	*48*	*35*	*0.11*	*9*				*18*
jura chartreuse 033	*5.391*	*45.8851*		*TP*	*124*	*-58*	*2*	*-18*	*83*	*25*	*0.84*	*7*				*18*
jura chartreuse 053	*5.5805*	*45.8726*		*P*	*126*	*0*	*36*	*14*	*37*	*-76*	*0.68*	*5*				*18*
jura chartreuse 057	*5.689*	*45.8751*		*P*	*109*	*4*	*20*	*-4*	*156*	*-84*	*0.33*	*9*				*18*

Site	Long.	Lat.	Age	Tectonic regime	σ_1 trend	σ_1 plunge	σ_2 trend	σ_2 plunge	σ_3 trend	σ_3 plunge	R	N	F	α	RUP	REF
jura chartreuse 061	*5.6604*	*45.8109*		*TP*	*105*	*-26*	*171*	*40*	*39*	*39*	*0.46*	*6*				*18*
jura chartreuse 074	*5.7288*	*45.7601*		*P*	*112*	*8*	*21*	*4*	*82*	*-81*	*0.55*	*4*				*18*
jura chartreuse 075	*5.7351*	*45.7592*		*SS*	*107*	*10*	*60*	*-76*	*15*	*10*	*0.23*	*9*				*18*
jura chartreuse 076b	*5.7493*	*45.7638*		*P*	*123*	*-7*	*30*	*-21*	*51*	*65*	*0.33*	*8*				*18*
jura chartreuse 080	*5.8437*	*45.7974*		*TP*	*108*	*-10*	*4*	*-55*	*24*	*33*	*0.19*	*5*				*18*
jura chartreuse 108	*6.0341*	*45.4309*		*TP*	*80*	*-9*	*0*	*40*	*162*	*42*	*0.16*	*5*				*18*
jura chartreuse 110	*6.0948*	*45.3846*		*P*	*64*	*-5*	*152*	*18*	*149*	*71*	*0.43*	*7*				*18*
P12b	*5.8936*	*43.9406*	*Mio-Pliocene*	*SS*	*139*	*7*	*56*	*-47*	*43*	*42*	*0.13*					*20*
P13	*5.7289*	*43.8675*	*L. Oligocene*	*SS*					*51*	*-4*	*0.98*					*20*
P25b	*5.4019*	*44.1753*	*Miocene*	*P*	*16*	*-3*	*106*	*0*			*0.7*					*20*
P26	*5.4108*	*44.1714*	*L. Cretaceous*	*SS*	*37*	*-10*	*142*	*-56*	*121*	*32*	*0.15*					*20*
P27	*5.4689*	*44.1872*	*Miocene*	*P*	*162*	*-8*	*69*	*-19*	*94*	*69*	*0.46*					*20*
P28	*5.7644*	*44.1675*	*L. Cretaceous*	*P*	*173*	*8*	*80*	*19*	*106*	*-69*	*0.71*					*20*
P29b	*5.9319*	*44.1644*	*L. Cretaceous*	*P*	*153*	*-2*	*64*	*18*	*56*	*-72*	*0.5*					*20*
P30b	*5.9372*	*44.1625*	*L. Cretaceous*	*P*	*138*	*20*					*0.01*					*20*
P31	*6.025*	*44.1022*	*Mio-Pliocene*	*SS*	*33*	*-18*	*98*	*53*	*134*	*-31*	*0.18*					*20*
P32	*6.0503*	*44.1847*	*Oligocene*	*SS*	*152*	*-8*	*39*	*-71*	*65*	*17*	*0.19*					*20*
P8b	*5.1961*	*44.24*		*SS*	*11*	*-27*	*72*	*44*	*121*	*-34*	*0.34*					*20*
BARAI	*6.8263*	*44.5552*		*SS*	*21*	*33*	*8*	*-57*	*107*	*-6*	*0.7*	*21*				*21*
BDTNO	*6.5208*	*44.7313*		*T*	*142*	*77*	*169*	*-18*	*78*	*-6*	*0.6*	*30*				*21*
BDTSU	*6.529*	*44.7147*		*T*	*108*	*83*	*176*	*-3*	*85*	*-6*	*0.4*	*25*				*21*
BEAUD	*6.689*	*44.8187*		*T*	*142*	*80*	*41*	*2*	*130*	*-1*	*0.3*	*26*				*21*
CERVI	*6.7505*	*44.8862*		*T*	*28*	*-76*	*133*	*-4*	*44*	*14*	*0.3*	*18*				*21*
CHENO	*6.753*	*44.9253*		*T*	*111*	*76*	*137*	*-13*	*46*	*-6*	*0.4*	*10*				*21*
COLSN	*6.841*	*44.4888*		*SS*	*22*	*-3*	*174*	*-57*	*104*	*13*	*0.6*	*15*				*21*
CROUS	*6.6552*	*44.7238*		*SS*	*15*	*16*	*157*	*7*	*102*	*-11*	*0.5*	*10*				*21*
CRXSA	*6.5508*	*44.8363*		*T*	*143*	*82*	*147*	*-8*	*57*	*-1*	*0.4*	*19*				*21*
CRXSA	*6.5508*	*44.8363*		*SS*	*169*	*32*	*173*	*-58*	*80*	*-2*	*0.5*	*20*				*21*
ESCNO	*6.7003*	*44.635*		*SS*	*19*	*1*	*96*	*-83*	*108*	*7*	*0.4*	*30*				*21*
ESCPE	*6.677*	*44.6393*		*SS*	*16*	*10*	*118*	*60*	*97*	*-27*	*0.2*	*25*				*21*
ESCRI	*6.6898*	*44.6428*		*SS*	*25*	*-38*	*10*	*52*	*110*	*7*	*0.9*	*34*				*21*

Site	Long.	Lat.	Age	Tectonic regime	σ_1 trend	σ_1 plunge	σ_2 trend	σ_2 plunge	σ_3 trend	σ_3 plunge	R	N	F	α	RUP	REF
ESCSU	*6.7163*	*44.6295*		*SS*	*15*	*2*	*111*	*73*	*104*	*-17*	*0.4*	*29*				*21*
FOUIL	*6.8003*	*44.5537*		*T*	*130*	*82*	*4*	*5*	*94*	*-6*	*0.4*	*11*				*21*
FOURN	*6.5443*	*44.7962*		*T*	*110*	*-80*	*33*	*0*	*113*	*10*	*0.4*	*25*				*21*
FREIS	*6.5357*	*44.7608*		*T*	*33*	*-83*	*149*	*-3*	*59*	*7*	*0.3*	*15*				*21*
HOUER	*6.7825*	*44.5877*		*SS*	*27*	*-29*	*62*	*56*	*124*	*-18*	*0.7*	*16*				*21*
JANES	*6.7385*	*44.9338*		*SS*	*172*	*4*	*43*	*83*	*82*	*-5*	*0.7*	*8*				*21*
LAUSE	*6.6652*	*44.8558*		*T*	*55*	*84*	*172*	*3*	*82*	*-5*	*0.3*	*17*				*21*
LONGE	*6.9487*	*44.65*		*T*	*81*	*70*	*116*	*-17*	*22*	*-11*	*0.2*	*16*				*21*
MALAM	*6.6433*	*44.7118*		*T*	*107*	*-81*	*34*	*3*	*125*	*8*	*0.2*	*36*				*21*
MROYN	*6.7297*	*44.6923*		*SS*	*32*	*18*	*24*	*-72*	*121*	*-2*	*0.8*	*10*				*21*
NEUFC	*6.7725*	*44.5713*		*SS*	*16*	*20*	*28*	*-70*	*108*	*4*	*0.6*	*12*				*21*
ORCEA	*6.5047*	*44.8017*		*T*	*15*	*-77*	*3*	*15*	*93*	*4*	*0.3*	*23*				*21*
ORCEB	*6.5043*	*44.8017*		*T*	*19*	*-75*	*2*	*14*	*93*	*4*	*0.1*	*16*				*21*
ORECE	*6.5042*	*44.8017*		*SS*	*20*	*-2*	*130*	*-83*	*111*	*7*	*0.8*	*17*				*21*
OREES	*6.5112*	*44.7963*		*T*	*15*	*77*	*178*	*13*	*89*	*-4*	*0.2*	*10*				*21*
OREES	*6.5112*	*44.7963*		*SS*	*23*	*-5*	*96*	*73*	*115*	*-16*	*0.2*	*10*				*21*
OREOU	*6.5115*	*44.7967*		*SS*	*12*	*-15*	*18*	*75*	*103*	*-1*	*0.5*	*26*				*21*
OROUA	*6.5215*	*44.7952*		*T*	*122*	*8*	*163*	*-7*	*72*	*-6*	*0.3*	*31*				*21*
OROUB	*6.5213*	*44.7952*		*T*	*144*	*75*	*0*	*12*	*88*	*-8*	*0.2*	*32*				*21*
PARPA	*6.6775*	*44.4968*		*T*	*176*	*74*	*157*	*-15*	*69*	*5*	*0.2*	*13*				*21*
PCHAT	*6.7878*	*44.54*		*SS*	*7*	*-2*	*13*	*69*	*98*	*-2*	*0.4*	*15*				*21*
PEYGU	*6.7403*	*44.8252*		*T*	*66*	*78*	*2*	*-5*	*93*	*-11*	*0.2*	*13*				*21*
PRORE	*6.5642*	*44.9053*		*T*	*154*	*70*	*135*	*-19*	*47*	*6*	*0.2*	*20*				*21*
ROBAR	*6.5698*	*44.808*		*T*	*15*	*86*	*159*	*3*	*69*	*-2*	*0.4*	*20*				*21*
RUBUR	*6.9732*	*44.3968*		*SS*	*2*	*3*	*80*	*-76*	*93*	*13*	*0.8*	*12*				*21*
VHOUE	*6.8242*	*44.5788*		*SS*	*24*	*40*	*23*	*-50*	*113*	*-1*	*0.8*	*17*				*21*
P39	*6.1533*	*44.0278*	*Mio-Pliocene*	*P*							*0.95*					*8*
P43b	*6.2017*	*43.8967*	*L. Cretaceous*	*SS*	*25*	*5*	*109*	*-51*	*119*	*38*	*0.6*					*8*
P44	*6.2047*	*43.8878*	*Mio-Pliocene*	*P*					*32*	*-70*	*0.97*					*8*
P45	*6.2008*	*43.8694*	*L. Quaternary*	*P*	*13*	*12*	*102*	*-4*	*175*	*77*	*0.68*					*8*
D16b	*6.5686*	*44.1031*	*U. Cretaceous*	*SS*	*11*	*-12*	*28*	*77*	*102*	*-4*	*0.62*					*20*

Site	Long.	Lat.	Age	Tectonic regime	σ_1 trend	σ_1 plunge	σ_2 trend	σ_2 plunge	σ_3 trend	σ_3 plunge	R	N	F	α	RUP	REF
D22b	*6.7461*	*44.2697*	*U. Cretaceous*	*SS*	*27*	*-2*	*169*	*-88*	*116*	*1*	*0.87*					*20*
D22c	*6.7461*	*44.2697*	*U. Cretaceous*	*SS*	*12*	*-31*	*30*	*58*	*107*	*-8*	*0.8*					*20*
D24b	*6.7494*	*44.31*	*U. Cretaceous*	*SS*	*9*	*-18*	*32*	*71*	*101*	*-7*	*0.73*					*20*
D29a2	*6.8472*	*44.3406*	*Cretaceous*	*SS*	*172*	*0*			*82*	*-8*	*0.35*					*20*
D29b4	*6.8472*	*44.3406*	*Cretaceous*	*SS*	*172*	*12*	*106*	*-61*	*76*	*25*	*0.11*					*20*
D34	*6.9417*	*44.3597*	*U. Jurassic*	*P*	*158*	*-30*	*71*	*5*	*170*	*60*	*0.11*					*20*
D35b	*6.9672*	*44.3775*	*M.U. Eocene*	*SS*	*177*	*-6*			*87*	*3*	*0.83*					*20*
D39b	*6.6322*	*44.2333*	*M. Cretaceous*	*P*	*178*	*7*					*0.01*					*20*
D45	*6.8969*	*44.3178*	*Hercynian*	*P*	*170*	*-9*	*83*	*19*	*54*	*-69*	*0.19*					*20*
D53	*6.8969*	*44.2856*	*Hercynian*	*P*	*11*	*-3*	*100*	*8*			*0.73*					*20*
D54	*7.0292*	*44.1911*	*Hercynian*	*P*	*14*	*-9*	*97*	*38*	*115*	*-51*	*0.31*					*20*
D56	*6.5478*	*44.0033*	*U. Cretaceous*	*SS*	*8*	*3*			*98*	*-5*	*0.47*					*20*
D58	*6.8667*	*44.1161*	*M. Jurassic*	*SS*	*175*	*14*	*174*	*-76*	*85*	*0*	*0.87*					*20*
BONNETTE	*6.2216*	*44.0927*		*P*	*50*	*0*	*140*	*0*	*69*	*-90*	*0.29*	*21*		*10*	*32*	*13*
CHAMPOURCIN	*6.2311*	*44.1165*		*SS*	*79*	*10*	*21*	*-71*	*167*	*-16*	*0.16*	*8*		*21*	*42*	*13*
CHAUVET	*6.2977*	*44.1828*		*P*	*98*	*1*	*9*	*-5*	*177*	*-85*	*0.6*	*18*		*8*	*20*	*13*
GD.COLLE	*6.2471*	*44.116*		*SS*	*70*	*-3*	*150*	*71*	*161*	*-19*	*0.08*	*20*		*11*	*32*	*13*
LA FONSE	*6.2496*	*44.0726*		*P*	*45*	*4*	*135*	*-4*	*177*	*85*	*0.01*	*21*		*11*	*34*	*13*
MEUNIERE	*6.244*	*44.124*		*P*	*62*	*-2*	*152*	*-6*	*134*	*83*	*0.34*	*25*		*10*	*38*	*13*
ROCHASSAS	*6.2468*	*44.116*		*P*	*66*	*2*	*155*	*-16*	*162*	*74*	*0.32*	*23*		*15*	*47*	*13*

ANNEXE 2 : OUTIL D'EXTRACTION SEMI-SUPERVISÉE DES ANOMALIES DE DRAINAGES

Un algorithme a été programmé en vue d'extraire les anomalies latérales et verticales du réseau hydrographique en recherchant les variations de directions d'écoulement ou de pente anomaliques. Il nécessite en entrée un modèle numérique de terrain et des données vectorielles SIG du réseau hydrographique et de la géologie.

L'utilisateur peut demander à ne pas prendre en compte les anomalies se trouvant à une distance définie d'un contact lithologique ou d'une confluence.

L'algorithme fourni en sortie le profil en long des cours d'eau analysés associé aux graphiques de pente, variation de pente, direction d'écoulement et variation de directions d'écoulement. Les valeurs anomaliques et leur localisation sont exportés dans un fichier de donnée vectorielle consultable et éditable dans un logiciel SIG.

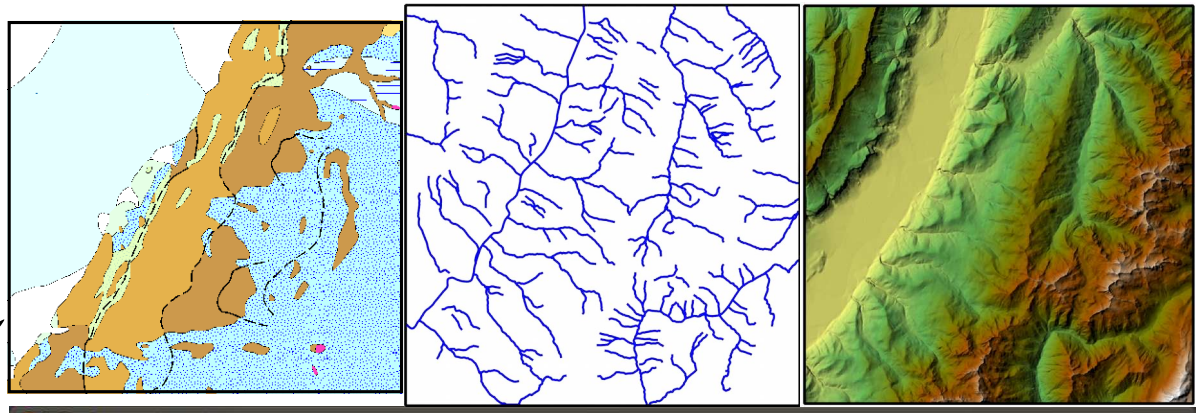

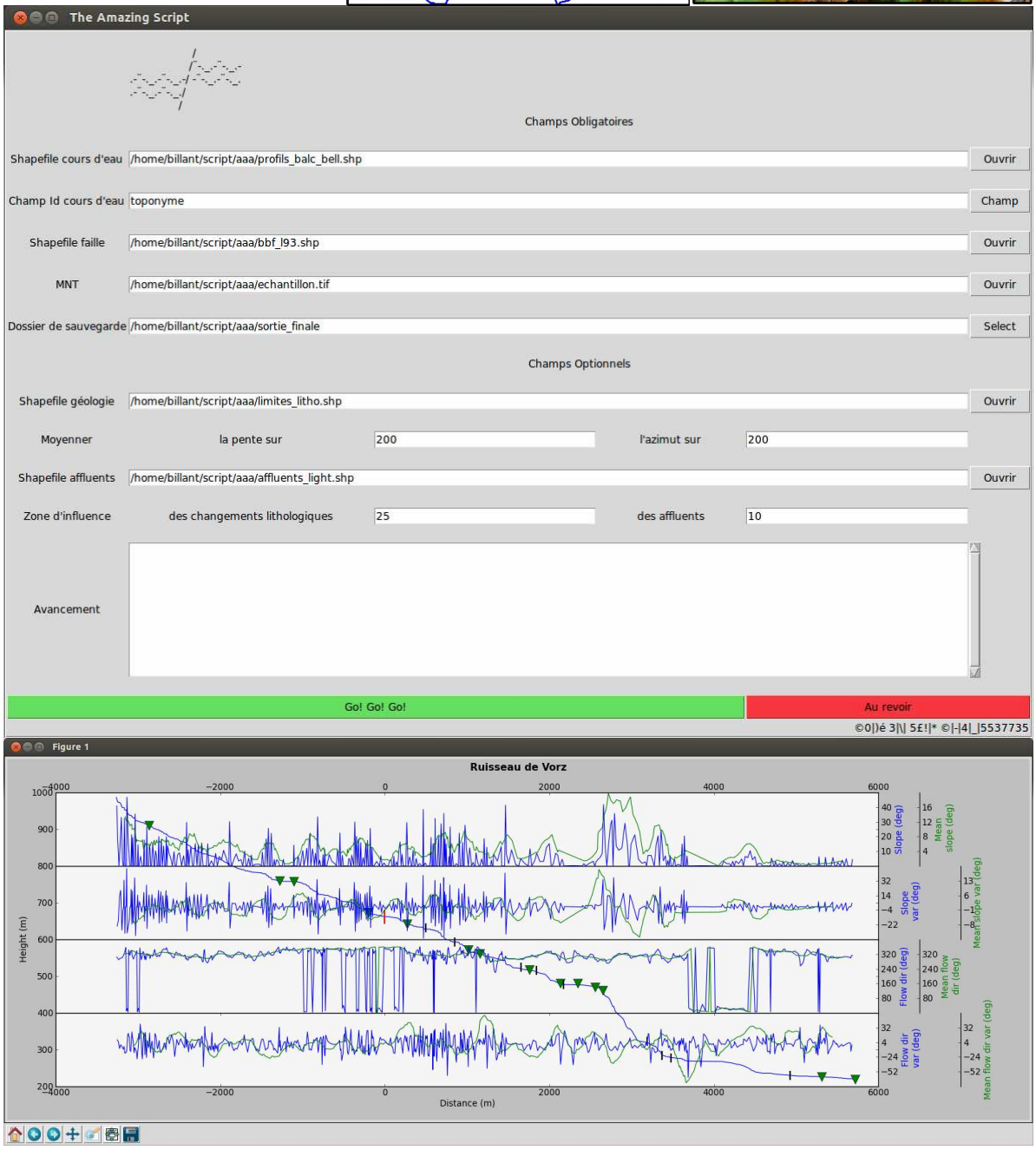
The Amazing Script
Champs Obligatoires
Shapefile cours d'eau
/home/billant/script/aaa/profils_balc_bell.shp
Ouvrir
Champ Id cours d'eau
toponyme
Champ
Shapefile faille
/home/billant/script/aaa/bbf_l93.shp
Ouvrir
MNT
/home/billant/script/aaa/echantillon.tif
Ouvrir
Dossier de sauvegarde
/home/billant/script/aaa/sortie_finale
Select
Champs Optionnels
Shapefile géologie
/home/billant/script/aaa/limites_litho.shp
Ouvrir
Moyenner
la pente sur
200
l'azimut sur
200
Shapefile affluents
/home/billant/script/aaa/affluents_light.shp
Ouvrir
Zone d'influence
des changements lithologiques
25
des affluents
10
Avancement
Go! Go! Go!
Au revoir
©0|}é 3|\| 5£!|* ©|-|4|_|5537735

Figure 1
Ruisseau de Vorz
Height (m)
Distance (m)
Slope (deg)
Mean slope (deg)
Slope var (deg)
Mean slope var (deg)
Flow dir (deg)
Mean flow dir (deg)
Flow dir var (deg)
Mean flow dir var (deg)

ANNEXE 3 : MESURES H/V ET COURBES H/V

Points	Pic Fréquence	Fenêtre de calcul (s)	Nombre de fenêtres de calcul	f0 (Hz)	Incertitude f0	Amplitude A0	Azimuth direction d'énergie (°)	WGS84 Latitude	WGS84 Longitude
S3-1	Oui, pic aplati	60	59	3,31325	0,317798	4,15758		44,903629	4,828529
S3-10	Oui, 2 pics	60	59	0,704439	0,121402	2,4599	150,0	44,901297686	4,829337814
S3-10	Oui, 2 pics	60	59	0,704439	0,121402	2,4599		44,901297686	4,829337814
S3-12	Non	60	47	0,728556	0,110475	1,86902		44,9027888730	4,829451857
S3-13	Oui, 2 pics	60	38	0,73381	0,0715615	3,58096	150,0	44,901711154	4,826840076
S3-14	Non	60	39	0,778347	0,150288	1,98252		44,899633383	4,815959789
S3-15	Non	60	46	0,649291	0,109137	3,37751		44,902235834	4,818066698
S3-16	**Oui**	60	41	0,729898	0,0529205	3,92977	110,0	44,903915938	4,821016874
S3-17	**Oui**	60	59	0,694153	0,0831441	2,82987	140,0	44,901727562	4,822807723
S3-2	**Oui**	60	41	0,720674	0,0311114	5,18589	130,0	44,902342	4,824178
S3-3	**Oui**	60	41	0,679719	0,0898895	3,34157	50,0	44,903341	4,819842
S3-4	**Oui**	60	59	0,712512	0,0523526	4,90446	150,0	44,897336	4,825158
S3-6	**Oui**	60	55	0,747224	0,0683009	3,86693	160,0	44,897843271	4,826446026
S3-7	Oui, 2 pics	60	45	0,757355	0,0957947	3,69717	170,0	44,898193442	4,827562993
S3-8	**Oui**	60	55	0,732428	0,0638669	3,33532	140,0	44,899444557	4,825268929
S3-9	Oui, 2 pics	60	48	0,741501	0,104475	2,2602	150,0	44,900700909	4,82830401
S4-1	Plusieurs pics	60	44	10,1288	0,621291	2,11947		44,900554	4,831712
S4-10	**Oui**	60	51	0,718295	0,049307	5,47707	140,0	44,901216947	4,825492791
S4-12	Non	60	33	0,63696	0,0900071	3,71293		44,903676789	4,827198345
S4-13	Non	60	59	2,36923	0,166998	4,55423		44,905677823	4,825623161
S4-14	Non	60	53	0,576157	0,0986374	3,2069		44,901795445	4,81688615
S4-16	Non	60	39	0,744585	0,0834483	2,2964		44,904368154	4,821874666
S4-17	**Oui**	60	51	0,735541	0,0873406	5,05319	130,0	44,903903744	4,823706291
S4-2	Plusieurs pics	60	59	6,62748	0,552969	4,23966		44,906504	4,826083
S4-3	Oui, 2 Pics	60	50	0,750123	0,052249	4,42359	160,0	44,900553	4,826939
S4-4	**Oui**	60	46	0,661934	0,0630468	3,6773	130,0	44,901432	4,821478
S4-5	Oui, 2 pics	60	43	1,05408	0,0802935	2,10385		44,901118	4,814709
S4-6	Non	60	33	0,688881	0,0853281	3,78677		44,899573822	4,830618717
S4-7	Oui, 2 pics	60	38	1,89626	0,17763	3,85271		44,897102847	4,824034081
S4-8	Non	60	43	5,6754	0,481273	4,56273		44,897419561	4,820108384
S4-9	**Oui**	60	48	0,710699	0,0762112	5,36784	140,0	44,899977648	4,826347299
S5-1	Plusieurs pics	60	36	0,709493	0,138615	1,76139		44,901948	4,83032
S5-10	**Oui**	60	47	0,674216	0,0666844	3,47387	160,0	44,902246617	4,828086787
S5-11	Oui, 2 pics	60	53	0,70714	0,0556321	3,9313	130,0	44,900113253	4,822157697
S5-12	**Oui**	60	52	0,708718	0,0535008	3,61424	130,0	44,903178336	4,825564779
S5-13	Non	60	43	2,21199	0,331257	1,8896		44,898832374	4,81859981
S5-14	Non	60	50	1,95163	0,323793	2,03021		44,899960627	4,817436569
S5-16	Non	60	59	0,701517	0,122001	2,76101		44,901068718	4,820450231
S5-2	**Oui**	60	59	0,689459	0,0620244	5,08146	150,0	44,905222	4,822215
S5-3	**Oui**	60	55	0,767553	0,0904557	4,03528	160,0	44,898564	4,828751
S5-4	**Oui**	60	53	0,701086	0,0514922	4,13374	160,0	44,899078	4,8237
S5-5	Plusieurs pics	60	36	1,30894	0,243065	1,88309		44,896102	4,819259
S5-6	Oui, 2 pics	60	41	0,753123	0,102294	2,8259	160,0	44,899148403	4,829981967
S5-7	Non	60	44	2,16428	0,255457	4,61412		44,896819814	4,822768971
S5-8	Non	60	35	2,17027	0,307393	1,91177		44,897913346	4,821510902
S5-9	**Oui**	60	37	3,72129	0,456819	2,77176		44,896126142	4,821226823

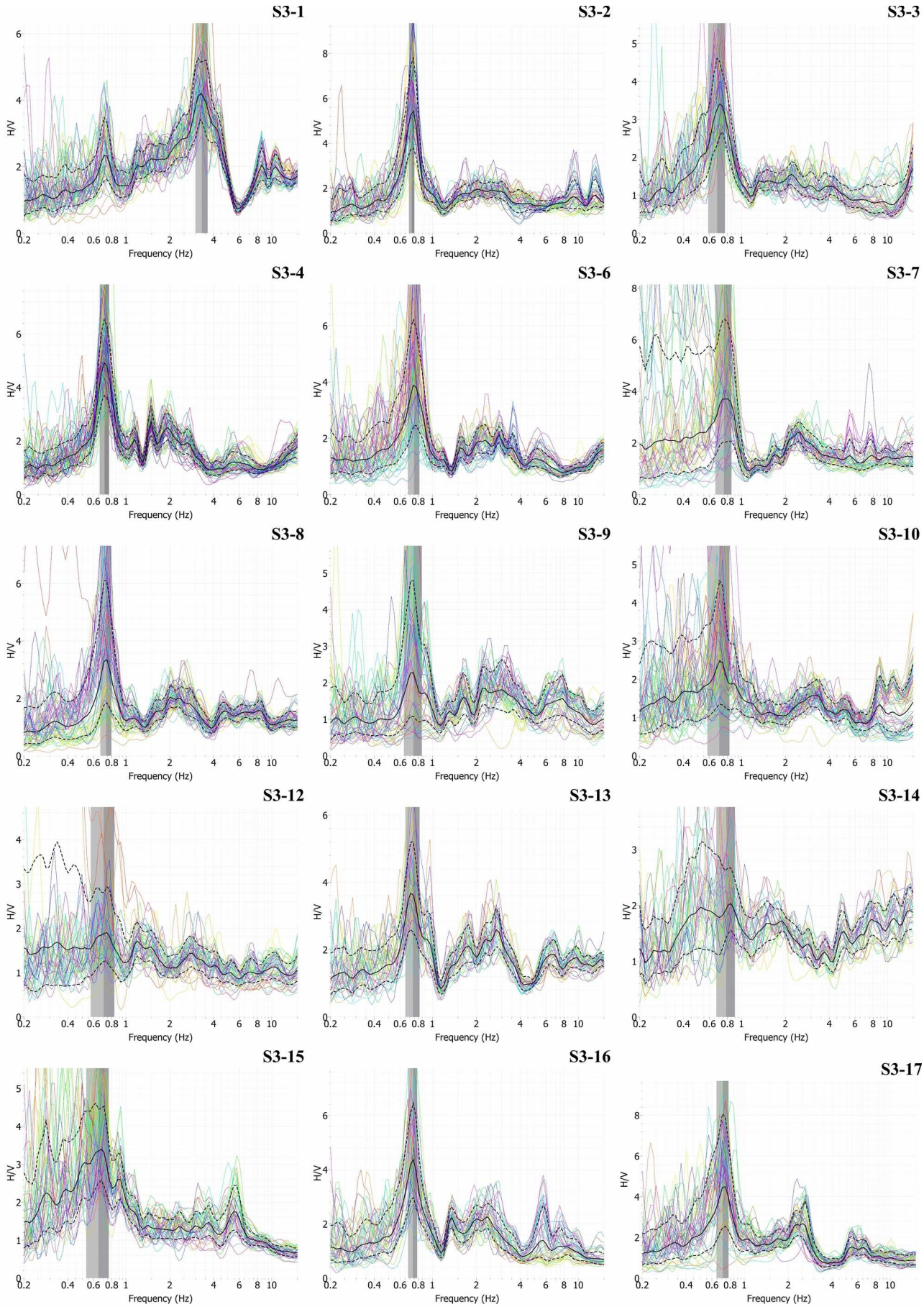
S3-1
S3-2
S3-3
S3-4
S3-6
S3-7
S3-8
S3-9
S3-10
S3-12
S3-13
S3-14
S3-15
S3-16
S3-17
H/V
Frequency (Hz)

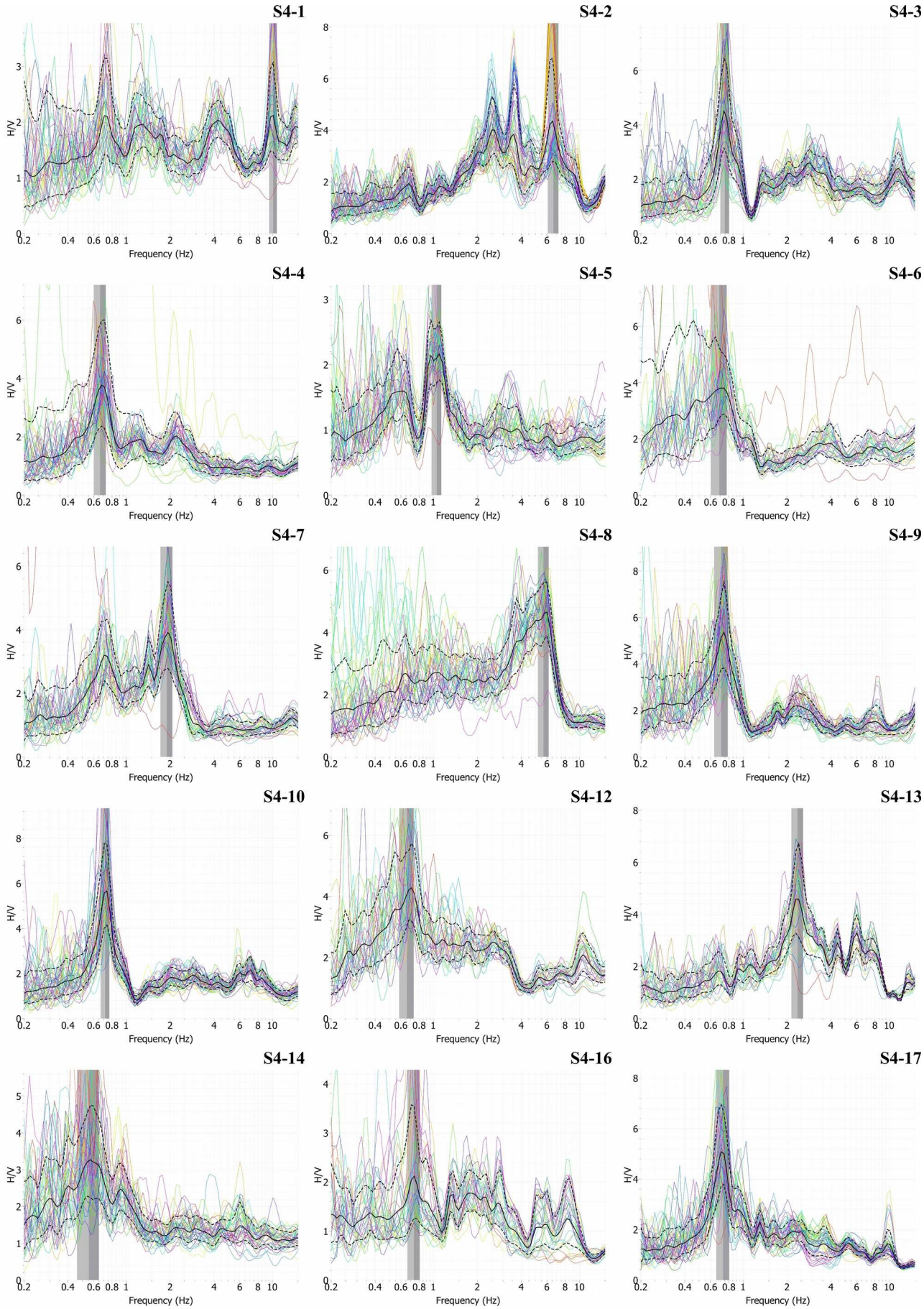
S4-1
S4-2
S4-3
S4-4
S4-5
S4-6
S4-7
S4-8
S4-9
S4-10
S4-12
S4-13
S4-14
S4-16
S4-17
H/V
Frequency (Hz)

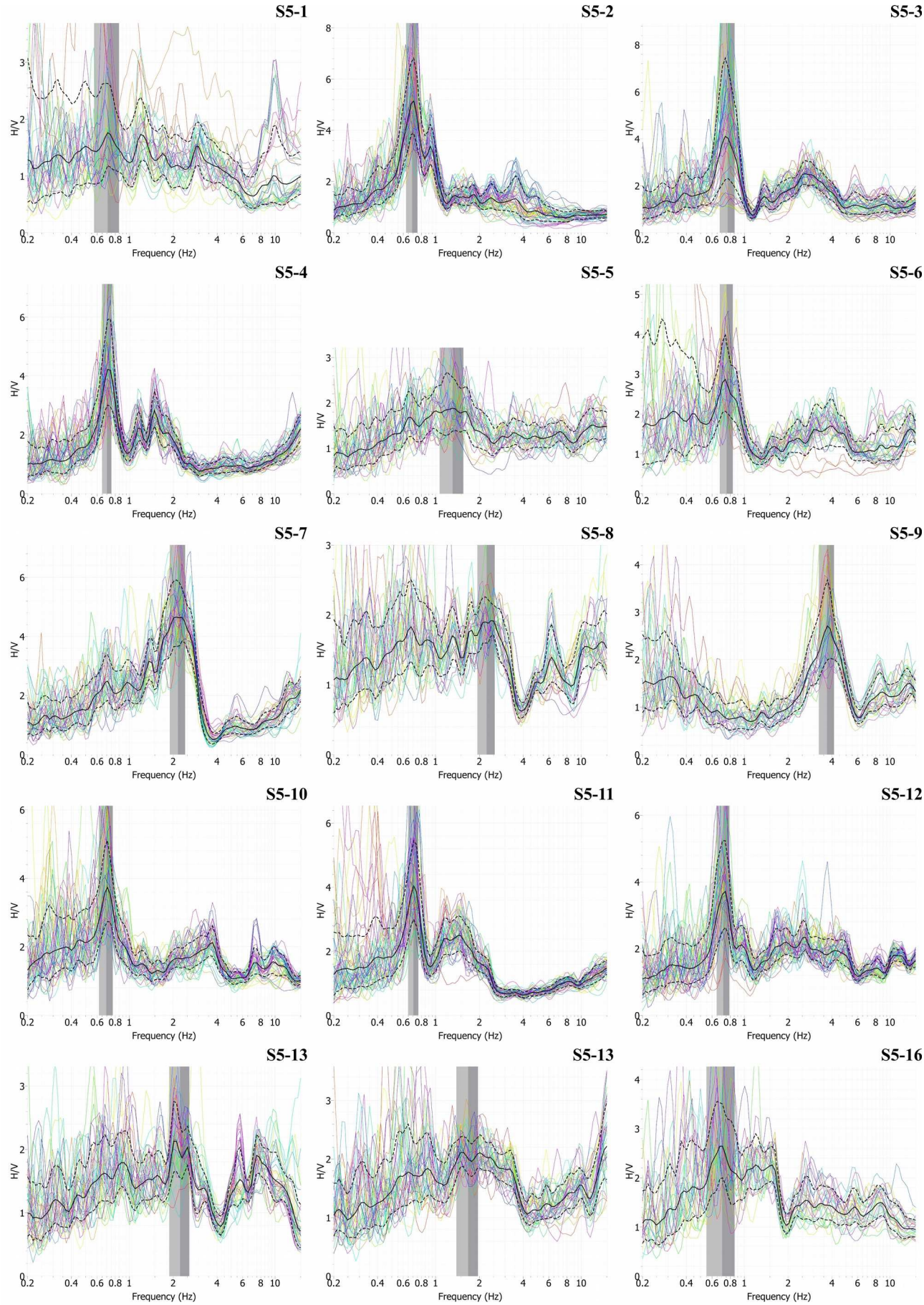
S5-1
S5-2
S5-3
S5-4
S5-5
S5-6
S5-7
S5-8
S5-9
S5-10
S5-11
S5-12
S5-13
S5-13
S5-16
H/V
Frequency (Hz)